COUPLED FLOW AND CONTAMINANT TRANSPORT MODELING IN LARGE WATERSHEDS

A Dissertation
Presented to
The Academic Faculty

By

Orhan Gunduz

In Partial Fulfillment
Of the Requirements for the Degree
Doctor of Philosophy in the
School of Civil and Environmental Engineering

Georgia Institute of Technology
April, 2004

COUPLED FLOW AND CONTAMINANT TRANSPORT MODELING IN LARGE WATERSHEDS

Approved by:

Dr. Mustafa M. Aral (Advisor)

Dr. Terry W. Sturm

Dr. Philip J. W. Roberts

Dr. Paul A. Work

Dr. Turgay Uzer

Date Approved:

April 5, 2004

To the loving memory of my grandmother,

Without her support, I could not have been the man I am today…

ACKNOWLEDGMENTS

I would like to express my sincere gratitude and appreciation to my research and academic advisor, Dr. Mustafa M. Aral, for his invaluable guidance, encouragement and continuous support throughout my graduate studies. Without his advice and guidance, this thesis would not have been completed. I enjoyed every moment of our discussions and certainly benefited a lot from his academic insight to complicated problems. I find myself extremely lucky to have the opportunity to have met him and worked with him.

I would also like to thank my committee members; Dr. Terry W. Sturm, Dr. Philip J. W. Roberts, Dr. Paul A. Work and Dr. Turgay Uzer, for their invaluable comments, suggestions and advice to improve this thesis to its final form.

I would like to express my sincere appreciation to the Turkish Council of Higher Education, Dokuz Eylul University and Georgia Sea Grant College Program of the National Sea Grant Program for providing financial and academic support during my studies in the United States.

I would also like to take this opportunity to express my appreciation and indebtedness to my father, Nuri G. Gunduz, for providing me the vision to pursue my dream; my mother, Nermin Gunduz, for her love and her support to achieve the best; my sister, Ozge Gunduz, for her smile and warm feelings, and my grandmother, Fikriye Yaman, for all the love, encouragement and dedication she has provided to me.

Finally, I would especially like to express my gratitude for my wife, Basak Gunduz, and my son, Batu O. Gunduz, whose love, encouragement, understanding, patience and endless support have made it all possible. Without you next to me, this work would have never been completed to the level it is now and my life would have not been so much full of love, fun and sharing.

TABLE OF CONTENTS

LIST OF TABLES

LIST OF FIGURES

LIST OF SYMBOLS

a : Location of sampling point in Gaussian quadrature (-) and local boundary coordinate (L)

A : Active cross-sectional area of channel flow (L^2)

A_o : Inactive cross-sectional area (off-channel storage) (L^2)

B : Active cross-sectional top width (L)

B_o : Inactive cross-sectional top width (L)

C : Specific moisture capacity in the unsaturated zone (L^{-1})

c_1 : Unit system dependent constant in Manning's equation (-)

C_{gD} : Specified contaminant concentration in groundwater (ML^{-3})

C_g : Vertically-averaged contaminant concentration in groundwater (ML^{-3})

$\hat{C}_g$: Approximate vertically-averaged contaminant concentration in groundwater (ML^{-3})

C_{g0} : Initial contaminant concentration in groundwater (ML^{-3})

C_I : Contaminant concentration in infiltrating water (ML^{-3})

C_o : Contaminant concentration in overland inflow to the river channel (ML^{-3})

C_r : Contaminant concentration in river channel (ML^{-3})

C_{r0} : Initial contaminant concentration in river channel (ML^{-3})

C_{ru} : Upstream boundary condition contaminant concentration in river channel (ML^{-3})

C_v : Contaminant concentration in the inflowing stream of variable boundary condition in groundwater (ML^{-3})

C_w : Contaminant concentration in point source (ML^{-3})

d : Water depth in the river channel (L)

D : Hydrodynamic dispersion coefficient in groundwater (L^2T^{-1})

D_L : Longitudinal dispersion coefficient in river channel (L^2T^{-1})

D_m : Molecular diffusion coefficient (L^2T^{-1})

D_{sed} : Vertical dispersion coefficient in the channel bed (L^2T^{-1})

E : Dummy parameter (-)

f : Arbitrary function (-)

g : Gravitational acceleration (LT^{-2})

g_x : The x-coordinate of the parametric equation defining the river in domain (-)

g_y : The y-coordinate of the parametric equation defining the river in domain (-)

h_d : Downstream boundary condition water surface elevation in river (L)

h_g : Vertically-averaged groundwater hydraulic head above a datum (L)

h_{g_0} : Initial groundwater head (L)

h_{gD} : Specified head boundary condition value in groundwater (L)

$\hat{h}_g$: Approximate groundwater hydraulic head above a datum (L)

$\left(\hat{h}_g\right)_{avg}$: Element average approximate groundwater head above a datum (L)

h_o : Overland flow water surface elevation (stage) above a datum (L)

h_{o0} : Initial overland flow water surface elevation (stage) above a datum (L)

h_{oD} : Initial overland flow water surface elevation (stage) above a datum (L)

h_r : Channel flow water surface elevation (stage) above a datum (L)

h_{r0} : Initial water surface elevation in channel (L)

h_T : Total head loss in a junction (L)

h_u : Upstream boundary condition water surface elevation in river channel (L)

H : Heaviside step function (-)

I : Infiltration rate (LT^{-1})

k : Decay coefficient of contaminant (T^{-1})

K : Channel conveyance (L^3T^{-1})

K_d : Partitioning coefficient (L^3M^{-1})

K_{ec} : Contraction/expansion coefficient (-)

K_g : Saturated hydraulic conductivity in groundwater (LT^{-1})

K_o : Diffusion coefficients in overland flow (L^2T^{-1})

K_r : Saturated hydraulic conductivity of channel bottom sediments (LT^{-1})

K_u : Unsaturated hydraulic conductivity in vertical direction (LT^{-1})

K_w : Biodegradation rate constant for contaminant (T^{-1})

L_d : Total channel flow domain length (L)

M : Mass loading (MT^{-1})

M_{L1} : Momentum flux due to lateral seepage inflow/outflow (L^3T^{-2})

M_{L2} : Momentum flux due to lateral overland inflow/outflow (L^3T^{-2})

m : Constant in kinematic wave equation (-)

m_r : Thickness of the channel bottom sediments (L)

m_v : Empirical constant in van Genuchten model (-)

n : Porosity of the medium (-)

n_c : Manning's roughness coefficient in channel ($L^{-1/3}T$)

n_o : Manning's roughness coefficient over land surface ($L^{-1/3}T$)

n_{sed} : Porosity of the channel bottom sediment (-)

n_r : Number of river channels in the domain (-)

n_v : Empirical constant in van Genuchten model (-)

n_w : Number of wells in the domain (-)

N : Total number of nodes in the entire channel network or in groundwater flow domain (-)

N_i : i^{th} weighing function (-)

N_j : j^{th} shape function (-)

N_k : Number of nodes in channel k (-)

q : Darcy flux ($L^3L^{-2}T^{-1}$)

q_{L1} : Lateral seepage inflow/outflow per channel length ($L^3L^{-1}T^{-1}$)

q_{L2} : Lateral overland inflow/outflow per channel length ($L^3L^{-1}T^{-1}$)

q_C : Head-dependent boundary condition flux value ($L^3L^{-1}T^{-1}$)

q_N : Specified flux boundary condition value ($L^3L^{-1}T^{-1}$)

q_v : Volumetric inflowing flux rate of variable boundary condition ($L^3L^{-2}T^{-1}$)

Q : Channel discharge (L^3T^{-1})

Q_0 : Initial channel discharge (L^3T^{-1})

Q_d : Downstream boundary condition discharge (L^3T^{-1})

Q_u : Upstream boundary condition discharge (L^3T^{-1})

Q_w : Point source (i.e., well) strength (L^3T^{-1})

R : Precipitation rate (LT^{-1})

$\tilde{R}$: Residual in the Galerkin method (variable in each model)

R_d : Retardation coefficient (-)

R_h : Hydraulic radius (L)

s : Scale parameter in under-relaxation coefficient (-)

s_c : Sinuosity factor for continuity equation (-)

s_m : Sinuosity factor for momentum equation (-)

S_{ec} : Contraction/expansion slope (-)

S_e : Effective saturation content (-)

S_f : Channel/floodplain boundary friction slope (-)

S_s : Specific storage coefficient ($L^3L^{-3}L^{-1}$)

S_w : Degree of saturation in unsaturated zone (-)

S_y : Specific yield of unconfined aquifer (-)

t : Time coordinate (T)

u : Parameter of the parametric equation defining sources and sinks (-)

v : Pore-water velocity in groundwater (LT^{-1})

V : Flow velocity in the river channel (LT^{-1})

V^* : Shear velocity in the river channel (LT^{-1})

w : Weighing constant in Gaussian quadrature (-)

w_r : Wetted perimeter of channel bed (L)

x : Global spatial coordinate in longitudinal direction (L)

y : Global spatial coordinate in transverse direction (L)

z : Global spatial coordinate in vertical direction (L)

z_b : Top elevation of bottom impervious layer above a datum (L)

z_g : Ground surface elevation above a datum (L)

z_r : Bottom elevation of channel bed above a datum (L)

z_{wt} : Water table elevation above a datum (L)

α : Weighing coefficient (-)

α_c : A weighing parameter in Newton-Raphson method used to evaluate the first estimate of the unknown variables (-)

α_k : A constant in kinematic wave equation ($L^{1/3}T^{-1}$)

α_L : Longitudinal dispersivity of porous medium (L)

α_T : Transverse dispersivity of porous medium (L)

α_v : Empirical constant in van Genuchten model (-)

β : Momentum correction coefficient for non-uniform velocity distribution (-)

δ : Kronecker delta (-) or Dirac delta function (argument^{-1})

γ : Iteration-dependent under-relaxation coefficient (-)

ε : Maximum change in hydraulic head for all nodes between two iterations (L)

η : Local transverse coordinate (L)

θ : Volumetric moisture content in unsaturated zone (L^3L^{-3})

θ_0 : Initial volumetric moisture content in unsaturated zone (L^3L^{-3})

θ_c : Angle of inclination of between principle and global coordinate axis (-)

θ_f : Weighing coefficient (-)

θ_r : Residual moisture content in unsaturated zone (L^3L^{-3})

θ_s : Saturation moisture content in unsaturated zone (L^3L^{-3})

ξ : Local longitudinal coordinate (L)

λ : Radioactive decay constant for contaminant (T^{-1})

ρ_b : Bulk density of the porous medium (ML^{-3})

τ : Tortuosity of porous medium (-)

Γ : Global groundwater flow domain boundary (L)

Γ_1 : Specified head boundary in groundwater flow model (L)

Γ_2 : Specified flux boundary in groundwater flow model (L)

Γ_3 : Head-dependent boundary in groundwater flow model (L)

υ_x : Velocity of overland flow in the direction of channel flow (LT^{-1})

ψ_f : Weighing coefficient (-)

ψ : Pressure head in unsaturated zone (L)

ψ_0 : Initial pressure head in unsaturated zone (L)

Ω : Global groundwater flow domain (L^2)

Ω_e : Local groundwater flow domain (L^2)

A : Global coefficient matrix

B : Global load vector

$\hat{\mathbf{C}}_\mathbf{g}$: Global approximate vector for contaminant concentration in groundwater

f : Vector of arbitrary functions

F : Load vector

$\hat{\mathbf{h}}_\mathbf{g}$: Global approximate vector for hydraulic head

J : Jacobian matrix in Newton-Raphson scheme

M : Mass matrix

n : Unit normal vector to the boundary

S : Stiffness matrix

x : Vector of unknown variables

i, j, k, l, m, o : Indices

SUMMARY

A hybrid surface/subsurface flow and transport model is developed that blends distributed parameter models with simpler lumped parameter models. The hybrid model solves the channel flow and saturated groundwater flow domains in continuous time using fully distributed physically-based formulations. This system is supplemented with the overland flow and unsaturated groundwater flow that uses lumped parameter descriptions in discrete time. This hybrid formulation decreases the computational requirements associated with overland and unsaturated zone domains in a large scale continuous watershed modeling task but still allows a representative description of the watershed flow processes.

In the proposed model, a one-dimensional channel flow model is dynamically coupled with a two-dimensional vertically-averaged groundwater flow model along the river bed. As an alternative to the commonly applied iterative solution technique, a so-called simultaneous solution procedure is developed to provide a better understanding to the coupled flow problem. This new methodology is based on the principle of solving the two flow domains within a single matrix structure in a simultaneous manner. The method eliminates the iterative scheme that is otherwise required to obtain the convergence of the solution and provides a faster solution.

In addition to the flow model, a coupled contaminant transport model is also developed to simulate the migration of contaminants between surface and subsurface domains. Based on its flow counterpart, the contaminant transport model dynamically couples a one-dimensional channel transport model with a two-dimensional vertically-averaged groundwater transport model. The coupling is performed at the river bed interface via advective and dispersive transport mechanisms. A modified extension of the proposed simultaneous solution procedure is also implemented to solve the coupled contaminant transport problem. The dynamic coupling provides the much needed understanding for the continuity of contaminants in strongly interacting surface/subsurface systems such as a river and an unconfined aquifer.

The coupled flow and transport models are applied to the lower Altamaha watershed in southern Georgia. The flow model is used to perform simulations of hydrologic and hydraulic conditions along the river and in the dynamically linked surfacial aquifer. The model predicted the flood patterns including the magnitude of peaks and their arrival times with accuracy. Under the given flow conditions, the transport model is then implemented to test alternative contaminant transport patterns both in the river and within the aquifer. It has been found that contaminated river water is much more likely to create significant consequences over the aquifer than would the contaminated aquifer water over the river due to the significant dilution of the river water over the contaminated seepage from the aquifer. Furthermore, it is observed that the channel network would serve as a conduit for rapid transport of contaminants within the aquifer to large distances in small time frames.

CHAPTER 1

INTRODUCTION

1.1. General

Since the early days of watershed modeling, hydrologists have separated and isolated the hydrology of the system into its subcomponents. They have implemented discrete models for various hydrologic processes in an effort to simulate the response of the watershed to a hydrologic disturbance. Such models have been studied and improved constantly for decades. Currently, these models reached a certain level of sophistication and many commercialized software packages became available to accurately simulate discrete flow and transport patterns in surface and subsurface flow pathways including rivers and aquifers.

It was perhaps in the early 1970s that hydrologic modelers realized that separating an otherwise strongly linked system would involve major errors in proper representation of the response characteristics. In this regard, the work of Freeze (1972a, 1972b) has been a milestone in the hydrologic simulation of watershed processes within the context of a 'single' entity. Surface and subsurface processes have thus begun to be modeled as parts of a complete system. It was not surprising to see that this development in hydrologic

modeling coincided with an era when computers and computing power started to become easily accessible to hydrologic modelers. Consequently, modelers have developed coupled models within the last two decades. This effort is still on-going and facing some tough challenges despite all computational advances achieved.

1.2. Integrated Watershed Modeling

The concept of integrated watershed modeling has emerged as a new understanding for the interactions between the surface and subsurface pathways of water. It defines the bidirectional linkage that implies the main rationale for the unity of the two systems. In this regard, surface flow processes such as channel and overland flow are integrated to subsurface flow processes in the unsaturated and saturated groundwater flow zones via the dynamic interactions at the ground surface and channel bed. Only with this kind of approach, can one successfully quantify the volumetric and mass flux balances between the domains.

The highly dynamic interactions between overland flow and unsaturated zone flow determine the amount of infiltrating/exfiltrating flux at the ground surface. Similar interactions also occur at the river bed where channel flow seeps into the underlying unconfined aquifer or vice versa. Both of these interactions are regarded as important links between the components of the hydrologic cycle and are responsible in maintaining the continuity of the entire cycle. While these interactions may operate as safety barriers to extreme conditions by decreasing the intensity and severity of major hydrological events such as floods and droughts, it is also likely that the opposite scenario is true and they tend to amplify the strength of such events and cause significant loss of life and

property. Therefore, it is of utmost importance to analyze these interactions systematically and develop management scenarios based on such quantitative assessments.

Modeling watershed processes in an integrated fashion is thus the ultimate goal. Although there is no doubt about the necessity of integrated watershed modeling, the process is a complicated task. Therefore, despite advances in computational speed and capacity, integrated watershed models still require extensive computational times for large scale applications, which in turn require the modeler to have a clear understanding of the temporal and spatial scales of the processes.

1.3. Temporal and Spatial Scales of Watershed Processes

Different flow pathways of the watershed experience entirely different time and space scales. These differences have a direct impact on the numerical discretizations of these sub-processes. One of the most evident of these differences is the time scale dissimilarities between the overland flow and the saturated groundwater flow. While the former is a much faster pathway requiring time steps on the order of seconds, the latter is a fairly slow process and calls for much larger time steps on the order of days or even months. Such differences create problems in the numerical solution procedures. Moreover, these problems are even more pronounced when the two sub-systems are solved in an integrated fashion. Similar concerns await the modeler in the spatial discretization of various domains. An example of a space scale problem is experienced in the unsaturated zone. Space scale requirements of the unsaturated zone models are

several orders of magnitude smaller than their saturated zone counterpart, which becomes a major concern in integrated modeling applications.

In addition to varying scales of subprocesses, the modeler also faces the critical issue of a representative time scale that is important to all watershed flow pathways. This directly leads to the problem of assigning a time frame for the overall analysis of the processes. For long term simulations (i.e., seasonal or annual simulations) that most modelers would prefer, the existence of the more dynamic subprocesses becomes an issue. An example is the overland flow process that only exists during a very short time frame compared to the other pathways. Additional problems are present in the simulation of overland flow when one considers the boundedness of the process in spatial and temporal dimensions. It is not easy to identify well-defined temporal and spatial extents of the overland flow pathway, hence a long term simulation of a large scale watershed clearly presents numerical difficulties when overland flow is included.

1.4. Research Needs and Objectives of the Study

Currently, integration of watershed processes are implemented at limited spatial and temporal scales. Many integrated models have been developed at the test bed scale to analyze the general consequences of interactions between flow pathways. Fewer models have been applied to small experimental watersheds. In this regard, there is an emerging need to develop models that can be applied to large scale watersheds using real-time data. Furthermore, the coupling mechanisms of the sub-processes are an important research area where the current methodologies are based on discrete solution of surface and subsurface flow systems. In discrete solution procedures, linkage between the domains is

achieved by (i) simplistic non-iterative methods in which results from the solution of one domain are directly fed into the other domain and do not accept any feedback from the other domain, or (ii) iterative methods where solutions from one domain are fed to the other in a cyclic manner until sufficient convergence is achieved between two consecutive solutions. Currently, iterative techniques are the state-of-the-art for coupling surface and subsurface flow processes. However, it is also believed that there is room for more sophisticated coupling procedures such as the advanced simultaneous solution of both processes, as proposed in this study.

Finally, despite efforts to couple flow processes, hydrological modelers were hesitant in coupling contaminant transport processes. There is no model available that performs coupled surface-subsurface contaminant transport modeling at the watershed scale. Although this may be partially attributed to the current immature state of flow coupling, it does not justify the lack of attention by hydrologic modelers. It is believed that at least some of the efforts spent on flow coupling could be re-routed towards analyzing the relationships between surface and subsurface processes in terms of contaminant transport.

Based on these facts, this study attempts to develop models that are directly applicable to large scale watershed systems. Coupled models of surface and subsurface flow processes are developed in an effort to provide a better understanding for the relative significance of the pathways that drive the hydrological cycle. Considering the numerical difficulties associated with mathematical representation and numerical solution of some of the flow processes, a hybrid modeling approach is proposed. This approach offers the much needed relief that fully physically-based distributed models suffer from

by compromising the process description of the problematic processes and proposing relatively simple empirical approaches in their representation.

Sophisticated coupling mechanisms are also studied in detail and a new, more efficient coupling mechanism is proposed and applied to large scale systems. This new simultaneous coupling technique attempts to solve surface and subsurface flow and transport processes simultaneously rather than implementing a sequential solution and an iterative improvement of the common parameters. In this regard, it is believed that this new methodology has wide applicability for coupled hydrological modeling. In addition, this study is possibly one of the first applications of coupled contaminant transport modeling in a large watershed. The proposed approach uses a semi-simultaneous coupling of surface and subsurface transport and provides linkage via not only the generally used advective transport mechanism but also the commonly neglected dispersive transport mechanism as well.

1.5. Thesis Organization

With the above mentioned objectives, this thesis is organized in 6 chapters and 12 appendices. The main text of each chapter is intentionally kept as short as possible in favor of easy reading and is written to include only the fundamental concepts and the new ideas. All details associated to the numerical solution procedures are given in the appendices. In Chapter 2, the thesis starts with a literature review where descriptions of watershed models as well as watershed flow and transport processes are presented. A summary of available coupling techniques and scale issues is also given in this chapter. Mathematical models of key watershed processes are discussed in Chapter 3, where the

governing equations, initial and boundary conditions and the implemented numerical solution procedures of each process are presented from the perspective of large scale watershed modeling. Two coupled models are studied in detail and a hybrid modeling approach is proposed. The details of the new simultaneous coupling procedure are also presented in this chapter. In Chapter 4, the focus switches to the major transport processes, and a coupled surface-subsurface contaminant transport model is presented. The governing equations, initial and boundary conditions and the numerical solution procedures of the proposed model are presented in this chapter of the thesis. As stated earlier, all the detailed derivations and formulations of the numerical solution schemes are given in the appendices. The new coupled models of flow and transport are then used to simulate the hydrological and hydrochemical characteristics of a large scale watershed. The details of this application are given in Chapter 5. Finally, the thesis concludes with a conclusion and recommendations section in Chapter 6.

CHAPTER 2

BACKGROUND AND LITERATURE REVIEW

In this chapter, background information on watershed processes and modeling principles are reviewed with special emphasis on different hydrologic pathways encountered in a watershed. The mathematical description of these processes and their numerical solution are reviewed along with a discussion of alternative coupling mechanisms utilized to link various pathways in a watershed. After coupling processes are introduced, a detailed analysis of scale problems in watersheds is presented including the spatial and temporal scales that are common to various pathways. The chapter concludes with a discussion of the data requirements of watershed models.

2.1. Characteristics of Watershed Models

Models that describe watershed hydrology are classified according to several criteria. One of the most significant of these classifications is based on the spatial variability of the parameters that define the flow processes (Abbott and Refsgaard, 1996). In this regard, a distributed parameter model takes into account the spatial variability in all parameters of concern, whereas a lumped parameter model assumes the watershed to

be single unit with variables and parameters representing average values for the entire catchment. From this perspective, a lumped parameter model downscales and simplifies a complex system to a single unit entity.

Another closely related classification of watershed models is based on system characteristics. Such a classification distinguishes models that are based on fundamental laws of physics from models that are solely based on certain empirical rules of input/output functions. In this regard, the so-called physically-based model describes the natural system using fundamental physics laws that define the movement of mass, momentum and energy by using complex mathematical representations (Abbott and Refsgaard, 1996). These mathematical relations are partial differential equations, integral-differential equations or integral equations including but not limited to the Saint Venant equations for channel and overland flow, Richards' equation for unsaturated zone flow and Boussinesq's equation for saturated groundwater flow. Such models are also known as 'white box' models expressing the fact that the details associated with the underlying processes are all known and clear to the modeler. Physically based models always display the characteristics of distributed models as they involve at least one spatial dimension and variations along this dimension. Well known examples of physically-based distributed models include the SHE model of Abbott et al. (1986a and 1986b), IHDM model of Beven et al. (1987), THALES model of Grayson et al. (1992) and MIKE SHE model of Refsgaard and Storm (1995).

On the opposite extreme, empirical models are developed with little or no consideration to the underlying physical theory and attempt to explain the natural behavior by using simple input-output relationships. In this regard, this type of a model is

generally called a “black box” model about which the modeler has often little or no physical understanding of its processes. It serves as a simple mechanism that converts the input information to some sort of an output response without any consideration of the internal characteristics of the process. Abbott and Refsgaard (1996) have further classified black box models into three main groups: (i) empirical hydrological methods; (ii) statistically-based methods; and, (iii) hydroinformatics-based methods. The empirical hydrological methods are amongst the best known black box models. Unit hydrograph theory and Soil Conservation Service (SCS) curve number method are examples of this type of model. The statistically-based methods include many models developed using regression and correlation analysis of the available data. These methods are also called the transfer function models that convert an input time series to some output time series. An example of this type of black box model is the antecedent precipitation index (API) model that correlates rainfall volume and duration, past days of rainfall and season of year to runoff. Finally, a new group of black box models called the hydroinformatics-based methods are developed in parallel with the recent advances in information technology such as artificial neural networks and genetic algorithms. It is, however, important to note that, regardless of the level of advancement achieved with an empirical model, it will always be one step behind the physics-based models as the latter provides a thorough and more correct description of the hydrological processes in a watershed. Furthermore, physics-based models also provide a suitable platform where all information associated with the watershed could be extracted without much difficulty.

Despite their drawbacks, however, empirically-based models are still extensively used due to the simplicity and speed of the analysis. Examples of empirically-based

distributed parameter models include the ones that are developed to perform simple rainfall-runoff analysis such as the SCS curve number method (Still and Shih, 1985) or the ones that are formulated to carry out fairly complicated watershed analysis such as the Hydrologic Simulation Program-Fortran (HSPF) model (Donigian et al., 1995).

Another possible classification for hydrological models is carried out based the time scale of the process. From a broader perspective, models could be continuous in time performing real time simulations or they could be discrete in time implementing simulations that are based on daily, monthly or even yearly-averaged values of model parameters (Singh, 1995). Nevertheless, this classification does not have clear-cut boundaries similar to the previously mentioned classifications due to the fact that even a continuous-in-time model uses certain time steps that, in essence, represent the average values within that time step. In this regard, one can argue that there would never be a continuous time model since the definition of the time step violates the continuity of the process. This discussion could further branch out when one realizes the fact that some of the watershed processes such as overland flow are so limited in time, when compared to others such as channel or groundwater flow, that continuous simulation of all watershed flow pathways in a simultaneous manner is simply not feasible with our current level of understanding. It is probably this motivation that forces the modelers to develop event-based models that run only during the time period when all watershed processes physically exist.

2.2. Hydrologic Flow Processes and Pathways in a Watershed

The hydrology of a watershed could be analyzed in two broad categories: (i) surface flow processes; and, (ii) subsurface flow processes. A combination of these two major flow categories defines the overall response of the system to a hydrologic input. The surface flow processes are further classified into channel and overland flow sub-systems where the surface flow depth, velocity and width clearly proposes the presence of two distinct domains which may or may not be analyzed separately depending on the purpose of the analysis. The channel flow is usually defined as the bulk movement of water in domains with relatively well-defined boundaries. It is considered to be the major conveyance medium in terms of the quantity of water transported downstream. The channel flow is characterized by high flow velocities and depths and is considered to be a fully-turbulent flow phenomenon (Chow, 1959). The overland flow subsystem, on the other hand, is defined over the entire surface area of the watershed with no well-defined boundaries. Although the small flow depths and velocities of overland flow suggest that the flow is in the laminar range, additional factors including rainfall impact, vegetation, channelized flow and the non-fixed bed phenomena complicate the problem. In this regard, a general consensus has been achieved among hydraulics experts that the overland flow covers both laminar and turbulent flows (Moore and Foster, 1990). Since overland flow occurs as an outcome of space and time variable precipitation input, it is represented by highly variable spatial distribution and temporal coverage. This major difficulty associated with overland flow becomes even more pronounced in the presence of small water depths and velocities and complicates accurate simulation of overland flow processes.

The subsurface flow is generally defined by the variably-saturated flow phenomena according to the level of saturation of the porous medium (Bear, 1979). The domain could be spatially and temporally variably-saturated depending on the overall flow behavior, boundary conditions and forcing functions. In general, the variably-saturated three-dimensional domain is subdivided into: (i) a saturated flow zone; and, (ii) an unsaturated flow zone according to the level of saturation of the porous medium. These two sub-systems are separated from each other by the groundwater table, below which a saturated groundwater flow zone develops and above which, an unsaturated groundwater flow zone occurs. As the position of the water table is spatially and temporally variable in a watershed, the domain that is considered to be saturated varies accordingly and any modeling effort must consider the associated consequences. Although the subsurface flow processes can be modeled as a single variably-saturated medium, it is generally treated as two separated systems linked to each other at the groundwater table. This artificial separation of variably-saturated subsurface flow phenomenon into saturated and unsaturated zones simplifies the analysis and provides a more straightforward understanding of the overall hydrologic conditions of the watershed.

In light of the above discussion, the major watershed processes of concern are considered to be: (i) the channel flow; (ii) the overland flow; (iii) the unsaturated zone groundwater flow; and, (iv) the saturated zone groundwater flow. The mathematical and physical characteristics as well as possible numerical solution methodologies of these watershed flow pathways are discussed in the following sections.

2.2.1. Channel Flow

The channel flow is characterized by small water depths when compared to other major systems such as seas, oceans and large inland lakes. While these large flow processes are described by the general three-dimensional hydrodynamic equations of fluid flow (i.e., the mass conservation equation and the Navier-Stokes equations of motion), many flow systems of interest to the hydrologic modeler, including channel flow, are characterized by small flow depths in the vertical dimension compared to their lateral and longitudinal flow dimensions. For such systems, the two-dimensional, depth-averaged hydrodynamic equations are generally deemed sufficient to describe this shallow water flow phenomenon as it occurs in rivers, estuaries, shallow lakes and over land surfaces. The shallow water equations that are used to model these flows are developed by vertically averaging the general three-dimensional equations of mass continuity and momentum (Dronkers, 1964; Chow and Ben-Zvi, 1973; Zhang and Cundy, 1989; Weiyan, 1992).

The channel flow is a good example of a shallow water flow system. It has a small vertical flow component when compared to its longitudinal and transverse flow dimensions (i.e., small depth to width and depth to length ratios). Furthermore, channel flow in small to moderate sized rivers is also characterized by small widths such that velocity and depth are assumed to vary only in the direction of flow and a single velocity and depth is assumed to govern the entire channel width. Under these assumptions, river channel flow is described by the one-dimensional analog of the three-dimensional hydrodynamics equations and is generally known as the Saint-Venant equations after

French hydraulic engineer B. de Saint-Venant who introduced them in late 19th century (Strelkoff, 1969).

The assumption of one-dimensional flow has been widely accepted and numerous models have been developed for analyzing unsteady, non-uniform flow in open channels (Liggett and Woolhiser, 1967; Baltzer and Lai, 1968; Strelkoff, 1970; Fread, 1993; Havno et al, 1995). Particularly for large scale applications such as watershed modeling, the one-dimensional flow assumption is the only practically available option to the hydrologic modeler (Refsgaard and Storm, 1995; Jha et al., 2000).

Even though the Saint-Venant equations form the basis of the general mathematical model of unsteady, non-uniform flow in channels, they should be modified for application to natural waterways since natural systems such as rivers and streams show significant variability from man-made channels in terms of channel geometry, channel bed roughness and river form. These characteristics are extremely important for alluvial systems where braiding and meandering are commonly observed. As a result, a number of researchers including Fread (1976) and DeLong (1986 and 1989) have modified the Saint-Venant equations so that they could be applied in river channels. They have introduced the effects of complex channel geometry (i.e., channel-floodplain system) and meandering pattern in the equations. Upon these modifications, the Saint-Venant equations became capable of accounting for the effects of the floodplain, inactive (off-channel or dead) storage and the meandering ratio (sinuosity factor) of the river.

Both the original and the modified Saint-Venant equations have various simplified forms, which are obtained by neglecting some of the terms in the one-dimensional conservation of momentum equation. These simplified forms of the

momentum equation coupled with the continuity equation yield a number of approximate distributed flow methods. Without any simplification, the full Saint-Venant equation is also known as the dynamic wave model. It is the only model that can accurately simulate the backwater effects in a channel, by allowing for propagation of the changes in discharge and water depth in the upstream direction. The local and convective acceleration terms as well as the pressure force term describe this upstream movement of these changes. The dynamic wave model is the model of choice when the backwater effects are significant or the channel slope is mild (Sturm, 2001). If the local and convective acceleration terms in the momentum equation are neglected, the so-called diffusion wave model is obtained. The diffusion wave model can also be used to simulate backwater effects only to a certain degree, via the pressure force term. Therefore, it cannot be the model of choice when significant backwater effects are present. The diffusion wave model is further simplified by neglecting the pressure force term to obtain the simple kinematic wave model that is known to be the simplest channel flow model. The kinematic wave model assumes that friction slope is equal to channel bed slope and does not allow the simulation of backwater effects as flood wave can only travel downstream (Sturm, 2001).

The complete Saint-Venant equations are a set of partial differential equations with two independent and two dependent variables. There is no analytical solution to these equations except in a few special cases. In general, the only choice of solution for these equations is through the application of numerical techniques, which are classified as: (i) method of characteristics; (ii) finite difference methods; and, (iii) finite element

methods. These methods can be further classified as explicit or implicit methods depending on the solution approach selected.

Among the three available solution procedures, the method of finite elements is seldom used to solve the Saint-Venant equations of unsteady flow (Cooley and Moin, 1976; Szymkiewicz, 1991; Blandford and Ormsbee, 1993). This is mainly due to the fact that the finite element method does not offer any advantages over the method of characteristics or the finite difference technique in a one-dimensional setup. The power of the finite element method becomes apparent in two- or three- dimensional treatment of unsteady flow routing in natural waterways, such as very wide river systems and estuaries.

The method of characteristics was the first successfully applied technique for the solution of the Saint-Venant equations. The application of this technique required a transformation of the original partial differential equations to their characteristic forms, which are ordinary differential equations. In the 1960's, Liggett and Woolhiser (1967) and Streeter and Wylie (1967) developed explicit solution techniques to the characteristic forms of the Saint-Venant equations. Similarly, Amein (1966) and Wylie (1970) worked out some implicit solution methods for the same characteristic forms of the original equations. The characteristic method is applied either on a characteristic (curvilinear) grid or a rectangular grid in the *x-t* solution plane. The former is not suitable for application in natural waterways with irregular geometry (Fread, 1985). The latter, also known as the Hartree method, requires the interpolation formulae meshed within the finite difference mesh. This restriction has limited the application of the method of characteristics to flood

routing (Fread, 1985). However, it is still used in explicit and implicit finite difference techniques for a more accurate approximation of boundary conditions (Sturm, 2001).

The finite difference methods are based on the principle of transforming the governing differential equations into algebraic equations by approximating the derivatives in terms of difference equations. In explicit finite difference methods, the solution of the Saint-Venant equations advances point by point along one time line in the *x-t* solution domain until all the unknowns associated with that time line have been evaluated. Then, the solution advances to the next time line. The numerical solution of the explicit method is quite straightforward and it is easily programmed. In implicit methods, the solution of the Saint-Venant equations advances from one time line to the next simultaneously for all points along the time line. Hence, the implicit method is numerically more complex and difficult to program. The major difference between the explicit and the implicit methods is the number of unknowns used from the time line where the solution is searched. In the explicit scheme, only the approximations of the time derivative involve the unknown variables, whereas in an implicit scheme, the approximations of all derivatives (i.e., time derivative, space derivative and non-derivative terms) contain the unknown variables and are solved simultaneously (Fread, 1985).

The development of explicit techniques began with the pioneering work of Stoker (1953) and followed by Liggett and Woolhiser (1967) and Strelkoff (1970). Even though the explicit scheme is relatively simple compared to the implicit scheme, it has serious restrictions in the size of the computational time step in order to achieve numerical stability. It was this motivation that led to the development of implicit schemes, the first

of which was originally formulated by Preissmann (1961). Following his work, Amein and Fang (1970), Chaudhry and Contractor (1973), Amein and Chu (1975) and Fread (1976) have also developed implicit schemes to solve flood routing problems. The implicit method of Preissmann (1961) later became the method of choice for channel flow analysis due to its flexibility in using large time steps with unconditional stability and was implemented in many studies after 1970s.

2.2.2. Overland Flow

Overland flow is another example of shallow water flow that can be analyzed with vertically-averaged equations. It is considered to be an important subprocess of watershed hydrology. Regardless of its source (i.e., infiltration excess or saturation excess), it is considered to be the major contributor of channel flow. However, unlike channel flow, it is characterized by even smaller water depths that are in the order of a less than a couple of centimeters which makes its analysis more difficult when compared to channel flow. Although small depths and velocities propose a laminar treatment of the process, other parameters such as the rainfall impact, highly variable roughness patterns and channelization favor a turbulent analysis for the process. It is because of these complications the overland flow is generally assumed to experience all possible aspects of flow hydraulics in a time and space dependent fashion. In the context of a general watershed model, however, such complications are generally lumped into one roughness parameter and the entire overland flow phenomenon is modeled as a turbulent flow similar to its channel flow counterpart. While this assumption may not be true at all times, it is the only feasible way to tackle the associated difficulties.

Another major characteristic of the overland flow is its temporarily discontinuous flow behavior. Unlike any other watershed flow processes, the overland flow is highly driven by external sources that are intermittent in time. While channel flow and groundwater flow are generally considered to be continuous flow processes, overland flow shows discontinuities in time and space as a direct consequence of the temporally and spatially non-uniform source/sink function. In this regard, overland flow does not have well-defined flow boundaries. It may be regarded as the only flow process that experiences a continuously changing flow domain, which is one of the reasons for the difficulties encountered in its numerical simulation.

Overland flow is generally modeled as a one- or two-dimensional process. Numerous one-dimensional models are used in simulating flows on idealized watersheds, laboratory flumes, or natural watersheds with well defined slopes in a particular direction. Such models include the works of Judah et al. (1975), Ross et al. (1977), Ross et al. (1979), Kawahara and Yokoyama (1980), Heatwole et al. (1982) and Shakill and Johnson (2000). Similarly, an extensive database exists in two-dimensional treatment of overland flows. Some selected examples of two-dimensional overland flow models are the studies of Chow and Zvi (1973), Katopodes and Strelkoff (1979), Hromadka and Lai (1985), Hromadka and Yen (1986), Akanbi and Katapodes (1988), Zhang and Cundy (1989), James and Kim (1990), Marcus and Julien (1990), Playan et al. (1994), Tayfur et al. (1993), Gottardi and Venutelli (1993b), Zhao et al. (1994), Di Giammarco et al. (1996), Gottardi and Venutelli (1997), Feng and Molz (1997), Hong and Mostaghimi (1997), Lal (1998), Esteves et al. (2000), Fiedler and Ramirez (2000), Chang et al. (2000) and Dutta et al. (2000).

Similar to the channel flow case, both the complete and the simplified forms of the two-dimensional Saint-Venant equations of overland flow are extensively used. Chow and Zvi (1973), Katopodes and Strelkoff (1979), Akanbi and Katopodes (1988), Zhang and Cundy (1989), Playan et al. (1994), Tayfur et al. (1993), Zhao et al. (1994), Hong and Mostaghimi (1997), Fiedler and Ramirez (2000) and Esteves et al. (2000) have preferred the full dynamic wave approach. However, their studies were all conducted on a limited spatial extent including laboratory experiments or test bed hypothetical runs. None of these studies were actually done at a realistic watershed scale. On the other hand, all overland flow models that are applied at the watershed scale used either the non-inertia wave or kinematic wave assumptions. These simplifications essentially made the process more suitable for large scale applications. The models of Hromadka and Lai (1985), Hromadka and Yen (1986), James and Kim (1990), Marcus and Julien (1990), Julien et al. (1995), Gottardi and Venutelli (1993b), Di Giammarco et al. (1996), Gottardi and Venutelli (1997), Feng and Molz (1997), Hong and Mostaghimi (1997), Lal (1998), Chang et al. (2000) and Dutta et al. (2000) can be listed in this line of work.

In general, two-dimensional overland flow can only be solved using numerical methods. Among the three available solution procedures, the method of characteristics is rarely applied due to the difficulties encountered in multi-dimensional characteristics methods. Except for the model of Katopodes and Strelkoff (1988), there is no bi-directional method of characteristic application of overland flow. On the other hand, both the finite element and the finite difference techniques have been widely used and have become the method of choice for two-dimensional overland flow modeling. While the works of Chow and Zvi (1973), Hromadka and Lai (1985), Hromadka and Yen (1986),

Zhang and Cundy (1989), James and Kim (1990), Tayfur et al. (1993), Playan et al. (1994), Julien et al. (1995), Feng and Molz (1997), Esteves et al. (2000), Fiedler and Ramirez (2000), Chang et al. (2000) and Dutta et al. (2000) have all used explicit and implicit finite difference methods; Akanbi and Katopodes (1988), Marcus and Julien (1990), Zhao et al. (1994), Hong and Mostaghimi (1997), Gottardi and Venutelli (1997) have preferred the finite element technique. Moreover, Di Giammarco et al. (1996), Gottardi and Venutelli (1997) and Lal (1998) have used the mass conservative control volume finite element method. As seen from the wide variety of studies, there is no direct preference for a particular method. However, the finite element method has obvious advantages over the finite difference method to discretize domains without any particular shape and size such as a watershed.

2.2.3. Unsaturated Zone Flow

The movement of moisture in the variably saturated flow is often modeled by using Richards' equation and closed by constitutive relations to describe the relationship among fluid pressures, saturations and hydraulic conductivities. When the groundwater flow is studied in two zones separated by the water table, the region of low saturation values between the ground surface and the water table is often called the unsaturated zone to distinguish it from its saturated counterpart that is found below the water table. The unsaturated zone is characterized by spatially and temporarily varying levels of water content below saturation and negative capillary pressure heads. A major characteristic of flow in the unsaturated zone is the dependency of the hydraulic conductivity of the medium on the level of saturation, which generally becomes a strong non-linear function

for many soil types. Therefore, in addition to the complexity of Richards' equation, the complexity of constitutive relationships that link the level of saturation to capillary pressure and hydraulic conductivity further complicates the governing equations and its numerical solution.

Although the unsaturated zone flow is three-dimensional in principle, it is often approximated with its one-dimensional counterpart along the vertical domain. This simplification essentially treats the unsaturated zone as a vertical link between the surface and the water table. As long as the source of moisture in this zone is either the infiltrating flux or rising water table, this simplification works fairly well. Particularly, in low land areas with mild surface topography, one can consider the unsaturated zone as columns of soil providing a conduit for bidirectional movement of soil moisture. Such an approach is widely used in large-scale watershed modeling including the SHE model of Abbott et al. (1986). A three-dimensional variably-saturated flow is practically not possible to implement in terms of computational resource limitations in large scale watershed models. Furthermore, Singh and Bhallamudi (1998) found out that the results don't show significant differences when the unsaturated zone is modeled one-dimensionally (i.e., vertical) as opposed to a possible two-dimensional (i.e., vertical-horizontal) treatment.

While Richards' equation is originally based on the capillary pressure as the dependent variable, numerous researchers have developed various modified forms by changing the dependent variable of the equation. Over the years, three different forms of Richards' equation have been widely applied by the soil scientist: (i) the pressure head-based equation; (ii) moisture content-based equation; and, (iii) mixed form of the

equation with both the pressure head and the water content explicitly appearing as dependent variables of the equation.

The original pressure-head based equation is applicable to all levels of saturation in the porous medium. It performs in a superior way under saturated conditions when some of the other forms fail to properly represent the flow conditions (Huang et al., 1996). This behavior is mostly related to the fact that the pressure head is a continuous function, both in saturated and unsaturated media under non-homogeneous soil profiles. Unfortunately, the pressure head-based equation does not perform as well as the water content-based equation under significantly dry conditions (Huang et al., 1996). Especially under the condition of infiltration to a very dry soil, the pressure-based form develops large mass balance errors due to the highly nonlinear nature of specific moisture capacity and notably underestimates the infiltration depth. Regardless of the limitations associated with it, this original form of the equation has been used extensively in solving both the unsaturated zone and variably saturated-unsaturated zone flow problems (Neuman, 1973; Narasimhan et al., 1978; van Genuchten, 1982; Milly, 1985; Feddes et al., 1988; Celia et al., 1990; Paniconi et al., 1991; Gottardi and Venutelli, 1993a; Rathfelder and Abriola, 1994; Pan and Wierenga, 1995; Pan et al., 1996; Romano et al., 1998; Williams et al., 2000; van Dam and Feddes, 2000).

To alleviate the problems associated with the pressure head-based form of the governing equation, a moisture-content based form was proposed as an alternative formulation of the unsaturated zone flow. This formulation is found to be superior in terms of mass conservation, particularly in the discrete approximations of its numerical solution such as finite element and finite difference methods (Hills et al., 1989; Gottardi

and Venutelli, 1993a; Pan and Wierenga, 1997). Moreover, the hydraulic functions are less nonlinear when expressed in terms of moisture content rather than capillary head, particularly when modeling infiltration into a relatively dry medium (Williams et al., 2000). However, the water content-based form of the equation was also limited in application to variably saturated-unsaturated flow since it was not able to properly simulate the saturated conditions. When the flow domain gets locally or completely saturated, the equation degenerates since the time rate of change of the moisture content becomes zero (Celia et al., 1990). In addition, using moisture content as the dependent variable introduces problems of continuity in the domain since it is not a state variable which is always continuous in space regardless of the soil inhomogeneities.

To overcome the difficulties associated with both the pressure-based and the moisture content-based forms of Richards' equation, a so-called mixed-form has been proposed, which uses both the moisture content and the pressure head as the dependent variables. The mixed form has both the superior mass conservation characteristics of the moisture content-based equation as well as the unlimited applicability to both saturated and unsaturated regions of flow that the pressure-based equation offers (Celia et al., 1990). In this regard, the numerical solution of the mixed form found wide applicability in the last decade and many researchers used this form to model the flow in variably saturated-unsaturated media (Celia et al., 1990; Gottardi and Venutelli, 1993a; Hong et al., 1994; Huang, et al., 1996; Tocci et al., 1997; Miller et al., 1998; Williams and Miller, 1999; Zhang and Ewen, 2000; Zhang et al, 2002).

Apart from these standard forms of the equations, some researchers did not directly use these three forms of the governing equation but rather applied certain

transformation functions to smooth the strong non-linearity of the constitutive functions (Pan and Wierenga, 1995; Pan et al., 1996; Pan and Wierenga, 1997; Williams and Miller, 1999; Williams et al., 2000). Even though these transformation techniques provide some relief to the problems associated with the numerical solution, they did not find wide applicability mainly due to the fact that they are only an approximation to the original equation and lack any underlying physical theory.

Regardless of the form of Richards' equation used, one needs to supplement the governing equation with the auxiliary equations to complete the mathematical representation of moisture movement in the unsaturated zone. These auxiliary relations are the soil-water retention and hydraulic conductivity relationships that rrelates the capillary pressure head to soil moisture and hydraulic conductivity (Bear, 1979). Although these relations are known to yield solutions to Richards' equation, it is rarely available in the extent that a distributed watershed model would require in terms of spatial variability. Therefore, researchers developed numerous empirical formulae to describe the relation between capillary pressure head and soil moisture as well as capillary pressure head and hydraulic conductivity. The most commonly used relations were proposed by Brooks and Corey (1964), Campbell (1974), Mualem (1976), Clapp and Hornberger (1978) and van Genuchten (1980). It is important to note that the original forms of these relations did not consider the phenomenon of hysteresis and pressure head is considered to be a single-valued function of moisture content.

The extreme variability and complexity of geological materials, dry initial conditions, varying boundary conditions and the strong non-linearity between the pressure head and moisture content as well as the pressure head and hydraulic

conductivity make the solution of Richards' equation quite a challenge, particularly within acceptable limits of accuracy and computational effort. Since analytical solutions are only possible when these nonlinear relationships are linearized and simplified (Tracy, 1995), numerical techniques are the only available method for the solution. In numerical solution of Richards' equation, the spatial discretization is commonly performed by: (i) finite difference; and, (ii) finite element methods (van Genuchten, 1982; Milly, 1985; Celia et al., 1990; Hong et al., 1994; Rathfelder and Abriola, 1994; Pan and Wierenga, 1995; Pan et al., 1996; Huang et al., 1996; Miller et al., 1998; van Dam and Feddes, 2000; Zhang and Ewen, 2000; Zhang et al., 2002). The standard temporal discretization technique used to approximate Richards' equation is the one-step Euler approach and the most common solution method uses a fully implicit time approximation of the time derivative. Recently, variable step size, variable time order integration methods are also used to discretize the temporal derivatives (Tocci et al., 1997; Miller et al., 1998; Williams and Miller, 1999).

2.2.4. Saturated Zone Flow

The saturated groundwater zone is defined as the domain below the water table. Since it is bounded by a dynamically changing water table, this zone is also known as the unconfined aquifer. The significance of this zone comes from the fact that it provides a link to other watershed processes such as the unsaturated zone as well as the channel flow zone. Therefore, it is a critically important part of the watershed hydrology. The saturated groundwater flow is modeled by Boussinesq's equation that describes the movement of

flow in porous medium. Darcy's law is the momentum equation embedded in the mass conservation equation (Bear, 1979).

The saturated zone flow could either be characterized by a three-dimensional groundwater flow model or a vertically-averaged two-dimensional groundwater flow model. Many modelers have used a three-dimensional representation of the groundwater flow such as Frind and Verge (1978), Huyakorn et al. (1986) and McDonald and Harbaugh (1988). Others such as Aral (1990) have preferred a vertically averaged two-dimensional representation considering the essentially two-dimensional horizontal flow pattern of groundwater in aquifer systems. It is, however, important to note that all of these models were developed as multi-layer aquifer models and are certainly applicable to deep aquifer systems. In the case of an unconfined aquifer, however, a three-dimensional representation might be necessary when the aquifer is under the influence of sources/sinks. In the close vicinity of wells, for example, flow becomes three dimensional. Vertically-averaged models are only suitable when the change in water table is not significant compared to the saturated aquifer thickness. Therefore, in cases where the assumption of vertical averaging might be violated, these models should be applied with utmost caution.

The numerical solution of the saturated groundwater flow equation is performed by finite element or finite difference methods. The finite element method has found a wide application in the field of groundwater modeling and numerous models used the finite element discretization (Huyakorn et al., 1986; Aral, 1990). The finite difference method is also applied commonly and the well-known groundwater flow model MODFLOW uses this discretization (McDonald and Harbaugh, 1988). Today, saturated

groundwater flow modeling has reached a certain level of sophistication where several commercial software packages have been developed and used with success.

2.3. Hydrologic Transport Processes and Pathways in a Watershed

The contaminant transport phenomenon in a watershed is a strong function of the flow pathways and their characteristics. It is generally not possible to consider a transport problem without properly identifying the governing flow patterns. Therefore, exactly the same approach needs to be applied when the transport problem is confronted. In this regard, one could analyze the transport of contaminants in surface and subsurface domains and implement proper linkages between these two systems. These two subsystems could further be classified as was done in flow analysis. It is, therefore, logical to analyze the contaminant transport in a watershed as channel and overland transport in the surface subsystem and saturated and unsaturated zone transport in the subsurface system.

2.3.1. Channel Transport

Contaminant transport in channels is the most studied aspect of the general mass transport process in a watershed. It is not only the fastest transport mechanism but also occurs in a medium (i.e., surface water) that is of utmost concern to humans. Consequently, many models have been developed to simulate the migration of contaminants along the channel. In the majority of these studies, the focus was directed towards the general characteristics of the transport equation.

Contaminant transport in a channel is a three dimensional phenomena. Even with the assumption of instantaneous vertical mixing, the transport process continues to be a two dimensional event until complete mixing is achieved in the transverse direction. Only after this point, the transport process can be effectively modeled with a one-dimensional behavior (Fischer et al., 1979). Although this condition limits the applicability of many models, one-dimensional transport modeling has been the choice of many researchers in analyzing transport phenomenon in channels and rivers. However, the modeler should always be concerned with the capabilities and the limitations of the one dimensional approach for contaminant transport modeling in channels.

Even with the simplifying one-dimensional approximation, the numerical solution of the advection-dispersion equation is still a complicated numerical problem. Unfortunately, the advances achieved in the field of numerical modeling of partial differential equations do not lead to a globally accepted efficient algorithm to solve the advection-dispersion equation. Even though the equation looks simple, it mathematically shows a dual behavior in terms of its characteristics, depending on the relative significance of various terms of the equation. For advection-dominated flows, the equation shows the characteristics of a hyperbolic equation, whereas it becomes a parabolic partial differential equation when the dispersion is the dominant term (Holly and Preissmann, 1977; Leonard, 1979). Considering the fact that this changing behavior of transport phenomenon could occur in a time- and space-dependent fashion, computational of the numerical solution becomes an extremely challenging task.

Several numerical solution techniques are implemented to solve the advection dispersion equation. These methods can be classified as: (i) Eulerian methods including

the finite difference, finite element or finite volume methods; (ii) Lagrangian methods; and, (iii) Eulerian-Lagrangian hybrid methods. As all major problems associated with the equation are linked to the advection operator, most of the literature is focused on handling the difficulties associated with the numerical solution of advection. Many researchers worked on finding more efficient algorithms to treat the advection component of the equation since the remaining terms, such as the dispersion and decay operators as well as the sink/source terms, do not pose any additional difficulties in the numerical solution. While some researchers focused on low (i.e., first and second) order conventional Eulerian techniques (Tucci and Chen, 1981; Bencala, 1983; Bencala and Walters, 1983; Leonard and Noye, 1989; Ristenpart and Wittenberg, 1991; Runkel and Chapra, 1993; Chen and Falconer, 1994; Jaque and Ball, 1994; Islam and Chaudhry, 1997; Wang and Lacroix, 1997; Geisdal and Teigland, 1998; Runkel, 1998, Zhang, 1998), some others preferred higher order conventional Eulerian techniques (Hirsch, 1975; Adam, 1977; Basco, 1984; Komatsu et al., 1985, Falconer and Liu, 1988; Leonard and Noye, 1989; Noye, 1990; Stamou, 1991; Leonard, 1991; Stamou, 1992; Chen and Falconer, 1992; Chu and Fan, 1998; Chu and Fan, 1999; Radwan, 1999; Spotz and Carey, 2001) to treat the advection operator. Although a common ground for all Eulerian methods is the fixed grid structure that these methods are based on and is the main reason why these methods are so popular, higher order methods utilize more nodes than the standard low order methods in an effort to reduce the false smearing and false oscillation problems of such methods particularly around steep front regions at the expense of computational power (Leonard, 1979).

In another line of work, several researchers proposed using Lagrangian and Eulerian-Lagrangian hybrid algorithms to treat the troublesome advection operator (Holly and Preissmann, 1977; Leonard, 1979; Glass and Rodi, 1982; Bedford et al., 1983; McBride and Rutherford, 1984; Jobson, 1987; Yu and Li, 1994; Oliveira and Baptista, 1995; Manson and Wallis, 1995; Manson and Wallis, 2000; Manson et al., 2001). Pure Lagrangian methods follow the natural motion of the water mass along a changing mesh, which makes them computationally cumbersome due to the necessity to keep track of moving coordinates. Hybrid techniques, on the other hand, combine the advantageous aspects of Eulerian and Lagrangian methods. They solve the advection operator with the powerful Lagrangian-based particle tracking algorithm over a fixed Eulerian grid. Despite the increasing popularity of hybrid schemes, some major drawbacks must be resolved before they can become a reliable contaminant transport method. One of the major limitations of such methods lies in the fact that Lagrangian treatment of flow still did not develop to become the method of choice mainly due to the difficulties involved in its coding and the lack of intuitive analysis capabilities that the Eulerian methods provide. Finally, they are implemented and experimented with relatively simple flows and have not been put to tests on real channel systems involving network of channels. They are not currently used in well-developed water quality models and the accurate algorithms are yet to be formulated for complex systems such as river networks before these models could be applied in large scale watershed modeling. Because of these difficulties, the fixed grid Eulerian schemes are still commonly implemented and improved as the most popular solution technique. Particularly, higher order schemes are increasingly used in Eulerian

framework to increase the accuracy of these methods under extreme conditions such as flows involving sharp concentration gradients.

2.3.2. Overland Transport

Overland transport of contaminants is vital for quantifying land-based distributed pollution such as the release of nutrients, pesticides and other dissolved hazardous chemicals from agricultural fields into surface runoff. The soil chemical loss to overland flow is an extremely complex phenomenon that is dependent on various factors including, but not limited to, the chemical application rate, soil chemical kinetics, mass transport in the soil matrix, mass transfer in overland flow and the overland flow pattern (Wallach and Shabtai, 1992). Within a watershed modeling framework, the analyst is mostly focused on determining the flow and mass transfer patterns of overland processes. From another perspective, the process becomes the concern of the watershed modeler after the contaminant is released from the soil.

The temporarily discontinuous behavior of overland flow over the land surfaces influences the transport of contaminants. The contaminant might be released and transported with the flow to a certain distance from its point of origin but then re-accumulate at this new point if overland flow is not persistent to reach to a channel and cease due to several loss mechanisms. This behavior further complicates the analysis of overland transport of contaminants.

Numerous models simulating overland transport characteristics are developed by various researchers including but not limited to Akan (1987), Yeh et al. (1998), Yan and Kahawita (2000), Garcia-Navarro et al. (2000) and Wallach et al. (2001). While the

studies of Yeh et al (1998) and Yan and Kahawita (2000) were based on two dimensional analysis of overland transport, Garcia-Navarro et al. (2000) and Wallach et al. (2001) worked on more simplistic one-dimensional models. Garcia-Navarro et al. (2000) and Yan and Kahawita (2000) have used a dynamic wave approach to model the overland flow patterns whereas Yeh et al. (1998) preferred non-inertia wave approach and Wallach et al. (2001) used a simpler kinematic wave approximation. These researchers have also implemented a variety of numerical solution schemes. While Yeh et al. (1998) have used a Eulerian-Lagrangian finite element method, Garcia-Navarro et al. (2000) implemented a Eulerian-Lagrangian finite difference method. On the other hand, Yan and Kahawita (2000) and Wallach et al. (2001) implemented standard Eulerian finite difference techniques to solve the transport equation. It is therefore clearly seen that no particular method is favorable compared to the other one. However, the general suitability of finite element methods to processes with irregular domains also applies to overland flow.

2.3.3. Unsaturated Zone Transport

Contaminant transport in the unsaturated zone plays an important role in many areas of agriculture and engineering. The analysis of the migration of fertilizers into the soil matrix and potentially becoming pollutants for the saturated groundwater system is one of these many areas. Therefore, a clear understanding of contaminant transport in the unsaturated zone, including proper quantification of the relevant transport processes is important for the engineer (van Genuchten, 1982). Although high dimensional modeling of the unsaturated zone transport is possible, the major pathway of concern within the unsaturated zone is the vertical movement of contaminants which eventually reaches and

pollutes the saturated groundwater reservoir. In this regard, the focus is kept on only the one dimensional unsaturated zone transport models.

The major transport mechanisms responsible for vertical migration of contaminants are again advection and dispersion. Hence, the one-dimensional transport equation has a very similar form to its counterpart in channel flow with the exception of the relative magnitudes of advection velocities and dispersion coefficients. Advection in the unsaturated zone occurs in a much slower fashion and this assists the modeler in terms of the success of the numerical algorithm. In this regard, standard Eulerian finite difference and finite element methods have generally been the method of choice in numerous models including HYDRUS (Simunek et al., 1998), TETRANS (Corwin and Waggoner, 1990) and VLEACH (Ravi and Johnson, 1993).

2.3.4. Saturated Zone Transport

The advection-dispersion equation describing the contaminant transport in saturated groundwater exhibits similar characteristics to its counterpart in a channel. Although the advection operator is still the major concern for numerical solution, the severity of the problem is generally milder in groundwater transport due to the significantly slower advection velocities in aquifers. It is generally accepted that there are at least 4-5 orders of magnitude difference between the advection velocities in the channel and in the aquifer. This condition provides a certain amount of immunity to the problems associated with the advection operator.

Similar to its flow counterpart, the contaminant transport in groundwater could be analyzed with either a three-dimensional model or a vertically-averaged two dimensional

model. The decision follows the same criteria depicted in the flow model selection and a similar approach is to be implemented to simulate the transport phenomenon.

The transport modeling in groundwater flow is generally done with: (i) standard Eulerian finite difference or finite element methods (Voss, 1984; Huyakorn et al., 1985; Faust et al., 1990; Simunek et al., 1998); (ii) Lagrangian methods (Bear and Verrujit, 1987; Tompson and Gelhar, 1990; LaBolle et al., 1996); and, (iii) mixed Eulerian-Lagrangian hybrid methods combining Lagrangian treatment of advection with the standard finite element or finite difference schemes for non-advection terms (Neuman, 1984; Celia et al., 1990; Yeh, 1990; Bentley and Pinder, 1992; Zhang et al., 1993;Yeh et al., 1993; Binning and Celia, 1995; Oliveira and Baptista, 1995). In spite of all the advances achieved and new techniques developed, there is not a single technique that can yield completely satisfactory solutions to the numerical solution of advection-dominated contaminant transport and it remains to be a difficult problem due to the often contradictory needs to suppress numerical dispersion, avoid artificial oscillation and conserve mass.

2.4. Coupling of Flow Mechanisms

During the last thirty-plus years of computerized modeling, many models have been developed to simulate the response of a watershed to an unsteady, non-uniform, spatially-variable precipitation event. Often, these models separated the watershed into surface and subsurface components and focused on only one of these hydrological processes. Although this artificial separation of an otherwise linked system helped to reduce most of the problems associated with physical process description as well as its

numerical solution, it failed to describe the system accurately and resulted in numerous discrete models of limited applicability. Therefore, an integration mechanism between surface and subsurface flows is particularly important for models of watershed hydrology where the response of the system is based on simultaneous interactions between these two major flow domains.

The analysis of the hydrologic cycle reveals the fact that surface and subsurface flow processes are linked at a number of interfaces. The most obvious one of these interfaces is the ground surface where overland flow and unsaturated zone flow are linked to each other via the infiltration/exfiltration flux. The direction of the interacting flux is not only dependent on the overland flow conditions but also a strong function of the level of saturation of soil moisture. The two overland flow initiation mechanisms (i.e., saturation from above and saturation from below) are strongly related to these interactions as well as other factors such as the topography, land cover/use and rate of precipitation. Another major interface linking surface and subsurface flow processes is the river channel bottom. The seepage flux is responsible for providing the linkage between the two systems. The direction of the flux is a function of the relative values of groundwater head and river water stage.

The mechanism that links surface and subsurface components at the ground surface is the interaction between soil water content and infiltration of water to the ground. In most of the surface flow models, infiltration is modeled as a sink for overland flow and approximated by semi-empirical infiltration formulae such as that of Green and Ampt (1911), Horton (1933) or Philip (1957). On the opposite end, most subsurface models take the infiltrated water as a source for groundwater flow. This separated

modeling approach is often deemed sufficient for watersheds with relatively low permeability soils (Freeze, 1972b). In watersheds with high permeability soils, interaction between surface and subsurface flow components becomes important especially during overland flow initiation (Morita and Yen, 2002). It has been observed that the surface flow is overestimated during the rising part of the hydrograph and underestimated during the recession part when surface-subsurface interaction is neglected (Wallach et al., 1997). In this regard, it is important to couple surface and subsurface components to obtain accurate and comprehensive watershed modeling (Morita and Yen, 2002).

Depending on the accuracy required and numerical and computational complexity allowed, there are numerous techniques to couple surface and subsurface flow components: (i) true simultaneous coupling; (ii) iterative (internal) coupling; (iii) non-iterative (external) coupling; and, (iv) sink function type coupling (i.e., also known as "no" coupling). Except for the sink function type coupling, all three methods are based on linking partial differential equations of surface and subsurface flow via infiltration and seepage as the internal boundary conditions. In sink function type coupling, however, infiltration is simulated with empirical equations, which are based on soil characteristics.

The true simultaneous coupling is the ultimate, most advanced method of interacting surface and subsurface flows. The technique is based on numerically solving the surface flow, subsurface flow and the common internal boundary condition between the two as a set of simultaneous equations at each time step. Since the equations are solved simultaneously, the result directly yields the unknown quantities. This type of coupling is extremely difficult and this study is believed to be one of the earliest examples of true simultaneous coupling of watershed processes. The works of Gunduz

and Aral (2003a, 2003b, 2004b) are early examples of models implementing this technique. The true simultaneous coupling of watershed flow processes is deemed to be very promising and there is a wide open field for further research. Particularly, with the ever increasing computational power of personal computers, watershed models based on true simultaneous coupling are expected to emerge in the near future.

In iterative (internal) coupling, the equations of surface and subsurface flows are solved separately but iteratively at each time step of the solution. The link between the two is supplied by the infiltration equation represented as a gradient-type expression. The technique provides fairly accurate solutions at the expense of computational cost. Furthermore, like any iterative solution procedure, the iterative coupling also requires the use of a pre-determined tolerance value below which the solution is assumed to converge. Morita and Yen (2002) presents a set of models that are based on iterative coupling of surface and subsurface flows. According to their study, the earliest examples of iterative coupling were the studies by Pinder and Sauer (1971) and Freeze (1972a). In the surface flow component, both included the solution of the one-dimensional dynamic wave equation along a rectangular channel. In the subsurface domain, Pinder and Sauer (1971) solved the two-dimensional horizontal groundwater flow equations in the saturated medium whereas Freeze (1972a) solved the three-dimensional Richards' equation in both unsaturated and saturated media. These studies are followed by Akan and Yen (1981a) where they solved the one-dimensional dynamic wave equation for overland flow and two-dimensional Richards' equation in unsaturated and saturated media. More recently, Govindaraju and Kavvas (1991) created an integrated model for hillslope hydrology, which included three flow pathways, including one-dimensional overland flow, one-

dimensional channel flow, and two-dimensional saturated/unsaturated subsurface flow component. A more complex simulation of overland flow is achieved by Bradford and Katopodes (1998) where they solved the two-dimensional turbulent Navier-Stokes equations for overland flow with the two-dimensional Richards' equation for groundwater flow. Recently, Morita and Yen (2002) developed a conjunctive two-dimensional surface and three-dimensional variably-saturated subsurface flow model by applying the two-dimensional non-inertia wave approximation of the Saint-Venant equations in overland flow component and the three-dimensional Richards' equation in unsaturated and saturated subsurface flow component.

In non-iterative (external) coupling, the surface and subsurface components are again solved separately at the same time step but in a non-iterative fashion. Even though the accuracy of the solution from a non-iterative coupling technique is less than the solution from an iterative technique, this method found wide applicability among modelers due to its comparably less computational time requirements. In non-iterative coupling, the surface flow model is generally solved first in each time step and the results are passed to the subsurface flow model. Once the solution procedure of the subsurface component is completed at the same time step, the control is progressed to the next time step without entering an iterative loop where the model tries to satisfy the convergence of common flow variables such as overland flow water depth or infiltration flux. Numerous modelers have developed models with non-iterative coupling. One of the earliest of these studies is the one by Smith and Woolhiser (1971), where they solved the one-dimensional kinematic wave equations for surface flow together with one-dimensional Richards' equation for the unsaturated subsurface domain. Abbott et al. (1986a and 1986b)

developed their well-known SHE model, which solved the two-dimensional non-inertia wave equations for the overland flow and the two-dimensional Richards' equation for groundwater flow components. In a more recent study, Di Giammarco et al. (1994) combined two-dimensional overland flow equations, one-dimensional channel flow equations and one- and two-dimensional groundwater flow equations to obtain an integrated model for watershed runoff. Motha and Wigham (1995) also developed an externally coupled model of one-dimensional overland flow and two-dimensional subsurface flow. Wallach et al. (1997) studied the errors in surface runoff prediction by neglecting the relationship between infiltration rate and overland flow depth. They applied a kinematic wave approximation of the Saint-Venant equations in their surface flow components and coupled it with the two-dimensional Richards' equation in their subsurface flow component. El-Hames and Richards (1998) combined three one-dimensional models of channel flow, overland flow and subsurface flow. They have used the full dynamic wave equations for channel flow, kinematic wave equations for overland flow and Richards' equation for subsurface flow. Similarly, Singh and Bhallamudi (1998) have coupled a one-dimensional dynamic wave model of overland flow with a two-dimensional subsurface flow model based on Richards' equation.

Finally, the sink function type coupling is regarded as a further simplification of non-iterative coupling where infiltration is now considered as a sink for the surface flow component. The one-dimensional downward movement of infiltration is modeled using a semi-empirical algebraic equation such as Horton, Philip or Green and Ampt formula. Generally, the subsurface flow is not even modeled with models that apply sink function type coupling. In rare cases where it is modeled, infiltration is included as a source to

groundwater flow. In this regard, it is clear that there is no direct link between surface and subsurface components and sink function type coupling is therefore known as the "no-coupling" approach. Due to its computational ease, there exist many models that used sink function type coupling. Both Akanbi and Katapodes (1988) and Playan et al. (1994) used the two-dimensional non-inertia wave equations in the surface flow component and Kostiakov equation in the infiltration sink function. Singh and Bhallamudi (1996) used the one-dimensional dynamic wave equation in the surface flow component and Kostiakov equation in infiltration function. On the other hand, Esteves et al. (2000), Yan and Kahawita (2000) and Tayfur et al. (1993) used Green and Ampt formula to model infiltration in their two-dimensional overland flow models. In three large scale applications, James and Kim (1990), Julien et al. (1995) and Chang et al. (2000) also used the Green and Ampt infiltration equation to model two-dimensional overland flow but applied the non-inertia wave approximation to the Saint-Venant equations to reduce computational costs.

Most of the time, the selection of the coupling technique is based on limitations of computational and data resources as well as the objectives of the study. Iterative coupling methods require significantly higher computational run-times when compared to non-iterative and sink function type coupling methods, even to complete simulations of moderate time scales. The non-iterative and sink function type techniques reduce run-times by eliminating the necessity to iterate on model variables at each time step at the cost of reducing the model realism. In most cases where data are the limiting factor of the modeling effort, such reduction in realism is tolerable. It is often a dilemma of the modeler to choose between coupling techniques of higher accuracy and techniques that

demand less data. Particularly for large scale modeling applications, this decision is biased towards techniques that require less data. In pilot or experimental scale studies, however, the modeler uses his luxury to implement models of high accuracy with unlimited data that he can collect from his ideal system. However, with the sophistication of remote sensing and geographic information systems, sophisticated coupling techniques started to become popular in large scale modeling efforts.

Apart from the coupling technique used, models of surface and subsurface flows are also classified according to the number of spatial dimensions used in discretizing the two flow domains. All surface flow models typically apply one- or two-dimensional discretization due to the relatively shallow water depths and well-defined flow paths. In channel flows, modelers almost always prefer the one-dimensional Saint-Venant equations or its approximations. In overland flows, both one and two-dimensional modeling are equally applied. The selection is mostly based on the complexity of the system under investigation and the available computer resources. Subsurface flow models, on the other hand, have a wide spectrum of spatial domain discretization. One-dimensional vertical flow models are mostly used with external and sink function type coupling techniques, where infiltration is mostly considered as a sink for overland flow phenomena. Two- and three-dimensional subsurface flow models are commonly applied with internal and simultaneous coupling methods.

Just like their discrete analogs, the coupled models also implement a wide array of numerical solution methods including the finite difference, finite element and method of characteristics. The selection of the solution approach is based on: (i) the characteristics of the physical domain; (ii) number of spatial dimensions; (iii) ability to handle numerical

problems; (iv) available computational resources; and, (v) the level of comfort the modeler feels with a particular technique.

Regardless of the wide spectrum of techniques that has been used to approximate surface and subsurface flows, there are still some particular methods that modelers concentrated on for particular domains. In essence, one-dimensional channel flow is mostly solved by finite difference techniques. Freeze (1972a), Pinder and Sauer (1971), Smith and Woolhiser (1971), Singh and Bhallamudi (1998) and El-Hames and Richards (1998) used explicit finite difference methods where as James and Kim (1990), Govindaraju and Kavvas (1991), Di Giammarco et al. (1994), Dutta et al. (2000), Chang et al. (2000) applied implicit finite difference methods. Although several examples of finite element method are published in discrete channel flow routing applications, it is generally not the method of choice for channel routing in coupled models. In one and two-dimensional overland flow modeling, Akan and Yen (1981), James and Kim (1990), Tayfur et al. (1993), Wallach et al. (1997), Feng and Molz (1997), Dutta et al. (2000) and Yan and Kahawita (2000) used implicit finite difference methods, where as Hromadka and Yen (1986), Zhang and Cundy (1989), Playan et al. (1994), Julien et al. (1995), El-Hames and Richards (1998), Singh and Bhallamudi (1998), Chang et al. (2000), Esteves et al. (2000), Gandolfi and Savi (2000) and Morita and Yen (2002) preferred explicit finite difference methods. On the other hand, Akanbi and Katapodes (1988), Motha and Wigham (1995) and Tisdale et al. (1998) have preferred finite element method. More recently, a new technique called the finite volume method found applicability in the area of overland flow modeling, which is a combination of finite element and finite difference methods. Lal (1998) applied this technique to an overland flow model, where as Bradford

and Sanders (2002) and Bradford and Katapodes (2002) used the technique in shallow water flooding in lowland areas and flood plains. In subsurface flow models, Smith and Woolhiser (1971), Pinder and Sauer (1971), Freeze (1972a), Akan and Yen (1981), Abbott et al. (1986a and 1986b), Motha and Wigham (1995), Wallach et al. (1997), El-Hames and Richards (1998) and Singh and Bhallamudi (1998) used a variation of explicit and implicit finite difference methods, where as Di Giammarco et al. (1994) and Motha and Wigham (1995) preferred finite element formulation. Of all the solution techniques implemented, the finite element and finite volume schemes showed to better suit the irregular boundaries of a watershed and also provided slightly better numerical accuracy.

2.5. Coupling of Transport Mechanisms

Despite the vast amount of literature describing the coupling of flow mechanisms, there is very limited information on how transport mechanisms of various domains must be linked together in a coupled modeling framework. It is the understanding of the author that coupled transport modeling is still a few steps behind its flow counterpart and there is a significant potential for development in this field. Only recently, a couple of studies emerged describing some level of coupling of surface and subsurface transport processes, including the works of Yeh et al. (1998), Ewen et al. (2000), Vanderkwaak and Loague (2001) and Lin and Medina (2003).

Since the information from the flow coupling, such as the volumetric transfer rate, is directly used in coupling transport processes, the coupling of transport mechanisms are done at exactly the same interfaces where flow coupling is carried out. Hence, the river bed, ground surface and water table are again used to link transport models to provide a

continuous representation of the movement of a contaminant in the watershed. However, it is important to note that flow coupling must be executed smoothly and accurately before transport coupling could be attempted. The relatively immature level of flow coupling might explain to some degree why researchers were hesitant to tackle the coupled transport problem.

Iterative and non-iterative coupling mechanisms are also used in linking contaminant transport in various domains. The idea behind coupling transport processes strictly follow flow coupling and relative heads are replaced by relative concentrations in different domains. The additional complication, however, arises from the nature of modeling transport processes and more sophisticated numerical algorithms with more computational requirements are generally necessary to obtain an equally accurate transport simulation.

2.6. Scale Issues

In a general definition, the term "scale" refers to the characteristic spatial or temporal dimensions at which entities, patterns, and processes can be observed and characterized to capture the important details of a hydrologic process. All hydrologic processes, large-scale or small-scale, have their own characteristic scales of reference, which is necessary to capture details of the processes modeled or observed. Independent of the size of the model used, all hydrologic models are based on some mathematical representation of a physical process which is scale dependent. When analysts use large-scale models to predict small-scale events, or when small-scale models are used to predict large-scale events, problems may arise. In the following sections, scale issues are

discussed from a general perspective and specific details associated with subprocesses are presented in details. These sections closely follow the work of Aral and Gunduz (2003).

2.6.1. Fundamental of Scales

From saturated-unsaturated groundwater flow and contaminant transport models to flow and transport in river channel networks, the hydrological processes occur at a wide range of scales and span about ten orders of magnitude in space and time. When an integrated system is modeled, the major question to be answered is whether to include all components of the hydrologic cycle into one system model. In a global sense, no component of the cycle could be separated from the overall system. However, the need for some artificial separation might be inevitable depending on the goals of the analysis and the importance of the contribution of the subprocess to the understanding and evaluation of that goal (Aral and Gunduz, 2003). In this regard, if one is not interested in observing or reflecting the effect of one subcomponent on the other, than one can easily isolate a hydrologic process and analyze that subcomponent alone. For example there are numerous groundwater flow and contaminant transport models which are extensively used in the literature just to study groundwater systems such as the MODFLOW model of McDonald and Harbaugh (1988) and the SAINTS model of Aral (1990). In this type of an analysis, groundwater would consider some input/output from surface water but would not influence the conditions in the surface flow. On the other hand, if the simulation of multi-pathway interaction of hydrologic processes is the goal, than an integrated system modeling approach becomes a necessity and therein lie the difficulties of integration of scales.

The transfer of data or information across scales or linking sub-process models through a unified scale is referred to as "scaling" in the literature. Up-scaling consists of taking information at smaller scales to derive processes at larger scales, while downscaling consists of decomposing information at one scale into its constituents at smaller scales (Jarvis, 1995). In the context of absolute space and time, scaling primarily involves a change in the geometric and temporal structure of the data and their corresponding attributes. The term "absolute scale" refers to the definitions used in an Eulerian coordinate system where distances between points in time and space are well defined geometric and differential entities. Thus, linking sub-process parameters within these well defined rules can be considered to be objective and to be independent of one's viewpoint or frame of reference in solving a problem. From the relative perspective, scaling becomes a more complex task than from the absolute framework. In the relative scale framework, one focuses on the sub hydrologic processes and defines the space and time as a measure of relationship between these sub-processes. In a way, one can interpret this definition as a Lagrangian frame of reference. Relative scales concept represents the transcending concepts that link processes at different levels of space and time. It entails a change in scale that identifies major factors operational on a given scale of observation, their congruency with those on the lower and higher scales, and the constraints and feedbacks on those factors (Caldwell et al., 1993). With this definition, one can observe that two processes that occur in close proximity by the definition of an absolute scale may be very distant from one another in a relative scale sense. An example could be the case of the two hydrologic processes such as overland flow and saturated groundwater flow zones separated by an unsaturated zone. These two hydrologic

processes could be close to each other in an absolute sense but in terms of their interaction with one another, these processes could be very distant from one another in relative space and time frame of reference due to limiting transfer rates that may exist in the unsaturated zone. In such cases, the relative frame of reference should take precedence when scaling is considered.

As expressed by Jarvis (1995), what makes scaling a real challenge is the non-linearity between processes and variables scaled, and the heterogeneity in properties that determines the rates of processes in a relative frame of reference. Therefore, it is important to realize that scaling requires an understanding of the complex hierarchical organization of the geographic and temporal worlds where different patterns and processes are linked to specific scales of observation, and where transitions across scales are based on geographically and temporarily meaningful rules (Marceau, 1999).

Scaling and its effects on hydrological modeling are commonly linked to heterogeneity of the system modeled. However, this link should also include the refinement necessary to resolve the mathematical non-linearities incorporated into a hydrologic process. The importance of mathematical non-linearities can be clearly seen in the components of a sub hydrologic model such as groundwater flow. Scale differences of saturated and unsaturated groundwater flow could be given as an example of this type of a problem. While dependence of hydraulic conductivity on saturation in unsaturated zone is a major source of mathematical non-linearity in the solution of the governing equation, spatially variable hydraulic conductivity of the saturated zone is a heterogeneity that needs to be addressed but does not significantly alter the solution characteristics of the governing equation. Thus, non-linearity and heterogeneity are the two important

factors that need to be considered in scaling. The greater the degree of heterogeneity and non-linearity, the smaller the scale one would have to use to represent such variability or resolve such non-linearity (Aral and Gunduz, 2003).

The other component of the scaling effect arises in the interpretation of field data. Integrated hydrologic models use a variety of parameters to represent the characteristics of a watershed. However, data on watershed parameters are only available at a limited number of locations. The task is then to transform this spatially limited data to a scale which can be used as input to a large scale watershed model. The problem then becomes the selection of a scale that can represent this data without losing accuracy during the extrapolation process. As the spatial scale of the model increases from a small area to a large area, the extrapolation of limited spatial data to a large scale system would introduce errors in the analysis from the start and should be avoided at all costs.

Singh (1995) defines scale as the size of a grid cell or sub watershed within which the hydrologic response can be treated as homogeneous. If this scale is too small, the process will be dominated by local physical features, if this scale is too large, the process will ignore significant hydrologic heterogeneity caused by spatial variability. As much as this definition is correct and reasonable, it does not incorporate the scale effects associated with the resolution of mathematical non-linearity issues associated with an integrated modeling effort of the type considered here, i.e. integrated overland, channel and groundwater flow and contaminant transport in large scale watershed systems. An optimum scale of an integrated watershed model should then reflect the functional scale that provides a compromise between the resolution of non-linearities of the mathematical model, availability and extrapolation of hydrologic data and the heterogeneity of system.

2.6.2. Scales of Watershed Subprocesses

Different scales of space and time govern the physical flow and transport phenomena in the hydrologic cycle. For integrated watershed models, these scales vary by several orders of magnitudes in terms of the computational step size, the simulation extent that is necessary to capture the important aspects of the hydrologic process modeled as well as the proper scales that are necessary to interpret the input data.

In the unsaturated groundwater flow in the vertical domain, the movement of moisture is relatively slow when compared to other sub-processes of the hydrological cycle. Simulation of this process is generally complicated by the existence of strong non-linearity in the properties of the medium for a large scale simulation. This non-linearity can be further complicated by the presence of a relatively dry medium where large hydraulic gradients may develop between the dry lower layers of the soil and the wet surface layers or visa versa. Hence, unsaturated zone modeling requires very small time and spatial discretization to handle both the strong non-linearity that often occur in layered soils and also to accurately capture the piston-like flow pattern at the wetting front. Small discretization is also essential for maintaining the water balance in a strongly non-linear system. In this regard, effective simulations in field applications in large watershed modeling typically require time and space scales on the order of 10^{-1}-10^{2} sec and 10^{-2}-10^{1} cm, respectively (Aral and Gunduz, 2003). This results in a system with a very large number of nodes and time steps to simulate even a relatively small domain. Further complications might occur when modeling includes processes such as root uptake and evaporation. To model such processes the scales may have to be further refined to

achieve numerically acceptable and physically meaningful results. In extreme case, it is possible that one might have to face almost real-time simulation run times, which is impractical from an engineering standpoint. Therefore, selecting a suitable spatial and temporal scale in an unsaturated flow domain can become one of the most challenging tasks of the modeler.

The overland flow is another challenging sub-process of the hydrologic cycle. The problem in this domain is the continuity of flow in this phase. While there is continuous flow in all other sub-processes, the overland flow pattern is highly discontinuous in time. Its behavior is a strong function of the intermittent and spatially distributed source pattern (i.e. precipitation). Furthermore, it is a temporally relatively short event when compared to other flow processes such as river flow and groundwater flow. Thus, the overland flow may best be described as a moving boundary problem, which requires sophisticated numerical solution strategies (Aral and Gunduz, 2003). In this type of application, discontinuities in time and space domains complicate the numerical solution of overland flow. Further difficulties arise from the small water depths associated with overland flow patterns. As a rule of thumb, it is highly uncommon to find overland flow depths larger than 2-3 cm, which produces small resistance coefficients (high resistance to flow). This characteristic of the flow combined with the strong, two-way and spatially-distributed interactions with the unsaturated zone might render the solution numerically unstable. Additional complications of the overland flow arise due to the tendency of overland flow to channelize, making it extremely difficult to define the flow boundaries. These difficulties of overland flow as well as the time and space scales of the forcing function

(i.e., precipitation) typical necessitate the use of 10^{-1} to 10^{2} sec time steps and 10^{1}-10^{4} cm spatial discretizations (Aral and Gunduz, 2003).

The saturated groundwater flow is perhaps the only sub-process that scale issues do not introduce extra complications for its solution. Since groundwater flow is slow when compared to surface flow processes, such as river and overland flow, one can use very large time steps such as 10^{3}-10^{6} secs or even higher (Aral and Gunduz, 2003). The spatial scales would generally depend on the non-linearity of the medium but are generally large compared to other processes such as 10^{3}-10^{6} cm (Aral and Gunduz, 2003). However, difficulties arise when the slowly moving groundwater flow is linked to other processes which are more dynamic. Therefore, it is possible to conclude that the numerical simulation of saturated groundwater flow can become extremely challenging when dynamic, real-time interactions with other sub-processes are included in an integrated model.

Finally, the river flow is the most dynamic flow pathway of the hydrologic cycle. In general, the simulation time scales are a strong function of the steepness of the hydrograph to be routed in the flow channel. Time steps of 10^{2}-10^{5} sec are used to simulate the flow patterns in moderate to large natural river networks (Aral and Gunduz, 2003). On the other hand, spatial scales are mostly a function of the channel characteristics including slope, flow cross section area and roughness coefficient. Spatial steps of 10^{3}-10^{6} cm are commonly used in simulations of gradually varied unsteady flow in river channels (Aral and Gunduz, 2003). Mainly due to the fact that the time and space scales are relatively large and mathematical procedures are well established, river flow modeling became well established within the overall watershed hydrology. Even with its

current level of advancement, river models face challenging simulations particularly with steep hydrographs and highly non-linear channel geometries, which in turn might require that the space and time scales given above are modified radically.

2.7. Data Requirements

The data requirements of watershed models are one of the major issues that the hydrologic modeler has to focus on. Depending on the type of the model, these requirements might occasionally reach to such levels that it might totally destroy the effort. Particularly, the distributed watershed models are very costly in terms of the operational data requirements. Since such models are based on spatial variability of parameters over the watershed area, the input data are expected to be compatible and satisfy the needs of each model component. Therefore, the data requirements of all the subprocesses included in an integrated model should be studied in details at the earlier stages where model formulation is done. Unless satisfactory data resources are found, a decision to include a watershed process in the integrated model is subjective and would not make much sense.

The channel flow domain is among the few for which data are easily accessible. The major data requirement in the one-dimensional channel flow model is the characterization of the channel that would involve the analysis of channel topographic features (i.e., reach lengths, bottom elevations above a datum and slopes) and channel conveyance characteristics (i.e., tables relating water surface elevation to channel top width and roughness coefficients). Another crucial data requirement for a channel flow model is the time dependent boundary condition data that drives the model. Access to

stage and discharge hydrographs or stage-discharge rating curves is extremely important for accurate simulations of channel flow processes. Finally, reasonably accurate initial condition data is also important for successful start up of a model. Without such data, the numerical model could easily create stability problems which would eventually invalidate the simulation.

The major data requirement of the overland flow model is the description of the overland surface. This description includes a basic topographic characterization of the watershed surface (i.e., surface elevation, slope, orientation) and a specification of overland roughness coefficients based on land use/cover data. Another crucial data requirement of the overland flow analysis is the source function specification. Access to spatially and temporarily distributed precipitation data is of vital importance for the success of the overland flow simulations. Using remote sensing technology such as weather radars and satellites, it is now not difficult to supply this data to overland flow models. The boundary condition data is generally not very important in overland flow analysis when the majority of the flow boundaries are taken as watershed boundaries that enforce a zero flow depth. Only at the outflow boundary, the conditions must be carefully determined and imposed on the model. Finally, the initial condition data of the overland flow domain is mostly supplied by a zero depth condition along the entire watershed as long as flow is purely a function of precipitation input and there exists no prior overland water accumulation on the watershed.

In the saturated groundwater flow domain, the aquifer characteristics are the most significant data requirement. The modeler must have a clear understanding of the geological features of the aquifer and make sure that his representation of the system is a

replica of the real situation in the field. Aquifer characterization would also involve the determination of the material properties of the aquifer (i.e., hydraulic conductivity and specific storage), without which, groundwater flow analysis is not possible. The specification of boundary conditions is another major data requirement that all groundwater flow models require. Time-dependent specification of head, flux or head-dependent boundary conditions must be done along the entire boundary of the modeling domain. Finally, a fairly accurate representation of initial hydraulic head is also crucial for successful modeling of groundwater flow patterns. However, the numerical solution of groundwater flow is generally more resistant to errors in initial conditions than channel flow models are.

The data requirements of the unsaturated zone groundwater flow model are very similar to the saturated zone. The material characteristics of the medium (i.e., the hydraulic conductivity and storage coefficient) are the major data source that must be supplied to any unsaturated zone model. The problem is generally more complicated compared to the saturated zone due to the additional difficulty arising from the dependency of model parameters to the saturation level in the domain. Therefore, the hydraulic conductivity values are to be quantified according to the level of saturation in the medium. When the relationships between soil-water parameters are not properly quantified using field data, approximate empirical models are to be used, reducing the level of accuracy of the results.

CHAPTER 3

COUPLED FLOW MODEL

In this chapter, watershed scale flow pathways are analyzed within the context of a coupled system approach. The governing equations, initial and boundary conditions, as well as the numerical solution schemes of each model component are first given to describe the physics of each flow pathway. Then, two possible coupled models of surface-subsurface flow processes are discussed comprehensively. A new simultaneous coupling methodology is proposed to solve the coupled system more accurately and with better representation of physical processes. The chapter concludes with the introduction of a 'hybrid' modeling concept to alleviate the difficulties of large scale, physically-based distributed watershed modeling.

3.1. One Dimensional Channel Flow Model

3.1.1. Governing Equations

The mathematical model of the one-dimensional channel flow is given by the continuity and momentum equations that are modified to include the effects of natural

channel geometry and characteristics of rivers (Fread, 1993). In this study, the momentum equation is based on the complete dynamic wave form of the unsteady non-uniform St. Venant equations:

$$\frac{\partial s_c (A + A_o)}{\partial t} + \frac{\partial Q}{\partial x} - q_{L1} - q_{L2} = 0 \tag{3.1}$$

$$\frac{\partial s_m Q}{\partial t} + \frac{\partial (\beta Q^2 / A)}{\partial x} + gA\left(\frac{\partial h_r}{\partial x} + S_f + S_{ec}\right) + M_{L1} + M_{L2} = 0 \tag{3.2}$$

where x is the longitudinal coordinate representing the distance along the channel/flood plain, t is the temporal coordinate, s_c and s_m are sinuosity factors for continuity and momentum equations, respectively, A is the active cross-sectional area of flow, A_o is the inactive (off-channel storage) cross-sectional area of the channel/floodplain, Q is the discharge, q_{L1} is the lateral seepage flow per channel length (positive for inflow and negative for outflow), q_{L2} is the lateral overland flow per channel length (positive for inflow and negative for outflow), β is the momentum coefficient for velocity distribution, g is the gravitational acceleration, h_r is the water surface elevation in the river (i.e., stage), M_{L1} is the momentum flux due to lateral seepage inflow/outflow, M_{L2} is the momentum flux due to lateral overland inflow/outflow; and, S_f and S_{ec} are channel/flood plain boundary friction slope and contraction/expansion slope, respectively. The momentum flux due to lateral seepage and overland flows, contraction/expansion slope and channel/flood plain boundary friction slope are evaluated as:

$$M_{L1} = \begin{cases} 0 & \text{for seepage inflow} \\ -\dfrac{Qq_{L1}}{2A} & \text{for seepage outflow} \end{cases} \tag{3.3}$$

$$M_{L2} = \begin{cases} -\beta v_x q_{L2} & \text{for overland inflow} \\ -\dfrac{Qq_{L2}}{A} & \text{for overland outflow} \end{cases} \tag{3.4}$$

$$S_{ec} = \frac{K_{ec}\Delta(Q/A)^2}{2g\Delta x} \tag{3.5}$$

$$S_f = \frac{n_c^2 |Q|Q}{c_1{}^2 A^2 R_h{}^{4/3}} = \frac{|Q|Q}{K^2} \tag{3.6}$$

where v_x is the velocity of the overland flow in the direction of channel flow, K_{ec} is the expansion/contraction coefficient, Δx is the reach length, c_1 is a unit system dependent constant (i.e., 1.0 in SI unit system and 1.486 in British unit system), n_c is the Manning's roughness coefficient in river channel, K is the flow conveyance factor and R_h is the hydraulic radius. The hydraulic radius is defined as the ratio of cross-sectional area to wetted perimeter but is approximated in this study as the ratio of cross-sectional area to top width for large rivers. The lateral flow that provides the link between the channel flow model and the saturated groundwater flow model is defined as:

$$q_{L1} = \begin{cases} -K_r w_r \dfrac{h_r - h_g}{m_r} & h_g > (z_r - m_r) \\ -K_r w_r \dfrac{h_r - (z_r - m_r)}{m_r} & h_g \le (z_r - m_r) \end{cases} \tag{3.7}$$

where K_r is the river bottom sediment hydraulic conductivity, m_r is the thickness of river bottom sediments, z_r is the river bottom elevation, w_r is the wetted perimeter of the river bed and h_g is the groundwater hydraulic head. The details of the coupling between river and groundwater flow systems are given in Section 3.5.1.

3.1.2. Initial Conditions

In order to start the transient solution, initial values of the unknowns (i.e., discharge and water surface elevation) are to be specified along the one-dimensional channel domain. The initial conditions can be obtained from: (i) field data; (ii) a previous unsteady model solution; or, (iii) solution of steady, non-uniform flow equation. In any case, the initial conditions are given as:

$$Q(x,0) = Q_0(x) \tag{3.8}$$

$$h_r(x,0) = h_{r0}(x) \tag{3.9}$$

where Q_0 and h_{r0} represent the discharge and water surface elevation in the channel at the beginning of the simulation, respectively.

3.1.3. Boundary Conditions

In the one-dimensional channel flow model, there are two different types of boundary conditions specified at: (i) external; and, (ii) internal boundaries of the domain. The external boundary conditions are given at the most upstream and downstream points

of the channel network, whereas the internal boundary conditions are specified at internal junction points of the channel network.

3.1.3.1. External Boundary Conditions

In this study, the proposed model is capable of modeling a network of river channels. The tree-like network is composed of several upstream and internal channels and a single downstream channel. Therefore, the model can accommodate several upstream boundary conditions and a single downstream boundary condition. In this regard, the model does not solve looped channel networks. At any upstream boundary, a discharge or a stage hydrograph can be used as the boundary condition. These conditions are expressed as discharge and stage time series and are given as:

$$Q(0,t) = Q_u(t) \tag{3.10}$$

$$h_r(0,t) = h_u(t) \tag{3.11}$$

where Q_u and h_u represent upstream boundary discharge and water surface elevation values, respectively. Similarly, the boundary condition at the downstream boundary can also be defined as a discharge or a stage hydrograph and specified as:

$$Q(L_d,t) = Q_d(t) \tag{3.12}$$

$$h_r(L_d,t) = h_d(t) \tag{3.13}$$

where Q_d and h_d represent downstream boundary discharge and water surface elevation values, and L_d is the total domain length. In addition, it is also possible to define the downstream boundary condition as a single-valued rating curve, a looped rating curve or a critical depth section. The single-valued rating curve maps a particular stage value to a corresponding discharge value and can be expressed by using linear interpolation within a table of stage-discharge data:

$$Q\left(L_d,t\right)=Q^k+\frac{Q^{k+1}-Q^k}{h_r^{k+1}-h_r^k}\left(h_d-h_r^k\right) \tag{3.14}$$

where Q^k, Q^{k+1}, $h_r{}^k$ and $h_r{}^{k+1}$ are consecutive tabular data sets of the rating curve and h_d is the stage at the downstream boundary. A looped rating curve, on the other hand, maps a stage value to several possible discharge values depending on the hydraulic conditions of the channel and can be expressed using the Manning's equation:

$$Q\left(L_d,t\right)=\frac{c_1}{n_c}AR_h^{2/3}S_f^{1/2} \tag{3.15}$$

where S_f is given by the modified momentum equation as:

$$S_f=-\frac{1}{gA}\frac{\partial Q}{\partial t}-\frac{1}{gA}\frac{\partial(Q^2/A)}{\partial x}-\frac{\partial h_r}{\partial x} \tag{3.16}$$

Finally, it is also possible to use critical depth as the downstream boundary condition when the most downstream point of the modeling domain is a controlling structure such as a weir. In this particular case, the critical depth is mapped to the critical discharge via the following equation:

$$Q(L_d, t) = \sqrt{\frac{g}{B}} A^{3/2} \tag{3.17}$$

where B is the cross-sectional top width of the channel.

3.1.3.2. Internal Boundary Conditions

Any two or more channels intersecting within a channel network form a junction where internal boundary conditions are specified to satisfy the mass and energy balances. In this study, the proposed model does not allow for looped networks and requires that there is always a single outflow channel from a junction. The mass balance equation at a junction can therefore be specified as:

$$\sum_{k=1}^{m} Q_k - Q_o = \frac{dS}{dt} \tag{3.18}$$

where m is the total number of inflowing channels to the junction, Q_k is the discharge at the end of the k^{th} inflowing channel to the junction, Q_o represents the discharge at the beginning of the outflowing channel from the junction, and dS/dt corresponds to the change in storage within the junction. For many modeling applications, it is a common

practice to assume that the change in storage within a junction is negligible compared to the change in storage within in a channel (Akan and Yen, 1981b; Fread, 1993; Jha et al., 2000). Consequently, the mass balance equation reduces to a simple continuity equation. On the other hand, the energy equation at a junction is written as:

$$(h_r)_k + \frac{V_k^2}{2g} = (h_r)_o + \frac{V_o^2}{2g} + h_T \qquad k = 1,2,\ldots,m \tag{3.19}$$

where $(h_r)_k$ and V_k are the stage and flow velocity at the end of the k^{th} inflowing channel to the junction, $(h_r)_o$ and V_o are the stage and flow velocity at the beginning of the outflowing channel from the junction and h_T is the total headloss in the junction. When all the flows in all the branches joining a junction are subcritical and the head lost in the junction is negligible, the equation simplifies to:

$$(h_r)_k = (h_r)_o \qquad k = 1,2,\ldots,m \tag{3.20}$$

and is commonly used in modeling channel networks (Akan and Yen, 1981b; Fread, 1993; Jha et al., 2000).

3.1.4. Numerical Solution Scheme

In general, the available numerical techniques for the solution of the expanded Saint-Venant equations can be given as: (i) method of characteristics; (ii) finite difference methods; and, (iii) finite element methods. Of these methods, the finite element method is rarely used when flow is approximated as one-dimensional such as in the case of Saint-

Venant equations. The other two methods have been commonly applied for the numerical solution of one-dimensional unsteady flow since 1960s. The finite difference methods can further be classified as explicit and implicit techniques, each of which holds distinct numerical characteristics. A major advantage of the implicit finite difference method over the method of characteristic and the explicit finite difference technique is its inherent stability without the requirement to satisfy the Courant condition, which sets the criteria for the maximum allowable time step. This requirement to satisfy Courant condition often makes the method of characteristics and explicit techniques very inefficient in terms of the use of computer time. Furthermore, certain implicit schemes such as the one proposed by Preissmann (1961) allow the use of variable time and spatial steps, which make the method extremely convenient for applications in routing of flood hydrographs in river systems (Sturm, 2001). Considering these advantages, the implicit finite difference technique is used to solve the channel flow equations given by equations (3.1) and (3.2).

Of the various implicit schemes that have been developed, the "weighted four-point" scheme of Preissmann is very valuable since it can readily be used with unequal distance steps that become particularly important for natural waterways where channel characteristics are highly variable even over short distances. Similarly, the possibility of unequal time steps is another important characteristic of this technique for hydrograph routing where floodwaters would generally rise relatively quickly and recess gradually in time.

The finite difference counterparts of the continuity, momentum and boundary condition equations are derived in Appendix A. In a channel network, the discretized

forms of equations (3.1) and (3.2) form the core of the channel flow model. These equations are written for each channel in the network, and supplemented by the discretized forms of the boundary condition equations. For each channel, the final form of the continuity equation written for an intermediate node is given as:

$$\begin{aligned}
&\frac{\Delta x_i}{2\Delta t^j}\left[s_{ci+1/2}^{\,j+1}\left(A+A_o\right)_{i+1}^{j+1} + s_{ci+1/2}^{\,j+1}\left(A+A_o\right)_{i}^{j+1} - s_{ci+1/2}^{\,j}\left(A+A_o\right)_{i+1}^{j} - s_{ci+1/2}^{\,j}\left(A+A_o\right)_{i}^{j} \right] \\
&+\theta_f\left[Q_{i+1}^{j+1} - Q_i^{j+1} - \Delta x_i\left[\left(-\frac{K_r w_r}{m_r} \right)_{i+1/2}^{j+1} \left(h_{ri+1/2}^{\,j+1} - h_{gi+1/2}^{\,j+1} \right) \right] - \Delta x_i \left(q_{L2}\right)_{i+1/2}^{j+1} \right] \\
&+\left(1-\theta_f\right)\left[Q_{i+1}^{j} - Q_i^{j} - \Delta x_i\left[\left(-\frac{K_r w_r}{m_r} \right)_{i+1/2}^{j} \left(h_{ri+1/2}^{\,j} - h_{gi+1/2}^{\,j} \right) \right] - \Delta x_i \left(q_{L2}\right)_{i+1/2}^{j} \right] = 0
\end{aligned} \tag{3.21}$$

Similarly, the finite difference form of the momentum equation written for an intermediate node is given as:

$$\begin{aligned}
&\frac{\Delta x_i}{2\Delta t^j}\left[s_{mi+1/2}^{\,j+1} Q_{i+1}^{j+1} + s_{mi+1/2}^{\,j+1} Q_i^{j+1} - s_{mi+1/2}^{\,j} Q_{i+1}^{j} - s_{mi+1/2}^{\,j} Q_i^{j} \right] \\
&+\theta_f\left[\begin{array}{l} \left(\beta Q^2/A\right)_{i+1}^{j+1} - \left(\beta Q^2/A\right)_{i}^{j+1} + \\ gA_{i+1/2}^{j+1}\left[h_{ri+1}^{\,j+1} - h_{ri}^{\,j+1} + \Delta x_i S_{f\,i+1/2}^{\,j+1} + \Delta x_i S_{eci+1/2}^{\,j+1} \right] + \\ \Delta x_i \left(M_{L1}\right)_{i+1/2}^{j+1} + \Delta x_i \left(M_{L2}\right)_{i+1/2}^{j+1} \end{array} \right] \\
&+\left(1-\theta_f\right)\left[\begin{array}{l} \left(\beta Q^2/A\right)_{i+1}^{j} - \left(\beta Q^2/A\right)_{i}^{j} + \\ gA_{i+1/2}^{j}\left(h_{ri+1}^{\,j} - h_{ri}^{\,j} + \Delta x_i S_{f\,i+1/2}^{\,j} + \Delta x_i S_{ei+1/2}^{\,j} \right) + \\ \Delta x_i \left(M_{L1}\right)_{i+1/2}^{j} + \Delta x_i \left(M_{L2}\right)_{i+1/2}^{j} \end{array} \right] = 0
\end{aligned} \tag{3.22}$$

where corresponding formulations developed in Appendix A are substituted for the slope terms S_f and S_{ec}, as well as the lateral flow terms M_{L1} and M_{L2} (depending on the direction of lateral flows) from equations (A.17), (A.18), (A.19) and (A.20), respectively. In equations (3.21) and (3.22), subscripts i and j represent the spatial and temporal indices, respectively. The terms with subscript j are known either from initial conditions or from the solution of Saint-Venant equations at the previous time step. Since cross sectional area and channel top width are functions of water surface elevation, the only unknown terms in these equations are discharge and water surface elevation at the $(j+1)^{th}$ time step at nodes (i) and ($i+1$). Therefore, there are only four unknowns in these two equations. All remaining terms are either constants or are functions of these unknowns. The resulting two algebraic equations obtained by the application of the weighted four-point scheme are nonlinear and an iterative solution technique is required.

When the finite difference forms of the continuity and momentum equations are solved for each channel grid shown in Appendix A, a system of $2(N_k-1)$ equations are formed for each time-step between the upstream and downstream boundary of channel k, where N_k represents the number of nodes in channel k. The two unknowns in each of these equations yield a total of $2N_k$ unknowns for each time line. The system of $2(N_k-1)$ equations with $2N_k$ unknowns requires two additional equations for the closure of the system. These two additional equations are supplied by the upstream and downstream boundary conditions of the channel. The discretized forms of these equations are also presented in Appendix A. When this procedure is repeated for each channel of the network, a total of $\Sigma(2N_k)=2N$ equations are formed, where k runs from 1 to the number of channels in the network, and N represents the total number of nodes in the entire

system. The resulting system of *2N* non-linear equations with *2N* unknowns is solved by a suitable non-linear matrix solution algorithm.

Of all the non-linear solution procedures, the Newton-Raphson method is one of the most common iterative techniques used for the solution of a system of non-linear equations. It provides an efficient means of converging to a root given a sufficiently good initial guess. For any channel network application, the system of equations can be denoted as *2N* functional relations to be zeroed that involve variables Q and h_r represented by x_k for $k=1,2,...,2N$:

$$f_k(x_1, x_2, x_3, ..., x_{2N}) = 0 \tag{3.23}$$

If **x** denotes the entire vector of unknown variables x_k and **f** denotes the entire vector of functions f_i, each of the functions f_i can be expanded as a Taylor series expansion in the neighborhood of **x**:

$$f_k(\mathbf{x} + \delta\mathbf{x}) = f_k(\mathbf{x}) + \sum_{m=1}^{2N} \frac{\partial f_k}{\partial x_m} \delta x_m + O(\delta\mathbf{x}^2) \tag{3.24}$$

where the matrix of first partial derivatives is called the Jacobian matrix, **J**. The elements of the Jacobian matrix for 2N unknowns are evaluated in Appendix B. In matrix notation, one can rewrite equation (3.24) as:

$$\mathbf{f}(\mathbf{x} + \delta\mathbf{x}) = \mathbf{f}(\mathbf{x}) + \mathbf{J} \cdot \delta\mathbf{x} + O(\delta\mathbf{x}^2) \tag{3.25}$$

Neglecting the higher order terms and setting the left hand-side equal to zero, one can obtain a set of linear equations that is written as:

$$\mathbf{J} \cdot \delta\mathbf{x} = -\mathbf{f} \tag{3.26}$$

This matrix equation is solved by a suitable matrix solver for the unknown $\delta\mathbf{x}$, and an improved estimate of the solution is obtained by:

$$\mathbf{x}^{j+1,k+1} = \mathbf{x}^{j+1,k} + \delta\mathbf{x}^{j+1,k} \tag{3.27}$$

where superscript k represents the level of iteration at the unknown time line. The iterative solution is tracked by finding the values of the unknowns Q and h_r so that the residuals given in equation (3.27) are forced to zero or very close to zero. It must be noted that the convergence process depends on a good first estimate for the unknown variables. Fread (1985) states that a reasonably good estimate for the first time step is to use the initial condition of discharge and water surface elevation. For all other time steps, the first estimates of the unknown variables can be obtained by using the linearly extrapolated values from solutions at previous time steps according to the algorithm given below:

$$\mathbf{x}^{j+1,1} = \mathbf{x}^{j} + \alpha_c \left(\mathbf{x}^{j} - \mathbf{x}^{j-1}\right)\frac{\Delta t^{j+1}}{\Delta t^{j}} \qquad \text{j} \neq 1 \tag{3.28}$$

where $\mathbf{x}^{j+1,1}$ is the first estimate of unknown variables at $(j+1)^{th}$ time line, $\mathbf{x}^{j}$ is the solution vector of Q and h_r values from previous time step, $\mathbf{x}^{j-1}$ is the solution vector of Q and h_r values from two previous time steps, α_c is a weighing factor from 0 to 1 and Δt^{j+1} and Δt^{j} are the two consecutive time step sizes.

3.1.5. Model Testing

The channel flow model is one of the most complicated partial differential equations in the computational fluid dynamics area. Since there are no known analytical solutions to the coupled continuity and momentum equations, the proposed model is tested against the popular HEC-RAS river analysis software developed by the U.S. Army Corps of Engineers Hydrologic Engineering Center (Brunner, 2002) and the previously published model of Choi and Molinas (1993).

Three tests are done to check the performance of the proposed model. In the first test, a triangular flood hydrograph is routed in a single channel. The 10000m long channel is rectangular in cross-section with a constant width of 20m and lies on the slope 0.001 m/m. A Manning's roughness coefficient of 0.020 is used throughout the channel. At the upstream boundary, the discharge hydrograph is used as the boundary condition. At the downstream boundary, a constant water depth of 2m is used throughout the simulations. The simulations are made with a constant grid spacing of 100m and a time step of 1hr. For this particular example, the results of the proposed model are compared with the results from both the HEC-RAS model and comparisons are made at the mid-point of the channel and at the most downstream point of the channel. The results of the comparison are given in figures 3.1 and 3.2.

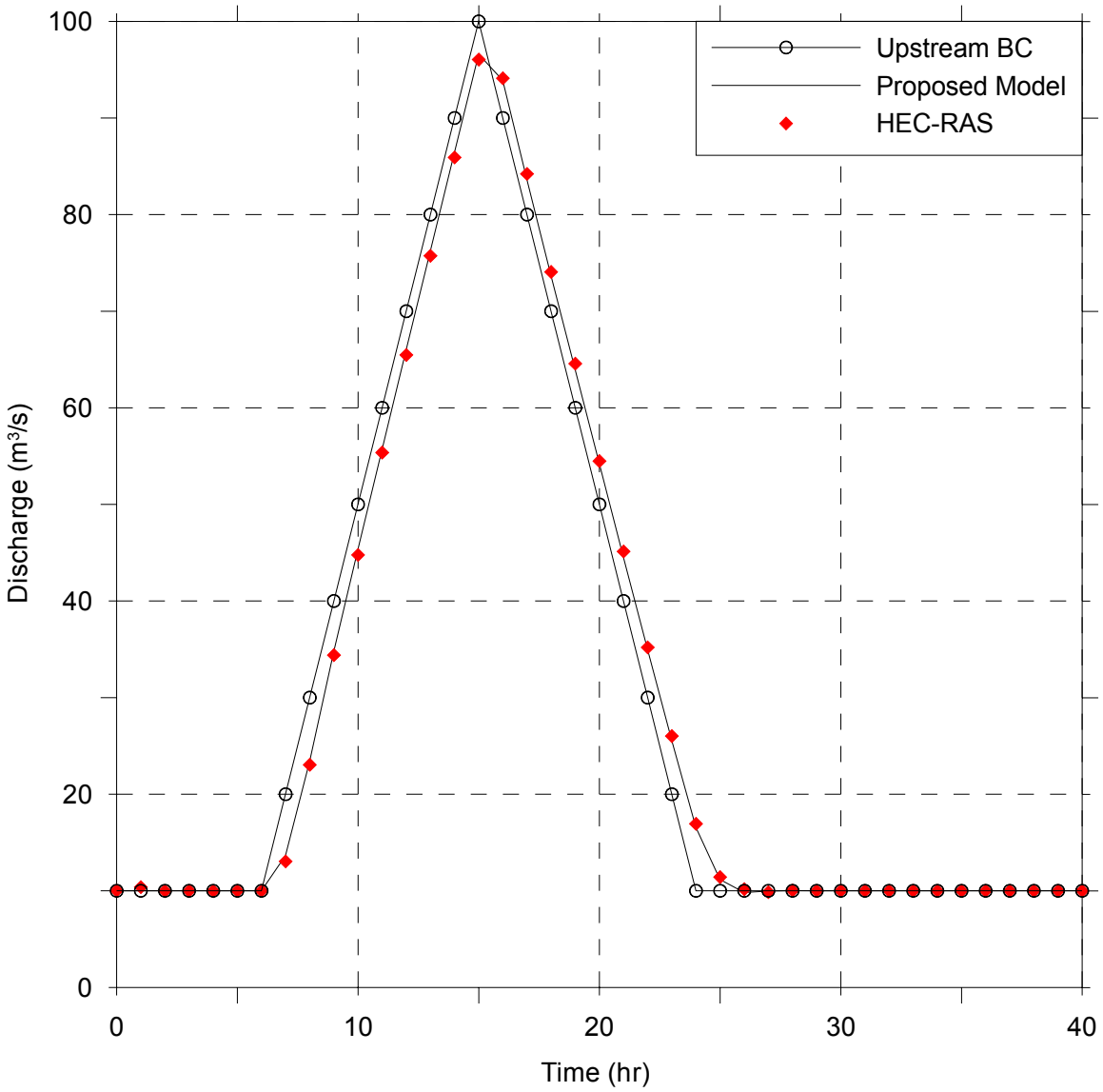

Figure 3.1. Comparison of single channel simulations at mid-point cross-section

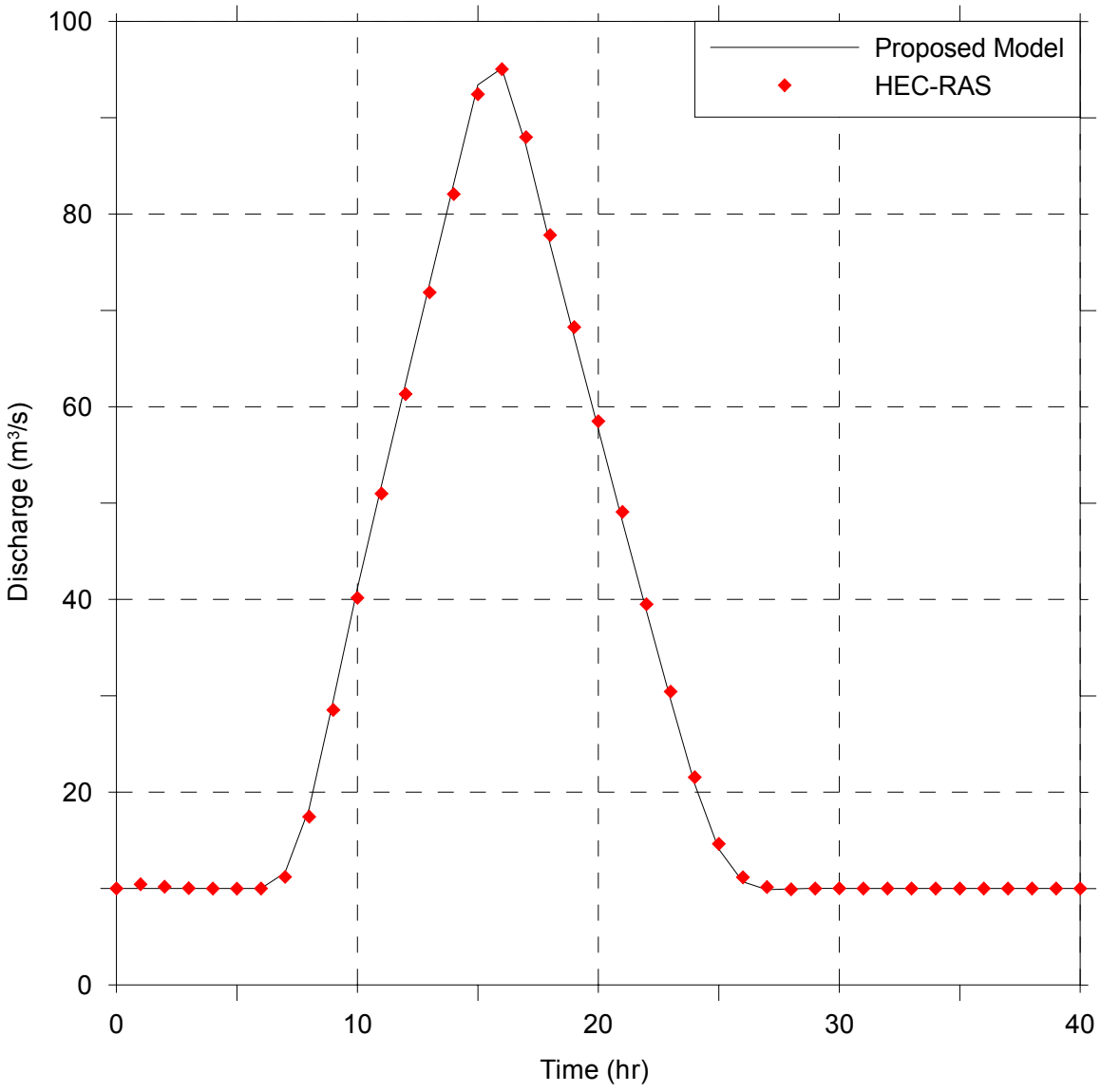

Figure 3.2. Comparison of single channel simulations at most downstream cross-section

As seen in figures 3.1 and 3.2, the proposed model and HEC-RAS give identical results both at the mid-point of the channel and at the most downstream point of the channel. Therefore, the proposed model is shown to simulate a single channel case correctly by propagating and attenuating the triangular discharge hydrograph.

In the second test, a simple channel network is simulated with the proposed model as well as the HEC-RAS model. The network contains 2 upstream channels, a junction, and a downstream channel (Figure 3.3). The upstream channels are 10,000m and 5,000m long respectively and have a slope of 0.001m/m. The downstream channel is 10,000m long and has slope of 0.001m/m. All channels have a roughness coefficient of 0.030. The channels are trapezoidal in cross-section with a base width of 10m and a side slope of 2 to 1. At the upstream boundaries of the upstream channels, single and double peaked triangular discharge hydrographs are used as the boundary conditions. At the most downstream point of the channel system, a constant water depth of 2m is used throughout the simulations. The simulations are made with a constant grid spacing of 100m and a time step of 1hr. Comparisons are made at the mid-point and at the exit point of the downstream channel. The results are given in figures 3.4 and 3.5.

The proposed model gives very similar results to the HEC-RAS model. The deviations in peaks and depressions are mainly due to the hydraulic radius evaluation differences in these two models. In the proposed model, the wetted perimeter of a cross-section is approximated with the top width which makes it only an estimate for hydraulic radius evaluation, where as HEC-RAS uses an exact evaluation method for the wetted perimeter and the hydraulic radius. The approximate procedure implemented in the proposed model is a widely applied technique for modeling real river systems (Fread,

1985; Fread, 1993; Jha et al., 2000). It may, however, create some discrepancies for applications to artificial channels where wetted perimeter is significantly different from the top width. Except for this problem, the two models practically generate identical results in terms of hydrograph timing.

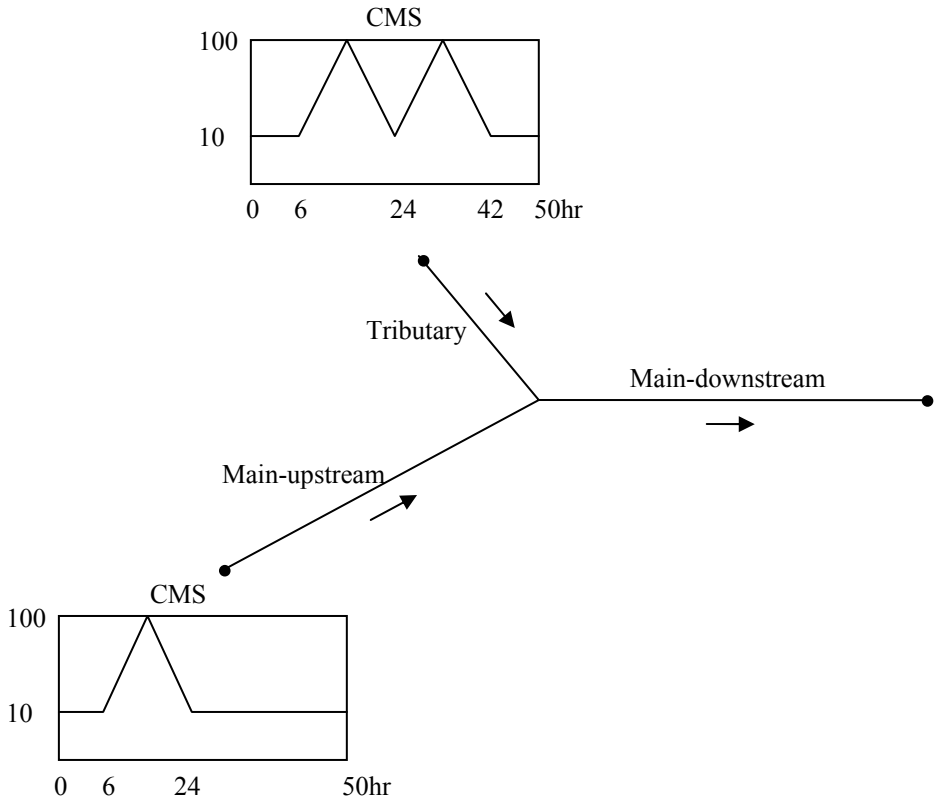

Figure 3.3. Simple network setup

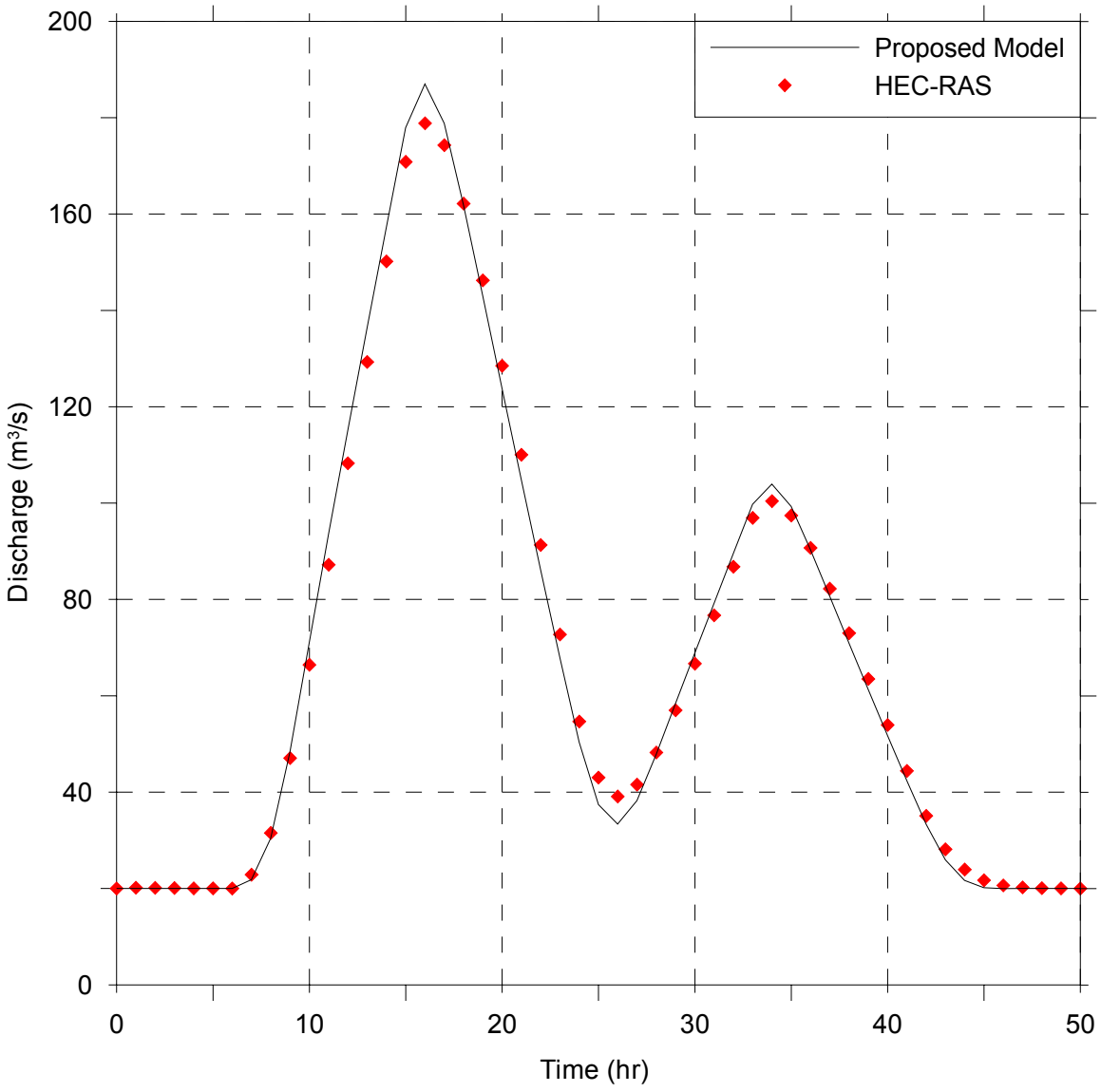

Figure 3.4. Comparison of simple network simulations at mid-point cross-section of downstream channel

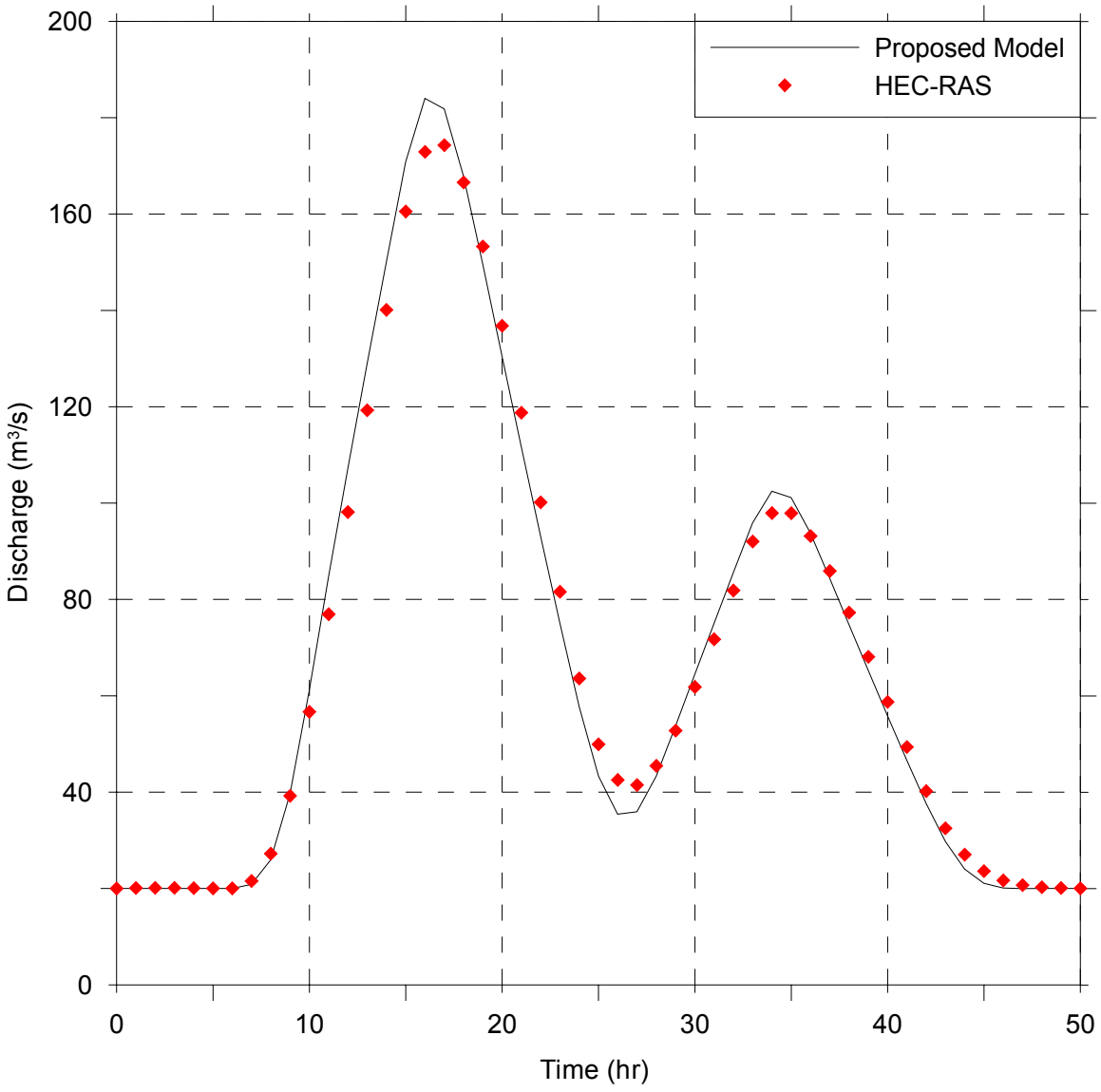

Figure 3.5. Comparison of simple network simulations at most downstream cross-section

The final test is taken from Choi and Molinas (1993) who analyzed a hypothetical dendritic system composed of five tributary channels and three main channels (Figure 3.6). A linear discharge variation with a maximum discharge of 2,300ft^3/s is used as the upstream boundary condition of all tributary channels. The tributary and main channel lengths were taken as 6mile long. The channel widths varied from 100ft for tributaries to 200ft for the reach downstream from tributaries 1 and 2, 400ft for the reach downstream of tributaries 3 and 4, to 500ft for the downstream main channel. The slope in each channel segment was taken to be 0.002ft/ft and the Manning's roughness coefficient was 0.04. The initial discharge per unit width was constant throughout the network. The simulations were performed with 10min time increments and 1mile spatial spacing. For the initial conditions, the same water depths are assumed in all branches and in the main channel. Comparisons are made at the most downstream point of the channel network. The results from the proposed model and HEC-RAS are overlaid on Choi and Molinas' results and are presented in Figure 3.7. Since Choi and Molinas did not provide a detailed output of their results, an overlay technique is used to compare the results of their model with the proposed model and HEC-RAS. In their study, they compare their dendritic model to sequential kinematic and sequential dynamic models and show that their dendritic model is capable of producing similar results. Comparisons of the proposed model, HEC-RAS and their dendritic model do not provide a definite bias towards a particular model. The proposed model, however, closely follows the results from the Choi and Molinas' dendritic model in the early parts of the rising limb of the hydrograph during which the HEC-RAS significantly creates a delay in the arrival of the rising limb. The proposed model then shows signs of delay in the later parts of the hydrograph rising

limb and creates a slightly delayed peak value when compared to the Choi and Molinas model and HEC-RAS. In the falling limb, however, the proposed model closely follows Choi and Molinas' dendritic model as well as HEC-RAS. In terms of the value of the peak, the proposed model estimates very closely to Choi and Molinas' model, whereas HEC-RAS slightly overestimates. An overall analysis of the results shown in Figure 3.7 reveal that the proposed channel flow model performs accurately compared to some other models. Exact comparisons are only possible with analytical solutions of the mathematical model that are currently not available.

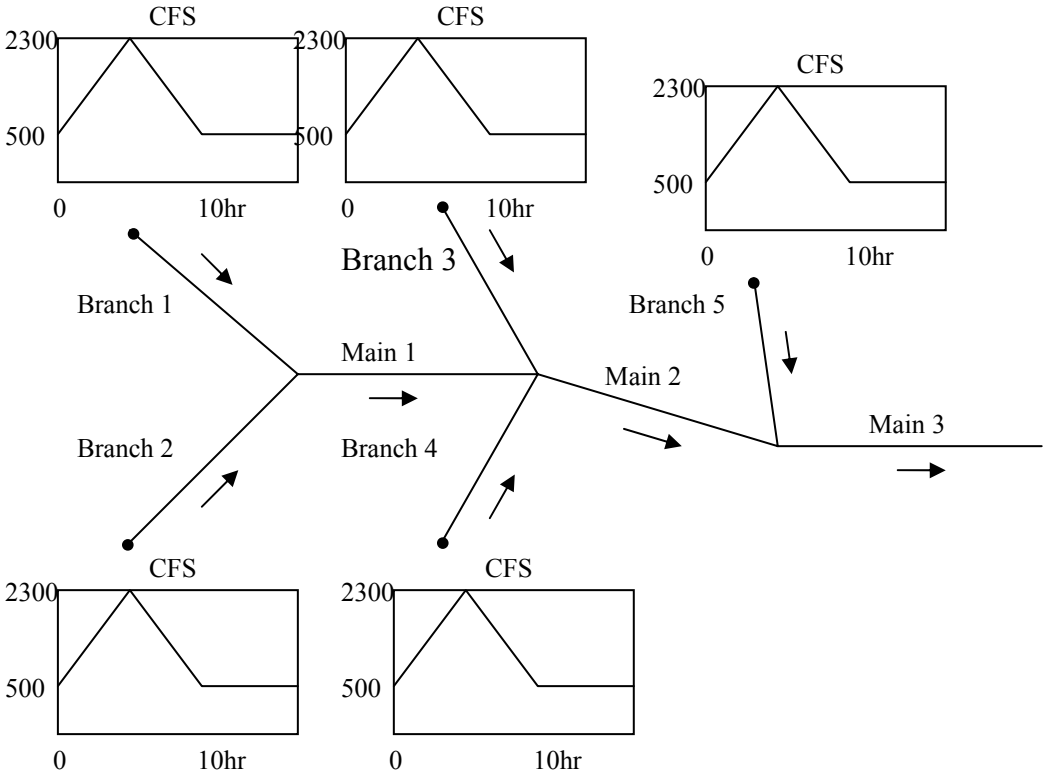

Figure 3.6. Choi and Molinas (1993) dendritic network setup

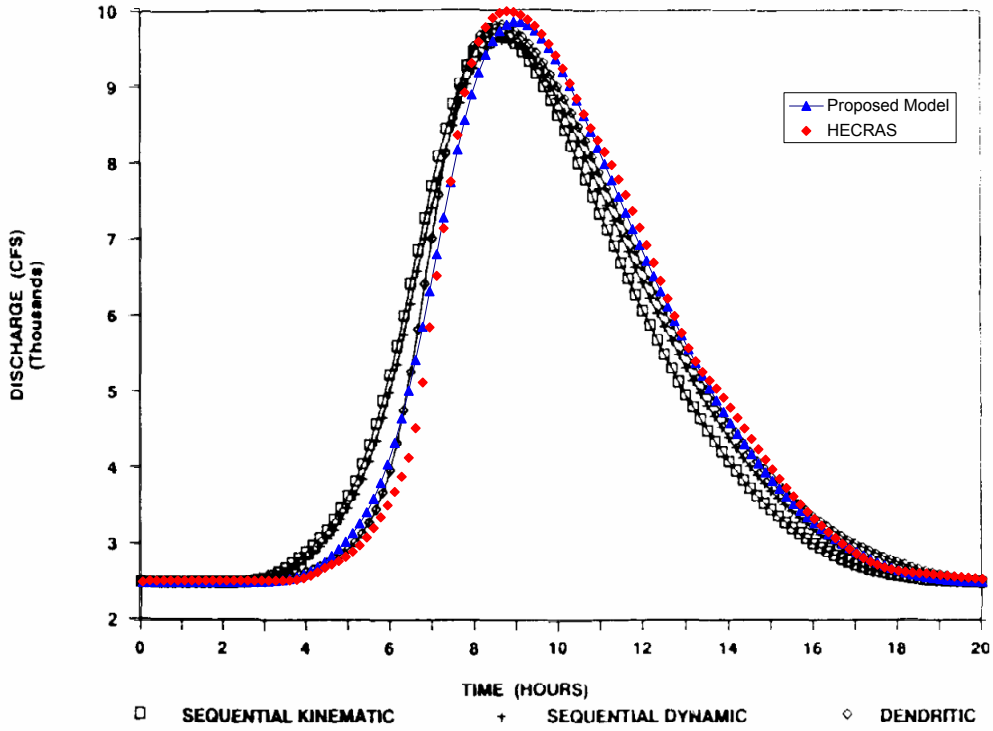

Figure 3.7. Comparison of results from Choi and Molinas (1993) with the proposed model and HECRAS

3.2. Two Dimensional Saturated Groundwater Flow Model

3.2.1. Governing Equations

The governing equation of two-dimensional vertically-averaged saturated groundwater flow is obtained by vertically integrating the general three-dimensional conservation of mass and momentum equations describing subsurface flow (Aral, 1990). The equation is later on modified by Gunduz and Aral (2004a) to include the effect of a line source/sink. For an anisotropic, non-homogeneous, unconfined aquifer with principle

permeability directions not matching the coordinate directions, the governing equation of vertically-averaged saturated groundwater flow is given by:

$$S_y \frac{\partial h_g}{\partial t} - \frac{\partial}{\partial x}\left[\left(h_g - z_b\right)\left(K_g\right)_{xx} \frac{\partial h_g}{\partial x} + \left(h_g - z_b\right)\left(K_g\right)_{xy} \frac{\partial h_g}{\partial y} \right]$$
$$- \frac{\partial}{\partial y}\left[\left(h_g - z_b\right)\left(K_g\right)_{yx} \frac{\partial h_g}{\partial x} + \left(h_g - z_b\right)\left(K_g\right)_{yy} \frac{\partial h_g}{\partial y} \right] + \sum_{k=1}^{n_w}\left[Q_{w,k}\,\delta\left(x - x_{w,k}\right)\delta\left(y - y_{w,k}\right)\right] \quad (3.29)$$
$$+ \sum_{m=1}^{n_r}\left[\int_0^1 q_{L1,m} \sqrt{\left(\frac{dg_{x,m}}{du}\right)^2 + \left(\frac{dg_{y,m}}{du}\right)^2}\,\delta\left(x - g_{x,m}(u)\right)\delta\left(y - g_{y,m}(u)\right) du \right] + I = 0$$

where x and y are the spatial coordinates in the horizontal domain, t is the temporal coordinate, S_y is the specific yield of the unconfined aquifer, h_g is the vertically-averaged hydraulic head, z_b is the top elevation of bottom impervious layer, K_g is the anisotropic saturated hydraulic conductivity, n_w is the number of wells in the domain, $Q_{w,k}$ is the well flow rate of the kth well located at ($x_{w,k}$,$y_{w,k}$) in the domain (i.e., positive for a discharging well and negative for an injecting well), δ is the Dirac Delta function, n_r is the number of river channels in the domain, q_{L1} is the lateral flow at the river-bottom interface defined by equation (3.7) (i.e., positive for lateral outflow from the aquifer and negative for lateral inflow to the aquifer), $g_{x,m}$ and $g_{y,m}$ are the Cartesian coordinate components of the parametric equation defining the mth river channel in the domain, u is the dimensionless parameter of the parametric equation and I is the infiltration/exfiltration rate (i.e., positive for exfiltration and negative for infiltration).

In general, the directions, along which the hydraulic conductivity measurements (i.e., the principle coordinate system) are made, are different from the assumed global

coordinate system on which the entire analysis is based. Under such circumstances, a transformation is necessary to make proper use of the hydraulic conductivity data obtained from field studies. Hence, if the values of hydraulic conductivity are known in the principle coordinate system (ξ,η), then their corresponding values in a global coordinate system (x,y) making an angle θ_c with the principle coordinate system are given as (Bear, 1979):

$$\begin{aligned}
\left(K_g\right)_{xx} &= \frac{\left(K_g\right)_{\xi\xi}+\left(K_g\right)_{\eta\eta}}{2}+\frac{\left(K_g\right)_{\xi\xi}-\left(K_g\right)_{\eta\eta}}{2}\cos 2\theta_c \\
\left(K_g\right)_{yy} &= \frac{\left(K_g\right)_{\xi\xi}+K_{\eta\eta}}{2}-\frac{\left(K_g\right)_{\xi\xi}-\left(K_g\right)_{\eta\eta}}{2}\cos 2\theta_c \\
\left(K_g\right)_{xy} &= \left(K_g\right)_{yx} = -\frac{\left(K_g\right)_{\xi\xi}-\left(K_g\right)_{\eta\eta}}{2}\sin 2\theta_c
\end{aligned} \tag{3.30}$$

3.2.2. Initial Conditions

The initial values of the hydraulic head, h_{g0}, are specified as the initial conditions of the groundwater flow model:

$$h_g(x,y,0) = h_{g0}(x,y) \tag{3.31}$$

which can be obtained from: (i) field measurements, (ii) a steady state flow simulation; and, (iii) a previous unsteady model solution.

3.2.3. Boundary Conditions

Three different types of boundary conditions can be specified along different external boundaries of the groundwater flow domain. Type-1 or specified head boundary conditions are used to model boundaries with known hydraulic head values. This is also known as a Dirichlet boundary condition and is given as:

$$h_g\left(x,y,t\right) = h_{gD}\left(x,y,t\right) \tag{3.32}$$

where h_{gD} is the known hydraulic head value. Type-2 or specified flux boundary conditions are used to model boundaries with known flux values. This is also known as a Neumann boundary condition and is given as:

$$q_N\left(x,y,t\right) = -\mathbf{n}\cdot\left(\left(h_g - z_b\right)\mathbf{K}_g\cdot\nabla h_g\right) \tag{3.33}$$

where q_N is the known flux value and $\mathbf{n}$ is the unit normal to the boundary. Finally, Type-3 or head-dependent boundary conditions are used to model boundaries on which the conditions depend on the changing hydraulic head such as streams, rivers or lakes at the external boundaries of the domain. It is also known as a Cauchy boundary condition and is given as:

$$q_C(x,y,t) = -\mathbf{n}\cdot\left(\left(h_g - z_b\right)\mathbf{K}_g \cdot \nabla h_g\right) = \begin{cases} -K_r w_r \dfrac{h_r - h_g}{m_r} & h_g > \left(z_r - m_r\right) \\ -K_r w_r \dfrac{h_r - \left(z_r - m_r\right)}{m_r} & h_g \le \left(z_r - m_r\right) \end{cases} \tag{3.34}$$

where q_C is the head-dependent flux value and is similar to the lateral seepage flow term defined internally in the domain and given in equation (3.7).

3.2.4. Numerical Solution Scheme

In the groundwater flow modeling literature, there exist numerous models implementing different numerical solution procedures. The most common of these procedures are the finite difference and finite element methods (Narasimhan and Witherspoon, 1977; Huyakorn et al., 1986; McDonald and Harbaugh, 1988; Aral, 1990; Yeh, 1999; Morita and Yen, 2002). The finite element method became a popular method due to the flexibility it offers in simulating large scale aquifer domains with irregular boundaries as well as heterogeneous aquifer properties. In this regard, the Galerkin finite element method based on the method of weighted residuals is used in this study to solve the groundwater flow.

The numerical procedure starts with the idealization of the solution domain by a finite number of distinct, non-overlapping regions, called the finite elements, over which the unknown variables are to be interpolated. In any idealization, the elements are selected such that the material properties of the domain, such as hydraulic conductivity and specific yield, are retained in individual elements. In two-dimensional finite element analysis, families of triangular and/or quadrilateral elements are generally used to

discretize the analysis domain. Although these elements can be linear, quadratic or cubic, using simple linear elements generally provides sufficient accuracy and a better solution strategy. Quadrilateral elements are superior as opposed to triangular elements due to the fact that they are computationally more efficient and they simplify the task of tiling the problem domain without introducing any bias that the triangular elements possess. For these reasons, linear irregular quadrilateral elements with four nodes are selected to discretize the domain and develop basis functions in this study. The details associated with the basis functions are given in Appendix C.

Following the idealization of domain and selection of the interpolating functions, an appropriate weak form of the problem is developed using the Galerkin weighted residual method as shown in Appendix D by using the standard steps of writing the weighted residual, integration by parts and incorporating the natural boundary conditions. The resulting finite element matrix equation obtained by applying the Galerkin procedure is given as:

$$\mathbf{S} \cdot \hat{\mathbf{h}}_{\mathbf{g}} + \mathbf{M} \cdot \frac{d\,\hat{\mathbf{h}}_{\mathbf{g}}}{dt} = \mathbf{F} \tag{3.35}$$

where **S**, **M** and **F** stand for global stiffness matrix, global mass matrix and global load vector, respectively, and $\hat{\mathbf{h}}_{\mathbf{g}}$ is the approximate hydraulic head vector. These global matrices and vectors are obtained by tiling their element counterparts according to the connectivity of elements within the solution domain. The explicit formulations of element matrices and vectors are derived in Appendix E. At this point, it is clearly seen that these element integrals are generally complex and cannot be integrated analytically. Hence, a

numerical integration scheme is required to evaluate these element integrals. In this study, a two-dimensional Gaussian quadrature technique is implemented to evaluate these integrals numerically. The details of this technique are discussed in Appendix F.

The ordinary differential equation (3.35) obtained as a result of finite element discretization could be solved using a number of techniques including the one-step finite difference approximations. Since the hydraulic head is a function of time, it is possible to define two positions, j and $j+1$, representing the known and unknown time steps, respectively. If one defines an intermediate point between the known and the unknown time step (i.e., $j+\alpha$ where $0 \le \alpha \le 1.0$), then the corresponding head could be calculated as a weighted average:

$$\hat{\mathbf{h}}_{\mathbf{g}}{}^{j+\alpha} = \alpha \hat{\mathbf{h}}_{\mathbf{g}}{}^{j+1} + (1-\alpha)\hat{\mathbf{h}}_{\mathbf{g}}{}^{j} \tag{3.36}$$

such that if the intermediate point is selected as the mid point between the two time steps (i.e., $\alpha=0.5$), the head becomes an arithmetic average of the two heads at two ends. When the Taylor series expansion of the hydraulic head around the intermediate point is done using the points j and $j+1$, one would obtain:

$$\hat{\mathbf{h}}_{\mathbf{g}}{}^{j+(1-\alpha)} = \hat{\mathbf{h}}_{\mathbf{g}}{}^{j} + \frac{(1-\alpha)\Delta t}{1!}\frac{\partial \hat{\mathbf{h}}_{\mathbf{g}}{}^{j}}{\partial t} + \frac{(1-\alpha)^2 \Delta t^2}{2!}\frac{\partial^2 \hat{\mathbf{h}}_{\mathbf{g}}{}^{j}}{\partial t^2} + O\left(\Delta t^3\right) \tag{3.37}$$

$$\hat{\mathbf{h}}_{\mathbf{g}}{}^{j+(1-\alpha)} = \hat{\mathbf{h}}_{\mathbf{g}}{}^{j+1} - \frac{\alpha \Delta t}{1!}\frac{\partial \hat{\mathbf{h}}_{\mathbf{g}}{}^{j+1}}{\partial t} + \frac{\alpha^2 \Delta t^2}{2!}\frac{\partial^2 \hat{\mathbf{h}}_{\mathbf{g}}{}^{j+1}}{\partial t^2} - O\left(\Delta t^3\right) \tag{3.38}$$

Neglecting the terms equal to or higher than second order and subtracting the second equation from the first yields:

$$0 = \hat{\mathbf{h}}_{\mathbf{g}}{}^{j} - \hat{\mathbf{h}}_{\mathbf{g}}{}^{j+1} + \frac{(1-\alpha)\Delta t}{1!}\frac{\partial \hat{\mathbf{h}}_{\mathbf{g}}{}^{j}}{\partial t} + \frac{\alpha \Delta t}{1!}\frac{\partial \hat{\mathbf{h}}_{\mathbf{g}}{}^{j+1}}{\partial t} \tag{3.39}$$

and after rearranging, reduces to:

$$\frac{\hat{\mathbf{h}}_{\mathbf{g}}{}^{j+1} - \hat{\mathbf{h}}_{\mathbf{g}}{}^{j}}{\Delta t} = (1-\alpha)\frac{\partial \hat{\mathbf{h}}_{\mathbf{g}}{}^{j}}{\partial t} + \alpha \frac{\partial \hat{\mathbf{h}}_{\mathbf{g}}{}^{j+1}}{\partial t} \tag{3.40}$$

Since it is always possible to write the ordinary differential equation for a particular time step, one would obtain the following equations for the two time steps:

$$\mathbf{S}^{j} \cdot \hat{\mathbf{h}}_{\mathbf{g}}{}^{j} + \mathbf{M}^{j} \cdot \frac{d\,\hat{\mathbf{h}}_{\mathbf{g}}{}^{j}}{dt} = \mathbf{F}^{j} \tag{3.41}$$

$$\mathbf{S}^{j+1} \cdot \hat{\mathbf{h}}_{\mathbf{g}}{}^{j+1} + \mathbf{M}^{j+1} \cdot \frac{d\,\hat{\mathbf{h}}_{\mathbf{g}}{}^{j+1}}{dt} = \mathbf{F}^{j+1} \tag{3.42}$$

When these equations are multiplied by the weighing parameters (1-α) and α, respectively and added together, one would obtain:

$$\alpha \mathbf{S}^{j+1} \cdot \hat{\mathbf{h}}_{\mathbf{g}}{}^{j+1} + (1-\alpha)\mathbf{S}^{j} \cdot \hat{\mathbf{h}}_{\mathbf{g}}{}^{j} + \alpha \mathbf{M}^{j+1} \cdot \frac{d\hat{\mathbf{h}}_{\mathbf{g}}{}^{j+1}}{dt} + (1-\alpha)\mathbf{M}^{j} \cdot \frac{d\hat{\mathbf{h}}_{\mathbf{g}}{}^{j}}{dt} = \alpha \mathbf{F}^{j+1} + (1-\alpha)\mathbf{F}^{j} \tag{3.43}$$

It must be noted that in saturated unconfined aquifer flow, the mass matrix, **M**, is a constant matrix which is not a function of hydraulic head and takes the same values for all time steps. Therefore, the above formulation can be simplified as:

$$\alpha \mathbf{S}^{j+1} \cdot \hat{\mathbf{h}}_{\mathbf{g}}{}^{j+1} + (1-\alpha)\mathbf{S}^{j} \cdot \hat{\mathbf{h}}_{\mathbf{g}}{}^{j} + \mathbf{M} \cdot \left(\alpha \frac{d\hat{\mathbf{h}}_{\mathbf{g}}{}^{j+1}}{dt} + (1-\alpha)\frac{d\hat{\mathbf{h}}_{\mathbf{g}}{}^{j}}{dt} \right) = \alpha \mathbf{F}^{j+1} + (1-\alpha)\mathbf{F}^{j} \tag{3.44}$$

It is now possible to substitute for the weighted averaged derivative terms given in equation (3.40) for the term in the parenthesis to obtain:

$$\alpha \mathbf{S}^{j+1} \cdot \hat{\mathbf{h}}_{\mathbf{g}}{}^{j+1} + (1-\alpha)\mathbf{S}^{j} \cdot \hat{\mathbf{h}}_{\mathbf{g}}{}^{j} + \mathbf{M} \cdot \left(\frac{\hat{\mathbf{h}}_{\mathbf{g}}{}^{j+1} - \hat{\mathbf{h}}_{\mathbf{g}}{}^{j}}{\Delta t} \right) = \alpha \mathbf{F}^{j+1} + (1-\alpha)\mathbf{F}^{j} \tag{3.45}$$

After rearrangement, the equation takes the following final from:

$$\left(\alpha \mathbf{S}^{j+1} + \frac{\mathbf{M}}{\Delta t} \right) \cdot \hat{\mathbf{h}}_{\mathbf{g}}{}^{j+1} = \alpha \mathbf{F}^{j+1} + (1-\alpha)\mathbf{F}^{j} - \left((1-\alpha)\mathbf{S}^{j} - \frac{\mathbf{M}}{\Delta t} \right) \cdot \hat{\mathbf{h}}_{\mathbf{g}}{}^{j} \tag{3.46}$$

From equation (3.46), one can obtain different time integration schemes depending on the value of the time weighing parameter. Even though infinitely many values of the weighing parameter are possible, several of these are particularly important and have significant properties With $\alpha=0$, the equation becomes an explicit scheme and it does not require the solution of any system of equations in order to advance the solution across time. However, explicit schemes often encounter numerical instabilities if the time step is taken too large. When $\alpha=0.5$, the scheme becomes the so-called Crank-Nicholson method, which implements a central-difference approximation between two time lines. It is known that this choice of the time weighing factor corresponds to the optimal sampling of the first temporal derivative over the time step. If the data associated the problem have sufficient continuity, this scheme exhibits its optimal accuracy properties and results in a very efficient method for handling the time-dependence of the transient problem. Unfortunately, the presence of any discontinuity in the data might lead to spurious oscillations of the computed solution. If $\alpha=1$, the scheme becomes a fully-implicit scheme and resists the development of solution oscillations better than any other one-step method. Therefore, it is commonly used for most difficult problems. However, it should be noted that this scheme is not fully accurate or especially efficient but it will dampen spurious high-frequency effects more strongly than the other schemes. Based on this discussion, a time-weighing parameter of 0.5 is selected to be used in this study.

The governing equation for an unconfined aquifer is non-linear since the saturated thickness is a function of hydraulic head. Therefore, the discretized equations are to be solved in an iterative manner. Common non-linear solution techniques such as the Newton-Raphson method or the successive substitution (Picard iteration) method can be

applied in this solution. Although the Newton-Raphson method is faster in convergence, it requires the computation of partial derivatives which is rather costly in a finite element framework. Hence, the relatively simple Picard iteration technique is applied in the solution of the groundwater flow model. The Picard method is a very simple technique and is based on successively substituting the latest values of the hydraulic head to compute new values until sufficient convergence is achieved. When the Picard method is applied, the discretized groundwater flow equation can be written as:

$$\left(\alpha\mathbf{S}^{j+1,k}+\frac{\mathbf{M}}{\Delta t}\right)\cdot\hat{\mathbf{h}}_{\mathbf{g}}{}^{j+1,k+1}=\alpha\mathbf{F}^{j+1,k}+(1-\alpha)\mathbf{F}^{j}-\left((1-\alpha)\mathbf{S}^{j}-\frac{\mathbf{M}}{\Delta t}\right)\cdot\hat{\mathbf{h}}_{\mathbf{g}}{}^{j} \qquad (3.47)$$

where superscripts k and k+1 represent previous and current iteration values of hydraulic head at the unknown time level. For all iterations, most recent values of the hydraulic heads are used to obtain an improved estimate of the heads at the unknown time level according to the following formula:

$$\hat{\mathbf{h}}_{\mathbf{g}}{}^{j+1,k+1}=\gamma\hat{\mathbf{h}}_{\mathbf{g}}{}^{j+1,k+1}+(1-\gamma)\hat{\mathbf{h}}_{\mathbf{g}}{}^{j+1,k} \qquad (3.48)$$

where γ is an iteration-dependent under-relaxation coefficient (or a damping parameter) taking values between 0 and 1. The left hand-side value at the $(k+1)^{th}$ iteration represents the improved estimate to be used in the next iteration. For very non-linear problems, head change in iterations might be large enough to cause the solution to oscillate. In such cases, a damping parameter can be used to restrict the head change from one iteration

cycle to the next (Huyakorn et al., 1986). In each iteration cycle, the value of the damping parameter is computed according to the following procedure:

$$\gamma = \begin{cases} \dfrac{3+s}{3+|s|} & s \geq -1 \\ \dfrac{1}{2|s|} & s < -1 \end{cases} \tag{3.49}$$

where s is a scale parameter evaluated according to the following rule:

$$s = \begin{cases} 1 & k = 1 \\ \dfrac{\varepsilon_{k+1}}{\gamma_{old}\varepsilon_k} & k > 1 \end{cases} \tag{3.50}$$

where ε_{k+1} and ε_k represent the hydraulic head change for iteration k+1 and k, respectively, that is largest in absolute value and γ_{old} is the value of the damping parameter at the previous iteration.

3.2.5. Model Testing

As there are no documented analytical solutions for unsteady groundwater flow in two dimensions, the proposed model is tested against two different sets of analytical solutions developed within a one dimensional framework. The first analytical solution is based on the simulation of a canal-aquifer system as shown in Figure 3.8. The water level in the canal as well as the aquifer is initially horizontal at a level h_{g1}. The water level in the canal is raised instantaneously to an elevation h_{g2} above the datum line and

maintained constant thereafter, creating an increase in the aquifer head, h_g. The one dimensional mathematical model of this bank storage flow problem is given as:

$$S_y \frac{\partial h_g}{\partial t} = K \frac{\partial}{\partial x}\left(h_g \frac{\partial h_g}{\partial x} \right) \tag{3.51}$$

with the following initial and boundary conditions:

$$\begin{aligned} h_g(x,0) &= h_{g1} \\ h_g(0,t) &= h_{g2} \\ h_g(\infty,t) &= h_{g1} \end{aligned} \tag{3.52}$$

where it is assumed that the aquifer has uniform hydraulic conductivity. The model assumes that the aquifer is homogeneous and isotropic and rests on a horizontal impervious base. In addition, the sediment layer between the canal and aquifer has the same conductivity as the aquifer.

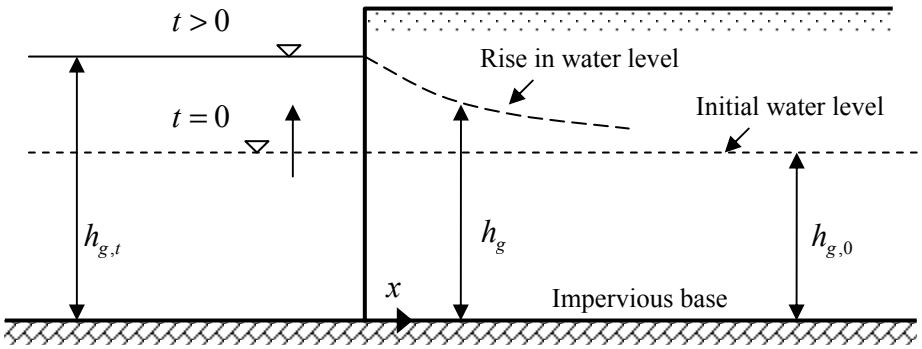

Figure 3.8. Rise of water level in a semi-infinite unconfined aquifer

Following suitable linearization, the governing equation can be written in the following form:

$$\frac{\partial h_g^2}{\partial t} = \bar{\upsilon} \frac{\partial^2 h_g^2}{\partial x} \tag{3.53}$$

where the parameter $\bar{\upsilon}$ is given as:

$$\bar{\upsilon} = \frac{K\bar{h}_g}{S_y} \tag{3.54}$$

with $\bar{h}_g$ is a weighted average of the depth of saturation during the period of flow. The analytical solution to this model is given by Marino and Luthin (1982):

$$h_g^2(x,t) = h_{g,0}^2 + \left(h_{g,t}^2 - h_{g,0}^2\right) erfc\left(\frac{x}{\sqrt{4\bar{\upsilon}t}}\right) \tag{3.55}$$

where *erfc* is the complimentary error function. To test the model's capability against this analytical solution, a hypothetical aquifer-canal system is constructed in which flow is assumed to be one directional. Linear square elements of 5m side length are assembled to create an unconfined aquifer 100m long such that the assumption of an infinite aquifer is satisfied during the 10-hr simulation period. A uniform hydraulic conductivity field of 0.001m/s is used in the simulations. The initial water level in the canal and in the aquifer is taken to be 5m. The water level in the aquifer is instantaneously increased to 7m and

kept constant at this level throughout the simulation. The groundwater movement in the aquifer is then simulated with the proposed model. The comparison of analytically computed and numerically simulated groundwater heads are given in Figure 3.9. As seen from the figure, the numerically simulated values are almost identical to the analytically calculated groundwater heads. It is also important to note that the goodness of fit does not deteriorate with time, which is an important issue in time-dependent solutions.

In the second test, the model is verified with the analytical solution of Marino (1967) that describes the growth and decay of groundwater ridges due to vertical percolation (i.e., infiltration). Figure 3.10 shows a cross-section of an unconfined aquifer assumed to be infinite in areal extent and receiving uniform vertical percolation. The rate of percolation is maintained by a spreading area in the form of an infinitely long strip located above the main unconfined aquifer. After sufficient time, a groundwater ridge develops and initiates groundwater flow. The mathematical model for this flow system is written as in two separate zones. Zone 1 is defined as the region where the infiltration occurs. Zone 2, on the other hand, starts from the edge of Zone 1 extending throughout the aquifer and does not receive infiltration. The mathematical model of this problem is defined by the following boundary value problem (Marino, 1967):

$$\begin{aligned}
&\text{ZONE}-1: && \frac{1}{\bar{\upsilon}}\frac{\partial h_{g1}^2}{\partial t} = \frac{\partial^2 h_{g1}^2}{\partial x^2} + Af(t) \\
& && f(t) = \begin{cases} 1 & 0 < t \le t_i \\ 0 & t > t_i \end{cases} \\
&\text{ZONE}-2: && \frac{1}{\bar{\upsilon}}\frac{\partial h_{g2}^2}{\partial t} = \frac{\partial^2 h_{g2}^2}{\partial x^2}
\end{aligned} \tag{3.56}$$

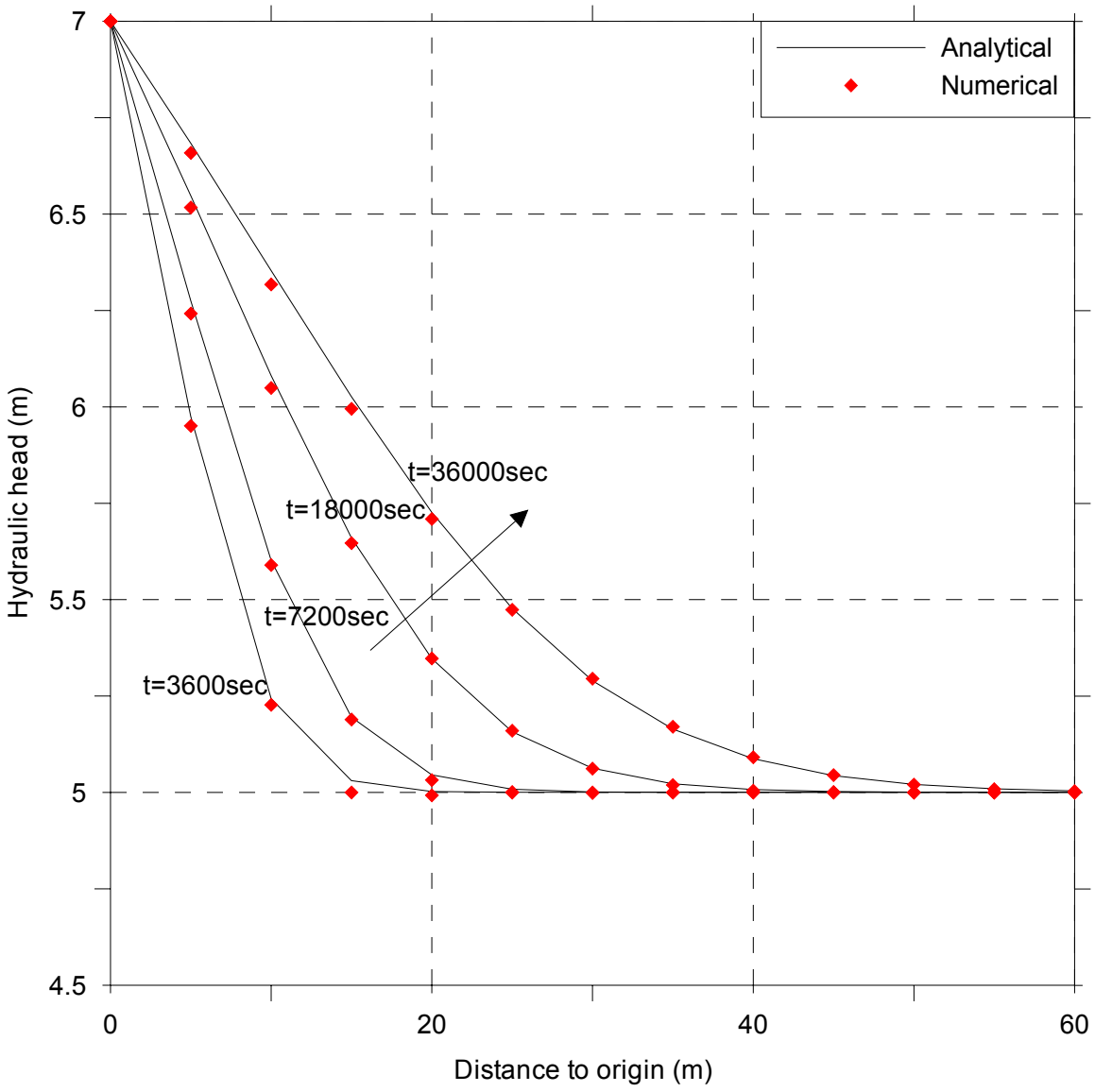

Figure 3.9. Comparison of simulated hydraulic heads and analytical solution of canal-aquifer system

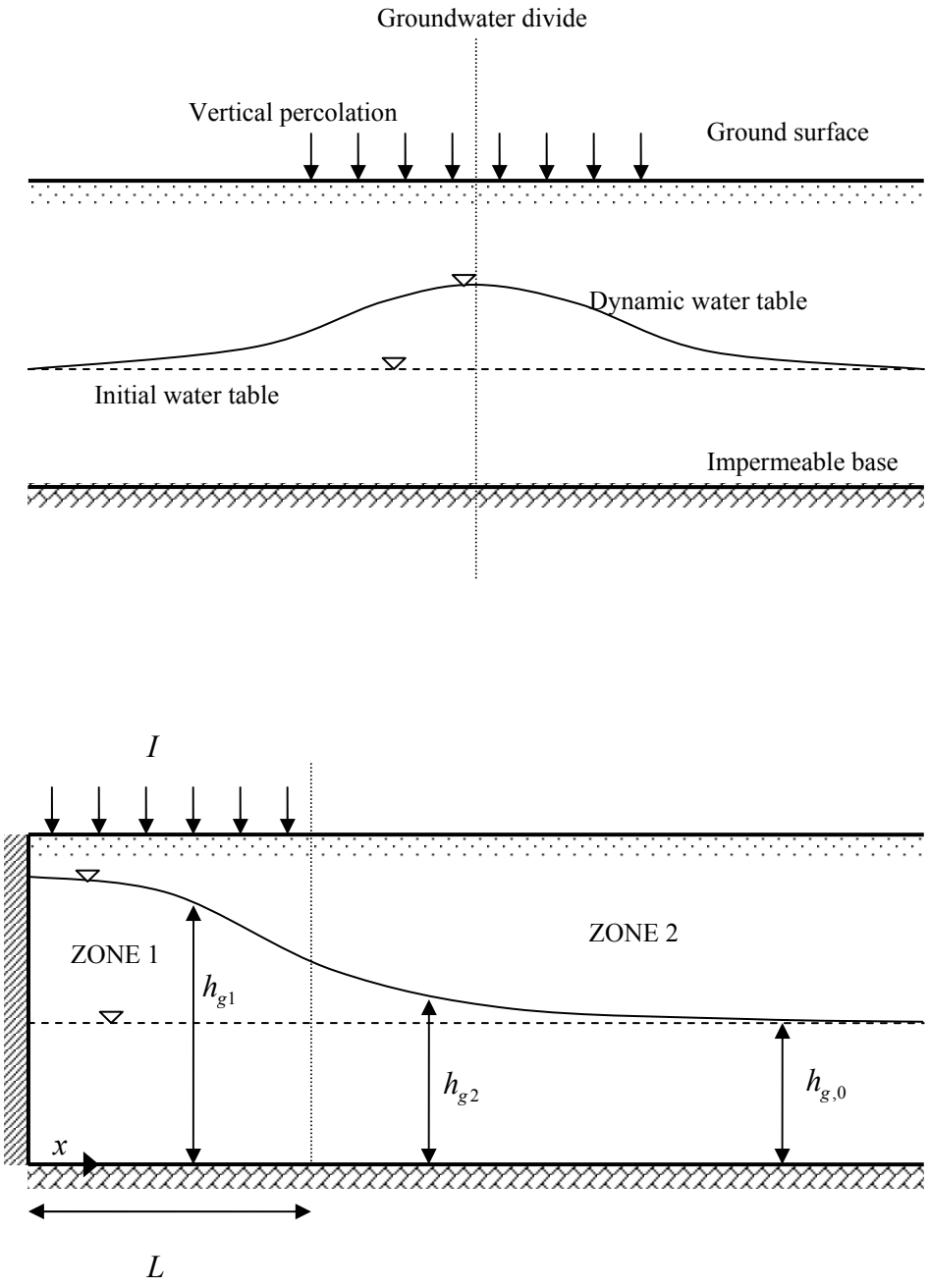

Figure 3.10. Schematic of growth and decay of groundwater ridges

where t_i is the time period during which vertical percolation or infiltration, I, occurs and the parameter A is equal to $2I/K$. The following initial and boundary conditions are used to supplement the equation:

$$\begin{aligned} &\text{ZONE}-1: && h_{g1}(x,0) = h_{g,o} \\ & && Kh_{g1}\left.\frac{\partial h_{g1}}{\partial x}\right|_{x=0,t>0} = 0 \\ &\text{ZONE}-2: && h_{g2}(x,0) = h_{g,o} \\ & && h_{g2}(\infty,t) = h_{g,o} \end{aligned} \tag{3.57}$$

At the internal boundary between zones 1 and 2 (i.e., $x=L$), it is possible to write the continuity of mass fluxes and equality of hydraulic heads such that:

$$\begin{aligned} h_{g1}(L,t) &= h_{g2}(L,t) \\ Kh_{g1}\left.\frac{\partial h_{g1}}{\partial x}\right|_{x=L,t>0} &= Kh_{g2}\left.\frac{\partial h_{g2}}{\partial x}\right|_{x=L,t>0} \end{aligned} \tag{3.58}$$

Marino (1967) developed the analytical solution for this problem by applying a Laplace transform with respect to t and presented the results both for the period when infiltration occurs and for the period after it ceases. During the infiltration period $0<t\leq t_i$, the analytical solution is written as:

$$h_{g1}^2 = h_{g,0}^2 + \frac{2I\bar{\upsilon}t}{K} - \frac{I\bar{\upsilon}t}{K}\left[4i^2 erfc\left(\frac{L-x}{\sqrt{4\bar{\upsilon}t}}\right) + 4i^2 erfc\left(\frac{L+x}{\sqrt{4\bar{\upsilon}t}}\right)\right]$$

$$h_{g2}^2 = h_{g,0}^2 + \frac{I\bar{\upsilon}t}{K}\left[4i^2 erfc\left(\frac{x-L}{\sqrt{4\bar{\upsilon}t}}\right) - 4i^2 erfc\left(\frac{x+L}{\sqrt{4\bar{\upsilon}t}}\right)\right] \tag{3.59}$$

Similarly, for $t>t_i$, the analytical solution becomes:

$$\begin{aligned} h_{g1}^2 = h_{g,0}^2 &+ \frac{2I\bar{\upsilon}t}{K} - \frac{I\bar{\upsilon}t}{K}\left[4i^2 erfc\left(\frac{L-x}{\sqrt{4\bar{\upsilon}t}}\right) + 4i^2 erfc\left(\frac{L+x}{\sqrt{4\bar{\upsilon}t}}\right)\right] \\ &- \frac{2I\bar{\upsilon}t'}{K} - \frac{I\bar{\upsilon}t'}{K}\left[4i^2 erfc\left(\frac{L-x}{\sqrt{4\bar{\upsilon}t'}}\right) + 4i^2 erfc\left(\frac{L+x}{\sqrt{4\bar{\upsilon}t'}}\right)\right] \end{aligned}$$

$$\begin{aligned} h_{g2}^2 = h_{g,0}^2 &+ \frac{I\bar{\upsilon}t}{K}\left[4i^2 erfc\left(\frac{x-L}{\sqrt{4\bar{\upsilon}t}}\right) - 4i^2 erfc\left(\frac{x+L}{\sqrt{4\bar{\upsilon}t}}\right)\right] \\ &- \frac{I\bar{\upsilon}t'}{K}\left[4i^2 erfc\left(\frac{x-L}{\sqrt{4\bar{\upsilon}t'}}\right) - 4i^2 erfc\left(\frac{x+L}{\sqrt{4\bar{\upsilon}t'}}\right)\right] \end{aligned} \tag{3.60}$$

where $t'=t-t_i$ is the time since the cessation of vertical percolation and $4i^2erfc(y)$ is the second repeated integral of the error function of the argument y (Carslaw and Jaeger, 1959).

The proposed groundwater flow model is tested against the analytical solution of Marino (1967) given in equation (3.60). In his paper, Marino compared his analytical solution with a laboratory scale experiment. His experimental setup included a 100cm long flume filled with a soil that has a conductivity value of 0.42cm/s. A 23.8cm long apparatus provided the uniform infiltration rate of 5.6E-2cm/s over the aquifer. The experiment was conducted with an initial groundwater head of 11.3cm. In his study,

Marino (1967) found a good fit between measured and analytically calculated hydraulic head values. In this study, a numerical model is constructed to duplicate the aquifer conditions of Marino (1967) and the results from his analytical solution and laboratory experiments are compared with the numerically computed values. In the numerical model, the spatial discretization of the experimental aquifer is done with square finite elements that have a side length of 5cm. The temporal discretization is done with 10sec to cover a total simulation period of 660sec. Marino (1967) used the observation points of his experimental setup to compute the values of the analytical solution and presented his analytical solution at these discrete points. Following Marino's approach, the analytical solution values are given discretely and the numerical solution is presented as a continuous line for comparison of the analytically computed and numerically simulated groundwater heads (Figure 3.11). When the figure is analyzed, one can see that a fairly close fit is obtained between the numerically computed results and Marino's analytical and experimental results. Although the maximum deviation is fairly small (i.e., less than 10%), the numerically simulated hydraulic head values start to deviate from the analytical solution as a function of time. It is interesting to note that the level of fit with the observed values is better then the level of fit with the analytical solution.

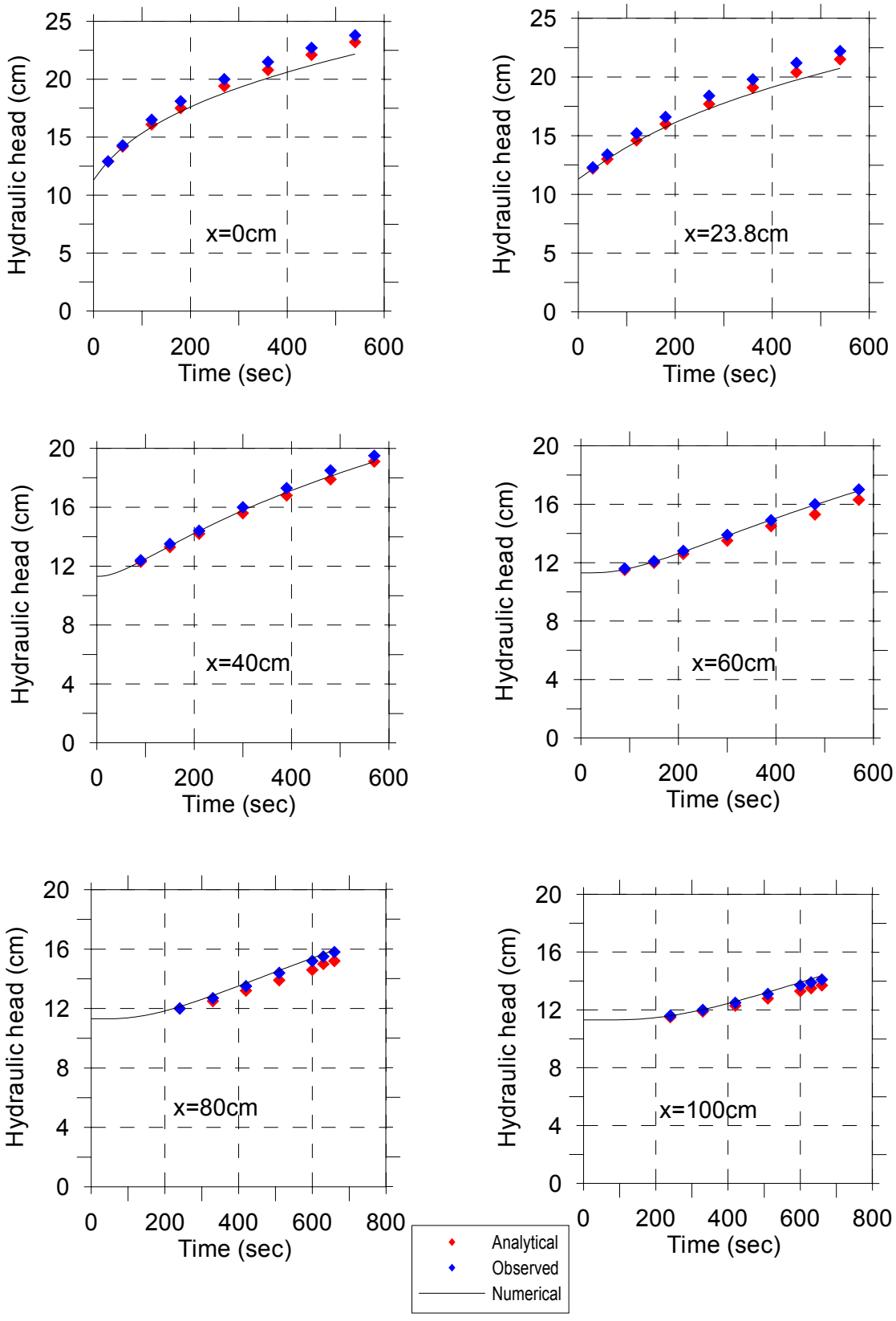

Figure 3.11. Comparison of simulated, observed and analytical hydraulic heads

3.3. Two Dimensional Overland Flow Model

3.3.1. Governing Equations

The governing equation of overland flow model is obtained by the introducing non-inertia wave-approximation to the general continuity and momentum equations of the two-dimensional shallow water flow. The non-inertia or diffusion wave approximation is suitable for areas with mild topography where downstream backwater effect is important but accelerations are relatively small. Numerous researchers have chosen the non-inertia wave approximation to simulate shallow water hydrodynamics in order to reduce computational efforts without sacrificing accuracy (Hromadka II and Yen, 1986; Feng and Molz, 1997; Morita and Yen, 2002). For an anisotropic, non-homogeneous ground surface with principle diffusion directions matching the coordinate directions, the governing equation for overland flow is written as:

$$\frac{\partial h_o}{\partial t} - \frac{\partial}{\partial x}\left(K_{ox} \frac{\partial h_o}{\partial x} \right) - \frac{\partial}{\partial y}\left(K_{oy} \frac{\partial h_o}{\partial y} \right) - R + I = 0 \tag{3.61}$$

where x and y are the spatial coordinates in the horizontal domain, t is the temporal coordinate, h_o is the water surface elevation of overland flow, R is the rainfall rate, I is the infiltration rate, and K_{ox} and K_{oy} are the diffusion coefficients in the x- and y- directions of flow given by:

$$K_{oi} = \frac{1}{(n_o)_i^2} \frac{(h_o - z_g)^{5/3}}{\left[\left(\frac{\partial h_o}{\partial x} \right)^2 \frac{1}{(n_o)_x^4} + \left(\frac{\partial h_o}{\partial y} \right)^2 \frac{1}{(n_o)_y^4} \right]^{1/4}} \qquad i = x, y \tag{3.62}$$

where z_g is the ground surface elevation and n_o is the Manning's roughness coefficient for overland flow. It is important to note that friction factors for overland flow in natural areas are difficult to conceptualize from pure theory alone. Except for flow over man-made surfaces such as asphalt or concrete, overland flow is usually a very complex hydraulic and geometric phenomenon. Ideally, different friction factors must be used to cover different flow regimes, and the dynamic effects of rainfall impact, channelization of flow, obstacles such as litter, crop ridges and rocks and erosion must all be considered during the formulation of a total friction coefficient. On the other hand, from a practical engineering standpoint, an "effective" coefficient of friction is adequate for applied cases of simulating an overland flow hydrograph or computing travel times.

Overland flow typically occurs in wide thin films with very small depths (i.e., less than a couple of centimeters) and relatively small velocities (i.e., less than 0.1 m/s). These typical values result in relatively small Reynolds numbers when compared to open channel flow. The flow is typically considered to be laminar if only the Reynolds number is considered as a factor. However, the hydraulics of overland flow are much more complicated and numerous additional factors are to be addressed when quantifying this complex flow such as the added turbulence due to rainfall impact, vegetation and channelized flow as well as non-fixed bed phenomena due to erosion (Dingman, 1994). In this regard, a general consensus has been achieved among hydraulics experts that the

overland flow covers both laminar and turbulent flows and is considered to change from laminar to turbulent and back to laminar during the rise and recession of a hydrograph (Engman, 1986).

The most theoretically sound friction formulae that can cover the entire flow spectrum is the Darcy-Weisbach relationship. This relationship was originally developed for pipe flow and has found wide applicability in pipe flow hydraulics. It included relative roughness and Reynolds number as two parameters required to find the roughness coefficient. However, the difficulty in obtaining an accurate roughness parameter helped other resistance expressions, such as the Manning and Chezy formulae, find wider applicability especially in open channel flow where flow is mostly characterized in the turbulent regime. Consequently, a wide collection of Manning and Chezy resistance coefficients accumulated over time, which further promoted their use in simulation models. Nevertheless, the Darcy-Weisbach relation still remained the method of choice when the flow is out of the turbulent regime and/or when there are sufficient data from the field.

Considering the scale of the modeling effort and the accuracy of the available data, it is practically wise to use a single value for the resistance coefficient that basically assumes that the overland flow is turbulent. In this context, the effect of rainfall impact, vegetation, channelized flow and all other possible factors are lumped into an effective friction coefficient. This approximation is clearly justifiable from an engineering perspective for a distributed hydrological model of watershed scale. Hence, it is possible to use the Manning resistance factor and equation to formulate the friction slope in non-inertia wave equations. Essentially, the Manning roughness coefficient not only includes

all the uncertainty in terms of process theory and data limitations but also covers our ignorance in terms of the effects of unsteadiness and non-uniformity of flow.

3.3.2. Initial Conditions

In the overland flow model, the initial conditions are given by specifying the water surface elevation at all points in the two-dimensional domain. In representing an initially dry overland surface, a very thin water film is assumed before the flow is initiated such that (Akan and Yen, 1981a):

$$h_o(x, y, 0) = h_{o0}(x, y) \tag{3.63}$$

This artificial assignment of an initial water depth facilitates the numerical solution procedure. As a rule of thumb, h_{o0} can be taken to be less than or equal to 0.1 mm to alleviate any possible numerical problems that might arise otherwise.

3.3.3. Boundary Conditions

Although overland flow is basically a source/sink driven flow mechanism, two different types of boundary conditions are still specified along different external boundaries of overland flow domain. Type-1 or specified head boundary conditions are generally used to model boundaries with known water surface elevation and are given as:

$$h_o(x, y, t) = h_{oD}(x, y, t) \tag{3.64}$$

where h_{oD} is the known water surface elevation. Type-2 or specified flux boundary conditions are used to model boundaries with known flux values. It is also known as a Neumann boundary condition and is given as:

$$q_N(x,y,t) = -\mathbf{n}\cdot(\mathbf{K}_o\cdot\nabla h_o) = -\mathbf{n}\cdot\left(\mathbf{V}\left(h_o - z_g\right)\right) \tag{3.65}$$

where q_N is the known flux value and **n** is the unit normal to the boundary. Although it is theoretically possible to define a head-dependent boundary condition for overland flow, it is generally not implemented for the sake of simplicity, since it is very difficult to keep track of changing stages over the land in a precipitation event.

3.3.4. Numerical Solution Scheme

In general, the finite difference and finite element methods are widely applied in overland flow modeling (Akan and Yen, 1981b; Hromadka and Yen, 1986; Akanbi and Katapodes, 1988; Zhang and Cundy, 1989; Motha and Wigham, 1995; Feng and Molz, 1997; Lal, 1998; Dutta et al., 2000; Gandolfi and Savi, 2000; Morita and Yen, 2002; Bradford and Sanders, 2002). For watershed-scale applications where topography is highly variable, the finite element method is proven to be more powerful compared to the finite difference method due to the flexibility it offers in simulating land surfaces with spatially variable land use/cover patterns and irregular boundaries. Hence, the Galerkin finite element method based on the method of weighted residuals is used in this study to solve the overland flow equation.

The overland flow surface is discretized with two-dimensional quadrilateral finite elements such that the material properties of the domain (i.e., the roughness coefficient) are retained in individual elements. Following the idealization of the domain and selection of the interpolating functions, an appropriate weak form of the problem is developed as shown in Appendix G. The resulting finite element matrix equation obtained by applying the Galerkin procedure is given as:

$$\mathbf{S} \cdot \hat{\mathbf{h}}_{\mathbf{o}} + \mathbf{M} \cdot \frac{d\,\hat{\mathbf{h}}_{\mathbf{o}}}{dt} = \mathbf{F} \tag{3.66}$$

where **S**, **M** and **F** stand for global stiffness matrix, global mass matrix and global load vector, respectively, and $\hat{\mathbf{h}}_{\mathbf{o}}$ is the overland flow stage vector. The explicit formulas for the element matrices and vectors are also derived in Appendix H. As these element integrals are generally complex and cannot be integrated analytically, a two-dimensional Gaussian quadrature technique is implemented to numerically integrate the integrals. When the same procedure implemented in the derivation of the groundwater flow equation is followed, one would obtain the final form of the discretized equation as:

$$\left(\alpha \mathbf{S}^{j+1} + \frac{\mathbf{M}}{\Delta t}\right) \cdot \hat{\mathbf{h}}_{\mathbf{o}}{}^{j+1} = \alpha \mathbf{F}^{j+1} + (1-\alpha)\mathbf{F}^{j} - \left((1-\alpha)\mathbf{S}^{j} - \frac{\mathbf{M}}{\Delta t}\right) \cdot \hat{\mathbf{h}}_{\mathbf{o}}{}^{j} \tag{3.67}$$

Although different time integration schemes are now possible, a Crank-Nicholson scheme with $\alpha=0.5$ is used in this study. This scheme provides the ideal approximation between the two time steps.

The overland flow equation is a highly non-linear equation since the diffusion coefficients are non-linear functions of the dependent variable (i.e., stage). To handle this non-linearity, the Picard iteration is used in this study such that the latest values of the stage are successively substituted to compute new values until sufficient convergence is achieved. When the Picard method is applied, the discretized overland flow equation can be written as:

$$\left(\alpha\mathbf{S}^{j+1,k}+\frac{\mathbf{M}}{\Delta t}\right)\cdot\hat{\mathbf{h}}_{\mathbf{o}}{}^{j+1,k+1}=\alpha\mathbf{F}^{j+1,k}+(1-\alpha)\mathbf{F}^{j}-\left((1-\alpha)\mathbf{S}^{j}-\frac{\mathbf{M}}{\Delta t}\right)\cdot\hat{\mathbf{h}}_{\mathbf{o}}{}^{j} \qquad (3.68)$$

where superscripts k and k+1 represent previous and current iteration values of stage at the unknown time level.

3.3.5. Model Testing

The overland flow model is probably the most difficult of the four major flow pathways discussed in this study. Even for a single event simulation, the model contains difficulties in defining the time dependent spatial extent of the flow phenomena as it changes continuously according to the flow characteristics and the spatially variability of the precipitation event. Although there are no analytical solutions to the two dimensional non-inertia wave form of the model, it is possible to write a simple analytical solution for the simplified kinematic wave form of the model in one-dimensional form (Stephenson and Meadows, 1986). The proposed model is tested against this analytical solution and the data collected from a test plot by Izzard (1946).

The kinematic wave model neglects not only the local and convective acceleration terms but also the pressure term in the momentum balance equation of the original St. Venant equations. It inherently assumes that the bed slope is equal to the friction slope in the channel. The kinematic wave model does not allow upstream migration of disturbances so is not suitable to systems with backwater effects. It is, however, found to be suitable for modeling overland flow in some upland watersheds as well as modeling channel flow in small streams with moderate to high bed slopes (Stephenson and Meadows, 1986).

The kinematic wave model is written using the continuity equation and the simplified momentum equation by using Manning's expression to define the velocity in the channel such that:

$$\frac{\partial d}{\partial t} + m\alpha_k \left(d\right)^{m-1} \frac{\partial d}{\partial x} = R - I \tag{3.69}$$

where d is the water depth in the channel, m is a constant that is equal to 5/3 and α_k is a constant that is a function of surface roughness and bed slope written as:

$$\alpha_k = \frac{\sqrt{S_o}}{n} \tag{3.70}$$

According to Stephenson and Meadows (1986), the analytical solution to the kinematic wave model in response to a uniform rainfall event with no infiltration is given as:

$$q = \begin{cases} \alpha (Rt)^m & for \quad 0 \le t \le t_c \\ \alpha (Rt_c)^m & for \quad t_c \le t \le t_r \\ RL - Rm\alpha^{1/m} q^{(m-1)/m} (t - t_r) & for \quad t_r \le t \le t_f \end{cases} \tag{3.71}$$

where q is the discharge per unit width, t_c is the time of concentration, t_r is the duration of the rainfall event and t_f is the total simulation time. The time of concentration is defined as the time at which the entire watershed starts to contribute to the outflow and is given by the expression:

$$t_c = \left(\frac{L}{\alpha R^{m-1}} \right)^{1/m} \tag{3.72}$$

The proposed model is verified using the above model on a hypothetical test bed with a length of 100 m and a bed slope of 0.001 m/m. The Manning's roughness coefficient is taken to be 0.02. A constant rainfall rate of 2.78E-6 m/s is applied for 8000sec over the entire test bed and the model is simulated for a total of 15000sec. The analytically computed and numerically simulated discharge per unit width values obtained at the outlet of the bed are shown in Figure 3.12. As seen from the figure, the proposed model gives a very close fit to the analytical solution. Only just before the time of concentration, the proposed model creates a much smoother transition to the peak value where as the analytical solution produces a sharper transition.

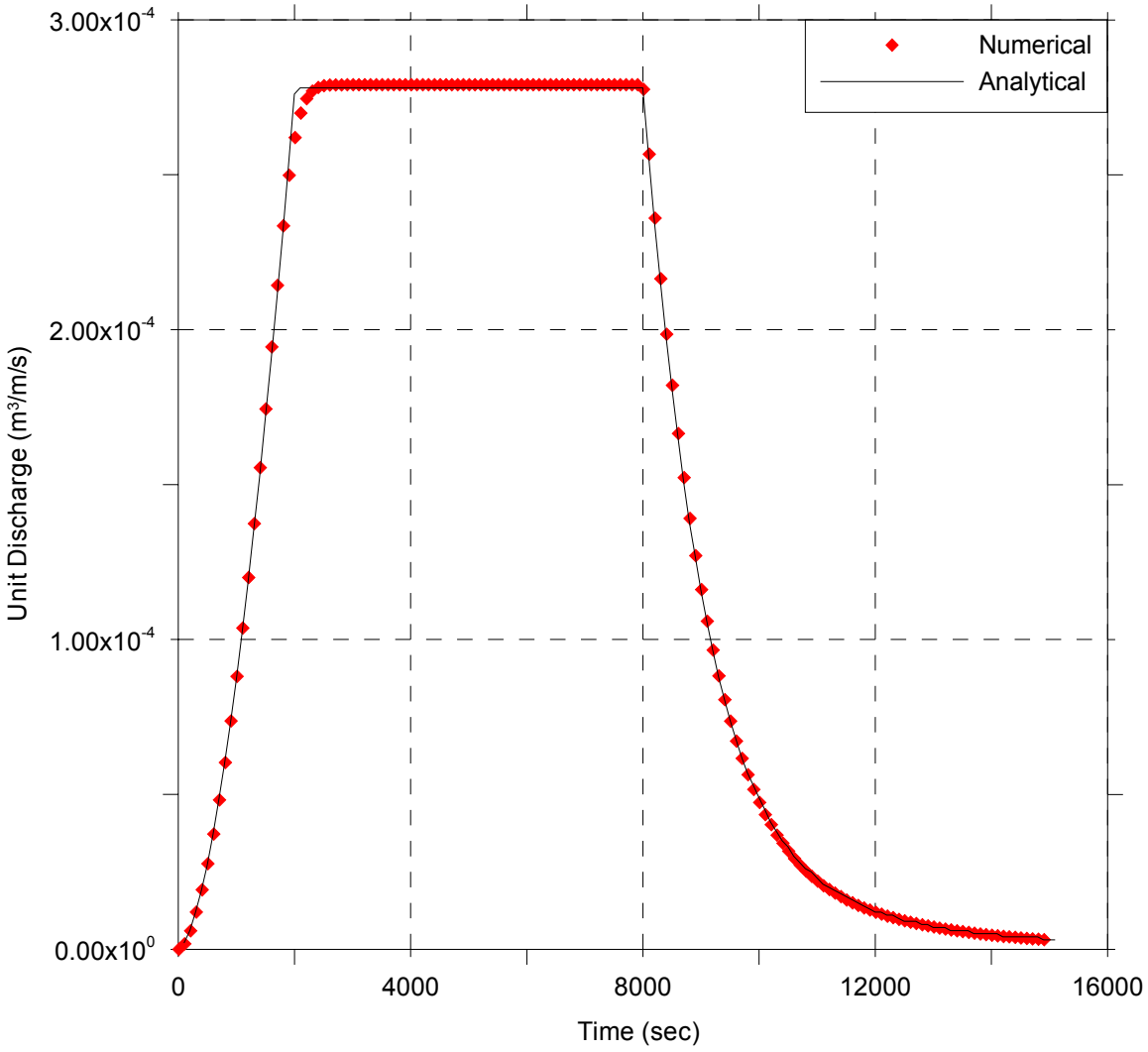

Figure 3.12. Comparison of simulated unit discharge and analytical solution of overland flow

In the second example, the proposed model is tested against the experimental work of Izzard (1946). Izzard analyzed the overland flow from paved and turf surfaces and performed a series of tests which he called 'runs'. Run-136 of Izzard (1946) is used to test the model. The experimental plot in his run was a 72 m long flume with 0.01 ft/ft bed slope. The flume was an asphalt plane with a Manning's roughness value of 0.024. In his Run-136, Izzard used a two stage rainfall event with both stages having a magnitude of 3.56 inch/hr. The proposed model is run with the same data and the results are compared in Figure 3.13.

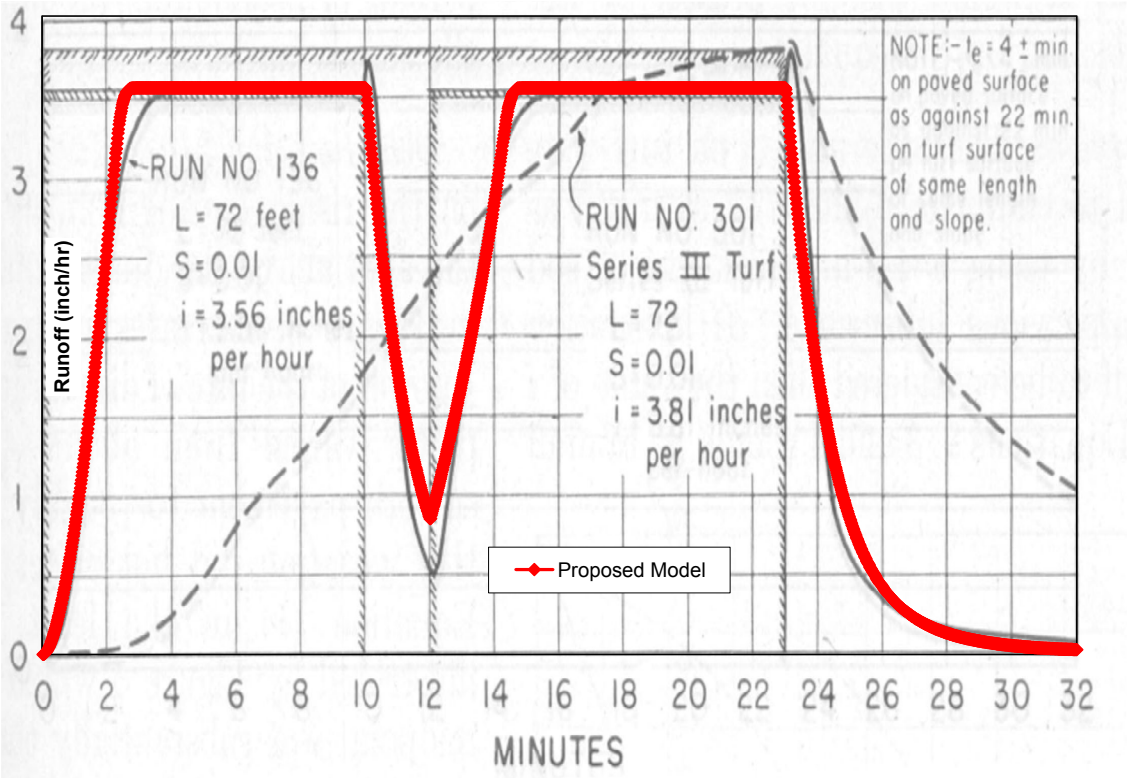

Figure 3.13. Comparison of simulated values of overland flow runoff with data from Izzard (1946)

As seen from this figure, the proposed model accurately predicts the peak discharge, time to peak and rising and falling limbs of the hydrograph. However, it shows slight deviations from Izzard's experimental data during the transition to the peak value and during the minimum flow period between the two rainfall steps. Overall, the level of prediction by the model is considered to be satisfactory.

3.4. One Dimensional Unsaturated Groundwater Flow Model

3.4.1. Governing Equations

The movement of soil moisture in the variably-saturated unsaturated zone is modeled using Richards' equation, which is supplemented by constitutive relations to describe the relationship among fluid pressure, water saturation and unsaturated hydraulic conductivity. In an anisotropic, non-homogeneous media, the mixed-form of the equation with both the water content and the pressure head as the dependent variables is given as (Miller et al., 1998):

$$S_w S_s \frac{\partial \psi}{\partial t} + \frac{\partial \theta}{\partial t} - \frac{\partial}{\partial z}\left(K_u \left(\frac{\partial \psi}{\partial z} + 1 \right) \right) = 0 \tag{3.73}$$

where z is the vertical coordinate, t is time, S_w is the degree of saturation, S_s is the specific storage coefficient, Ψ is the capillary pressure head, θ is the volumetric water content and K_u is the unsaturated hydraulic conductivity in the vertical direction. To complete the mathematical representation of moisture movement in the unsaturated zone, soil-water retention and hydraulic conductivity relationships that relate the capillary pressure head

to soil moisture and hydraulic conductivity must also be provided such as the ones shown in Figure 3.14.

Although the relationships developed by Brooks and Corey (1964), Campbell (1974), Mualem (1976), Clapp and Hornberger (1978) and van Genuchten (1980) are used extensively in the solution of Richards' equation, detailed analysis reveals that only the expressions of van Genuchten (1980) would describe the entire pressure spectrum including the saturated portion above the bubbling pressure. Therefore, the θ-ψ and K-ψ relations of van Genuchten (1980) are used in this study:

$$S_e = \frac{\theta - \theta_r}{\theta_s - \theta_r} = \left[1 + \left(\alpha_v |\psi|\right)^{n_v}\right]^{-m_v} \tag{3.74}$$

$$K_u(\psi) = \left(K_g\right)_z \frac{\left\{1 - \left(\alpha_v |\psi|\right)^{n_v - 1}\left[1 + \left(\alpha_v |\psi|\right)^{n_v}\right]^{-m_v}\right\}^2}{\left[1 + \left(\alpha_v |\psi|\right)^{n_v}\right]^{m_v/2}} \tag{3.75}$$

where S_e is the effective saturation, θ_r is the residual water content, θ_s is the saturated water content, K_g is the saturated hydraulic conductivity, n_v and m_v are constants that depend on soil type and m_v is equal to $\left(1 - 1/n_v\right)$.

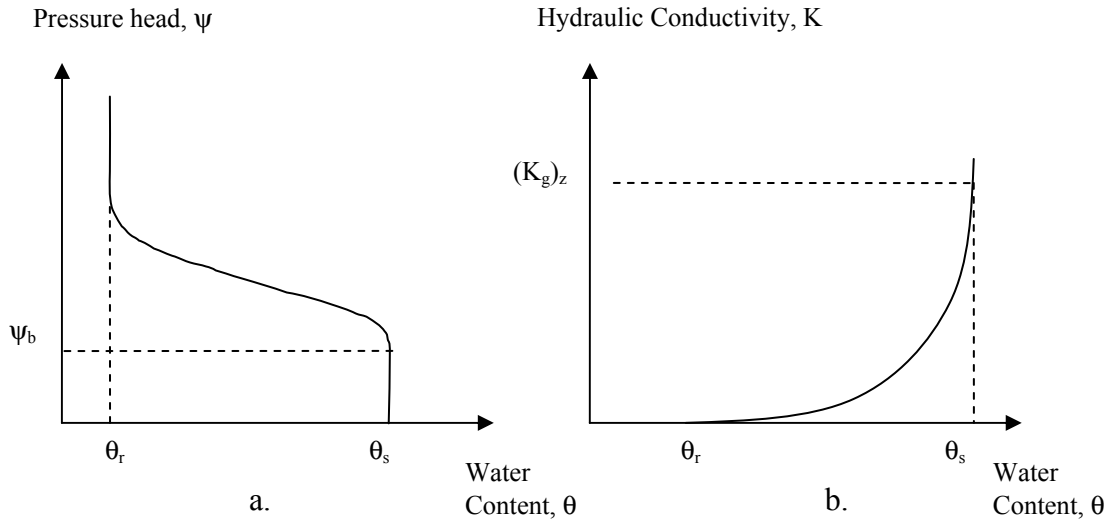

Figure 3.14. Typical soil water retention curves for (a) hydraulic conductivity and (b) water content in unsaturated porous media

3.4.2. Initial Conditions

The initial conditions describe the capillary pressure head and/or soil moisture at all points in the vertical domain at the beginning of the simulation. Therefore, if z_g and z_{wt} represent the elevations of the ground surface and the water table, respectively, the initial conditions can be written as a function of pressure head or water content such that:

$$\psi(z,0) = \psi_0(z) \quad \text{for} \quad z_{wt} \le z \le z_g \tag{3.76}$$

$$\theta(z,0) = \theta_0(z) \quad \text{for} \quad z_{wt} \le z \le z_g \tag{3.77}$$

where ψ_0 is the initial capillary pressure head and θ_0 is the initial water content within the domain.

3.4.3. Boundary Conditions

The boundary conditions are defined at the top and bottom of the domain. In this study, the top boundary condition is at the soil surface and the bottom boundary condition is defined at the groundwater table. At the ground surface, the boundary condition switches between specified head and specified flux depending on the conditions of the overland flow (Gunduz and Aral, 2003c):

$$\begin{aligned} \psi\left(z_g, t\right) &= \psi_g\left(t\right) \\ -K\left(\psi\right)\frac{\partial\left(\psi + z\right)}{\partial z} &= q_g\left(t\right) \end{aligned} \tag{3.78}$$

where ψ_g is the positive overland flow depth over the ground surface and q_g is the infiltration/exfiltration flux at the surface. At the water table, on the other hand, a zero pressure head boundary condition is defined at all times:

$$\psi\left(z_{wt}, t\right) = 0 \tag{3.79}$$

3.4.4. Numerical Solution Scheme

In the numerical solution of Richards' equation, the spatial discretization is commonly performed by (i) finite difference and (ii) finite element methods (Celia et al., 1990; Gottardi and Venutelli, 1993a; Rathfelder and Abriola, 1994; Pan et al., 1996; Miller et al., 1998; Van Dam and Feddes, 2000; Zhang et al., 2002). Both methods are commonly used in the literature and neither method really surpasses the other. Regardless

of the spatial discretization method used, the time approximation commonly involves a fully implicit approximation of the time derivative.

The Picard iteration, Modified Picard iteration or Newton-Raphson iteration techniques are frequently used to resolve the nonlinearities in Richards' equation. While the first two converge linearly, the Newton iteration converges quadratically in the vicinity of the solution, which might lead to more efficient solutions depending on the type of nonlinearity. Paniconi et al. (1991) and Miller et al. (1998) studied the numerical properties of iterative methods and found that both the linearly-converging and the quadratically-converging methods provide similar convergence rates, especially for strongly nonlinear situations with linearly-converging methods requiring much less computational power.

In this study, the numerical solution of Richards' equation is done with a standard central difference control volume finite difference approximation to discretize the spatial derivatives and a first-order backward finite difference approximation to discretize the time derivatives. The modified Picard iteration of Celia et al. (1990) is then implemented to solve for the nonlinearity. The details of the numerical solution method are given in Appendix I. The discretized form of equation (3.73) is the core of the unsaturated zone flow model. This equation is written for each intermediate node of the domain, and supplemented by the discretized forms of the boundary condition equations at the top and bottom of the domain. For each intermediate node, the final form of the discretized Richards' equation is written as:

$$\left(S_w S_s\right)_i^{j+1,k}\left[\frac{\psi_i^{j+1,k+1}-\psi_i^{j}}{\Delta t}\right]+\left[\frac{\theta_i^{j+1,k}+C_i^{j+1,k}\left(\psi_i^{j+1,k+1}-\psi_i^{j+1,k}\right)-\theta_i^{j}}{\Delta t}\right]$$
$$-\frac{1}{\Delta z_i}\left[\left(K_u\right)_{i+1/2}^{j+1,k}\left(\frac{\psi_{i+1}^{j+1,k+1}-\psi_i^{j+1,k+1}}{\Delta z_{i+1/2}}+1\right)-\left(K_u\right)_{i-1/2}^{j+1,k}\left(\frac{\psi_i^{j+1,k+1}-\psi_{i-1}^{j+1,k+1}}{\Delta z_{i-1/2}}+1\right)\right]=0 \tag{3.80}$$

where subscripts *i*, *j* and *k* represent the spatial, temporal and iteration indices, respectively. The three pressure heads at nodal points *i*-1, *i* and *i*+1 at the unknown iteration level are the unknowns in the above equation. When written for all intermediate nodes, one would obtain a system of *N-2* nonlinear equations with *N* unknowns. Upon including the two equations for the top and bottom boundary conditions, the system could be written as:

$$\left[\alpha\mathbf{A}^{j+1,k}+\left(1-\alpha\right)\mathbf{A}^{j}\right]\cdot\mathbf{x}^{j+1,k+1}=\alpha\mathbf{f}^{j+1,k}+\left(1-\alpha\right)\mathbf{f}^{j} \tag{3.81}$$

where **A** is the coefficient matrix, **x** is the unknown vector and **f** is the known right hand side vector. This matrix equation is then solved by a suitable matrix solver. Due to the three-diagonal structure of the coefficient matrix, the efficient Thomas algorithm provides the best solution for this system.

3.4.5. Model Testing

The one-dimensional unsaturated groundwater flow equation is a difficult non-linear partial differential equation due to the strong dependency of both the hydraulic conductivity and the water content on the capillary pressure. The empirical soil-water retention and conductivity relationships such as the van Genuchten model are the source

of this non-linearity. In this regard, there are no known analytical solutions to the one-dimensional Richards' equation with realistic soil-water relationships. Nevertheless, numerous researchers including Philip (1969), Warrick (1975), Sander et al. (1988), Warrick et al. (1990), Srivastava and Yeh (1991), Warrick et al. (1991), Barry et al (1993), Tracy (1995), Marinelli and Durnford (1998), Hogarth and Parlange (2000) and Chen et al. (2003) have developed various forms of exact solutions under fairly strict limitations. In all of these studies, the problematic soil-water relations are simplified and linearized by using various transformations and/or trouble-free linear functions. Therefore, it is believed that these solutions have very limited applicability in testing a practical model based on strongly non-linear soil-water relations such as the one of van Genuchten. In addition, these exact solutions are almost always extremely complicated, and require numerical methods which sometimes make them more labor intensive than the original numerical model used to solve the governing partial differential equation.

Considering the factors discussed above, the proposed unsaturated zone flow model is tested against a well-documented and verified commercial programs such as HYDRUS-1D (Simunek et al., 1998) and the results from a benchmark paper by Celia et al. (1990). Three different tests are simulated with both the HYDRUS model and the proposed model to test the proposed model's capabilities with different soil types and soil hydraulic parameters as well as different boundary conditions. The first test is called the Skagg's column infiltration test and is intended to simulate infiltration into a 60cm column having -150cm initial pressure head. Constant pressure head values of -150cm and -1cm are applied at the bottom and top of the column as constant head boundary conditions, respectively. The hydraulic parameters of the soil are given in Table 3.1. The

moisture is allowed to migrate along the column for 2.5hrs and the advancing front is tracked within the column. The pressure head distribution is simulated with both HYDRUS and the proposed model and the results are shown in Figure 3.15 for various instances in time.

Table 3.1. Soil Hydraulic Parameters of Test Cases

	Saturation Water Content θ_s(-)	Residual Water Content θ_r(-)	Van Genuchten parameter α (cm^{-1})	Van Genuchten parameter n (-)	Saturated Conductivity K_s (cm/hr)
TEST 1	0.3500	0.020	0.0410	1.964	2.5992000
TEST 2	0.4300	0.078	0.0360	1.560	1.0400004
TEST 3	0.3308	0.000	0.0143	1.506	25.000000

The first test case demonstrates the capabilities of the proposed model in simulating the characteristics of infiltration into a moderately dry soil. It can be seen from Figure 3.15 that the model performs extremely well in simulating the vertical movement of soil moisture in vertical direction. It is clearly seen that the results obtained from the proposed model are indistinguishable from the HYDRUS model. Moreover, the downward movement of the wetting front is accurately captured by the proposed model both in space and in time.

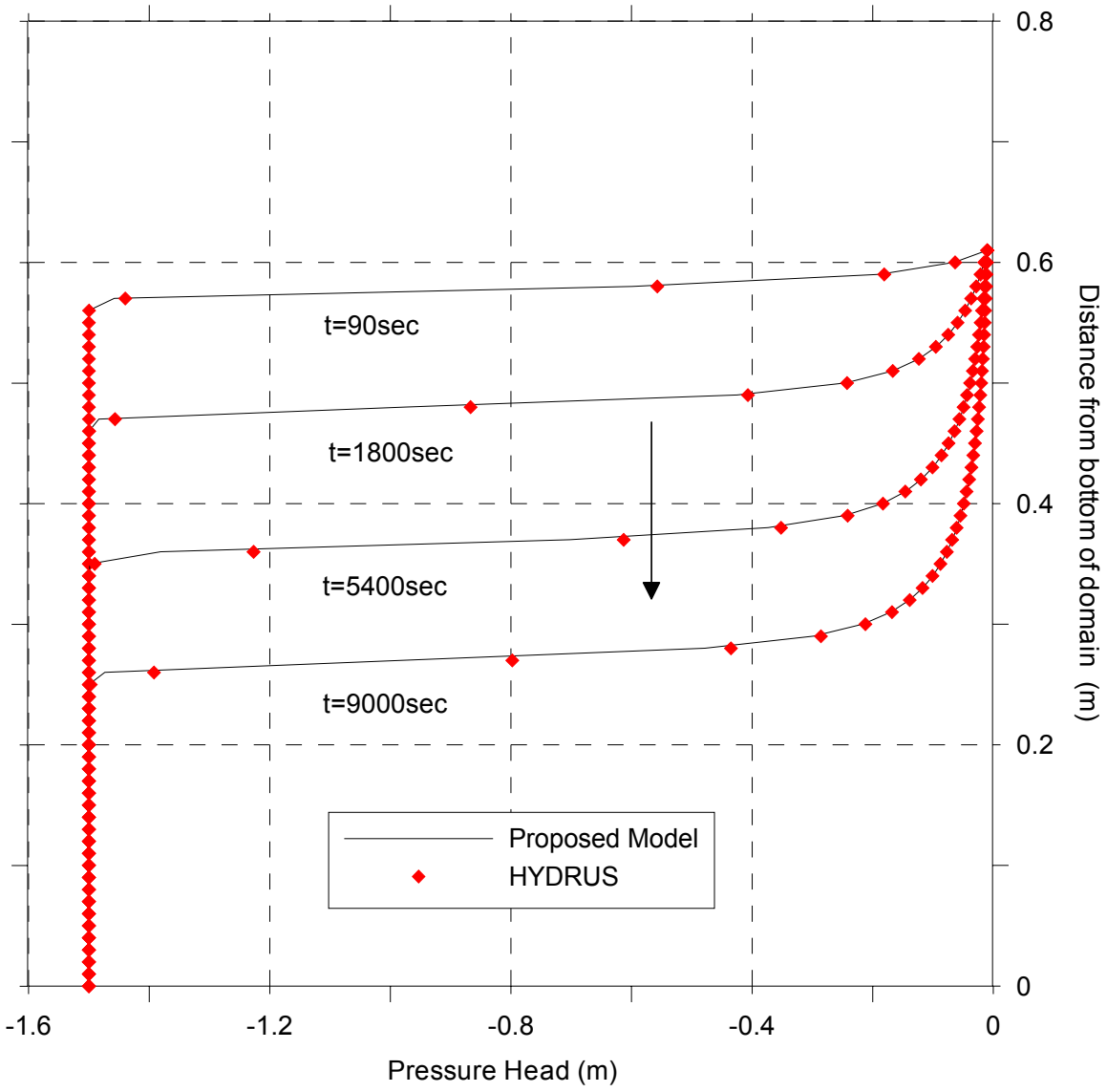

Figure 3.15. Comparison of pressure heads in TEST-1

The second test is a demonstration of an exfiltration condition, where moisture movement is opposite to the direction of gravitational acceleration. It is a condition in which the vertical drainage is overcome by the strong pressure gradient between the surface and the bottom boundary conditions. A 7.6cm column of soil is discretized in a non-uniform fashion such that the highly variable pressure head conditions at the bottom boundary could be captured accurately. A dry initial condition (i.e., -750cm pressure head) is used to start the simulation. The bottom boundary condition is selected to be a -1cm constant head that is used to drive the upward movement of soil moisture. On the other hand, a zero flux condition is enforced at the top boundary. The soil hydraulic parameters of the test are given in Table 3.1. The upward migration of soil moisture is simulated for 3hrs and the results of pressure head distributions of HYDRUS and the proposed model are summarized in Figure 3.16 for various instances in time.

The results from Figure 3.16 clearly represent the high accuracy achieved by the proposed model in simulating the exfiltration behavior in an extremely dry soil that is saturated from below. This test is a perfect example to observe the movement of soil moisture towards the surface by overcoming the pull of gravity. It is even possible to see fully saturated conditions developing in the domain towards the end of the simulation (i.e., $t>7200$sec). Just like in Test-1, the position of the advancing front is accurately predicted by the proposed model in both space and time.

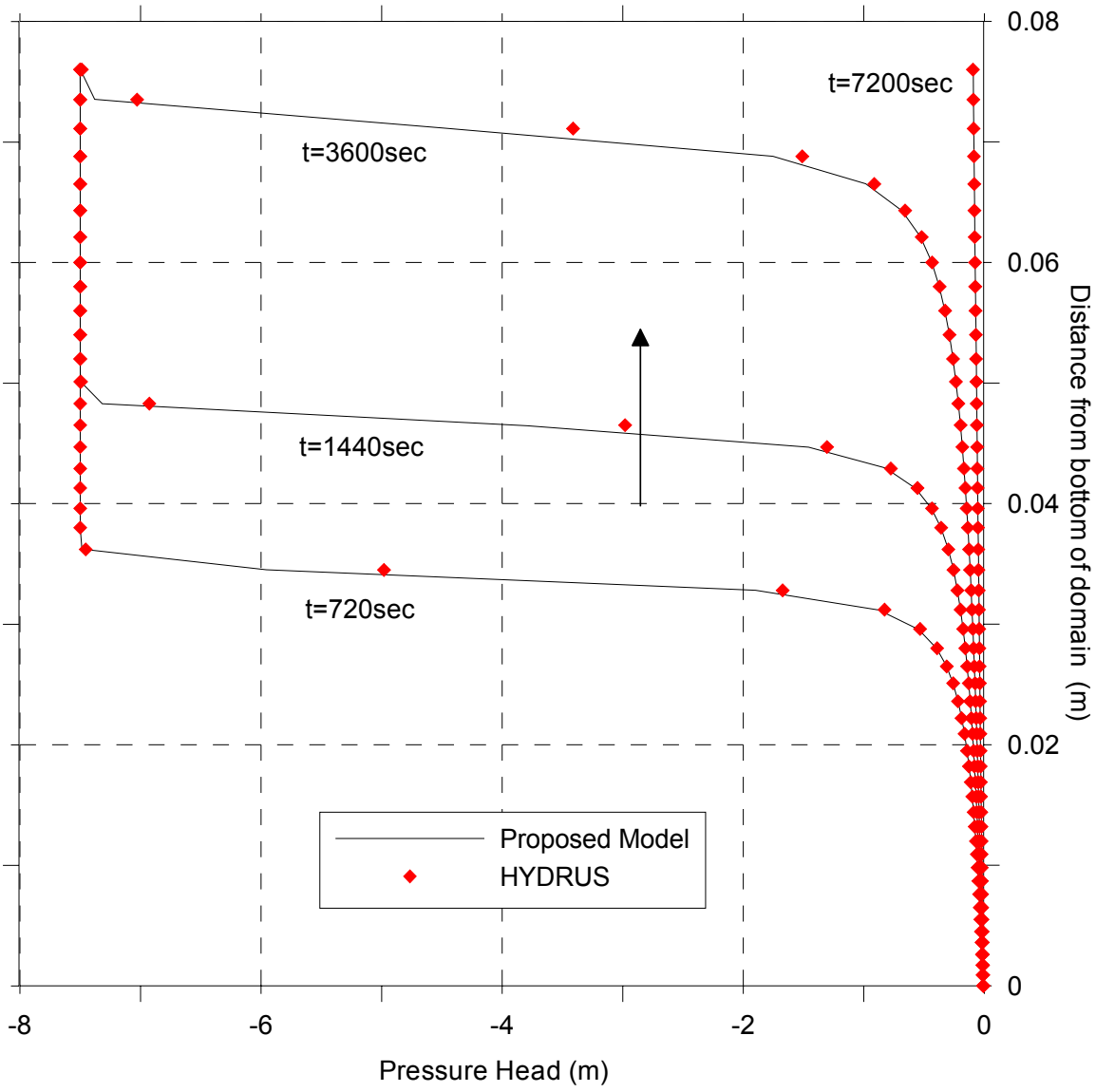

Figure 3.16. Comparison of pressure heads in TEST-2

In the third test, the drainage in a 6m-long caisson is simulated for 100hrs to analyze the effect to gravitational drainage on soil-water distribution. To simulate this condition, a fully saturated soil column (i.e., 0m pressure head initially) is allowed to drain due to gravity. While a zero flux boundary condition is implemented at the top of the domain, the bottom of the domain is allowed to be saturated at all times and solved assuming a constant pressure head condition. The soil hydraulic parameters used in this test are given in Table 3.1. It is clearly seen from the table that the conductivity of the soil in this test is very high and represents a sandy soil which allows relatively fast changes in soil moisture. The pressure head distribution is simulated with both HYDRUS and the proposed model, and the results are shown in Figure 3.17 for various times.

The drainage of soil moisture in a long caisson is simulated for relatively extended periods of time compared to the other test cases. The vertical drainage of upper layers creates dry conditions and negative pressure heads. It is seen from Figure 3.17 that the proposed model simulates the temporal and spatial distribution of soil moisture accurately and gives almost identical results to HYDRUS model.

Finally, the proposed model is also tested against one of the simulations presented in the benchmark paper of Celia et al. (1990). The simulations are based on the van Genuchten model with a saturated hydraulic conductivity of 33.2cm/hr, saturated water content of 0.368, residual water content of 0.102 and n and α values of 2.0 and 0.0335, respectively. Uniform initial conditions were set at -10m. The upper and lower boundaries are simulated with a -0.75m and -10m constant pressure head, respectively.

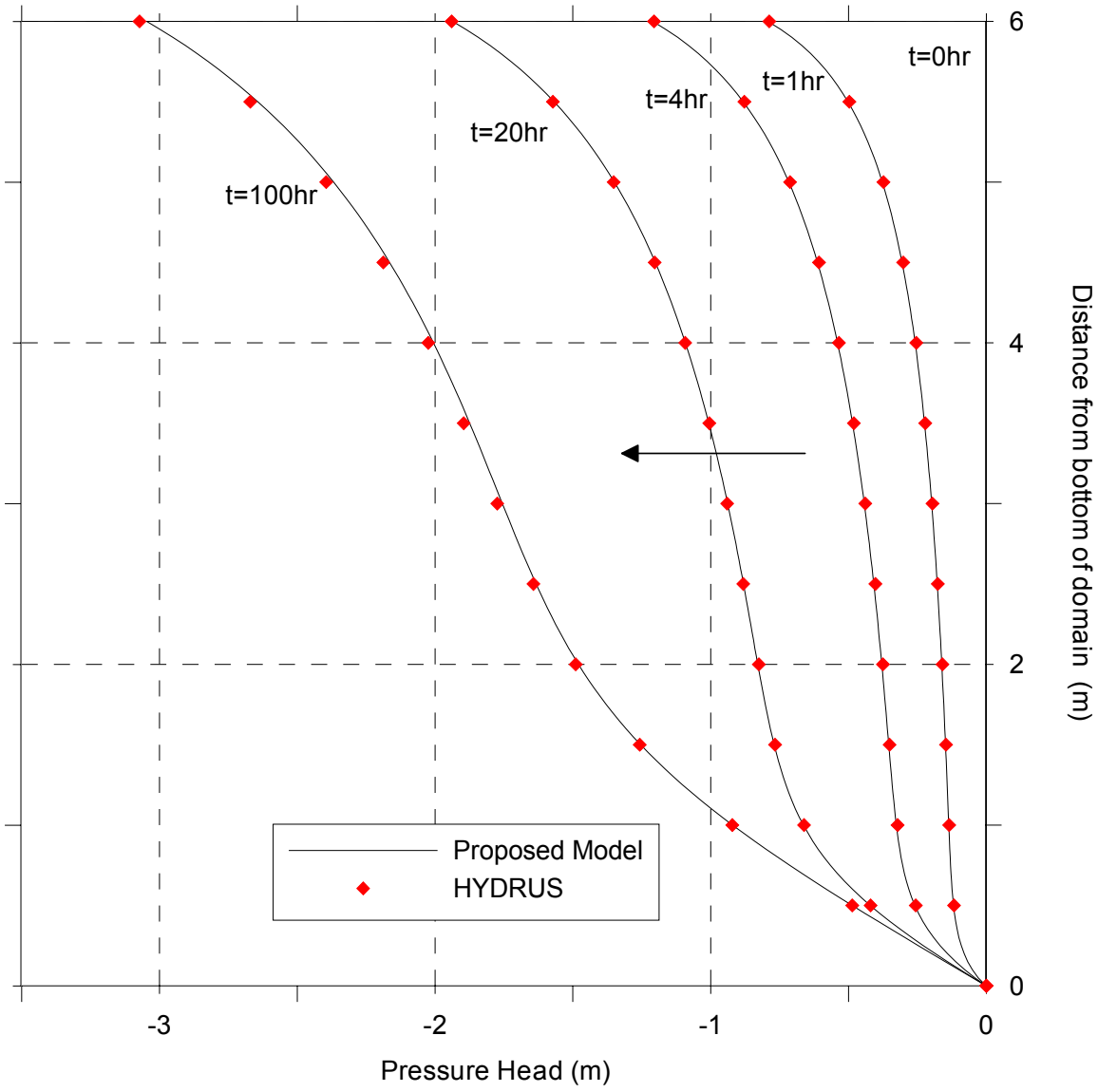

Figure 3.17. Comparison of pressure heads in TEST-3

In this example, the intention of Celia et al. (1990) was to compare finite difference and finite element methods as well as the effect of temporal discretization. They compared several simulations using different time steps with the results of a dense grid simulation. Therefore, the results of the proposed model are also compared to their dense grid simulation shown in Figure 3.18. It is clearly seen that the proposed model produces results that are very close to the dense grid results of Celia et al. (1990). Both the timing and position of the wetting front simulated by this model match properly with their results.

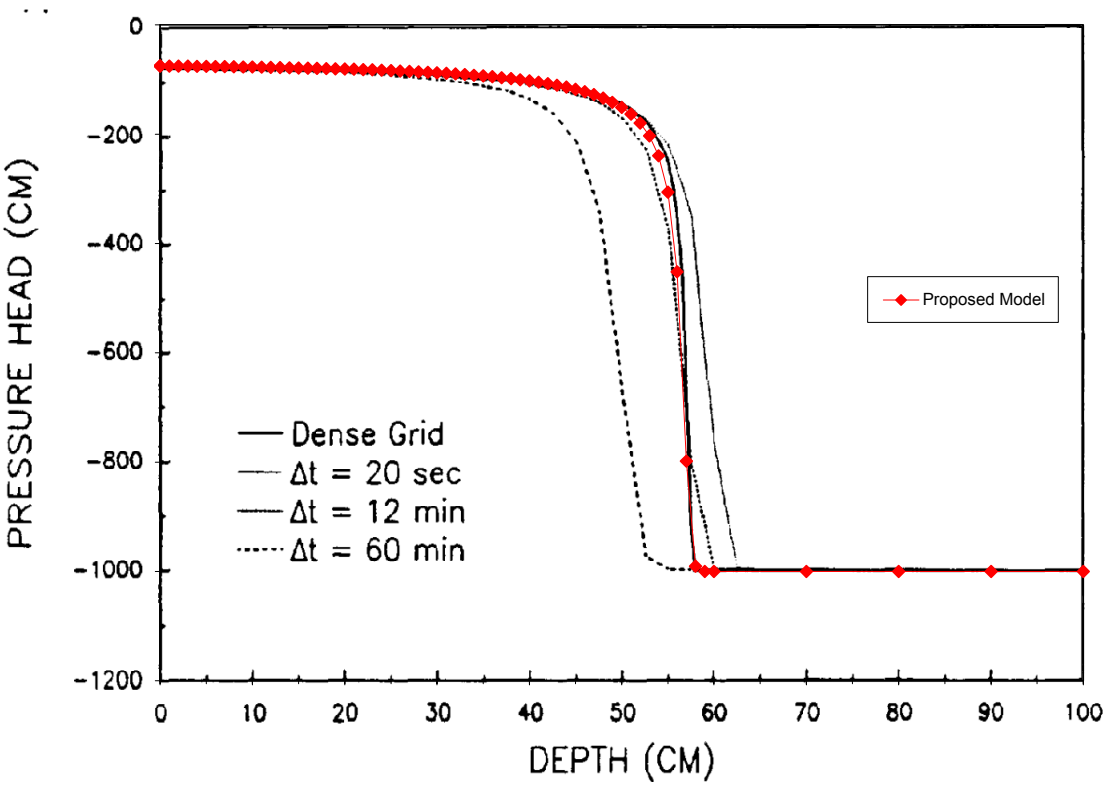

Figure 3.18. Comparison of simulated pressure heads with Celia et al. (1990)

3.5. Coupled Surface-Subsurface Flow Model-1

The river bed is one of the most significant interfaces between surface and subsurface flow systems. The seepage along the river bed not only provides the minimum flow in the river during low flow periods but also attenuates the severity of flood event via bank storage during high flow episodes. It also supplies significant recharge to the aquifer when groundwater heads fall below the river bed. Due to its significance in regulating the river flows and in providing the much needed recharge to the aquifer, it is imperative to accurately analyze the characteristics of the two systems in a coupled fashion and quantify volumetric transfer between these two domains. In order to satisfy these objectives, a coupled surface-subsurface flow model is developed to link the one-dimensional channel flow with the two-dimensional vertically-averaged saturated groundwater flow. The following discussion closely follows the previous work of Gunduz and Aral (2003a, 2003b).

3.5.1. Coupling at River Bed

The lateral seepage flow between the channel flow and the groundwater flow domains provides the coupling mechanism at the river bed interface (Figure 3.19). The lateral flow term appears as a source/sink term in both the channel flow and the saturated groundwater flow equations. The analysis of the lateral flow expression given in equation (3.7) reveals that lateral seepage flow is a direct function of river water surface elevation and groundwater head. Therefore, several possibilities arise depending on the relative values of the river water surface elevation and the groundwater head:

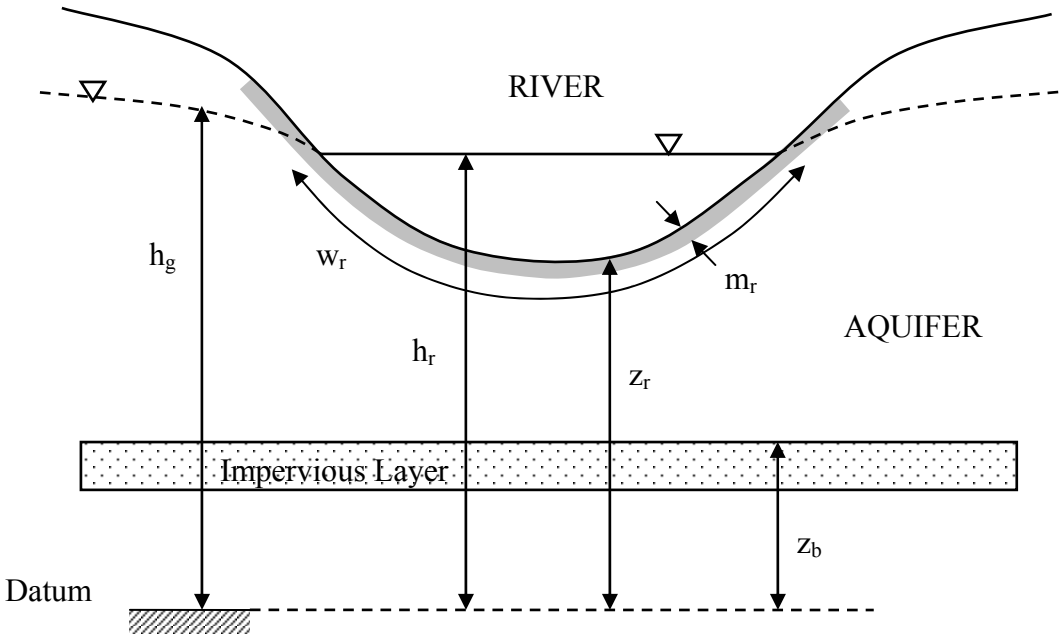

Figure 3.19. Channel flow / groundwater flow interaction

- $h_r > h_g$

  Seepage occurs from the channel to the groundwater flow domain. Hence, it becomes a lateral outflow for the channel flow model and an inflow for the groundwater flow model.

- $h_r = h_g$

  No seepage occurs between the two domains. Hence, the lateral inflow/outflow term in equations (3.1) and (3.29) becomes zero representing a no flux condition for both models.

- $h_r < h_g$

  Seepage occurs from the groundwater flow domain to the channel. Hence, it becomes a lateral inflow for the channel flow model and an outflow for the groundwater flow model.

One can see from these conditions that seepage is generally a head-dependent phenomenon for the coupled system. However, when the groundwater head falls below the bottom elevation of river sediments, the second condition applies in equation (3.7) as the (z_r - m_r) term becomes constant. It then becomes no longer a head-dependent phenomenon and seepage flow is treated as a constant flux condition within the numerical solution. It is, however, important to note that if the groundwater head falls too far below the channel, the link between the two systems is essentially broken and possibly an unsaturated transition zone would develop. Under such conditions, the analysis is no longer based on the first order gradient expression given in equation (3.7) and the entire coupling mechanism described herein must be modified.

It is also important to note that the coupling mechanism proposed in this study is based on the assumption that the movement of water at the river bed is at a steady state. If it cannot be assumed that an equilibrium condition is reached at the river bed, this analysis would yield erroneous results. Under such circumstances, flow within the channel bed must be analyzed with a one-dimensional unsteady vertical flow model. However, the equilibrium assumption is valid for most large scale practical analysis of surface-subsurface flow interactions.

3.5.2. Proposed Simultaneous Solution Method

As discussed in Chapter 2, iterative (implicit) and non-iterative (explicit) coupling techniques are commonly used to establish the interactions between the surface and subsurface flow systems. While iterative algorithms are considered to be the most advanced coupling mechanisms for today's modeler, they can be computationally costly

for large systems due to the extra iteration loop in the solution. Moreover, they may be inaccurate at times when the convergence criterion is set at a high value to reduce computational run times.

Considering the limitations of current coupling mechanisms, a new simultaneous coupling technique is proposed by the author in an effort to link surface-subsurface flow systems at the river bed interface. The idea of the method is based on the simultaneous solution of the discretized forms of the two systems rather than the sequential solution that both the iterative and non-iterative coupling methods implement (Gunduz and Aral, 2003a). Although a theoretically similar approach might have already been applied in other branches of science, it is believed that the method is truly original in terms of its formulation in a coupled river-aquifer model framework.

The initial step for the simultaneous solution of the coupled model is discretizing the analysis domain. In this procedure, the channel network is discretized first considering the stability requirements of the channel flow model. Then, the groundwater flow domain is discretized considering the heterogeneity of the aquifer. During the discretization of the groundwater flow domain, each node of the channel flow model is selected such that it coincides with a node in the groundwater flow model as seen in Figure 3.20. This one-to-one correspondence of the nodes along the channel network is essential for the proposed simultaneous solution of the coupled model (Gunduz and Aral, 2003a). If there is a requirement for finer discretization of the groundwater flow domain at any point along the channel network due to highly variable aquifer properties, the discretization of the channel flow model must also be modified to satisfy the one-to-one correspondence of the nodes. In this regard, the simultaneous solution of the coupled

model is always based on finest discretized domain that either model enforces along the channel network (Gunduz and Aral, 2003a). For any other point in the analysis domain, the discretization is solely based on the requirements of the groundwater flow model.

The only exception to the one-to-one correspondence of nodes is observed at the channel junction points. At any junction with k inflowing channels and one outflowing channel, the numerical discretization of the channel flow model requires that k+1 nodes are used to properly represent the k downstream boundary nodes of the inflowing channels and one upstream boundary node of the outflowing channel. Since all k+1 nodes physically represent the same junction point, they all correspond to a single point in the groundwater flow model. Therefore, at junction points, k+1 nodes of the channel flow model corresponds to one node of the groundwater flow model.

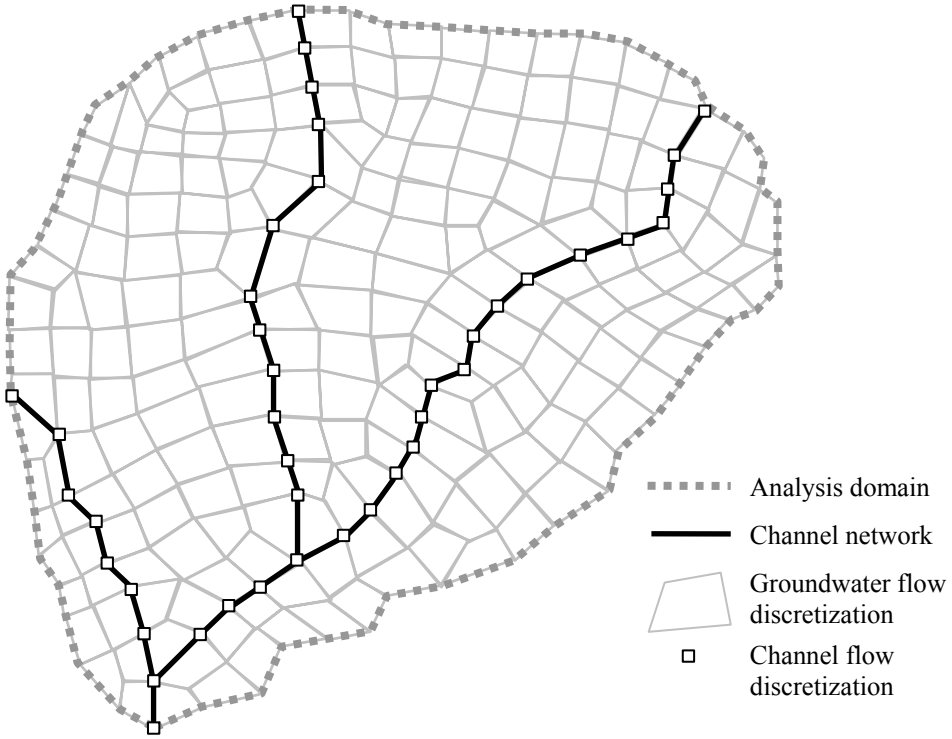

Figure 3.20. General discretization of the domain

The second step of the simultaneous solution of the coupled model is to write discretized equations of channel and groundwater flow equations. These are given in equations (3.26) and (3.46), respectively. When these equations are written for all nodes of channel and groundwater flow domains, a system of equations is obtained for both channel and groundwater flow system. At this point, if the standard iterative coupling scheme is implemented to solve this system, one would have two separate matrix solutions to solve each domain separately by using the latest values of the common parameter from the other domain (i.e., river water surface elevation for groundwater flow model and groundwater head for channel flow model). Following each solution, a convergence check is performed with respect to a pre-determined criterion. Once the check is satisfied the solution proceeds to the next time level. In the proposed simultaneous solution of the coupled model, however, the systems of equations obtained from the channel flow and groundwater flow models are assembled together within a single system so that they can be solved together in a simultaneous manner inside a single matrix structure. The assembled final matrix equation is shown in Figure 3.21. In the assembled global matrix equation, **A** is the global coefficient matrix, **B** is the global load vector and **x** is the global unknown vector. As seen from Figure 21, the global matrix and vectors are obtained by combining their separate blocks obtained from channel and groundwater flow model. These separate blocks are written as:

$$\mathbf{A}^{GW} = \alpha \mathbf{S}^{j+1,k} + (1/\Delta t)\mathbf{M} \tag{3.82}$$

$$\mathbf{A}^{RIVER} = \mathbf{J}^{j+1,k} \tag{3.83}$$

$$\mathbf{B}^{GW} = \alpha \mathbf{F}^{j+1,k} + (1-\alpha)\mathbf{F}^{j} - \left((1-\alpha)\mathbf{S}^{j} - (1/\Delta t)\mathbf{M}\right)\cdot \hat{\mathbf{h}}_{\mathbf{g}}{}^{j} \tag{3.84}$$

$$\mathbf{B}^{RIVER} = -\mathbf{f}^{j+1,k} \tag{3.85}$$

$$\mathbf{x}^{GW} = \hat{\mathbf{h}}_{\mathbf{g}}^{\,j+1,k+1} \tag{3.86}$$

$$\mathbf{x}^{RIVER} = \delta\mathbf{x}^{j+1,k+1} \tag{3.87}$$

Although the global matrix is shown in full-matrix format, the calculations are performed using a banded matrix structure to reduce computer memory required to store and solve the system. The total bandwidth of the global matrix depends on the relative magnitudes of the bandwidths of channel flow and groundwater flow models. Therefore, the size of the global matrix is determined by the size of the bigger bandwidth. In general, the bandwidth of the groundwater flow model is bigger than the bandwidth of the channel flow model (Gunduz and Aral, 2003a).

$$\left[\begin{array}{c|c} \left[\mathbf{A}^{\mathrm{GW}}\right] & \mathbf{0} \\ \hline \mathbf{0} & \left[\mathbf{A}^{\mathrm{RIVER}}\right] \end{array}\right] \left\{\begin{array}{c} \mathbf{x}^{\mathrm{GW}} \\ \hline \mathbf{x}^{\mathrm{RIVER}} \end{array}\right\} = \left\{\begin{array}{c} \mathbf{B}^{\mathrm{GW}} \\ \hline \mathbf{B}^{\mathrm{RIVER}} \end{array}\right\}$$

Figure 3.21. Global matrix equation and component blocks

It is crucial to emphasize that the global matrix solution directly solves the unknown variable in groundwater flow domain (i.e., hydraulic head) whereas it solves for the change in unknown variables between two iterations in channel flow domain (i.e., change in discharge and stage). Therefore, one has to evaluate the actual values of the unknown values after each solution of the global matrix equation before the global coefficient matrix and the load vector are re-assembled for the next solution. It is also important to note that since the global system is non-linear due to the non-linearities in channel flow and groundwater flow, it is solved several times for each time step until sufficient convergence is achieved for the unknown parameters. Hence, the global matrix solution involves an iterative portion to handle the non-linearity of the governing equations of both models. However, this iterative non-linear solution does not affect the simultaneous solution behavior of the overall coupled system. The iterative solution is only used to treat the non-linearity in the two sub-systems. The convergence of the non-linear solution is checked using two separate criteria for channel flow and groundwater flow components. Therefore, although the systems are solved together, the convergence of the solution is tested with respect to different criteria since the degree of the non-linearity in channel flow is generally much higher than the degree of non-linearity in groundwater flow. Typically, 2 to 3 iterations are found to be sufficient for the convergence of two sub-domain models (Gunduz and Aral, 2003a).

Even though the two hydrologic systems coupled in this model have significantly different time scales, their simultaneously coupled solution, unlike an iteratively coupled solution, requires a common time step in numerical discretization. Since the behavior of a channel flow model is generally more dynamic than the overall response of a

groundwater flow model, this constraint could occasionally create long simulation periods with the proposed algorithm. However, it is always faster than the iterative solution approach that utilizes the same time step size (Gunduz and Aral, 2003a).

3.5.3. Model Testing

As there are no analytical solutions to verify against, two sets of hypothetical simulations are performed using the proposed model and the solution algorithm. In the first application, a hypothetical test case is simulated to test the model's capabilities and limitations with a rectangular groundwater flow domain and an overlying single channel domain. In the second application, the same hypothetical test case is modified to analyze the model's response with the presence of a channel network.

Single Channel-Aquifer System:

The coupled channel/groundwater flow model is first applied to a hypothetical single channel stream-aquifer system to demonstrate the performance of the proposed simultaneous solution algorithm. The physical setup of the hypothetical domain is shown in Figure 3.22. In this application, the stream is a 30m wide, 10km long uniform rectangular channel with a constant slope of 0.0001m/m and divides the aquifer into two equal portions 2000m wide on each side of the channel. The Manning's roughness coefficient of the stream is uniform throughout the channel and has a value of 0.025. At steady flow conditions, the channel carries $100 m^3/s$ discharge at the uniform flow depth of 3.56m. The thickness of the sediments at the bottom of the channel is 0.3m and the hydraulic conductivity of the deposits is 1.0E-6m/s. The channel bottom elevation at the most upstream point is given as 30m above mean sea level. To visualize results easily,

the 10km long and 4 km wide unconfined aquifer is assumed to have a uniform and isotropic hydraulic conductivity of 1.0E-3m/s and the aquifer base is set at mean sea level. The stream flow model is discretized into 100m long elements giving a total of 101 nodes. The groundwater flow model domain is discretized by square elements with a side length of 100m giving a total of 4141 nodes and 4000 square elements. Furthermore, a constant time step of 1hr is used in simulations.

In the channel flow model, the upstream boundary condition for the channel is given by a trapezoidal discharge hydrograph with a base discharge of $100m^3/s$, a peak discharge of $350m^3/s$ and a time to peak of 10 days (Figure 3.23). The downstream boundary condition is given by a single-valued rating curve that maps the discharge to its normal depth. In the groundwater flow model, the boundaries parallel to the stream are specified as constant head condition and the boundaries perpendicular to the stream are specified as no-flux condition. Moreover, the internal boundary, where the stream runs through, is specified as a head-dependent line source. The initial conditions in the stream flow model is given as uniform flow conditions (i.e., $100m^3/s$ of discharge and a corresponding 3.56m of depth) at all nodes. In the groundwater flow model, two different sets of initial hydraulic head surfaces are used. In the first simulation, the initial groundwater head in the aquifer is chosen to be at 32m at all nodes. This simulation illustrates a condition where lateral flow occurs from the stream to the aquifer. In the second simulation, the opposite scenario is simulated and the initial groundwater head in the aquifer is chosen to be 35m, illustrating a condition where the lateral flow occurs from the aquifer to the stream. These two simulations are referred to as Scenario-1 and Scenario-2, respectively and are abbreviated as S1 and S2 in the following discussion.

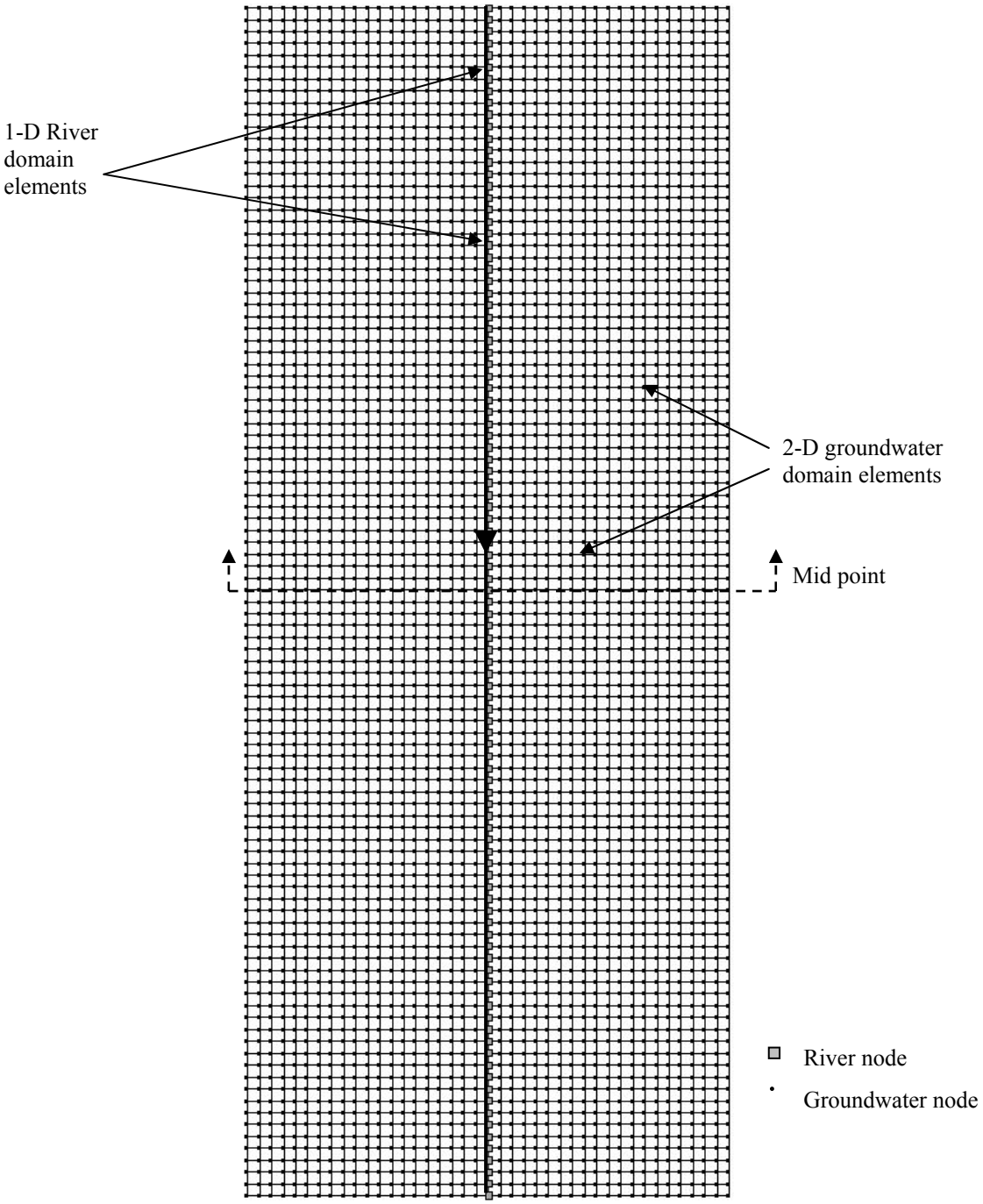

Figure 3.22. Physical setup of hypothetical domain, single channel

In both scenarios, the point comparisons of groundwater head and stream stage are presented in figures 3.23 and 3.25 at the mid point of the analysis domain (i.e., 5000m from the upper boundary of the aquifer, which also corresponds to the mid point of the stream). The spatial distribution of groundwater heads are also presented in figures 3.24 and 3.26 along the line ($-2000m \leq x \leq 2000m$; $y = 5000m$). Analysis of groundwater head time series in figures 3.23 and 3.25 reveals that the passage of the flood wave creates an increase in the groundwater heads by creating a mound near the river as long as the stream stages are higher than the groundwater heads for a sufficiently long period of time. This mound is the result of lateral inflow to the aquifer (Figure 3.24). It is also seen that the mound subsides and the bank storage is drained back to the stream when the stream stage falls below the groundwater heads. It is also seen from figures 3.23 and 3.25 that there is a lag between the peak values of the hydraulic head and the stream stage which clearly represents the dynamic behavior of the stream flow as opposed to the groundwater flow.

The response of the coupled system to a flood wave is directly related to the initial conditions in the stream and the aquifer. A comparison of figures 3.24 and 3.26 demonstrate the effect of initial groundwater head in the aquifer and its position relative to the stage in the stream. When the hydraulic head in the aquifer is higher than the stream stage (Figure 3.26), a discharge from bank storage occurs in the first 5 days of the simulation creating a drawdown near the stream. During the second 5 day period, stream stages increases due to the arrival of the flood peak and this creates a flow reversal towards the aquifer (Figure 3.26).

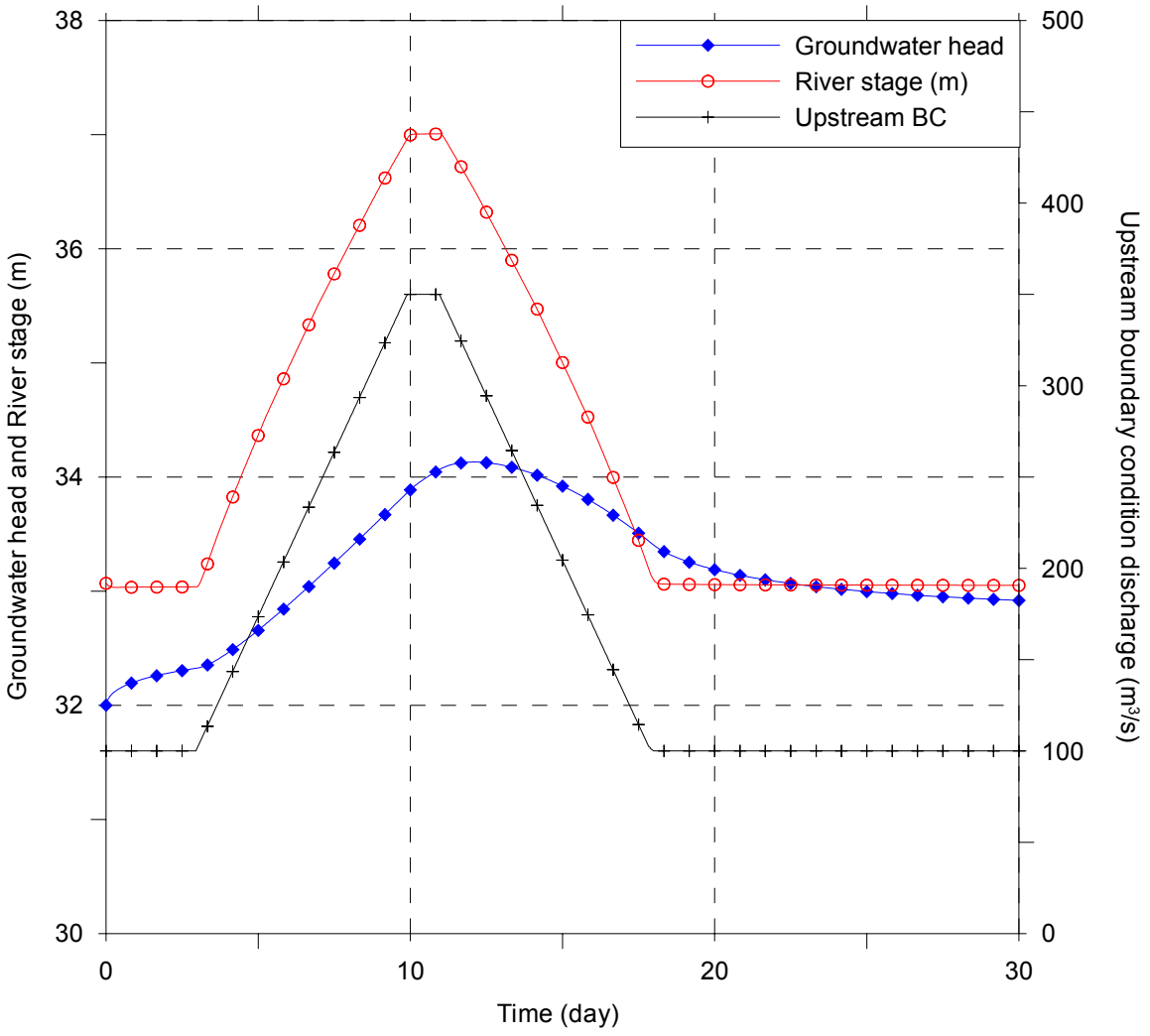

Figure 3.23. Groundwater head and river stage at the mid-point and river discharge at the upstream boundary for Scenario-1

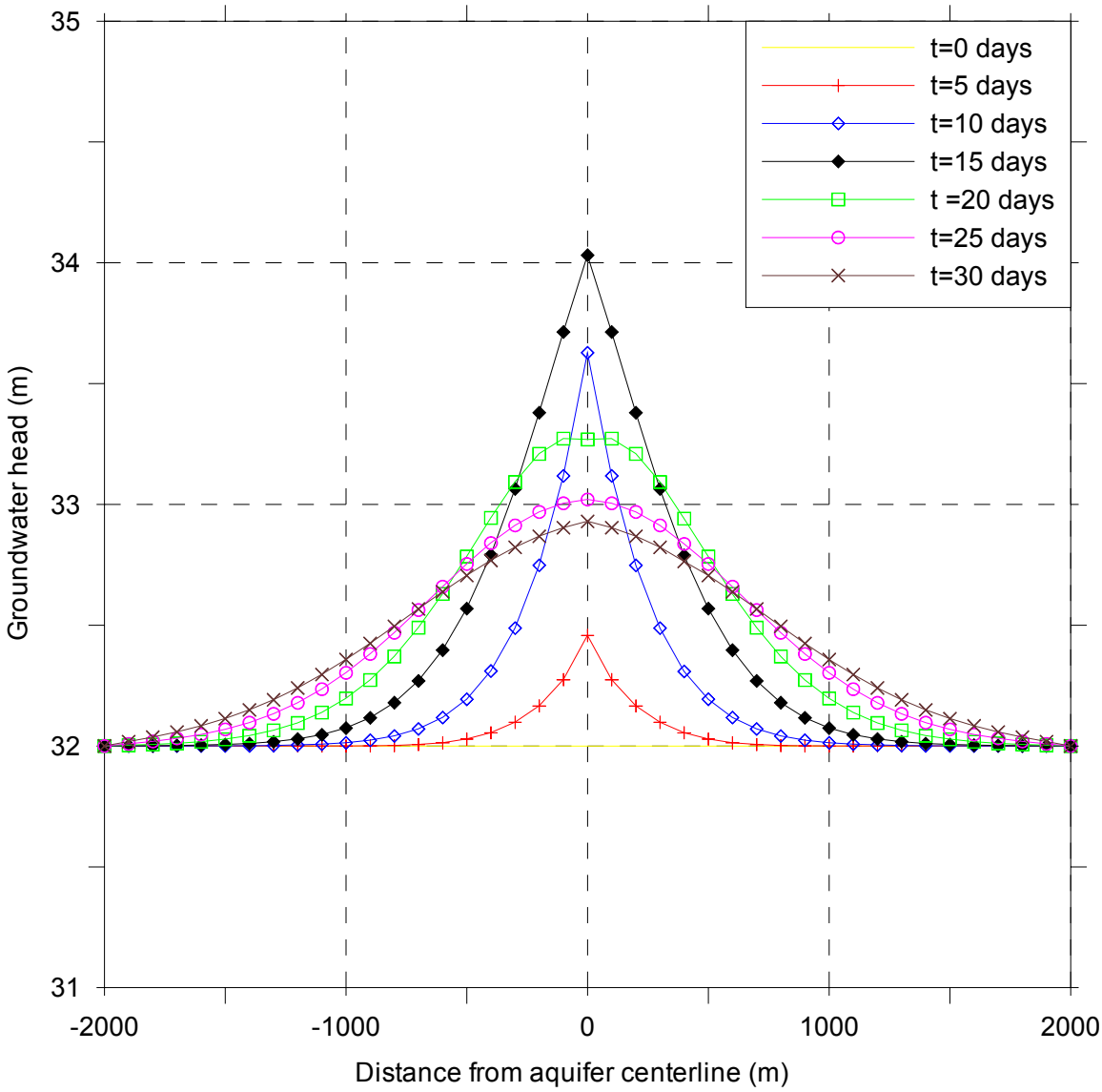

Figure 3.24. Groundwater head profiles at various times along mid point for Scenario-1

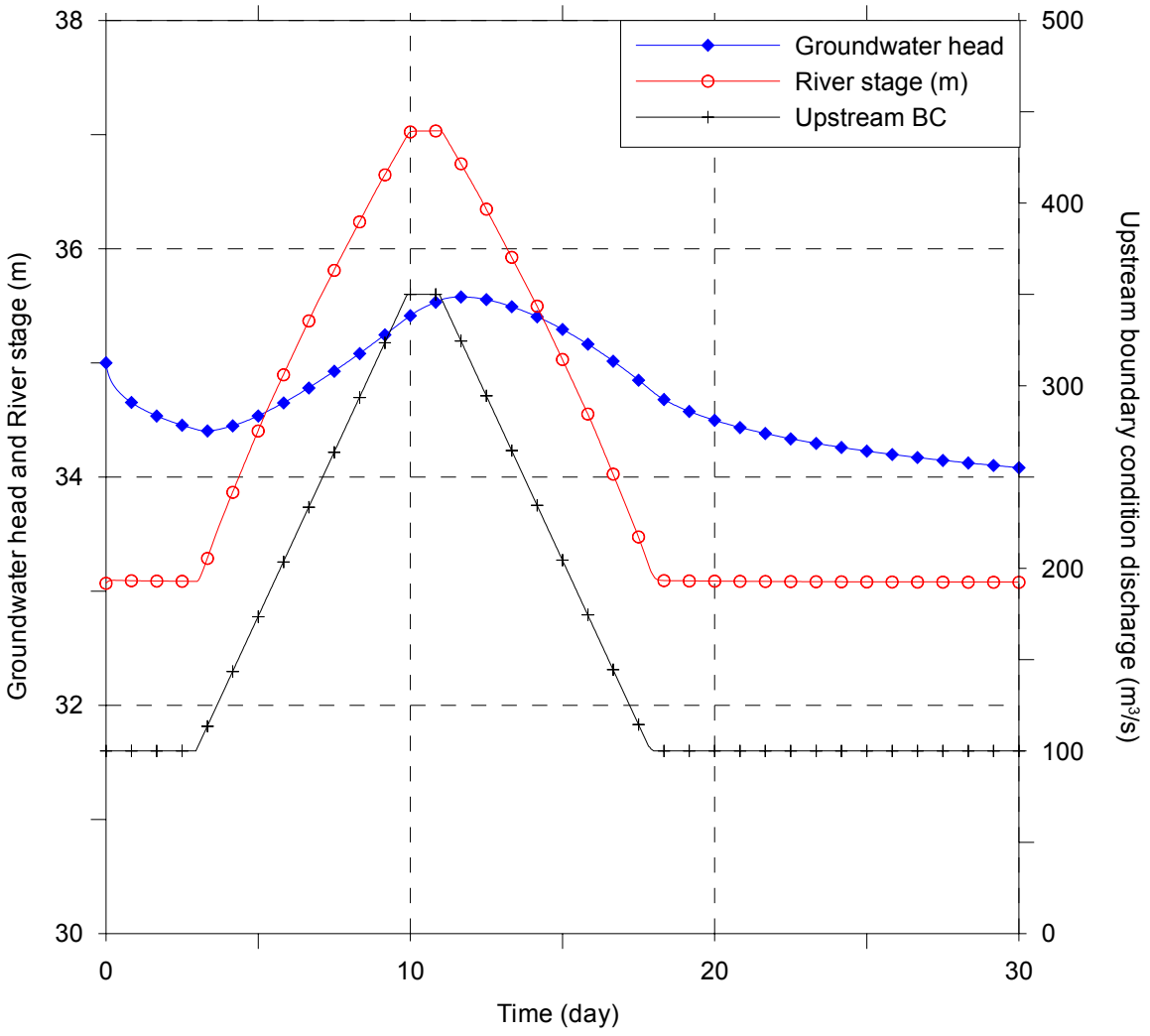

Figure 3.25. Groundwater head and river stage at the mid-point and river discharge at the upstream boundary for Scenario-2

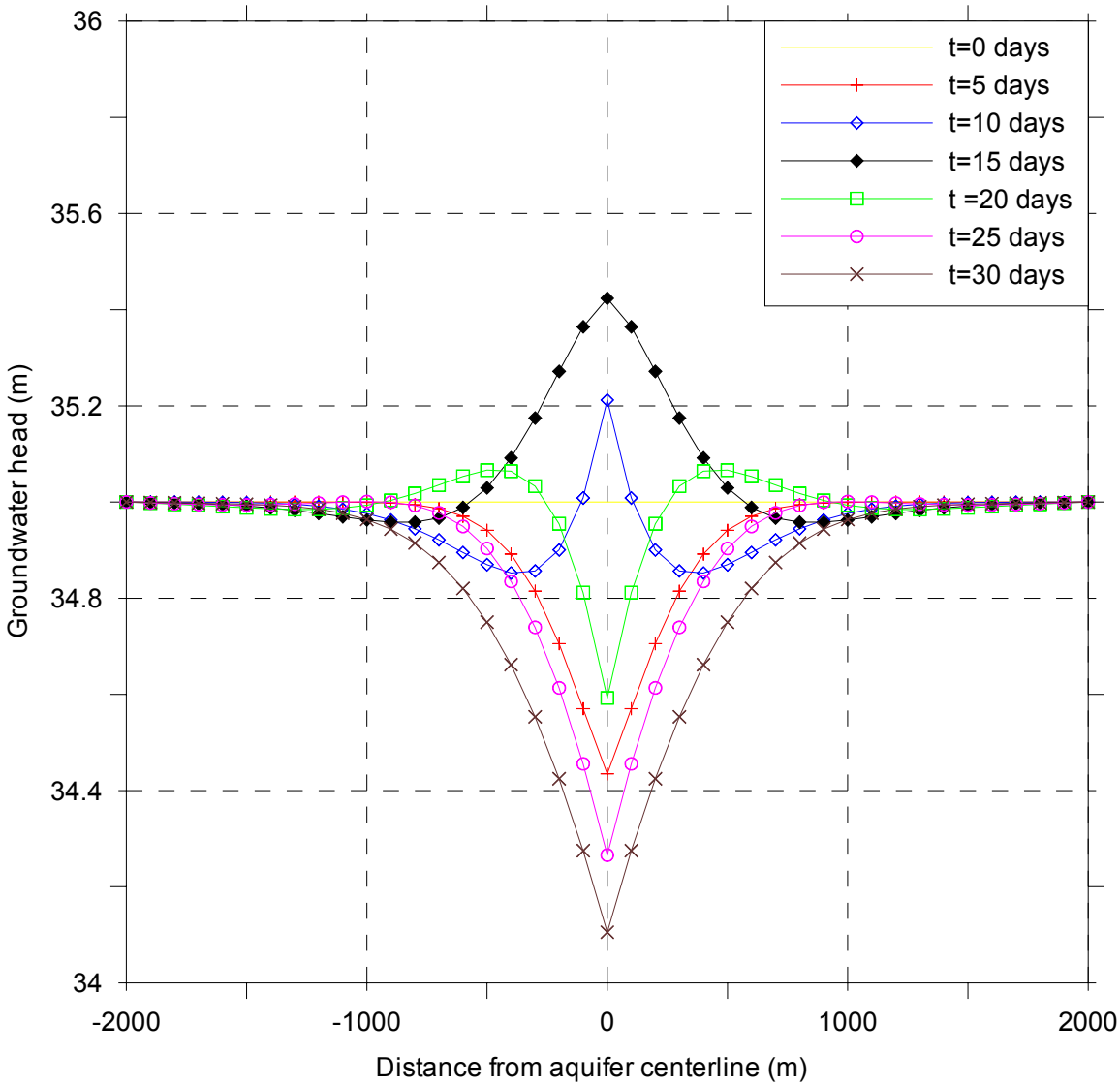

Figure 3.26. Groundwater head profiles at various times along mid point for Scenario-2

Channel Network-Aquifer System:

In the second application, the coupled channel/groundwater flow model is applied to a hypothetical stream network-aquifer system to demonstrate the performance of the proposed simultaneous solution algorithm to multiple channel applications. The physical setup of the hypothetical domain is shown in Figure 3.27. In this application, two stream channels (i.e., channels 1 and 2) meet and form a larger channel (i.e., channel 3) at the junction point shown in Figure 3.27. The two upstream tributaries are 30m wide and 7071m long uniform rectangular channels with a constant slope of 0.00015m/m. The downstream stream is 45m wide and 5000m long uniform rectangular channel with a constant slope of 0.0001m/m. The two upstream channels confluence at the mid-point of the domain and creates the junction. The Manning's roughness coefficients of all channels are uniform through out the domain and have a value of 0.025. At steady flow conditions, the two upstream channels carry $100m^3/s$ whereas the downstream channel carries $200m^3/s$. The thickness of the sediments at the bottom of the channel is 0.3m and the hydraulic conductivity of the deposits is 1.0E-6m/s. To visualize results easily, the 10km long and 4 km wide unconfined aquifer is assumed to have a uniform and isotropic hydraulic conductivity of 1.0E-3m/s and the aquifer base is set at mean sea level. The stream flow model is discretized by variable length elements giving a total of 155 nodes. The groundwater flow model domain is discretized by quadrilateral elements with variable side lengths giving a total of 4161 nodes and 4022 elements. A constant time step of 1hr is used in simulations.

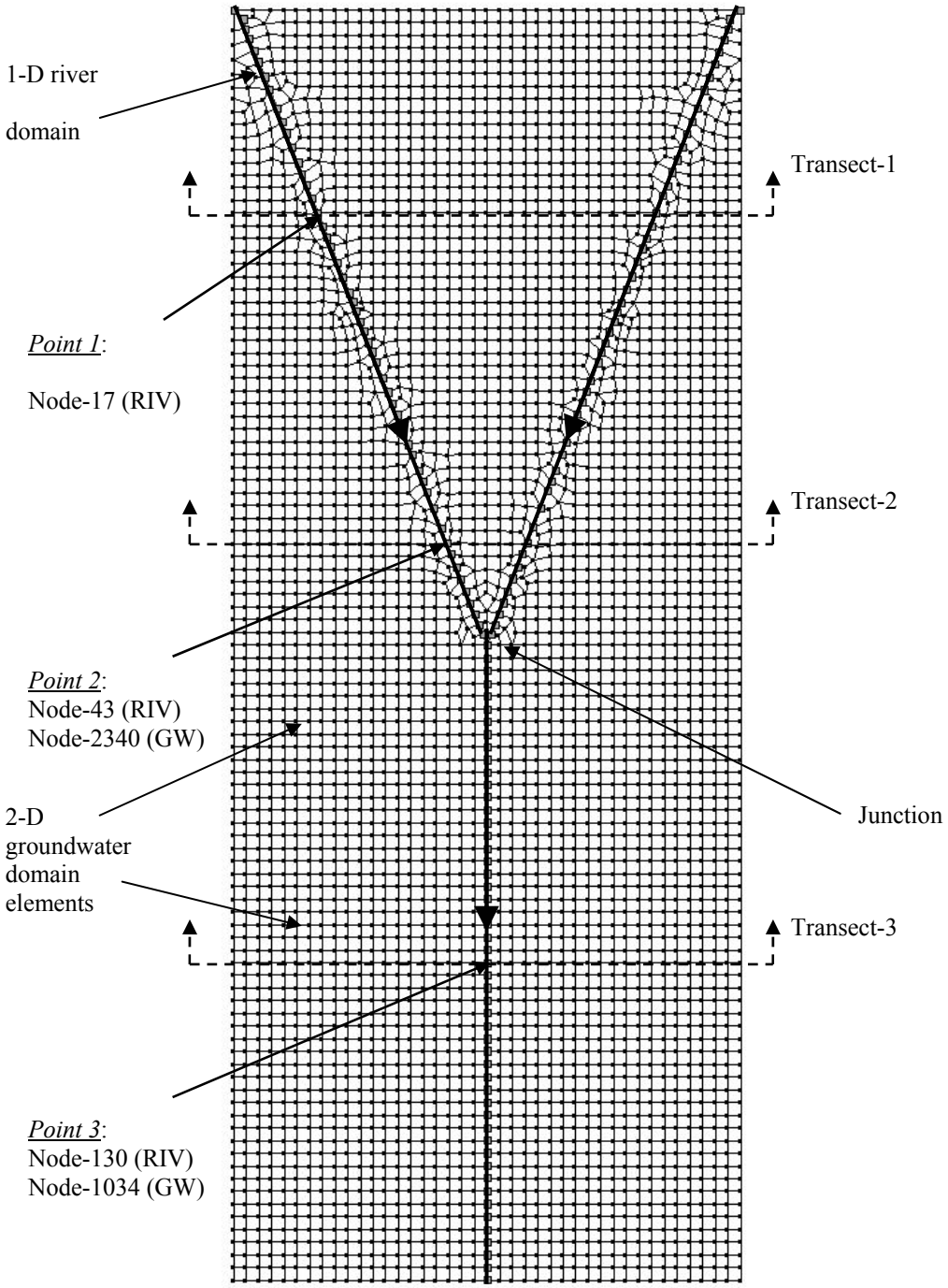

Figure 3.27. Physical setup of hypothetical domain, channel network

In the channel flow model, the upstream boundary conditions are given by a trapezoidal discharge hydrograph with a base discharge of $100m^3/s$, a peak discharge of $350m^3/s$ and a time to peak of 10 days (Figure 3.29). The downstream boundary condition is given by a single-valued rating curve that maps the discharge to its normal depth. In the groundwater flow model, the boundaries parallel to the stream are specified as constant head condition and the boundaries perpendicular to the stream are specified as no-flux condition. Moreover, the internal boundary, where the stream runs through, is specified as a head-dependent line source. The initial conditions in the stream flow model are given as uniform flow conditions at all nodes. In the groundwater flow model, two different sets of initial hydraulic head surfaces are used. In the first simulation, the initial groundwater head in the aquifer is chosen to be at 32m at all nodes. This simulation illustrates a condition where lateral inflow occurs from the stream to the aquifer. In the second simulation, the opposite scenario is simulated and the initial groundwater head in the aquifer is chosen to be 35m, illustrating a condition where the lateral inflow occurs from the aquifer to the stream. These two simulations are referred to as Scenario-1 and Scenario-2, respectively and are abbreviated as S1 and S2 in the following discussion.

In both scenarios, the point comparisons of groundwater head and stream stage are presented in figures 3.28 and 3.32 at three points in the analysis domain. These points are shown in Figure 3.27. Among these three points, points 1 and 2 are on the left upstream channel and are situated 1745m and 4537m from the most upstream point of channel 1. On the other hand, point 3 is on the downstream channel and is situated at the mid point between the junction and the channel's most downstream point (i.e., 2500m from the junction). These three points are also positioned on the three transects depicted

in Figure 3.27 (i.e., 1600m, 4200m, and 7500m from the upper boundary of the aquifer). These transects are used to present the spatial distributions of groundwater heads along the aquifer.

Analysis of groundwater head time series in figures 3.29 through 3.31 and 3.33 through 3.35 reveal that the passage of the flood wave creates an increase in the groundwater heads by creating a mound near the river as long as the stream stages are higher than the groundwater heads for a sufficiently long period of time. This mound is the result of lateral inflow to the aquifer. It is also seen that the mound subsides and the bank storage is drained back to the stream when the stream stage falls below the groundwater heads. The spatial distribution of groundwater heads in transects 1 and 2 illustrate a symmetric response behavior since the physical characteristics of the upstream channels and their boundary conditions are exactly identical as a function of time. Any difference between these characteristics would clearly create an asymmetric hydraulic head distribution in the upper half of the aquifer.

In S1, the initial groundwater head in all three transects are below the initial river stages. This situation creates a lateral outflow from stream channels towards the groundwater domain, creating an increase in groundwater heads as seen in figures 3.29, 3.30 and 3.31. Then, the flood wave arrives and this increase is even more pronounced. Once the flood wave starts receding, the groundwater heads start falling. Since the water surface elevation decrease in channel is much more dynamic than the groundwater head decrease, a flow reversal is observed creating a lateral inflow to stream channels from the groundwater domain. This behavior is present in all transects after 15 days in figures 3.29, 3.30 and 3.31. In S2, on the other hand, the initial groundwater head in all three

transects are above the initial river stages. Hence, an immediate lateral inflow to the stream channels starts to develop. In the absence of a flood wave, this situation creates a decrease in groundwater heads in the immediate vicinity of the channels. Therefore, it is possible to observe the drawdown associated with this behavior in all transects in the first 5 days of the simulation in figures 3.33, 3.34 and 3.35. After the 5^{th} day, the arrival of the flood wave forces an increase in the groundwater heads due to lateral outflow from the channel.

It is important to mention the fact that a relatively high hydraulic conductivity value and a relatively smoothly-increasing upstream discharge hydrograph are used to promote a rapid response behavior so that the results could be analyzed in a simpler and idealized fashion. In real time simulations, however, the aquifer conductivity values are generally much smaller and the hydrographs are commonly much steeper on the rising limb. Such a situation is presented in the application chapter of this study.

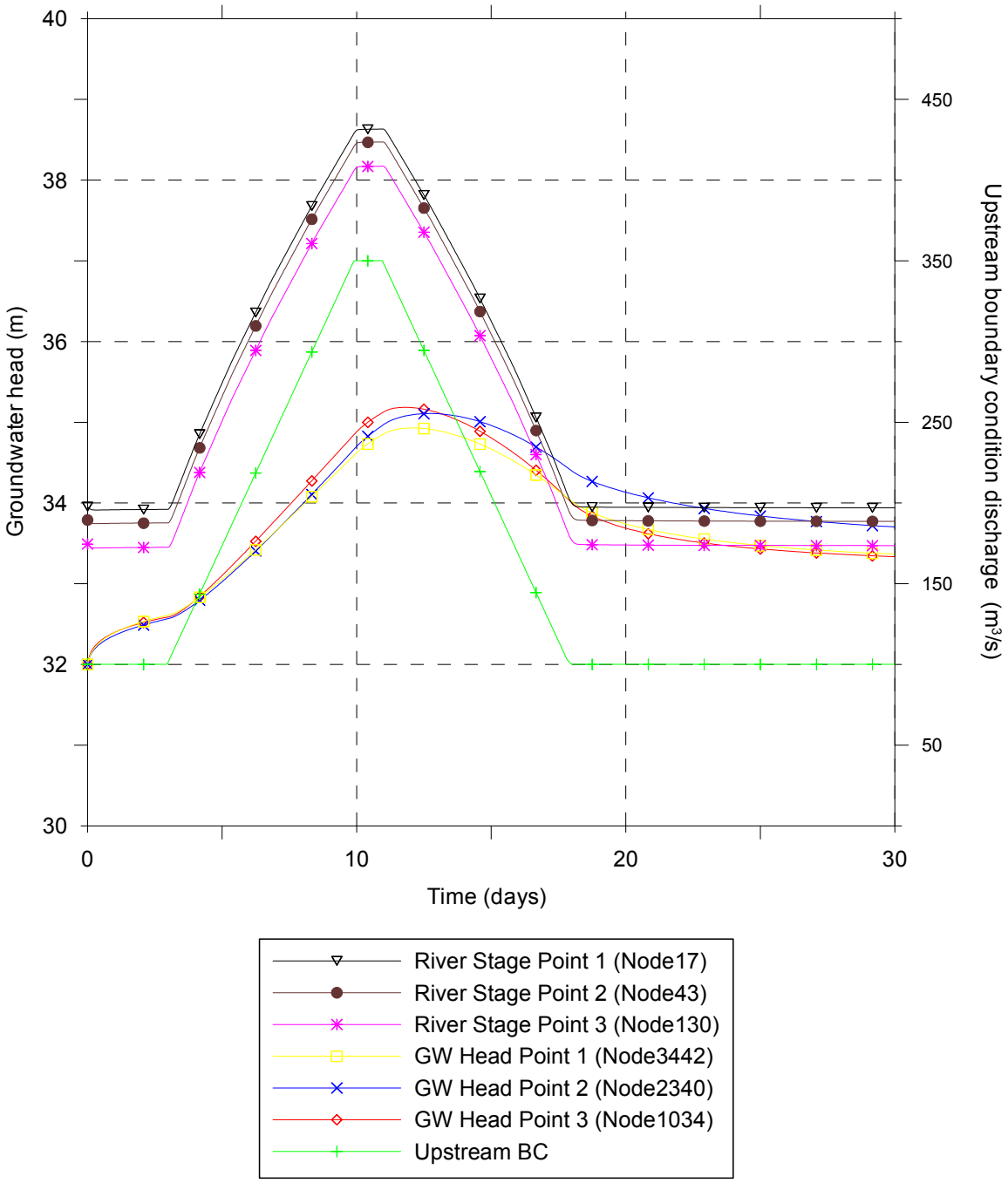

Figure 3.28. Groundwater head and river stage at various points in domain and river discharge at the upstream boundary in Run-1

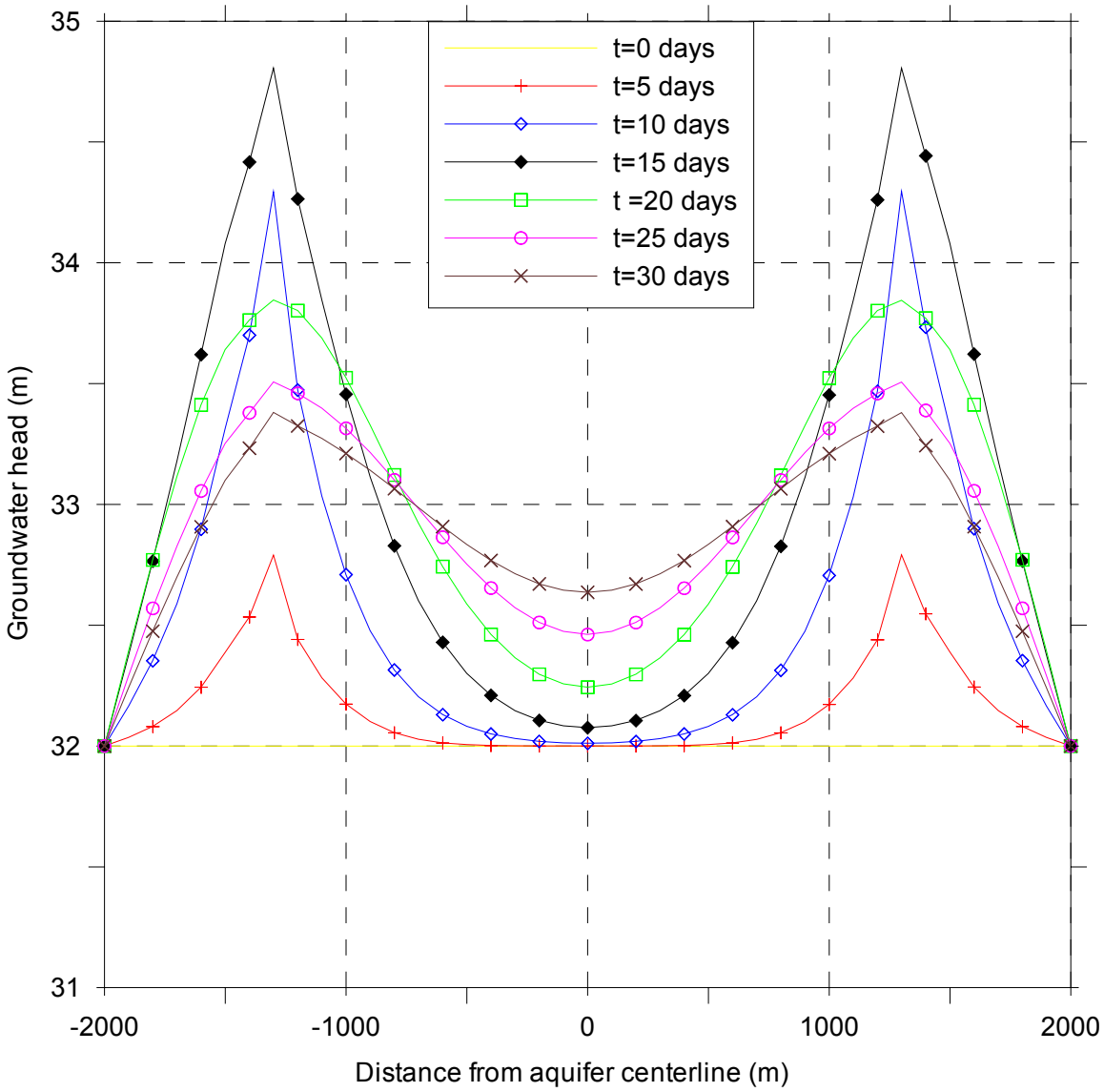

Figure 3.29. Groundwater head profiles at various times at transect-1 in Run-1

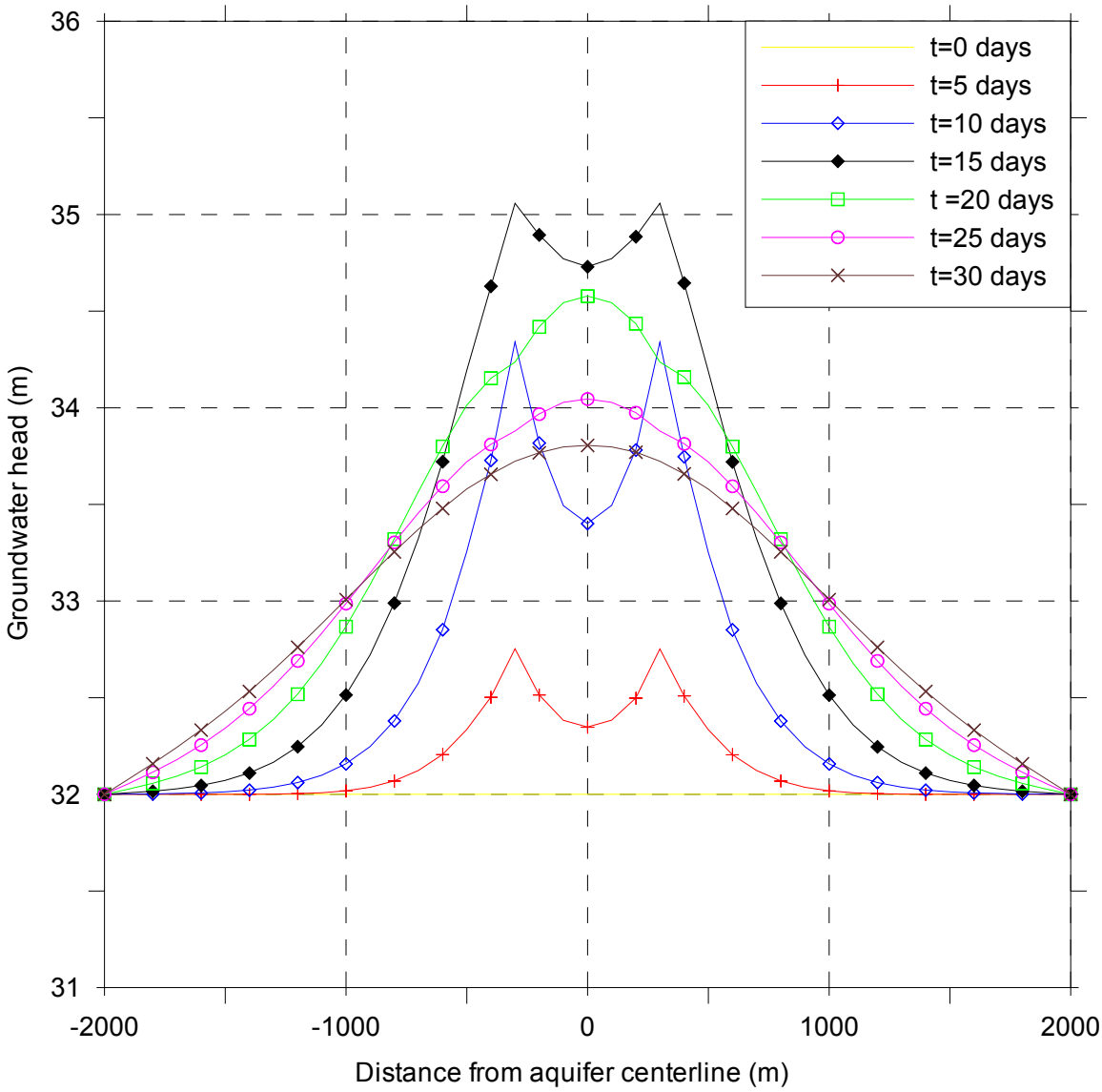

Figure 3.30. Groundwater head profiles at various times at transect-2 in Run-1

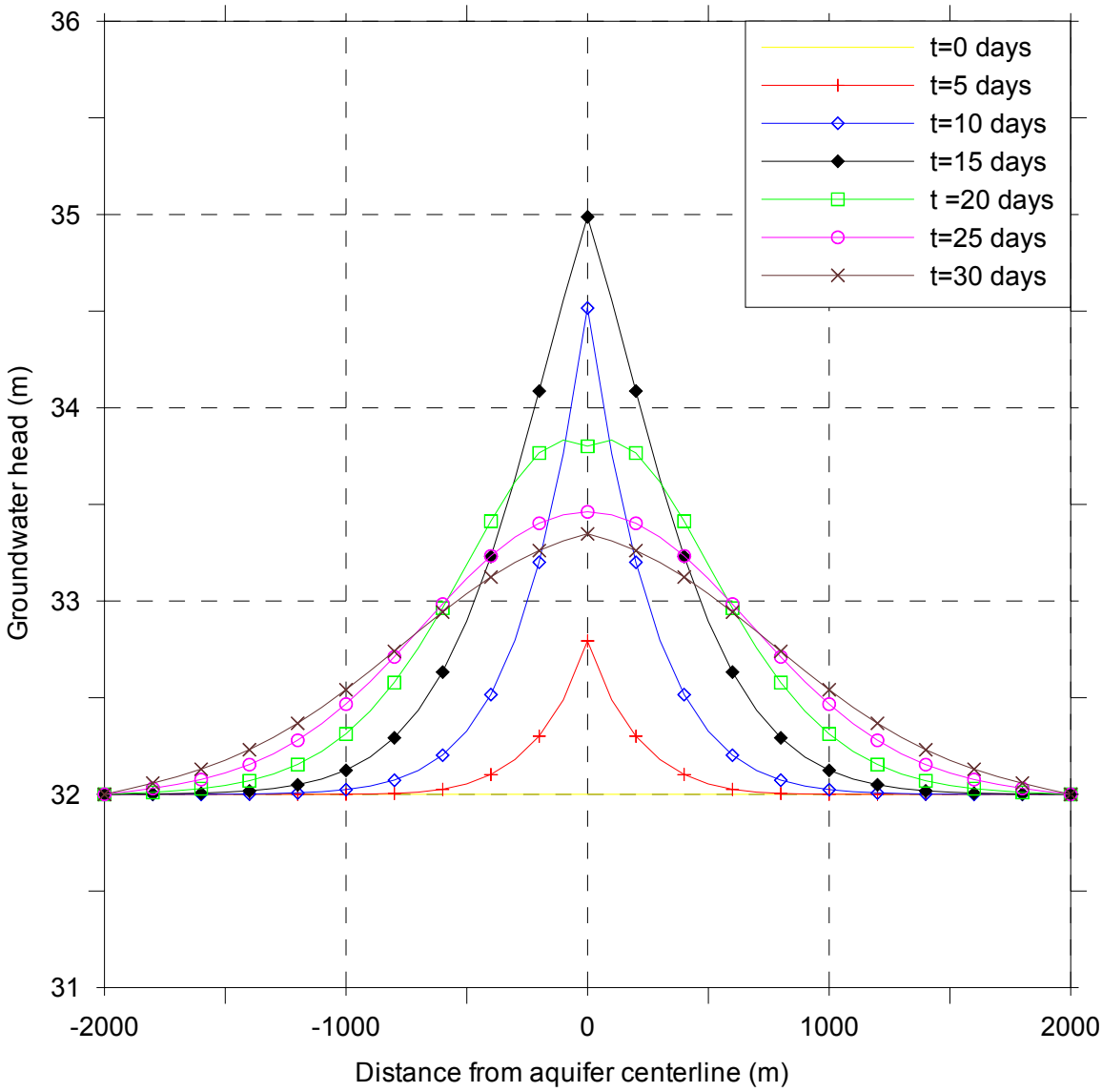

Figure 3.31. Groundwater head profiles at various times at transect-3 in Run-1

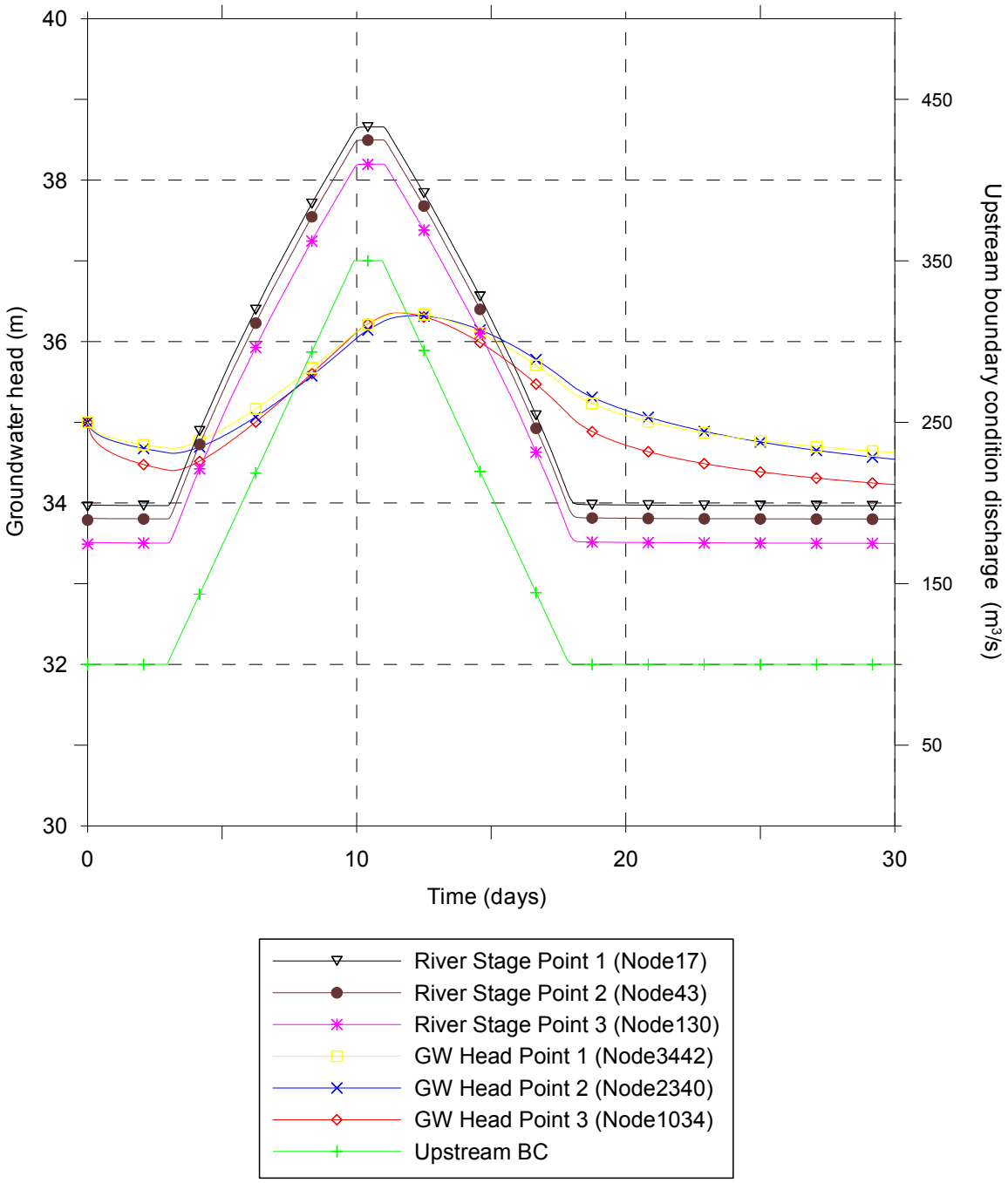

Figure 3.32. Groundwater head and river stage at various points in domain and river discharge at the upstream boundary in Run-2

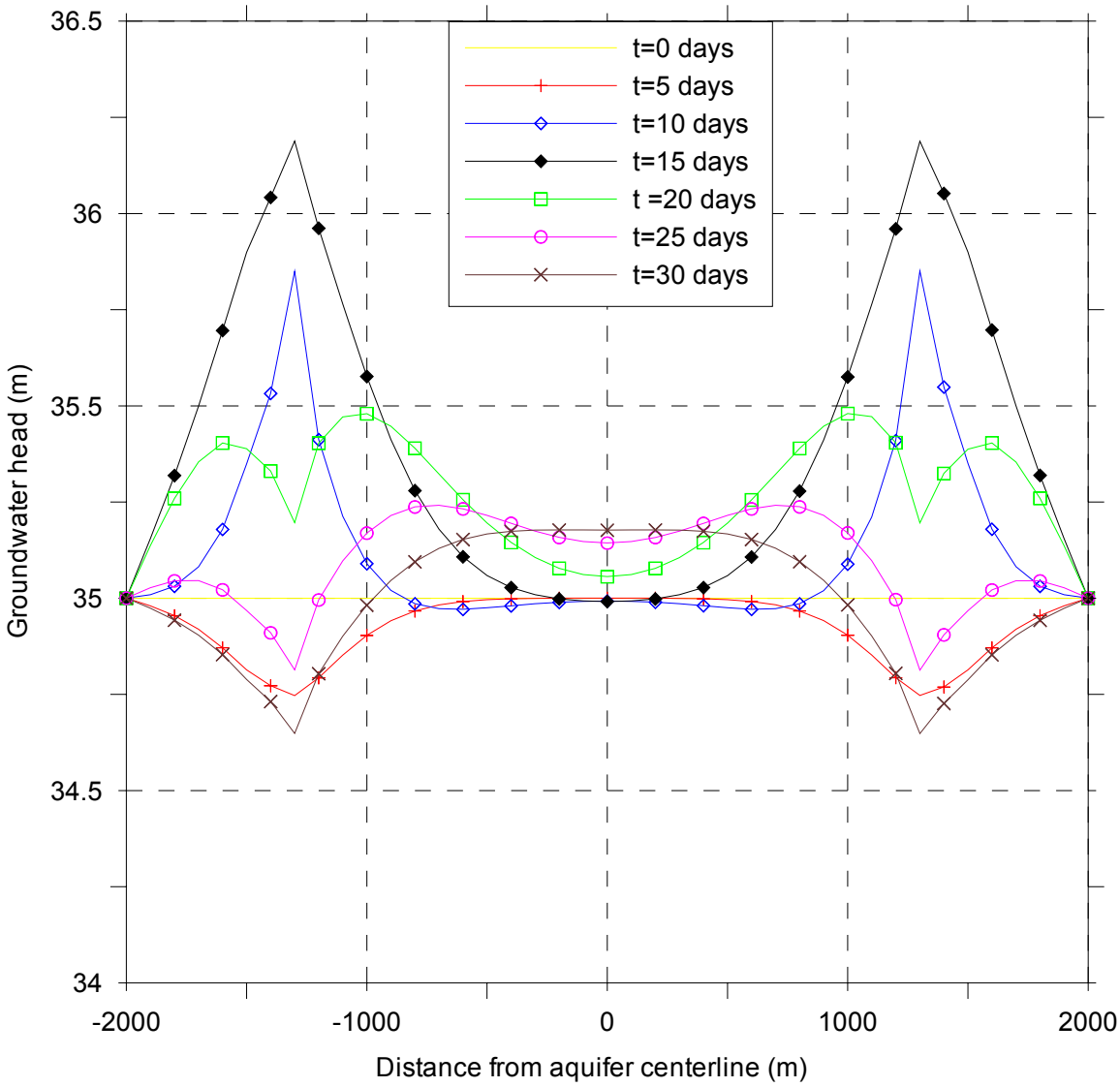

Figure 3.33. Groundwater head profiles at various times at transect-1 in Run-2

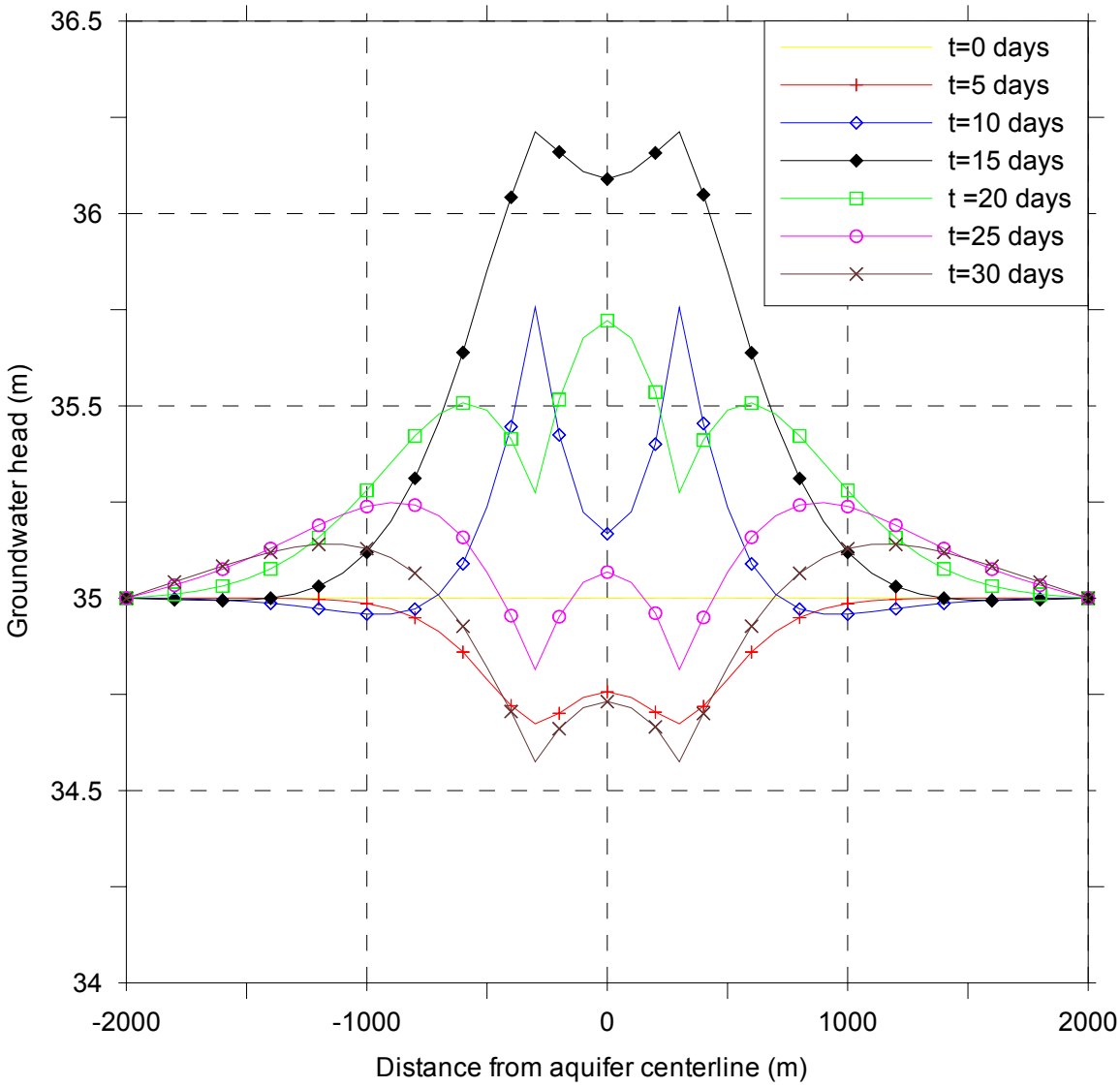

Figure 3.34. Groundwater head profiles at various times at transect-2 in Run-2

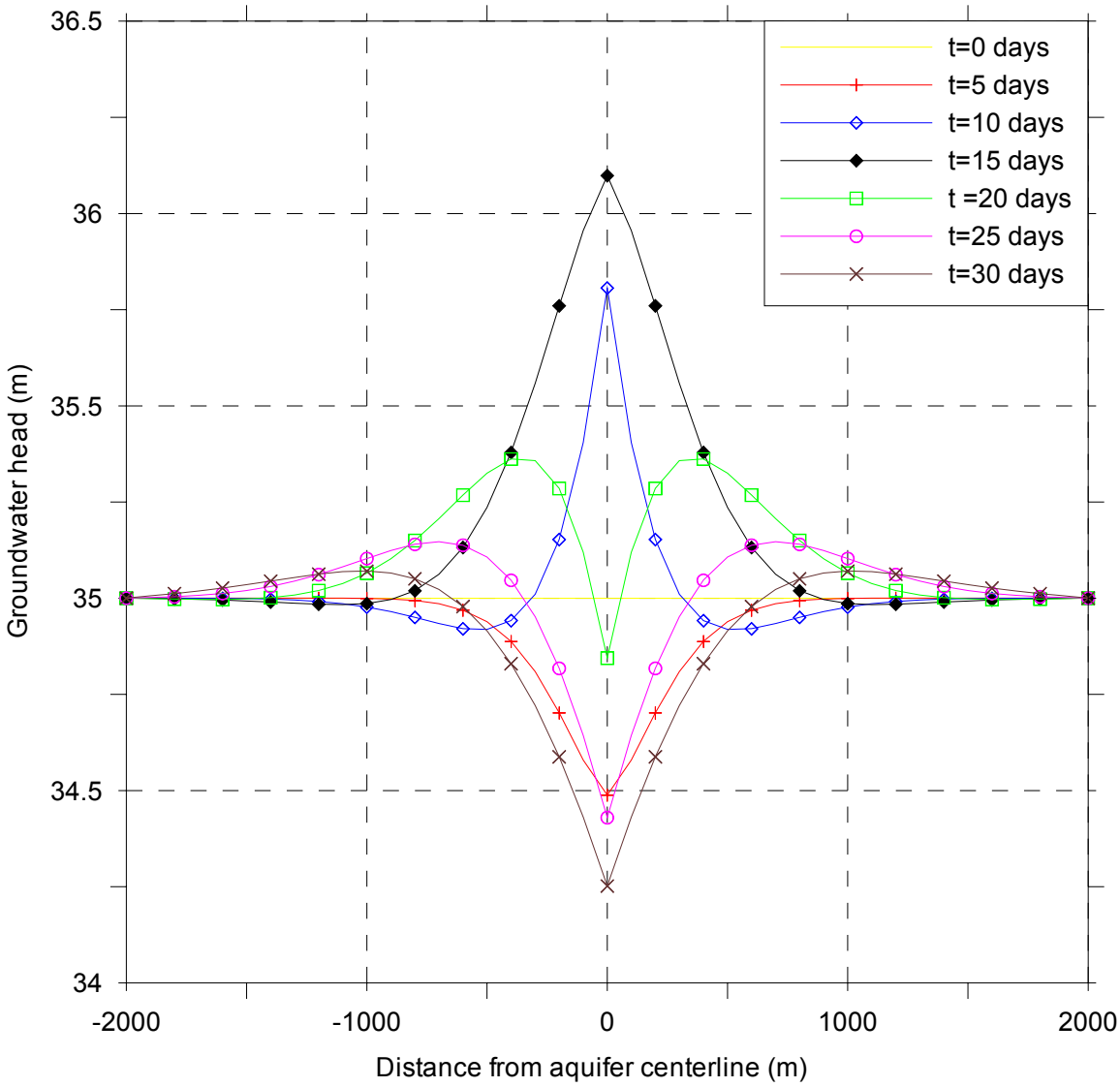

Figure 3.35. Groundwater head profiles at various times at transect-3 in Run-2

3.6. Coupled Surface-Subsurface Flow Model-2

In addition to the river bed interface, surface and subsurface flows are also linked at the ground surface which has the largest areal extent for surface-subsurface interactions. The ground surface serves as the first point-of-contact for the incoming meteorological input and is the place where it is distributed into various components. It essentially provides the medium for runoff generation which makes it an important part of the hydrologic cycle. Furthermore, if a saturated-unsaturated zone separation is made in groundwater flow, as has been done in this study, the water table would become another interface of importance to the hydrologist, where the unsaturated zone is divided from the saturated zone. In order to analyze the interactions between the overland flow zone, unsaturated groundwater flow zone and the saturated groundwater flow zone, a second coupled model is developed and presented in the following sections. This discussion closely follows the previous work of Gunduz and Aral (2003c).

3.6.1. Coupling at Ground Surface and Water Table

In this second coupled model, the infiltration/exfiltration flux between the overland flow and general groundwater flow domains provides the coupling mechanism at the ground surface and at the water table. A schematic of this model is shown in Figure 3.36. As seen from the figure, the overland flow domain is stacked on top of an unsaturated zone, which also lies above a saturated groundwater flow zone. This triple structure is dynamically linked at the ground surface and at the water table (Gunduz and Aral, 2003c).

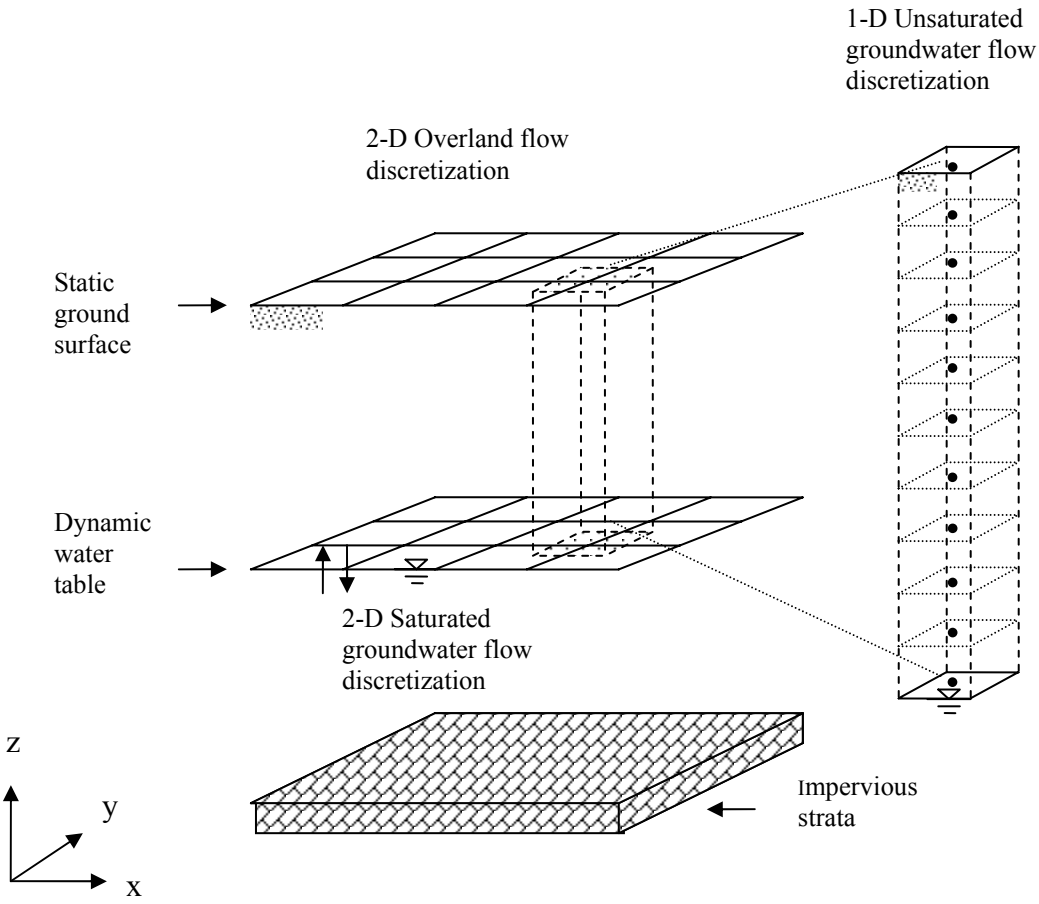

Figure 3.36. Coupling at ground surface and water table

As the groundwater flow domain is separated into a saturated and unsaturated zone, one should pay special attention to the interactions between these two systems. Depending on the moisture levels in the ground, the unsaturated zone may totally diminish if the water table rises to the surface. In this regard, while the overland flow and saturated groundwater flow domains exist continuously in this model, the presence and/or the extent of the unsaturated zone flow domain is a fully dynamic process and becomes a function of the corresponding hydrologic conditions over the land surface and below the water table. In essence, these dynamic conditions determine the existence of 'saturation from below' or "saturation from above" mechanisms of overland flow generation and represent the highly dynamic behavior of surface-subsurface flow interactions.

In the set up shown in Figure 3.36, the overland flow and saturated groundwater flow discretizations coincide in the two-dimensional horizontal domain such that an overland flow node and a saturated groundwater flow node are located at the same x-y position. The soil column between these two nodes is considered to be the one-dimensional unsaturated zone. Therefore, the overall discretization yields a total of N unsaturated columns, where N is the total number of overland or saturated groundwater nodes. In this formation, it is important to note that the unsaturated zone columns are disconnected from each other and there is no flux in the x- or y- directions. This approach is the foundation for the proposed quasi three-dimensional structure (Gunduz and Aral, 2003c). The alternative is a completely three-dimensional variably-saturated groundwater flow model coupled with the two-dimensional overland flow. In such a setup, the water table becomes a part of the solution and there is no deliberate separation between unsaturated and saturated groundwater flow zones. The three-dimensional groundwater

flow model is, however, not suitable for large scale watershed modeling applications due to computational limitations due to the large number of nodes required.

At the ground surface, the overland flow model is coupled with the unsaturated zone model via the infiltration/exfiltration flux. Depending on the relative magnitudes of potential infiltration and water supply rate (i.e., the sum of rainfall rate and overland flow depth expressed as a rate within a time step), the top boundary condition of the unsaturated zone is set as a specified head or specified flux. Therefore, the unsaturated zone top boundary condition of the coupled model possibly switches from a specified head condition to a specified flux condition or vice versa within the course of a simulation (Gunduz and Aral, 2003c). When a specified flux condition is used at the top boundary of the unsaturated zone, the same flux value is also directly used in the overland flow equation. On the other hand, if a specified head condition is required at the top boundary, then the corresponding flux is evaluated according to Darcy's law. The computed flux value is then used in the overland flow equation.

In a similar manner, the unsaturated and saturated zone groundwater flow models are linked to each other with the infiltration/exfiltration flux evaluated at the water table. In the setup shown in Figure 3.36, the bottom of the unsaturated zone is always fixed to be the water table. Hence, the boundary condition becomes a zero pressure head condition. The flux computed at the bottom of the unsaturated zone is then used as the infiltration/exfiltration term in the saturated groundwater flow equation (Gunduz and Aral, 2003c). When the groundwater table elevation increases or decreases, the corresponding unsaturated zone depth decreases or increases, respectively. Consequently, the unsaturated zone discretization must be adjusted to the growing/shrinking domain

size. This adjustment would require adding new nodes or removing existing nodes at the bottom of the domain when the water table moves down and up, respectively. In this regard, a sophisticated dynamic mesh update routine is integrated to the coupled model and the unsaturated zone mesh is updated at each time step of the simulation.

Although the initial idea was to implement the new simultaneous coupling idea in the solution of the current model, computational limitations became so severe that an iterative coupling idea had to be used. The unsaturated column between each overland/groundwater node couple increased not only the memory requirements of the model but also created extremely large matrices that were deemed impossible to solve within reasonable time frames. Consequently, the iterative coupling is used as an alternative solution method.

While one of the advantages of iterative coupling is the ability to use different time step sizes for each component of the model, the minimum time step requirement of all processes is used in solving all three components of the coupled model. Despite the increased run-times, this method is believed to better represent the influence of the highly dynamic behavior of the overland flow process on unsaturated zone flow process much. For all time steps, first the unsaturated zone model is solved for each column using the corresponding overland flow stage and groundwater head values from previous time step. As the spatial discretization in the unsaturated zone is updated at every time step according to the relative time-dependent positions of the water table, the domain is essentially constant within each time step. After obtaining the top and bottom fluxes from the unsaturated model, they are used as inputs to the overland and saturated groundwater models. Then, the overland and saturated groundwater flows are solved to find the

overland flow depths and aquifer heads. Once the depths and water table elevations are computed, they are re-substituted to the unsaturated zone boundary condition values to solve all unsaturated zone columns again. This procedure is continued iteratively until sufficient convergence is achieved between two consecutive values of overland flow depth and groundwater head. Typically, one to two iteration cycles are sufficient to reach a converged solution due to the relatively slow response times of the saturated groundwater flow (Gunduz and Aral, 2003c).

3.6.2. Model Testing

The coupled model is applied to a rectangular test plot to demonstrate the performance of the different model components and the interactions in between. In this application, a 40 m wide and 500 m long rectangular plane (Figure 3.37) with a slope of 0.001m/m in the longitudinal direction and 0.0 m/m in the transverse direction is used to model the response of a precipitation event shown in Figure 3.38. The response of the watershed is simulated for both sand and clay soils to demonstrate the effect of soil type on overland flow generation and groundwater recharge. The van Genuchten model parameters for both soils are taken from the statistically averaged values given by Carsel and Parrish (1988) and given in Table 3.2.

Table 3.2. Soil Hydraulic Parameters of Sand and Clay Soils (Carsel and Parrish, 1988)

	Saturation Water Content θ_s(-)	Residual Water Content θ_r (-)	Van Genuchten parameter α (cm^{-1})	Van Genuchten parameter n (-)	Saturated Conductivity K_s (cm/hr)
Sand	0.430	0.045	0.145	2.680	29.70
Clay	0.380	0.068	0.008	1.090	0.20

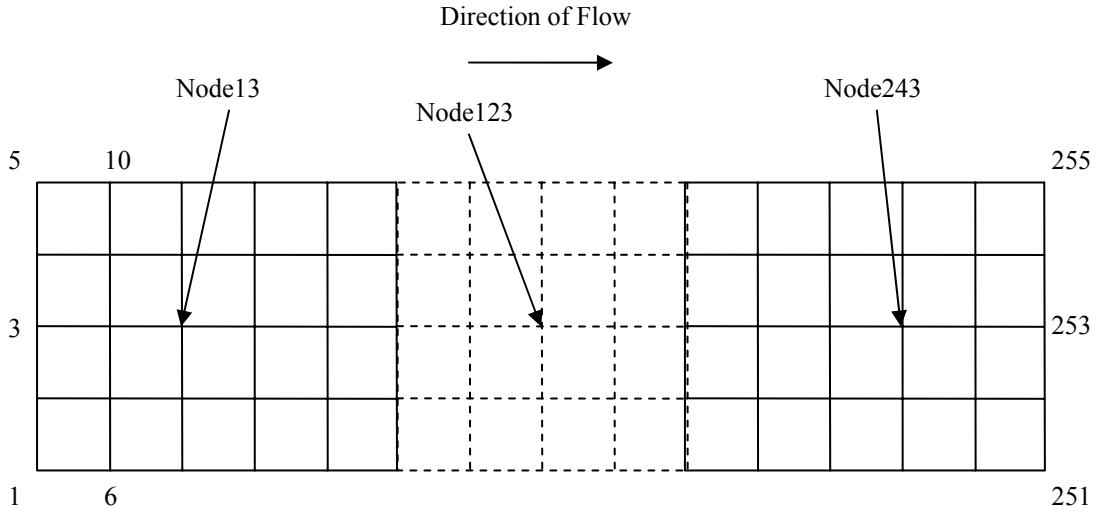

Figure 3.37. Test bed modeling domain in coupled model-2

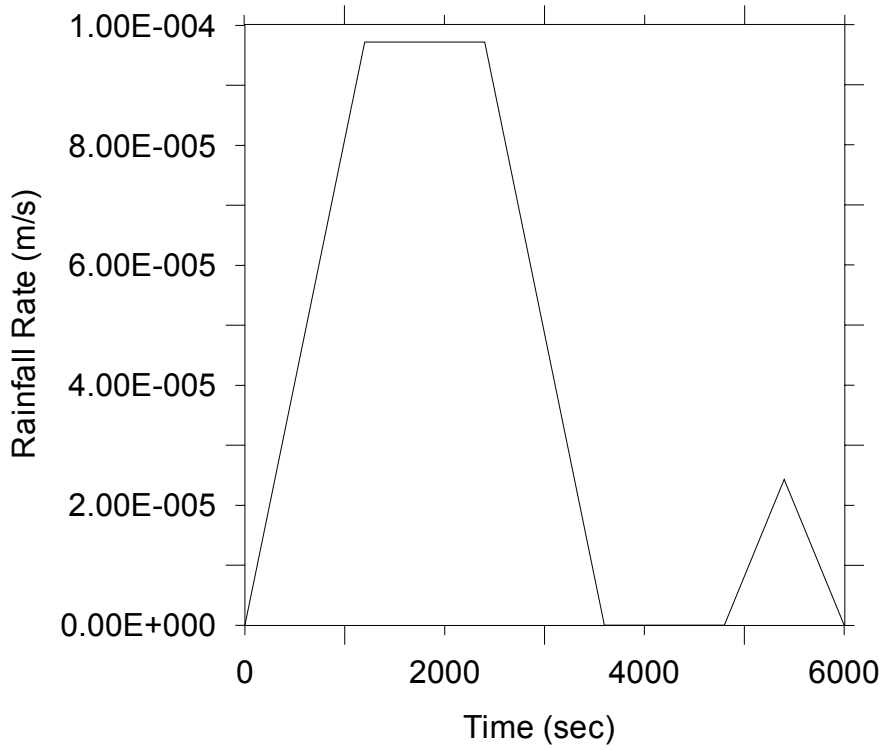

Figure 3.38. Precipitation event used in model

Both the overland and saturated groundwater domains are discretized by square quadrilateral elements of 10m side length creating a total of 200 elements and 255 nodes (Figure 3.37). Each of these 255 unsaturated soil columns is discretized with a vertical spacing of 1 cm but the number of nodes varied during the solution according to the relative surface and groundwater table elevations for each column.

In the overland flow model, critical depth conditions are used at the outflow side of the domain and no flux conditions are used along all other sides of the domain. An initial flow depth of 1.0E-4m is used to avoid numerical singularity for the first time step. In the saturated groundwater flow model, a fixed head condition is used beneath the outflow side of the overland flow model and no flux conditions are used at all other sides. A horizontal initial water table of 89.5 m is used in the simulation. The bottom boundary condition of the unsaturated zone is always taken to be a zero specified head condition at the water table. The top boundary condition, however, switches between a specified head and a specified flux condition depending on the presence of overland flow. An initial pressure head profile of -50 cm up to the capillary fringe of 3-4 cm is used to represent a moderately dry soil in all unsaturated soil columns. A constant time step of 1 sec is used in the simulation.

The following results are presented at three nodes (i.e., 13, 123, 243) in the two dimensional domain. These nodes represent an upstream, a midstream and a downstream point along the flow direction. The overland flow depth time series and the groundwater head time series of both soils are shown in figures 3.39 and 3.40, respectively. The unsaturated zone profiles at t=9000sec and t=18000sec of simulation are shown for nodes 13, 123 and 243 in figures 3.41, 3.42 and 3.43, respectively.

The simulations reveal that the selected rainfall event is intensive enough to create overland flow on both soil types. In the early stages of the simulation, the generated overland flow is governed by the saturation of the top soil layers and is therefore regarded as a "saturation from above" type overland flow. It is seen that the overland flow depths are larger in clay soils, which permits relative smaller amounts of infiltration compared to sandy soils. As seen from Figure 3.40, clay soil did not create any significant recharge to the groundwater since the hydraulic conductivity of clay is two orders of magnitude smaller than that of sandy soil. Consequently, considerable amounts of infiltration did not occur during the simulation period. On the other hand, it is seen from Figure 3.40 that sandy soil created significant recharge to the groundwater, particularly towards the downstream nodes where groundwater table reached very close to the surface. Hence, any further precipitation event will likely create a "saturation from below" type overland flow especially in down slope, lowland area. Particularly, the unsaturated zone profile of node 243 shown in Figure 3.43 demonstrates the fact that such lowland areas get saturated in a faster rate than the upland areas and create a potential recharge zone for the groundwater domain. This finding is consistent with the generally accepted overland flow generation mechanisms where highland areas mostly contribute to runoff via saturation from above and lowland areas are generally responsible for creating runoff via saturation from below (Dingman, 1994).

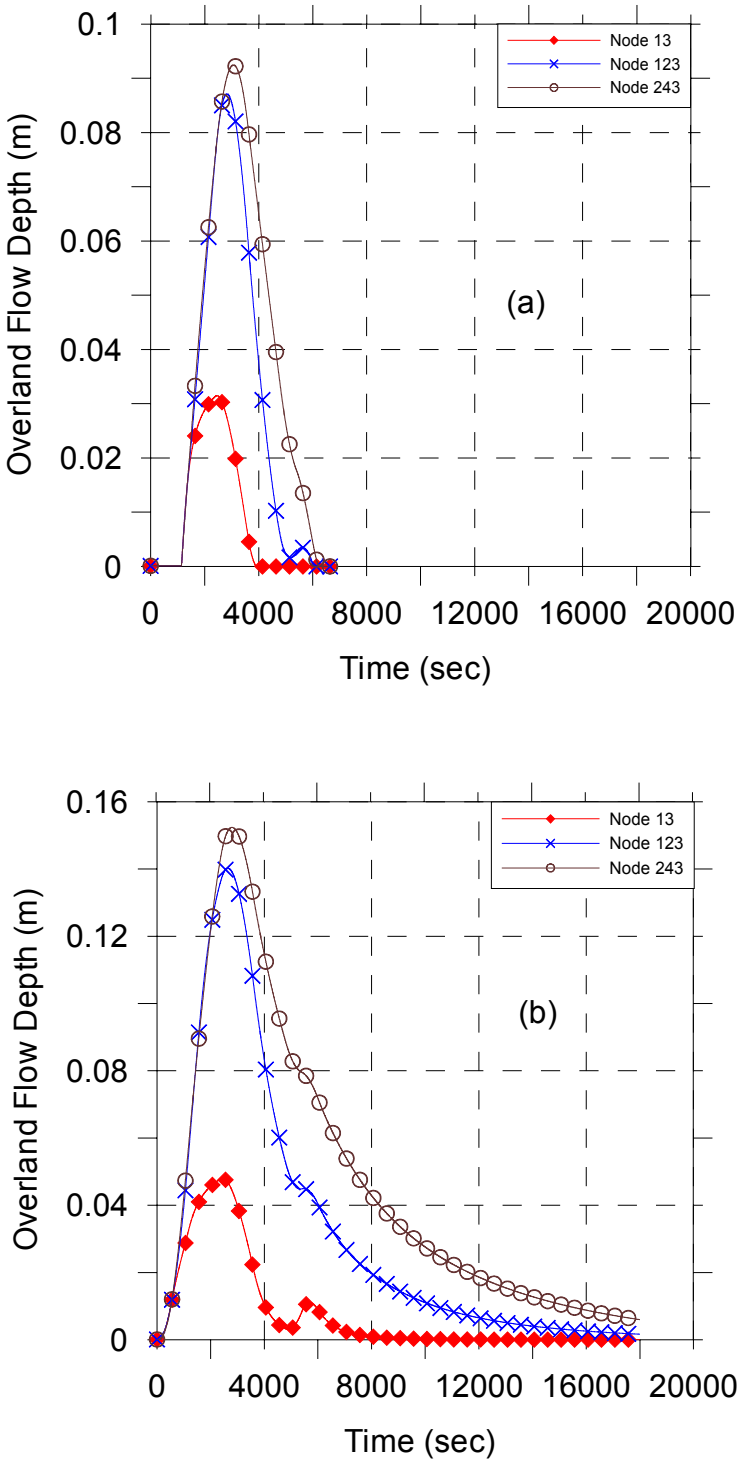

Figure 3.39. Overland flow depth time series in (a) sand and (b) clay soils at different nodes in the domain

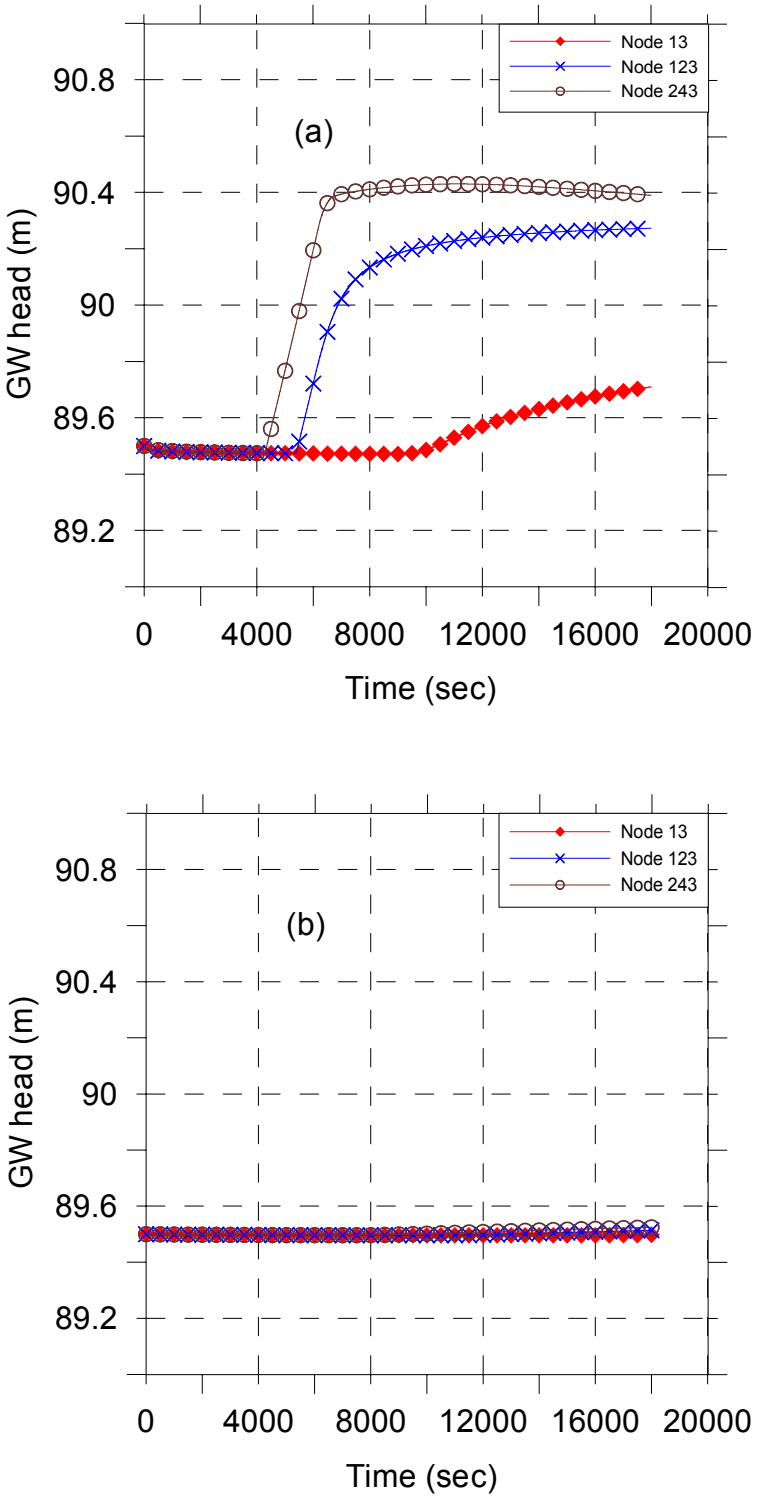

Figure 3.40. Groundwater head time series in (a) sand and (b) clay soils at different nodes in the domain

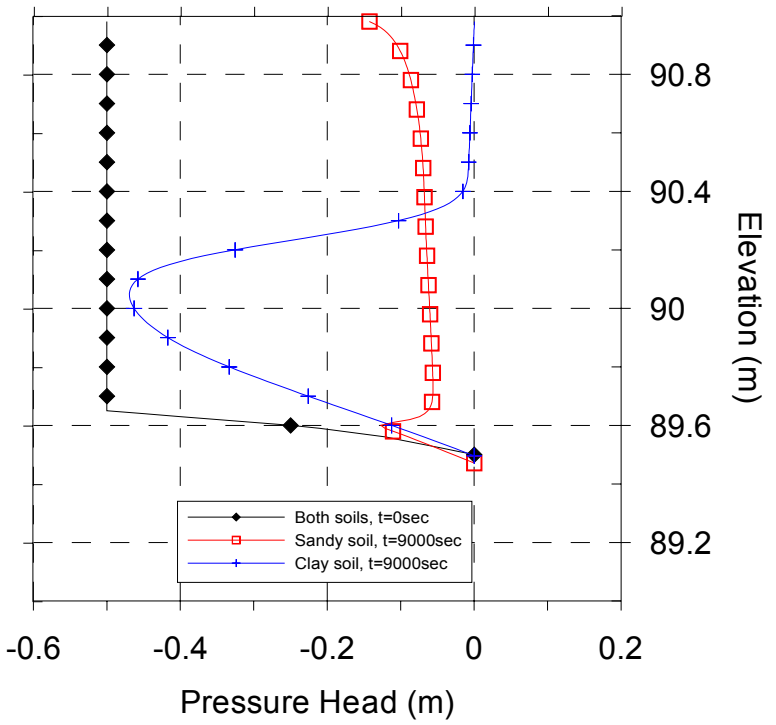

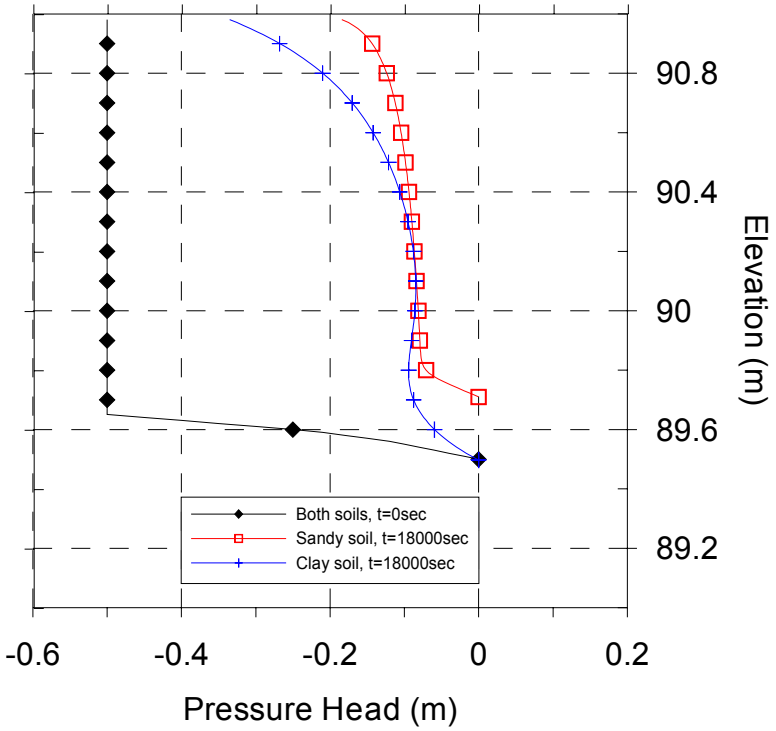

Figure 3.41.Unsaturated zone profiles of clay and sand soils at an upstream node (Node 13) at t=9000sec and t=18000sec

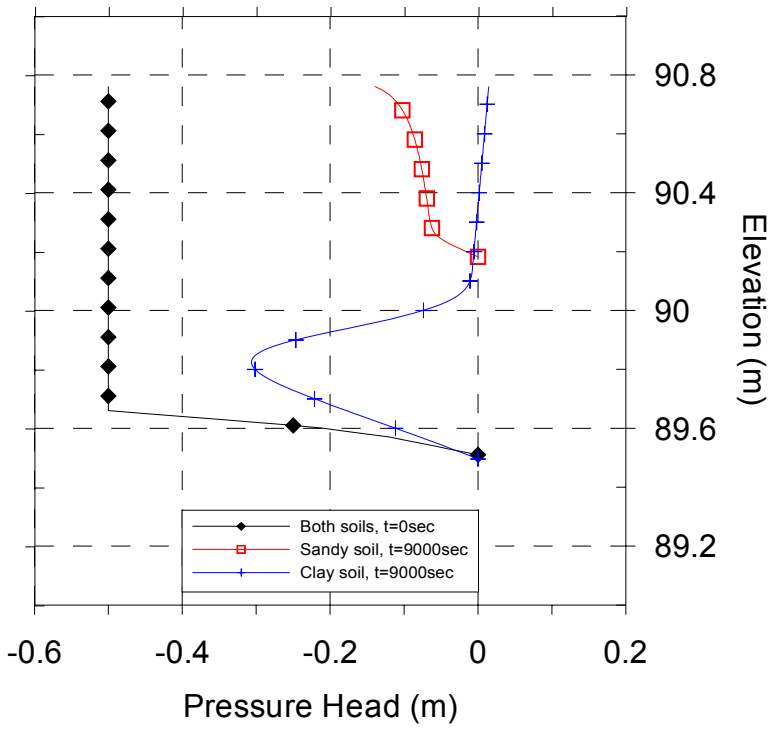

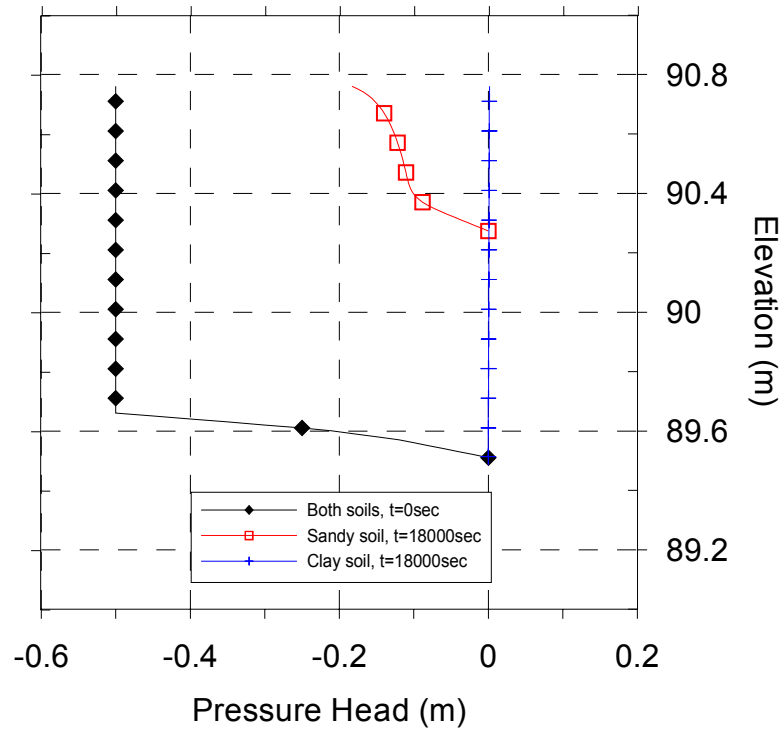

Figure 3.42.Unsaturated zone profiles of clay and sand soils at a midstream node (Node 123) at t=9000sec and t=18000sec

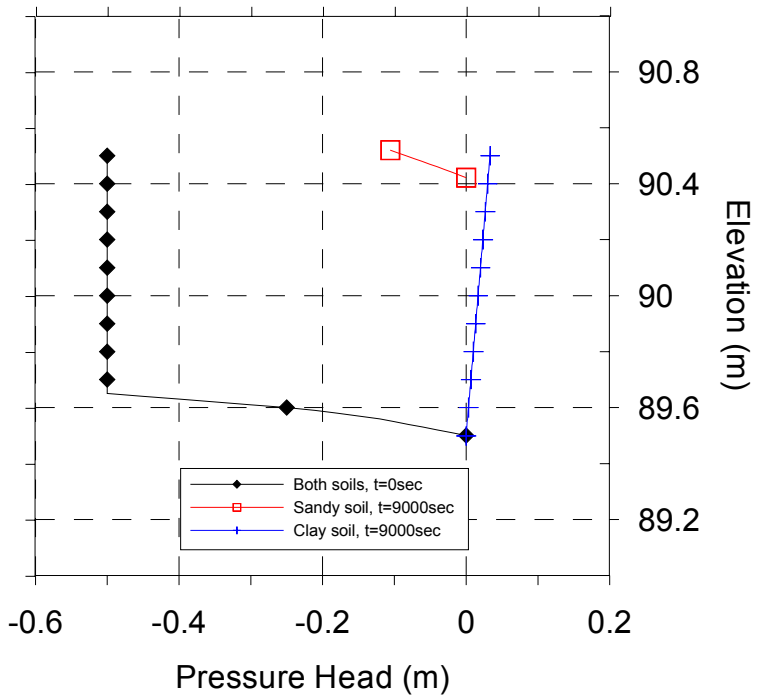

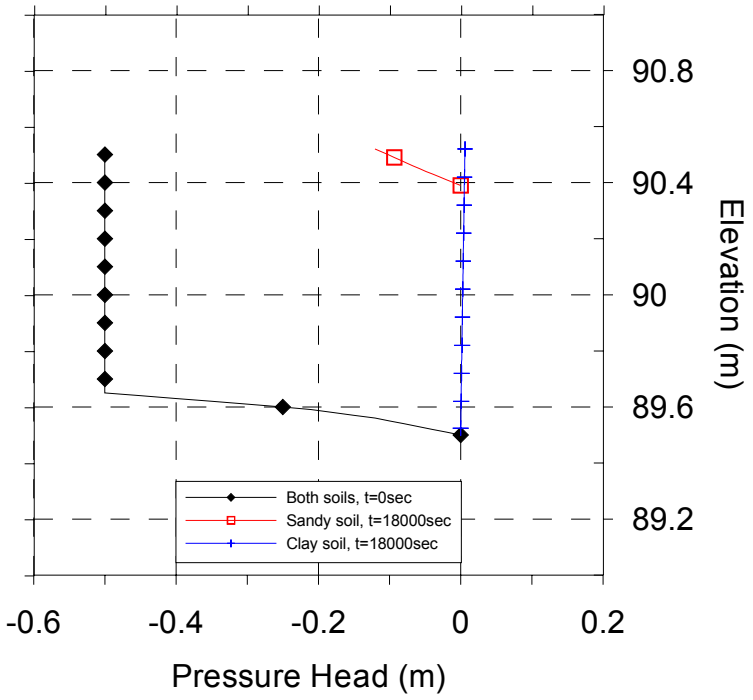

Figure 3.43. Unsaturated zone profiles of clay and sand soils at a downstream node (Node 243) at t=9000sec and t=18000sec

3.7. Analysis of Coupled Models

The sub-processes defining the hydrologic system are linked via the interfaces located at: (i) the groundwater table; (ii) ground surface; and, (iii) river bed. Of these, the river bed is the only interface which may have a certain thickness and may involve a sediment layer along the river bottom that may allow a delayed exchange between river and groundwater flow domains. All others are "zero-width" interfaces where water exchange occurs instantaneously. Although the river bottom sediment is considered to be a layered interface, it is assumed that the interactions occur instantly due to the relatively small thickness of the sediment layer. This assumption simplifies the overall coupling analysis (Aral and Gunduz, 2003).

An important aspect of integrating various sub-processes is the selection of the method applied to solve the matrix equations defining the system. Even though coupling via iterative solution and coupling via simultaneous solution are the most advanced levels of solving the sub-processes in an integrated fashion, iterative solution requires much smaller matrices to solve than the simultaneous solution. In iterative solutions, each sub-process model is integrated sequentially and solved separately by using the contributions from the other sub-processes. After each sub-model is solved, the common parameters linking these systems are checked for convergence (i.e., deviation from the previous iteration's solution). If the solutions of these common parameters are not sufficiently close, the procedure is repeated until the differences between subsequent solutions are below a pre-determined convergence criteria. This iterative coupling idea is slow, especially when more than two sub-processes are linked together. On the other hand this

approach would be less restrictive from the perspective of scaling concerns since each sub-process can possibly be analyzed within its own scale.

In the simultaneous solution approach proposed in this study, all sub-process models are solved together using a common time step. In this approach, all sub-model solution matrices are grouped into a single matrix structure and solved at once. Hence, this method requires the use of the smallest time step of all sub-models, which makes it impractical for the coupling processes requiring time steps from the two extremes (i.e., linking processes such as saturated groundwater flow and unsaturated groundwater flow). Attempting to solve such a system simultaneously results in very small time step requirements and creates numerical incompatibility between systems. On the other hand, this approach is more accurate than the iterative method since it does not involve improvement of the solution by iterating on the common parameters of the sub-models.

The wide array of time scales required to efficiently simulate the flow pathways is the most important problem of the watershed modeling. The incompatibility of the sub-process time scales makes the overall coupling of the system difficult and sometimes impractical. As described before, unsaturated flow numerically requires small time steps on the order of seconds to describe the vertical movement of moisture in the unsaturated domain, whereas the groundwater flow can be run with time steps on the order of days. If a simultaneous solution technique is used to couple these two systems, then the entire system would need to be run with the time step of the unsaturated zone. This condition is computationally costly and inefficient for the groundwater flow simulation. Moreover, including the entire unsaturated zone discretization to the overall matrix structure would simply make the matrix sizes impractical to solve with current computational power,

which is why the second coupled model discussed above is not solved with the simultaneous solution approach.

Nevertheless, regardless of the method used, it is the understanding of the author that coupling of a process requiring large time steps with a process requiring small time steps over a large watershed application is still not practical with the current level of computational power. Small time step requirements of certain processes including the unsaturated zone and overland flow zone practically create very large simulation times to simulate watershed scale events (i.e., large areal extent and long temporal periods). When this is the case, certain engineering judgments are to be made to either simplify or totally neglect the processes that create the bottle neck. Although these judgments might violate the proper representation of the system, it would still allow the modeler to gain an insight of the system with optimal model performance. It is believed, without these shortcuts, large scale watershed modeling is still not feasible when distributed models are used in sub-process modeling and non iterative solution processes are selected in solving the integrated model.

The problem of spatial scale compatibility between models is not as significant as the problem of time scale compatibility, discussed above. The spatial scale compatibility becomes most significant within the simultaneous solution framework where sub-processes must be discretized to have common nodes. In the first model discussed above (i.e., coupled river/groundwater flow model), the system is composed of a common set of nodes representing the river discretization, which are also a member of the unconfined aquifer discretization. The corresponding dependent variables of both models (i.e., river water surface elevation and the groundwater head) at these nodes essentially perform the

simultaneous coupling. While the iterative coupling method does not require having common nodes, it would still be more convenient for the modeler to work with two dependent variables at the same point without the need to go through the task of interpolation.

The situation is much worse in the second coupled model discussed above (i.e., coupled overland flow/unsaturated zone/saturated zone model). Similar spatial scale compatibility issues become more pronounced within the solution of this model. Coinciding overland and saturated groundwater nodal points are used to effectively link the vertical distance between the groundwater table and ground surface with an unsaturated zone model with variable nodal points. The coinciding nature of nodal points is required to have an unsaturated zone in between and to guarantee correct volume balance within the unsaturated zone model. However, it is impractical to use the many discretized unsaturated zone nodes between each node-couple of overland/saturated zone model and solve a huge system matrix at each time step, a simultaneous solution algorithm is definitely not the method of choice with current level of computer speed.

3.8. Hybrid Model

The analysis of the two coupled models reveals some key features that have to be addressed for accurate understanding of the system. The problems associated with the scales of sub-processes and their coupled counterparts are probably the most significant difficulty in integrated watershed modeling. As shown in sections 3.5 and 3.6, it is theoretically possible to couple all processes if computational cost is not an issue. However, for large scale applications such as catchment modeling, the small scale

requirements of overland and unsaturated zone flow domains exhibit severe limitations on efforts in fully integrating the system (Aral and Gunduz, 2003). Furthermore, the issues discussed in Chapter 2 further complicate the large scale applications of both overland and unsaturated zone flow modeling. Consequently, a hybrid modeling approach is proposed in this study in which distributed and lumped parameter models are essentially linked and blended to obtain a semi-distributed watershed model. In such models, the overland flow and unsaturated zone models are replaced with their lumped parameter empirical counterparts in an effort to simplify the overall analysis. When issues like computational limitations, proper mathematical formulation of physical processes and data requirements are addressed accurately and sufficiently, these systems would be included in the analysis as shown in sections 3.5 and 3.6.

CHAPTER 4

COUPLED CONTAMINANT TRANSPORT MODEL

In this chapter, a coupled contaminant transport model that is based on the proposed hybrid flow model given in Chapter 3 is presented. The coupled contaminant transport model is one of the earliest attempts to model multi-pathway contaminant transport phenomena. It essentially links the surface and subsurface transport processes and couples them in a semi-simultaneous manner. The difficulties associated with the numerical solution of the advection dispersion equation would presently not allow fully simultaneous coupling of these transport processes.

4.1. One Dimensional Channel Transport Model

4.1.1. Governing Equations

The mathematical model of the one-dimensional channel contaminant transport is given by the mass conservation equation, including extra terms for lateral mass contribution from overland and seepage flows. As the contribution from seepage flows is not considered in previous studies, this study can be considered as a first attempt to

incorporate the impact of subsurface transport on surface transport of contaminants. In addition, the following governing equation not only considers the effect of advective seepage transport but also formulates a dispersive component of transport as a first order Fickian process over the thickness of the river bed. With these additions, the one-dimensional advection-dispersion equation in channel flow can be written by using a control volume approach and presented in the following conservation form:

$$\frac{\partial (C_r A)}{\partial t} + \frac{\partial}{\partial x}(VAC_r) - \frac{\partial}{\partial x}\left(AD_L \frac{\partial C_r}{\partial x} \right) + kC_r A - q_{L1} C^*_{L1} + \; n_{sed} D_{sed} \frac{C_g - C_r}{m_r} w_r - q_{L2} C^*_{L2} = 0 \quad (4.1)$$

where x is the longitudinal coordinate representing the distance along the channel, t is the temporal coordinate, C_r is the contaminant concentration in the channel, A is flow area, V is the cross-sectionally averaged flow velocity, D_L is the longitudinal dispersion coefficient in the channel, k is the decay coefficient, q_{L1} and q_{L2} are the lateral seepage and overland flows per channel length (positive for inflow and negative for outflow), C^*_{L1} and C^*_{L2} are the contaminant concentration associated with lateral seepage and overland flows, respectively, n_{sed} is the porosity of the sediment layer, D_{sed} is the vertical dispersion coefficient in the sediment layer, m_r is the thickness of the sediment layer and w_r is the wetter perimeter of the river. It is important to note that the values of C^*_{L1} and C^*_{L2} change according to the direction of the lateral flow terms such that when lateral flow is towards the channel (i.e., inflow to the channel), these values take the associated concentrations coming from the groundwater (i.e., C_g) and overland flow domains (i.e., C_o) whereas they become the concentration in the channel (i.e., C_r) when the lateral flow is away from the channel (i.e., outflow from the channel):

$$C_{L1}^{*} = \begin{cases} C_r & when \quad q_{L1} < 0 \\ C_g & when \quad q_{L1} > 0 \end{cases} \tag{4.2}$$

$$C_{L2}^{*} = \begin{cases} C_r & when \quad q_{L2} < 0 \\ C_o & when \quad q_{L2} > 0 \end{cases} \tag{4.3}$$

The value of the longitudinal dispersion coefficient is an important parameter in the overall distribution of the contaminant within the channel network. It may become the major transport mechanism in mildly moving or stagnant sections of the channel such as ponds or small tributary inflow sites to the main channel. Although the ideal way to obtain the value of the longitudinal dispersion coefficient is to perform tracer tests, it is only available for selected reaches of only a small number of rivers. Therefore, water quality modelers often use empirical formulations that are mainly based on the easily measured hydraulic and channel characteristics. Following the early works of Taylor (1954) and Elder (1959), numerous researchers including Fischer (1966, 1968, 1975, 1979), McQuivey and Keefer (1974), Liu (1977) and Aral et al. (1980) have developed methods to estimate the longitudinal dispersion coefficient. Their efforts were later followed by Magazine et al. (1988), Iwasa and Aya (1991), Kousis and Rodriguez-Mirasol (1998), Seo and Cheong (1998), Deng et al. (2001) and Kashefipour and Falconer (2002), who have also developed both semi-analytical and empirical equations for estimating the longitudinal dispersion in river channels. Despite the vast amount of published work, there is no globally accepted formulation that is used extensively. In this study, the most recent study conducted by Kashefipour and Falconer (2002) is implemented. They have analyzed the available data via regression analysis and proposed

their version of an empirical formula for the longitudinal dispersion coefficient that can be written as:

$$D_L = 10.612\left(\frac{V}{V^*}\right)Vd \tag{4.4}$$

where d is the water depth in the channel and V^* is the shear velocity defined as:

$$V^* = \sqrt{gR_hS_f} \tag{4.5}$$

They have obtained a coefficient of determination value of 0.84 for a data set including more than 30 major rivers in the United States. Following comparisons with the results obtained from Seo and Cheong's equation (Seo and Cheong, 1998), they choose to combine the two equations in a linear manner to estimate the longitudinal dispersion coefficient more accurately. By comparison of predicted vs. measured dispersion coefficients, they proposed the following form of the equation as their second formulation for dispersion coefficient:

$$D_L = \left[7.428 + 1.775\left(\frac{B}{d}\right)^{0.620}\left(\frac{V}{V^*}\right)^{0.572}\right]\left(\frac{V}{V^*}\right)Vd \tag{4.6}$$

Upon further investigation with the two alternative forms, Kashefipour and Falconer (2002) recommended the use of the first equation for open channel flows with width to

depth (i.e. B/d) ratios in excess of 50 and the use of second equation for open channel flows with width to depth ratios less than 50.

4.1.2. Initial Conditions

In order to start the transient solution, initial values of the contaminant concentration are to be specified along the one-dimensional channel domain such that:

$$C_r\left(x,0\right) = C_{ro}\left(x\right) \tag{4.7}$$

where C_{ro} is the initial concentration distribution along the channel network.

4.1.3. Boundary Conditions

Similar to the one-dimensional channel flow model, the contaminant transport model also have two different types of boundary conditions specified at (i) external; and, (ii) internal boundaries of the domain. The external boundary conditions are given at the most upstream and downstream points of the channel network, whereas the internal boundary conditions are specified at internal junction points of the channel network.

4.1.3.1. External Boundary Conditions

In this study, the contaminant transport model can accommodate several upstream boundary conditions and a single downstream boundary condition. Thus, the model does not solve looped channel networks. At any upstream boundary, a specified concentration time series can be used as the boundary condition. The concentration time series is either

available from continuous measurement (i.e., specified concentration) or from simple contaminant mass loading computation (i.e., specified mass flux):

$$C_r(0,t) = C_{ru}(t) = \frac{M(t)}{Q(t)} \tag{4.8}$$

where *M(t)* is the mass loading rate from some upstream source, *Q(t)* is the river flow at the upstream boundary and C_{ru} is the corresponding upstream boundary concentration time series. At the downstream boundary, a zero concentration gradient is generally used as the boundary condition when the boundary is far away from the contaminant zone:

$$A D_L \left.\frac{\partial C_r}{\partial x}\right|_{x=L_d} = 0 \tag{4.9}$$

which states that advection dominates at the outflow and the contaminant propagates out of the domain unhindered. When the boundary is not far and the outflow concentration is measured, a specified total mass flux, *f*, is used as the downstream boundary condition:

$$QC - A D_L \left.\frac{\partial C}{\partial x}\right|_{x=L_d} = f \tag{4.10}$$

4.1.3.2. Internal Boundary Conditions

Any two or more channels intersecting within a channel network forms a junction where internal boundary conditions are specified to satisfy the contaminant mass balance.

In this study, the proposed contaminant transport model follows its flow counterpart and does not allow for looped networks. Hence, it requires that there is always a single outflow channel from a junction. The mass balance equation at a junction can then be specified as:

$$\sum_{k=1}^{m} A_k J_k - A_o J_o = \frac{dM}{dt} \tag{4.11}$$

where m is the total number of inflowing channels to the junction, J_k and A_k are the total mass flux and the area at the end of the k^{th} inflowing channel to the junction, J_o and A_o represent the total mass flux and the area at the beginning of the outflowing channel from the junction, and dM/dt corresponds to the change in mass within the junction. Following the basic assumption applied in many modeling applications, the change in mass storage within a junction is assumed to be negligible compared to the change in mass within in a channel. Consequently, the mass balance equation can be written as:

$$\sum_{k=1}^{m} A_k J_k - A_o J_o = 0 \tag{4.12}$$

Furthermore, the continuity of concentration at the junction guarantees that all the concentrations must be equal to each other at the junction:

$$(C_r)_k = (C_r)_o \qquad k = 1,2,\ldots,m \tag{4.13}$$

4.1.4. Numerical Solution Scheme

There are numerous numerical solution techniques for solving the advection-dispersion equation. These techniques can be classified as: (i) Eulerian methods, including finite difference, finite element or finite volume methods; (ii) Lagrangian methods; and, (iii) Hybrid methods. When the limitations of these methods discussed in Chapter 2 are considered, it is tempting to use fixed grid methods for the solution of the advection-dispersion equation. One of the key criteria behind this selection lies in the fact that the flow model that would supply the necessary flow data to the contaminant transport model is based on an Eulerian framework. Therefore, information obtained from the flow model at fixed points can best be used in the transport model at the same grid points. Hence, the one-to-one correlation of flow and transport model discretizations greatly simplifies the implementation of the contaminant transport model and possibly increases its accuracy since it would not require unnecessary interpolations that would otherwise be inevitable. Furthermore, systematic modeling of complex channel networks is still only viable with fixed-grid methods.

Based on this discussion, the advection-dispersion equation describing the transport of contaminants in a river channel is solved using a fixed grid control-volume finite difference scheme. In the context of this scheme and similar other fixed grid methods, it is widely accepted by the numerical modeler that the dispersion component of the equation could generally be solved without any problems using a variety of schemes. The problem generally arises from the advection component of the equation, particularly for highly advective transport of contaminants with sharp fronts, where the numerical methods start to lose accuracy and computational efficiency. While dispersion favors

implicit solution algorithms with possible use of large time steps, advection modeling generally utilizes an explicit algorithm with time steps limited by the Courant number criteria. Hence, the two major contaminant transport processes essentially behave in a contradictory manner. Since dispersion modeling could also be done with an explicit algorithm, a fully explicit scheme for the entire advection-dispersion equation is possible. However, such a scheme would not allow a simultaneous solution for the transport equation in a river with the transport equation in groundwater and is not favorable for this study. Rather, the matrix solution of implicit schemes is necessary to simultaneously solve the two transport systems. The only exception to this setup would be the problematic advection component of the river transport that should be solved using an explicit scheme. It is this motivation that forces to separate the two processes and solve them in two steps. Using a fairly recent development in the area that results in the formulation of the so-called 'split operator' approach, one can now separate the advection operator from the dispersion and the rest of the operators and solve them using the most suitable scheme possible for each operator. Although this approach appears to be a violation of the principle of "simultaneous presence" of these processes in nature, it provides a very powerful technique to handle the numerical difficulties associated with each particular operator. Essentially, this procedure provides a sound methodology that gives mathematically identical results to the traditional compact operator methods. Consequently, one could discretize the equation by evaluating the advection term explicitly in time and the remaining terms implicitly in time. The discretized form of the equation would then become:

$$(C_rA)_i^{j+1} = (C_rA)_i^j + \Delta t\left[-\frac{\partial}{\partial x}(VAC_r)\right]^j + \Delta t\left[\frac{\partial}{\partial x}\left(AD_L\frac{\partial C_r}{\partial x}\right) - kC_rA + q_{L1}C_{L1}^* - n_{sed}D_{sed}\frac{C_g - C_r}{\Delta z}w_r + q_{L2}C_{L2}^*\right]^{j+1} \quad (4.14)$$

which gives cell-average values of (C_rA) in each control volume, i, at the future time line j+1, based on the cell-average values of (C_rA) in each control volume at the current time line j, as well as the mass influx and outflux to/from the control volume. The square brackets represent some form of spatial discretization. Since the advection term is treated explicitly, the equation may be rewritten in two substeps without compromising the algorithmic integrity:

$$(C_rA)_i^* = (C_rA)_i^j + \Delta t\left[-\frac{\partial}{\partial x}(VAC_r)\right]^j \quad (4.15)$$

$$(C_rA)_i^{j+1} = (C_rA)_i^* + \Delta t\left[\frac{\partial}{\partial x}\left(AD_L\frac{\partial C_r}{\partial x}\right) - kC_rA + q_{L1}C_{L1}^* - n_{sed}D_{sed}\frac{C_g - C_r}{\Delta z}w_r + q_{L2}C_{L2}^*\right]^{j+1} \quad (4.16)$$

In essence, this procedure of splitting the operators first allows the fluid to advect for a time step, and then lets it disperse and decay in its new advected location. With this approach, it is possible to use a suitable solution scheme for advection and other operators. In this regard, the highly accurate Quadratic Upstream Interpolation for Convective Kinematics with Estimated Streaming Terms (QUICKEST) algorithm could be used to model the advection operator, while the dispersion operator is discretized with a standard central difference scheme. The remaining terms are just algebraic terms

evaluated at the $(j+1)^{th}$ time line. The details associated with the discretizations of the advection operator with the QUICKEST scheme and the dispersion operator with the central difference scheme are given in Appendix J. The formulations of the boundary conditions as well as the treatment of the junctions are also given in this appendix. Using the formulations given in the appendix, the channel transport equation becomes:

$$\begin{aligned}\left(C_r A\right)_i^{j+1} &= \left(C_r A\right)_i^{*} \\ &+ \frac{\Delta t}{0.5\left(\Delta x_{i-1} + \Delta x_i\right)}\left[\left(A_f^{j+1}\left(D_L\right)_f \frac{\left(C_r\right)_{i+1}^{j+1} - \left(C_r\right)_i^{j+1}}{\Delta x_i}\right) - \left(A_b^{j+1}\left(D_L\right)_b \frac{\left(C_r\right)_i^{j+1} - \left(C_r\right)_{i-1}^{j+1}}{\Delta x_{i-1}}\right)\right] \\ &+ \Delta t\left[\begin{array}{l} -k\left(C_r\right)_i^{j+1} A_i^{j+1} + \left(q_{L1}\right)_i^{j+1}\left(C_{L1}^{*}\right)_i^{j+1} \\ \qquad -\left(n_{sed} D_{sed}\right)_i \dfrac{\left(C_g\right)_i^{j+1} - \left(C_r\right)_i^{j+1}}{\Delta z}\left(w_r\right)_i^{j+1} + \left(q_{L2}\right)_i^{j+1}\left(C_{L2}^{*}\right)_i^{j+1} \end{array}\right]\end{aligned} \tag{4.17}$$

where $(C_rA)^*$ is the result of the advection operator using the explicit QUICKEST algorithm as given in Appendix J.

4.1.5. Model Testing

The one-dimensional channel contaminant transport model is tested against the available analytical solutions in a single channel framework. Since there are no analytical solutions that define the transport of contaminants in a channel network, model testing of contaminant transport in channel networks is performed by a number of supplementary tests for various hypothetical conditions of pure advection and pure dispersion.

The single channel verification of the proposed channel contaminant transport model is done with the exact solution originally developed by Ogata and Banks (1961)

and later modified by Bear (1972) and van Genuchten and Alves (1982). The original one-dimensional mathematical model is written as:

$$\frac{\partial C_r}{\partial t} + V\frac{\partial C_r}{\partial x} - D_L\frac{\partial^2 C_r}{\partial x^2} + kC_r = 0 \tag{4.18}$$

that defines not only the advective-dispersive transport but also the first order decay of contaminants in a simple channel. The initial and boundary conditions of the problem can also be given as:

$$\begin{aligned} &C_r(x,0) = C_o && for && x \geq 0 \\ &C_r(0,t) = \begin{cases} C_{ru} & for \quad 0 < t < t^* \\ 0 & for \quad t \geq t^* \end{cases} \\ &\frac{\partial C_r}{\partial x}(\infty,t) = 0 && for && t \geq 0 \end{aligned} \tag{4.19}$$

which defines the conditions for a continuous source of a finite duration, t*. The analytical solution of this problem for conservative species (*k=0*) can then be written as:

$$C_r(x,t) = \begin{cases} C_o + (C_{ru} - C_o)\,A(x,t) & 0 < t \leq t^* \\ C_o + (C_{ru} - C_o)\,A(x,t) - C_{ru}A(x,t-t^*) & t > t^* \end{cases} \tag{4.20}$$

where:

$$A(x,t)=\frac{1}{2}erfc\left(\frac{x-Vt}{\sqrt{4D_Lt}}\right)+\frac{1}{2}\exp\left(\frac{Vx}{D_L}\right)erfc\left(\frac{x+Vt}{\sqrt{4D_Lt}}\right) \tag{4.21}$$

For non-conservative species ($k\neq0$), the solution is slightly modified as:

$$C_r(x,t)=\begin{cases}C_oA(x,t)+C_{ru}B(x,t) & 0<t\le t^*\\ \\ C_oA(x,t)+C_{ru}B(x,t)-C_{ru}B(x,t-t^*) & t>t^*\end{cases} \tag{4.22}$$

where the functions A(x,t) and B(x,t) are defined as:

$$A(x,t)=\exp(-kt)\left[1-\frac{1}{2}erfc\left(\frac{x-Vt}{\sqrt{4D_Lt}}\right)-\frac{1}{2}\exp\left(\frac{Vx}{D_L}\right)erfc\left(\frac{x+Vt}{\sqrt{4D_Lt}}\right)\right] \tag{4.23}$$

$$B(x,t)=\frac{1}{2}\exp\left(\frac{Vx}{2D_L}(1-\Gamma)\right)erfc\left(\frac{x-Vt\Gamma}{\sqrt{4D_Lt}}\right)+\frac{1}{2}\exp\left(\frac{Vx}{2D_L}(1+\Gamma)\right)erfc\left(\frac{x+Vt\Gamma}{\sqrt{4D_Lt}}\right) \tag{4.24}$$

The term Γ in function B(x,t) is given as:

$$\Gamma=\sqrt{1+\frac{4kD_L}{V^2}} \tag{4.25}$$

To test the proposed model with the analytical solution given above, a hypothetical rectangular channel domain is created so that steady uniform flow will prevail in the channel at all times. A constant discharge of $10m^3/s$ is passed through a

10000m long rectangular channel that has a base width of 20m. The channel lies on a 0.001m/m bed slope and carries the discharge at a uniform depth of 0.5m with a constant velocity of 1m/s. Initially, the channel is assumed to contain no contaminants. A constant specified concentration boundary condition of 1mg/L is implemented at the upstream boundary of the channel. The contaminant is allowed to advect, disperse and/or decay within the channel as a function of time. The results of numerical simulations and analytical solutions are compared in figures 4.1 through 4.6.

In the first set of tests, the basic transport characteristics of the contaminant are analyzed and the decay of the contaminant is not allowed. Three different tests are performed with different dispersion coefficients representing (i) an essentially pure advection flow with very low dispersion (D_L=1.0E-8 m^2/s); (ii) a medium dispersion (D_L=30 m^2/s) flow; and, (iii) a high dispersion (D_L=100 m^2/s) flow. The numerically simulated vs. analytically computed results are compared in figures 4.1, 4.2 and 4.3. In the first test shown in Figure 4.1, a very small amount of dispersion is allowed and the contaminant transport is mainly an advection dominated event. It can be seen that the pattern and timing of the sharp front is properly captured with the proposed model in three different positions in time. Hence, it is possible to conclude that the model can accurately simulate advection dominated contaminant transport. The second test is performed with a moderate amount of dispersion representative of most of the flow patterns found in nature. As seen at all three times presented in Figure 4.2, the simulated results are either identical or very close to the analytical solution. Therefore, it can be concluded that the proposed model accurately captures the expected advection and dispersion patterns of the contaminant plume. Finally in the third test, simulations are

performed with a significantly high dispersion value. The dispersion coefficient is so high that the plume shows a ±3000m deviation from its center of gravity (Figure 4.3). Similar to the previous two tests, the comparison of simulated and calculated results also reveals an excellent fit and demonstrates the prediction power of the proposed model.

In the second set of tests, the basic transport characteristics of the contaminant are analyzed under the influence of contaminant decay. Three different tests are performed with different dispersion and decay coefficients representing (i) a high decay rate in an essentially pure advection flow (k=3.0E-4 s^{-1}); (ii) a low decay rate in a medium dispersion flow (k=1.0E-4 s^{-1}); and, (iii) a high decay rate in a medium dispersion flow (k=3.0E-4 s^{-1}). The numerically simulated vs. analytically computed results are compared in figures 4.4, 4.5 and 4.6. As seen from the figures, the simulated and calculated results are almost identical or very close to each other which represent the predictive capabilities of the proposed model with decay. In all three cases, decay acts as an additional smoothing mechanism on the sharp contaminant profile that is already smoothened by the dispersion.

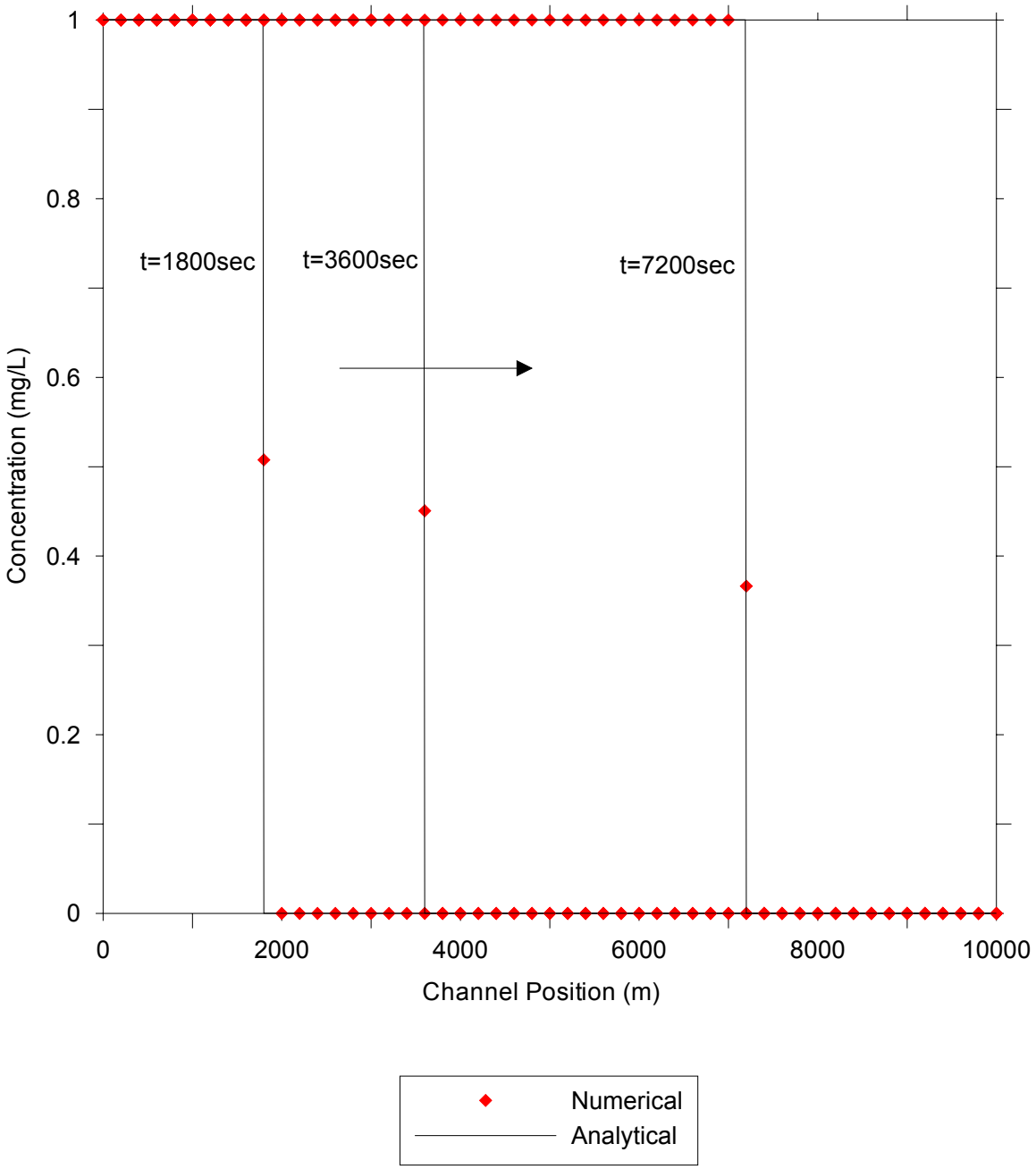

Figure 4.1. Comparison of numerically simulated and analytically computed concentrations in an advection dominated flow (D_L=1.0E-8 m^2/s)

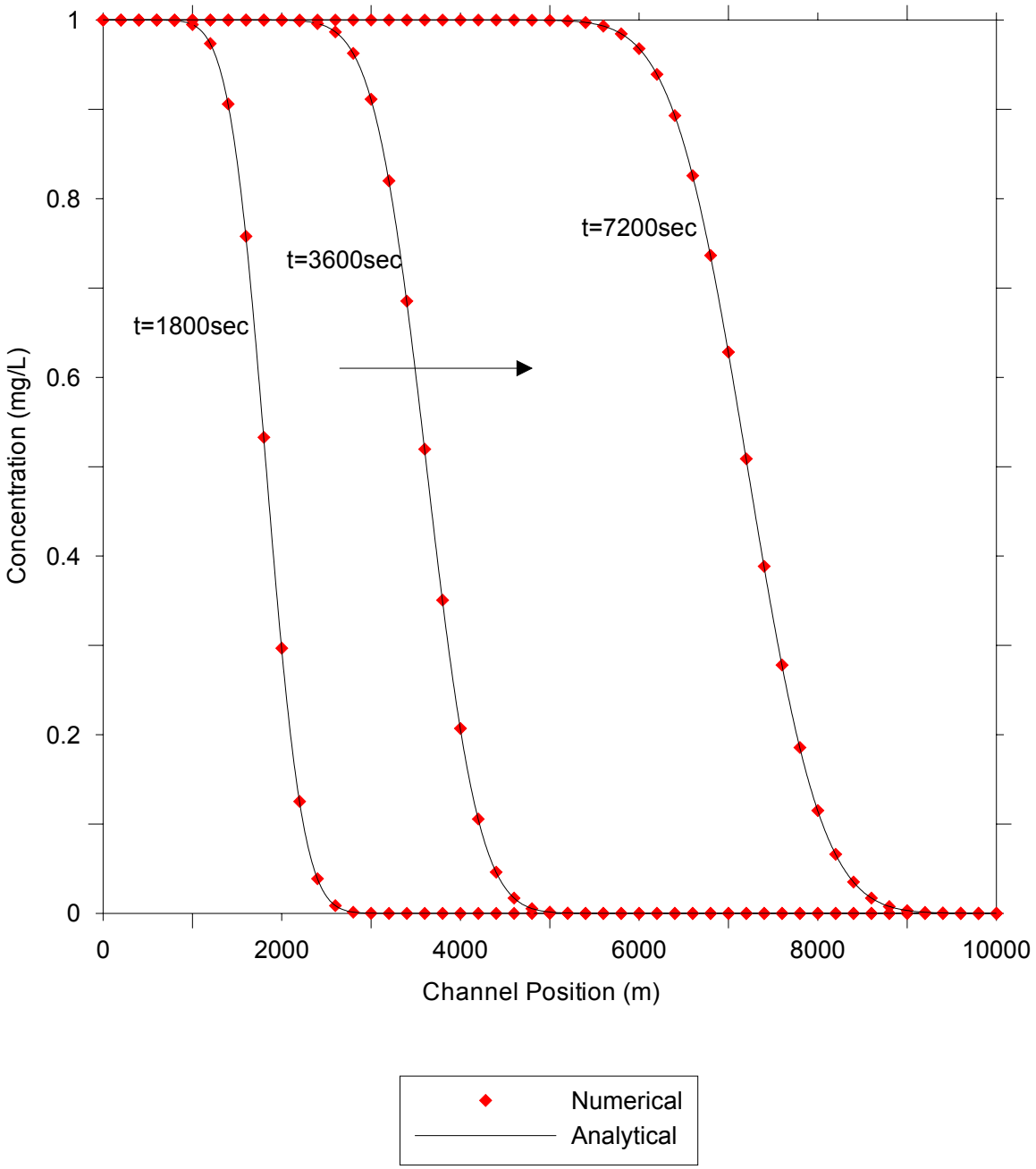

Figure 4.2. Comparison of numerically simulated and analytically computed concentrations in a moderate dispersion flow (D_L=30 m^2/s)

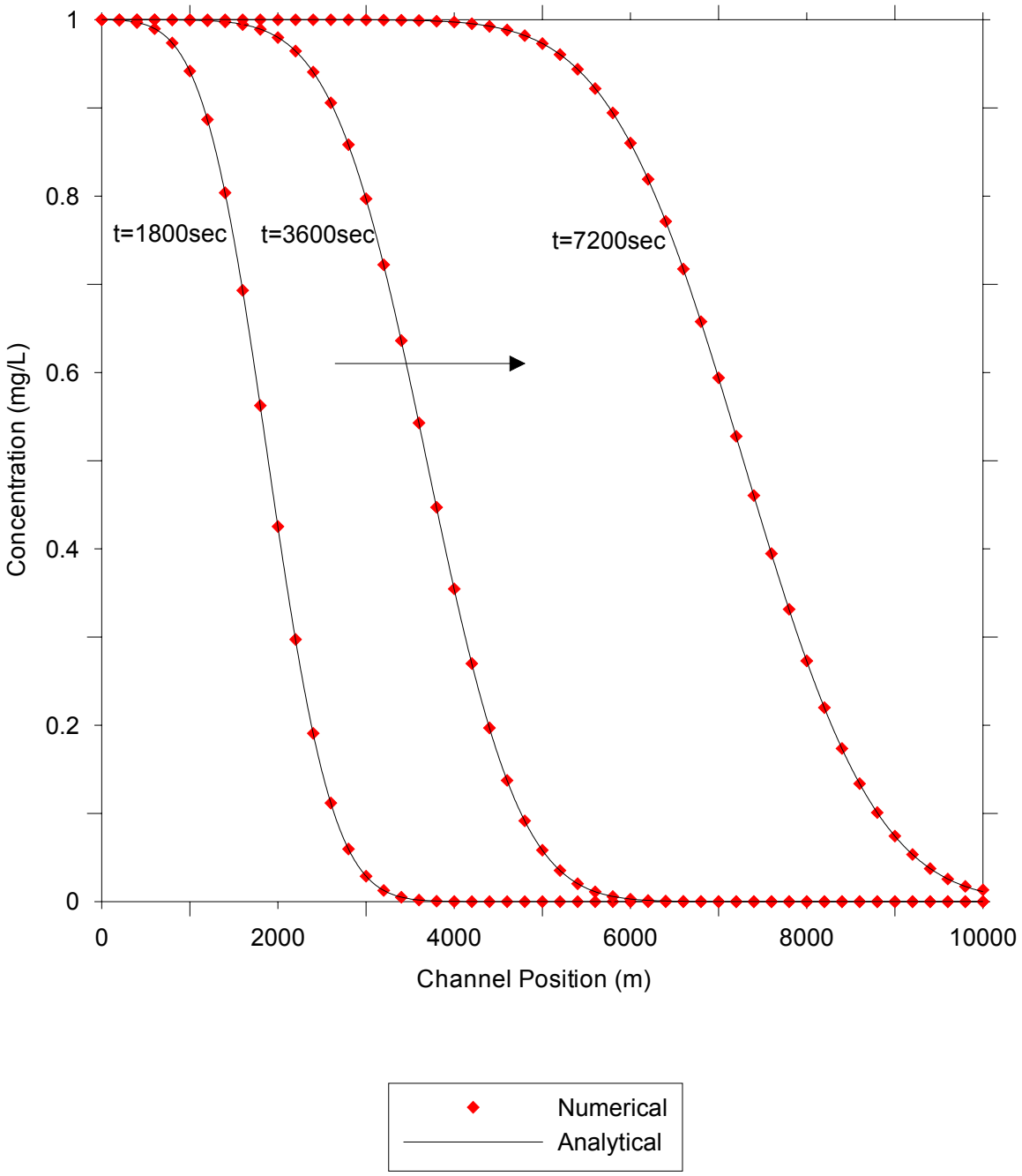

Figure 4.3. Comparison of numerically simulated and analytically computed concentrations in a high dispersion flow (D_L=100 m^2/s)

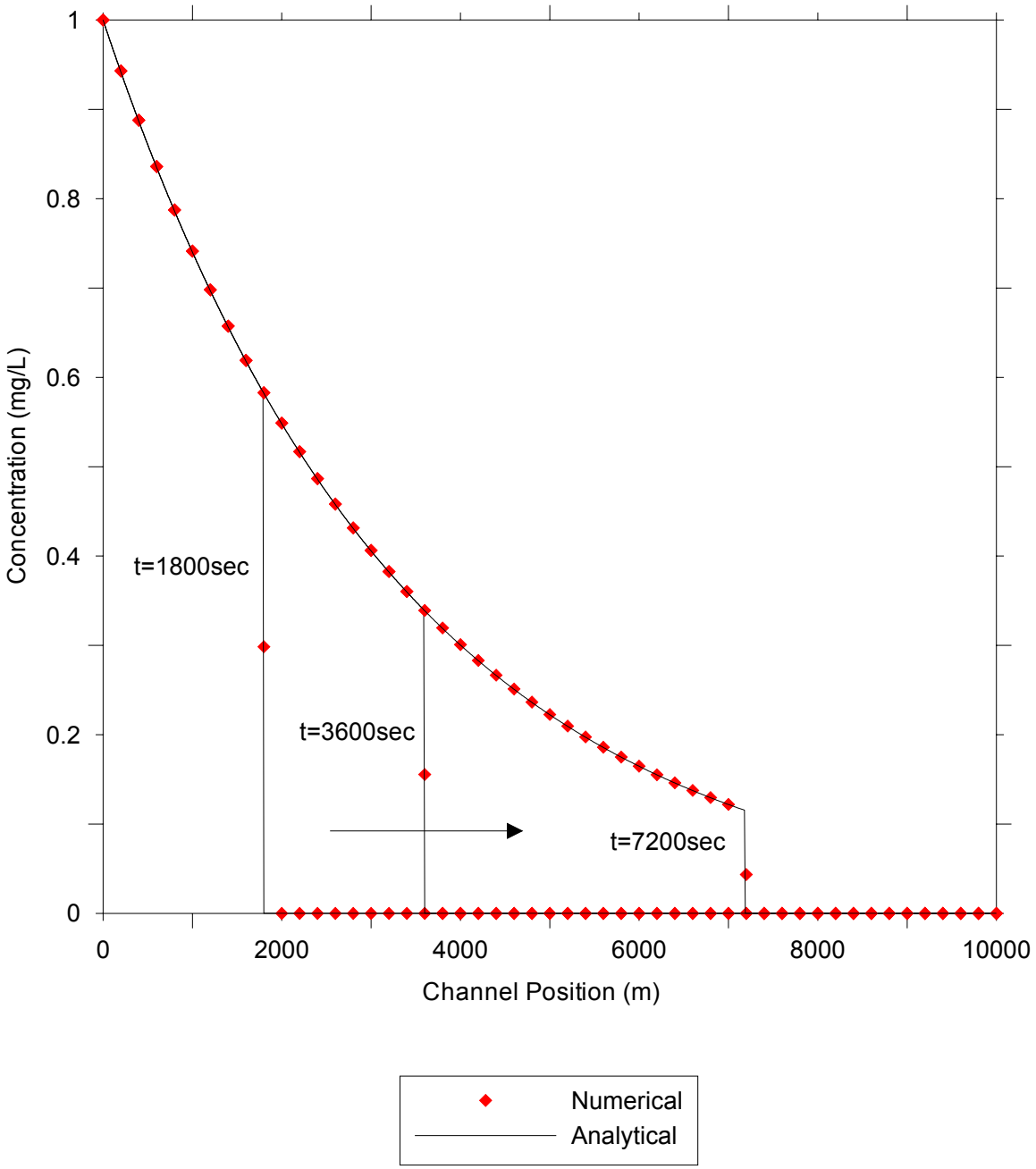

Figure 4.4. Comparison of numerically simulated and analytically computed concentrations in an advection dominated flow (D=1.0E-8 m^2/s) with decay (k=3.0E-4 s^{-1})

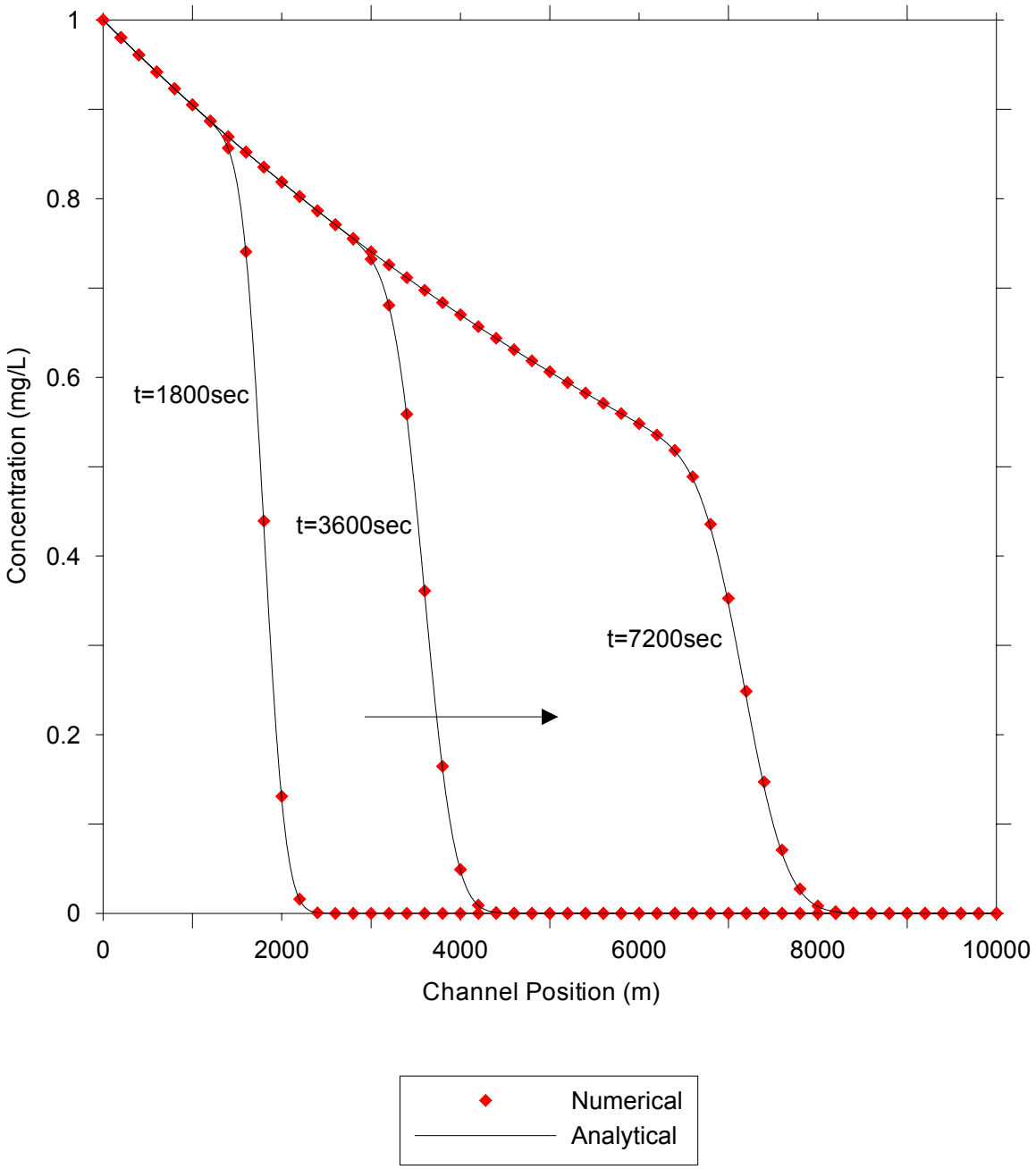

Figure 4.5. Comparison of numerically simulated and analytically computed concentrations in a moderate dispersion (D=10 m^2/s) flow with moderate decay (k=1.0E-4 s^{-1})

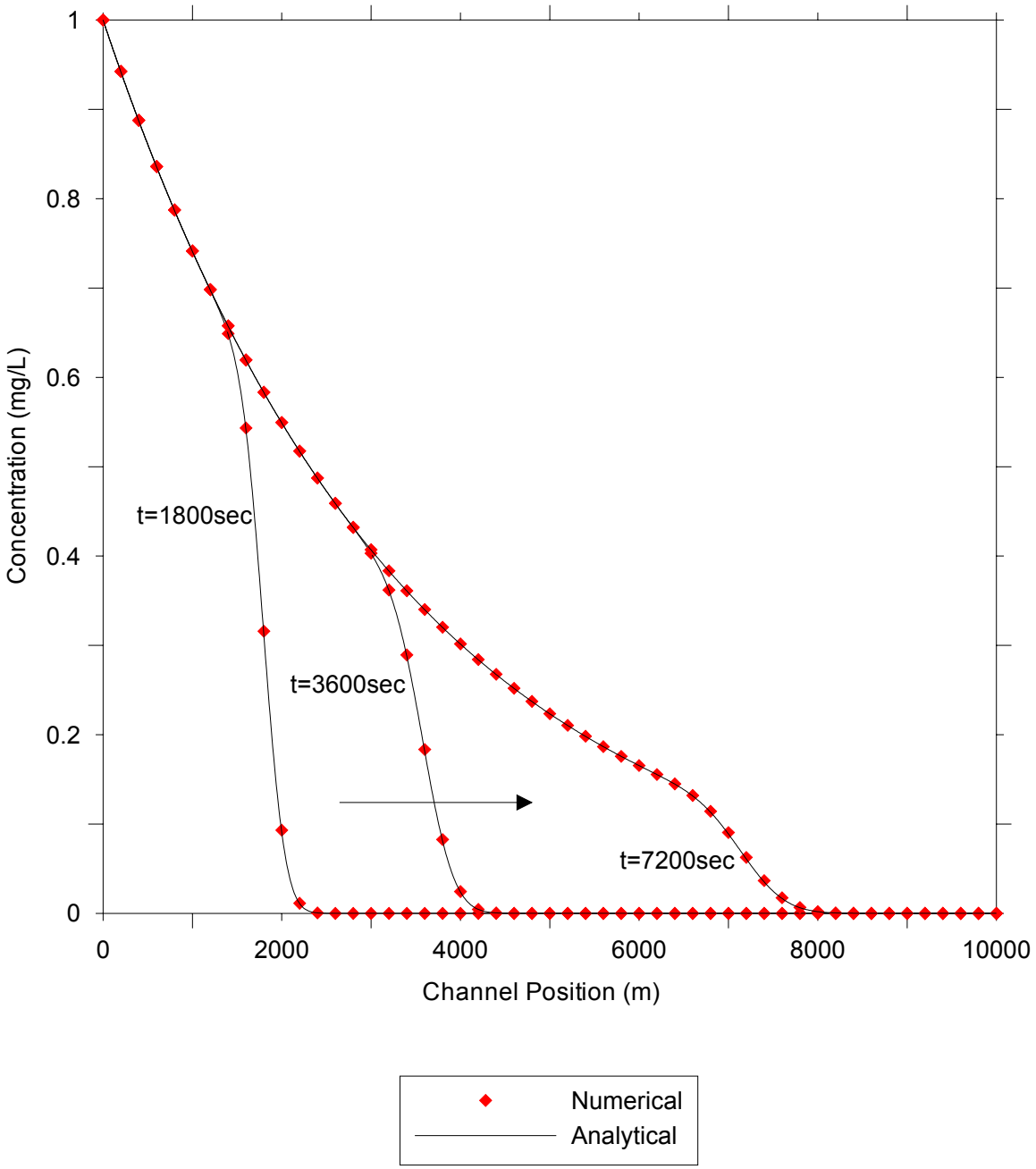

Figure 4.6. Comparison of numerically simulated and analytically computed concentrations in a moderate dispersion (D_L=10 m^2/s) flow with high decay (k=3.0E-4 s^{-1})

In a channel network setup, there are no analytical solutions that the model could be tested against when advection, dispersion and/or decay are the governing mechanisms of fate and transport. It is, however, possible to perform simple benchmark tests when the steady uniform channel flow only allows advection of contaminants. Although such a situation is of no practical value, it is believed to provide an important test condition for the numerical model within a network setup. To test the simulation capabilities of the proposed model in a channel network under simple advection, a three channel network with two upstream tributaries and a downstream channel is used as shown in Figure 4.7.

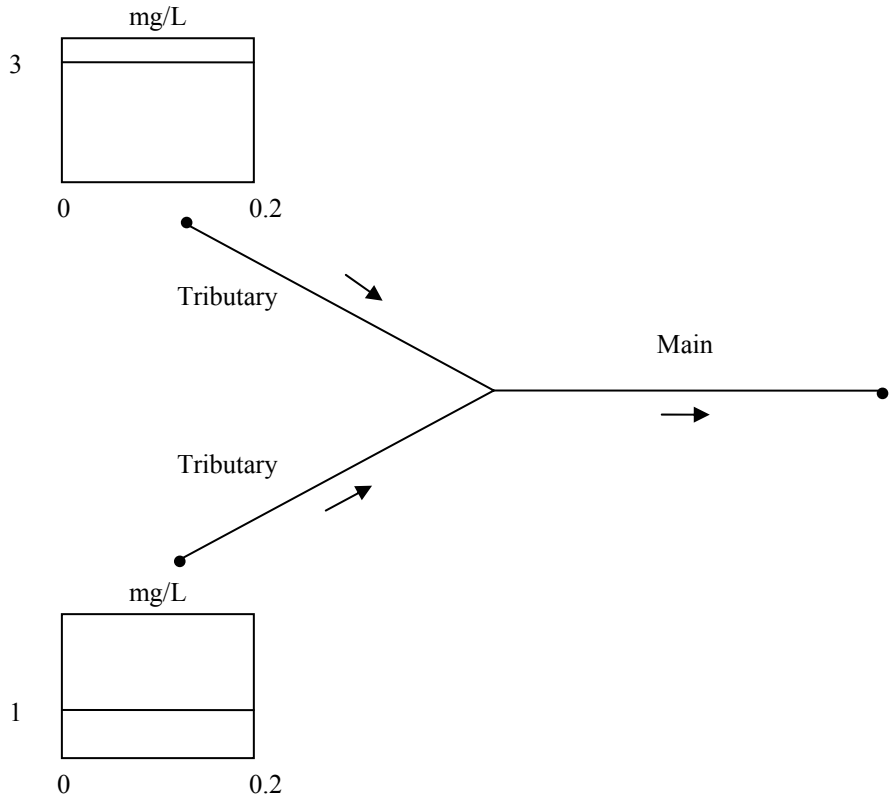

Figure 4.7. Simple channel network for testing pure advective transport

The hypothetical channel network consists of three 10000m long rectangular channels laid on a 0.001m/m bed slope. The upstream tributaries and the downstream main channels have top widths of 20m and 40m and carry a discharge of $10m^3/s$ and $20m^3/s$, respectively. The steady uniform flow creates a normal depth of 0.5m and a velocity of 1m/s in all three channels. Initially, all channels contain zero contaminant concentration. Then, the first tributary starts to receive constant 1mg/L while the second tributary gets constant 3mg/L throughout the rest of the simulation period of 0.2 days. Since flow in the channel system is steady and uniform and advection is the only means of transport, it is expected that the two concentration streams blend in the junction and travel downstream with the volumetric average concentration. Considering the fact that both tributaries carry an equal amount of discharge, the blended main channel concentration is expected to balance out at 2mg/L and still continue to travel downstream as a step function based on the assumption that the mixing of the two streams occur instantaneously. The results of numerical simulation exactly follow this intuitive expectation. Figure 4.8 shows results before and after blending of the two streams.

Although the channel network would not allow a similar intuitive analysis for pure diffusion/dispersion, the proposed model is still used to simulate the channel network shown in Figure 4.7, so that the results could at least be analyzed from a general perspective. In this test, however, the second tributary is assumed free of contamination and is assumed to have a zero concentration boundary condition at the most upstream point. Since the second tributary does not carry any contaminant, one would expect dispersion towards not only along the main channel but also towards the second tributary once the contaminant reaches the junction. Therefore, a symmetric pattern is expected

beyond the junction. The results of pure diffusion/dispersion test verify this expectation, as shown in Figure 4.9. The contaminant is allowed to diffuse from the upstream point of the first tributary for 30 days and the corresponding contaminant concentration is calculated at all points along the channel network. It is important to note that this test is performed with a diffusion coefficient of $10m^2/s$, which corresponds to an unrealistically high diffusion coefficient since dispersion is not a transport mechanism in stagnant water. It is, however, convenient to test the numerical functioning of the code rather than drawing any physical results. The results clearly demonstrate the symmetric behavior beyond the junction and follow an error function trend. It is therefore possible to conclude that the proposed model functions properly in the case of pure diffusion in a channel network setup.

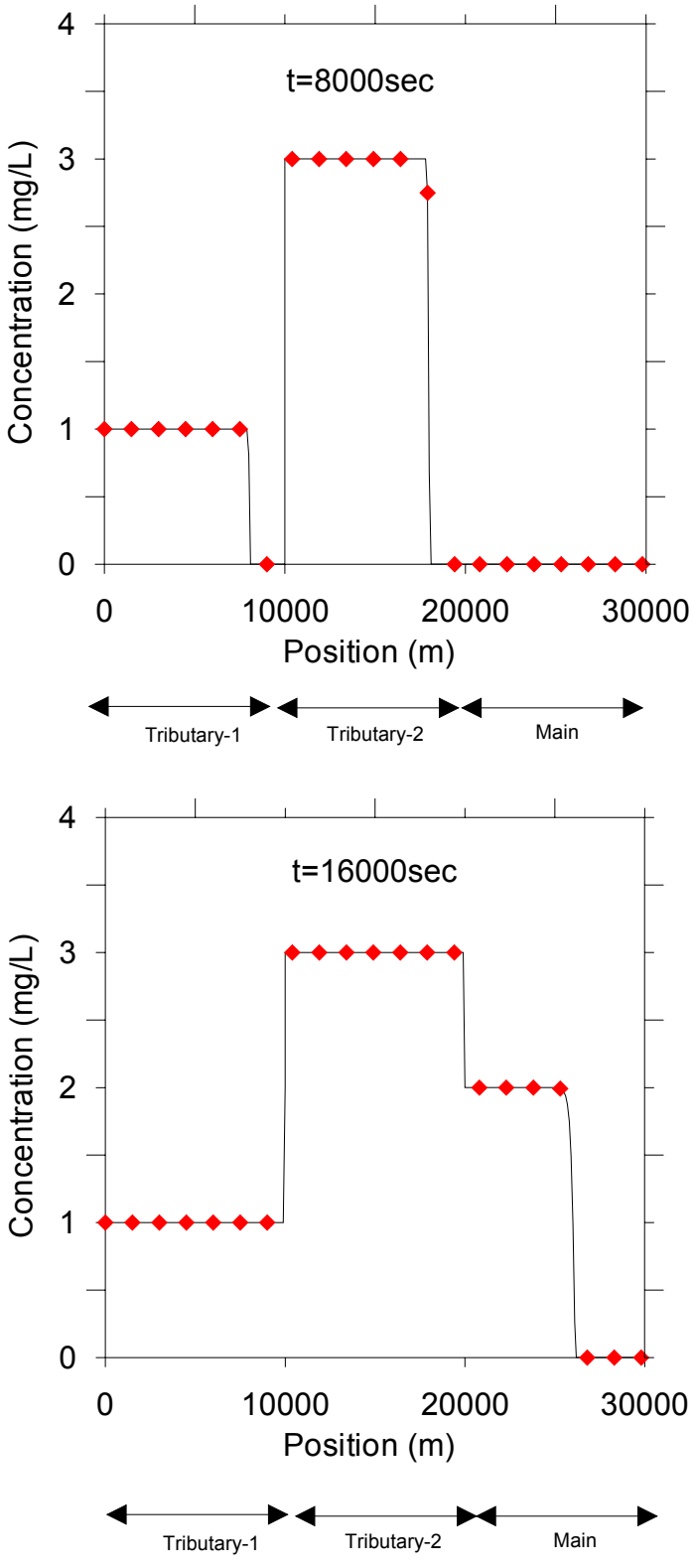

Figure 4.8. Pure advective transport in a channel network

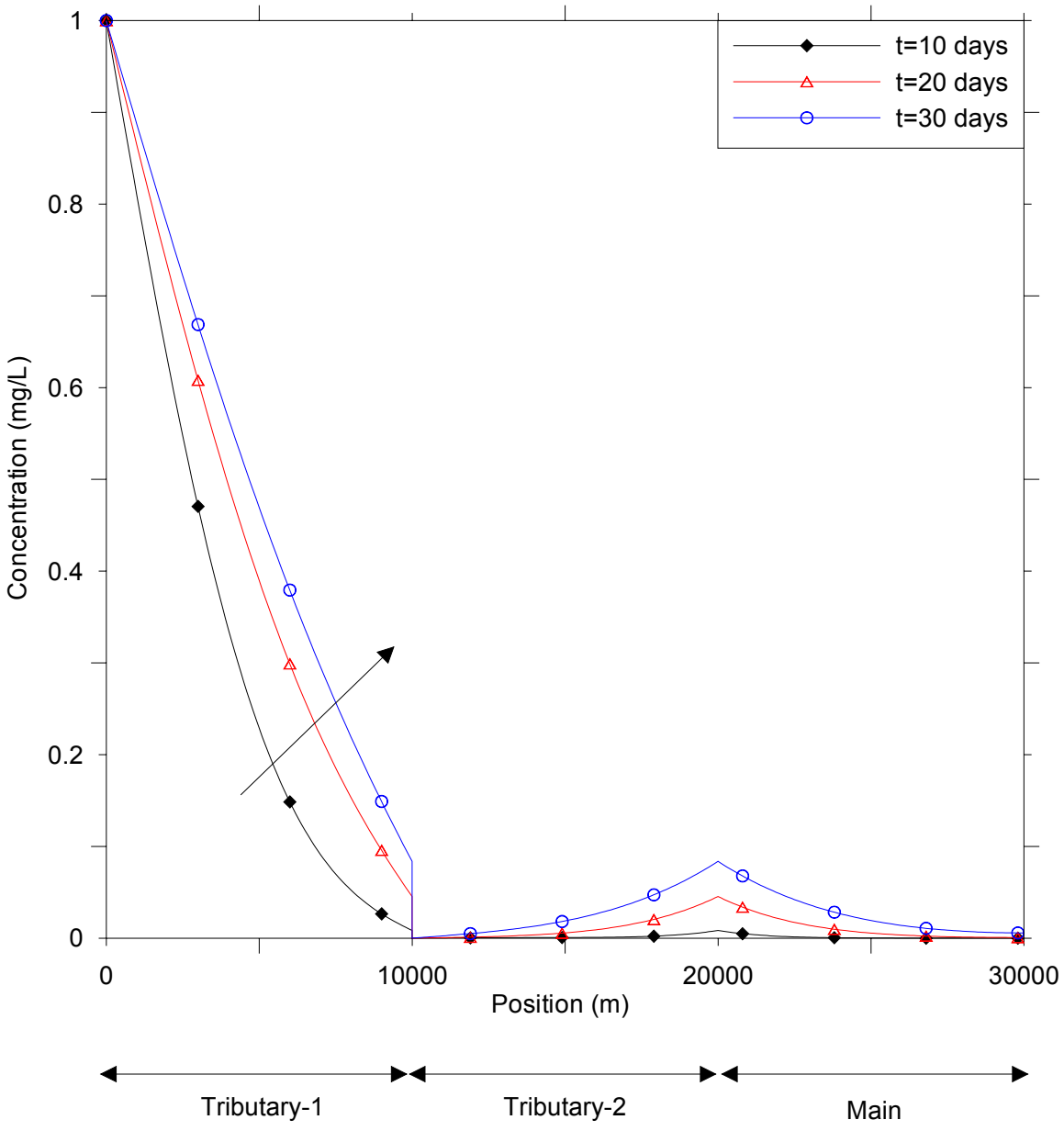

Figure 4.9. Pure diffusion/dispersion in a channel network

4.2. Two Dimensional Saturated Groundwater Transport Model

4.2.1. Governing Equations

The governing equation for contaminant transport in a two-dimensional vertically-averaged groundwater flow is obtained by vertically integrating the general three-dimensional conservation of mass equation in the groundwater. The equation is later modified to include the effect of line source/sink following the original idea proposed by Gunduz and Aral (2004a). For an anisotropic, non-homogeneous unconfined aquifer with principle permeability directions not matching the coordinate directions, the governing equation of contaminant transport in groundwater is given by:

$$
\begin{aligned}
&nR_d\left(h_g-z_b\right)\frac{\partial C_g}{\partial t}+\left(h_g-z_b\right)q_x\frac{\partial C_g}{\partial x}+\left(h_g-z_b\right)q_y\frac{\partial C_g}{\partial y}\\
&-\frac{\partial}{\partial x}\left[\left(h_g-z_b\right)nD_{xx}\frac{\partial C_g}{\partial x}\right]-\frac{\partial}{\partial x}\left[\left(h_g-z_b\right)nD_{xy}\frac{\partial C_g}{\partial y}\right]\\
&-\frac{\partial}{\partial y}\left[\left(h_g-z_b\right)nD_{yx}\frac{\partial C_g}{\partial x}\right]-\frac{\partial}{\partial y}\left[\left(h_g-z_b\right)nD_{yy}\frac{\partial C_g}{\partial y}\right]\\
&+I\left(C_I^*-C_g\right)+\lambda nR_d\left(h_g-z_b\right)C_g+K_w n\left(h_g-z_b\right)C_g-C_gS_y\frac{\partial h_g}{\partial t}\\
&+\sum_{k=1}^{n_w}\left[Q_{w,k}\left(C_{w,k}^*-C_g\right)\delta\left(x-x_{w,k}\right)\delta\left(y-y_{w,k}\right)\right]\\
&+\sum_{m=1}^{n_r}\left[\int_0^1\left[q_{L1,m}\left(C_{L1,m}^*-C_g\right)-n_{sed,m}D_{sed,m}\frac{C_{r,m}-C_g}{\left(m_r\right)_m}\left(w_r\right)_m\right]\right.\\
&\left.\sqrt{\left(\frac{dg_{x,m}}{du}\right)^2+\left(\frac{dg_{y,m}}{du}\right)^2}\,\delta\left(x-g_{x,m}(u)\right)\delta\left(y-g_{y,m}(u)\right)du\right]=0
\end{aligned}
\tag{4.26}
$$

where x and y are the spatial coordinates in the horizontal domain, t is the temporal coordinate, C_g is the vertically-averaged contaminant concentration, n is the porosity of the medium, q is the vertically-averaged Darcy flux, D is the hydrodynamic dispersion coefficient, h_g is the vertically-averaged hydraulic head, z_b is the elevation of the bottom impervious layer, I is the infiltration/exfiltration rate (i.e., positive for exfiltration and negative for infiltration), C^*_I is the contaminant concentration associated with the filtrating water, λ is the radioactive decay constant for a radioactive contaminant, K_w is the biochemical decay constant for a biodegradable contaminant, S_y is the specific yield of the unconfined aquifer, n_w is the number of wells in the domain, $Q_{w,k}$ is the well flow rate of the kth well located at ($x_{w,k}$, $y_{w,k}$) in the domain (i.e., positive for a discharging well and negative for an injecting well), $C^*_{w,k}$ is the contaminant concentration associated with the kth well, δ is the Dirac Delta function, n_r is the number of river channels in the domain, $q_{L1,m}$ is the lateral seepage flow between the groundwater and river flow domains in the mth river channel (positive for outflow from the aquifer or inflow to the river and negative for inflow to the aquifer or outflow from the river), $C^*_{L1,m}$ is the contaminant concentration associated the mth river channel, $C_{r,m}$ is the contaminant concentration in the mth river channel, n_{sed} is the porosity of the sediment layer, D_{sed} is the vertical dispersion coefficient in the sediment layer, m_r is the thickness of the sediment layer, w_r is the wetted perimeter of the mth river channel, $g_{x,m}$ and $g_{y,m}$ are the Cartesian coordinate components of the parametric equation defining the mth river channel in the domain, u is the dimensionless parameter of the parametric equation and R_d is the retardation coefficient given by:

$$R_d = 1 + \frac{\rho_b K_d}{n} \tag{4.27}$$

where ρ_b is the bulk density of the porous medium and K_d is the portioning coefficient. It is important to note that the values of C^*_I, $C^*_{w,k}$ and $C^*_{L1,m}$ change according to the direction of the volumetric flux driving the mass transport. Accordingly, when the volumetric flux is towards the aquifer, these values take the associated concentrations in the infiltrating water (i.e., C_I), the well recharge (i.e., $C_{w,k}$) and the lateral seepage flow (i.e., $C_{r,m}$) where as they become the concentration in the groundwater (i.e., C_g) when the corresponding volumetric fluxes are away from the aquifer:

$$C^*_I = \begin{cases} C_g & when \quad I > 0 \quad \text{(exfiltration)} \\ C_I & when \quad I < 0 \quad \text{(infiltration)} \end{cases} \tag{4.28}$$

$$C^*_{w,k} = \begin{cases} C_g & when \quad Q_{w,k} > 0 \quad \text{(discharging well)} \\ C_{w,k} & when \quad Q_{w,k} < 0 \quad \text{(recharging well)} \end{cases} \tag{4.29}$$

$$C^*_{L1,m} = \begin{cases} C_g & when \quad q_{L1,m} > 0 \quad \text{(outflow from aquifer)} \\ C_{r,m} & when \quad q_{L1,m} < 0 \quad \text{(inflow to aquifer)} \end{cases} \tag{4.30}$$

Despite the vast number of alternative empirical formulations in open channels, the theory of dispersion is much better developed in groundwater systems. The developed equations are generally globally accepted and implemented in many modeling applications. The theory is based on the concept of a hydrodynamic dispersion coefficient that is defined as the sum of mechanical dispersion and molecular diffusion. Bear (1972) has formulated the hydrodynamic dispersion coefficient as:

$$D = \tau D_m + \alpha_L v \tag{4.31}$$

where τ is the tortuosity of the medium, D_m is the molecular diffusion coefficient, α_L is the longitudinal dispersivity and v is the average pore velocity defined by the ratio of Darcy velocity and porosity of the medium. When the relative importance of mechanical dispersion and molecular diffusion is studied, it is seen that the mechanical dispersion is almost always the major contributor of hydrodynamic dispersion coefficient under field conditions. In the last 30 years, Bear's analysis has become the industry standard for the analysis of dispersion in groundwater systems, which describes the following three-dimensional dispersion tensor:

$$D_{ij} = D_m \tau \delta_{ij} + \alpha_T |v| \delta_{ij} + (\alpha_L - \alpha_T) \frac{v_i v_j}{|v|} \tag{4.32}$$

where α_L and α_T are the longitudinal and transverse dispersivities, respectively, and δ_{ij} is the Kronecker delta. In a vertically-averaged two-dimensional setup, the hydrodynamic dispersion coefficient reduces to a second order tensor and is given as:

$$\begin{aligned} D_{xx} &= \alpha_L \frac{v_x^2}{|v|} + \alpha_T \frac{v_y^2}{|v|} + D_m \tau \\ D_{yy} &= \alpha_T \frac{v_x^2}{|v|} + \alpha_L \frac{v_y^2}{|v|} + D_m \tau \\ D_{xy} &= D_{yx} = (\alpha_L - \alpha_T) \frac{v_x v_y}{|v|} \end{aligned} \tag{4.33}$$

4.2.2. Initial Conditions

The initial values of the contaminant concentration, C_{g0}, are specified as the initial conditions of the groundwater contaminant transport model:

$$C_g(x, y, 0) = C_{g0}(x, y) \tag{4.34}$$

which is generally taken to be zero, representing a contaminant release into an otherwise uncontaminated domain, or is obtained from: (i) field measurements, (ii) a steady state contaminant transport simulation; or, (iii) a previous unsteady model solution.

4.2.3. Boundary Conditions

Two different types of boundary conditions can be specified along different external boundaries of the groundwater domain. Type-1 or specified concentration boundary conditions are used to model boundaries with known contaminant concentration values. This is also known as a Dirichlet boundary condition and is given as:

$$C_g(x, y, t) = C_{gD}(x, y, t) \tag{4.35}$$

where C_{gD} is the known concentration. It is also possible to define a variable boundary condition, which becomes a zero dispersive flux for a volumetric outflow and a specified mass influx for a volumetric inflow:

$$
\begin{aligned}
&-\mathbf{n}\cdot\left[\left(h_g - z_b\right) n\mathbf{D}\cdot\nabla C_g\right] = 0 && \textit{for} \quad \left(h_g - z_b\right)\mathbf{q}\cdot\mathbf{n} > 0 \\
&\left(h_g - z_b\right)\mathbf{n}\cdot\left[\mathbf{q}C_g - n\mathbf{D}\cdot\nabla C_g\right] = \left(h_g - z_b\right) q_v C_v && \textit{for} \quad \left(h_g - z_b\right)\mathbf{q}\cdot\mathbf{n} < 0
\end{aligned}
\tag{4.36}
$$

where q_v is the volumetric inflow rate and C_v is the contaminant concentration in the inflowing stream.

4.2.4. Numerical Solution Scheme

Although the form of the groundwater contaminant transport equation is very similar to the channel transport equation, the difficulties associated with the numerical solution are not as significant as the channel transport equation. This finding is mainly due to the fairly small advection velocities that govern the groundwater transport. The relative magnitudes of the advective and dispersive transport mechanisms are much closer to each other than their counterparts in channel flow. Hence, fixed grid finite element and finite difference models are still widely applied in groundwater transport modeling. Similar to its flow counterpart, the finite element method became a popular method due to the flexibility it offers in simulating aquifer domains with irregular boundaries as well as heterogeneous aquifer properties. In this regard, the Galerkin finite element method based on the method of weighted residuals is used in this study to solve the groundwater contaminant transport. The weak form of the problem is developed in Appendix K. Using the same discretization that its flow counterpart uses; the contaminant transport model also implements linear interpolating functions and quadrilateral elements. The resulting finite element matrix equation obtained by applying the Galerkin procedure is given as:

$$\mathbf{S}\cdot\hat{\mathbf{C}}_{\mathbf{g}}+\mathbf{M}\cdot\frac{d\hat{\mathbf{C}}_{\mathbf{g}}}{dt}=\mathbf{F} \tag{4.37}$$

where **S**, **M** and **F** stand for global stiffness matrix, global mass matrix and global load vector, respectively, and $\hat{\mathbf{C}}_{\mathbf{g}}$ is the approximate contaminant concentration vector. These global matrices and vectors are obtained by tiling their element counterparts according to the connectivity of elements within the solution domain. The explicit formulas of element matrices and vectors are derived in Appendix L. The element integrals are evaluated with the same numerical integration scheme used in the flow model.

The ordinary differential in (4.37) is obtained as a result of finite element discretization and can be solved using a number of techniques including the one-step finite difference approximations. Since the concentration is a function of time, it is possible to define two positions, j and j+1, representing the known and unknown time lines, respectively. If one defines an intermediate point between the known and the unknown time line (i.e., $j+\alpha$ where $0\leq\alpha\leq1.0$), then the corresponding concentration could be calculated as a weighted average:

$$\hat{\mathbf{C}}_{\mathbf{g}}{}^{j+\alpha}=\alpha\hat{\mathbf{C}}_{\mathbf{g}}{}^{j+1}+(1-\alpha)\hat{\mathbf{C}}_{\mathbf{g}}{}^{j} \tag{4.38}$$

such that if the intermediate point is selected as the mid point between the two time lines (i.e., $\alpha=0.5$), the concentration becomes an arithmetic average of the two concentrations

at two ends. Following the same procedure used in the flow model, one can obtain the final form as:

$$\left(\alpha \mathbf{S}^{j+1} + \frac{\mathbf{M}^{j+1}}{\Delta t}\right) \cdot \hat{\mathbf{C}}_{\mathbf{g}}{}^{j+1} = \alpha \mathbf{F}^{j+1} + (1-\alpha)\mathbf{F}^{j} - \left((1-\alpha)\mathbf{S}^{j} - \frac{\mathbf{M}^{j}}{\Delta t}\right) \cdot \hat{\mathbf{C}}_{\mathbf{g}}{}^{j} \tag{4.39}$$

Since the transport equation is linear, solution does not require a non-linear solver as its flow counterpart does and the equation given above is solved by a suitable linear matrix solver.

4.2.5. Model Testing

Similar to its flow counterpart, there are no documented analytical solutions for the unsteady groundwater contaminant transport in two dimensions. Therefore, the proposed model is tested against the analytical solutions developed within a one dimensional framework. The analytical solution is very similar to the one showed in channel contaminant transport with slight modification with respect to the retardation coefficient. Following the works of Ogata and Banks (1961) and van Genuchten and Alves (1982), the one-dimensional mathematical model for groundwater contaminant transport is written as:

$$R_d \frac{\partial C_g}{\partial t} + \frac{q_x}{n}\frac{\partial C_g}{\partial x} - D_x \frac{\partial^2 C_g}{\partial x^2} + K_w C_g = 0 \tag{4.40}$$

in which advection, dispersion and decay are the three mechanisms of fate and transport. The initial and boundary conditions of the problem can also be given as:

$$\begin{aligned} &C_g(x,0) = C_o \qquad for \qquad x \geq 0 \\ &C_g(0,t) = \begin{cases} C_{gD} & for \quad 0 < t < t^* \\ 0 & for \quad t \geq t^* \end{cases} \\ &\frac{\partial C_g}{\partial x}(\infty,t) = 0 \qquad for \qquad t \geq 0 \end{aligned} \tag{4.41}$$

which defines the conditions for a continuous source of finite duration. The analytical solution of this problem for conservative species ($K_w=0$) is slightly modified from the solution of channel transport and is written as:

$$C_g(x,t) = \begin{cases} C_o + (C_{gD} - C_o) A(x,t) & 0 < t \leq t^* \\ \\ C_o + (C_{gD} - C_o) A(x,t) - C_{gD} A(x, t - t^*) & t > t^* \end{cases} \tag{4.42}$$

where the function A(x,t) is now written as::

$$A(x,t) = \frac{1}{2} erfc\left(\frac{R_d x - (q_x / n) t}{\sqrt{4 D_x R_d t}} \right) + \frac{1}{2} \exp\left(\frac{(q_x / n) x}{D_x} \right) erfc\left(\frac{R_d x + (q_x / n) t}{\sqrt{4 D_x R_d t}} \right) \tag{4.43}$$

For non-conservative species ($K_w \neq 0$), the solution is given as:

$$C_g(x,t)=\begin{cases} C_o A(x,t)+C_{gD}B(x,t) & 0<t\le t^* \\ C_o A(x,t)+C_{gD}B(x,t)-C_{gD}B(x,t-t^*) & t>t^* \end{cases} \tag{4.44}$$

where the functions A(x,t) and B(x,t) are defined as:

$$A(x,t)=\exp\left(-\frac{K_w t}{R_d}\right)\left[1-\frac{1}{2}erfc\left(\frac{R_d x-(q_x/n)t}{\sqrt{4D_x R_d t}}\right)-\frac{1}{2}\exp\left(\frac{(q_x/n)x}{D_x}\right)erfc\left(\frac{R_d x+(q_x/n)t}{\sqrt{4D_x R_d t}}\right)\right] \tag{4.45}$$

$$B(x,t)=\frac{1}{2}\exp\left(\frac{(q_x/n)x}{2D_x}(1-\Gamma)\right)erfc\left(\frac{R_d x-(q_x/n)t\Gamma}{\sqrt{4D_x R_d t}}\right)+\frac{1}{2}\exp\left(\frac{(q_x/n)x}{2D_x}(1+\Gamma)\right)erfc\left(\frac{R_d x+(q_x/n)t\Gamma}{\sqrt{4D_x R_d t}}\right) \tag{4.46}$$

The term Γ in function B(x,t) is given as:

$$\Gamma=\sqrt{1+\frac{4K_w D_x}{(q_x/n)^2}} \tag{4.47}$$

To test the proposed model with the analytical solution given above, a two-dimensional hypothetical rectangular aquifer is created so that steady uniform flow will prevail in the aquifer at all times. The 100m long aquifer is structured in such a way that the flow is essentially one-dimensional in the two dimensional domain between two fixed head boundaries creating a hydraulic gradient of 0.1m/100m. The unconfined aquifer

flow would then result in a constant Darcy velocity of 1.0E-5m/s when a uniform hydraulic conductivity value of 0.01m/s is used throughout the domain. The relative values of the aquifer conductivity and hydraulic gradient are deliberately selected to be on the high end to allow rapid response from the aquifer. In the following tests, a retardation coefficient of 1.2 and two dispersion coefficients of 1.0E-4m^2/s and 1.0E-5m^2/s are used in the simulations. Moreover, a decay coefficient of 1.0E-6s^{-1} is also used to simulate the removal of contaminants from the aquifer. The simulations used a specified constant contaminant concentration of 1mg/L as the boundary condition of the transport module. On the opposite side of the domain, a zero concentration gradient boundary condition is implemented. The contaminant is allowed to advect, disperse and/or decay within the channel as a function of time. The results of numerical simulations and analytical solutions are compared in figures 4.10 through 4.13.

The numerical solution demonstrates a perfect fit with the analytical solution for both moderate and low dispersion flows. Since high dispersion flows are always easier to simulate than low dispersion flows, it is not difficult to predict that dispersion values higher than the ones used herein will not create any problems. For pure advection flows, however, the spatial and temporal discretization used in these simulations must be further refined or a more sophisticated higher order numerical algorithm must be implemented to avoid numerical oscillations. Such conditions are not common and as problematic as in channel flow due to significantly lower advection velocities observed in groundwater flow. The simulated and computed results also demonstrate very good fit when 1.0E-6s^{-1} of decay is added to the simulation. Therefore, the proposed model performs accurately when simulating contaminant transport in saturated groundwater flow domain.

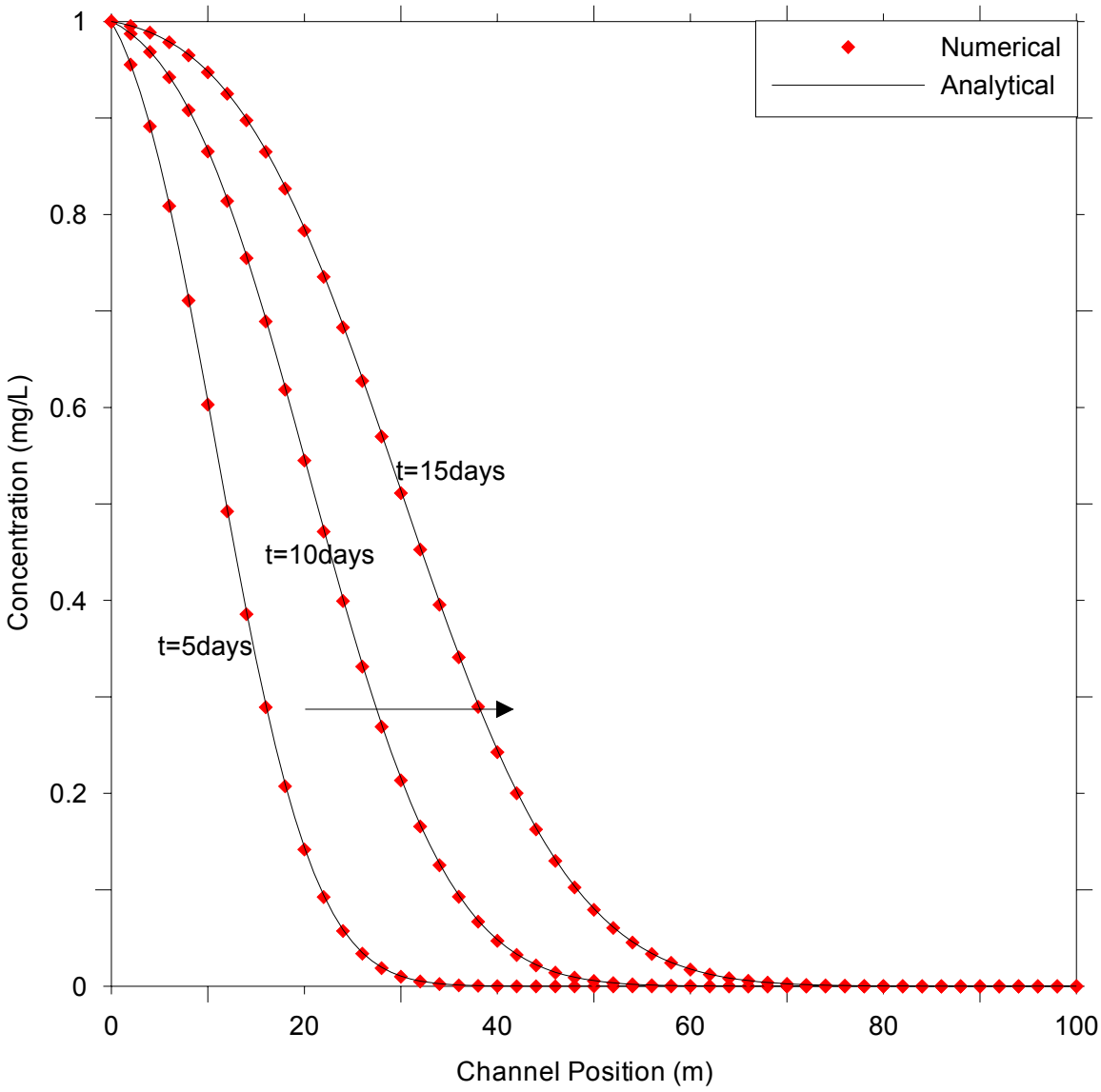

Figure 4.10. Comparison of numerically simulated and analytically computed concentrations for D_x=1.0E-4 m^2/s

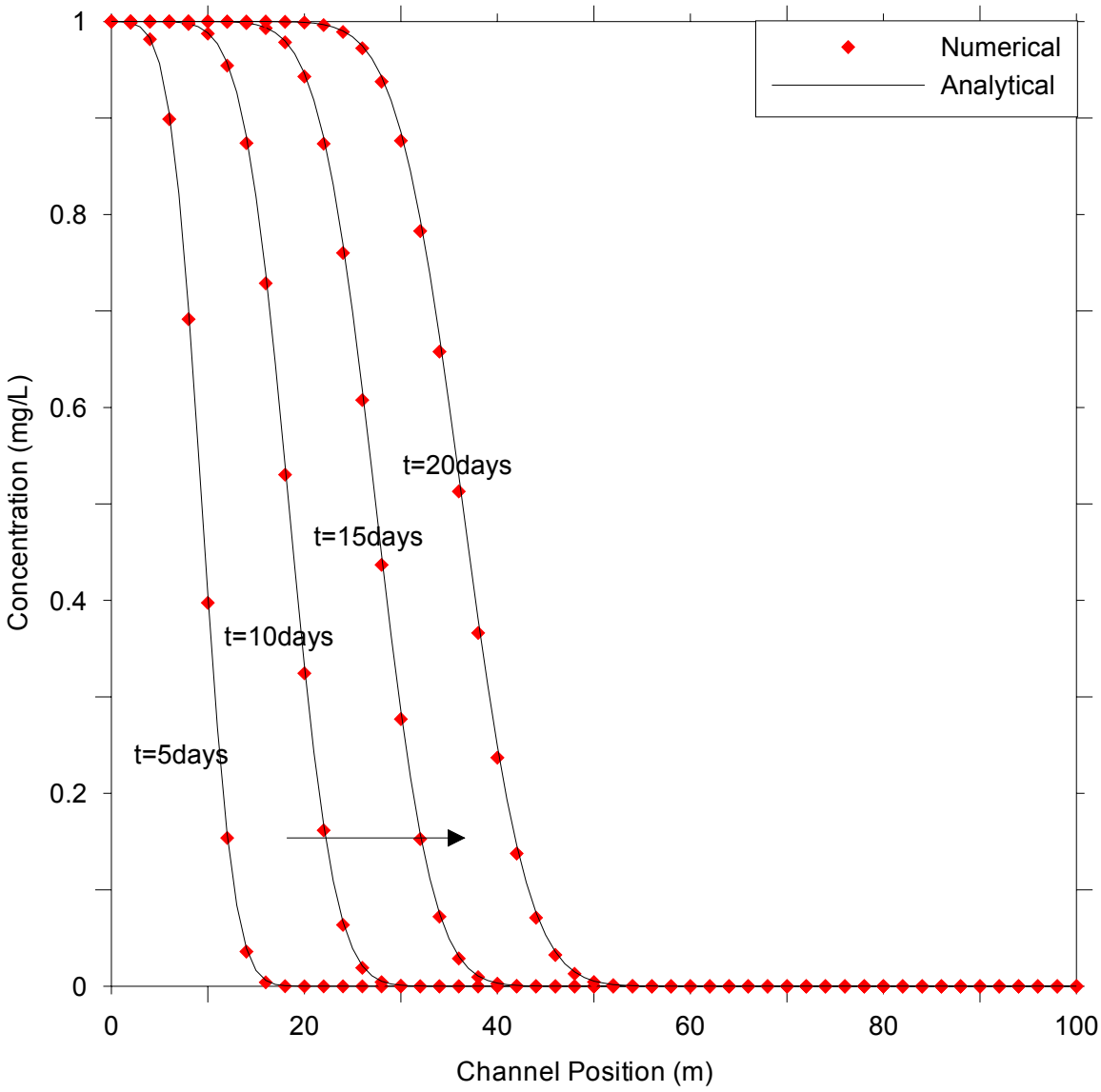

Figure 4.11. Comparison of numerically simulated and analytically computed concentrations for D_x=1.0E-5 m^2/s

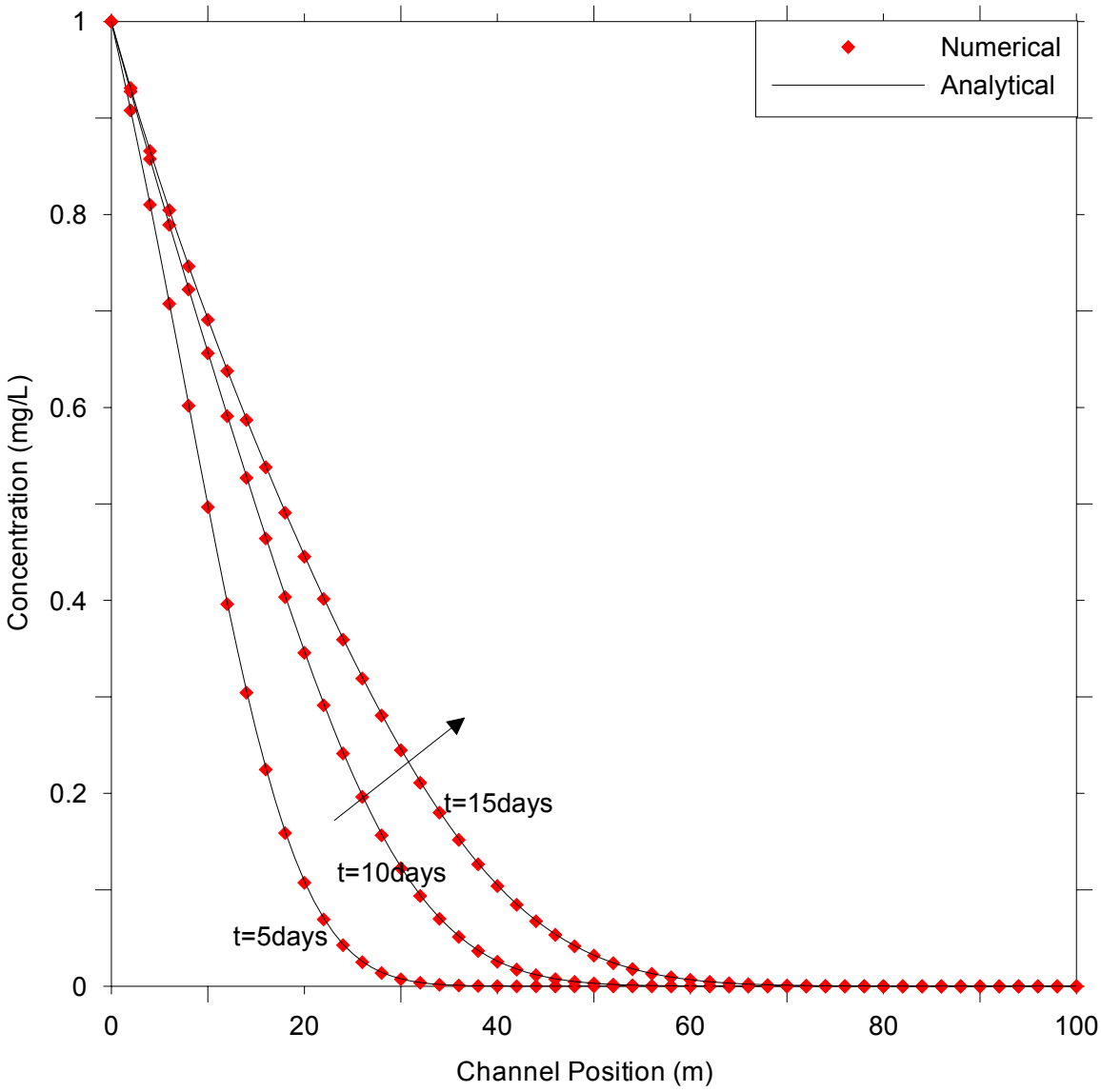

Figure 4.12. Comparison of numerically simulated and analytically computed concentrations for D_x=1.0E-4 m^2/s and K_w=1.0E-6 s^{-1}

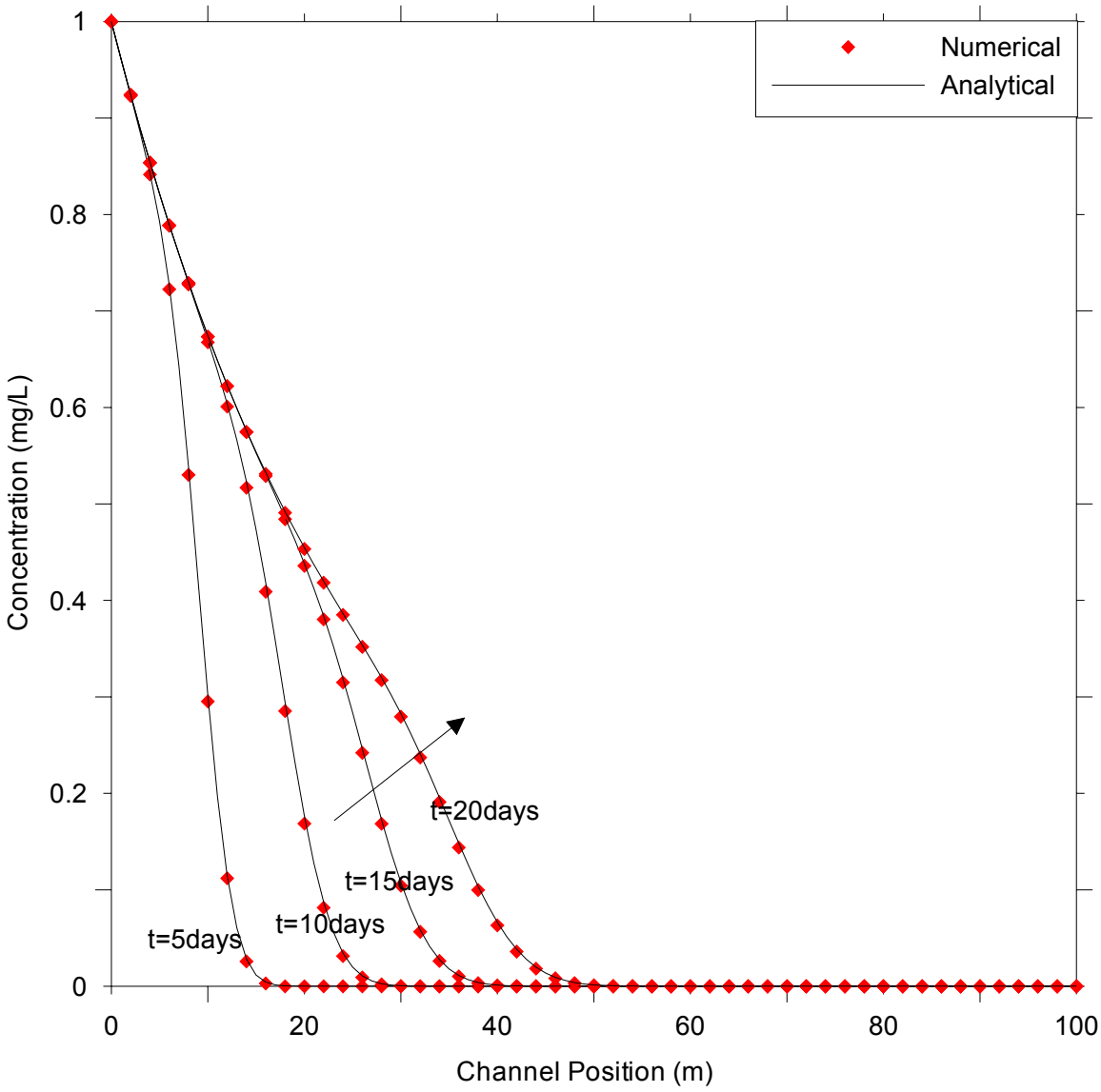

Figure 4.13. Comparison of numerically simulated and analytically computed concentrations for D_x=1.0E-5 m^2/s and K_w=1.0E-6 s^{-1}

4.3. Coupled Surface-Subsurface Contaminant Transport Model

Even though there are many discrete contaminant transport models that describe the fate and transport of contaminant in rivers and aquifers, no coupled analysis has ever been attempted before to the best of the author's knowledge. In this regard, this study is believed to be one of the earliest efforts to couple the surface and subsurface contaminant transport process.

The proposed coupled surface-subsurface transport model follows the hybrid approach discussed in Chapter 3. The two systems are coupled at the river bed using both the advective and the dispersive transport mechanisms. These mechanisms provide possible pathways for the transfer of contaminants between the two domains. This is one of the crucial points of the proposed contaminant transport model since one or both of these mechanisms might be working to transport the contaminant. In previous studies of contaminant transport modeling in discrete systems, only the advective transport mechanism was considered, where the impact of other domains was included as source/sink terms possibly due to its relatively larger contribution compared to dispersive transport. Although this approach is reasonable when the interactions with other domains are only vaguely attempted and the focus is on one particular domain, it might yield to an incorrect treatment of the simultaneous interactions if the dispersive component is neglected from the analysis.

4.3.1. Coupling at the River Bed

In this analysis, the total mass flux along the river bed interface is considered to be a function of (i) the groundwater hydraulic head; (ii) river water surface elevation or

stage; (iii) contaminant concentration in the river; and, (iv) contaminant concentration in the groundwater:

$$Total\ \ mass\ \ flux = f\left(h_r, h_g, C_r, C_g\right) \tag{4.48}$$

While the first two of these parameters determine the magnitude and the direction of the advective flux, the remaining two are responsible for the magnitude and the direction of dispersive flux. The vector sum of the advective and dispersive fluxes would then give the total mass flux between the two domains. It is important to note that the advective flux is a direct function of the water flow between the two domains and is always in the direction of the lower head. As the values of river water surface elevation and the groundwater head changes dynamically, the direction of the volumetric flux and the advective transport changes. On the other hand, the dispersive flux is a function of the concentration gradient and is always towards the domain with lower contaminant concentration based on the Fickian description of dispersion. The direction of the dispersive flux also changes when the contaminant concentration in the channel or in the aquifer changes. This situation represents a highly variable transport phenomenon and is a strong function of the dynamically varying flow conditions. Based on this discussion, one of the following alternative conditions would describe the interactions between the river and the aquifer at all times:

- $h_r > h_g \;\; and \;\; C_r > C_g$

  Both the advective and the dispersive fluxes are towards the aquifer since the river stage is larger than the groundwater head and the concentration in river is larger than the concentration in groundwater.

- $h_r > h_g \;\; and \;\; C_r < C_g$

  The advective flux is towards the aquifer since the river stage is larger than the groundwater head. The dispersive flux, on the other hand, is towards the river since the groundwater domain has a higher contaminant concentration than river.

- $h_r < h_g \;\; and \;\; C_r > C_g$

  The advective flux is towards the river since the groundwater head is larger than the river stage. The dispersive flux, on the other hand, is towards the aquifer since the river has a higher contaminant concentration than the aquifer.

- $h_r < h_g \;\; and \;\; C_r < C_g$

  Both the advective and the dispersive fluxes are towards the river since the groundwater head is larger than the river stage and the concentration in groundwater is larger than the concentration in river.

- $h_r = h_g \;\; and \;\; C_r > C_g$

  The advective flux does not exist since both heads are equal. The dispersive flux is the only available transport mechanism and it is towards the aquifer since the concentration in river is larger than the concentration in aquifer.

- $h_r = h_g \;\; and \;\; C_r < C_g$

  The advective flux does not exist since both heads are equal. The dispersive flux is the only available transport mechanism and it is towards the river since the concentration in aquifer is larger than the concentration in river.

- $h_r > h_g \;\; and \;\; C_r = C_g$

  The dispersive flux does not exist since both domains have the same contaminant concentrations. The advective flux is the only available transport mechanism and it is towards the aquifer since the river stage is larger than the groundwater head.

- $h_r < h_g \;\; and \;\; C_r = C_g$

  The dispersive flux does not exist since both domains have the same contaminant concentrations. The advective flux is the only available transport mechanism and it is towards the river since the groundwater head is larger than the river stage.

- $h_r = h_g \;\; and \;\; C_r = C_g$

  Both the advective and the dispersive flux do not exist and there is no mass transfer between the two domains.

In any one of the cases discussed above, the total mass flux is the summation of the relative contributions from advective and dispersive components. In general, the advective transport mechanism is much larger than the dispersive transport mechanism. Therefore, the direction of the total mass flux typically follows that of the volumetric flux. Only under the condition that the river water surface elevation is in equilibrium with the groundwater head, the dispersive flux dominates the transport phenomenon.

It is important to note that the coupling mechanism for the contaminant transport model is similar to that proposed in the flow model. It is also based on the assumption that the vertical movement of contaminants at the river bed is at a steady state. If it is not possible to assume that an equilibrium condition is reached at the river bed, this analysis would yield erroneous results. Under such circumstances, contaminant transport within the channel bed must be analyzed with a one-dimensional unsteady vertical transport model at the river bed. However, the equilibrium assumption is valid for most large scale practical analysis of surface-subsurface interactions.

The coupling of the contaminant transport model is provided with a modified form of the new simultaneous solution algorithm discussed in Chapter 3. Although the algorithm could have been directly used as discussed in flow coupling, the numerical solution of the advective transport mechanism enforced an explicit solution algorithm which in turn violated the full simultaneous coupling of the surface and subsurface flow processes. When an equally accurate implicit algorithm is devised to solve the advection mechanism of channel transport model, one can apply the fully simultaneous coupling of Chapter 3. Until that time, a semi-simultaneous algorithm is implemented in this study. In the proposed semi-simultaneous algorithm, the advection mechanism of channel contaminant transport model is solved as a separate event prior to the other processes. In a sense, water packet is first advected to its new position in channel. Then, the dispersion, source/sink and decay mechanisms of the channel transport model are solved in a fully simultaneous manner with all mechanisms of the groundwater transport model.

4.3.2. Model Testing

The proposed coupled contaminant transport model is applied to a hypothetical river/aquifer system to demonstrate its performance and the proposed semi-simultaneous solution algorithm. The numerical mesh of the problem is shown in Figure 4.14. In this figure, two densely meshed regions are identified for detailed analysis. In this application, the stream is a 20m wide 5km long uniform rectangular channel with a constant slope of 0.0001m/m and a Manning's roughness coefficient of 0.020. At steady flow conditions, the channel carries $100m^3/s$ discharge at the uniform flow depth of 4.12m. The thickness of the sediments at the bottom of the channel is 0.3m and the hydraulic conductivity of the deposits is 7.0E-6m/s. The river lies at the center of a 5km long and 0.8km wide unconfined aquifer which is formed by clay and gravel layers. The clay layer is located at the center of the aquifer ($600 \leq x \leq 1400$ and $2400 \leq y \leq 4700$) and has a hydraulic conductivity value of 5.5E-8m/s. Two gravel layers are located to the north ($600 \leq x \leq 1400$ and $1000 \leq y \leq 2400$) and south ($600 \leq x \leq 1400$ and $4700 \leq y \leq 6000$) of the clay layer and have a hydraulic conductivity value of 1.0E-3m/s.

The hydraulics of the aquifer is arranged so that it would be a discharging aquifer at the upstream portions of the river and a recharging aquifer at the downstream portions of the river as shown in Figure 4.15. With this particular setup, it is possible to analyze the potential of the river to serve as a fast transport medium for contaminants in the aquifer. Accordingly, any contaminant plume in the vicinity of the upstream reaches of the river will first be transported to the river and will then be quickly conveyed to the lower portions of the aquifer where the reversed seepage flow direction will reintroduce the contaminants to the aquifer.

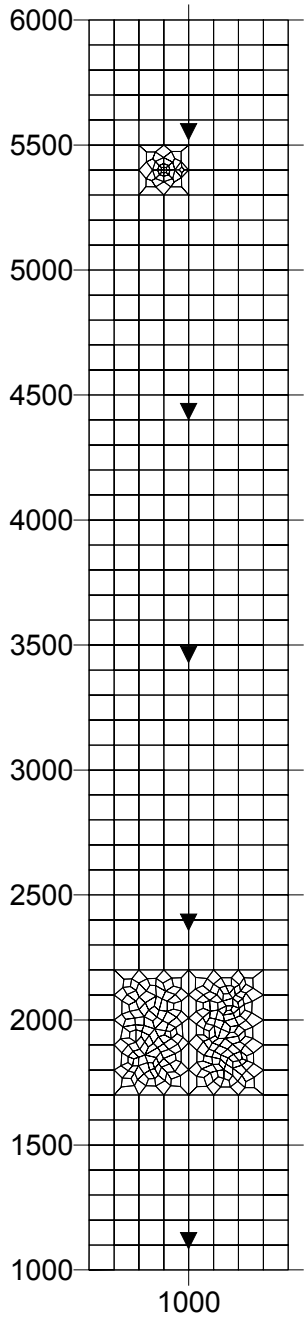

Figure 4.14. Physical setup of hypothetical domain

In this setup, the hydraulics of the river are of little concern and is driven by a steady 100m^3/s discharge at the upstream boundary throughout the simulation period. At the downstream boundary, a normal depth boundary condition is implemented. The hydraulics of the aquifer shown in Figure 4.15 is governed by fixed head boundary conditions on the left and right boundaries and no flux conditions at the top and bottom boundaries. Hence, the aquifer feeds the river in the upper 2500m, whereas the river feeds the aquifer in the lower 2500m. Therefore, any contaminant introduced from the upper region will first reach the river, transported with river flow and be later reintroduced to the aquifer in the lower region.

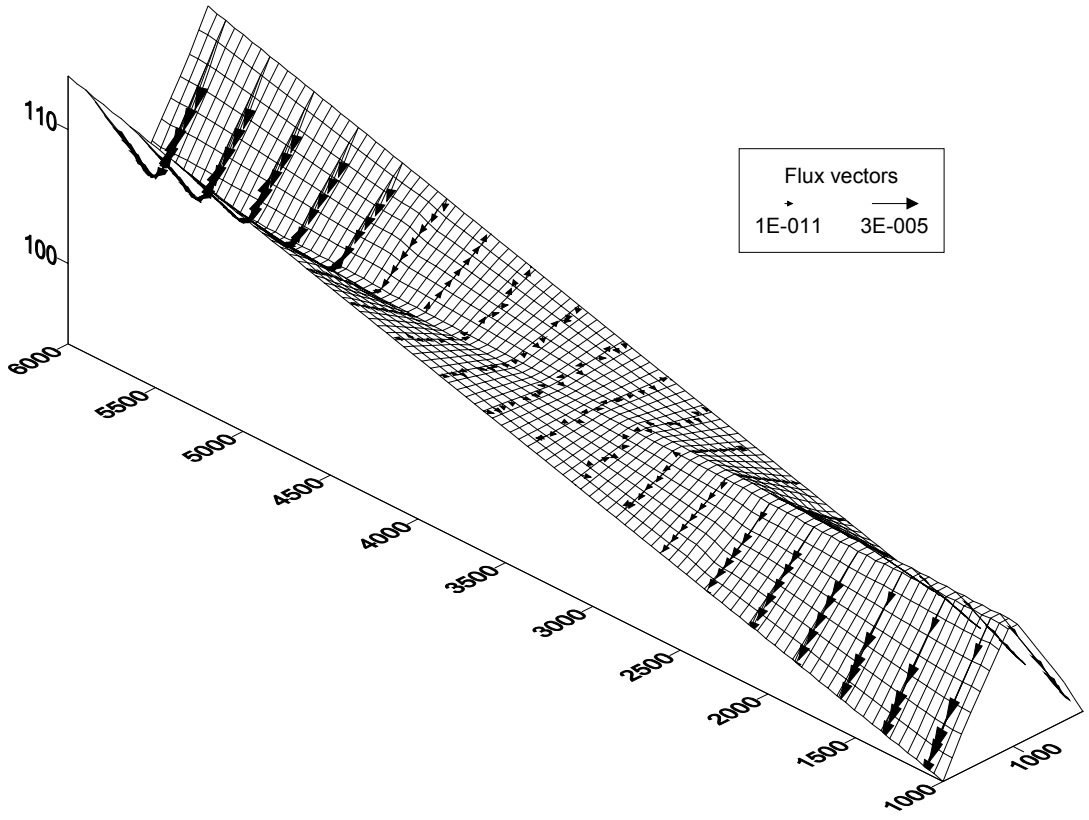

Figure 4.15. Hydraulic head distribution and flux pattern within the domain

In this study, a contaminated area covering a 20m by 20m area is located at the upper densely meshed zone centered at (900,5400) as shown in Figure 4.14. This zone is called the upper analysis zone in the following discussion and covers a 100m X 100m are on the left bank of the river. It is assumed that the contaminated area located at the core of the zone continuously releases a conservative contaminant of 1.0E+5mg/L throughout the simulation. Due to the dominant aquifer flow towards the river, the contaminant plume is then transported towards the river mainly by advective transport. Along the river bed, the contaminant passes through the bed sediments and pollutes the otherwise pristine river water. From this point of contamination, the contaminant is transported further downstream by river flow and quickly affects the lower portions of the aquifer. The analysis is focused on the lower portions of the aquifer on the lower densely meshed area located 3.5km downstream from the original contamination area. This region covers a 300m X 300m are and is centered at position (1000,1950) as shown in Figure 4.14. It is also called the lower analysis zone in the following discussion. The migration of contaminant in the upper and lower analysis zones are analyzed as a function of time.

Before reviewing the results, it is important to stress that fact that the physical setup shown in Figure 4.14 and discussed above is deliberately chosen to demonstrate the impact of a river passing through a contaminated aquifer. In general, it is well known that the travel time of a contaminant in an aquifer could easily be on the order of tens of years to cover a distance of a couple of kilometers under favorable geological settings. The purpose of this application, however, is to show that this commonly accepted belief might be totally wrong with the presence of a river in the system and suitable hydrological conditions.

Following the introduction of the contaminant, it is transported towards the river mainly due to the advective transport governed by the general flow field in the upstream portions of the aquifer where seepage velocities are observed to be in the order of 3.0E-5m/s due to high conductivity value of gravel and large hydraulic head gradient between the boundaries of the aquifer and the river. The contaminant then starts to seep into the river waters where it is heavily diluted and transported downstream. The analysis reveals that the contaminant concentration underneath the river reaches a value of 2.0E+4mg/L in less than 25 days. After the contaminant reaches the river, it only takes about 0.8hrs to reach the point of analysis in the downstream reaches of the river due to the 1.2m/s average flow velocity in the river. Therefore, the river acts as a conduit for rapid transport of contaminants. The hydraulic head conditions in the lower portions of the aquifer favors seepage inflow to the aquifer as shown in Figure 4.14. This hydrologic pattern re-introduces the contaminants to the otherwise uncontaminated portions of the aquifer. It must be mentioned that, without the river, the contamination in the aquifer cannot reach the lower analysis zone which is located about 3.5km downstream. Furthermore, the clay layer in between the two gravel layers acts as an additional barrier for the contamination to reach the lower analysis zone even in long time periods.

First, the migration of the contaminant towards the river is analyzed as shown in Figure 4.16. The spatial distribution of time-dependent change in contaminant concentration in the upper analysis zone reveals the fact that contaminant quickly reaches the river due to the large advective and dispersive transport. The advection velocity in this zone is in the order of 7.0E-5m/s, which allows the contaminant to move about 6m/day. Moreover, the dispersivity of the medium is taken to be 50m, which also

significantly contributes to the overall rapid movement of the contaminant. As soon as the contaminant reaches the river, it starts to cross the river bed via advective and dispersive transport and mix into the river waters. At this point, the advective transport is a function of the lateral seepage velocity where as the dispersive flux is based on the concentration gradient between the two domains. It is important to note that the dilution effect of the river is generally significant since it is a function of river discharge and total seepage from the aquifer. The contaminant concentration distribution in the river is shown in Figure 4.17 as a function of time and space. From this figure, it is seen that the river concentration is effectively constant from the point where the contamination zone is located as there is no reaction involved. The amount of dispersion in the channel allows is to migrate backwards towards the upstream boundary of the channel where a zero concentration is specified.

Due to the fast travel times in the river channel, the contaminant is quickly transported downstream where it finds an opportunity to seep back into the aquifer according to the hydraulic head distribution in the region. However, the large dilution in the river reduced the concentration of the contaminant and is at least 5 orders of magnitude smaller when reintroduced to the aquifer. The spatial distribution of time-dependent change in contaminant concentration in the lower analysis zone is shown in Figure 4.18. Since the river acts as a line source for the otherwise pristine lower zone of the aquifer, the contaminant migrates almost perpendicular to the governing flux direction.

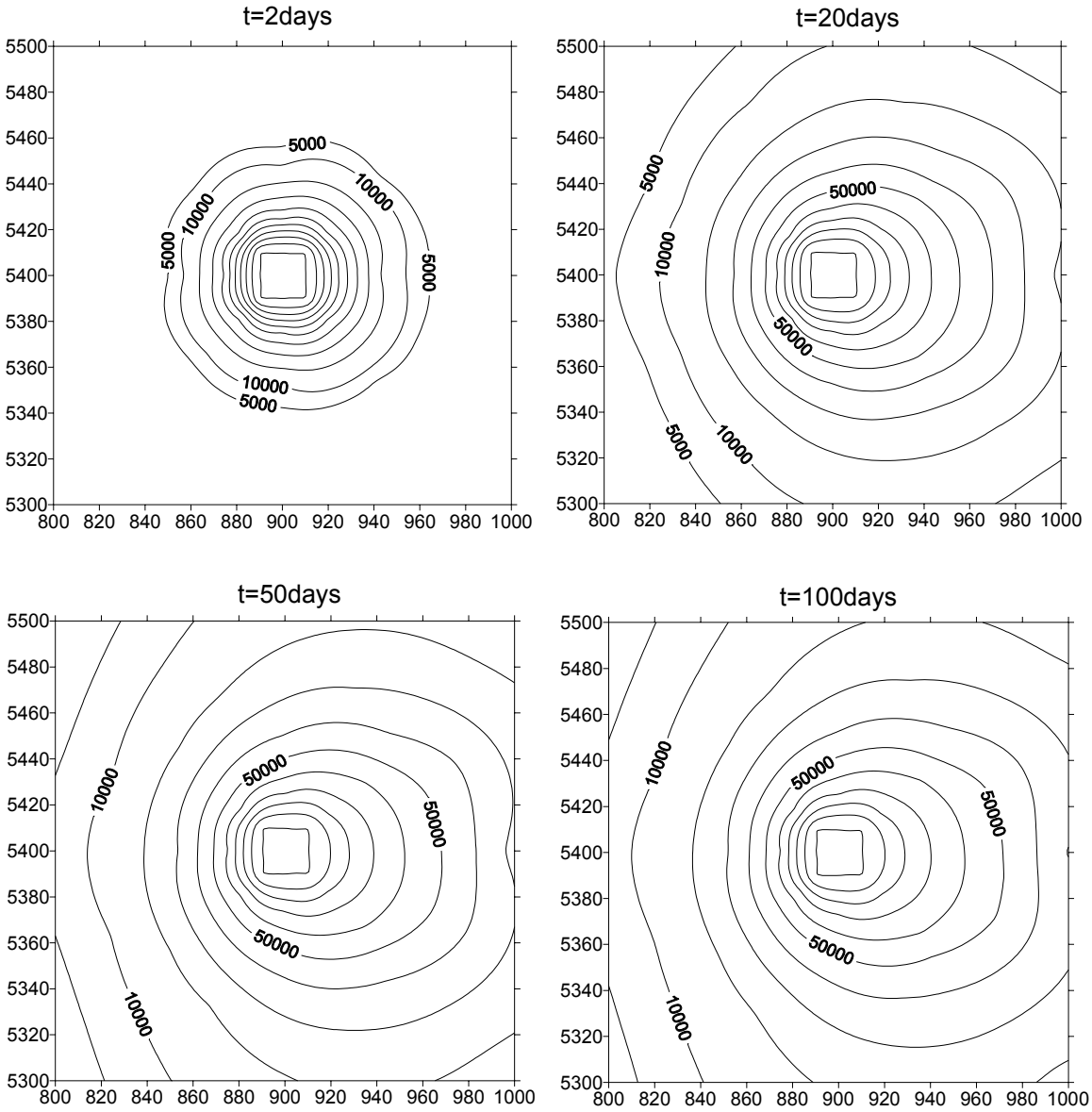

Figure 4.16. Spatial distribution of time-dependent change in contaminant concentration (mg/L) in upper analysis zone

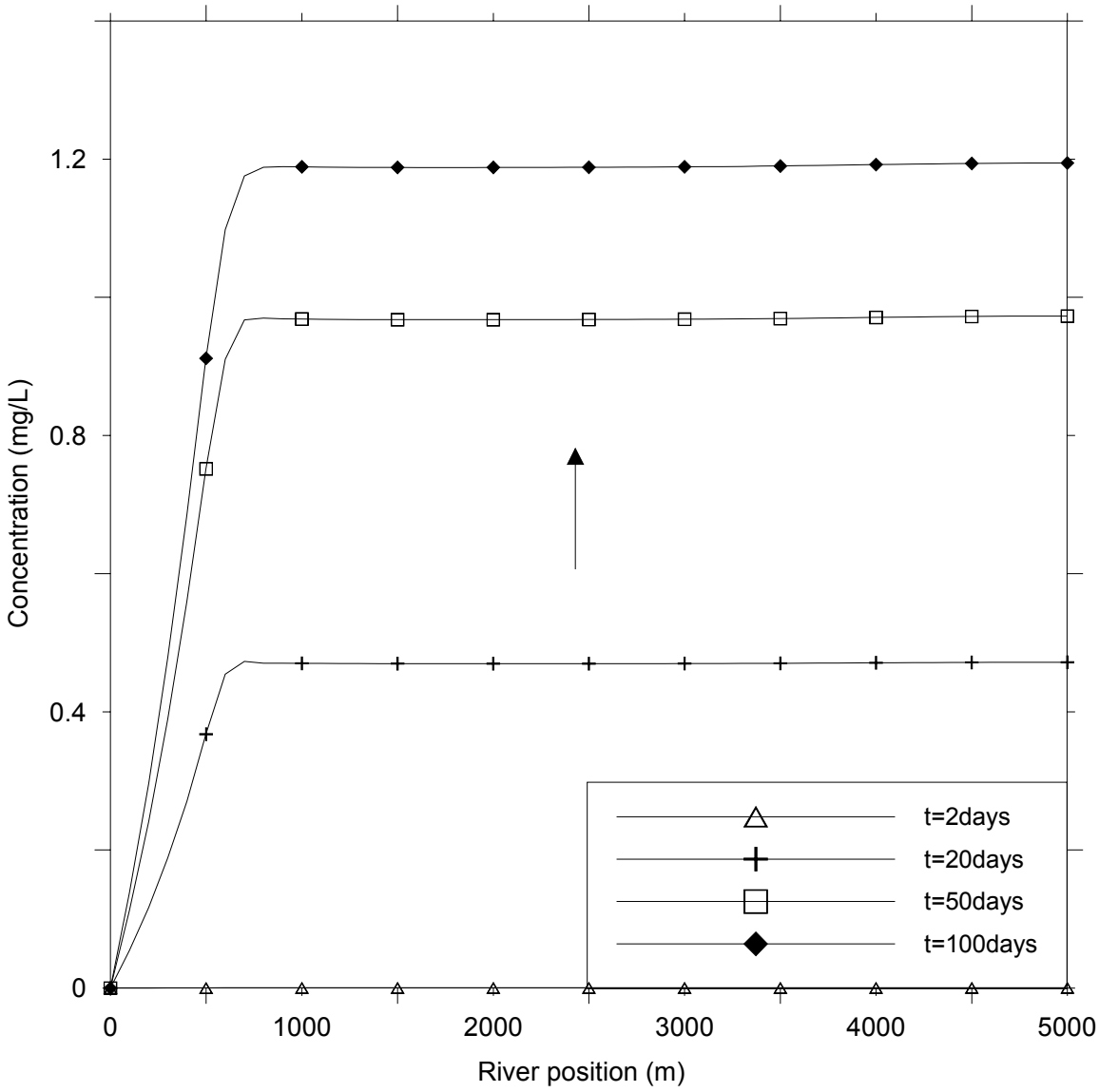

Figure 4.17. Time-dependent change in contaminant concentration in river

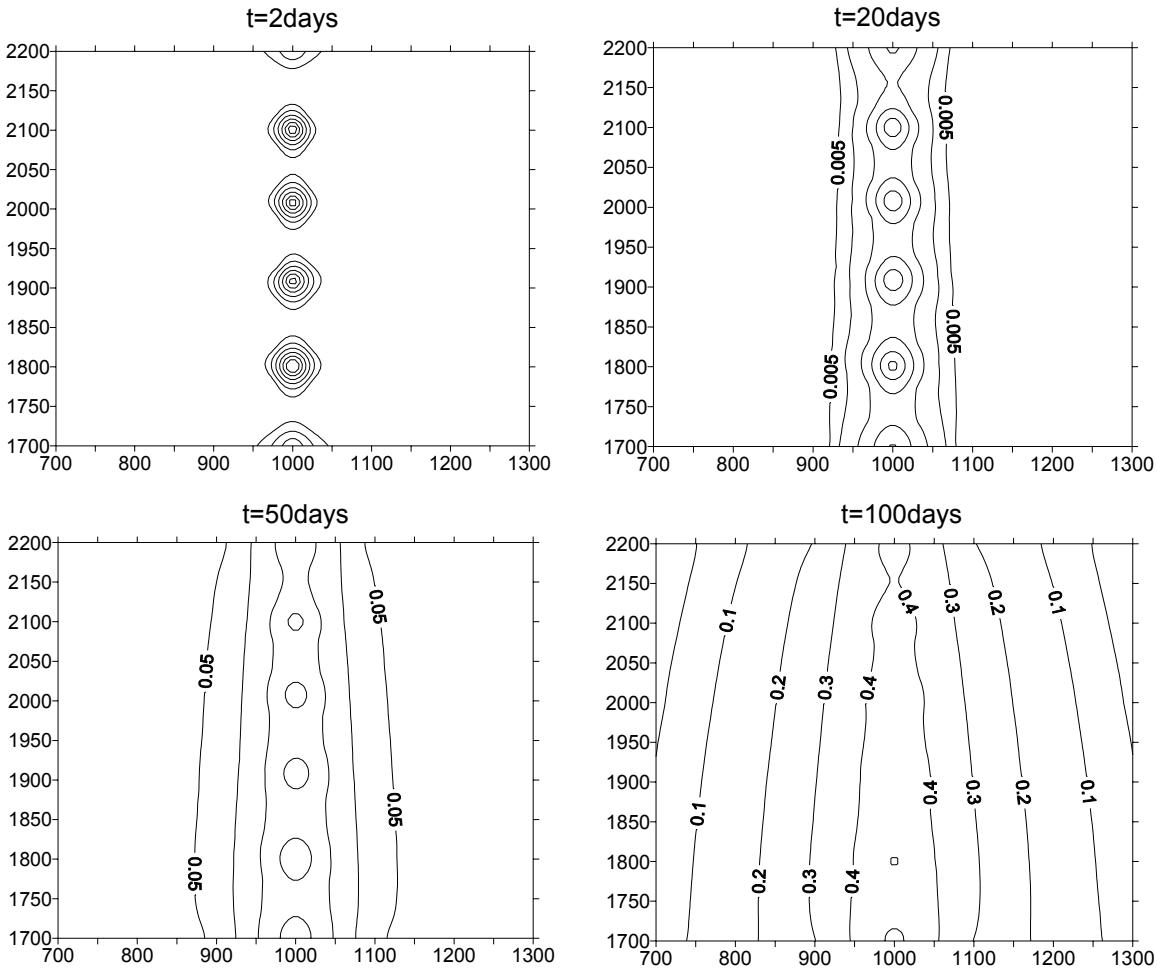

Figure 4.18. Spatial distribution of time-dependent change in contaminant concentration (mg/L) in lower analysis zone

CHAPTER 5

MODEL APPLICATION

In this chapter, the coupled flow and contaminant transport model developed earlier is applied to a large scale watershed to demonstrate the versatility and applicability of the proposed modeling system in a field application using site specific field data. The selected watershed is located in southern Georgia and is a part of the greater Altamaha river basin. The flow model is calibrated and verified with field data from several gaging stations operated by the U.S. Geological Survey. The transport model is then applied with this flow solution to test the consequences of various scenarios based on different contaminant loading conditions. These applications demonstrate the potential use of the model developed in this study in understanding and evaluating the environmental impacts of critical contaminant loading conditions in this watershed which is a relatively underdeveloped watershed otherwise.

5.1. Data Requirements of the Proposed Model

The proposed model requires significant amounts of data mainly due to the distributed nature of the hydrologic and hydraulic processes modeled as well as the

physics-based representation of the fundamental flow and contaminant transport laws defining these processes. For the successful application of the proposed model, these data requirements must be satisfied accurately and realistically. The model data are stored in several input files that are organized according to the flow pathway and characteristics. All files are standard text files with special formatting applied for easy preparation and retrieval of the data. A list of the required data files for the flow and transport model are given in Table 5.1.

Table 5.1. Data files for the Proposed Model

Component	Module	Data file
Main	Common module	time_data.txt general_data.txt
Flow Model	Channel flow module	RIVflow_parameters.txt RIVflow_xs_data.txt RIVflow_channel_data.txt RIVflow_junction_data.txt RIVflow_initial_cond.txt Overland_flow.txt *Boundary condition data files**
	Groundwater flow module	GWflow_parameter.txt GWflow_nodes.txt GWflow_elements.txt GWflow_infilt.txt GWflow_lines.txt GWflow_wells.txt GWflow_bc1.txt GWflow_bc2.txt GWflow_bc3.txt
Transport Model	Channel transport module	RIVtrans_parameters.txt RIVtrans_channel_data.txt RIVtrans_initial_cond.txt Overland_conc.txt *Boundary condition data files**
	Groundwater transport module	GWtrans_parameter.txt GWtrans_nodes.txt GWtrans_elements.txt GWtrans_infilt.txt GWtrans_lines.txt GWtrans_wells.txt GWtrans_bc1.txt GWtrans_bc2.txt

** The names of these files are application specific and are provided in channel data file.*

The common data files (i.e., *general_data.txt* and *time_data.txt*) are used by both flow and transport models. The time parameters file specify the temporal simulation data including the starting and ending date and time as well as maximum, minimum and standard time steps to be used in variable time stepping algorithm. The minimum and maximum iteration boundaries used to alter the time step are also specified in the time parameters file. The general data file specifies the use of the model (i.e., flow simulation or flow and transport simulation) and the convergence criteria for transport model.

The flow parameters in the channel and groundwater flow domains are specified in *RIVflow_parameters.txt* and *GWflow_parameters.txt*, respectively. These files include the total number of flow related parameters such as the total number of nodes, elements, boundary conditions, lines sources and wells in the groundwater flow domain as well as the total number of cross-sections, channels, junctions, data lines, overland flow contributions and boundary conditions in the channel flow domain. These files also include the tolerance values for the associated non-linear solvers.

The cross-section data file *RIVflow_xs_data.txt* contains the major input information for the river flow model. This file is assembled to contain elevation vs. top width information at each user-specified cross-section along the channel network. The top width information is further classified as main channel, left and right floodplain and inactive storage widths. The file also includes elevation dependent Manning's roughness coefficients as well as the straight and meandering distances of each cross-section to the starting position of each channel within the system.

The channel data file *RIVflow_channel_data.txt* includes one line of information specific to each channel within the network. For single channel systems, this file contains

a single line of data. The data file contains the name, first and last cross-section number and order of the channel. It also specifies the types of boundary conditions at both ends of the particular channel as well as the names of the input files associated with these boundary condition types. The junction data file *RIVflow_junction_data.txt* contains one line of information for each junction within the channel network. This file is not used for single channel systems. For all networks, this file specifies the total number of inflowing channels to the particular junction and their channel identification numbers. In addition, the file also contains the identification number of the outflowing channel from the particular junction.

The initial conditions along channel are specified in the *RIVflow_initial_cond.txt* file and contain the initial depth and discharge values observed at each cross-section of the system. These values are used to initiate the simulation and therefore are extremely important for the stability and accuracy of model solutions.

If a channel has an external boundary condition at any end, a boundary condition data file is specified. The names of these files are supplied in the channel data file. It is important to note that only a single channel system would have two boundary conditions at the upstream and downstream ends of the channel. For all networks, a minimum of three boundary conditions are specified both at the upstream nodes of first order channels and the downstream node of the most downstream channel. The files would include the associated data type such as a discharge time series or stage time series or a rating curve as specified the channel data file.

The model also requires a data file if overland flow is present in the system. The small creeks and tributaries could be modeled as overland flow if the reach length that

this flow discharges is selected to be small compared to the regular length of a reach. When such a condition is modeled, then the overland flow input file *overland_flow.txt* must be prepared to include the time-dependent discharge value and the reach number it discharges to.

The data associated with each node in the two dimensional groundwater flow domain is specified in the *GWflow_nodes.txt* file. This file contains the x- and y- position of the node, the initial hydraulic head elevation prior at starting time of the simulation and the top elevation of the bottom impervious layer. Similarly, the data associated with each quadrilateral element of the two dimensional groundwater flow domain is specified in the *GWflow_elements.txt* file. This file contains the nodal connectivity of the element as well as the specified yield, hydraulic conductivity and angle of inclination between the global and the principle coordinate systems. The infiltration rate acting on each element of the domain is specified in the *GWflow_infilt.txt* file as a function of time.

The river/aquifer interface data is provided in the *GWflow_lines.txt* file. This file includes the connectivity of the nodes in river and groundwater flow domains. It also contains the river bottom sediment hydraulic conductivity and thickness information together with the initial values of average river stage in the corresponding reaches of the channel network. The data associated with any discharge or recharge well in the aquifer is specified in the *GWflow_wells.txt* file. This file contains the node value of the well as well as the time-dependent flow rate value of the well.

The three types of boundary conditions of the groundwater flow domain are specified in the files *GWflow_bc1.txt*, *GWflow_bc2.txt* and *GWflow_bc3.txt*. In the first type boundary condition file, the nodal value and the associated time-dependent specified

hydraulic head are provided in the data file. In the second type boundary condition file, the two nodes of the boundary side on which the condition applies are given together with the time-dependent specified flux value. Finally, in the third type boundary condition, the two nodes of the boundary side on which the head-dependent boundary condition applies are given with the hydraulic conductivity of the interface as well as the thickness, wetted perimeter, bottom elevation and time-dependent external head value.

The data files associated with the transport models are very similar to their flow counter parts. In the *RIVtrans_parameters.txt* and *GWtrans_parameters.txt* files, the same discretization related parameters are repeated in addition to some global constants such as the biochemical and radioactive decay coefficients in channel and groundwater flow domains. In addition, the groundwater parameters file also includes the molecular diffusion coefficient.

The *RIVtrans_channel_data.txt* and *RIVtrans_initial_cond.txt* files contain channel specific connectivity data as well as the types of boundary conditions at both ends of the particular channel with the names of the input files associated with these boundary condition types and the initial contaminant concentration values at each cross-section of the channel network.

The model also requires a data file if any overland inflow is present in the system. The small creeks and tributaries carrying contaminants could be modeled as overland flow if the reach length that this flow discharges is selected to be small compared to the regular length of a reach. When such a condition is modeled, then the contaminant concentration in the overland flow is input in the file *overland_conc.txt*. In addition to the time-dependent contaminant concentration value, the file also contains the reach number

it discharges. It is important to note that this file is only prepared for overland inflow to the channel. For overland outflow from the channel, the concentration is fixed and is equal to the river concentration and hence does not require an input file.

The *GWtrans_nodes.txt* data file contains the initial contaminant concentration values at all nodes of the groundwater domain. The *GWtrans_elements.txt* data file includes the longitudinal and transverse dispersivity values, the density and porosity of the soil matrix as well as the portioning coefficient within the element. The contaminant concentration in the infiltration water is specified in the *GWtrans_infilt.txt* file for each element of the domain as a function of time.

At the river/aquifer interface, the vertical dispersivity and the porosity of the river sediments are provided in the *GWtrans_lines.txt* file. It also contains the initial values of average contaminant concentration in river at the corresponding reaches of the channel network. The data associated with any discharge or recharge well in the aquifer is specified in the *GWtrans_wells.txt* file. This file contains the node value of the well as well as the time-dependent contaminant concentration value of the recharging well.

The two types of boundary conditions of the groundwater transport are specified in the files *GWtrans_bc1.txt* and *GWtrans_bc2.txt*. In the first type boundary condition file, the nodal value and the associated time-dependent specified concentration are provided in the data file. In the second type boundary condition file, the two nodes of the boundary side, on which the condition applies, are given together with the time-dependent specified mass flux value.

5.2. Applicability of the Model

The applicability of a model is an important criterion to be ensured before performing any simulations in a watershed. The proposed model has several assumptions and limitations that must be considered carefully for each particular application. The most important of these assumptions is the vertically-averaged nature of the coupled model. Therefore, the proposed model is not applicable when vertical variations in surface and subsurface flow and contaminant transport domains become significant such as in the immediate vicinity of significant water recharge/withdrawal from the aquifer or when the river channel is deep enough to allow vertically stratified flow patterns. Moreover, the coupling between these two pathways is provided by the lateral seepage, which is modeled as a head-dependent line source term. It is, however, well-known that the river channel is essentially of finite width and this width could sometimes become significant with respect to the overall modeling domain width. In this regard, the ratio of average river width to watershed width must be carefully assessed for each application. The user must be aware that the proposed model results might deviate from reality when a wide river channel in a narrow floodplain aquifer is modeled. Under such conditions, the line source assumption is violated and the river channel must be modeled as an area source, which cannot be handled with the current model structure.

5.3. General Description of the Lower Altamaha Watershed and Project Area

The greater Altamaha river basin is the largest watershed in the State of Georgia draining about 25% of the state's area. It is also the third largest basin draining to the Atlantic Ocean. It is formed by the confluence of the Ocmulgee, Oconee and Ohoopee

rivers (Figure 5.1). From the confluence point of Ocmulgee and Oconee rivers down to the Atlantic Ocean, the river system is known as the Altamaha river. It is only this most downstream part of this large basin, which is referred as the Lower Altamaha watershed. This particular application of the coupled flow and transport model focuses on this lower section of the entire Altamaha basin, including portions of the Altamaha and Ohoopee rivers as shown in Figure 5.1.

The lower Altamaha watershed has a drainage area of about 3900 square kilometers compared to the total 35200 square kilometers of the entire Altamaha basin. The project area, on the other hand, covers an area of about 2500 square kilometers, which roughly corresponds to 64% of the lower Altamaha watershed. Looking at the overall hypsographic features of the entire Altamaha basin, it can be seen that, with an average width of 26 kilometers, the Lower Altamaha basin is like an 'outflow pipe' or a 'conduit' discharging the combined flows of the Ocmulgee and Oconee rivers with some contribution from its own drainage area (Figure 5.1). The basin has an average elevation of 50m and an average annual precipitation of approximately 115cm. At the U.S. Geological Survey gaging station located at Doctortown, GA, the long term mean annual flow of the Altamaha river is measured to be about 400 cubic meters per second.

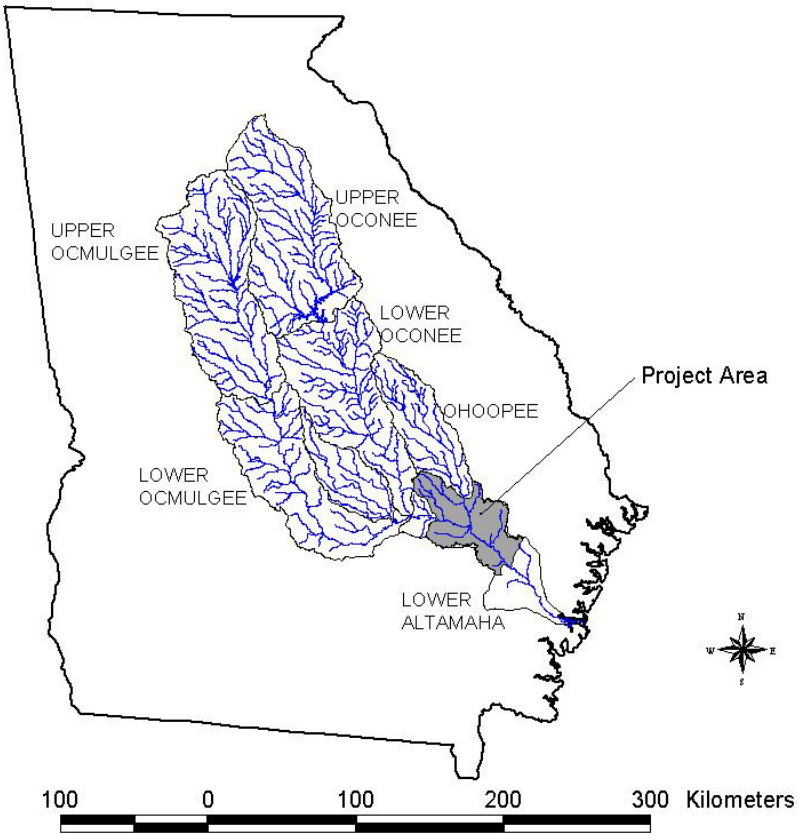

Figure 5.1. Altamaha river drainage area and project area

The lower Altamaha watershed has characteristics typical of lowlands with gentle slopes. The maximum elevation difference between the lowest and highest points of the watershed is approximately 90m, representing a very mild topography. The main features of the drainage network show a gently meandering pattern in this low land area with a relatively mild slope. This pattern is reflected in Altamaha river with an average slope of 0.0002 m/m below the confluence point of Ocmulgee and Oconee to Doctortown, GA.

Wetlands are commonly observed in the low gradient areas, especially along the river banks and in the coastal region. The contour map of the Lower Altamaha watershed illustrates three distinct topographic zones: (i) the (relatively) highlands; (ii) the transition

zone, and (iii) the lowlands or the coastal plains. The topography of the region also shows the gradual increase in floodplain width as the river flows towards the lowland zone. Although the Altamaha river is the main drainage feature of the lower Altamaha watershed, the drainage pattern becomes extremely complex particularly in the coastal plains downstream of Jesup, GA. In this particular section, Altamaha river does not have a significant drainage area but rather resembles a 'conduit' composed of several inter-connected channels to convey the combined flows of Ocmulgee, Oconee and Ohoopee.

The project area covers a portion of the lower Altamaha watershed drainage area bounded by the U.S. Geological Survey stream gaging stations located at Baxley, Reidsville and Doctortown (Figure 5.2). The drainage pattern in this region is governed by Altamaha river which is later confluenced by Ohoopee river about midway between Baxley and Jesup. The sections of the Altamaha-Ohoopee river system within this area have a total reach length of about 90 km within a sinuous channel of about 115 km.

To implement the proposed flow and transport model, this area is discretized by 6,828 quadrilateral finite elements giving a total of 7,031 nodal points. The average element side length along the river sections varies from 150 m to 400 m and about 1000 m elsewhere. On the other hand, the river network that is formed by three channels (i.e., the upstream channel of Altamaha river before the Ohoopee confluence, the Ohoopee river channel and the downstream channel of Altamaha after the Ohoopee confluence) and a single junction is discretized by 391 river reaches giving a total of 394 nodal points. The discretized modeling domain for the proposed model is shown in Figure 5.2. The channel profiles are given in Figure 5.3. As can be seen from the figure, the Ohoopee river channel has the biggest bottom slope compared to the mildly sloping Altamaha.

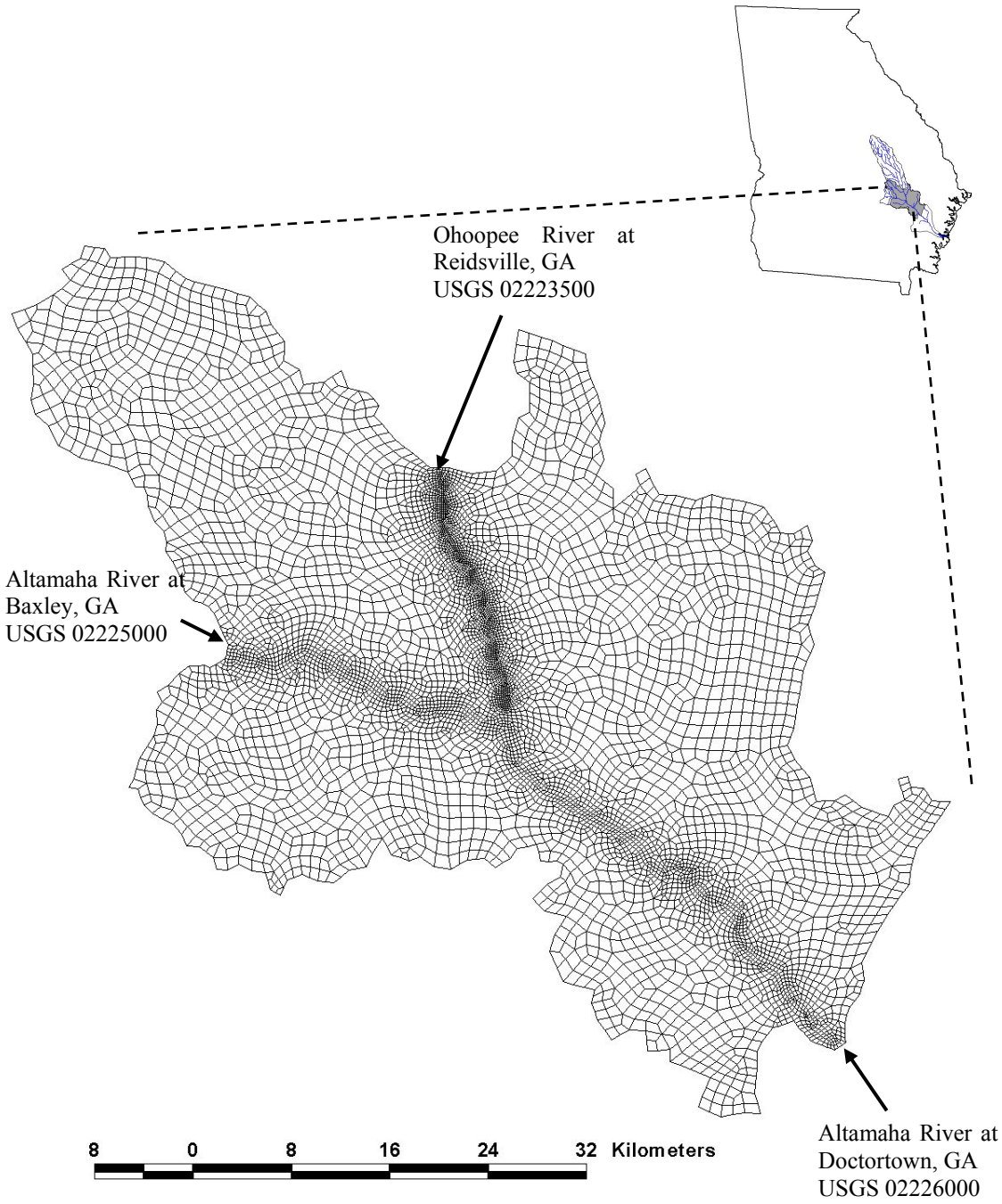

Figure 5.2. Discretized map of the project area in lower Altamaha river basin

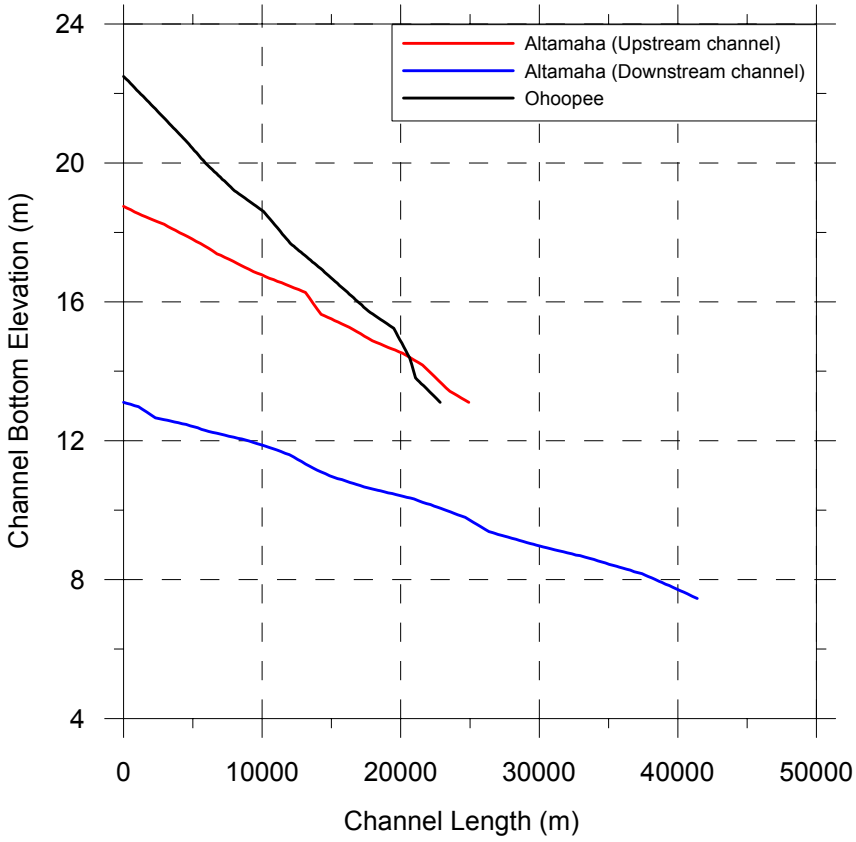

Figure 5.3. River channel profiles

The channel network is discretized by 394 cross-sections. The required data at these nodes are obtained by using: (i) the measurements taken at three gaging stations by USGS; (ii) the profiles of highway bridges along the river channels; and, (iii) the topographic maps of the area. For all intermediate nodes where no specific feature is present to aid the collect the cross-section data, linear interpolation is performed between the nearest upstream and downstream cross-section with specific data. The top widths are then verified with map readings for consistency. For this particular application, each cross-section is described with 10 sets of elevation-top width pairs starting with thalweg elevation and bottom width of the river.

The Manning's roughness coefficients are generally considered to be the calibration parameter for channel flow models. Following a series of test runs on the Altamaha river system, a range of Manning's roughness coefficients are used in the simulations. These values varied between 0.020 to 0.030 within the main channel and 0.030 to 0.070 along the floodplain. Considering the accuracy of the timing of the flood peaks, these values are considered to be very close to the actual roughness values in the river. Unless actual field measurements are obtained, these values could be used as general figures in flood routing simulations in Altamaha and Ohoopee rivers.

Three boundary conditions are specified for the channel flow model. The upstream nodes of the upper channel of Altamaha as well as the Ohoopee river is modeled with a discharge time-series that are obtained from the Baxley and Reidsville river gaging stations operated by the U.S. Geological Survey as shown in Figure 5.2. At the most downstream point of the network, a depth-discharge rating curve is used as the boundary condition. This rating curve is obtained from the Doctortown gaging station (Figure 5.2). The rating curve is generated by the U.S. Geological Survey staff for use in their modeling studies and is given in Figure 5.4.

The initial discharge and stage conditions in the river network are determined by running the model for sufficiently long periods of time with time invariant constant boundary conditions. This method of obtaining the initial conditions is well-defined and documented in the literature (Fread, 1985). As river hydraulics are extremely dynamic compared to groundwater hydraulics, the initial conditions smooth out very rapidly after the real-time boundary conditions imposed on the system. Therefore, any possible errors in the initial conditions quickly fade away and the model returns to accurate real-time

operation. On the other hand, the initial conditions are very crucial on the stability of the model in the early phases of the simulation such that they should still be as accurate as possible to provide a stable start-up.

An unconfined surfacial aquifer overlying the Upper Floridian aquifer is considered to be present in the entire project area, with an average thickness of about 40 m. The groundwater flow domain is assumed to follow the surface drainage boundary line. Hence, the watershed boundary is also believed to be to a flux boundary for the groundwater flow domain. While this assumption may not be true for deep aquifers, it is generally accepted that surfacial aquifers demonstrate a replica of the surface topography. With this consideration, the groundwater flow domain is discretized by 6,828 quadrilateral finite elements and 7,031 nodal points as shown in Figure 5.2.

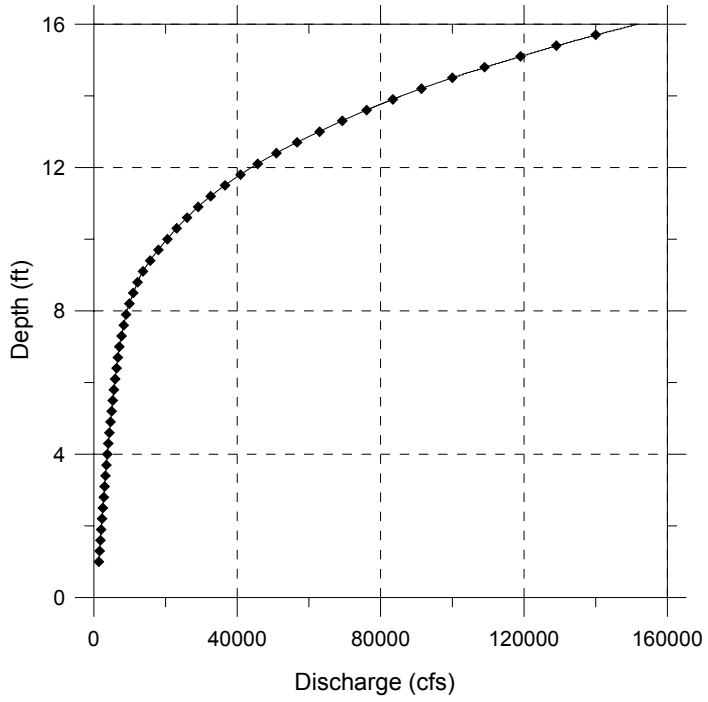

Figure 5.4. USGS rating curve at Doctortown gaging station

The soil types in the aquifer were determined using the State Soils Geographic Database (STATSGO) of Georgia developed by the U.S. Department of Agriculture (STATSGO, 1998). Accordingly, the surfacial aquifer consists primarily of unconsolidated, well sorted sand and silt soils. The spatially distributed soil map of the project area is presented in Figure 5.5. The saturated hydraulic conductivities of these soils are assumed to follow the statistically averaged values provided by Carsel and Parrish (1988). The conductivity values used in the proposed model were selected to be 1.25E-6m/s for silt loam soils, 4.05E-5m/s for loamy sand soils and 1.23E-5 m/s for sandy loam soils. In addition, a 0.3m thickness of river bottom sediments is estimated to be uniformly present along the channel system with a hydraulic conductivity of 6.94E-7m/s, representing silt material deposited in channel bottoms.

The Altamaha river system is modeled as a head-dependent line source that creates lateral in/out flow to/from the groundwater flow domain according to the relative values of the river stage and groundwater head. The natural and artificial lakes and ponds in the basin are modeled as constant-head boundary conditions. Moreover, the external watershed boundary is simulated as a no-flux boundary condition except for the immediate vicinity of the Altamaha River near Doctortown gage that is mostly characterized as marshland and modeled as a constant head boundary condition. Although there are several water extractions within the watershed, including the paper and pulp mill near Doctortown, these are not done from the surfacial aquifer that the proposed model focuses on. Therefore, such extractions are not considered in this study.

The initial conditions in the aquifer is simulated by running the model for extended periods of time with time invariant boundary conditions as well as steady state conditions in the river system since there exists no hydraulic head measurements in the surface aquifer that could serve as initial values of simulations. Considering the strong dynamic link of the aquifer with the surface water features (i.e., primarily the Altamaha river system), this technique of obtaining initial hydraulic head distribution is deemed sufficient.

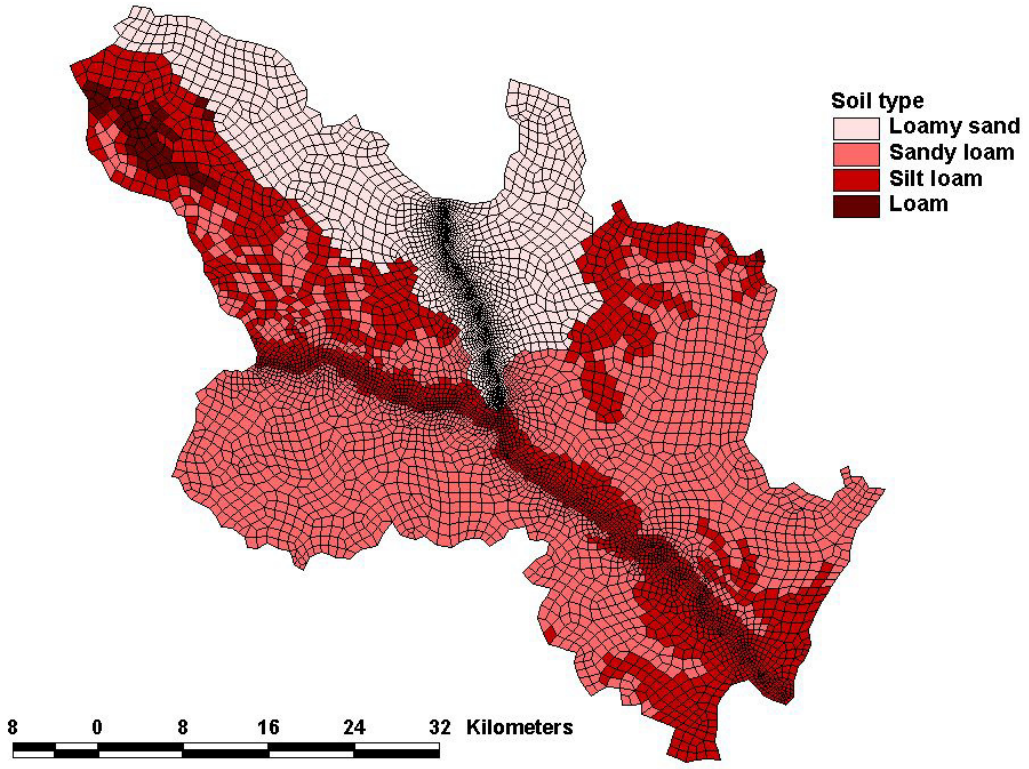

Figure 5.5. Soil type distribution in simulation area

The overland flow contributions to the model are obtained from the simulation results of an empirical model i.e., the Hydrologic Simulation Program-Fortran (HSPF). The HSPF model is a comprehensive, continuous, lumped parameter model developed for U.S. EPA to simulate watershed hydrology and water quality for both conventional and toxic organic pollutants. The HSPF model uses information such as the time history of rainfall, temperature and solar radiation; land surface characteristics such as land-use patterns; and land management practices to simulate the processes that occur in a watershed. The result of this simulation is a time history of the quantity and quality of runoff from an urban or agricultural watershed. Flow rate, sediment load, and nutrient and pesticide concentrations are predicted. HSPF includes an internal database management system to process the large amounts of simulation input and output.

The HSPF is used to simulate the surface and subsurface hydrology of the project area. The results from the overland flow and unsaturated zone flow pathways are then used as input data to the simulations of the proposed model. The overland flow generation scheme of HSPF is used to obtain the flow of several small creeks and tributaries discharging to Altamaha and Ohoopee rivers (Valenzuela and Aral, 2004). The discharge hydrographs of these overland flow contributions are supplied to the model as approximate figures and are not expected to represent the real overland flow discharges. However, the simulation results are shown to get better even with these approximate results and is, therefore, included in the analysis. It is believed that once an accurate and physically-based overland flow algorithm is derived for large scale applications, the results of the analysis would probably improve to a greater extent. For this particular study, a total of 28 point loads representing the main tributaries of Altamaha and

Ohoopee rivers are used in model simulations. The locations of these inputs of overland flow associated with small tributaries and creeks are shown in Figure 5.6. The HSPF-simulated discharge hydrographs for the three major tributary are presented in Figure 5.7.

The simulations are performed over two different time periods. The first phase covers a three-year period starting with 01/01/1988 through 31/12/1990. The second phase, on the other hand, covers a four-year period starting with 01/01/1991 through 12/31/1994. While the first phase is used as the calibration period, the second is used as a verification period.

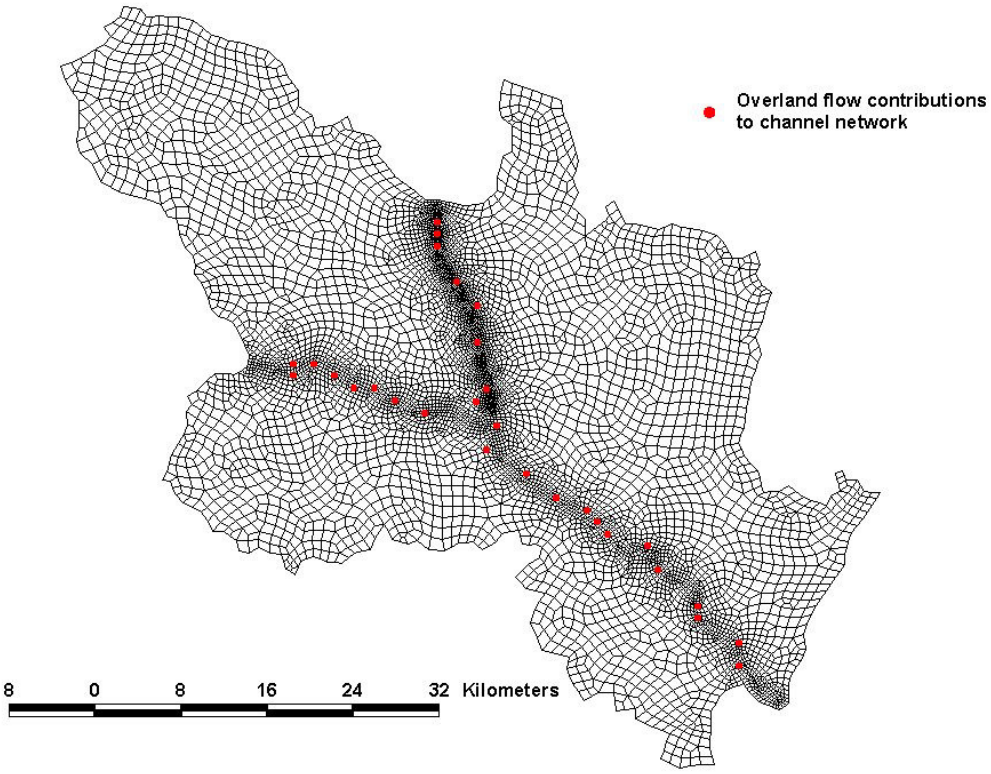

Figure 5.6. Overland flow input points to the channel network

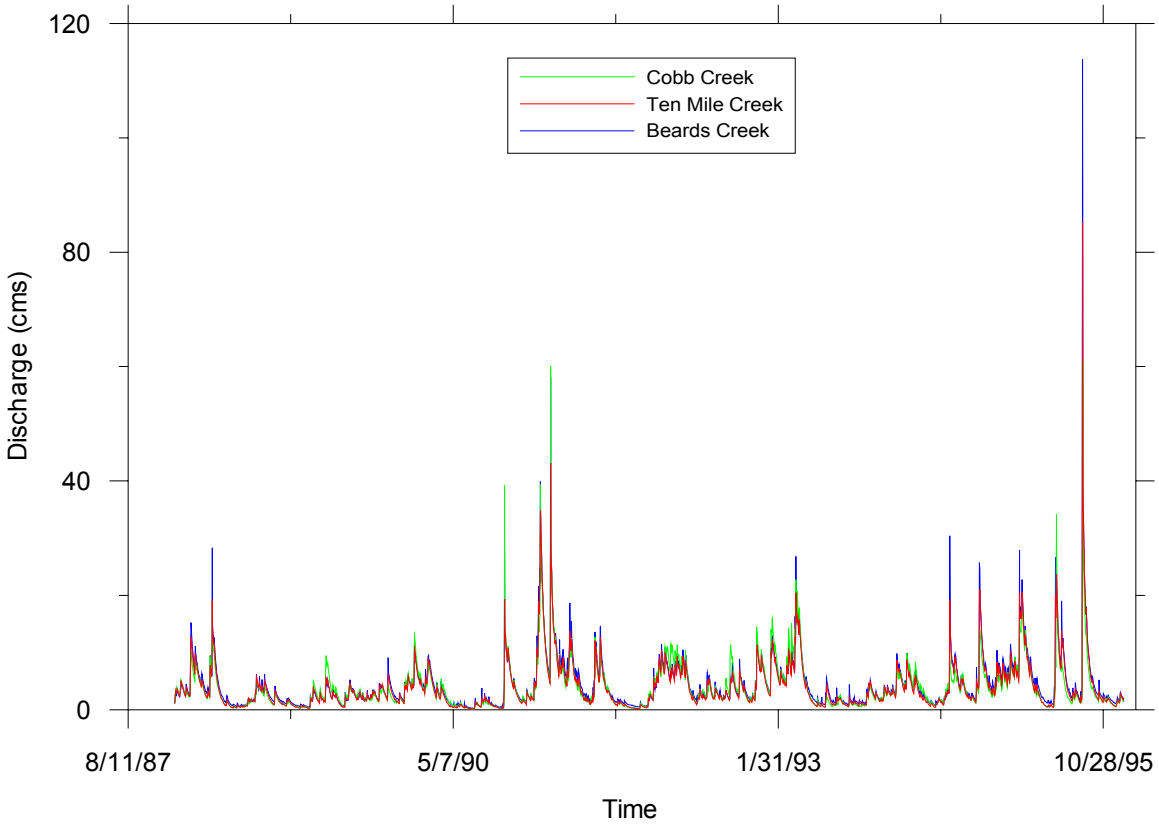

Figure 5.7. Discharge hydrographs of three major tributaries of the Altamaha-Ohoopee system simulated by HSPF model

In all calibration and verification simulations, a maximum time step of 86400secs is used to run the coupled flow model. The minimum time step below which the model is coded to stop simulations is selected to be 1secs for this particular application. All simulations initially started with a time step value of 86400secs, which is later modified dynamically within the simulation according to the convergence requirements of the channel flow model as well the number of iterations performed to converge. Commonly the model experiences a wide range of time steps during a simulation depending on the characteristics of the boundary conditions and the flood wave in the channel. The groundwater flow model generally did not impose any limits on the time step due to the

relatively slow response times in aquifers. In this regard, the coupled flow model is limited by the time step requirements of the channel flow model. The simulations are performed on an Intel Pentium IV computer with a clock time of 2.4GHz and 1.0GB RAM. The Altamaha river simulations take about 5secs per iteration. On the other hand, the number of iterations per time step and the value of the time step are highly variable and are a strong function of the flood wave that is routed in the channel as well as the boundary conditions. The time-weighing parameter used in the four-point Preissmann scheme of channel flow model is also important in the total number of iterations required for convergence. In this study, a weighing parameter value of 0.72 is used during calibration and verification periods.

Simulations in calibration and verification periods revealed the fact that the lower Altamaha river watershed is mostly a boundary condition driven system and the model is highly sensitive to boundary condition data. Therefore, the accuracy of the boundary condition data is very critical for successful simulations of the watershed. In addition, several test runs in the watershed also revealed that the model is also relatively sensitive to other parameters including the Manning's roughness coefficient in channel flow domain and hydraulic conductivity in subsurface flow domain.

5.4. Coupled Flow Simulation

The proposed model is used to simulate the flow conditions in the project area shown in Figure 5.2. Two different sets of runs are performed for calibration and verification purposes. The model calibration and verification is performed with respect to the Doctortown gaging station at the most downstream point of the domain (Figure 5.2).

Although more then one calibration point would generally provide a better assessment of the simulation results, the data availability in the Altamaha system imposes a single point calibration. In this regard, a midstream calibration point would have been a better option for calibrating the results. Nevertheless, the level of accuracy comparisons with a single calibration point is still believed to provide high standards when particularly in data scarce conditions such as the Altamaha river basin. The simulated vs. observed values of the three-year long calibration period is given in Figure 5.8.

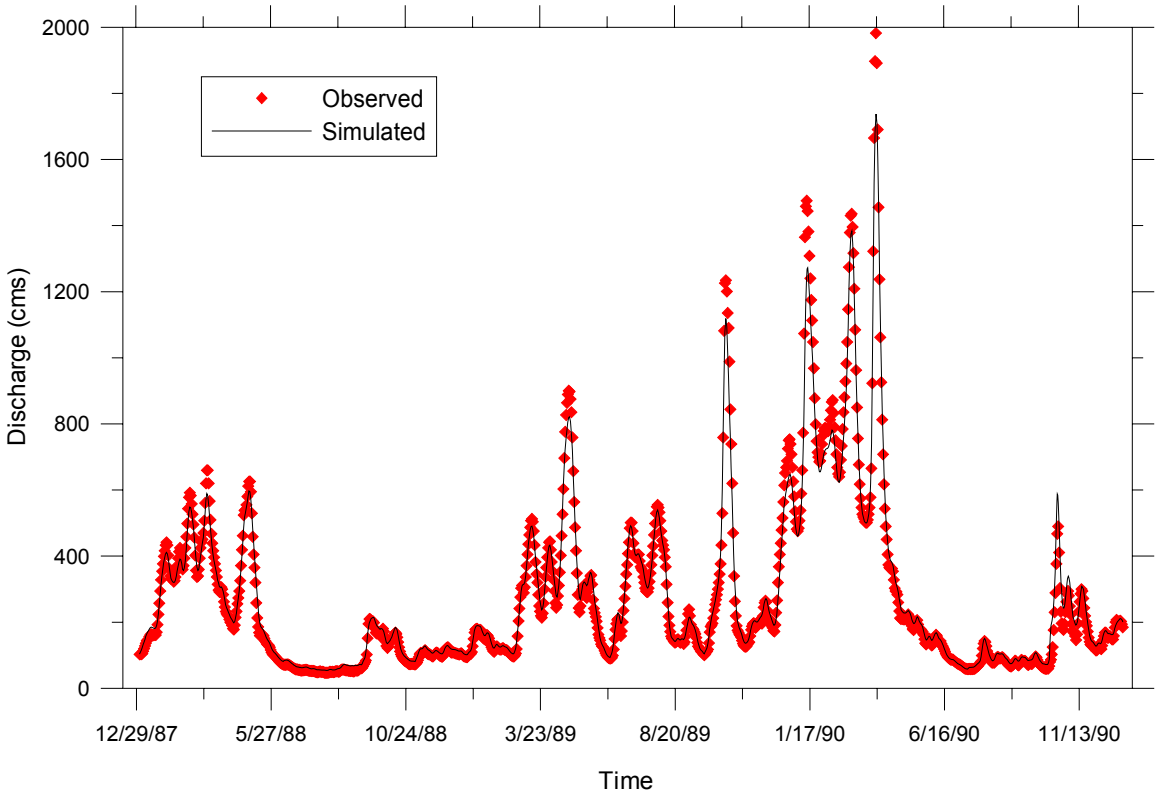

Figure 5.8. Observed vs. simulated results in the calibration period (01/01/1988 – 12/31/1990)

As seen from the figure, the proposed coupled flow provides very good results when compared to the observed values at the Doctortown gage. However, the results are further divided into three separate years to show detailed comparison and to reduce the effect of time scale on the presented graph. These results are shown in figures 5.9a, 5.9b and 5.9c for years 1988, 1989 and 1990, respectively. The detailed comparisons further verify the high level of accuracy achieved by the model. Both the timing and the magnitude of the flood waves are properly captured. Slight deviations are observed at the peak values which are known to be high flow periods by definition. During these extreme events, the overland flow discharges from the small creeks and tributaries reach to considerable levels that would influence the simulation results. During these periods, a more sophisticated overland flow module is necessary to fully capture the flood peak values. It is clear that, in such high flow periods, the watershed becomes a critical contributor to the river flow in the system as opposed to the general boundary condition driven nature of the system. Therefore, it is possible to conclude that with an accurate overland flow algorithm or with measured discharge data of these creeks and tributaries, one could achieve an almost perfect fit using the proposed model.

Unfortunately there exist no measurements to verify the spatial distribution of discharge and/or depth along the channel network. Nevertheless, the discharge distribution along the main Altamaha river is presented in figures 5.10a and 5.10b, representing low and high flow periods, respectively. It is clearly seen from this figure that there are small increases in the channel discharge due to overland flow contributions from the tributaries. The spike at the mid-channel is the point where Ohoopee river joins the Altamaha river.

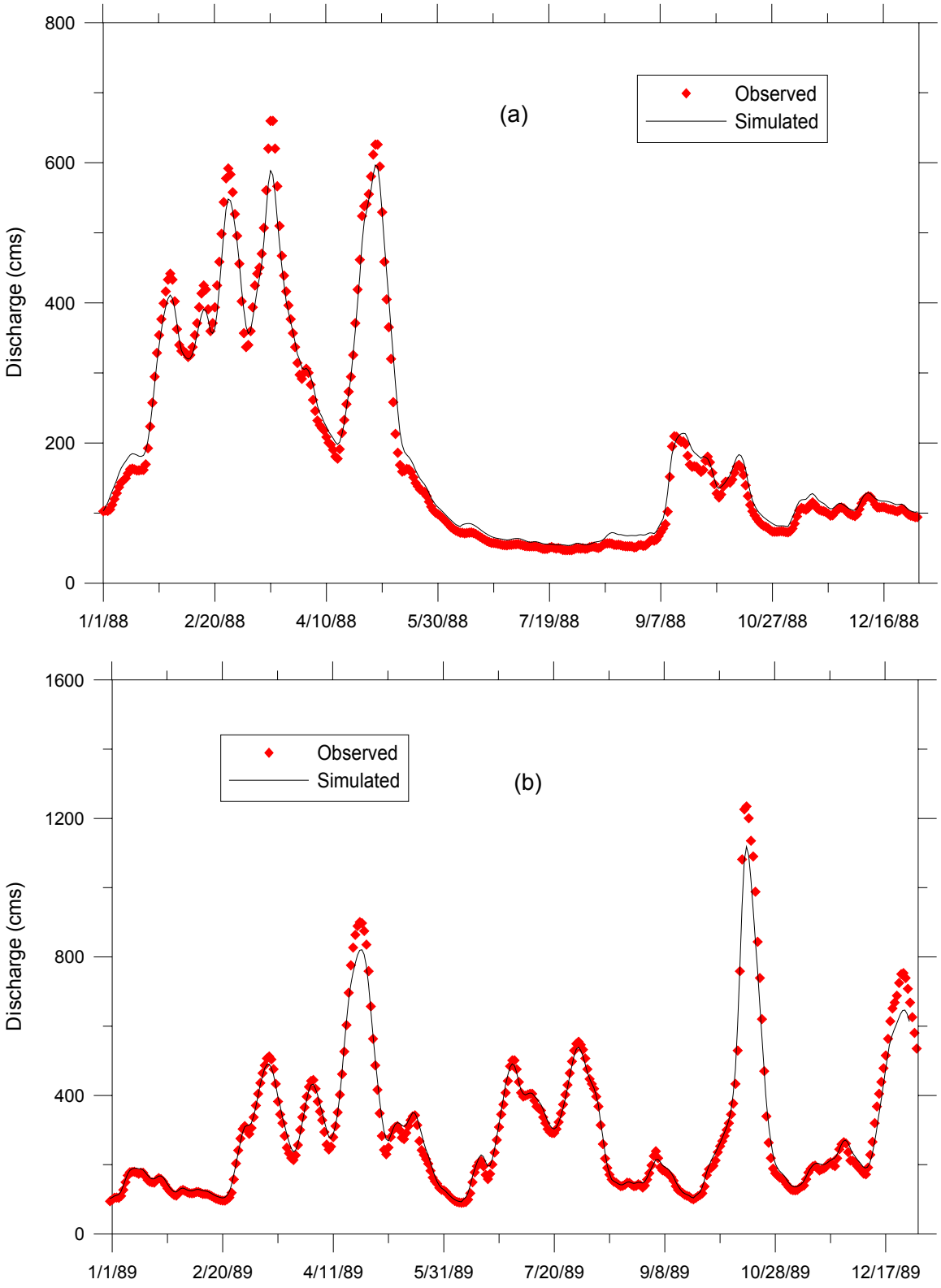

Figure 5.9. Observed vs. simulated results in (a) 1988, (b) 1989 and (c) 1990

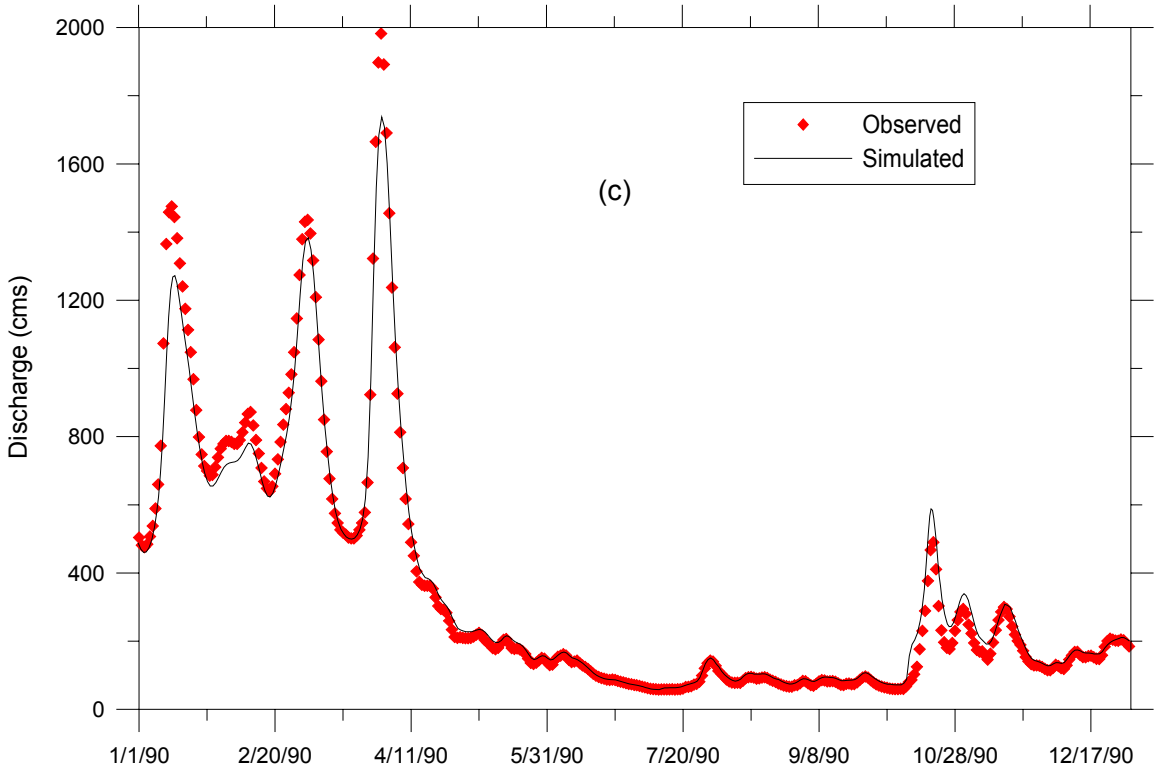

Figure 5.9 (cont'd).

The response of the groundwater to the dynamic hydrologic and hydraulic variations in river channels could be analyzed by focusing on some of the groundwater nodes in the immediate vicinity of the channel network. The lateral seepage to/from the river in these sections determines the hydraulic head distribution in these areas of the surfacial aquifer. This analysis would also help to understand the significance of bank storage on flood peak attenuation in the Altamaha river system. The temporal variation of lateral seepage between cross-sections 45 and 46 in the upstream channel of Altamaha river is shown in Figure 5.11. The figure also presents the discharge hydrograph at cross-section 46. The correlation between lateral seepage and channel discharge conditions is particularly obvious when a major flood event occurs after a relatively steady flow period. In this regard, one could observe the significant lateral outflux from the channel

around 9/10/88. When the flood wave arrives, it disturbs equilibrium that was achieved in the relatively steady flow period that covers a couple of months before the event. As a result of the flood event, the stage in the channel increases and creates a lateral outflow from the channel.

The lateral seepage responses could also be seen in the early parts of the year when consecutive floods arrive to the particular location. However, these interactions are not as clear as the event in September 1988 as the interactions are very dynamic and strongly effected from the earlier events. The model could also predict the impact of bank storage on flood attenuation. Laterally seeping waters from the river are temporarily stored in the immediate vicinity of the channel and is released back to the channel when flood wave passes and river waters recede.

Finally, the groundwater distribution in the watershed is demonstrated in Figure 5.12. The hydraulic head distribution in the figure corresponds to the data at the end of 1988. Since the groundwater flow domain does not experience major changes, a temporal variation in hydraulic head distribution is not meaningful to present. Only in the vicinity of the river channels, the hydraulic head distribution in the aquifer shows variation in accordance with the dynamic link with the river hydraulics.

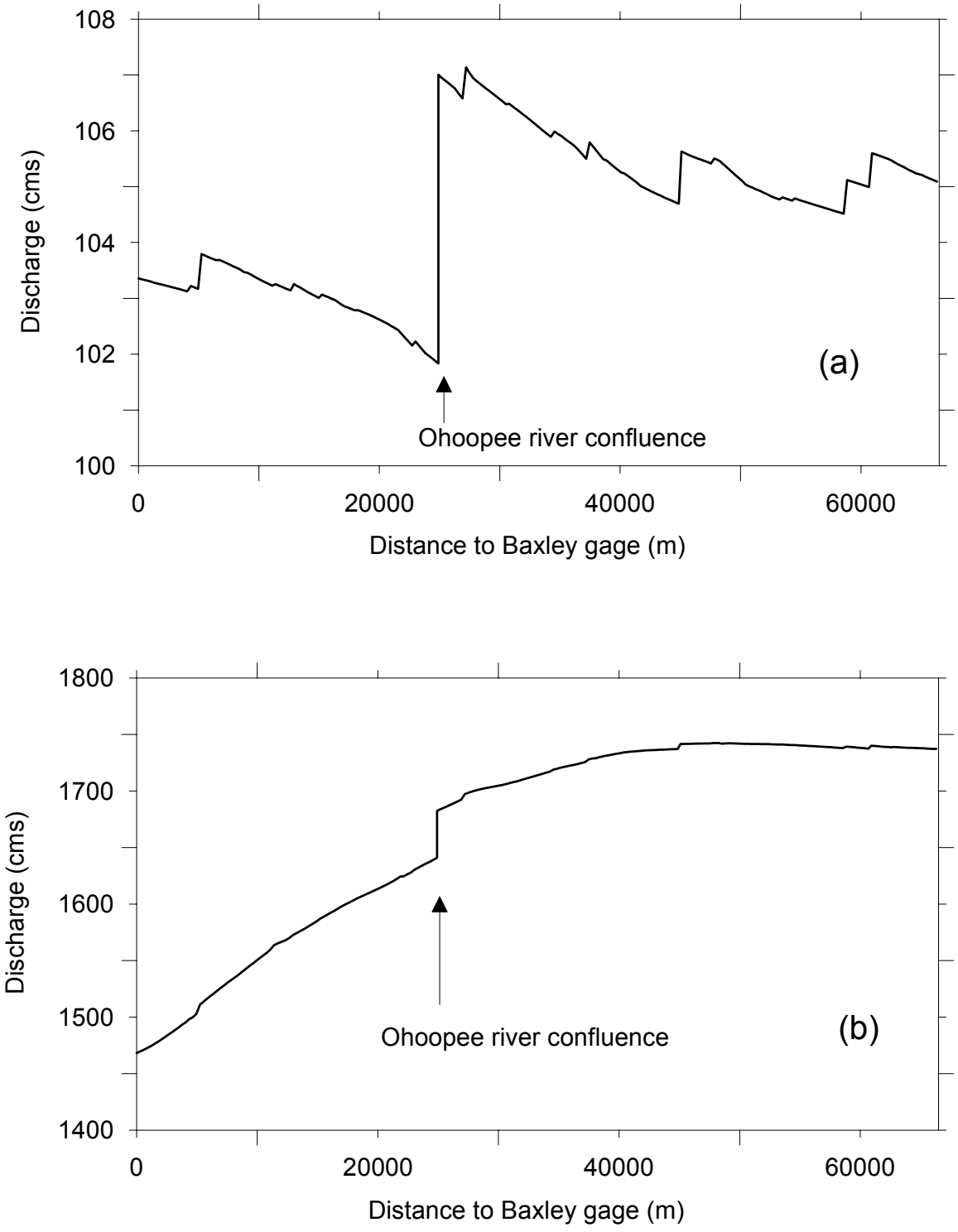

Figure 5.10. Spatial distribution of discharge along the Altamaha river (a) 12/31/1988 and (b) 03/31/1990

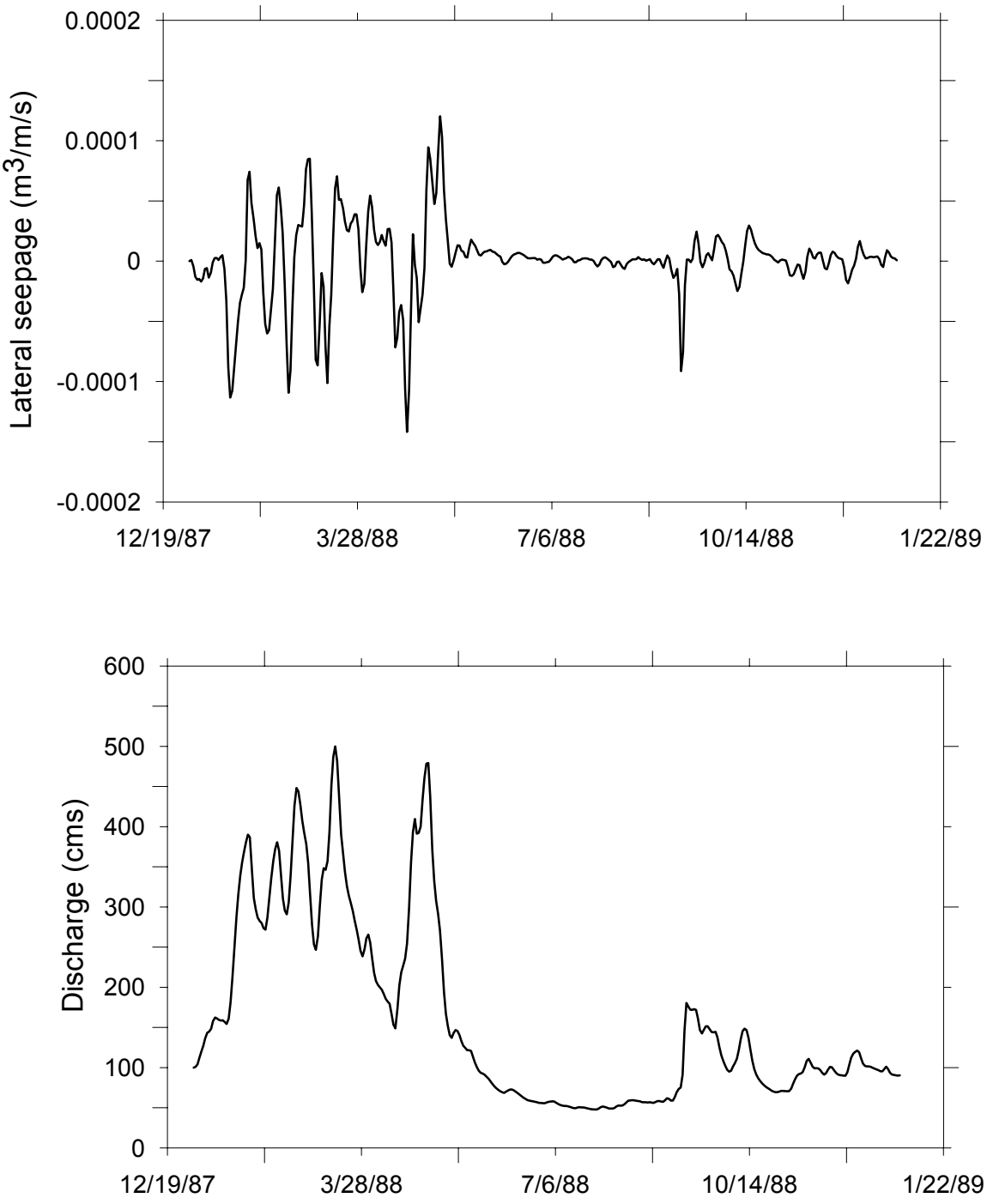

Figure 5.11. Temporal variations in lateral seepage and its correlation with channel flow at Node-46 in upstream channel of Altamaha river

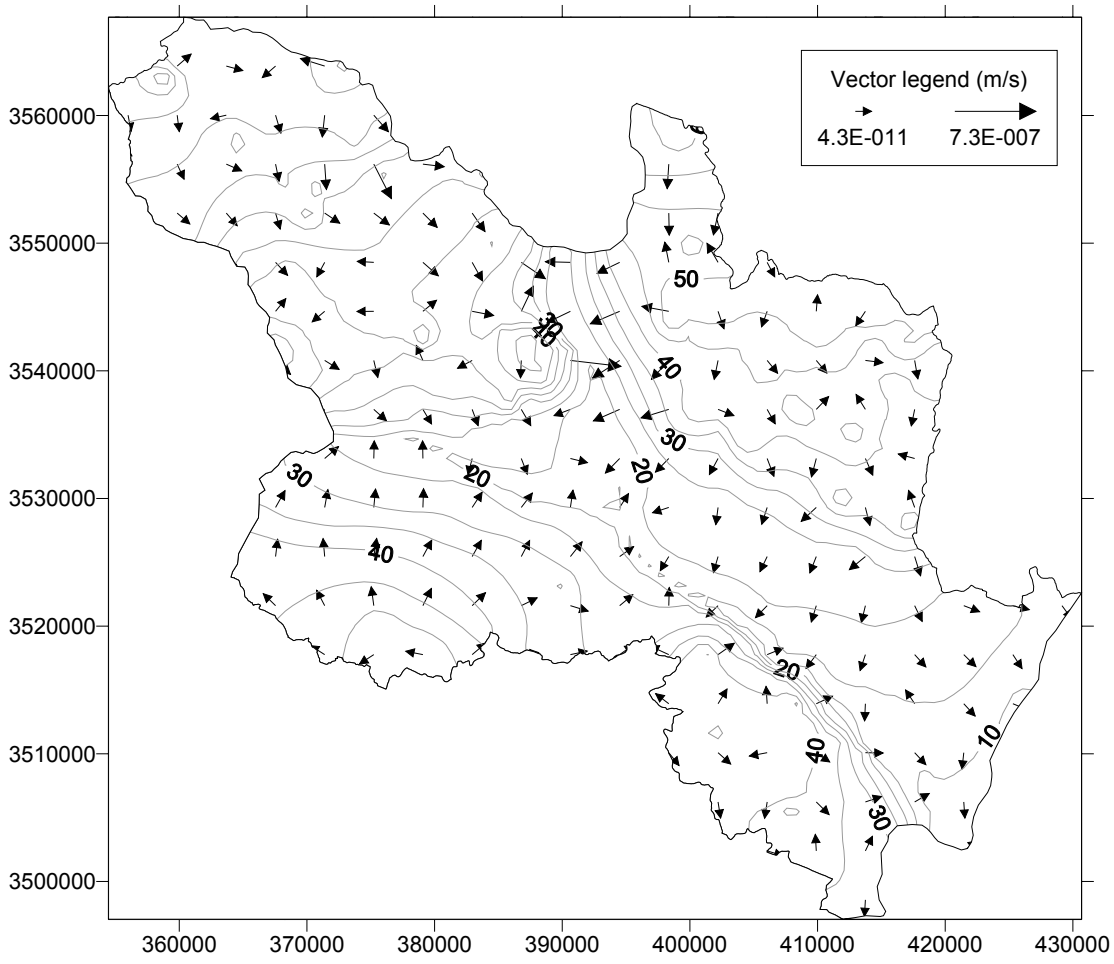

Figure 5.12. Simulated hydraulic head distribution in the watershed at 12/31/1988

Following the calibration runs, a verification run is also performed to validate the proposed coupled flow model. The verification period covers a four-year period between 1991 and 1995. The simulated vs. observed values of the verification period is given in Figure 5.13. As can be seen from the figure, the model performs accurately in the verification run as well. The flood wave is properly routed in the channel system. The discrepancies between observed and simulated extreme events are still visible in the verification run. Considering relatively insignificant, directionally variable contributions of groundwater seepage, these discrepancies are mainly attributed to the lack of an

accurate overland flow simulator. The contribution of overland flow becomes particularly important in extreme events where even small tributaries could carry large discharges.

As seen from the figure, the proposed coupled flow provides very good results in the verification period as well. The results are further divided into four years to show detailed comparison and to reduce the effect of time scale on the presented graph. These results are shown in figures 5.14a, 5.14b, 5.14c and 5.14d for years 1991, 1992, 1993 and 1994, respectively. The detailed comparisons also demonstrate the high level of accuracy achieved by the model. The discrepancies between observed and simulated peak flows are still present in the verification period and are most likely associated with significant overland inflow to the channel from tributaries. Finally, the hydraulic head distribution in the watershed is shown in Figure 5.15 which corresponds to the data at the end of 1991.

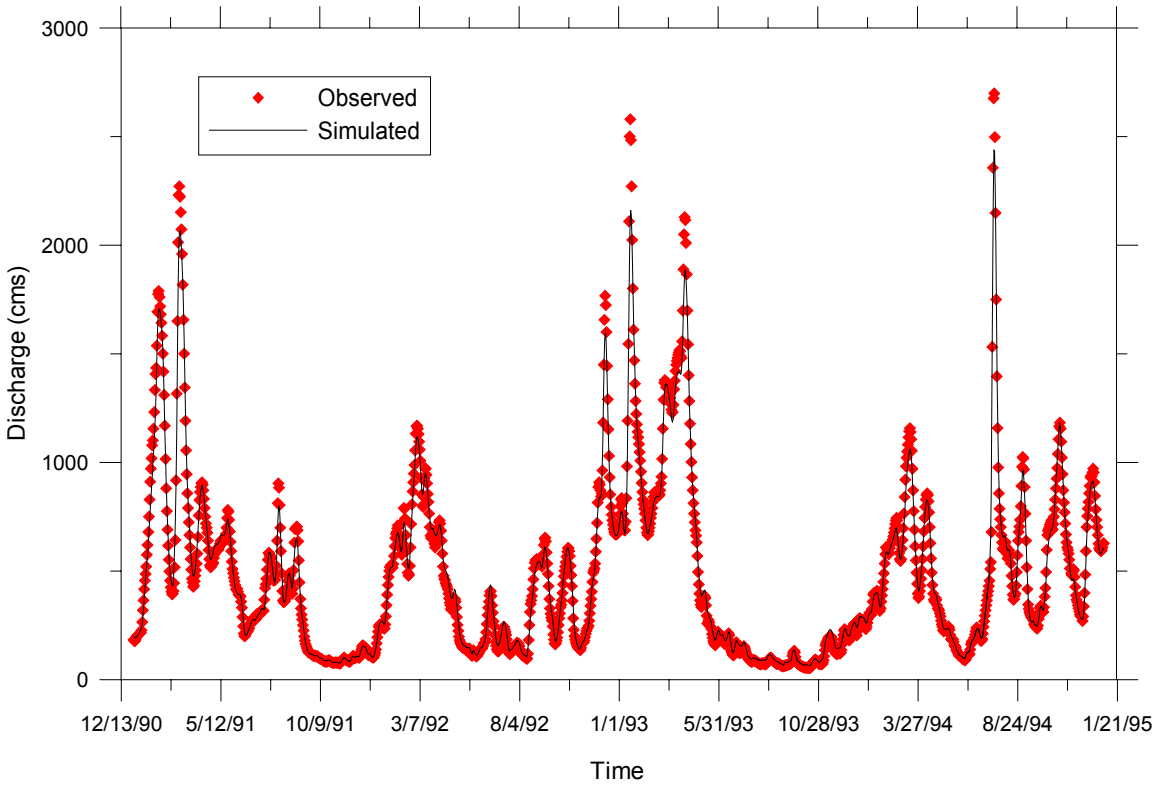

Figure 5.13. Observed vs. simulated results in the verification period (01/01/1991 – 12/31/1994)

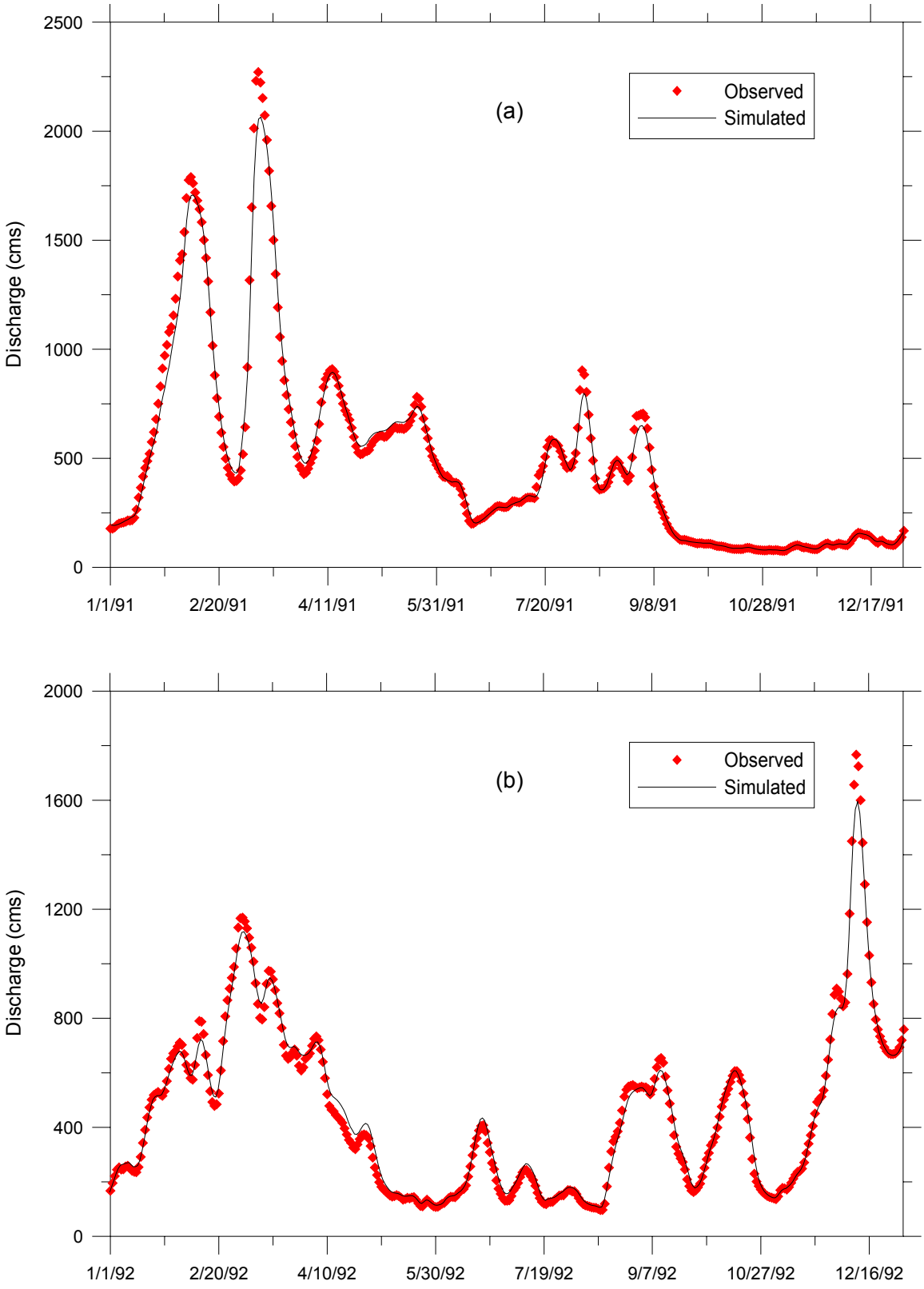

Figure 5.14. Observed vs. simulated results in (a) 1991, (b) 1992, (c) 1993 and (d) 1994

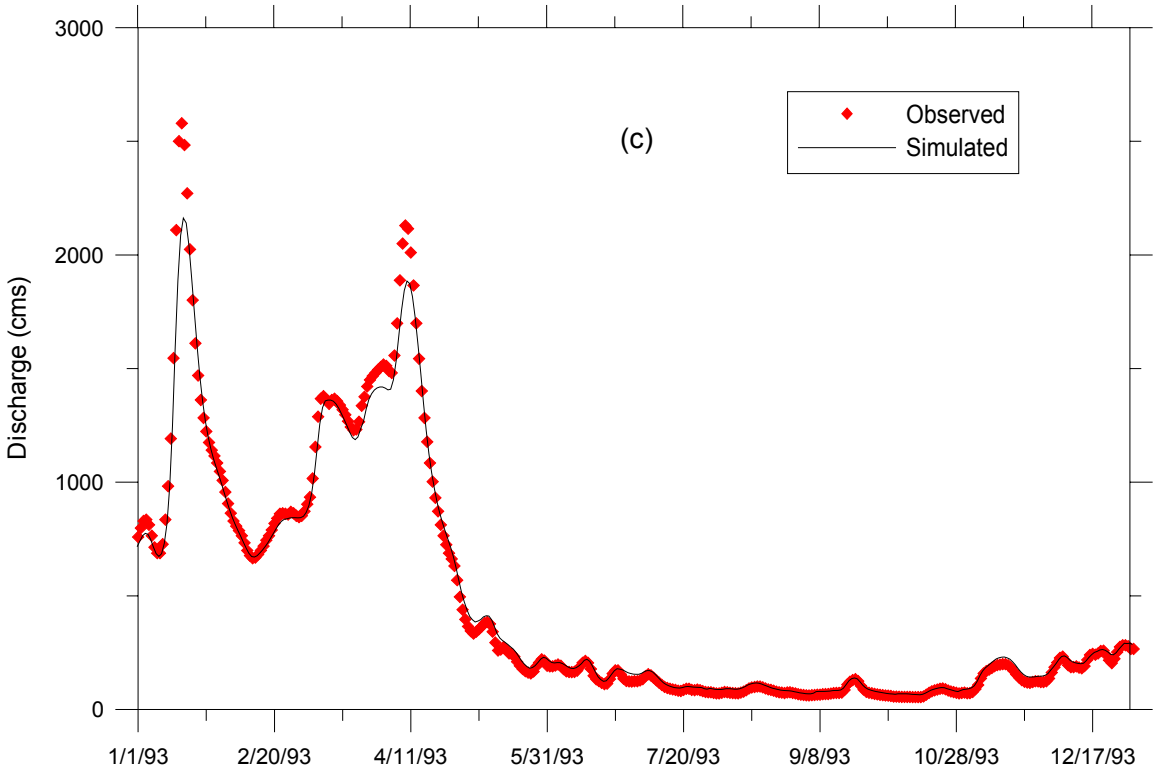

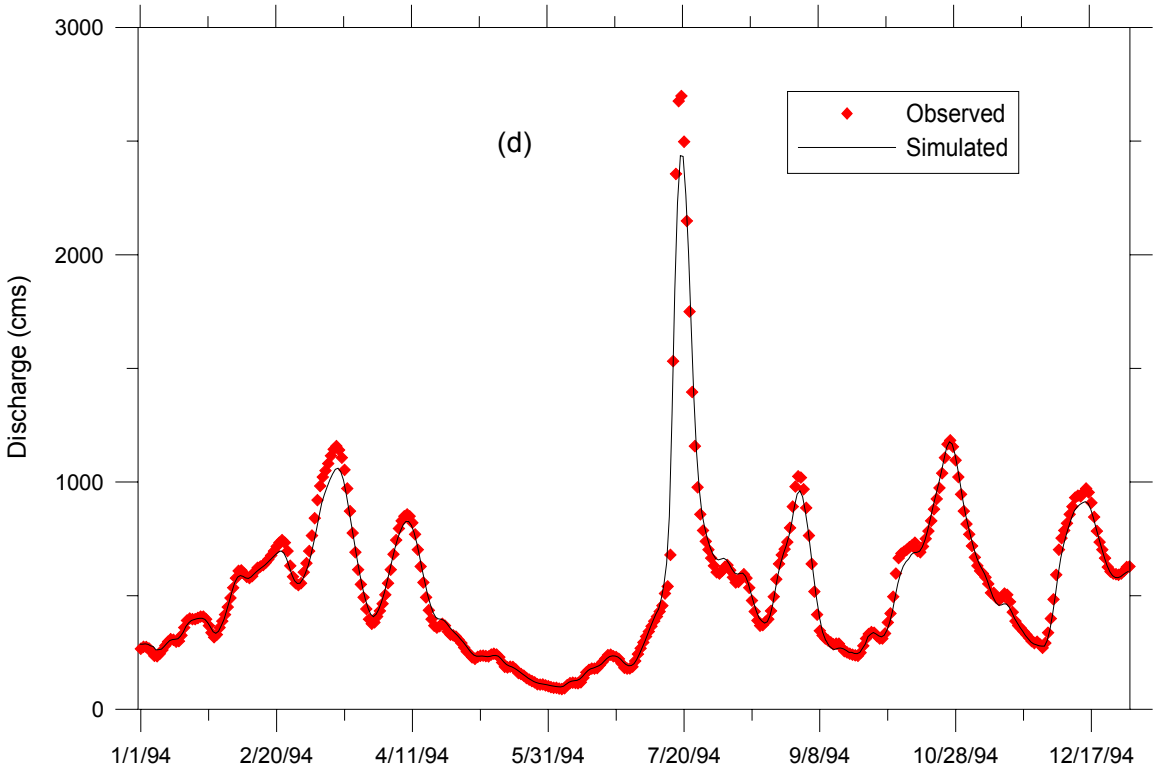

Figure 5.14 (cont'd).

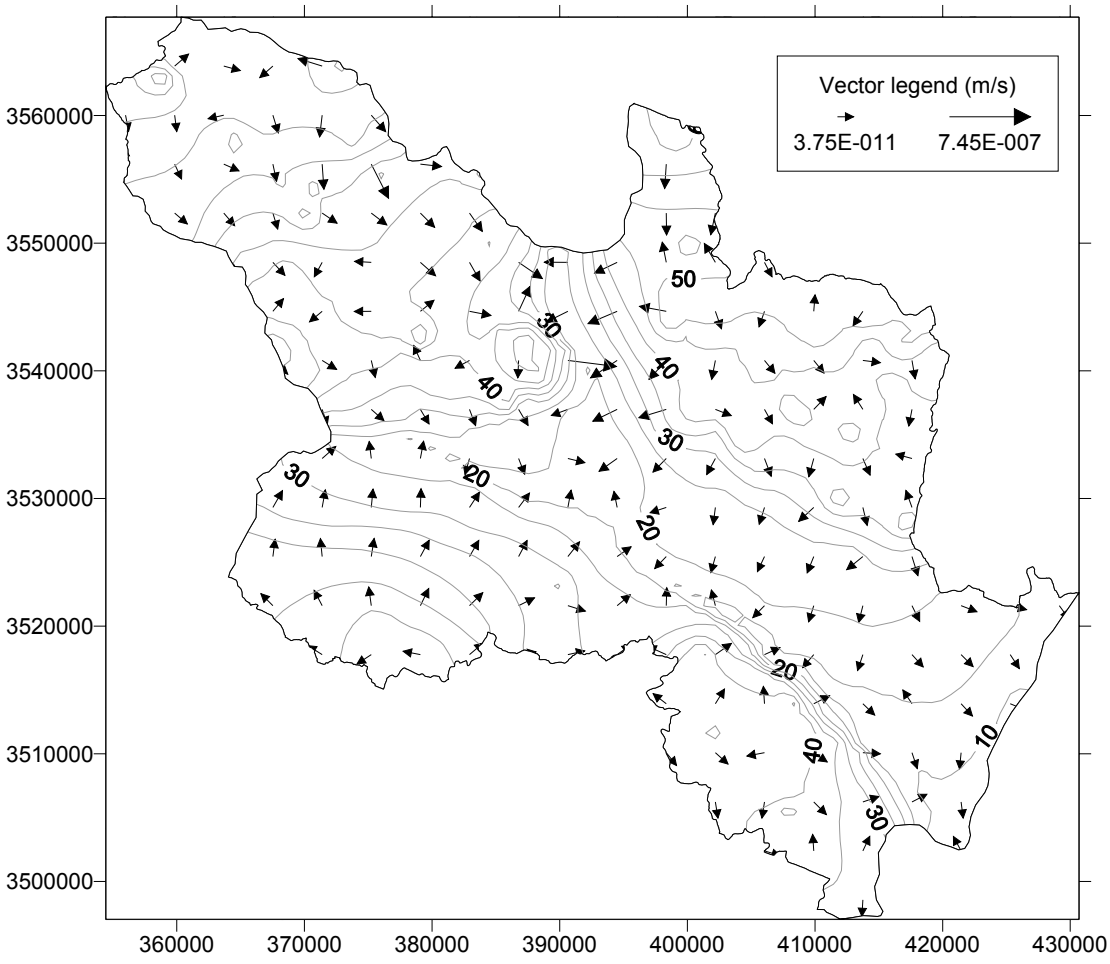

Figure 5.15. Simulated hydraulic head distribution in the watershed at 12/31/1991

Overall, one could conclude that the coupled surface/subsurface flow model performs satisfactorily. About 4-8% of peak flows are missed at the most downstream location of the watershed where the calibration and verification is made. This discrepancy is expected to be lower in any intermediate point within the system. Nevertheless, this level of agreement is deemed normal for a large scale modeling effort such as the one discussed here. It is further believed that these discrepancies are mainly attributed to the relatively inaccurate overland flow discharge values used in this study that are obtained from an empirical model. Once proper mathematical formulation and cost-effective numerical simulation of overland flow is achieved (i.e., in a similar format shown in

second coupled model in Chapter 3), the large-scale watershed modeling efforts would most likely yield better results.

5.5. Coupled Contaminant Transport Simulation

The coupled contaminant transport model is applied in the lower Altamaha river basin. Since there are no water quality measurements in the project area, the model is primarily operated as a general tool to understand the overland contaminant transport patterns inside the system with particular focus on the interactions between the river network and the surfacial aquifer. The contaminant transport equations presented herein are all based on the calibrated and verified flow simulations presented in Section 5.3. Therefore, it is believed that the transport simulations would provide valuable insight to the potential transport of contaminants within the watershed. Furthermore, various scenario conditions could be tested with the proposed model and potential vulnerable points to contamination could be determined to assist the watershed management processes. In this regard, the results from the current Altamaha application of the transport model must be viewed from a general perspective and the focus should be on a broad understanding of system characteristics rather than on specific numerical values.

Two important contamination scenarios are analyzed in this section. In the first scenario, the contamination is assumed to initiate from the river system. In this context, the upstream Altamaha river channel is assumed to receive a constant 100mg/L conservative contaminant continuously. The Ohoopee river channel, on the other hand, is considered to be uncontaminated throughout the simulation. The initial conditions in both the river network and the aquifer are taken to be zero. In the second scenario, the

contamination is assumed to initiate from the surfacial aquifer at a point close to the Ohoopee river channel. The contaminant area is assumed to sustain 100,000mg/L representing a continuously leaking source. The river system and the rest of the aquifer are considered to be clean and free of any contamination.

These two conditions are simulated with the flow solution of the first 2 months of 1988. The selection of the simulation period was arbitrary since any reasonably long period would cover all possible hydrologic interaction conditions (i.e., river system recharging the aquifer or aquifer discharging to the river system) along the river network. With this simulation period and with the above mentioned two scenarios, it is possible to analyze the influence of contaminated river waters on aquifer water quality and the influence of contaminated aquifer waters on river water quality.

In the first scenario, the contamination is assumed to be entering the system from the upstream boundary of the domain at Baxley gaging station. The analysis of this contaminant is studied in two phases. The first phase covers the first 1-2 days of the simulation during which the contaminant advects and disperses within the channel network until a steady state is reached and the contaminant distribution stabilizes in the network. During this first phase, contaminant does not start to significantly affect the aquifer due to the relatively small response time the groundwater system. On the other hand, the second phase covers the entire extended simulation period where the major focus is on the dynamic interactions of contaminated waters between surface and subsurface systems.

The time-dependent migration of the contaminant in the channel network is shown in Figure 5.16. As can be seen from the figure, the contamination enters the

otherwise clean system as a step function, which by itself is a numerically difficult problem to solve. It is then advected and dispersed in the system. The dilution effects of the Ohoopee waters are clearly seen from the figure. The influence of the clean overland flow contributions are not observed as strictly as the Ohoopee river due to the relatively small discharges these tributaries carry as opposed to the main Altamaha river discharge at any particular instant in time. By the end of the second day of simulation, the contamination essentially covers the entire Altamaha river network except for most of the Ohoopee channel that does not receive any contaminant from upstream. Under the hydrologic conditions of this period, the contaminant concentration in the downstream Altamaha channel stabilizes around 94mg/L. The effect of dispersion on the otherwise clean Ohoopee channel is also seen from Figure 5.16. The immediate vicinity of the junction is contaminated via the dispersed contaminants from Altamaha waters.

After the initial phase in which the river contaminant concentration stabilizes throughout the channel network, the focus is switched to the contaminant migration in the aquifer. This second phase of the simulation demonstrates the difficulties associated with time scale differences in coupled contaminant transport modeling of the surface and subsurface processes. While the surface contaminant transport is a rapid phenomenon as seen from the first phase of the simulation, the subsurface response is fairly slow and requires longer times for representative output. In this regard, coupled simulation of these two processes necessitates significant computer time. A particular reason for this drawback is the explicit algorithm required to handle the problematic advection operator in the channel transport model as discussed in Chapter 4.

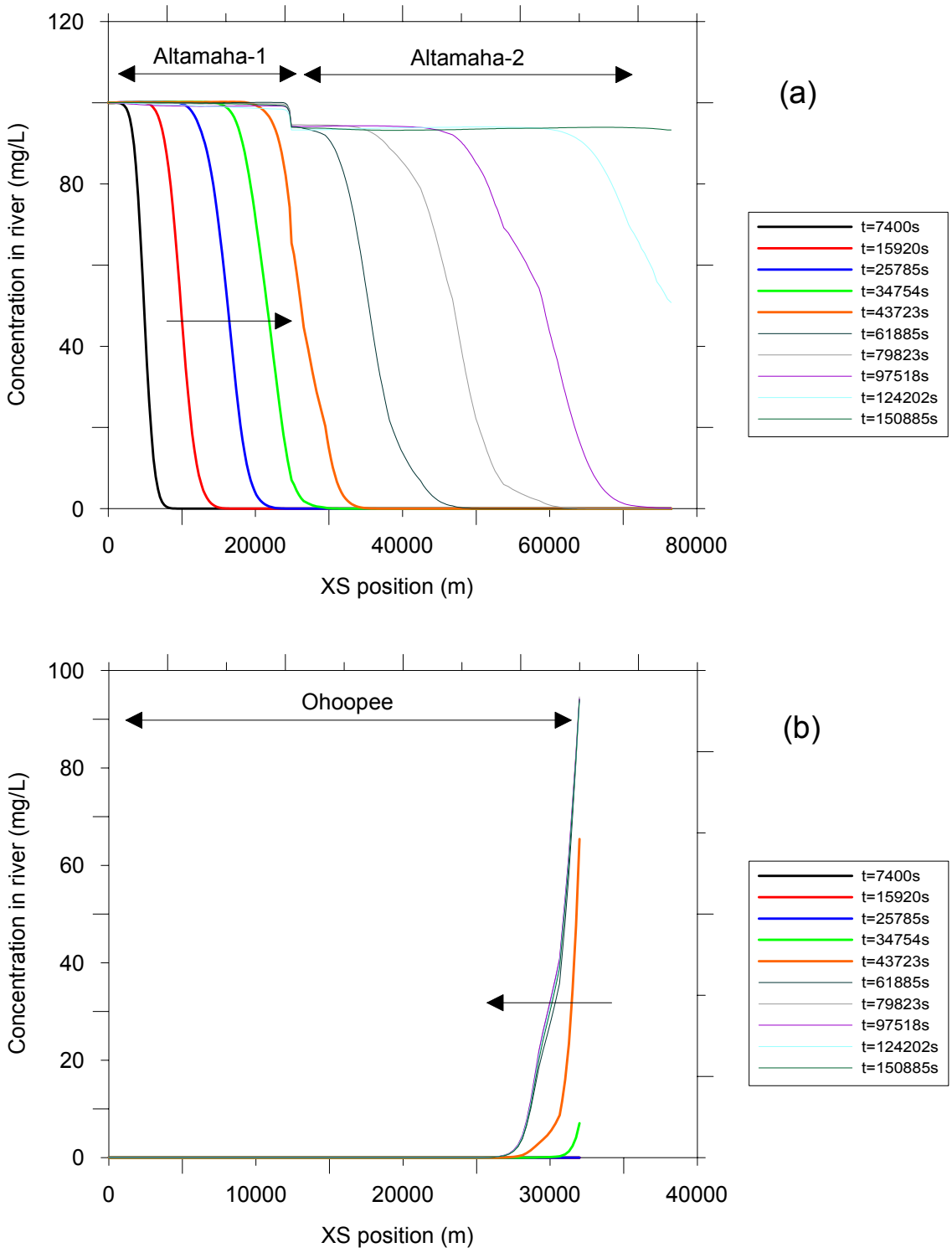

Figure 5.16. Time dependent migration of contamination (a) in upstream and downstream Altamaha river channels and (b) in Ohoopee river channel

Based on the above discussion, one could conclude that coupled surface/subsurface contaminant transport modeling would become much more feasible when sufficiently accurate implicit algorithms are found to handle the advection related numerical problems. Nevertheless, coupled contaminant transport simulations are still feasible in the current form of the model given enough computational time.

In the second phase, the river contaminant concentrations are spatially and temporarily variable only as a function of the Ohoopee river and overland flow discharges. With their zero-concentration values, Ohoopee and tributary flows act as dilution mechanisms to the contaminant in main Altamaha channels (i.e., upstream and downstream). Therefore, the temporal concentration variations are the only major fluctuations observed within the system in response to time-dependent discharge values in these streams. However, these fluctuations are not significant considering their relatively small magnitudes. It is thus possible to conclude that the system operates on a quasi-steady state as long as the specified concentration boundary condition is continuously enforced on the upstream end. Furthermore, the time scales in the channel domain are much smaller than their groundwater counterparts such that possible slight variations in channel concentrations do not create long enough changes that could in turn affect the groundwater concentrations. The aquifer contaminant concentration distributions at the end of the first and second months are shown in figures 5.17 and 5.18. It is clearly seen from the figures that both the spatial extent of the contaminated zone as well as the strength of contaminant concentration in these locales increased due to longer exposure to contaminated river waters.

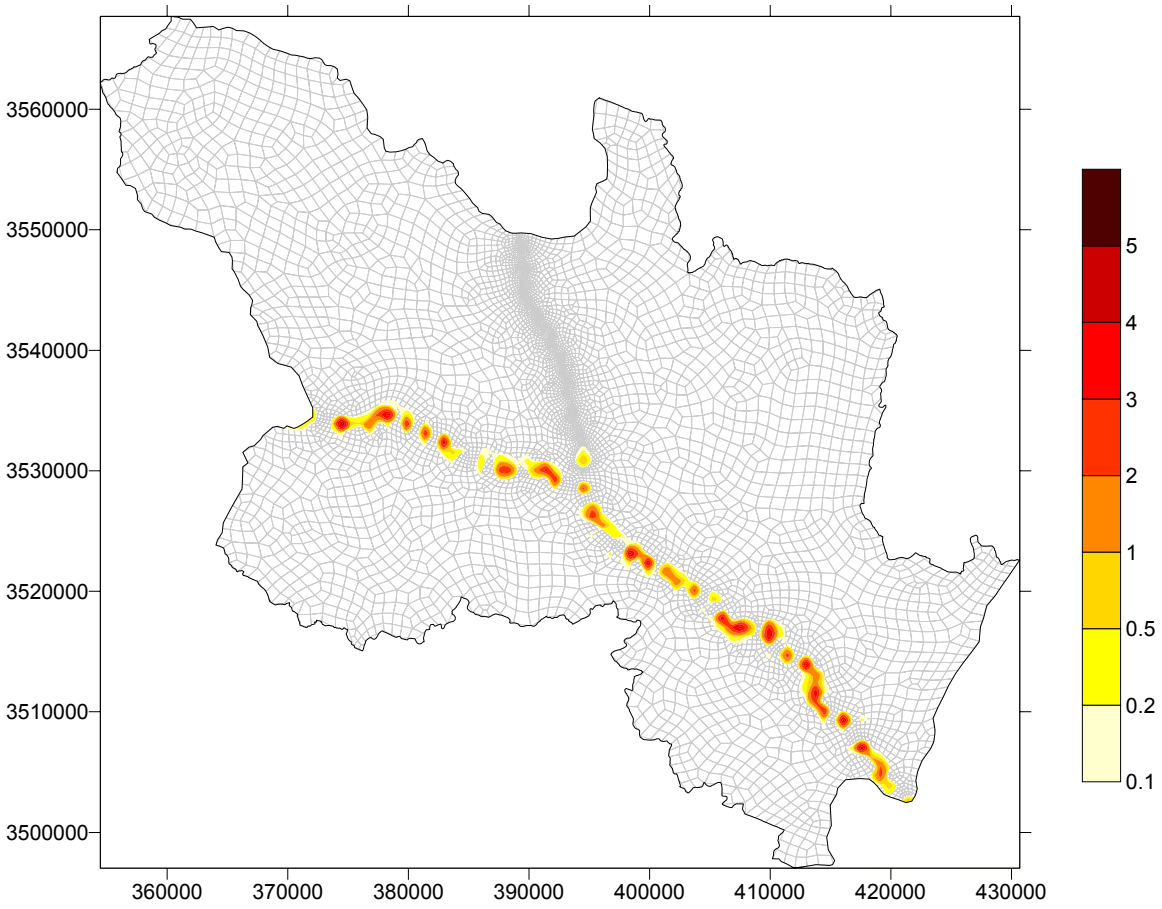

Figure 5.17. Contaminant concentration (mg/L) in aquifer after 1 month of simulation

In the second scenario, the contaminant is introduced to the aquifer at a position that is likely to reach the river network. The selected locale is one of the several alternatives that experiences highest Darcy velocities. The selected area is located in the vicinity of the Ohoopee river roughly at the midstream position between the Reidsville gaging station and the Altamaha confluence point. The contaminated zone covers an area of about 0.2km^2 in the Ohoopee flood plain and is about 150m away from the river channel as shown in Figure 5.19.

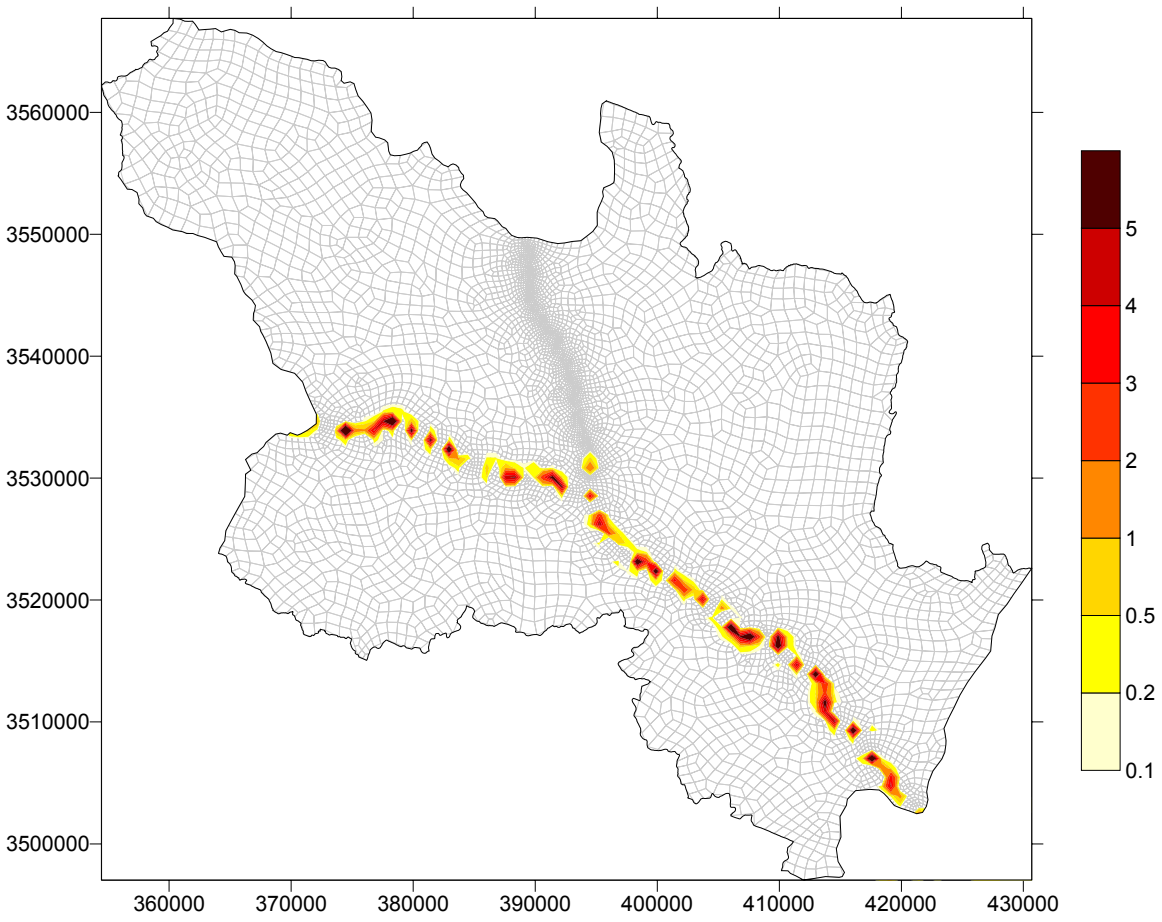

Figure 5.18. Contaminant concentration (mg/L) in aquifer after 2 month of simulation

It is assumed that this area is contaminated with 100,000mg/L of a conservative contaminant. The source zone is selected to be a continuous zone to demonstrate the long term consequences of contamination in the river network and other portions of the aquifer. The contaminated zone is deliberately selected close to the river channel and in an area governed by high groundwater flow velocities towards the river such that the contaminant would quickly reach the river. In this regard, it only takes about 15days for the aquifer concentration to reach a value of 1000mg/L underneath the river channel as a result of large groundwater flow velocities as well as high dispersion coefficient (i.e., a dispersivity value of 50m is used in the simulations).

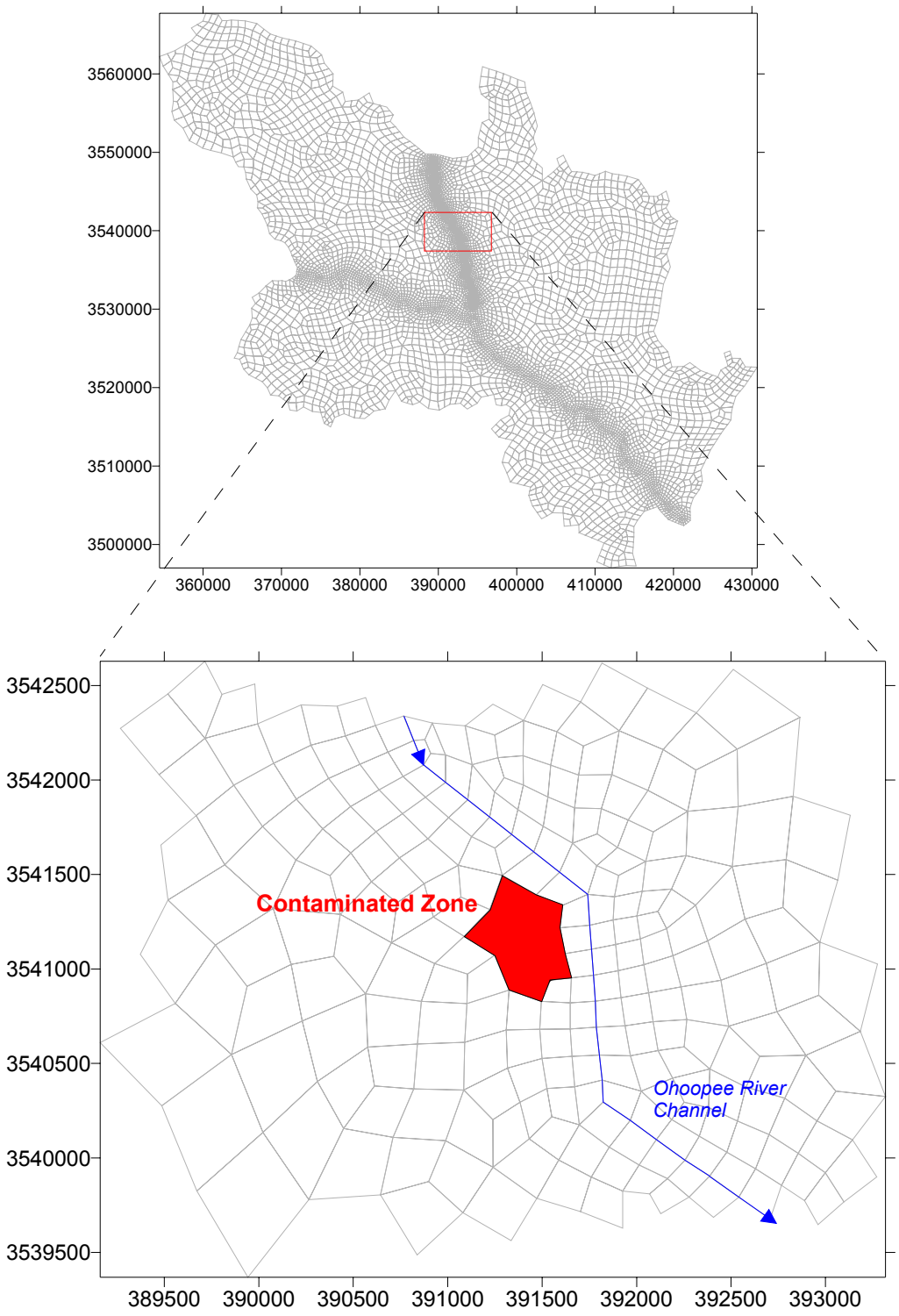

Figure 5.19. Contaminated zone location in Scenario-2

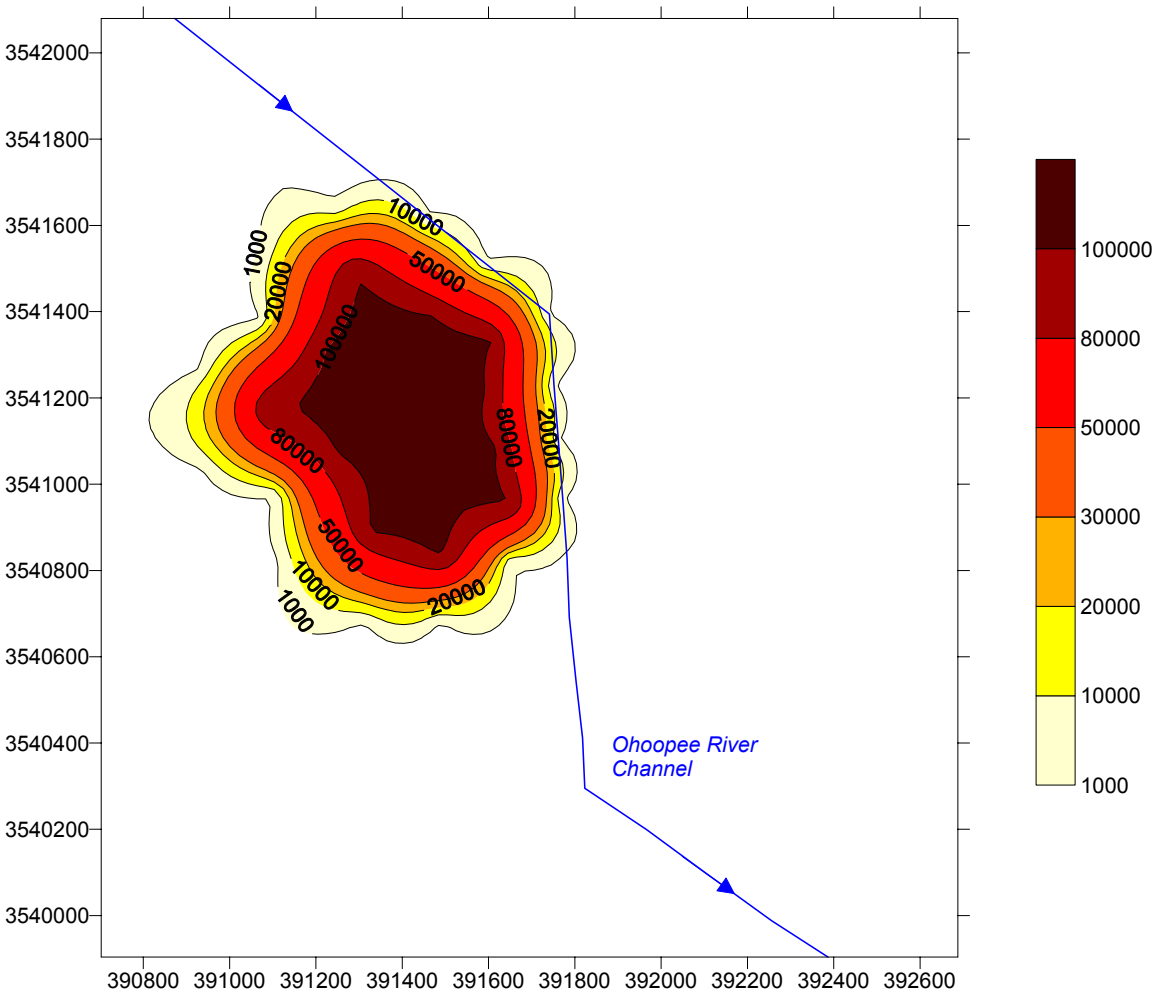

Figure 5.20. Contaminant concentration (mg/L) in the immediate vicinity of the source area after 1 month of simulation

The contaminant concentration at the end of one month of simulation in the immediate vicinity of the source area is presented in Figure 5.20. As seen from the figure, the contaminant reaches to high concentrations underneath the river, working as a significant source for the river pollution under suitable hydrologic conditions.

As the concentration in the aquifer below the river increases, the dispersive flux between the aquifer and river increases since the river is supplying contaminant free waters from the upstream boundary. The lateral seepage towards the river also facilitates the migration of the contaminant to the Ohoopee channel. It is important to note that the

mass flux in the lateral seepage flow is a direct function of the direction of the seepage flux. Hence, the contamination affects the river only when the lateral seepage is towards the river. When the river stage increases due to the arrival of a flood wave, the lateral seepage reverses and river starts to feed the aquifer. The time series graph of lateral seepage in the vicinity of the source zone is shown in Figure 5.21. The dynamic nature of the seepage is clearly reflected in the figure. The dips in the figure correspond to sequential flood waves that enter the reach as shown in Figure 5.22. Consequently, the increased river stage creates a seepage outflux from the river. The timing of seepage outflux dips are directly correlated with the arrival of the flood peaks. Once the wave is past the reach, the river stage retreats and seepage is reversed.

In accordance to the above correlation between lateral seepage and river hydrology, the influence of contaminated aquifer water over the river is an intermittent phenomenon. Once the flood wave passes, the river stage retreats, seepage and corresponding advective contaminant transport is reversed. Despite this dynamic behavior of advective flux, the dispersive flux continuously transfers from the high concentration domain (i.e., the aquifer) to the low concentration domain (i.e., the river) and creates a general transport trend independent of the hydrologic conditions of the system. It is important to note however that the magnitude of mass transported with dispersion is small compared to mass transported with advection (i.e., lateral seepage).

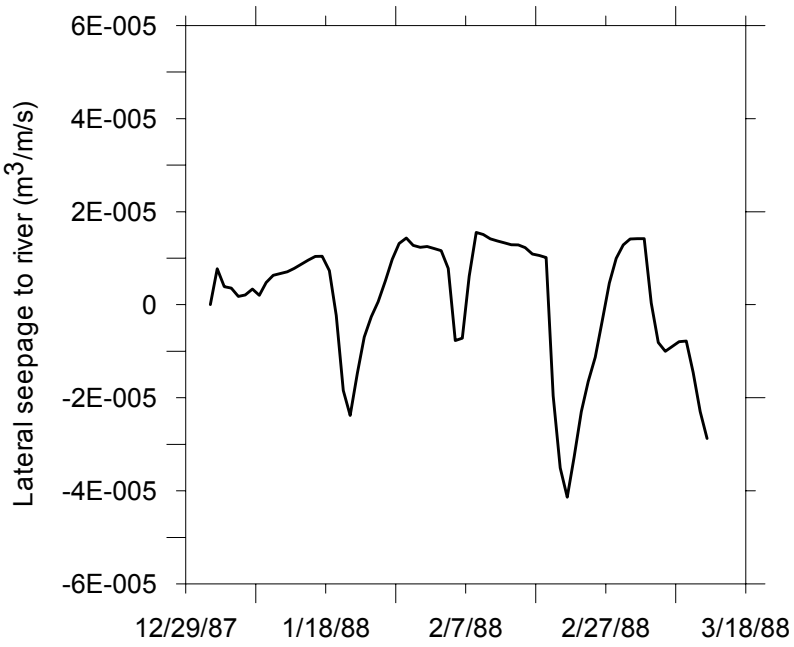

Figure 5.21. Lateral seepage near the contamination zone

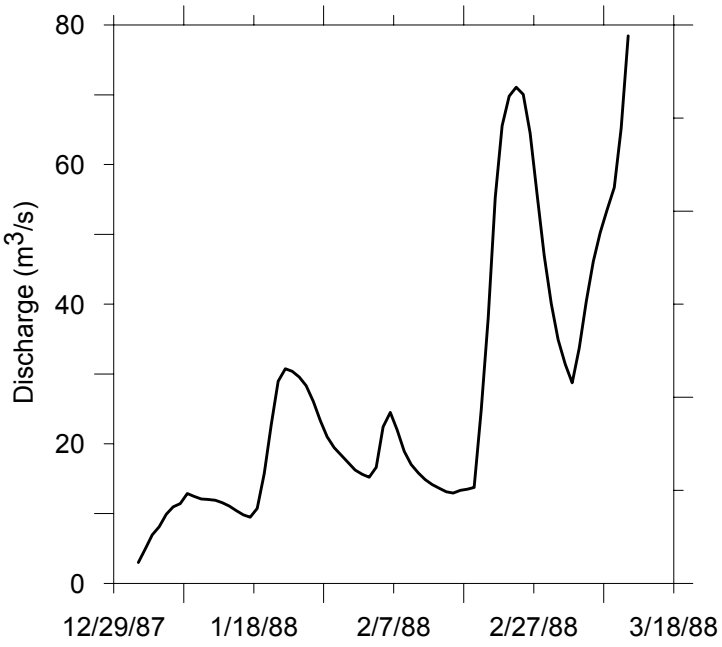

Figure 5.22. Discharge in the reach near the contamination zone

Another consequence of the variable lateral seepage direction is a highly variable contaminant concentration within the river. Since the main source of river contamination is lateral seepage-dependent-mass flux (i.e., due to pristine upstream conditions in the river), the river concentration downstream also shows dynamic variations as a direct result of both seepage and upstream discharge variability. The river concentrations downstream the contaminated area is shown in Figure 5.23. The seepage-dependent intermittent behavior of concentration is clearly observed in this figure.

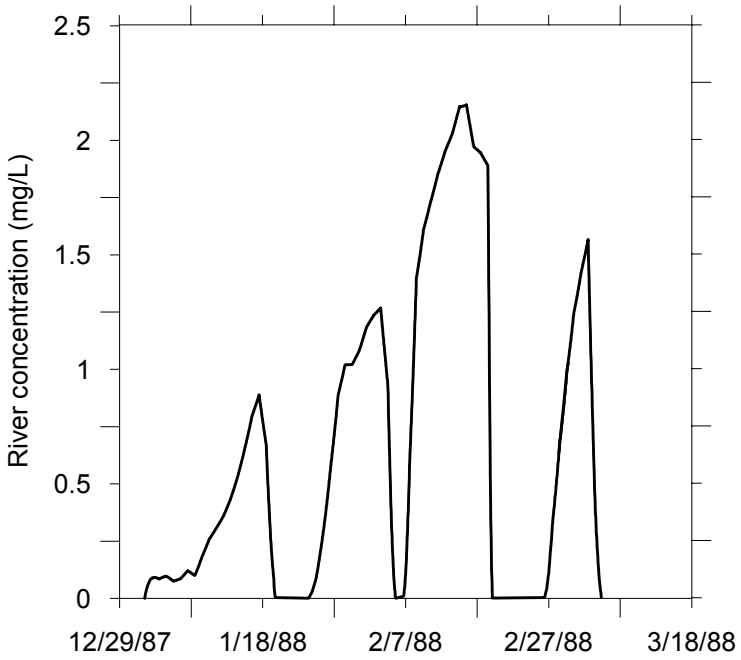

Figure 5.23. Contaminant concentration in the river at the contaminated zone

Once the contaminant reaches the river, it is quickly transported downstream. Since the source is next to the Ohoopee river and the upstream Altamaha channel is clean, a significant amount of dilution occurs at the Ohoopee-Altamaha junction. The Ohoopee channel concentrations are significantly diluted with pristine Altamaha waters and continue their downstream transport. The lateral seepage along the downstream Altamaha channel allows the re-introduction of contaminated waters back to the aquifer. Therefore, the river system acts as a conduit for fast transport of contaminants. The contaminant distribution within the aquifer after one and two months of simulation are shown in figures 5.24 and 5.25. As can be seen from the figures, the contaminant is slowly entering the otherwise clean aquifer downstream of the contamination zone. The spatially patchy distribution of contaminant concentration in the aquifer is due to the spatially variable seepage between river and groundwater flow domains that transports contaminated water from the river to the aquifer. The high concentration patches along the river channel essentially coincides with areas with lateral seepage outflow from the river channel towards the aquifer. It is also clearly seen that the contamination is limited to the immediate vicinity of the river channels. Any further migration towards the inner regions of the aquifer did not occur in these time periods as the general groundwater flow direction is mostly directed towards the main river network in the watershed. Only during flood events, intermittent flow reversals allow rapid contaminant transport towards the inner regions of the aquifer. In all other hydrologic conditions, the magnitude of dispersive flux, which is independent of the dynamic hydrology of the system, is not deemed to be sufficient to create extensive migration of contaminants to such inner regions of the aquifer. Therefore, it can be concluded that depending on the hydrology of

Altamaha system, the contamination in the river might migrate large distance inside the aquifer particularly for extremely wet years that are characterized by the river system feeding the surfacial aquifer.

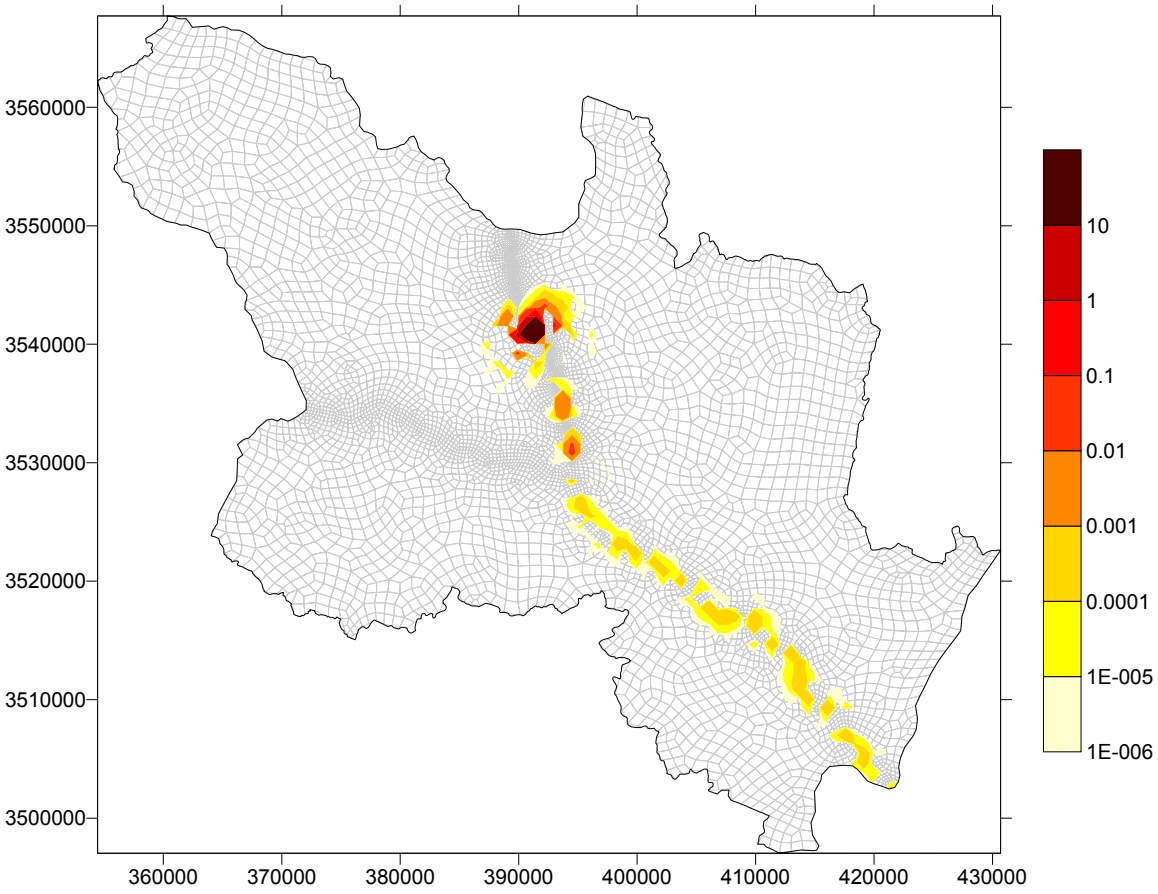

Figure 5.24. Contaminant concentration (mg/L) in aquifer after 1 month of simulation

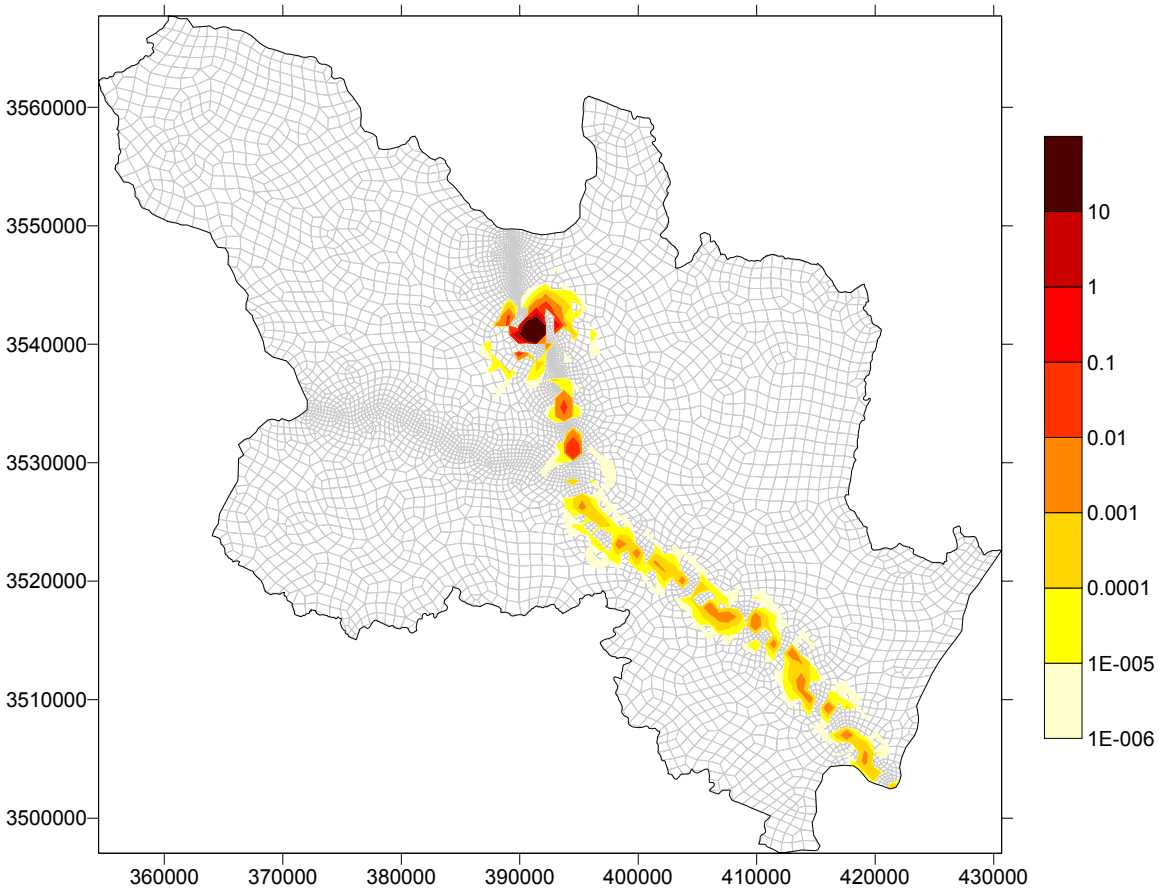

Figure 5.25. Contaminant concentration (mg/L) in aquifer after 2 month of simulation

CHAPTER 6

CONCLUSIONS AND RECOMMENDATIONS

6.1. Conclusions

Large scale watershed modeling has long been an important challenge for the hydrologist. Numerous models have been developed to analyze possible flow patterns in a watershed in response to a precipitation event. Although most of these models used empirically-based, lumped parameter formulations neglecting or oversimplify the underlying physical processes, they have provided basic data without needing a detailed analysis. In recent years, the trend has switched to more fundamental understandings of the processes affecting the overall response of the watershed, and hydrologic modelers have focused to physically-based distributed parameter models. These models are based on rigorous mathematical formulations of physical laws defining the flow of water over a watershed and provide better description of the watershed processes. Nevertheless, their application to large scale watersheds is severely limited by their computational requirements. Mainly due to the distributed nature of these models and the numerical solution techniques implemented to capture the flow patterns, these models require fine discretizations, which in turn increases the size of the overall matrix to be solved in each

computational time step. Therefore, both computational speed and memory requirements can become unmanageable given the limits of today's computers. A good example of such limitations is the overland flow domain. Due to its spatially and temporally discontinuous flow pattern, very small water depths as well as strong non-linearity associated with land characteristics, overland flow models require finer spatial and temporal discretization. Furthermore, the flow boundaries are not as well-defined as other processes such as the channel flow or groundwater flow. Another example is groundwater flow in the unsaturated zone. The moisture movement in this zone is strongly non-linear due to the dependency of hydraulic conductivity and pressure head on moisture content. Effectively capturing this dependency requires fine discretization which becomes a problem in large scale watershed models.

Considering these limitations, this study attempts to blend the powerful distributed parameter models with relatively simple lumped parameter models to form a so-called hybrid model to solve the major flow pathways in a distributed sense and simplify others in a lumped format. The proposed hybrid model considers the channel flow and groundwater flow as major pathways and treats them in a fully distributed sense using physically based formulations. The proposed model also implements full coupling of these flow processes along the river bed using lateral seepage. On the other hand, the model considers overland flow and unsaturated zone flow in a lumped parameter fashion without the details of these processes in a distributed modeling sense.

When watershed processes are analyzed in an integrated fashion, coupling becomes a major issue. Coupling provides the link between different flow pathways and maintains the continuity of the system. As essential as it is, coupling is a computationally

costly procedure where the common parameters are generally iteratively improved until convergence is achieved with respect to some pre-determined criterion. Previous studies implemented iterative algorithms, which became a standard procedure for coupling flow pathways. In this study, a new simultaneous solution procedure is proposed to couple surface and subsurface flow along the river bed via the lateral seepage flow. This new technique does not rely on iterative improvement; making it a faster procedure compared to the iterative technique. The method is based on solving channel flow and groundwater flow equations within a single matrix structure, considering the interacting terms within the equations. Although the method requires solution of larger matrices, it is still faster and more accurate than other methods available. As the two systems are essentially solved simultaneously, it is also a more physically realistic technique to handle inter-pathway interactions within the hydrologic cycle.

This study is believed to be one of the first examples of coupled contaminant transport modeling. A coupled surface-subsurface contaminant transport model is formulated to provide a basic understanding for contaminant transfers between interacting domains. The proposed transport model uses the coupled flow solution and implements an advective-dispersive mass transport function along the river bed. This coupled analysis of contaminant transport is thought to be an important mechanism for strongly interacting systems under suitable hydrological conditions. The numerical difficulties associated with the advection operator in the channel transport model hinder the use of the proposed simultaneous solution algorithm. As an explicit solution procedure is necessary to capture the behavior of contaminants in advection dominant systems, an operator splitting algorithm is implemented to separate the explicit advection

from the remaining operators. Although this numerical separation scheme appears to violate the simultaneous presence of two physical transport processes, it is mathematically sound and essential for accurate analysis of transport in advection dominant systems. In this regard, the proposed simultaneous solution algorithm is modified such that the advection operator is solved discretely before the all other operators, which are then solved simultaneously with the groundwater transport equation in a single matrix structure. Because of this, the transport solution algorithm is called the semi-simultaneous solution method. The method could, however, be made fully simultaneous without much difficulty if an implicit advection algorithm is developed that would numerically yield accurate results without the restrictions of its explicit counterpart.

The proposed coupled flow and transport models were applied to the lower Altamaha watershed in southern Georgia. Long term flow and contaminant transport simulations were performed to analyze the hydrologic and geo-hydrologic characteristics of the watershed. The coupled flow simulations revealed a dynamic and spatially variable interaction pattern between the river and the surfacial unconfined aquifer. Seepage rates are found to be a strong function of the hydrologic conditions in the river. The flow simulations show a good match with the observed data obtained from the downstream gauging station. The simulated values are capture the timing and magnitude of observed flood hydrographs accurately. The calibrated flow patterns in the river channels and in the aquifer are then used to test several contaminant transport scenarios for the watershed. The results from the contaminant transport simulations showed that contaminated river water is much more likely to create significant consequences over the aquifer than would

the contaminated aquifer water over the river due to the significant dilution of the river water over the contaminated seepage from the aquifer. Furthermore, it is observed that the immediate vicinity of the river channels is most likely to experience the highest contaminant concentrations under suitable hydrologic conditions due to the slow movement of groundwater. Therefore, an accidental instantaneous spill to the river is not likely to create significant groundwater pollution as the contaminants are quickly washed away by the fast flowing river waters. On the other hand, any potential continuous source of contamination near a discharging section of the aquifer (e.g., a leaking tank) is likely to create problems in otherwise clean river waters despite the diluting effect of the river. In this regard, it is believed that the coupled flow and transport model could allow more detailed analysis of possible sources and migration patterns of contamination in the lower Altamaha watershed.

6.2. Recommendations

Although this study provides a new approach to watershed modeling by introducing the concept of hybrid models, the future of watershed modeling still necessitates a fully distributed approach in all possible subprocesses of the water cycle. In the future, mathematical representation and numerical solution procedures of these processes could evolve to such a degree that the modeler will not have to compromise the fully physically-based distributed approach. In this regard, the author believes that there will be two major areas of work that the future hydrologic modeler will focus on. One of these would involve better representation of flow pathways with more accurate models,

and the other would focus on development of better numerical techniques for these sophisticated mathematical models.

There is work to be done in better describing the overland flow component. This must not only represent the temporal discontinuity accurately but also must incorporate it in a suitable format so that long term simulations would be possible after including the overland flow domain in the overall simulations. It is believed that time-dependent moving boundary analysis and temporal Dirac delta representations could become the hot topics in overland flow modeling. Better numerical algorithms will be required to accurately handle the moving boundary problem, small water depths and wetting-drying conditions in the three-dimensional topography of the watershed.

The current state of the proposed model could be improved by incorporating more sophisticated descriptions of subprocesses. These would certainly require more computational power and data. For example, a variably-saturated three-dimensional groundwater model will be an improvement of flow processes in porous media. This would not only eliminate the one-dimensional representation of the unsaturated zone but would also solve the entire soil column as a whole in a variably-saturated fashion. However, the data requirements would be extremely large compared to the present model and it could only be applied over a very limited spatial domain unless sophisticated data collection and analysis methods are developed and made available to the modeler in an easy to access fashion. In the long run, a two-dimensional river model might be linked to this three-dimensional variably saturated groundwater model. Such an improvement would probably constitute what is called the ‘ultimate watershed model’. However, better

coupling mechanisms would need to be developed before the interactions between the river and the aquifer can be accurately simulated.

It is believed that enhanced numerical algorithms would have to be incorporated into river and groundwater transport models for more accurate results and for more general applicability of the model. Such algorithms would better handle the dual-nature of the advective-dispersive transport equation. However, compromises might need to be made in terms of using such algorithms versus using the simultaneous solution techniques since such algorithms generally require the use of explicit components to handle the advective transport that, in theory, violates the idea of simultaneous solution. In this regard, high-accuracy implicit schemes have to be developed before a fully simultaneous coupling of surface and subsurface transport processes could be done similar to their flow counterpart.

Further research is also necessary on scale issues of coupled hydrologic modeling. Separate model components with different spatial and temporal scales are difficult to couple dynamically. In particular, scale issues associated with slow and fast hydrologic processes create problems in terms of computer resources and data availability. Therefore, only after computational speed reaches a point where the entire watershed hydrology could be modeled with the smallest time scale requirement, could one achieve an ultimate simultaneous coupling of all processes.

An essential part of watershed modeling is the requirement for calibration and verification data. Such data sets are only available for small experimental watersheds. At larger scales, researchers are faced with data insufficiency to calibrate and verify their models. Therefore, additional resources should be allocated to provide not only extensive

field studies but also to increase the density of standard data collection facilities that are currently available. These efforts must be geared towards obtaining better subsurface data, since surface flow data are more abundant.

Finally, the author firmly believes that, in the long term, the hydrology and hydraulics of watersheds will be modeled as a whole in a fully coupled way using three-dimensional models. Such a comprehensive model would simultaneously couple all processes and would solve them as a single system considering all their interactions without the need to introduce artificially separated flow domains. This study is an initial step towards such an approach.

APPENDIX A

FINITE DIFFERENCE EQUATIONS OF CHANNEL FLOW

APPENDIX A

FINITE DIFFERENCE EQUATIONS OF CHANNEL FLOW

The finite difference forms of continuity, momentum and boundary condition equations of channel flow are derived in this appendix. For each channel of the network, the continuity and momentum equations given in equations (3.1) and (3.2) are discretized in the *x-t* plane using the "four-point" weighted difference scheme. Two additional equations are then used to represent the conditions in the upstream and downstream boundaries of the channel. When this procedure is done for all channels, a system of *2N* equations is formed, which is then solved to evaluate the unknown discharge and stage at the nodes of the discretization. The discretized forms of the continuity, momentum and boundary condition equations are given in the following sections.

Channel Network

In the discussion that follows, in order to assist the derivation, the sample network shown in Figure A.1 is used. This network contains 5 channels and 2 junctions. The channel numbering scheme starts from the most upstream channel and follows the direction of flow. When a junction is reached, the node numbering continues from the

most upstream node of the next channel and follows sequentially down to the junction until all inflowing channels of the junction is numbered. When all inflowing channels are numbered for a particular junction, node numbering continues with the most upstream node of the outflowing channel. This procedure is continued until the entire system is numbered.

Discretized forms of continuity and momentum equations

The finite difference discretization of continuity and momentum equations is done for each channel as shown in Figure A.2. It can be seen from this figure that the solution plane for channel k is represented by a total of N_k nodes with local node numbers starting from 1 and running through N_k. In the four-point scheme, the approximations of derivatives and constant terms are given in equations (A.1), (A.2) and (A.3) for a dummy parameter E:

$$\frac{\partial E}{\partial t} = \psi_f \frac{E_{i+1}^{j+1} - E_{i+1}^{j}}{\Delta t^j} + \left(1 - \psi_f\right) \frac{E_i^{j+1} - E_i^j}{\Delta t^j} \tag{A.1}$$

$$\frac{\partial E}{\partial x} = \theta_f \frac{E_{i+1}^{j+1} - E_i^{j+1}}{\Delta x_i} + \left(1 - \theta_f\right) \frac{E_{i+1}^{j} - E_i^j}{\Delta x_i} \tag{A.2}$$

$$E = \theta_f \frac{E_{i+1}^{j+1} + E_i^{j+1}}{2} + \left(1 - \theta_f\right) \frac{E_{i+1}^{j} + E_i^j}{2} \tag{A.3}$$

where i and j are subscripts representing spatial and temporal positions, respectively, ψ_f and θ_f are weighing factors between 0 and 1, and Δx_i and Δt^j are reach lengths between nodes i and i+1, and time step between timelines j and j+1, respectively. It is possible to

create different schemes using different values for the weighing factors. While θ_f value of 0.0 corresponds to an "explicit" scheme, one could create a so-called "box" scheme by setting θ_f to 0.5. Similarly, a scheme with a θ_f value of 1.0 is known as the "fully-implicit" scheme in space. Several researchers preferred using a ψ_f value of 0.5 and approximated the time derivative at the center of grid between $(j)^{th}$ and $(j+1)^{th}$ time lines (Amein and Fang, 1970; Chaudhry and Contractor, 1973) where as others used varying values depending on the particular application (Fread, 1985).

Fread (1974) has shown that the weighted four-point implicit scheme is unconditionally stable for any time step if the value of θ_f is selected between 0.5 and 1.0. In addition to stability criteria, he also analyzed the influence of the weighing factor on the accuracy of computations and found out that the accuracy decreases as θ_f departs from 0.5 and approaches to 1.0. He reported that this effect became more pronounced as the magnitude of the computational time step increased. Furthermore, his analysis revealed that a θ_f value of between 0.55 and 0.6 provided unconditional stability and good accuracy, which makes this scheme superior compared to the explicit scheme that requires time steps of less than a critical value determined by the Courant condition.

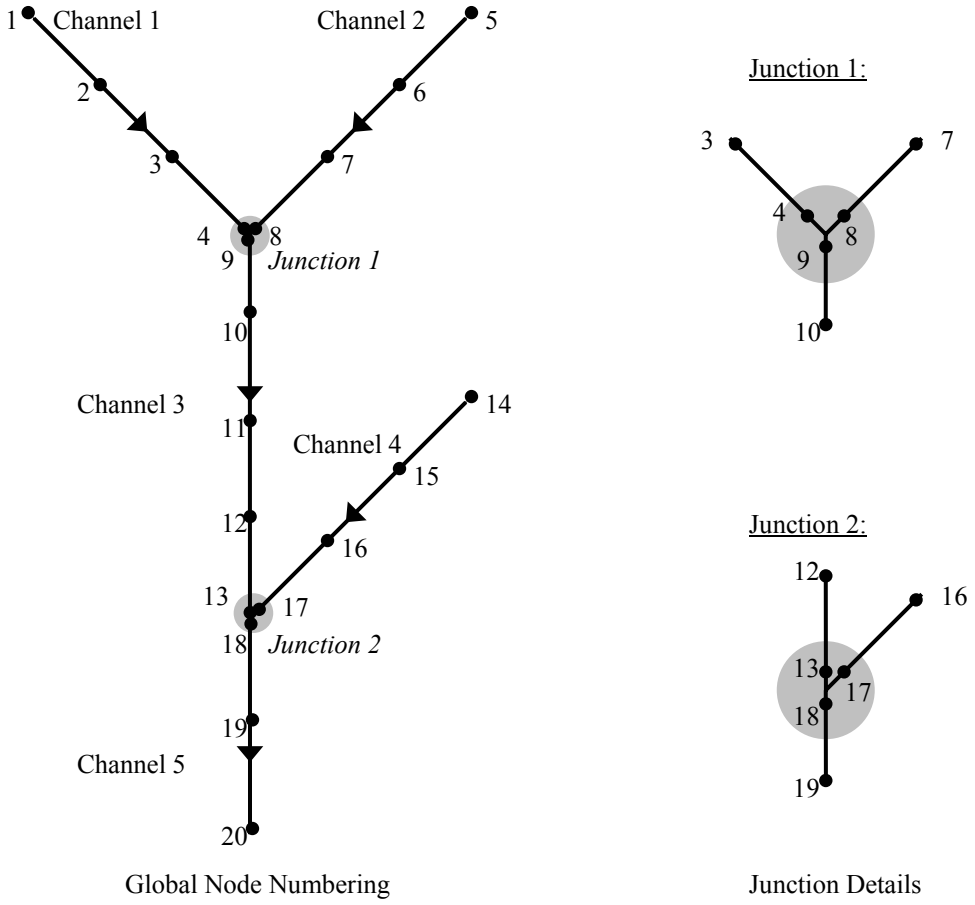

Figure A. 1. Sample channel network and node numbering scheme

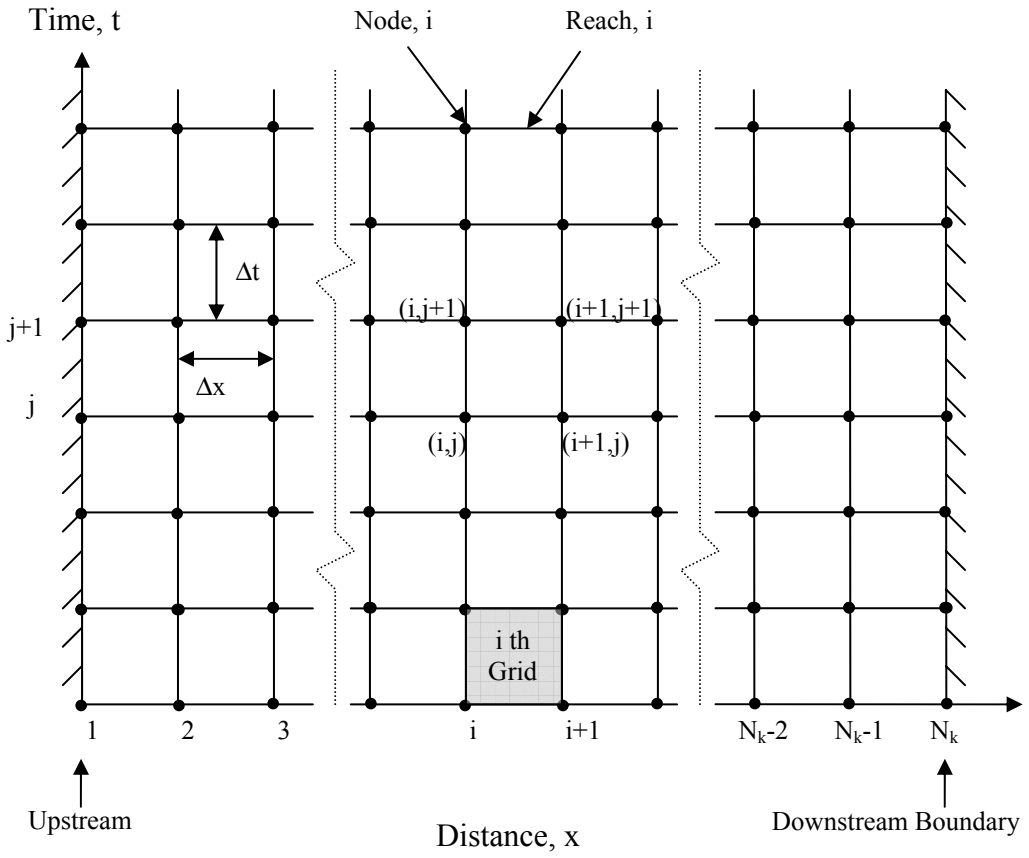

Figure A. 2. The distance-time grid used to formulate the implicit finite difference scheme for channel k (Fread, 1974)

With the templates given in equations (A.1), (A.2) and (A.3), the space derivatives in Equations (3.1) and (3.2) are approximated as:

$$\frac{\partial Q}{\partial x} = \theta_f \frac{Q_{i+1}^{j+1} - Q_i^{j+1}}{\Delta x_i} + \left(1-\theta_f\right)\frac{Q_{i+1}^{j} - Q_i^{j}}{\Delta x_i} \tag{A.4}$$

$$\frac{\partial h_r}{\partial x} = \theta_f \frac{h_{ri+1}^{\ j+1} - h_{ri}^{\ j+1}}{\Delta x_i} + \left(1-\theta_f\right)\frac{h_{ri+1}^{\ j} - h_{ri}^{\ j}}{\Delta x_i} \tag{A.5}$$

$$\frac{\partial\left(\beta Q^2 / A\right)}{\partial x} = \theta_f \frac{\left(\beta Q^2 / A\right)_{i+1}^{j+1} - \left(\beta Q^2 / A\right)_i^{j+1}}{\Delta x_i} + \left(1-\theta_f\right)\frac{\left(\beta Q^2 / A\right)_{i+1}^{j} - \left(\beta Q^2 / A\right)_i^{j}}{\Delta x_i} \tag{A.6}$$

Similarly, the time derivatives are approximated as:

$$\frac{\partial s_c\left(A+A_o\right)}{\partial t} = \frac{s_{c\,i+1/2}^{\ j+1}\left(A+A_o\right)_{i+1}^{j+1} - s_{c\,i+1/2}^{\ j}\left(A+A_o\right)_{i+1}^{j}}{2\Delta t^{\,j}} + \frac{s_{c\,i+1/2}^{\ j+1}\left(A+A_o\right)_{i}^{j+1} - s_{c\,i+1/2}^{\ j}\left(A+A_o\right)_{i}^{j}}{2\Delta t^{\,j}} \tag{A.7}$$

$$\frac{\partial s_m Q}{\partial t} = \frac{s_{m\,i+1/2}^{\ j+1} Q_{i+1}^{j+1} - s_{m\,i+1/2}^{\ j} Q_{i+1}^{j}}{2\Delta t^{\,j}} + \frac{s_{m\,i+1/2}^{\ j+1} Q_{i}^{j+1} - s_{m\,i+1/2}^{\ j} Q_{i}^{j}}{2\Delta t^{\,j}} \tag{A.8}$$

Finally, the constant terms such as q_{L1}, q_{L2}, S_f, S_e, M_{L1}, M_{L2} and A are approximated as:

$$q_{L1} = \theta_f \left(q_{L1}\right)_{i+1/2}^{j+1} + \left(1-\theta_f\right)\left(q_{L1}\right)_{i+1/2}^{j} \tag{A.9}$$

$$q_{L2} = \theta_f \left(q_{L2}\right)_{i+1/2}^{j+1} + \left(1-\theta_f\right)\left(q_{L2}\right)_{i+1/2}^{j} \tag{A.10}$$

$$S_f = \theta_f S_{f\,i+1/2}^{\ j+1} + \left(1-\theta_f\right) S_{f\,i+1/2}^{\ j} \tag{A.11}$$

$$S_{ec} = \theta_f S_{eci+1/2}^{\,j+1} + \left(1-\theta_f\right) S_{eci+1/2}^{\,j} \tag{A.12}$$

$$M_{L1} = \theta_f \left(M_{L1}\right)_{i+1/2}^{j+1} + \left(1-\theta_f\right)\left(M_{L1}\right)_{i+1/2}^{j} \tag{A.13}$$

$$M_{L2} = \theta_f \left(M_{L2}\right)_{i+1/2}^{j+1} + \left(1-\theta_f\right)\left(M_{L2}\right)_{i+1/2}^{j} \tag{A.14}$$

$$A = \theta_f \frac{A_{i+1}^{j+1} + A_i^{j+1}}{2} + \left(1-\theta_f\right)\frac{A_{i+1}^{j} + A_i^{j}}{2} = \theta_f A_{i+1/2}^{j+1} + \left(1-\theta_f\right) A_{i+1/2}^{j} \tag{A.15}$$

where the variables with subscripts (i+½) are defined for the reach between nodes (i) and (i+1) as an average of the two nodal values. The following formulations are used to define the above variables:

$$\left(q_{L1}\right)_{i+1/2} = -K_{ri+1/2} w_{ri+1/2} \frac{h_{ri+1/2} - h_{g_{i+1/2}}}{m_{ri+1/2}} \tag{A.16}$$

$$\left(S_f\right)_{i+1/2} = \frac{n_{i+1/2}^2 \left|Q_{i+1/2}\right| Q_{i+1/2}}{c_1^{\,2} A_{i+1/2}^2 R_{hi+1/2}^{\,4/3}} = \frac{\left|Q_{i+1/2}\right| Q_{i+1/2}}{K_{i+1/2}^2} \tag{A.17}$$

$$\left(S_{ec}\right)_{i+1/2} = \frac{K_{eci+1/2}}{2g\Delta x_i}\left[\left(\frac{Q}{A}\right)_{i+1}^2 - \left(\frac{Q}{A}\right)_i^2\right] \tag{A.18}$$

$$\left(M_{L1}\right)_{i+1/2} = \begin{cases} 0 & \text{for seepage inflow} \\ -\dfrac{Q_{i+1/2}\left(q_{L1}\right)_{i+1/2}}{2A_{i+1/2}} & \text{for seepage outflow} \end{cases} \tag{A.19}$$

$$\left(M_{L2}\right)_{i+1/2} = \begin{cases} -\beta v_{xi+1/2}\left(q_{L2}\right)_{i+1/2} & \text{for overland inflow} \\ -\dfrac{Q_{i+1/2}\left(q_{L2}\right)_{i+1/2}}{A_{i+1/2}} & \text{for overland outflow} \end{cases} \tag{A.20}$$

$$Q_{i+1/2} = \frac{Q_i + Q_{i+1}}{2} \tag{A.21}$$

$$R_{hi+1/2} = \frac{A_{i+1/2}}{w_{ri+1/2}} \approx \frac{A_{i+1/2}}{B_{i+1/2}} \tag{A.22}$$

$$A_{i+1/2} = \frac{A_i + A_{i+1}}{2} \tag{A.23}$$

$$B_{i+1/2} = \frac{B_i + B_{i+1}}{2} \tag{A.24}$$

$$K_{i+1/2} = \frac{K_i + K_{i+1}}{2} \tag{A.25}$$

$$K_{ri+1/2} = \frac{K_{ri} + K_{ri+1}}{2} \tag{A.26}$$

$$w_{ri+1/2} = \frac{w_{ri} + w_{ri+1}}{2} \approx \frac{B_i + B_{i+1}}{2} \tag{A.27}$$

$$h_{ri+1/2} = \frac{h_{ri} + h_{ri+1}}{2} \tag{A.28}$$

$$h_{gi+1/2} = \frac{h_{gi} + h_{gi+1}}{2} \tag{A.29}$$

The finite difference form of continuity equation is obtained when equations (A.4) through (A.29) are substituted into (3.1) and rearranged for each channel in the network:

$$\begin{aligned}
&\frac{\Delta x_i}{2\Delta t^j}\left[s_{ci+1/2}^{\,j+1}\left(A+A_o\right)_{i+1}^{j+1} + s_{ci+1/2}^{\,j+1}\left(A+A_o\right)_{i}^{j+1} - s_{ci+1/2}^{\,j}\left(A+A_o\right)_{i+1}^{j} - s_{ci+1/2}^{\,j}\left(A+A_o\right)_{i}^{j} \right] \\
&\quad + \theta_f \left[Q_{i+1}^{j+1} - Q_i^{j+1} - \Delta x_i \left[\left(-\frac{K_r w_r}{m_r} \right)_{i+1/2}^{j+1} \left(h_{ri+1/2}^{\,j+1} - h_{gi+1/2}^{\,j+1} \right) \right] - \Delta x_i \left(q_{L2} \right)_{i+1/2}^{j+1} \right] \\
&\quad + \left(1-\theta_f\right) \left[Q_{i+1}^{j} - Q_i^{j} - \Delta x_i \left[\left(-\frac{K_r w_r}{m_r} \right)_{i+1/2}^{j} \left(h_{ri+1/2}^{\,j} - h_{gi+1/2}^{\,j} \right) \right] - \Delta x_i \left(q_{L2} \right)_{i+1/2}^{j} \right] = 0
\end{aligned} \tag{A.30}$$

Similarly, the finite difference form of the momentum equation is obtained when equations (A.4) through (A.29) are substituted into (3.2) and rearranged for each channel in the network:

$$\begin{aligned}
&\frac{\Delta x_i}{2\Delta t^j}\left[s_{m\,i+1/2}^{\;\;j+1} Q_{i+1}^{j+1} + s_{m\,i+1/2}^{\;\;j+1} Q_i^{j+1} - s_{m\,i+1/2}^{\;\;j} Q_{i+1}^{j} - s_{m\,i+1/2}^{\;\;j} Q_i^{j} \right] \\
&+\theta_f \left[\begin{array}{l} \left(\beta Q^2 / A\right)_{i+1}^{j+1} - \left(\beta Q^2 / A\right)_{i}^{j+1} + \\ g A_{i+1/2}^{j+1} \left[h_{r\,i+1}^{\;\;j+1} - h_{r\,i}^{\;\;j+1} + \Delta x_i S_{f\,i+1/2}^{\;\;j+1} + \Delta x_i S_{ec\,i+1/2}^{\;\;j+1} \right] + \\ \Delta x_i \left(M_{L1}\right)_{i+1/2}^{j+1} + \Delta x_i \left(M_{L2}\right)_{i+1/2}^{j+1} \end{array} \right] \\
&+\left(1-\theta_f\right) \left[\begin{array}{l} \left(\beta Q^2 / A\right)_{i+1}^{j} - \left(\beta Q^2 / A\right)_{i}^{j} + \\ g A_{i+1/2}^{j} \left(h_{r\,i+1}^{\;\;j} - h_{r\,i}^{\;\;j} + \Delta x_i S_{f\,i+1/2}^{\;\;j} + \Delta x_i S_{e\,i+1/2}^{\;\;j} \right) + \\ \Delta x_i \left(M_{L1}\right)_{i+1/2}^{j} + \Delta x_i \left(M_{L2}\right)_{i+1/2}^{j} \end{array} \right] = 0
\end{aligned} \tag{A.31}$$

where corresponding explicit formulations are substituted for the slope terms S_f and S_{ec}, as well as the lateral flow terms (depending on the direction of lateral flows) M_{L1} and M_{L2} from equations (A.17), (A.18), (A.19) and (A.20), respectively.

Discretized forms of external boundary condition equations

At any external upstream boundary of a channel, a discharge or a stage hydrograph can be used as the boundary condition equation. The discretized forms of these equations are given as:

$$Q_m^{j+1} - Q_u(t) = 0 \tag{A.32}$$

$$h_{r\,m}^{\;\;j+1} - h_u(t) = 0 \tag{A.33}$$

where subscript *m* represents the global upstream node number of the channel. For a single channel system, *m* takes the value 1. In the sample network, channels 1, 2 and 4 have external upstream conditions and *m* takes values 1, 5 and 14, respectively. Since the proposed model does not allow looped networks, only one external downstream boundary condition is required in the model. The boundary condition at the external downstream boundary can also be defined as a discharge or a stage hydrograph. The discretized forms of these equations are given as:

$$Q_N^{j+1} - Q_d(t) = 0 \tag{A.34}$$

$$h_{rN}^{j+1} - h_d(t) = 0 \tag{A.35}$$

where *N* represents the last node in the entire network. In the case of the sample network shown in Figure A.1, *N* takes the value of 20. In addition to the stage and discharge conditions, the external downstream boundary condition can also be specified as a single-valued rating curve, a looped-rating curve and a critical depth section. If a single-valued rating curve is used as the downstream boundary condition, the discretized form becomes:

$$\mathrm{Q}_N^{j+1} - \left[Q^k + \frac{Q^{k+1} - Q^k}{h_r^{k+1} - h_r^k} \left[h_{rN}^{j+1} - h_r^k \right] \right] = 0 \tag{A.36}$$

where subscript *k* represents the values from the rating curve data. If a looped-valued rating curve is used as the downstream boundary condition, the discretized form becomes:

$$Q_N^{j+1} - c_1 \left(\frac{AR_h^{2/3}}{n_c} \right)_N^{j+1} \left(S_f^{1/2} \right)_{N-1/2}^{j+1} = 0 \tag{A.37}$$

where the friction slope is approximated using the known values of discharge and stage at the downstream reach:

$$\left(S_f \right)_{N-1/2}^{j+1} \approx -\frac{1}{gA_N^j} \left(\frac{Q_N^j - Q_N^{j-1}}{\Delta t^{j-1}} \right) - \frac{1}{gA_N^j} \left(\frac{\left(Q^2 / A \right)_N^j - \left(Q^2 / A \right)_{N-1}^j}{\Delta x_{N-1}} \right) - \left(\frac{h_{rN}^{\ j} - h_{rN-1}^{\ j}}{\Delta x_{N-1}} \right) \tag{A.38}$$

Finally, if a critical depth section is used as the downstream boundary condition, the discretized form becomes:

$$Q_N^{j+1} - \sqrt{\frac{g}{B_N^{j+1}}} \left(A^{3/2} \right)_N^{j+1} = 0 \tag{A.39}$$

Discretized forms of internal boundary condition equations

When the external boundary conditions are implemented, it is observed that certain channels do not have any upstream or downstream boundary condition. These missing conditions occur at the junction points of these channels. Therefore, internal

boundary conditions are written to satisfy the mass and momentum balance at these junctions. For any junction with m inflowing channels, it is required to specify a total of m+1 internal boundary condition. These conditions are specified as m downstream boundary conditions for each inflowing channel and one upstream boundary condition for the outflowing channel. In this regard, one momentum equation is written for each inflowing channel satisfying the continuity in stages.

$$h_{ri}^{j+1} - h_{ro}^{j+1} = 0 \tag{A.40}$$

where subscript i now represent the last node of the particular inflowing channel to the junction and subscript o represent the first node of the outflowing channel from the junction. When equation (A.40) is written is for all inflowing channels, a total of m equations are written for the junction and the missing internal downstream boundary conditions of all inflowing channels are completed. Finally, one last condition is specified to get the missing internal upstream boundary condition of the outflowing channel. This condition is satisfied by writing the continuity equation for the junction:

$$\sum_{k=1}^{m}\left(Q_{i,k}^{j+1}\right) - Q_{o}^{j+1} = 0 \tag{A.41}$$

where i represents the last node of channel k. For the first junction of the particular network shown in Figure A.1, the internal downstream boundary conditions of the inflowing channels 1 and 2 is specified by:

$$h_{r4}^{j+1} - h_{r9}^{j+1} = 0 \tag{A.42}$$

$$h_{r8}^{j+1} - h_{r9}^{j+1} = 0 \tag{A.43}$$

and the internal upstream boundary condition of the outflowing channel 3 is specified by:

$$Q_4^{j+1} + Q_8^{j+1} - Q_9^{j+1} = 0 \tag{A.44}$$

Similarly, for the second junction of the particular network shown in Figure A.1, the internal downstream boundary conditions of inflowing channels 3 and 4 is specified by:

$$h_{r13}^{j+1} - h_{r18}^{j+1} = 0 \tag{A.45}$$

$$h_{r17}^{j+1} - h_{r18}^{j+1} = 0 \tag{A.46}$$

and the internal upstream boundary condition of the outflowing channel 5 is specified by:

$$Q_{13}^{j+1} + Q_{17}^{j+1} - Q_{18}^{j+1} = 0 \tag{A.47}$$

APPENDIX B

PARTIAL DERIVATIVES OF THE FINITE DIFFERENCE EQUATIONS OF CHANNEL FLOW

APPENDIX B

PARTIAL DERIVATIVES OF THE FINITE DIFFERENCE EQUATIONS OF CHANNEL FLOW

The Newton-Raphson technique is based on the analytical or numerical differentiation of the continuity and momentum equations to evaluate the partial derivative terms of the Jacobian matrix. The difference forms of continuity and momentum equations given in (3.21) and (3.22) are partially differentiated with respect to the unknown terms h_r and Q at the $(j+1)^{th}$ time line for the nodal points (i) and (i+1). In the following derivations, the continuity and momentum equations are represented by the letters "C" and "M", and the external upstream and external downstream boundary condition equations are represented by the letters "UB" and "DB", respectively, for clarity. Similarly, the internal boundary condition equations are represented by "IB".

Partial Derivatives of the Continuity Equation

The partial derivatives of the continuity equation with respect to the unknown terms (i.e., h_{ri}, h_{ri+1}, Q_i and Q_{i+1} at $(j+1)^{th}$ time line) are computed as follows:

$$\frac{\partial C}{\partial h_{ri}^{j+1}} = -\theta_f \Delta x_i \left(-\frac{K_r}{m_r} \right)_{i+1/2}^{j+1} \left[\frac{1}{2} B_{i+1/2}^{j+1} + \frac{1}{2} \frac{\Delta B_i^{j+1}}{\Delta h_{ri}^{j+1}} \left(h_{ri+1/2}^{j+1} - h_{g_{i+1/2}}^{j+1} \right) \right] + \frac{\Delta x_i}{2\Delta t^j} \left[s_{ci+1/2}^{j+1} \left(B + B_o \right)_i^{j+1} \right] \tag{B.1}$$

$$\frac{\partial C}{\partial h_{ri+1}^{j+1}} = -\theta_f \Delta x_i \left(-\frac{K_r}{m_r} \right)_{i+1/2}^{j+1} \left[\frac{1}{2} B_{i+1/2}^{j+1} + \frac{1}{2} \frac{\Delta B_{i+1}^{j+1}}{\Delta h_{ri+1}^{j+1}} \left(h_{ri+1/2}^{j+1} - h_{g_{i+1/2}}^{j+1} \right) \right] + \frac{\Delta x_i}{2\Delta t^j} \left[s_{ci+1/2}^{j+1} \left(B + B_o \right)_{i+1}^{j+1} \right] \tag{B.2}$$

$$\frac{\partial C}{\partial Q_i^{j+1}} = -\theta_f \tag{B.3}$$

$$\frac{\partial C}{\partial Q_{i+1}^{j+1}} = \theta_f \tag{B.4}$$

Partial Derivatives of the Momentum Equation

The partial derivatives of the momentum equation with respect to unknown terms (i.e., $(h_r)_i$, $(h_r)_{i+1}$, Q_i and Q_{i+1} at $(j+1)^{th}$ time line) are computed as follows:

$$\frac{\partial M}{\partial h_{r_i}^{j+1}} = \theta_f \left[\begin{array}{l} \left(\frac{\beta Q^2 B}{A^2} \right)_i^{j+1} + g A_{i+1/2}^{j+1} \left(-1 + \Delta x_i \frac{\partial S_{f_{i+1/2}}^{j+1}}{\partial h_{ri}^{j+1}} + \Delta x_i \frac{\partial S_{eci+1/2}^{j+1}}{\partial h_{ri}^{j+1}} \right) \\ + \frac{1}{2} g B_i^{j+1} \left(h_{ri+1}^{j+1} - h_{ri}^{j+1} + S_{f_{i+1/2}}^{j+1} \Delta x_i + S_{eci+1/2}^{j+1} \Delta x_i \right) \\ + \Delta x_i \frac{\partial \left(M_{L1} \right)_{i+1/2}^{j+1}}{\partial h_{ri}^{j+1}} + \Delta x_i \frac{\partial \left(M_{L2} \right)_{i+1/2}^{j+1}}{\partial h_{ri}^{j+1}} \end{array} \right] \tag{B.5}$$

where:

$$\frac{\partial S_{f_{i+1/2}}^{\ j+1}}{\partial h_{ri}^{\ j+1}} = S_{f_{i+1/2}}^{\ j+1}\left[\frac{2}{n_{ci+1/2}^{j+1}}\frac{\Delta n_{ci+1/2}^{\ j+1}}{\Delta h_{ri}^{\ j+1}} - \frac{5}{3}\frac{B_i^{j+1}}{A_{i+1/2}^{j+1}} + \frac{2}{3B_{i+1/2}^{j+1}}\frac{\Delta B_i^{j+1}}{\Delta h_{ri}^{\ j+1}}\right] \tag{B.6}$$

$$\frac{\partial S_{eci+1/2}^{\ j+1}}{\partial h_{ri}^{\ j+1}} = \frac{K_{eci+1/2}^{\ j+1}\left(Q^2\right)_i^{j+1} B_i^{j+1}}{g\Delta x_i \left(A^3\right)_i^{j+1}} \tag{B.7}$$

$$\frac{\partial \left(M_{L1}\right)_{i+1/2}^{j+1}}{\partial h_{ri}^{\ j+1}} = \begin{cases} 0 \\ -\dfrac{Q_{i+1/2}^{j+1}\left(q_{L1}\right)_{i+1/2}^{j+1}}{2A_{i+1/2}^{j+1}}\left[-\dfrac{B_i^{j+1}}{2A_{i+1/2}^{j+1}} + \dfrac{1}{2B_{i+1/2}^{j+1}}\dfrac{\Delta B_i^{j+1}}{\Delta h_{ri}^{\ j+1}} + \dfrac{1}{2\left(h_{ri+1/2}^{\ j+1} - h_{g_{i+1/2}}^{\ j+1}\right)}\right] \end{cases} \tag{B.8}$$

$$\frac{\partial \left(M_{L2}\right)_{i+1/2}^{j+1}}{\partial h_{ri}^{\ j+1}} = \begin{cases} 0 \\ -\dfrac{Q_{i+1/2}^{j+1}\left(q_{L2}\right)_{i+1/2}^{j+1}}{A_{i+1/2}^{j+1}}\left[-\dfrac{B_i^{j+1}}{2A_{i+1/2}^{j+1}}\right] \end{cases} \tag{B.9}$$

$$\frac{\partial M}{\partial h_{ri+1}^{\ j+1}} = \theta_f \begin{bmatrix} -\left(\dfrac{\beta Q^2 B}{A^2}\right)_{i+1}^{j+1} + gA_{i+1/2}^{j+1}\left(1 + \Delta x_i \dfrac{\partial S_{f_{i+1/2}}^{\ j+1}}{\partial h_{ri+1}^{\ j+1}} + \Delta x_i \dfrac{\partial S_{eci+1/2}^{\ j+1}}{\partial h_{ri+1}^{\ j+1}}\right) \\ +\dfrac{1}{2} gB_{i+1}^{j+1}\left(h_{ri+1}^{\ j+1} - h_{ri}^{\ j+1} + S_{f_{i+1/2}}^{\ j+1}\Delta x_i + S_{eci+1/2}^{\ j+1}\Delta x_i\right) \\ +\Delta x_i \dfrac{\partial \left(M_{L1}\right)_{i+1/2}^{j+1}}{\partial h_{ri+1}^{\ j+1}} + \Delta x_i \dfrac{\partial \left(M_{L2}\right)_{i+1/2}^{j+1}}{\partial h_{ri+1}^{\ j+1}} \end{bmatrix} \tag{B.10}$$

where:

$$\frac{\partial S_{f_{i+1/2}}^{\ j+1}}{\partial h_{ri+1}^{\ j+1}} = S_{f_{i+1/2}}^{\ j+1}\left[\frac{2}{n_{ci+1/2}^{j+1}}\frac{\Delta n_{ci+1/2}^{\ j+1}}{\Delta h_{ri+1}^{\ j+1}} - \frac{5}{3}\frac{B_{i+1}^{j+1}}{A_{i+1/2}^{j+1}} + \frac{2}{3B_{i+1/2}^{j+1}}\frac{\Delta B_{i+1}^{j+1}}{\Delta h_{ri+1}^{\ j+1}}\right] \tag{B.11}$$

$$\frac{\partial S_{eci+1/2}^{\ j+1}}{\partial h_{ri+1}^{\ j+1}} = \frac{K_{eci+1/2}^{\ j+1}(Q^2)_{i+1}^{j+1} B_{i+1}^{j+1}}{g\Delta x_i (A^3)_{i+1}^{j+1}} \tag{B.12}$$

$$\frac{\partial\left(M_{L1}\right)_{i+1/2}^{j+1}}{\partial h_{ri+1}^{j+1}}=\begin{cases}0\\ -\dfrac{Q_{i+1/2}^{j+1}\left(q_{L1}\right)_{i+1/2}^{j+1}}{2A_{i+1/2}^{j+1}}\left[-\dfrac{B_{i+1}^{j+1}}{2A_{i+1/2}^{j+1}}+\dfrac{1}{2B_{i+1/2}^{j+1}}\dfrac{\Delta B_{i+1}^{j+1}}{\Delta h_{ri+1}^{j+1}}+\dfrac{1}{2\left(h_{ri+1/2}^{j+1}-h_{gi+1/2}^{j+1}\right)}\right]\end{cases} \tag{B.13}$$

$$\frac{\partial\left(M_{L2}\right)_{i+1/2}^{j+1}}{\partial h_{ri+1}^{j+1}}=\begin{cases}0\\ -\dfrac{Q_{i+1/2}^{j+1}\left(q_{L2}\right)_{i+1/2}^{j+1}}{A_{i+1/2}^{j+1}}\left[-\dfrac{B_{i+1}^{j+1}}{2A_{i+1/2}^{j+1}}\right]\end{cases} \tag{B.14}$$

$$\frac{\partial M}{\partial Q_i^{j+1}}=\frac{\Delta x_i}{2\Delta t^j}s_{mi+1/2}^{\ j+1}+\theta_f\left[\begin{array}{r}-\left(\dfrac{2\beta Q}{A}\right)_i^{j+1}+gA_{i+1/2}^{j+1}\left(\Delta x_i\dfrac{\partial S_{f\,i+1/2}^{\ j+1}}{\partial Q_i^{j+1}}+\Delta x_i\dfrac{\partial S_{ec\,i+1/2}^{\ j+1}}{\partial Q_i^{j+1}}\right)\\ +\Delta x_i\dfrac{\partial\left(M_{L1}\right)_{i+1/2}^{j+1}}{\partial Q_i^{j+1}}+\Delta x_i\dfrac{\partial\left(M_{L2}\right)_{i+1/2}^{j+1}}{\partial Q_i^{j+1}}\end{array}\right] \tag{B.15}$$

where:

$$\frac{\partial S_{f\,i+1/2}^{\ j+1}}{\partial Q_i^{j+1}}=S_{f\,i+1/2}^{\ j+1}\left[\frac{1}{n_{ci+1/2}^{j+1}}\frac{\Delta n_{i+1/2}^{j+1}}{\Delta Q_{i+1/2}^{j+1}}+\frac{1}{Q_{i+1/2}^{j+1}}\right] \tag{B.16}$$

$$\frac{\partial S_{ec\,i+1/2}^{\ j+1}}{\partial Q_i^{j+1}}=\frac{-K_{ec\,i+1/2}^{\ j+1}Q_i^{j+1}}{g\Delta x_i(A^2)_i^{j+1}} \tag{B.17}$$

$$\frac{\partial\left(M_{L1}\right)_{i+1/2}^{j+1}}{\partial Q_i^{j+1}}=\begin{cases}0\\ -\dfrac{\left(q_{L1}\right)_{i+1/2}^{j+1}}{4A_{i+1/2}^{j+1}}\end{cases} \tag{B.18}$$

$$\frac{\partial\left(M_{L2}\right)_{i+1/2}^{j+1}}{\partial Q_i^{j+1}}=\begin{cases}0\\ -\dfrac{\left(q_{L2}\right)_{i+1/2}^{j+1}}{2A_{i+1/2}^{j+1}}\end{cases} \tag{B.19}$$

$$\frac{\partial M}{\partial Q_{i+1}^{j+1}} = \frac{\Delta x_{i+1/2}}{2\Delta t^{j+1/2}} s_{m\,i+1/2}^{\;\;j+1} + \theta_f \left[\begin{array}{r} \left(\frac{2\beta Q}{A}\right)_{i+1}^{j+1} + gA_{i+1/2}^{j+1}\left(\Delta x_i \frac{\partial S_{f\,i+1/2}^{\;\;j+1}}{\partial Q_{i+1}^{j+1}} + \Delta x_i \frac{\partial S_{ec\,i+1/2}^{\;\;j+1}}{\partial Q_{i+1}^{j+1}} \right) \\ + \Delta x_i \frac{\partial \left(M_{L1}\right)_{i+1/2}^{j+1}}{\partial Q_{i+1}^{j+1}} + \Delta x_i \frac{\partial \left(M_{L2}\right)_{i+1/2}^{j+1}}{\partial Q_{i+1}^{j+1}} \end{array} \right] \quad \text{(B.20)}$$

where:

$$\frac{\partial S_{f\,i+1/2}^{\;\;j+1}}{\partial Q_{i+1}^{j+1}} = S_{f\,i+1/2}^{\;\;j+1}\left[\frac{1}{n_{ci+1/2}^{j+1}} \frac{\Delta n_{i+1/2}^{j+1}}{\Delta Q_{i+1/2}^{j+1}} + \frac{1}{Q_{i+1/2}^{j+1}} \right] \quad \text{(B.21)}$$

$$\frac{\partial S_{ec\,i+1/2}^{\;\;j+1}}{\partial Q_{i+1}^{j+1}} = \frac{-K_{ec\,i+1/2}^{\;\;j+1} Q_{i+1}^{j+1}}{g\Delta x_i (A^2)_{i+1}^{j+1}} \quad \text{(B.22)}$$

$$\frac{\partial \left(M_{L1}\right)_{i+1/2}^{j+1}}{\partial Q_{i+1}^{j+1}} = \begin{cases} 0 \\ -\dfrac{\left(q_{L1}\right)_{i+1/2}^{j+1}}{4A_{i+1/2}^{j+1}} \end{cases} \quad \text{(B.23)}$$

$$\frac{\partial \left(M_{L2}\right)_{i+1/2}^{j+1}}{\partial Q_{i+1}^{j+1}} = \begin{cases} 0 \\ -\dfrac{\left(q_{L2}\right)_{i+1/2}^{j+1}}{2A_{i+1/2}^{j+1}} \end{cases} \quad \text{(B.24)}$$

Partial Derivatives of the External Boundary Conditions

At upstream boundaries, a discharge or a stage hydrograph can be implemented as the boundary condition. When a discharge hydrograph is used as the upstream boundary condition, the partial derivatives of Jacobian become:

$$\frac{\partial UB}{\partial Q_i^{j+1}} = 1 \tag{B.25}$$

$$\frac{\partial UB}{\partial h_{ri}^{j+1}} = 0 \tag{B.26}$$

where subscript *i* represent the upstream node number of the channel. However, if a stage hydrograph is used as the upstream boundary condition, then the partial derivatives become:

$$\frac{\partial UB}{\partial Q_i^{j+1}} = 0 \tag{B.27}$$

$$\frac{\partial UB}{\partial h_{ri}^{j+1}} = 1 \tag{B.28}$$

At the downstream boundary, a discharge hydrograph, a stage hydrograph, a single-valued rating curve, a looped rating curve or a critical depth section can be implemented as the boundary condition. If a discharge hydrograph is used as the downstream boundary condition, the partial derivatives become:

$$\frac{\partial DB}{\partial Q_N^{j+1}} = 1 \tag{B.29}$$

$$\frac{\partial DB}{\partial h_{rN}^{j+1}} = 0 \tag{B.30}$$

If a stage hydrograph is used as the downstream boundary condition, the partial derivatives become:

$$\frac{\partial DB}{\partial Q_N^{j+1}} = 0 \tag{B.31}$$

$$\frac{\partial DB}{\partial h_{r\,N}^{\;j+1}} = 1 \tag{B.32}$$

For the single-valued rating curve, the partial derivatives become:

$$\frac{\partial DB}{\partial Q_N^{j+1}} = 1 \tag{B.33}$$

$$\frac{\partial DB}{\partial h_{r\,N}^{\;j+1}} = -\left(\frac{Q^{k+1} - Q^k}{h_r^{k+1} - h_r^k} \right) \tag{B.34}$$

If a looped rating curve is used, the partial derivatives are written as:

$$\frac{\partial DB}{\partial Q_N^{j+1}} = 1 + Q' \left(\frac{1}{n_c} \frac{\Delta n_c}{\Delta Q} \right)_N^{j+1} \tag{B.35}$$

$$\frac{\partial DB}{\partial h_{r\,N}^{\;j+1}} = Q' \left(\frac{1}{n_c} \frac{\Delta n_c}{\Delta h_r} - \frac{5}{3} \frac{B}{A} + \frac{2}{3B} \frac{\Delta B}{\Delta h_r} \right)_N^{j+1} \tag{B.36}$$

where:

$$Q' = c_1 \left(\frac{AR_h^{2/3}}{n_c} \right)_N^{j+1} \left(S_f^{1/2} \right)_{N-1/2}^{j+1} \tag{B.37}$$

Finally, if a critical section is used at the downstream boundary, the partial derivatives are written as:

$$\frac{\partial DB}{\partial Q_N^{j+1}} = 1 \tag{B.38}$$

$$\frac{\partial DB}{\partial h_{r\,N}^{j+1}} = Q_{cr} \left(-\frac{3}{2} \frac{B}{A} + \frac{1}{2B} \frac{\Delta B}{\Delta h_r} \right)_N^{j+1} \tag{B.39}$$

where:

$$Q_{cr} = \sqrt{\frac{g}{B_N^{j+1}}} \left(A^{3/2} \right)_N^{j+1} \tag{B.40}$$

Partial Derivatives of the Internal Boundary Conditions

At any junction with m inflowing channels, a total of $m+1$ internal boundary conditions are specified. The partial derivatives of the junction momentum equation shown in equation (A.40) written for each inflowing channel become:

$$\frac{\partial IB}{\partial Q_i^{j+1}} = 0 \tag{B.41}$$

$$\frac{\partial IB}{\partial h_{r_i}^{j+1}} = 1 \tag{B.42}$$

where subscript *i* represents the last node of the particular inflowing channel to the junction. Similarly, the partial derivatives of the junction momentum equation shown in equation (A.40) written for the outflowing channel become:

$$\frac{\partial IB}{\partial Q_o^{j+1}} = 0 \tag{B.43}$$

$$\frac{\partial IB}{\partial h_{r_o}^{j+1}} = -1 \tag{B.44}$$

where the subscript *o* represents the first node of the outflowing channel from the junction. The partial derivatives of the junction continuity equation shown in equation (A.41) written for each inflowing channels become:

$$\frac{\partial IB}{\partial Q_i^{j+1}} = 1 \tag{B.45}$$

$$\frac{\partial IB}{\partial h_{r_i}^{j+1}} = 0 \tag{B.46}$$

where the subscript *i* represents the last node of the particular inflowing channel to the junction. Similarly, the partial derivatives of the junction continuity equation shown in equation (A.41) written for the outflowing channel become:

$$\frac{\partial IB}{\partial Q_o^{j+1}} = -1 \tag{B.47}$$

$$\frac{\partial IB}{\partial h_{r_o}^{j+1}} = 0 \tag{B.48}$$

APPENDIX C

INTERPOLATING FUNCTIONS IN GALERKIN FINITE ELEMENT METHOD

APPENDIX C

INTERPOLATING FUNCTIONS IN GALERKIN FINITE ELEMENT METHOD

Interpolating (or basis/shape) functions form the core of the finite element analysis. There is a one-to-one relation between basis functions and nodes in the discretized domain. A basis function that is identified at a particular node is zero over any element unless that node is associated with the element of concern.

Theoretically, basis functions can be written in global or local coordinates. However, it is practical to use a local coordinate system with quadrilateral elements, which is the element type selected in this study, to simplify the integrations and differentiations of the basis functions. In this regard, a local coordinate system together with a master element concept is implemented in this study (Figure C.1). A direct consequence of this approach is the necessity to formulate a transformation function between global and local coordinates. Unfortunately, this transformation is not linear for an irregular quadrilateral element and hence a numerical integration scheme is normally required to evaluate the integrals in the finite element analysis.

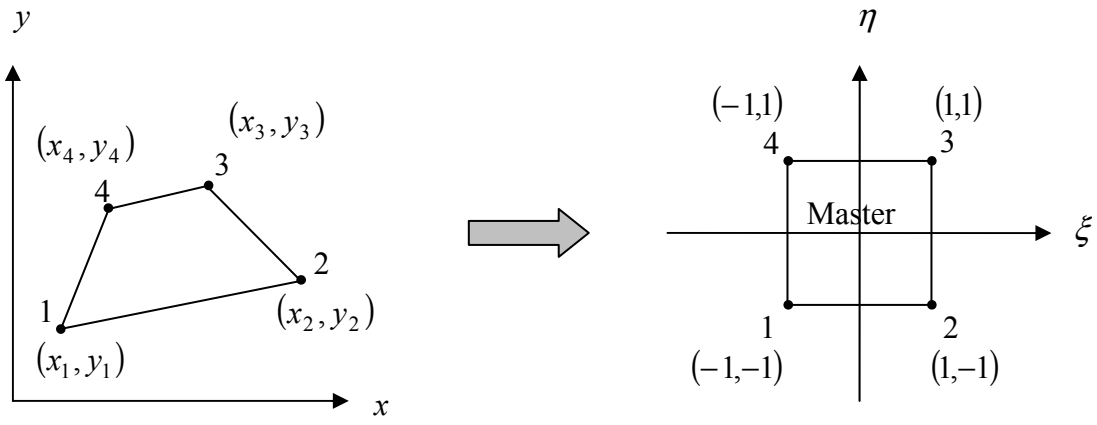

Figure C. 1. Global and local coordinate systems and the master element concept

In this method, the two-dimensional domain is globally discretized using irregular quadrilateral elements. Then, coordinates of the nodes of each element is mapped to a local coordinate system via the master element concept. The master element is a 2X2 square located at the center of the local coordinate axes with nodes at each corner. The corner coordinates of the master element are (-1,-1), (1,-1), (1,1) and (-1,1). Therefore, all integrations can be done on the master element using the limits $-1 \leq \xi \leq +1$ and $-1 \leq \eta \leq +1$. The general formula for the shape functions of a quadrilateral element can be obtained by taking the tensor product of the two shape functions for the linear line element and is given by the expression:

$$N_i(\xi,\eta) = \frac{1}{4}(1+\xi\xi_i)(1+\eta\eta_i) \tag{C.1}$$

where ξ and η define the local coordinate system used with the master element concept. Using this formula and the local coordinates of the master element, it is possible to write the four shape functions of the quadrilateral element shown in Figure C.1 as:

$$\begin{aligned} N_1(\xi,\eta) &= \frac{1}{4}(1-\xi)(1-\eta) \\ N_2(\xi,\eta) &= \frac{1}{4}(1+\xi)(1-\eta) \\ N_3(\xi,\eta) &= \frac{1}{4}(1+\xi)(1+\eta) \\ N_4(\xi,\eta) &= \frac{1}{4}(1-\xi)(1+\eta) \end{aligned} \tag{C.2}$$

There are two important modifications that should be done before the master element concept can be used in finite element analysis. The first one of these modifications is to transform the derivatives of the integrands into local coordinates. In order to implement this transformation from global to local coordinates, derivatives of these shape functions with respect to local coordinates are evaluated using the chain rule of differentiation:

$$\begin{aligned} \frac{\partial N_i}{\partial x} &= \frac{\partial N_i}{\partial \xi}\frac{\partial \xi}{\partial x} + \frac{\partial N_i}{\partial \eta}\frac{\partial \eta}{\partial x} \\ \frac{\partial N_i}{\partial y} &= \frac{\partial N_i}{\partial \xi}\frac{\partial \xi}{\partial y} + \frac{\partial N_i}{\partial \eta}\frac{\partial \eta}{\partial y} \end{aligned} \tag{C.3}$$

which can be represented in matrix form as:

$$\begin{bmatrix} \dfrac{\partial N_i}{\partial x} \\ \dfrac{\partial N_i}{\partial y} \end{bmatrix} = \begin{bmatrix} \dfrac{\partial \xi}{\partial x} & \dfrac{\partial \eta}{\partial x} \\ \dfrac{\partial \xi}{\partial y} & \dfrac{\partial \eta}{\partial y} \end{bmatrix} \begin{bmatrix} \dfrac{\partial N_i}{\partial \xi} \\ \dfrac{\partial N_i}{\partial \eta} \end{bmatrix} \tag{C.4}$$

The derivatives of the shape functions with respect to local coordinates can easily be computed as follows:

$$\begin{aligned} \frac{\partial N_1}{\partial \xi} &= -\frac{1}{4}(1-\eta) & \frac{\partial N_1}{\partial \eta} &= -\frac{1}{4}(1-\xi) \\ \frac{\partial N_2}{\partial \xi} &= +\frac{1}{4}(1-\eta) & \frac{\partial N_2}{\partial \eta} &= -\frac{1}{4}(1+\xi) \\ \frac{\partial N_3}{\partial \xi} &= +\frac{1}{4}(1+\eta) & \frac{\partial N_3}{\partial \eta} &= +\frac{1}{4}(1+\xi) \\ \frac{\partial N_4}{\partial \xi} &= -\frac{1}{4}(1+\eta) & \frac{\partial N_4}{\partial \eta} &= +\frac{1}{4}(1-\xi) \end{aligned} \tag{C.5}$$

The coefficient matrix, however, requires a functional relationship that maps the global coordinates to local coordinates. This transformation from global to local coordinates is obtained by using shape functions to interpolate the global coordinates. Hence, one can write:

$$\begin{aligned} x &= x(\xi,\eta) = \sum_{i=1}^{4} x_i N_i(\xi,\eta) \\ y &= y(\xi,\eta) = \sum_{i=1}^{4} y_i N_i(\xi,\eta) \end{aligned} \tag{C.6}$$

If the derivatives of these expressions are taken with respect to the local coordinates, one would obtain a 2X2 matrix that is commonly known as the Jacobian matrix:

$$[J]=\begin{bmatrix}\dfrac{\partial x}{\partial \xi} & \dfrac{\partial x}{\partial \eta}\\ \dfrac{\partial y}{\partial \xi} & \dfrac{\partial y}{\partial \eta}\end{bmatrix}=\begin{bmatrix}\displaystyle\sum_{i=1}^{4} x_i \frac{\partial N_i}{\partial \xi} & \displaystyle\sum_{i=1}^{4} x_i \frac{\partial N_i}{\partial \eta}\\ \displaystyle\sum_{i=1}^{4} y_i \frac{\partial N_i}{\partial \xi} & \displaystyle\sum_{i=1}^{4} y_i \frac{\partial N_i}{\partial \eta}\end{bmatrix} \tag{C.7}$$

The determinant of the Jacobian is an important quantity and is extensively used in the master element integrations using local coordinates.

$$\det[J]=|J|=\left(\sum_{i=1}^{4} x_i \frac{\partial N_i}{\partial \xi}\right)\left(\sum_{i=1}^{4} y_i \frac{\partial N_i}{\partial \eta}\right)-\left(\sum_{i=1}^{4} x_i \frac{\partial N_i}{\partial \eta}\right)\left(\sum_{i=1}^{4} y_i \frac{\partial N_i}{\partial \xi}\right) \tag{C.8}$$

It should be noted, however, that the matrix required to transform the derivatives in global coordinates to derivatives in local coordinates is not exactly the Jacobian matrix given above. The link between these two matrices can be established if an identity matrix is written such that:

$$\begin{bmatrix}1 & 0\\ 0 & 1\end{bmatrix}=\begin{bmatrix}\dfrac{\partial \xi}{\partial x} & \dfrac{\partial \eta}{\partial x}\\ \dfrac{\partial \xi}{\partial y} & \dfrac{\partial \eta}{\partial y}\end{bmatrix}\begin{bmatrix}\dfrac{\partial x}{\partial \xi} & \dfrac{\partial y}{\partial \xi}\\ \dfrac{\partial x}{\partial \eta} & \dfrac{\partial y}{\partial \eta}\end{bmatrix} \tag{C.9}$$

In the above equation, the second matrix is simply the transpose of the Jacobian matrix. Since the identity matrix is obtained by multiplying a matrix and its inverse, the first matrix then becomes the inverse of the Jacobian transpose.

$$\begin{bmatrix} \frac{\partial \xi}{\partial x} & \frac{\partial \eta}{\partial x} \\ \frac{\partial \xi}{\partial y} & \frac{\partial \eta}{\partial y} \end{bmatrix} = \left[J^T\right]^{-1} = \frac{1}{|J|} \begin{bmatrix} \sum_{i=1}^{4} y_i \frac{\partial N_i}{\partial \eta} & -\sum_{i=1}^{4} y_i \frac{\partial N_i}{\partial \xi} \\ -\sum_{i=1}^{4} x_i \frac{\partial N_i}{\partial \eta} & \sum_{i=1}^{4} x_i \frac{\partial N_i}{\partial \xi} \end{bmatrix} \tag{C.10}$$

It is now possible to complete the transformation of the shape function derivatives by using this matrix and the derivatives of the shape functions with respect to local coordinates. The second modification that is required to use the master element concept in finite element analysis is to convert the integration variables into local coordinates. The basic formula for a change of integration variables is given as:

$$\iint_{\substack{global \\ element}} f(x,y)dxdy = \iint_{\substack{master \\ element}} f\left(x(\xi,\eta), y(\xi,\eta)\right)|J|d\xi d\eta \tag{C.11}$$

where the determinant of the Jacobian is used explicitly. It should be noted that this change in integration variables does not pose any extra difficulty as long as the determinant of the Jacobian is a constant. For non-linear coordinate transformations, such as the one used here in quadrilateral elements, the Jacobian is not a constant and the above integration can only be done using a numerical integration scheme.

APPENDIX D

DERIVATION OF GALERKIN FORM OF GROUNDWATER FLOW EQUATION

APPENDIX D

DERIVATION OF GALERKIN FORM OF GROUNDWATER FLOW EQUATION

The first step of the derivation of the weak form is to approximate the unknown function over the domain using interpolating functions, $N_j(x,y)$, of the form:

$$h_g(x,y,t) \approx \hat{h}_g(x,y,t) = \sum_{j=1}^{N} \left(\hat{h}_g(t)\right)_j N_j(x,y) \tag{D.1}$$

where $\hat{h}_g(t)$ is the approximate value of the hydraulic head and N is the total number of nodes in the two-dimensional groundwater flow domain. In essence, the temporal and spatial discretizations are separated from each other in the approximate solution. The nodal values, $(\hat{h}_g(t))_j$, becomes only a function of time and the shape function, $N_j(x,y)$, is now only a function of space. It is also important to note that the shape functions are defined only for its corresponding node. They are zero elsewhere in the domain.

Since the Galerkin method is an approximate technique, the solution given in equation (D.1) does not satisfy the differential equation exactly and a residual occurs. The method states that the weighted average of this residual over the whole domain

becomes zero. If the approximate solution is substituted in the differential equation, one can write the total residual, $\check{R}$, as:

$$\begin{aligned}\tilde{R}(x,y,t) = {} & S_y \frac{\partial \hat{h}_g}{\partial t} - \frac{\partial}{\partial x}\left[\left(\hat{h}_g - z_b\right)\left(K_g\right)_{xx}\frac{\partial \hat{h}_g}{\partial x} + \left(\hat{h}_g - z_b\right)\left(K_g\right)_{xy}\frac{\partial \hat{h}_g}{\partial y}\right] \\ & - \frac{\partial}{\partial y}\left[\left(\hat{h}_g - z_b\right)\left(K_g\right)_{yx}\frac{\partial \hat{h}_g}{\partial x} + \left(\hat{h}_g - z_b\right)\left(K_g\right)_{yy}\frac{\partial \hat{h}_g}{\partial y}\right] \\ & + \sum_{k=1}^{n_w}\left[Q_{w,k}\,\delta\left(x - x_{w,k}\right)\delta\left(y - y_{w,k}\right)\right] \\ & + \sum_{m=1}^{n_r}\left[\int_0^1 q_{L1,m}\sqrt{\left(\frac{dg_{x,m}}{du}\right)^2 + \left(\frac{dg_{y,m}}{du}\right)^2}\,\delta\left(x - g_{x,m}(u)\right)\delta\left(y - g_{y,m}(u)\right)du\right] + I\end{aligned} \tag{D.2}$$

The Galerkin finite element method is based on the idea of minimizing this residual over the solution domain by letting the weighed integral residual tend to zero. In this formulation the weighing functions are selected as the interpolating functions used in element level:

$$\iint_{\Omega} \tilde{R}(x,y,t)\,N_i(x,y)\,d\Omega = 0 \qquad i = 1,2,3,...,N \tag{D.3}$$

For the sake of clarity, the description of the index *i* running from *1* to *N* is not repeated in the following equations. When the expression for the residual is substituted in equation (D.3) and the square root expression is written as the norm of the gradient of parametric vector equation $\mathbf{g} = g_x\mathbf{i} + g_y\mathbf{j}$, the integral simplifies to:

$$\iint_{\Omega}\left\{\begin{array}{l} S_y\dfrac{\partial \hat{h}_g}{\partial t}-\dfrac{\partial}{\partial x}\left[\left(\hat{h}_g-z_b\right)\left(K_g\right)_{xx}\dfrac{\partial \hat{h}_g}{\partial x}+\left(\hat{h}_g-z_b\right)\left(K_g\right)_{xy}\dfrac{\partial \hat{h}_g}{\partial y}\right] \\ -\dfrac{\partial}{\partial y}\left[\left(\hat{h}_g-z_b\right)\left(K_g\right)_{yx}\dfrac{\partial \hat{h}_g}{\partial x}+\left(\hat{h}_g-z_b\right)\left(K_g\right)_{yy}\dfrac{\partial \hat{h}_g}{\partial y}\right] \\ +\sum_{k=1}^{n_w}\left[Q_{w,k}\delta\left(x-x_{w,k}\right)\delta\left(y-y_{w,k}\right)\right] \\ +\sum_{m=1}^{n_r}\left[\int_0^1 q_{L1,m}\left|\nabla \mathbf{g}\right|\delta\left(x-g_{x,m}(u)\right)\delta\left(y-g_{y,m}(u)\right)du\right]+I \end{array}\right\}N_i d\Omega=0 \qquad \text{(D.4)}$$

The integration by parts is now applied to the second order derivative terms in the above integral to reduce them to first order and incorporate the natural boundary conditions:

$$\begin{aligned}\iint_{\Omega}\left\{\frac{\partial}{\partial x}\left[\left(\hat{h}_g-z_b\right)\left(K_g\right)_{xx}\frac{\partial \hat{h}_g}{\partial x}+\left(\hat{h}_g-z_b\right)\left(K_g\right)_{xy}\frac{\partial \hat{h}_g}{\partial y}\right]\right\}N_i d\Omega = \\ -\iint_{\Omega}\left(\hat{h}_g-z_b\right)\left[\left(K_g\right)_{xx}\frac{\partial \hat{h}_g}{\partial x}+\left(K_g\right)_{xy}\frac{\partial \hat{h}_g}{\partial y}\right]\frac{\partial N_i}{\partial x}d\Omega \\ +\int_{\Gamma}\left(\hat{h}_g-z_b\right)\left[\left(K_g\right)_{xx}\frac{\partial \hat{h}_g}{\partial x}+\left(K_g\right)_{xy}\frac{\partial \hat{h}_g}{\partial y}\right]N_i n_x d\Gamma\end{aligned} \qquad \text{(D.5)}$$

$$\begin{aligned}\iint_{\Omega}\left\{\frac{\partial}{\partial y}\left[\left(\hat{h}_g-z_b\right)\left(K_g\right)_{yx}\frac{\partial \hat{h}_g}{\partial x}+\left(\hat{h}_g-z_b\right)\left(K_g\right)_{yy}\frac{\partial \hat{h}_g}{\partial y}\right]\right\}N_i d\Omega = \\ -\iint_{\Omega}\left(\hat{h}_g-z_b\right)\left[\left(K_g\right)_{yx}\frac{\partial \hat{h}_g}{\partial x}+\left(K_g\right)_{yy}\frac{\partial \hat{h}_g}{\partial y}\right]\frac{\partial N_i}{\partial y}d\Omega \\ +\int_{\Gamma}\left(\hat{h}_g-z_b\right)\left[\left(K_g\right)_{yx}\frac{\partial \hat{h}_g}{\partial x}+\left(K_g\right)_{yy}\frac{\partial \hat{h}_g}{\partial y}\right]N_i n_y d\Gamma\end{aligned} \qquad \text{(D.6)}$$

where n_x and n_y represent the x and y components of unit normal vector. Substituting these expressions and rearranging gives:

$$\begin{aligned}
&\iint_{\Omega}\left(\hat{h}_g - z_b\right)\left\{\left[\left(K_g\right)_{xx}\frac{\partial \hat{h}_g}{\partial x}+\left(K_g\right)_{xy}\frac{\partial \hat{h}_g}{\partial y}\right]\frac{\partial N_i}{\partial x}+\left[\left(K_g\right)_{yx}\frac{\partial \hat{h}_g}{\partial x}+\left(K_g\right)_{yy}\frac{\partial \hat{h}_g}{\partial y}\right]\frac{\partial N_i}{\partial y}\right\}d\Omega\\
&-\int_{\Gamma}\left(\hat{h}_g - z_b\right)\left\{\left[\left(K_g\right)_{xx}\frac{\partial \hat{h}_g}{\partial x}+\left(K_g\right)_{xy}\frac{\partial \hat{h}_g}{\partial y}\right]N_i n_x+\left[\left(K_g\right)_{yx}\frac{\partial \hat{h}_g}{\partial x}+\left(K_g\right)_{yy}\frac{\partial \hat{h}_g}{\partial y}\right]N_i n_y\right\}d\Gamma\\
&+\iint_{\Omega}\left\{\sum_{k=1}^{n_w}\left[Q_{w,k}\delta\left(x-x_{w,k}\right)\delta\left(y-y_{w,k}\right)\right]\right\}N_i d\Omega\\
&+\iint_{\Omega}\left\{\sum_{m=1}^{n_r}\left[\int_0^1 q_{L1,m}\left|\nabla \mathbf{g}\right|\delta\left(x-g_{x,m}(u)\right)\delta\left(y-g_{y,m}(u)\right)du\right]\right\}N_i d\Omega\\
&+\iint_{\Omega} IN_i d\Omega+\iint_{\Omega} S_y\frac{\partial \hat{h}_g}{\partial t}N_i d\Omega = 0
\end{aligned} \tag{D.7}$$

In the above form, the boundary integral can be split into two parts, according to the boundary conditions along Γ_2 and Γ_3:

$$\int_{\Gamma}(...)N_i d\Gamma = \int_{\Gamma_2}(...)N_i d\Gamma_2+\int_{\Gamma_3}(...)N_i d\Gamma_3 \tag{D.8}$$

where these boundaries are known as specified flux boundary and head dependent boundary, respectively, and are called the natural boundary conditions. In addition to these second and third type boundaries, the domain might also have first type boundaries where the known hydraulic head is specified. Such boundaries form the essential boundary conditions. At the nodes of essential boundary conditions, the solution is known and the residual vanishes. When the expressions in the specified flux and head

dependent boundary conditions are substituted in the integrals of (D.8), one would obtain the following simplified form for the boundary integrals:

$$-\int_{\Gamma}\left(\hat{h}_g - z_b\right)\left\{\left[\left(K_g\right)_{xx}\frac{\partial \hat{h}_g}{\partial x}+\left(K_g\right)_{xy}\frac{\partial \hat{h}_g}{\partial y}\right]N_i n_x+\left[\left(K_g\right)_{yx}\frac{\partial \hat{h}_g}{\partial x}+\left(K_g\right)_{yy}\frac{\partial \hat{h}_g}{\partial y}\right]N_i n_y\right\}d\Gamma = \int_{\Gamma_2} q_N N_i d\Gamma_2 + \int_{\Gamma_3} q_C N_i d\Gamma_3 \quad \text{(D.9)}$$

It is also possible to write the head-dependent boundary integral using the flux expression between the river and the aquifer when the hydraulic head is greater than river bottom sediment lower elevation (z_r - m_r):

$$\int_{\Gamma_3} q_C N_i d\Gamma_3 = -\int_{\Gamma_3} K_r w_r \frac{h_r - \hat{h}_g}{m_r} N_i d\Gamma_3 = -\int_{\Gamma_3} \frac{K_r w_r h_r}{m_r} N_i d\Gamma_3 + \int_{\Gamma_3} \frac{K_r w_r}{m_r}\hat{h}_g N_i d\Gamma_3 \quad \text{(D.10)}$$

Otherwise, the flux is no longer head dependent and is treated as a constant flux integral. From this point on, the derivation is based on the case where a head-dependent flux exists and does not collapse to a constant flux. With these modifications, equation simplifies to:

$$\iint_{\Omega}\left(\hat{h}_g - z_b\right)\left\{\left[\left(K_g\right)_{xx}\frac{\partial \hat{h}_g}{\partial x}+\left(K_g\right)_{xy}\frac{\partial \hat{h}_g}{\partial y}\right]\frac{\partial N_i}{\partial x}+\left[\left(K_g\right)_{yx}\frac{\partial \hat{h}_g}{\partial x}+\left(K_g\right)_{yy}\frac{\partial \hat{h}_g}{\partial y}\right]\frac{\partial N_i}{\partial y}\right\}d\Omega$$
$$+\int_{\Gamma_2} q_N N_i d\Gamma_2 - \int_{\Gamma_3}\frac{K_r w_r h_r}{m_r}N_i d\Gamma_3 + \int_{\Gamma_3}\frac{K_r w_r}{m_r}\hat{h}_g N_i d\Gamma_3$$
$$+\iint_{\Omega}\left\{\sum_{k=1}^{n_w}\left[Q_{w,k}\delta\left(x-x_{w,k}\right)\delta\left(y-y_{w,k}\right)\right]\right\}N_i d\Omega \qquad \text{(D.11)}$$
$$+\iint_{\Omega}\left\{\sum_{m=1}^{n_r}\left[\int_0^1 q_{L1,m}\left|\nabla \mathbf{g}\right|\delta\left(x-g_{x,m}(u)\right)\delta\left(y-g_{y,m}(u)\right)du\right]\right\}N_i d\Omega$$
$$+\iint_{\Omega} IN_i d\Omega + \iint_{\Omega} S_y\frac{\partial \hat{h}_g}{\partial t}N_i d\Omega = 0$$

When lateral flow, q_{L1}, is written according to the first condition of equation (3.7), one would obtain the weak form of the boundary-value problem:

$$\iint_{\Omega}\left(\hat{h}_g - z_b\right)\left[\begin{array}{l}\left(K_g\right)_{xx}\dfrac{\partial \hat{h}_g}{\partial x}\dfrac{\partial N_i}{\partial x}+\left(K_g\right)_{xy}\dfrac{\partial \hat{h}_g}{\partial y}\dfrac{\partial N_i}{\partial x}\\ \qquad +\left(K_g\right)_{yx}\dfrac{\partial \hat{h}_g}{\partial x}\dfrac{\partial N_i}{\partial y}+\left(K_g\right)_{yy}\dfrac{\partial \hat{h}_g}{\partial y}\dfrac{\partial N_i}{\partial y}\end{array}\right]d\Omega$$
$$+\int_{\Gamma_2} q_N N_i d\Gamma_2 - \int_{\Gamma_3}\frac{K_r w_r h_r}{m_r}N_i d\Gamma_3 + \int_{\Gamma_3}\frac{K_r w_r}{m_r}\hat{h}_g N_i d\Gamma_3$$
$$+\iint_{\Omega}\left\{\sum_{k=1}^{n_w}\left[Q_{w,k}\delta\left(x-x_{w,k}\right)\delta\left(y-y_{w,k}\right)\right]\right\}N_i d\Omega \qquad \text{(D.12)}$$
$$+\iint_{\Omega}\left\{\sum_{m=1}^{n_r}\left[\int_0^1\left(-K_r w_r\frac{h_r-\hat{h}_g}{m_r}\right)_m\left|\nabla \mathbf{g}\right|\delta\left(x-g_{x,m}(u)\right)\delta\left(y-g_{y,m}(u)\right)du\right]\right\}N_i d\Omega$$
$$+\iint_{\Omega} IN_i d\Omega + \iint_{\Omega} S_y\frac{\partial \hat{h}_g}{\partial t}N_i d\Omega = 0$$

It is seen that this boundary-value problem is non-linear due to the term ($\hat{h}_g$-z_b). Therefore, it is required to use an iterative solution technique and a suitable convergence

criterion. In this study, this term is treated as a constant by using an element average value for each iteration step. Hence, it is possible to write this term as:

$$\left(\hat{h}_g - z_b\right) \approx \left(\left(\hat{h}_g\right)_{avg} - z_b\right) \tag{D.13}$$

With this simplification, we obtain the following expression when the approximate solution in (D.1) is substituted in the weak from:

$$\begin{aligned}
&\iint_{\Omega}\left(\left(\hat{h}_g\right)_{avg} - z_b\right)\left[\begin{array}{l}
\left(K_g\right)_{xx}\dfrac{\partial}{\partial x}\left[\sum_{j=1}^{N}\left(\hat{h}_g\right)_j N_j\right]\dfrac{\partial N_i}{\partial x} + \left(K_g\right)_{xy}\dfrac{\partial}{\partial y}\left[\sum_{j=1}^{N}\left(\hat{h}_g\right)_j N_j\right]\dfrac{\partial N_i}{\partial x} \\
\qquad + \left(K_g\right)_{yx}\dfrac{\partial}{\partial x}\left[\sum_{j=1}^{N}\left(\hat{h}_g\right)_j N_j\right]\dfrac{\partial N_i}{\partial y} + \left(K_g\right)_{yy}\dfrac{\partial}{\partial y}\left[\sum_{j=1}^{N}\left(\hat{h}_g\right)_j N_j\right]\dfrac{\partial N_i}{\partial y}
\end{array}\right] d\Omega \\
&+\int_{\Gamma_2} q_N N_i d\Gamma_2 - \int_{\Gamma_3}\frac{K_r w_r h_r}{m_r} N_i d\Gamma_3 + \int_{\Gamma_3}\frac{K_r w_r}{m_r}\left[\sum_{j=1}^{N}\left(\hat{h}_g\right)_j N_j\right] N_i d\Gamma_3 \\
&+\iint_{\Omega}\left\{\sum_{k=1}^{n_w}\left[Q_{w,k}\,\delta\left(x - x_{w,k}\right)\delta\left(y - y_{w,k}\right)\right]\right\} N_i d\Omega \\
&+\iint_{\Omega}\left\{\sum_{m=1}^{n_r}\left[\int_0^1\left[\begin{array}{l}
\left(-\dfrac{K_r w_r}{m_r}\right)_m\left(h_r - \left[\sum_{j=1}^{N}\left(\hat{h}_g\right)_j N_j\right]\right)_m \\
\qquad\qquad |\nabla \mathbf{g}|\,\delta\left(x - g_{x,m}(u)\right)\delta\left(y - g_{y,m}(u)\right)
\end{array}\right] du\right]\right\} N_i d\Omega \\
&+\iint_{\Omega} I N_i d\Omega + \iint_{\Omega} S_y\frac{\partial}{\partial t}\left[\sum_{j=1}^{N}\left(\hat{h}_g\right)_j N_j\right] N_i d\Omega = 0
\end{aligned} \tag{D.14}$$

Since the nodal values are only a function of time and the shape functions are only a function of space, the above expression can be simplified by taking some of the terms out of the derivatives:

$$\iint_{\Omega}\left(\left(\hat{h}_g\right)_{avg}-z_b\right)\left[\begin{array}{l}\left(K_g\right)_{xx}\sum_{j=1}^{N}\left(\hat{h}_g\right)_j\frac{\partial N_j}{\partial x}\frac{\partial N_i}{\partial x}+\left(K_g\right)_{xy}\sum_{j=1}^{N}\left(\hat{h}_g\right)_j\frac{\partial N_j}{\partial y}\frac{\partial N_i}{\partial x}\\ \quad+\left(K_g\right)_{yx}\sum_{j=1}^{N}\left(\hat{h}_g\right)_j\frac{\partial N_j}{\partial x}\frac{\partial N_i}{\partial y}+\left(K_g\right)_{yy}\sum_{j=1}^{N}\left(\hat{h}_g\right)_j\frac{\partial N_j}{\partial y}\frac{\partial N_i}{\partial y}\end{array}\right]d\Omega$$
$$+\int_{\Gamma_2}q_N N_i d\Gamma_2-\int_{\Gamma_3}\frac{K_r w_r h_r}{m_r}N_i d\Gamma_3+\int_{\Gamma_3}\frac{K_r w_r}{m_r}\left[\sum_{j=1}^{N}\left(\hat{h}_g\right)_j N_j\right]N_i d\Gamma_3$$
$$+\iint_{\Omega}\left\{\sum_{k=1}^{n_w}\left[Q_{w,k}\delta\left(x-x_{w,k}\right)\delta\left(y-y_{w,k}\right)\right]\right\}N_i d\Omega$$
$$+\iint_{\Omega}\left\{\sum_{m=1}^{n_r}\left[\int_0^1\left[\begin{array}{l}\left(-\frac{K_r w_r}{m_r}\right)_m\left(h_r-\sum_{j=1}^{N}\left(\hat{h}_g\right)_j N_j\right)_m\\ \quad\left|\nabla\mathbf{g}\right|\delta\left(x-g_{x,m}(u)\right)\delta\left(y-g_{y,m}(u)\right)\end{array}\right]du\right]\right\}N_i d\Omega$$
$$+\iint_{\Omega}IN_i d\Omega+\iint_{\Omega}S_y\sum_{j=1}^{N}N_j\frac{\partial\left(\hat{h}_g\right)_j}{\partial t}N_i d\Omega=0 \qquad \text{(D.15)}$$

Simplifying further, one could obtain:

$$\iint_{\Omega}\left\{\sum_{j=1}^{N}\left(\hat{h}_g\right)_j\left(\left(\hat{h}_g\right)_{avg}-z_b\right)\left[\begin{array}{l}\left(K_g\right)_{xx}\frac{\partial N_j}{\partial x}\frac{\partial N_i}{\partial x}+\left(K_g\right)_{xy}\frac{\partial N_j}{\partial y}\frac{\partial N_i}{\partial x}\\ \quad+\left(K_g\right)_{yx}\frac{\partial N_j}{\partial x}\frac{\partial N_i}{\partial y}+\left(K_g\right)_{yy}\frac{\partial N_j}{\partial y}\frac{\partial N_i}{\partial y}\end{array}\right]\right\}d\Omega$$
$$+\int_{\Gamma_2}q_N N_i d\Gamma_2-\int_{\Gamma_3}\frac{K_r w_r h_r}{m_r}N_i d\Gamma_3+\int_{\Gamma_3}\left\{\sum_{j=1}^{N}\frac{K_r w_r}{m_r}\left(\hat{h}_g\right)_j N_i N_j\right\}d\Gamma_3$$
$$+\iint_{\Omega}\left\{\sum_{k=1}^{n_w}\left[Q_{w,k}\delta\left(x-x_{w,k}\right)\delta\left(y-y_{w,k}\right)\right]\right\}N_i d\Omega$$
$$+\iint_{\Omega}\left\{\sum_{m=1}^{n_r}\left[\int_0^1\left[\begin{array}{l}\left(-\frac{K_r w_r}{m_r}\right)_m\left(h_r-\sum_{j=1}^{N}\left(\hat{h}_g\right)_j N_j\right)_m\\ \quad\left|\nabla\mathbf{g}\right|\delta\left(x-g_{x,m}(u)\right)\delta\left(y-g_{y,m}(u)\right)\end{array}\right]du\right]\right\}N_i d\Omega$$
$$+\iint_{\Omega}IN_i d\Omega+\iint_{\Omega}\sum_{j=1}^{N}N_j S_y\frac{\partial\left(\hat{h}_g\right)_j}{\partial t}N_i d\Omega=0 \qquad \text{(D.16)}$$

Since N_i is defined such that it is non-zero only over elements adjacent to node i, the integrations may be performed piecewise over each element and subsequently summed.

$$\sum_{e=1}^{n_e}\left[\iint_{\Omega^e}\left\{\sum_{j=1}^{N}\left(\hat{h}_g\right)_j\left(\left(\hat{h}_g\right)_{avg}-z_b\right)\left[\begin{array}{l}\left(K_g\right)_{xx}\dfrac{\partial N_j}{\partial x}\dfrac{\partial N_i}{\partial x}+\left(K_g\right)_{xy}\dfrac{\partial N_j}{\partial y}\dfrac{\partial N_i}{\partial x}\\ \qquad\qquad +\left(K_g\right)_{yx}\dfrac{\partial N_j}{\partial x}\dfrac{\partial N_i}{\partial y}+\left(K_g\right)_{yy}\dfrac{\partial N_j}{\partial y}\dfrac{\partial N_i}{\partial y}\end{array}\right]\right\}d\Omega^e\right]$$
$$+\sum_{e=1}^{n_e}\left[\int_{\Gamma_2^e}q_N N_i d\Gamma_2^e\right]-\sum_{e=1}^{n_e}\left[\int_{\Gamma_3^e}\frac{K_r w_r h_r}{m_r}N_i d\Gamma_3^e\right]+\sum_{e=1}^{n_e}\left[\int_{\Gamma_3^e}\left\{\sum_{j=1}^{N}\frac{K_r w_r}{m_r}\left(\hat{h}_g\right)_j N_j N_i\right\}d\Gamma_3^e\right]$$
$$+\sum_{e=1}^{n_e}\left[\iint_{\Omega^e}\left\{\sum_{k=1}^{n_w}\left[Q_{w,k}\delta\left(x-x_{w,k}\right)\delta\left(y-y_{w,k}\right)\right]\right\}N_i d\Omega^e\right]$$
$$+\sum_{e=1}^{n_e}\left[\iint_{\Omega^e}\sum_{m=1}^{n_r}\left[\int_0^1\left[\begin{array}{l}\left(-\dfrac{K_r w_r}{m_r}\right)_m\left(h_r-\sum_{j=1}^{N}\left(\hat{h}_g\right)_j N_j\right)_m\\ \qquad\qquad \left|\nabla\mathbf{g}\right|\delta\left(x-g_{x,m}(u)\right)\delta\left(y-g_{y,m}(u)\right)\end{array}\right]du\right]N_i d\Omega^e\right]$$
$$+\sum_{e=1}^{n_e}\left[\iint_{\Omega^e}IN_i d\Omega^e\right]+\sum_{e=1}^{n_e}\left[\iint_{\Omega^e}\sum_{j=1}^{N}N_j S_y\frac{\partial\left(\hat{h}_g\right)_j}{\partial t}N_i d\Omega^e\right]=0 \qquad \text{(D.17)}$$

The element integrals can now be written in matrix form:

$$\mathbf{S^e}\cdot\hat{\mathbf{h}}_\mathbf{g}+\mathbf{M^e}\cdot\frac{d\,\hat{\mathbf{h}}_\mathbf{g}}{dt}=\mathbf{F^e} \qquad \text{(D.18)}$$

where $\hat{\mathbf{h}}_\mathbf{g}$ is the unknown hydraulic head vector and $\mathbf{S^e}$, $\mathbf{M^e}$ and $\mathbf{F^e}$ are element matrices and vectors defined as follows:

$$\mathbf{S^e} = \iint_{\Omega^e} \left\{ \left(\left(\hat{h}_g \right)_{avg} - z_b \right) \begin{bmatrix} \left(K_g \right)_{xx} \dfrac{\partial N_j}{\partial x} \dfrac{\partial N_i}{\partial x} + \left(K_g \right)_{xy} \dfrac{\partial N_j}{\partial y} \dfrac{\partial N_i}{\partial x} \\ + \left(K_g \right)_{yx} \dfrac{\partial N_j}{\partial x} \dfrac{\partial N_i}{\partial y} + \left(K_g \right)_{yy} \dfrac{\partial N_j}{\partial y} \dfrac{\partial N_i}{\partial y} \end{bmatrix} \right\} d\Omega^e$$
$$+ \int_{\Gamma_3^e} \frac{K_r w_r}{m_r} N_j N_i d\Gamma_3^e \tag{D.19}$$
$$- \iint_{\Omega^e} \sum_{m=1}^{n_r} \left[\int_0^1 \begin{bmatrix} \left(-\dfrac{K_r w_r}{m_r} \right)_{m,e} N_j \left| \nabla \mathbf{g} \right| \\ \delta\left(x - g_{x,m,e}(u) \right) \delta\left(y - g_{y,m,e}(u) \right) \end{bmatrix} du \right] N_i d\Omega^e$$

$$\mathbf{F^e} = - \int_{\Gamma_2^e} q_N N_i d\Gamma_2^e + \int_{\Gamma_3^e} \frac{K_r w_r h_r}{m_r} N_i d\Gamma_3^e - \iint_{\Omega^e} I N_i d\Omega^e$$
$$- \iint_{\Omega^e} \left\{ \sum_{k=1}^{n_w} \left[Q_{w,k} \delta\left(x - x_{w,k} \right) \delta\left(y - y_{w,k} \right) \right] \right\} N_i d\Omega^e \tag{D.20}$$
$$- \iint_{\Omega^e} \sum_{m=1}^{n_r} \left[\int_0^1 \left(-\frac{K_r w_r}{m_r} h_r \right)_{m,e} \left| \nabla \mathbf{g} \right| \delta\left(x - g_{x,m,e}(u) \right) \delta\left(y - g_{y,m,e}(u) \right) du \right] N_i d\Omega^e$$

$$\mathbf{M^e} = \iint_{\Omega^e} S_y N_j N_i d\Omega^e \tag{D.21}$$

Finally, the global assembly of these matrices would yield the following matrix equation:

$$\mathbf{S} \cdot \hat{\mathbf{h}}_\mathbf{g} + \mathbf{M} \cdot \frac{d \hat{\mathbf{h}}_\mathbf{g}}{dt} = \mathbf{F} \tag{D.22}$$

where **S**, **M** and **F** is generally known as stiffness matrix, mass matrix and load vector, respectively, from the structural mechanics analogy.

APPENDIX E

DERIVATION OF ELEMENT INTEGRAL EQUATIONS FOR GROUNDWATER FLOW

APPENDIX E

DERIVATION OF ELEMENT INTEGRAL EQUATIONS FOR GROUNDWATER FLOW

The key point in finite element analysis is the derivation of element matrices and vectors that are obtained as a result of element level integrations. These element level matrices and vectors are then later assembled sequentially to obtain their global counterparts. In this study, the element matrices and vectors are [4X4] and {4X1} systems, respectively, since four-nodal linear quadrilateral elements are used to discretize the domain. In what follows first the evaluation of element domain integrals are discussed followed by the discussion of element boundary integrals. Each integral given in equations (D.19), (D.20) and (D.21) are split and written separately with a bullet. They are analyzed such that a procedure for their numerical evaluation is presented.

Derivation of Element Matrices and Vectors for the Element Domain

For all elements in the domain, a series of integrals presented in (D.19), (D.20) and (D.21) are evaluated to obtain the members of the [4X4] element stiffness and mass

matrices and {4X1} element load vector. Hence, in what follows, each integral is analyzed individually in which subscripts *i* and *j* run from 1 to 4.

- $$\iint_{\Omega^e} \left\{ \left(\left(\hat{h}_g \right)_{avg} - z_b \right) \left[\begin{array}{l} \left(K_g \right)_{xx} \dfrac{\partial N_j}{\partial x} \dfrac{\partial N_i}{\partial x} + \left(K_g \right)_{xy} \dfrac{\partial N_j}{\partial y} \dfrac{\partial N_i}{\partial x} \\ \qquad + \left(K_g \right)_{yx} \dfrac{\partial N_j}{\partial x} \dfrac{\partial N_i}{\partial y} + \left(K_g \right)_{yy} \dfrac{\partial N_j}{\partial y} \dfrac{\partial N_i}{\partial y} \end{array} \right] \right\} d\Omega^e$$

This integral is associated with the flux term in *x*- and *y*- directions due to the changes in hydraulic head in *x*- and *y*- directions as shown in equation (D.19). The basic assumption is that the hydraulic conductivity components and average hydraulic head are taken to be constant over the element. Therefore, these terms can be taken out of the integral and the integral is separated into its components.

$$\begin{array}{l} \left(\left(\hat{h}_g \right)_{avg} - z_b \right) \left(K_g \right)_{xx} \iint_{\Omega^e} \dfrac{\partial N_j}{\partial x} \dfrac{\partial N_i}{\partial x} d\Omega^e + \left(\left(\hat{h}_g \right)_{avg} - z_b \right) \left(K_g \right)_{xy} \iint_{\Omega^e} \dfrac{\partial N_j}{\partial y} \dfrac{\partial N_i}{\partial x} d\Omega^e + \\ \left(\left(\hat{h}_g \right)_{avg} - z_b \right) \left(K_g \right)_{yx} \iint_{\Omega^e} \dfrac{\partial N_j}{\partial x} \dfrac{\partial N_i}{\partial y} d\Omega^e + \left(\left(\hat{h}_g \right)_{avg} - z_b \right) \left(K_g \right)_{yy} \iint_{\Omega^e} \dfrac{\partial N_j}{\partial y} \dfrac{\partial N_i}{\partial y} d\Omega^e \end{array} \quad \text{(E.1)}$$

Each integral in (E.1) could then be written in local coordinates using the determinant of the Jacobian matrix and the master element concept. At this stage, it is important to transform the partial derivatives with respect to the global coordinates to the partial derivatives with respect to the local coordinates. For example, the derivatives in the first integral could be written as follows as using the chain rule of differentiation and the transformation matrix:

$$\frac{\partial N_i}{\partial x} = \frac{1}{|J|}\left[\left(\sum_{k=1}^{4} y_k \frac{\partial N_k}{\partial \eta}\right)\frac{\partial N_i}{\partial \xi} - \left(\sum_{k=1}^{4} y_k \frac{\partial N_k}{\partial \xi}\right)\frac{\partial N_i}{\partial \eta}\right]$$
$$\frac{\partial N_j}{\partial x} = \frac{1}{|J|}\left[\left(\sum_{k=1}^{4} y_k \frac{\partial N_k}{\partial \eta}\right)\frac{\partial N_j}{\partial \xi} - \left(\sum_{k=1}^{4} y_k \frac{\partial N_k}{\partial \xi}\right)\frac{\partial N_j}{\partial \eta}\right] \quad \text{(E.2)}$$

In these two equations, all the derivatives are partial derivatives of the shape functions with respect to local coordinates and can be computed easily. Substituting these two derivatives and writing the integral in terms of local coordinates, one would obtain:

$$\iint_{\Omega^e} \frac{\partial N_j}{\partial x}\frac{\partial N_i}{\partial x} d\Omega^e = \int_{-1}^{1}\int_{-1}^{1} \left\{ \begin{array}{l} \frac{1}{|J|}\left[\left(\sum_{k=1}^{4} y_k \frac{\partial N_k}{\partial \eta}\right)\frac{\partial N_i}{\partial \xi} - \left(\sum_{k=1}^{4} y_k \frac{\partial N_k}{\partial \xi}\right)\frac{\partial N_i}{\partial \eta}\right] * \\ \frac{1}{|J|}\left[\left(\sum_{k=1}^{4} y_k \frac{\partial N_k}{\partial \eta}\right)\frac{\partial N_j}{\partial \xi} - \left(\sum_{k=1}^{4} y_k \frac{\partial N_k}{\partial \xi}\right)\frac{\partial N_j}{\partial \eta}\right] \end{array} \right\} |J| d\xi d\eta \quad \text{(E.3)}$$

If the whole expression inside the integral is simplified and written as some function *f*:

$$f(\xi,\eta) = \frac{1}{|J|}\left[\left(\sum_{k=1}^{4} y_k \frac{\partial N_k}{\partial \eta}\right)\frac{\partial N_i}{\partial \xi} - \left(\sum_{k=1}^{4} y_k \frac{\partial N_k}{\partial \xi}\right)\frac{\partial N_i}{\partial \eta}\right] * \left[\left(\sum_{k=1}^{4} y_k \frac{\partial N_k}{\partial \eta}\right)\frac{\partial N_j}{\partial \xi} - \left(\sum_{k=1}^{4} y_k \frac{\partial N_k}{\partial \xi}\right)\frac{\partial N_j}{\partial \eta}\right] \quad \text{(E.4)}$$

the first integral simplifies to:

$$\iint_{\Omega^e} \frac{\partial N_j}{\partial x}\frac{\partial N_i}{\partial x} d\Omega^e = \int_{-1}^{1}\int_{-1}^{1} f(\xi,\eta) d\xi d\eta \quad \text{(E.5)}$$

and evaluated using the Gaussian quadrature:

$$\int_{-1}^{1}\int_{-1}^{1} f(\xi,\eta)d\xi d\eta = \sum_{l=1}^{NSP}\sum_{m=1}^{NSP} w_l w_m f(\xi_m,\eta_l) \tag{E.6}$$

When the above procedure is implemented for all integrals, one could obtain the final form of the flux integral. The difference between the integrals occurs from the differentiation with respect to x and y coordinates of the shape functions and their corresponding forms in local coordinates. Hence, the function f takes a different form for each of the four integrals such that:

$$f_1(\xi,\eta) = \frac{1}{|J|}\left[\left(\sum_{k=1}^{4} y_k \frac{\partial N_k}{\partial \eta}\right)\frac{\partial N_i}{\partial \xi} - \left(\sum_{k=1}^{4} y_k \frac{\partial N_k}{\partial \xi}\right)\frac{\partial N_i}{\partial \eta}\right] * \left[\left(\sum_{k=1}^{4} y_k \frac{\partial N_k}{\partial \eta}\right)\frac{\partial N_j}{\partial \xi} - \left(\sum_{k=1}^{4} y_k \frac{\partial N_k}{\partial \xi}\right)\frac{\partial N_j}{\partial \eta}\right] \tag{E.7}$$

$$f_2(\xi,\eta) = \frac{1}{|J|}\left[-\left(\sum_{k=1}^{4} x_k \frac{\partial N_k}{\partial \eta}\right)\frac{\partial N_j}{\partial \xi} + \left(\sum_{k=1}^{4} x_k \frac{\partial N_k}{\partial \xi}\right)\frac{\partial N_j}{\partial \eta}\right] * \left[\left(\sum_{k=1}^{4} y_k \frac{\partial N_k}{\partial \eta}\right)\frac{\partial N_i}{\partial \xi} - \left(\sum_{k=1}^{4} y_k \frac{\partial N_k}{\partial \xi}\right)\frac{\partial N_i}{\partial \eta}\right] \tag{E.8}$$

$$f_3(\xi,\eta) = \frac{1}{|J|}\left[\left(\sum_{k=1}^{4} y_k \frac{\partial N_k}{\partial \eta}\right)\frac{\partial N_j}{\partial \xi} - \left(\sum_{k=1}^{4} y_k \frac{\partial N_k}{\partial \xi}\right)\frac{\partial N_j}{\partial \eta}\right] * \left[-\left(\sum_{k=1}^{4} x_k \frac{\partial N_k}{\partial \eta}\right)\frac{\partial N_i}{\partial \xi} + \left(\sum_{k=1}^{4} x_k \frac{\partial N_k}{\partial \xi}\right)\frac{\partial N_i}{\partial \eta}\right] \tag{E.9}$$

$$f_4(\xi,\eta)=\frac{1}{|J|}\left[-\left(\sum_{k=1}^{4}x_k\frac{\partial N_k}{\partial \eta}\right)\frac{\partial N_j}{\partial \xi}+\left(\sum_{k=1}^{4}x_k\frac{\partial N_k}{\partial \xi}\right)\frac{\partial N_j}{\partial \eta}\right]* \left[-\left(\sum_{k=1}^{4}x_k\frac{\partial N_k}{\partial \eta}\right)\frac{\partial N_i}{\partial \xi}+\left(\sum_{k=1}^{4}x_k\frac{\partial N_k}{\partial \xi}\right)\frac{\partial N_i}{\partial \eta}\right] \tag{E.10}$$

where *f1*, *f2*, *f3* and *f4* represent the local functional form of each integrand of the original element integral. Finally, one could obtain the final integral when the corresponding values of the hydraulic conductivity and element averaged saturated thickness are substituted in the original integral giving a final outcome of a [4X4] element matrix.

- $\iint\limits_{\Omega^e} S_y N_j N_i d\Omega^e$

This integral is associated with the time rate of change of the hydraulic head over an element as shown in equation (D.21). The basic assumption is that the specific yield is constant over an element. Therefore, this term can be taken out of the integral. Furthermore, the integral is written in local coordinates using the determinant of the Jacobian matrix and the master element concept.

$$\iint\limits_{\Omega^e} S_y N_j N_i d\Omega^e = S_y \iint\limits_{\Omega^e} N_j N_i d\Omega^e = S_y \int_{-1}^{1}\int_{-1}^{1} N_j(\xi,\eta)N_i(\xi,\eta)|J|d\xi d\eta \tag{E.11}$$

If the integral is evaluated using the Gaussian quadrature, one would obtain:

$$\int_{-1}^{1}\int_{-1}^{1} N_j(\xi,\eta)N_i(\xi,\eta)|J|d\xi d\eta = \sum_{l=1}^{NSP}\sum_{m=1}^{NSP} w_l w_m N_j(\xi_m,\eta_l)N_i(\xi_m,\eta_n)|J(\xi_m,\eta_l)| \qquad \text{(E.12)}$$

Finally, the element matrix is written using the above formula and substituting the specific yield. The final outcome of the integral is a [4X4] matrix from each element.

- $\iint_{\Omega^e} IN_i d\Omega^e$

This integral represents the contribution of infiltration over an element as shown in equation (D.20). The basic assumption is that infiltration is taken to be constant over an element. Therefore, it can be taken out of the integral. Furthermore, the integral is written in local coordinates using the determinant of the Jacobian matrix and the master element concept.

$$\iint_{\Omega^e} IN_i d\Omega^e = I\iint_{\Omega^e} N_i d\Omega^e = I\int_{-1}^{1}\int_{-1}^{1} N_i(\xi,\eta)|J|d\xi d\eta \qquad \text{(E.13)}$$

If the integral is evaluated using the Gaussian quadrature, one would obtain:

$$\int_{-1}^{1}\int_{-1}^{1} N_i(\xi,\eta)|J|d\xi d\eta = \sum_{l=1}^{NSP}\sum_{m=1}^{NSP} w_l w_m N_i(\xi_m,\eta_l)|J(\xi_m,\eta_l)| \qquad \text{(E.14)}$$

Finally, the element vector is written using the above formula and substituting the infiltration value. The final outcome of the integral is a {4X1} vector from each element.

- $\iint\limits_{\Omega^e}\left\{\sum_{k=1}^{n_w}\left[Q_{w,k}\delta\left(x-x_{w,k}\right)\delta\left(y-y_{w,k}\right)\right]\right\}N_i d\Omega^e$

This term represents the contribution of discharge/recharge wells in the domain as shown in equation (D.20). The basic assumption is that well locations coincide with the nodal points. The domain integral of point source term associated with wells can be simplified using the sifting property of the Dirac-δ function. After implementing the property for each delta function, one would obtain:

$$\iint\limits_{\Omega}\sum_{k=1}^{n_w}\left[Q_{w,k}\delta\left(x-x_{w,k}\right)\delta\left(y-y_{w,k}\right)\right]N_i d\Omega=\sum_{k=1}^{n_w}Q_{w,k}\left(x_{w,k},y_{w,k}\right)N\left(x_{w,k},y_{w,k}\right) \quad \text{(E.15)}$$

Since the interpolating function takes the value of 1 at the particular node, the expression simplifies to:

$$\iint\limits_{\Omega}\sum_{k=1}^{n_w}\left[Q_{w,k}\delta\left(x-x_{w,k}\right)\delta\left(y-y_{w,k}\right)\right]N_i d\Omega=\sum_{k=1}^{n_w}Q_{w,k}\left(x_{w,k},y_{w,k}\right) \quad \text{(E.16)}$$

which is evaluated without any difficulty.

- $$\iint_{\Omega^e} \sum_{m=1}^{n_r} \left[\int_0^1 \left(-\frac{K_r w_r}{m_r} \right)_{m,e} N_j \left| \nabla \mathbf{g} \right| \delta\left(x - g_{x,m,e}(u) \right) \delta\left(y - g_{y,m,e}(u) \right) du \right] N_i d\Omega^e$$

This integral represents the contribution of head-dependent part of the line source as shown in (D.19). When linear quadrilateral elements are used to discretize the domain, the sides of the element are straight lines between two nodal points. Therefore, the river (i.e., the line source) becomes a combination of several straight line segments. Each of these segments is defined by the two end points such that the parametric equation of each line segment is written as:

$$\begin{aligned} x &= g_x(u) = x_A + (x_B - x_A)u \\ y &= g_y(u) = y_A + (y_B - y_A)u \end{aligned} \tag{E.17}$$

where points $A(x_A,y_A)$ and $B(x_B,y_B)$ define the global coordinates of the end points of a line segment. For a straight line, the gradient of parametric vector equation **g** is evaluated to be the length of the line segment:

$$\left| \nabla \mathbf{g} \right| = \sqrt{\left(\frac{dg_x}{du} \right)^2 + \left(\frac{dg_y}{du} \right)^2} = \sqrt{(x_B - x_A)^2 + (y_B - y_A)^2} = L_{AB} \tag{E.18}$$

It is assumed that the lateral flow associated with each line segment is constant along the segment and is not a function of the parameter u. Therefore, both the gradient term and

the lateral flow term can be taken out of the integral with respect to u such that the line source integral becomes:

$$\iint_{\Omega^e} \sum_{m=1}^{n_r} \left[L_{AB,e,m} \left(-\frac{K_r w_r}{m_r} \right)_{m,e} \int_0^1 N_j \delta\left(x - g_{x,m,e}(u)\right) \delta\left(y - g_{y,m,e}(u)\right) du \right] N_i d\Omega^e \quad \text{(E.19)}$$

Since N_j is not a function of u, it can also be taken out of the u integral and the integration with respect to u can now be performed using any one of the Dirac-δ function expressions. After substituting the expressions for g_x and g_y given in equation (E.31), the integral becomes:

$$\int_0^1 \delta\left(x - x_{A,e,m} + \left(x_{A,e,m} - x_{B,e,m}\right)u\right) \delta\left(y - y_{A,e,m} + \left(y_{A,e,m} - y_{B,e,m}\right)u\right) du \quad \text{(E.20)}$$

If the x-component is selected to perform the integration, the y-component of the Dirac-δ function can be written as some function $h(u)$ such that the integral becomes:

$$\int_0^1 h(u) \delta\left(x - x_{A,e,m} + \left(x_{A,e,m} - x_{B,e,m}\right)u\right) du \quad \text{(E.21)}$$

The expression in the Dirac-δ function can now be rearranged to give:

$$\delta\left(x - x_{A,e,m} + \left(x_{A,e,m} - x_{B,e,m}\right)u\right) = \delta\left(\left(x_{A,e,m} - x_{B,e,m}\right) \left[\frac{x - x_{A,e,m}}{x_{A,e,m} - x_{B,e,m}} + u \right] \right) \quad \text{(E.22)}$$

Since the term ($x_{A,e,m}$-$x_{B,e,m}$) is a constant, it can be written as:

$$\delta\left(x-x_{A,e,m}+\left(x_{A,e,m}-x_{B,e,m}\right)u\right)=\frac{1}{\left|x_{A,e,m}-x_{B,e,m}\right|}\delta\left(\left[\frac{x-x_{A,e,m}}{x_{A,e,m}-x_{B,e,m}}+u\right]\right) \tag{E.23}$$

Rewriting the Dirac-δ function gives:

$$\delta\left(x-x_{A,e,m}+\left(x_{A,e,m}-x_{B,e,m}\right)u\right)=\frac{1}{\left|x_{A,e,m}-x_{B,e,m}\right|}\delta\left(u-\frac{x-x_{A,e,m}}{x_{B,e,m}-x_{A,e,m}}\right) \tag{E.24}$$

Since the derivative of the Dirac-δ function is the Heaviside step function by using the sifting property (Harris and Stocker, 1998), the integration over *u* yields:

$$\begin{aligned}\int_0^1 h(u)\frac{1}{\left|x_{A,e,m}-x_{B,e,m}\right|}\delta\left(u-\frac{x-x_{A,e,m}}{x_{B,e,m}-x_{A,e,m}}\right)du \\ =\frac{1}{\left|x_{A,e,m}-x_{B,e,m}\right|}h\left(\frac{x-x_{A,e,m}}{x_{B,e,m}-x_{A,e,m}}\right)H\left(u-\frac{x-x_{A,e,m}}{x_{B,e,m}-x_{A,e,m}}\right)\Bigg|_{u=0}^{u=1}\end{aligned} \tag{E.25}$$

where *H* is the Heaviside step function. Evaluating this function at two points gives:

$$H\left(u-\frac{x-x_{A,e,m}}{x_{B,e,m}-x_{A,e,m}}\right)\Bigg|_{t=0}^{t=1}=H\left(\frac{x_{B,e,m}-x}{x_{B,e,m}-x_{A,e,m}}\right)-H\left(\frac{x-x_{A,e,m}}{x_{B,e,m}-x_{A,e,m}}\right) \tag{E.26}$$

Along the line where $x_{A,e,m} \leq x \leq x_{B,e,m}$, the Heaviside function expression above is calculated to be 1, and 0 elsewhere. After evaluating the function *h(u)* and substituting, the integral with respect to parameter *u* yields:

$$\begin{aligned}&\int_0^1 \delta\left(x - x_{A,e,m} + \left(x_{A,e,m} - x_{B,e,m}\right)u\right)\delta\left(y - y_{A,e,m} + \left(y_{A,e,m} - y_{B,e,m}\right)u\right)du \\ &= \frac{1}{\left|x_{A,e,m} - x_{B,e,m}\right|}\delta\left(y - y_{A,e,m} + \left(y_{A,e,m} - y_{B,e,m}\right)\left(\frac{x - x_{A,e,m}}{x_{B,e,m} - x_{A,e,m}}\right)\right)\end{aligned} \tag{E.27}$$

This term can now be substituted back in the general line source term to give:

$$\iint_{\Omega^e}\left[L_{AB,e,m}\left(-\frac{K_r w_r}{m_r}\right)_{e,m}\frac{1}{\left|x_{A,e,m} - x_{B,e,m}\right|}N_j \delta\left(y - y_{A,e,m} + \left(y_{A,e,m} - y_{B,e,m}\right)\left(\frac{x - x_{A,e,m}}{x_{B,e,m} - x_{A,e,m}}\right)\right)\right]N_i d\Omega^e \tag{E.28}$$

Taking the constant terms out of the domain integral and rearranging gives:

$$\frac{L_{AB,e,m}}{\left|x_{A,e,m} - x_{B,e,m}\right|}\iint_{\Omega^e}\left(-\frac{K_r w_r}{m_r}\right)_{e,m} N_j N_i \delta\left(y - y_{A,e,m} + \left(y_{A,e,m} - y_{B,e,m}\right)\left(\frac{x - x_{A,e,m}}{x_{B,e,m} - x_{A,e,m}}\right)\right)d\Omega^e \tag{E.29}$$

Focusing on the domain integral, the expression in front of the Dirac-δ function is treated as a function and the element integral can be evaluated using the sifting property and the Heaviside function:

$$\iint_{\Omega^e}\left(-\frac{K_r w_r}{m_r}\right)_{e,m} N_j N_i \delta\left(y - y_{A,e,m} + \left(y_{A,e,m} - y_{B,e,m}\right)\left(\frac{x - x_{A,e,m}}{x_{B,e,m} - x_{A,e,m}}\right)\right) d\Omega^e =$$

$$\int_{x^e}\begin{bmatrix}\left(-\frac{K_r w_r}{m_r}\right)_{e,m}\left(x, y_{A,e,m} + \left(y_{B,e,m} - y_{A,e,m}\right)\left(\frac{x - x_{A,e,m}}{x_{B,e,m} - x_{A,e,m}}\right)\right) \\ N_j\left(x, y_{A,e,m} + \left(y_{B,e,m} - y_{A,e,m}\right)\left(\frac{x - x_{A,e,m}}{x_{B,e,m} - x_{A,e,m}}\right)\right) \\ N_i\left(x, y_{A,e,m} + \left(y_{B,e,m} - y_{A,e,m}\right)\left(\frac{x - x_{A,e,m}}{x_{B,e,m} - x_{A,e,m}}\right)\right)\end{bmatrix} dx^e \tag{E.30}$$

where the parenthesis after the terms $K_r w_r/m_r$, N_j and N_i show at which (x,y) position they are evaluated. In this equation, all terms are reduced to a single variable (i.e., x) that is valid along the line segment. Therefore, the integral with respect to x will be performed between the two end points of the line segment. If one assumes that the $K_r w_r/m_r$ term is constant along the line segment and the functional parenthesis is dropped out for N_j and N_i for simplicity, one would obtain the following:

$$\left(-\frac{K_r w_r}{m_r}\right)_{e,m} \int_{x_{A,e,m}}^{x_{B,e,m}} N_j N_i dx^e \tag{E.31}$$

It is important to note that the shape functions are evaluated along the line segment. The integration of the shape functions along the line can be done using global coordinates or local coordinates. The result is a [2X2] matrix. Below, a sample integration using global coordinates is shown for the (1,1) position such that:

$$\int_{x_{A,e,m}}^{x_{B,e,m}} N_j N_i dx^e = \int_{x_{A,e,m}}^{x_{B,e,m}} \left(\frac{x - x_{A,e,m}}{x_{B,e,m} - x_{A,e,m}} \right) \left(\frac{x - x_{A,e,m}}{x_{B,e,m} - x_{A,e,m}} \right) dx^e = \frac{1}{3} \left(x_{B,e,m} - x_{A,e,m} \right) \quad \text{(E.32)}$$

The other positions follow the same idea. When the result of the integration is substituted in the original term and necessary simplifications are made, one would obtain:

$$\left(\frac{K_r w_r}{m_r} \right)_{e,m} \frac{L_{AB,e,m}}{3} \quad \text{(E.33)}$$

The coefficient of the length of the line changes for other positions such that it is 1/3 for positions i = j and 1/6 for i ≠ j.

- $$\iint_{\Omega^e} \sum_{m=1}^{n_r} \left[\int_0^1 \left(-\frac{K_r w_r}{m_r} h_r \right)_{m,e} |\nabla \mathbf{g}| \, \delta\left(x - g_{x,m,e}(u) \right) \delta\left(y - g_{y,m,e}(u) \right) du \right] N_i d\Omega^e$$

This integral represents the contribution of constant part of the line source as shown in equation (D.20). Following the steps shown in the above integral, the problem reduces to the evaluation of the following integral:

$$\int_{x^e} N_i dx^e = \int_{x_{A,e,m}}^{x_{B,e,m}} N_i dx^e \quad \text{(E.34)}$$

The integration of the shape functions along the line can be done using global coordinates or local coordinates. The result is now a {2X1} vector. Below, the integration is shown for the (1,1) position such that:

$$\int_{x_{A,e,m}}^{x_{B,e,m}} N_i dx^e = \int_{x_{A,e,m}}^{x_{B,e,m}} \left(\frac{x - x_{A,e,m}}{x_{B,e,m} - x_{A,e,m}} \right) dx^e = \frac{1}{2}\left(x_{B,e,m} - x_{A,e,m}\right) \tag{E.35}$$

When the result of the integration is substituted in the original term, one would obtain:

$$\left(\frac{K_r w_r}{m_r} h_r \right)_{e,m} \frac{L_{AB,e,m}}{2} \tag{E.36}$$

The result is the same for the other position (2,1).

Derivation of Element Matrices and Vectors for the Element Boundaries

Elements involving a boundary, where a natural boundary condition (i.e., Neumann or Cauchy type) is specified, require the computation of the three boundary integrals shown in Appendix D. In these integrals, the integration is performed over the global boundary coordinate $d\Gamma^e$ along the boundary of the element. To simplify the integration process, the integrands of these integrals must be written on the master element using the local coordinate system and must also be specified for a particular side of the element, which in turn requires that the shape functions are expressed for the particular boundary side of the element. As seen in Figure E.1, the boundary of the

element can be any side of the quadrilateral depending on its position in the analysis domain. In order to write the shape functions along each side, appropriate values of ξ and η are substituted for the general shape function formulae.

The global boundary coordinate Γ is mapped to the local boundary coordinate a (i.e, $-1 \le a \le 1$) for each side as shown in Figure E.1. The local coordinates holds the values $\xi = a, \eta = -1$ for side 1, $\xi = 1, \eta = a$ for side 2, $\xi = -a, \eta = 1$ for side 3 and $\xi = -1, \eta = -a$ for side 4. Using these values, one would obtain the following four shape functions for each side of the element:

$$\begin{aligned} SIDE \quad 1: \quad & \left[\frac{1-a}{2}, \frac{1+a}{2}, 0, 0\right] \\ SIDE \quad 2: \quad & \left[0, \frac{1-a}{2}, \frac{1+a}{2}, 0\right] \\ SIDE \quad 3: \quad & \left[0, 0, \frac{1-a}{2}, \frac{1+a}{2}\right] \\ SIDE \quad 4: \quad & \left[\frac{1+a}{2}, 0, 0, \frac{1-a}{2}\right] \end{aligned} \tag{E.37}$$

If the values of -1 and +1 are substituted for a in the above formulae, one would indeed obtain the fact that shape functions are equal to 1 at the node it is written for and 0 at all other nodes of the element. The integral over the element in global coordinates must also be transformed to an integral over the master element in local coordinates. This transformation introduces the determinant of the Jacobian between global boundary and local boundary coordinates.

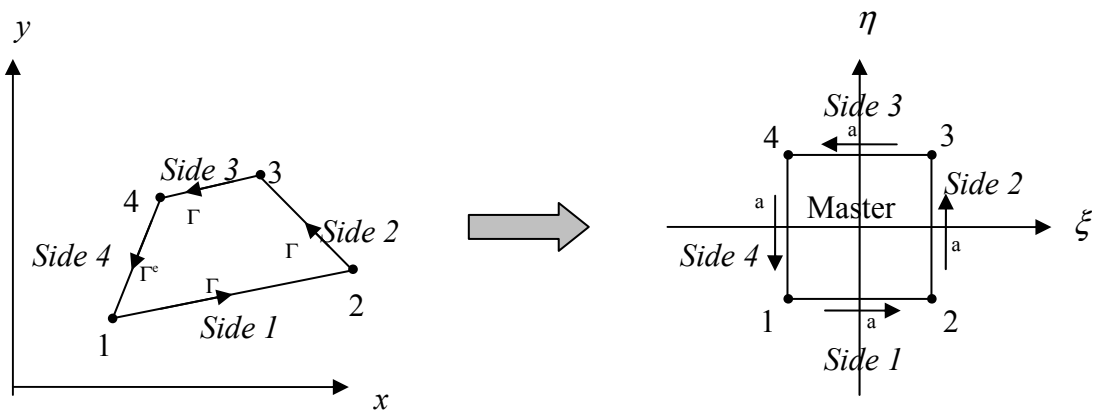

GLOBAL COORDINATE SYSTEM LOCAL COORDINATE SYSTEM

Figure E. 1. Boundary coordinates on the master and actual element

$$\int_{\Gamma^e} f(B)d\Gamma^e = \int_{-1}^{1} f(a)|J_a|da \tag{E.38}$$

where J_a is the Jacobian of the boundary. The incremental boundary coordinate in global coordinate system, $d\Gamma$, can be written as follows according to the Figure E.2:

$$d\Gamma = \sqrt{(dx)^2 + (dy)^2} \tag{E.39}$$

Dividing both sides of this relationship with differential length, *da*, would give the following relationship between the global and local boundary coordinate:

$$\frac{d\Gamma}{da} = \sqrt{\left(\frac{dx}{da}\right)^2 + \left(\frac{dy}{da}\right)^2} \qquad \Rightarrow \qquad d\Gamma = J_a da \tag{E.40}$$

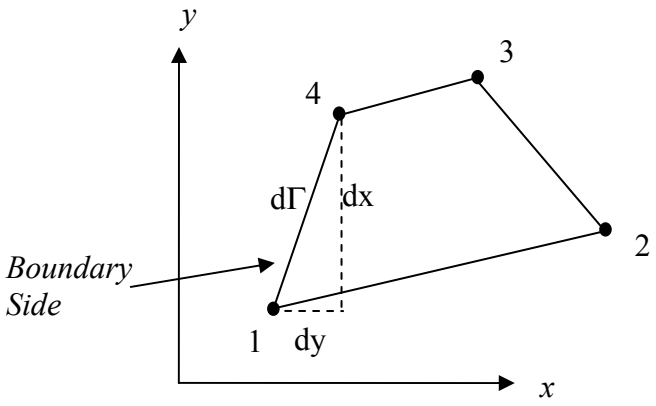

Figure E. 2. Incremental boundary coordinate in global coordinate system

Therefore, the Jacobian of the boundary is written as:

$$J_a = \sqrt{\left(\frac{dx}{da}\right)^2 + \left(\frac{dy}{da}\right)^2} \tag{E.41}$$

where *da* will always take the value of 2 since it is the length of any side on the master element. Using these fundamental concepts, the boundary integrals can be evaluated as follows:

- $\int_{\Gamma_2^e} q_N N_i d\Gamma_2^e$

This integral represents the contribution of Neumann boundary condition as shown in equation (D.20). The basic assumption is that flux is taken to be a constant over the boundary side of the element. Therefore, the q_N term can be taken out of the integral.

$$\int_{\Gamma_2^e} q_N N_i d\Gamma_2^e = q_N \int_{\Gamma_2^e} N_i d\Gamma_2^e \tag{E.42}$$

Furthermore, the integral is written in local coordinates using the determinant of the Jacobian matrix and the master element concept. At this stage, it is important to transform the shape functions with respect to the global coordinates to the shape function with respect to the local coordinates.

$$\int_{\Gamma_2^e} N_i d\Gamma_2^e = \int_{-1}^{1} N_i |J_a| da \tag{E.43}$$

and can further be simplified since the Jacobian is simply one half the length of the boundary side.

$$\int_{\Gamma_2^e} N_i d\Gamma_2^e = \frac{L_e}{2} \int_{-1}^{1} N_i da \tag{E.44}$$

It is important to note that this integral is simple and does not need numerical integration. It can be integrated exactly to obtain 1 regardless of the side and the associated nodes of the element. Therefore, the final outcome of this boundary integral is a {2X1} vector from each boundary element.

- $\int_{\Gamma_3^e} \frac{K_r w_r h_r}{m_r} N_i d\Gamma_3^e$

This integral represents the contribution of head dependent boundary condition due to the constant term as shown in equation (D.20). The basic assumption is that the $K_r w_r h_r / m_r$ term is taken to be a constant over the boundary side of the element. Therefore, it can be taken out of the integral to yield:

$$\int_{\Gamma_3^e} \frac{K_r w_r h_r}{m_r} N_i d\Gamma_3^e = \frac{K_r w_r h_r}{m_r} \int_{\Gamma_3^e} N_i d\Gamma_3^e \tag{E.45}$$

Furthermore, the integral is written in local coordinates using the determinant of the Jacobian matrix and the master element concept. At this stage, it is important to transform the shape functions with respect to the global coordinates to the shape function with respect to the local coordinates.

$$\int_{\Gamma_3^e} N_i d\Gamma_3^e = \int_{-1}^{1} N_i \left| J_a \right| da \tag{E.46}$$

and can further be simplified since the Jacobian is simply one half the length of the boundary side.

$$\int_{\Gamma_3^e} N_i d\Gamma_2^e = \frac{L_e}{2} \int_{-1}^{1} N_i da \tag{E.47}$$

As before, this integral is simple and does not need numerical integration. It can be integrated exactly to obtain 1 regardless of the side and the associated nodes of the element. Therefore, the final outcome of this boundary integral is a {2X1} vector from each boundary element.

- $\int_{\Gamma_3^e} \frac{K_r w_r}{m_r} N_j N_i d\Gamma_3^e$

Finally, this integral represents the contribution of head dependent boundary condition due to the variable groundwater head as shown in equation (D.19). It must be noted, however, that this term might also reduce to a constant flux term if the hydraulic head is below the bottom elevation of the river sediments. In such a case, the integral is evaluated as an added contribution to the constant flux integral. Otherwise, this integral is treated as a head-dependent boundary condition. In its head-dependent form, the basic assumption is that the $K_r w_r / m_r$ term is taken to be a constant over the boundary side of the element. Therefore, it can be taken out of the integral to yield:

$$\int_{\Gamma_3^e} \frac{K_r w_r}{m_r} N_j N_i d\Gamma_3^e = \frac{K_r w_r}{m_r} \int_{\Gamma_3^e} N_j N_i d\Gamma_3^e \qquad \text{(E.48)}$$

Furthermore, the integral is written in local coordinates using the determinant of the Jacobian matrix and the master element concept. At this stage, it is important to transform

the shape functions with respect to the global coordinates to the shape function with respect to the local coordinates.

$$\int_{\Gamma_3^e} N_j N_i d\Gamma_3^e = \int_{-1}^{1} N_j N_i |J_a| da \tag{E.49}$$

and can further be simplified since the Jacobian is simply one half the length of the boundary side.

$$\int_{\Gamma_3^e} N_j N_i d\Gamma_2^e = \frac{L_e}{2} \int_{-1}^{1} N_j N_i da \tag{E.50}$$

As before, this integral is simple and does not need numerical integration. It can be integrated exactly using the non-zero shape functions to obtain 2/6 for i = j and 1/6 for i ≠ j, regardless of the side and the associated nodes of the element. Therefore, the final outcome of this boundary integral is a [2X2] vector from each boundary element.

APPENDIX F

NUMERICAL INTEGRATION OF ELEMENT INTEGRAL EQUATIONS

APPENDIX F

NUMERICAL INTEGRATION OF ELEMENT INTEGRAL EQUATIONS

Element integral equations obtained after transformation to local coordinates are generally not evaluated by analytic integration since the integrands are very complicated non-linear functions of local coordinates due to the presence of non-constant Jacobian and its inverse. Particularly for irregular quadrilateral elements, a numerical integration scheme involving various numbers of integration points and corresponding weights is the only viable method of integration. The most common numerical integration scheme is the Gauss quadrature formula. In a one-dimensional setup, this formula takes the following form:

$$\int_{-1}^{1} f(\xi) d\xi = \sum_{j=1}^{NSP} f(a_j) w_j \tag{F.1}$$

where *NSP* is the total number of sampling locations, $f(a_j)$ is any function evaluated at sampling location a_j and w_j is the corresponding weighing constant. The sampling locations and corresponding weighing coefficients in Gauss quadrature formula are given in Table F.1 for the commonly applied schemes of less than six points.

Table F. 1. Integration Points and Weighing Coefficients in Gauss Quadrature Formula (Zienkiewicz and Taylor, 1989)

Number of Sampling Point (NSP)	Sampling Location (a)	Weighing Coefficient (w)
1	0.000 000 000 000 000	2.000 000 000 000 000
2	± 0.577 350 269 189 626	1.000 000 000 000 000
3	± 0.774 596 669 241 483 0.000 000 000 000 000	0.555 555 555 555 556 0.888 888 888 888 889
4	± 0.861 136 311 594 953 ± 0.339 981 043 584 856	0.347 854 845 137 454 0.652 145 154 862 546
5	± 0.906 179 845 938 664 ± 0.538 469 310 105 683 0.000 000 000 000 000	0.236 926 885 056 189 0.478 628 670 499 366 0.568 888 888 888 889
6	± 0.932 469 514 203 152 ± 0.661 209 386 466 265 ± 0.238 619 186 083 197	0.171 324 492 379 170 0.360 761 573 048 139 0.467 913 934 572 691

In general, a one-dimensional Gauss quadrature scheme with *NSP* sampling locations integrates any polynomial of *2*NSP-1* order exactly on the interval [-1,1]. Therefore, a two-point scheme will integrate a 3rd order polynomial exactly. Integration in two-dimensions is done based on the same analogy according to the following formula:

$$\int_{-1}^{1}\int_{-1}^{1} f(\xi,\eta)d\xi d\eta = \sum_{i=1}^{NSP}\sum_{j=1}^{NSP} w_i w_j f(\xi_j,\eta_i) \tag{F.2}$$

The inner integral is evaluated first by taking the η variable constant. The evaluated expression is then integrated with respect to the ξ variable. Generally, the same number of sampling points is used in both integration directions. In this study, the numerical integration is performed by using a three-point Gaussian quadrature formula.

APPENDIX G

DERIVATION OF GALERKIN FORM OF OVERLAND FLOW EQUATION

APPENDIX G

DERIVATION OF GALERKIN FORM OF OVERLAND FLOW EQUATION

The first step of the derivation of the weak form is to approximate the unknown function over the domain using interpolating functions, $N_j(x,y)$, of the form:

$$h_o(x,y,t) \approx \hat{h}_o(x,y,t) = \sum_{j=1}^{N} \left(\hat{h}_o(t)\right)_j N_j(x,y) \tag{G.1}$$

where $\hat{h}_o(t)$ is the approximate value of the water surface elevation and N is the total number of nodes in the two-dimensional overland flow domain. In essence, the temporal and spatial discretizations are separated from each other in the approximate solution. The nodal values, $(\hat{h}_o(t))_j$, becomes only a function of time and the shape function, $N_j(x,y)$, is now only a function of space. It is also important to note that the shape functions are defined only for its corresponding nodes. They are zero elsewhere in the domain.

Since the Galerkin method is an approximate technique, the solution given in equation (G.1) does not satisfy the differential equation exactly and a residual occurs. The method states that the weighted average of this residual over the whole domain

becomes zero. If the approximate solution is substituted in the differential equation, one can write the total residual, $\check{R}$, as:

$$\tilde{R}(x,y,t) = \frac{\partial \hat{h}_o}{\partial t} - \frac{\partial}{\partial x}\left(K_{ox} \frac{\partial \hat{h}_o}{\partial x} \right) - \frac{\partial}{\partial y}\left(K_{oy} \frac{\partial \hat{h}_o}{\partial y} \right) - R + I \qquad \text{(G.2)}$$

The Galerkin finite element method is based on the idea of minimizing this residual over the solution domain by letting the weighed integral residual tend to zero. In this formulation the weighing functions are selected as the interpolating functions used in element level:

$$\iint_{\Omega} \tilde{R}(x,y,t) N_i(x,y) d\Omega = 0 \qquad i = 1,2,3,...,N \qquad \text{(G.3)}$$

For the sake of clarity, the description of the index *i* running from *1* to *N* is not repeated in the following equations. When the expression for the residual is substituted in equation (G.3), the integral simplifies to:

$$\iint_{\Omega} \left\{ \frac{\partial \hat{h}_o}{\partial t} - \frac{\partial}{\partial x}\left(K_{ox} \frac{\partial \hat{h}_o}{\partial x} \right) - \frac{\partial}{\partial y}\left(K_{oy} \frac{\partial \hat{h}_o}{\partial y} \right) - R + I \right\} N_i d\Omega = 0 \qquad \text{(G.4)}$$

The integration by parts is now applied to the second order derivative terms in the above integral to reduce them to first order and incorporate the natural boundary conditions:

$$\iint_{\Omega}\left\{\frac{\partial}{\partial x}\left(K_{ox}\frac{\partial \hat{h}_o}{\partial x}\right)N_i\right\}d\Omega=-\iint_{\Omega}K_{ox}\frac{\partial \hat{h}_o}{\partial x}\frac{\partial N_i}{\partial x}d\Omega+\int_{\Gamma}K_{ox}\frac{\partial \hat{h}_o}{\partial x}N_i n_x d\Gamma \qquad \text{(G.5)}$$

$$\iint_{\Omega}\left\{\frac{\partial}{\partial y}\left(K_{oy}\frac{\partial \hat{h}_o}{\partial y}\right)N_i\right\}d\Omega=-\iint_{\Omega}K_{oy}\frac{\partial \hat{h}_o}{\partial y}\frac{\partial N_i}{\partial y}d\Omega+\int_{\Gamma}K_{oy}\frac{\partial \hat{h}_o}{\partial y}N_i n_y d\Gamma \qquad \text{(G.6)}$$

where n_x and n_y represent the x and y components of unit normal vector. Substituting these expressions and rearranging gives:

$$\begin{aligned}&\iint_{\Omega}K_{ox}\frac{\partial \hat{h}_o}{\partial x}\frac{\partial N_i}{\partial x}d\Omega+\iint_{\Omega}K_{oy}\frac{\partial \hat{h}_o}{\partial y}\frac{\partial N_i}{\partial y}d\Omega\\&-\int_{\Gamma}\left[K_{ox}\frac{\partial \hat{h}_o}{\partial x}N_i n_x+K_{oy}\frac{\partial \hat{h}_o}{\partial y}N_i n_y\right]d\Gamma\\&-\iint_{\Omega}(R-I)N_i d\Omega+\iint_{\Omega}\frac{\partial \hat{h}_o}{\partial t}N_i d\Omega=0\end{aligned} \qquad \text{(G.7)}$$

In the above form, the boundary integral can be written as a specified flux boundary condition, Γ_2:

$$\int_{\Gamma}(...)N_i d\Gamma=\int_{\Gamma_2}(...)N_i d\Gamma_2 \qquad \text{(G.8)}$$

where it becomes the natural boundary conditions. In addition to the second type boundary, the domain might also have first type boundaries where the known stage is specified. Such boundaries form the essential boundary conditions. At the nodes of essential boundary conditions, the solution is known and the residual vanishes. When the

expression in the specified flux is substituted in (G.8), one would obtain the following simplified form for the boundary integral:

$$-\int_{\Gamma}\left[K_{ox}\frac{\partial\hat{h}_o}{\partial x}N_i n_x + K_{oy}\frac{\partial\hat{h}_o}{\partial y}N_i n_y\right]d\Gamma = \int_{\Gamma} q_N N_i d\Gamma \tag{G.9}$$

After simplifications and further manipulations, one could obtain the following weak from of the equation as:

$$\begin{aligned}\int_{\Gamma} q_N N_i d\Gamma + \iint_{\Omega} K_{ox}\frac{\partial\hat{h}_o}{\partial x}\frac{\partial N_i}{\partial x}d\Omega + \iint_{\Omega} K_{oy}\frac{\partial\hat{h}_o}{\partial y}\frac{\partial N_i}{\partial y}d\Omega \\ -\iint_{\Omega}(R-I)N_i d\Omega + \iint_{\Omega}\frac{\partial\hat{h}_o}{\partial t}N_i d\Omega = 0\end{aligned} \tag{G.10}$$

When the approximate solution in (G.1) is substituted in the weak from, the equation is written as:

$$\begin{aligned}\int_{\Gamma} q_N N_i d\Gamma + \iint_{\Omega} K_{ox}\frac{\partial}{\partial x}\left[\sum_{j=1}^{N}\left(\hat{h}_o\right)_j N_j\right]\frac{\partial N_i}{\partial x}d\Omega + \iint_{\Omega} K_{oy}\frac{\partial}{\partial y}\left[\sum_{j=1}^{N}\left(\hat{h}_o\right)_j N_j\right]\frac{\partial N_i}{\partial y}d\Omega \\ -\iint_{\Omega}(R-I)N_i d\Omega + \iint_{\Omega}\frac{\partial}{\partial t}\left[\sum_{j=1}^{N}\left(\hat{h}_o\right)_j N_j\right]N_i d\Omega = 0\end{aligned} \tag{G.11}$$

Since the nodal values are only a function of time and the shape functions are only a function of space, the above expression can be simplified by taking some of the terms out of the derivatives:

$$\int_{\Gamma} q_N N_i d\Gamma + \iint_{\Omega} \sum_{j=1}^{N} \left(\hat{h}_o\right)_j K_{ox} \frac{\partial N_j}{\partial x} \frac{\partial N_i}{\partial x} d\Omega + \iint_{\Omega} \sum_{j=1}^{N} \left(\hat{h}_o\right)_j K_{oy} \frac{\partial N_j}{\partial y} \frac{\partial N_i}{\partial y} d\Omega$$
$$- \iint_{\Omega} (R - I) N_i d\Omega + \iint_{\Omega} \sum_{j=1}^{N} N_j \frac{\partial \left(\hat{h}_o\right)_j}{\partial t} N_i d\Omega = 0 \qquad \text{(G.12)}$$

Since N_i is defined such that it is non-zero only over elements adjacent to node *i*, the integrations may be performed piecewise over each element and subsequently summed.

$$\sum_{e=1}^{n_e} \left[\int_{\Gamma^e} q_N N_i d\Gamma^e \right] + \sum_{e=1}^{n_e} \left[\iint_{\Omega^e} \sum_{j=1}^{N} \left(\hat{h}_o\right)_j K_{ox} \frac{\partial N_j}{\partial x} \frac{\partial N_i}{\partial x} d\Omega^e \right]$$
$$+ \sum_{e=1}^{n_e} \left[\iint_{\Omega^e} \sum_{j=1}^{N} \left(\hat{h}_o\right)_j K_{oy} \frac{\partial N_j}{\partial y} \frac{\partial N_i}{\partial y} d\Omega^e \right] - \sum_{e=1}^{n_e} \left[\iint_{\Omega^e} (R - I) N_i d\Omega^e \right] \qquad \text{(G.13)}$$
$$+ \sum_{e=1}^{n_e} \left[\iint_{\Omega^e} \sum_{j=1}^{N} N_j \frac{\partial \left(\hat{h}_o\right)_j}{\partial t} N_i d\Omega^e \right] = 0$$

The element integrals can now be written in matrix form:

$$\mathbf{S^e} \cdot \hat{\mathbf{h}}_\mathbf{o} + \mathbf{M^e} \cdot \frac{d\ \hat{\mathbf{h}}_\mathbf{o}}{dt} = \mathbf{F^e} \qquad \text{(G.14)}$$

where $\hat{\mathbf{h}}_\mathbf{g}$ is the unknown hydraulic head vector and $\mathbf{S^e}$, $\mathbf{M^e}$ and $\mathbf{F^e}$ are element matrices and vectors defined as follows:

$$\mathbf{S^e} = \iint_{\Omega^e} \left[K_{ox} \frac{\partial N_j}{\partial x} \frac{\partial N_i}{\partial x} + K_{oy} \frac{\partial N_j}{\partial y} \frac{\partial N_i}{\partial y} \right] d\Omega^e \tag{G.15}$$

$$\mathbf{F^e} = -\int_{\Gamma^e} q_N N_i d\Gamma^e + \iint_{\Omega^e} (R - I) N_i d\Omega^e \tag{G.16}$$

$$\mathbf{M^e} = \iint_{\Omega^e} N_j N_i d\Omega^e \tag{G.17}$$

Finally, the global assembly of these matrices would yield the following matrix equation:

$$\mathbf{S} \cdot \hat{\mathbf{h}}_\mathbf{o} + \mathbf{M} \cdot \frac{d\ \hat{\mathbf{h}}_\mathbf{o}}{dt} = \mathbf{F} \tag{G.18}$$

where **S**, **M** and **F** is generally known as stiffness matrix, mass matrix and load vector, respectively, from the structural mechanics analogy.

APPENDIX H

DERIVATION OF ELEMENT INTEGRAL EQUATIONS FOR OVERLAND FLOW

APPENDIX H

DERIVATION OF ELEMENT INTEGRAL EQUATIONS FOR OVERLAND FLOW

The key point in finite element analysis is the derivation of element matrices and vectors that are obtained as a result of element level integrations. These element level matrices and vectors are then later assembled sequentially to obtain their global counterparts. In this study, the element matrices and vectors are [4X4] and {4X1} systems, respectively, since four-nodal linear quadrilateral elements are used to discretize the domain. In what follows first the evaluation of element domain integrals are discussed followed by the discussion of element boundary integrals. Each integral given in equations (G.15), (G.16) and (G.17) are split and written separately with a bullet. They are analyzed such that a procedure for their numerical evaluation is presented.

Derivation of Element Matrices and Vectors within the Domain

For all elements in the domain, a series of integrals presented in (G.15), (G.16) and (G.17) are evaluated to obtain the members of the [4X4] element stiffness and mass

matrices and {4X1} element load vector. Hence, in what follows, each integral is analyzed individually in which subscripts *i* and *j* run from 1 to 4.

- $$\iint_{\Omega^e}\left[K_{ox}\frac{\partial N_j}{\partial x}\frac{\partial N_i}{\partial x}+K_{oy}\frac{\partial N_j}{\partial y}\frac{\partial N_i}{\partial y}\right]d\Omega^e$$

This integral is associated with the flux term in *x*- and *y*- directions due to the changes in overland flow stage in *x*- and *y*- directions as shown in equation (G.15). The basic assumption is that the diffusion coefficients are taken to be constant over the element. Therefore, these terms can be taken out of the integral and the integral is separated into its components.

$$\iint_{\Omega^e}\left[K_{ox}\frac{\partial N_j}{\partial x}\frac{\partial N_i}{\partial x}+K_{oy}\frac{\partial N_j}{\partial y}\frac{\partial N_i}{\partial y}\right]d\Omega^e = K_{ox}\iint_{\Omega^e}\frac{\partial N_j}{\partial x}\frac{\partial N_i}{\partial x}d\Omega^e + K_{oy}\iint_{\Omega^e}\frac{\partial N_j}{\partial y}\frac{\partial N_i}{\partial y}d\Omega^e \quad \text{(H.1)}$$

Each integral in (H.1) could then be written in local coordinates using the determinant of the Jacobian matrix and the master element concept. At this stage, it is important to transform the partial derivatives with respect to the global coordinates to the partial derivatives with respect to the local coordinates. For example, the derivatives in the first integral could be written as follows as using the chain rule of differentiation and the transformation matrix:

$$\frac{\partial N_i}{\partial x} = \frac{1}{|J|}\left[\left(\sum_{k=1}^{4} y_k \frac{\partial N_k}{\partial \eta}\right)\frac{\partial N_i}{\partial \xi} - \left(\sum_{k=1}^{4} y_k \frac{\partial N_k}{\partial \xi}\right)\frac{\partial N_i}{\partial \eta}\right]$$
$$\frac{\partial N_j}{\partial x} = \frac{1}{|J|}\left[\left(\sum_{k=1}^{4} y_k \frac{\partial N_k}{\partial \eta}\right)\frac{\partial N_j}{\partial \xi} - \left(\sum_{k=1}^{4} y_k \frac{\partial N_k}{\partial \xi}\right)\frac{\partial N_j}{\partial \eta}\right] \quad \text{(H.2)}$$

In these two equations, all the derivatives are simple partials of the shape functions with respect to local coordinates and can be computed easily. Substituting these two derivatives and writing the integral in terms of local coordinates, one would obtain:

$$\iint_{\Omega^e} \frac{\partial N_j}{\partial x}\frac{\partial N_i}{\partial x} d\Omega^e = \int_{-1}^{1}\int_{-1}^{1} \left\{ \begin{array}{l} \frac{1}{|J|}\left[\left(\sum_{k=1}^{4} y_k \frac{\partial N_k}{\partial \eta}\right)\frac{\partial N_i}{\partial \xi} - \left(\sum_{k=1}^{4} y_k \frac{\partial N_k}{\partial \xi}\right)\frac{\partial N_i}{\partial \eta}\right] * \\ \frac{1}{|J|}\left[\left(\sum_{k=1}^{4} y_k \frac{\partial N_k}{\partial \eta}\right)\frac{\partial N_j}{\partial \xi} - \left(\sum_{k=1}^{4} y_k \frac{\partial N_k}{\partial \xi}\right)\frac{\partial N_j}{\partial \eta}\right] \end{array} \right\} |J| d\xi d\eta \quad \text{(H.3)}$$

If the whole expression inside the integral is simplified and written as some function *f*:

$$f(\xi,\eta) = \frac{1}{|J|}\left[\left(\sum_{k=1}^{4} y_k \frac{\partial N_k}{\partial \eta}\right)\frac{\partial N_i}{\partial \xi} - \left(\sum_{k=1}^{4} y_k \frac{\partial N_k}{\partial \xi}\right)\frac{\partial N_i}{\partial \eta}\right] * \left[\left(\sum_{k=1}^{4} y_k \frac{\partial N_k}{\partial \eta}\right)\frac{\partial N_j}{\partial \xi} - \left(\sum_{k=1}^{4} y_k \frac{\partial N_k}{\partial \xi}\right)\frac{\partial N_j}{\partial \eta}\right] \quad \text{(H.4)}$$

then the integral simplifies to:

$$\iint_{\Omega^e} \frac{\partial N_j}{\partial x}\frac{\partial N_i}{\partial x} d\Omega^e = \int_{-1}^{1}\int_{-1}^{1} f(\xi,\eta) d\xi d\eta \quad \text{(H.5)}$$

and evaluated using the Gaussian quadrature:

$$\int_{-1}^{1}\int_{-1}^{1} f(\xi,\eta)d\xi d\eta = \sum_{l=1}^{NSP}\sum_{m=1}^{NSP} w_l w_m f(\xi_m,\eta_l) \tag{H.6}$$

When the above procedure is implemented for the other integral, one could obtain the final form of the flux integral. The only difference between the integrals is the form of the function *f* which now becomes:

$$f(\xi,\eta) = \frac{1}{|J|}\left[-\left(\sum_{k=1}^{4} x_k \frac{\partial N_k}{\partial \eta}\right)\frac{\partial N_j}{\partial \xi} + \left(\sum_{k=1}^{4} x_k \frac{\partial N_k}{\partial \xi}\right)\frac{\partial N_j}{\partial \eta}\right] * \left[-\left(\sum_{k=1}^{4} x_k \frac{\partial N_k}{\partial \eta}\right)\frac{\partial N_i}{\partial \xi} + \left(\sum_{k=1}^{4} x_k \frac{\partial N_k}{\partial \xi}\right)\frac{\partial N_i}{\partial \eta}\right] \tag{H.7}$$

Finally, one could obtain the final integral when the corresponding values of the diffusion coefficient are substituted in the original integral giving a final outcome of a [4X4] element matrix.

- $\iint_{\Omega^e} N_j N_i d\Omega^e$

This integral is associated with the time rate of change of the water surface elevation over an element as shown in equation (G.17). When the integral is written in local coordinates using the determinant of the Jacobian matrix and the master element concept, one obtains:

$$\iint_{\Omega^e} N_j N_i d\Omega^e = \int_{-1}^{1}\int_{-1}^{1} N_j(\xi,\eta)\, N_i(\xi,\eta) |J| d\xi d\eta \qquad \text{(H.8)}$$

If the integral is evaluated using the Gaussian quadrature, one would obtain:

$$\int_{-1}^{1}\int_{-1}^{1} N_j(\xi,\eta) N_i(\xi,\eta) |J| d\xi d\eta = \sum_{l=1}^{NSP}\sum_{m=1}^{NSP} w_l w_m N_j(\xi_m,\eta_l) N_i(\xi_m,\eta_n) |J(\xi_m,\eta_l)| \qquad \text{(H.9)}$$

Finally, the element matrix is written using the above formula. The final outcome of the integral is a [4X4] matrix from each element.

- $\iint_{\Omega^e} (R-I) N_i d\Omega^e$

This integral represents the contribution of effective precipitation over an element as shown in equation (G16). The basic assumption is that both the precipitation and the infiltration are taken to be constant over an element. Therefore, the effective precipitation can be taken out of the integral. Furthermore, the integral is written in local coordinates using the determinant of the Jacobian matrix and the master element concept.

$$\iint_{\Omega^e} (R-I) N_i d\Omega^e = (R-I) \iint_{\Omega^e} N_i d\Omega^e = (R-I) \int_{-1}^{1}\int_{-1}^{1} N_i(\xi,\eta) |J| d\xi d\eta \qquad \text{(H.10)}$$

If the integral is evaluated using the Gaussian quadrature, one would obtain:

$$\int_{-1}^{1}\int_{-1}^{1} N_i(\xi,\eta)|J|d\xi d\eta = \sum_{l=1}^{NSP}\sum_{m=1}^{NSP} w_l w_m N_i(\xi_m,\eta_l)|J(\xi_m,\eta_l)| \qquad \text{(H.11)}$$

Finally, the element vector is written using the above formula and substituting the effective infiltration value. The final outcome of the integral is a 4X1 vector from each element.

Derivation of Element Matrices and Vectors along the Boundaries

Elements involving a boundary, where a natural boundary condition is specified, require the computation of the boundary integral shown in Appendix G. In this integral, the integration is performed over the global boundary coordinate $d\Gamma^e$ along the boundary of the element. To simplify the integration process, the integrands of these integrals must be written on the master element using the local coordinate system and must also be specified for a particular side of the element, which in turn requires that the shape functions are expressed for the particular boundary side of the element. As seen in Figure E.1, the boundary of the element can be any side of the quadrilateral depending on its position in the analysis domain. In order to write the shape functions along each side, appropriate values of ξ and η are substituted for the general shape function formulae. The global boundary coordinate Γ is mapped to a local boundary coordinate a ($-1 \le a \le 1$) for each side as shown in Figure E.1. The local coordinates holds the values ξ = a, η = -1 for side 1, ξ = 1, η = a for side 2, ξ = -a, η = 1 for side 3 and ξ = -1, η = -a for side 4. Using

these values, one would obtain the following four shape functions for each side of the element:

$$\begin{aligned} SIDE\quad 1: &\quad \left[\frac{1-a}{2},\frac{1+a}{2},0,0\right] \\ SIDE\quad 2: &\quad \left[0,\frac{1-a}{2},\frac{1+a}{2},0\right] \\ SIDE\quad 3: &\quad \left[0,0,\frac{1-a}{2},\frac{1+a}{2}\right] \\ SIDE\quad 4: &\quad \left[\frac{1+a}{2},0,0,\frac{1-a}{2}\right] \end{aligned} \tag{H.12}$$

If the values of -1 and +1 are substituted for a in the above formulae, one would indeed obtain the fact that shape functions are equal to 1 at the node it is written for and 0 at all other nodes of the element. The integral over the element in global coordinates must also be transformed to an integral over the master element in local coordinates. This transformation introduces the determinant of the Jacobian between global boundary and local boundary coordinates.

$$\int_{\Gamma^e} f(B)d\Gamma^e = \int_{-1}^{1} f(a)|J_a|da \tag{H.13}$$

where J_a is the Jacobian of the boundary and the incremental boundary coordinate in global coordinate system, $d\Gamma$, can be written as follows according to the Figure E.2:

$$d\Gamma = \sqrt{(dx)^2 + (dy)^2} \tag{H.14}$$

Dividing both sides of this relationship with differential length, *da*, would give the following relationship between the global and local boundary coordinate:

$$\frac{d\Gamma}{da} = \sqrt{\left(\frac{dx}{da}\right)^2 + \left(\frac{dy}{da}\right)^2} \qquad \Rightarrow \qquad d\Gamma = J_a da \tag{H.15}$$

Therefore, the Jacobian of the boundary is written as:

$$J_a = \sqrt{\left(\frac{dx}{da}\right)^2 + \left(\frac{dy}{da}\right)^2} \tag{H.16}$$

where *da* will always take the value of 2 since it is the length of any side on the master element. Using these fundamental concepts, the boundary integrals can be evaluated as follows:

- $\int_{\Gamma_2^e} q_N N_i d\Gamma_2^e$

This integral represents the contribution of Neumann boundary condition as shown in equation (G.16). The basic assumption is that flux is taken to be a constant over the boundary side of the element. Therefore, the q_N term can be taken out of the integral.

$$\int_{\Gamma_2^e} q_N N_i d\Gamma_2^e = q_N \int_{\Gamma_2^e} N_i d\Gamma_2^e \tag{H.17}$$

Furthermore, the integral is written in local coordinates using the determinant of the Jacobian matrix and the master element concept. At this stage, it is important to transform the shape functions with respect to the global coordinates to the shape function with respect to the local coordinates.

$$\int_{\Gamma_2^e} N_i d\Gamma_2^e = \int_{-1}^{1} N_i \left| J_a \right| da \tag{H.18}$$

and can further be simplified since the Jacobian is simply one half the length of the boundary side.

$$\int_{\Gamma_2^e} N_i d\Gamma_2^e = \frac{L_e}{2} \int_{-1}^{1} N_i da \tag{H.19}$$

It is important to note that this integral is simple and does not need numerical integration. It can be integrated exactly to obtain 1 regardless of the side and the associated nodes of the element. Therefore, the final outcome of this boundary integral is a {2X1} vector from each boundary element.

APPENDIX I

FINITE DIFFERENCE EQUATIONS OF UNSATURATED GROUNDWATER FLOW

APPENDIX I

FINITE DIFFERENCE EQUATIONS OF UNSATURATED GROUNDWATER FLOW

The finite difference form of unsaturated zone flow model is derived in this appendix. For each column of unsaturated zone, the governing equation of flow given in equation (3.73) is discretized in the *z-t* plane using the control volume finite difference method. Two additional equations are then used to represent the conditions at the top and bottom of the unsaturated column. This procedure creates a system of *N* equations for *N* unknowns, which is then solved to evaluate the unknown pressure head at all nodes of the discretization. The discretized form of the governing equation is derived below for both an intermediate node and for top and bottom boundary nodes.

The one-dimensional modeling domain used in the discretization is bounded by the soil surface at the top of the domain and by the water table at the bottom of the domain as shown in Figure I.1. The computational nodes are located at the centers of the control volumes or cells and are numbered from 1 to *N* starting from the lower boundary. The fluxes between cells are defined at the upper and lower boundaries of each control volume. This type of a discretization is extremely convenient when infiltration is the

upper boundary condition, allowing it to be defined right at the surface (i.e., at the upper boundary of top control volume). However, it requires special treatment when overland flow initiates and a certain amount of water depth is developed above the surface.

Following the work of Celia et al. (1990), the mixed form of Richards' equation has become popular for modeling the unsaturated zone flow. This form eliminates the mass balance errors associated with the classical head-based form of Richards equation. Simple Picard iteration is used to handle the non-linearity in the equation. Time stepping is done via the classical backward Euler method and a second order central differencing is used to discretize the spatial derivative.

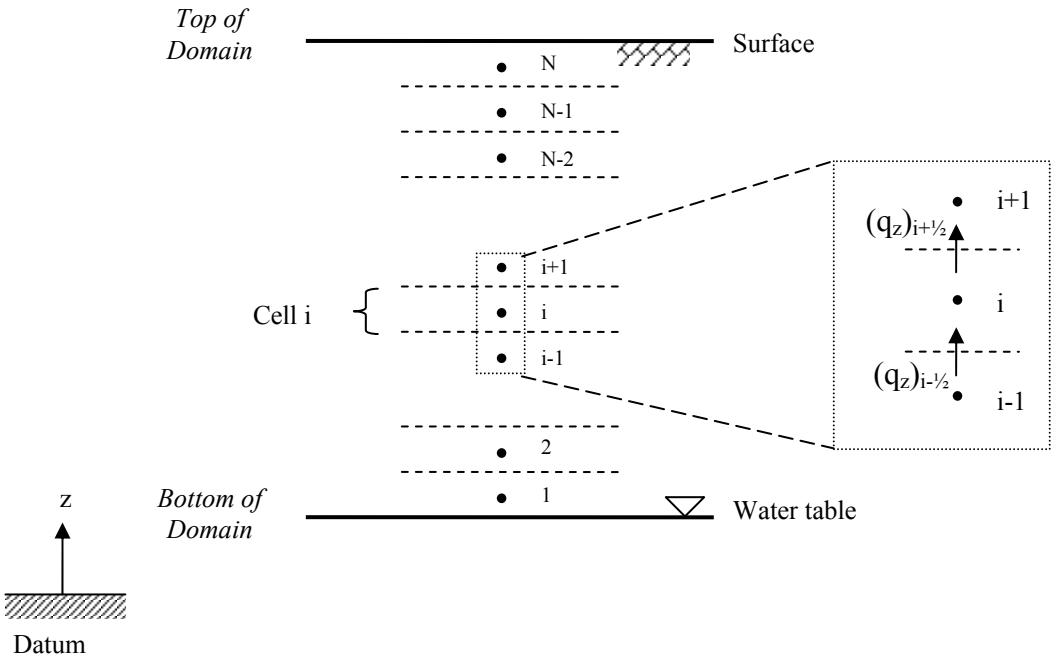

Figure I. 1. One-dimensional discretization in unsaturated zone

Discretized form of equation

Using the setup discussed above, the one-dimensional unsaturated zone equation is discretized for an intermediate spatial node *i* to give:

$$\left(S_w S_s\right)_i^{j+1,k}\left[\frac{\psi_i^{j+1,k+1}-\psi_i^{j}}{\Delta t}\right]+\left[\frac{\theta_i^{j+1,k+1}-\theta_i^{j}}{\Delta t}\right]= \frac{1}{\Delta z_i}\left[\left(K_u\right)_{i+1/2}^{j+1,k}\left(\frac{\psi_{i+1}^{j+1,k+1}-\psi_i^{j+1,k+1}}{\Delta z_{i+1/2}}+1\right)-\left(K_u\right)_{i-1/2}^{j+1,m}\left(\frac{\psi_i^{j+1,k+1}-\psi_{i-1}^{j+1,k+1}}{\Delta z_{i-1/2}}+1\right)\right] \quad \text{(I.1)}$$

where the subscripts *j* and *k* represent the known time and iteration levels where as *j*+1 and *k*+1 represent the unknown time and iteration levels, respectively. In addition, Δz_i is the thickness of control volume *i*, $\Delta z_{i+1/2}$ and $\Delta z_{i-1/2}$ are the distance between nodes *i*+1 and *i* and *i* and *i*-1, respectively, as shown in Figure I.1. There are several available approaches to compute internodal hydraulic conductivities, $(K_u)_{i+1/2}$ and $(K_u)_{i-1/2}$. Of these methods, the arithmetic mean, geometric mean, harmonic mean, arithmetic mean saturation and upwinding are the most commonly applied techniques to evaluate the value of the unsaturated hydraulic conductivity at cell faces. Although each method has its advantages and disadvantages, they all perform well for uniform soils. In the case of non-uniform soils, however, only an integral approach gives accurate results (Williams and Miller, 1999). Since a uniform soil profile is assumed in this study, a computationally simple arithmetic averaging technique is used to evaluate the internodal hydraulic conductivities.

It is clearly seen from the above formulation that all nonlinear occurrences of the unknowns are treated at the $(k)^{th}$ iteration level where as all linear occurrences of the

unknowns are computed at the $(k+1)^{th}$ iteration level. The key to the modified Picard iteration of Celia et al. (1990) is the expansion of the term $\theta_i^{j+1,k+1}$ in a truncated Taylor series with respect to Ψ, about the point $\Psi_i^{j+1,k}$:

$$\theta_i^{j+1,k+1} = \theta_i^{j+1,k} + \left.\frac{d\theta}{d\psi}\right|^{j+1,k} \left(\psi_i^{j+1,k+1} - \psi_i^{j+1,k}\right) + H.O.T \tag{I.2}$$

The derivative of moisture content with respect to the pressure head is actually the specific moisture capacity (C). If the higher order terms are neglected and this equation is substituted in the discretization, one would obtain:

$$\left(S_w S_s\right)_i^{j+1,k}\left[\frac{\psi_i^{j+1,k+1} - \psi_i^{j}}{\Delta t}\right] + \left[\frac{\theta_i^{j+1,k} + C_i^{j+1,k}\left(\psi_i^{j+1,k+1} - \psi_i^{j+1,k}\right) - \theta_i^{j}}{\Delta t}\right] = \frac{1}{\Delta z_i}\left[\left(K_u\right)_{i+1/2}^{j+1,k}\left(\frac{\psi_{i+1}^{j+1,k+1} - \psi_i^{j+1,k+1}}{\Delta z_{i+1/2}} + 1\right) - \left(K_u\right)_{i-1/2}^{j+1,k}\left(\frac{\psi_i^{j+1,k+1} - \psi_{i-1}^{j+1,k+1}}{\Delta z_{i-1/2}} + 1\right)\right] \tag{I.3}$$

In this form, both the degree of saturation in the left hand side and the internodal conductivities in the right hand side of the equation are treated at the known iteration level (k). Therefore, these terms become constants for the solution of the unknown iteration level ($k+1$).

Bottom Boundary Conditions

In this study, a specified zero pressure head is implemented at the bottom of the domain since water table is selected as the bottom boundary of the domain. Figure I.2 depicts the situation at the bottom boundary. Since there is not a node located precisely at the boundary, specifying a head condition at the boundary requires some extra work. Although there are several alternative treatments of the boundary, one of most commonly applied treatment is to pass an interpolating polynomial between the points 1, 2 and the boundary. Once this polynomial is quantified, it can be differentiated with respect to z to obtain the term necessary for computing the boundary flux value that is required for the analysis:

$$q_{1/2} = q_{bottom} = -K_{bottom} \left. \frac{\partial(\psi + z)}{\partial z} \right|_{bottom} \tag{I.4}$$

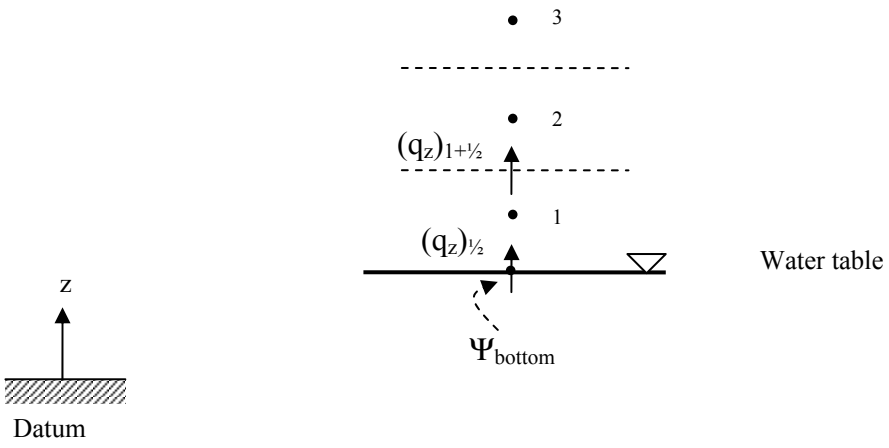

Figure I. 2. Bottom boundary condition

The computation of the hydraulic conductivity at the bottom boundary is not required when the bottom boundary condition is specified at the groundwater table because of the fact that this point is always saturated and the hydraulic conductivity always takes its saturated value. Multiplying the first derivative of the polynomial with the saturated hydraulic conductivity would give the flux needed to run the standard scheme given above.

In general, Lagrange polynomials can be used to interpolate between precise data points. For this particular application, the equation of a general second order Lagrange polynomial can be written as follows:

$$f(x)=\frac{(x-x_1)(x-x_2)}{(x_0-x_1)(x_0-x_2)}f(x_0)+\frac{(x-x_0)(x-x_2)}{(x_1-x_0)(x_1-x_2)}f(x_1)+\frac{(x-x_0)(x-x_1)}{(x_2-x_0)(x_2-x_1)}f(x_2) \quad \text{(I.5)}$$

where x_0, x_1 and x_2 are the known data points and $f(x_0)$, $f(x_1)$ and $f(x_2)$ are the corresponding values of the function (Chapra and Canale, 2002). When pressure head is taken as the function and the elevations of the points above a certain datum are used as the independent variable, the above polynomial can be written as:

$$\psi(z)=\frac{(z-z_1)(z-z_2)}{(z_0-z_1)(z_0-z_2)}\psi(z_0)+\frac{(z-z_0)(z-z_2)}{(z_1-z_0)(z_1-z_2)}\psi(z_1)+\frac{(z-z_0)(z-z_1)}{(z_2-z_0)(z_2-z_1)}\psi(z_2) \quad \text{(I.6)}$$

If points z_0, z_1 and z_2 are taken the bottom of domain, node*1* and node *2*, respectively, one can substitute the differences and take the derivative with respect to *z* at the bottom of the domain to obtain:

$$\left.\frac{\partial \psi}{\partial z}\right|_{z=z_b} = \frac{\left(-3/2\Delta z_1 - 1/2\Delta z_2\right)}{\left(-1/2\Delta z_1\right)\left(-\Delta z_1 - 1/2\Delta z_2\right)}\psi_{bottom} + \frac{\left(-\Delta z_1 - 1/2\Delta z_2\right)}{\left(1/2\Delta z_1\right)\left(-1/2\Delta z_1 - 1/2\Delta z_2\right)}\psi_1 + \frac{\left(-1/2\Delta z_1\right)}{\left(\Delta z_1 + 1/2\Delta z_2\right)\left(1/2\Delta z_1 + 1/2\Delta z_2\right)}\psi_2 \tag{I.7}$$

It should be noted that this polynomial simplifies to the following form when uniform nodal spacing are used in the discretization:

$$\left.\frac{\partial \psi}{\partial z}\right|_{z=z_b} = \frac{1}{\Delta z}\left[-\frac{8}{3}\psi_{bottom} + 3\psi_1 - \frac{1}{3}\psi_2\right] \tag{I.8}$$

Using this term and the hydraulic conductivity, the flux at the bottom of the domain is now written as:

$$q_{1/2} = q_{bottom} = -K_{bottom}\left[\frac{-\frac{8}{3}\psi_{bottom} + 3\psi_1 - \frac{1}{3}\psi_2}{\Delta z} + 1\right] \tag{I.9}$$

which further simplifies to:

$$q_{1/2} = q_{bottom} = -K_z\left[\frac{3\psi_1 - \frac{1}{3}\psi_2}{\Delta z} + 1\right] \tag{I.10}$$

since $K_{bottom}=(K_g)_z$ and $\psi_{bottom}=0$ when the bottom boundary condition is defined at the groundwater table. Therefore, the discretized equation for the bottom boundary node can be written as:

$$\left(S_w S_s\right)_1^{j+1,k}\left[\frac{\psi_1^{j+1,k+1}-\psi_1^{j}}{\Delta t}\right]+\left[\frac{\theta_1^{j+1,k}+C_1^{j+1,k}\left(\psi_1^{j+1,k+1}-\psi_1^{j+1,k}\right)-\theta_1^{j}}{\Delta t}\right]= \frac{1}{\Delta z_1}\left[K_{1+1/2}^{j+1,k}\left(\frac{\psi_2^{j+1,k+1}-\psi_1^{j+1,k+1}}{\Delta z_{1+1/2}}+1\right)-\left(-q_{bottom}\right)\right] \tag{I.11}$$

<u>*Top boundary condition*</u>

The top boundary of domain is always taken as the soil surface and either a specified head or a specified flux condition can be implemented. Figure I.3 depicts the situation at the top boundary for both head and flux conditions. Since there is not a node at the ground surface, specifying a head condition at the boundary requires some extra work. The flux condition is straightforward since it is specified at the upper boundary of the top control volume. Therefore, the specified flux value is simply substituted in the discretization to give:

$$\left(S_w S_s\right)_N^{j+1,k}\left[\frac{\psi_N^{j+1,k+1}-\psi_N^{j}}{\Delta t}\right]+\left[\frac{\theta_N^{j+1,k}+C_N^{j+1,k}\left(\psi_N^{j+1,k+1}-\psi_N^{j+1,k}\right)-\theta_N^{j}}{\Delta t}\right]= \frac{1}{\Delta z_N}\left[\left(-q_{surface}\right)-K_{N-1/2}^{j+1,k}\left(\frac{\psi_N^{j+1,k+1}-\psi_{N-1}^{j+1,k+1}}{\Delta z_{N-1/2}}+1\right)\right] \tag{I.12}$$

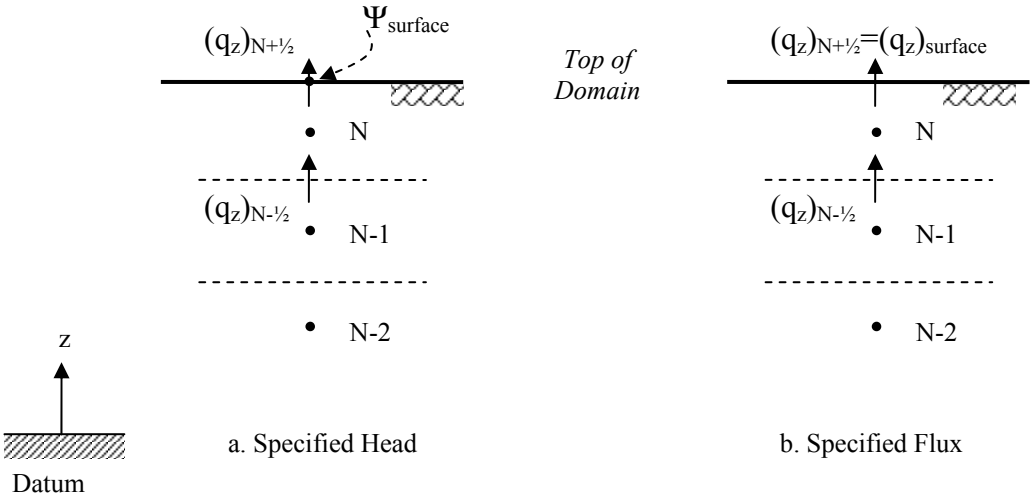

Figure I. 3. Top boundary condition

The discretization of the specified head condition is not as simple as the flux condition. The main difficulty is the fact that the head condition is specified at the boundary of a control volume. Hence, the classical treatment of the fluxes is not possible since such treatment requires the use of an upper node outside the modeling domain. In this regard, a similar idea that is used for the bottom boundary condition is also implemented in the top boundary. A Lagrange interpolating polynomial is passed between the points *N*-1, *N* and the boundary. Once this polynomial is quantified, it can be differentiated with respect to *z* to obtain the term necessary for computing the boundary flux value that is required for the analysis:

$$q_{N+1/2} = q_{surface} = -K_{surface} \left. \frac{\partial(\psi + z)}{\partial z} \right|_{surface} \tag{I.13}$$

The hydraulic conductivity at the surface is computed using the specified pressure head at this particular point. Applying a procedure similar to the one used in bottom boundary condition, the points z_0, z_1 and z_2 are taken at node *N-1*, node *N* and the top of domain, respectively, the differences are substituted and the derivative with respect to *z* at the bottom of the domain is calculated to obtain:

$$\left.\frac{\partial \psi}{\partial z}\right|_{z=z_s} = \frac{\left(1/2\Delta z_N\right)}{\left(-1/2\Delta z_{N-1} - 1/2\Delta z_N\right)\left(-\Delta z_N - 1/2\Delta z_{N-1}\right)}\psi_{N-1} + \frac{\left(\Delta z_N + 1/2\Delta z_{N-1}\right)}{\left(1/2\Delta z_N + 1/2\Delta z_{N-1}\right)\left(-1/2\Delta z_N\right)}\psi_N + \frac{\left(3/2\Delta z_N + 1/2\Delta z_{N-1}\right)}{\left(\Delta z_N + 1/2\Delta z_{N-1}\right)\left(1/2\Delta z_N\right)}\psi_{surface} \tag{I.14}$$

Again, it should be noted that this polynomial simplifies to the following form when uniform nodal spacing are used in the discretization:

$$\left.\frac{\partial \psi}{\partial z}\right|_{z=z_s} = \frac{1}{\Delta z}\left[\frac{1}{3}\psi_{N-1} - 3\psi_N + \frac{8}{3}\psi_{surface}\right] \tag{I.15}$$

Using this term and the hydraulic conductivity, the flux at the top of the domain is now written as:

$$q_{N+1/2} = q_{surface} = -K_{surface}\left[\frac{\frac{1}{3}\psi_{N-1} - 3\psi_N + \frac{8}{3}\psi_{surface}}{\Delta z} + 1\right] \tag{I.16}$$

where the hydraulic conductivity at the surface is computed by:

$$K_{surface} = K\left(\psi_{surface}\right) \tag{I.17}$$

When the general non-uniform expression for flux term is substituted in the discretization, one would obtain:

$$\left(S_w S_s\right)_N^{j+1,k}\left[\frac{\psi_N^{j+1,k+1}-\psi_N^{j}}{\Delta t}\right]+\left[\frac{\theta_N^{j+1,k}+C_N^{j+1,k}\left(\psi_N^{j+1,k+1}-\psi_N^{j+1,k}\right)-\theta_N^{j}}{\Delta t}\right]= \frac{1}{\Delta z_N}\left[\left(-q_{surface}\right)-K_{N-1/2}^{j+1,k}\left(\frac{\psi_N^{j+1,k+1}-\psi_{N-1}^{j+1,k+1}}{\Delta z_{N-1/2}}+1\right)\right] \tag{I.18}$$

APPENDIX J

FINITE DIFFERENCE EQUATIONS OF CHANNEL TRANSPORT

APPENDIX J

FINITE DIFFERENCE EQUATIONS OF CHANNEL TRANSPORT

In this appendix, the finite difference solution of the mass balance and boundary condition equations of contaminant transport in channels are presented. For each channel of the network, advection, dispersion, decay and source/sink operators of the contaminant mass balance equation given in equation (4.1) are discretized in the *x*-*t* plane using the most suitable scheme for each process. In this regard, the numerical solution of the advection operator is performed with the explicit QUICKEST algorithm. A standard fully implicit differencing algorithm is then implemented to solve dispersion, decay and source/sink operator. Additional equations are also used to represent the conditions in the upstream and downstream boundaries of the channel as well as the channel junctions. The discretized forms of these equations are given in the following sections.

Numerical solution of advection operator

In the control-volume finite difference method, each node represents a control-volume within which, mass is conserved. A control-volume for node *i* is shown in Figure J.1. The left-backward and right-forward cell faces of the control volume are represented

by the letters *b* and *f*. When similar control volumes are defined for all nodes of the domain, the domain is fully discretized in the control-volume sense guaranteeing mass balance. For volume *i*, the discretized equation could be written as:

$$\left(C_r A\right)_i^* = \left(C_r A\right)_i^j + \frac{\Delta t}{\frac{1}{2}\left(\Delta x_{i-1} + \Delta x_i\right)}\left[\left(VAC_r\right)_f^j - \left(VAC_r\right)_b^j\right] \tag{J.1}$$

where the subscript '*f*' and '*b*' represent the corresponding values of the variables at the forward and backward walls of the control volume. One of the key issues is to determine the parameter to advect along the channel. In the conservative form of advection-dispersion equation, the parameter (C_rA) is to be advected that also properly captures the unsteady behavior of the flow. However, it is important to note that the variation of the parameter (C_rA) may be totally different from C_r along the channel. Therefore, the numerical algorithm must be suitable to handle such variations and possible non-monotonic behavior.

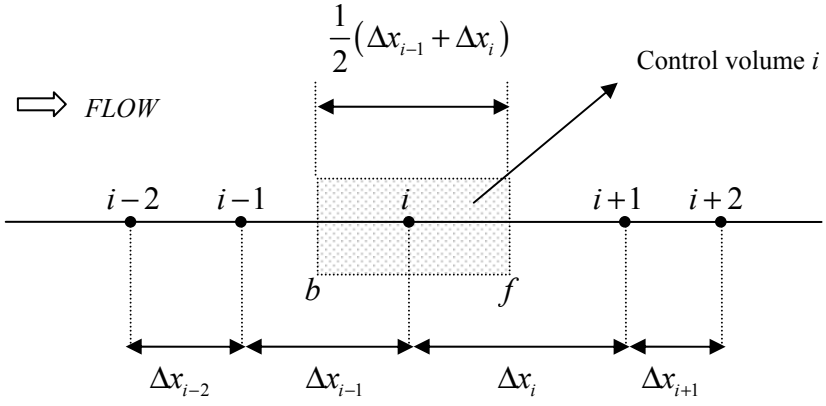

Figure J. 1. Numerical discretization of the domain for QUICKEST algorithm

The solution of the contaminant concentrations in the above equation is based on the principle of properly representing the parameters along the cell faces. In the equation given above, the flow variables V and A are obtained from the solution of the channel flow model and are known values for the transport solution. In general, the implicit flow model would allow much larger time steps than the explicit advection model shown here. Hence, for each flow model solution, numerous transport model solutions are to be made. In all of these transport solution steps, two techniques can be used to extract the flow data. One first is to linearly interpolate the flow information between the two time levels of flow solution data according to the transport time step. The second way is to use constant values of all flow parameters from the current or future time level within the transport solution. When the variation of flow variables within a flow time step is significant, then the first method may be more suitable. Otherwise, using constant values of flow parameters would give sufficient results.

Once flow parameters are defined at all node points for each transport time line, then the next step is to find the cell wall values of these parameters. When (C_rA) is solved in the equation, a higher order interpolator is used to solve (C_rA) value and an extra interpolation (i.e., simple linear or higher order) is done to find the cell face values of the velocity. When C_r is solved in the equation, a higher order interpolator is used to solve for the concentration and separate extra interpolations (i.e., simple linear or higher order) are used to find the cell face values of the velocity and the area. Regardless of the dependent variable of the equation, it is generally accepted that the remaining flow parameters (i.e., V when C_rA is the dependent variable; or V and A when C_r is the dependent variable) can be linearly interpolated with sufficient accuracy. Since A is a

known parameter to the transport model and very small time steps are enforced due to the explicit nature of the numerical scheme where A varies very mildly, the dependent variable of the equation can be reduced to C_r without violating the conservative behavior of the algorithm. Then one can write the equation as:

$$\left(C_r\right)_i^* A_i^{j+1} = \left(C_r\right)_i^j A_i^j + \frac{\Delta t}{\frac{1}{2}\left(\Delta x_{i-1} + \Delta x_i\right)}\left[\left(C_r\right)_f^j V_f^j A_f^j - \left(C_r\right)_b^j V_b^j A_b^j\right] \tag{J.2}$$

where the cell wall values of flow parameters are evaluated as:

$$\begin{aligned} V_f^j &= \frac{V_{i+1}^j + V_i^j}{2} \qquad & A_f^j &= \frac{A_{i+1}^j + A_i^j}{2} \\ V_b^j &= \frac{V_i^j + V_{i-1}^j}{2} \qquad & A_b^j &= \frac{A_i^j + A_{i-1}^j}{2} \end{aligned} \tag{J.3}$$

The cell face values of the concentration are evaluated using a higher order interpolator such as the QUICKEST scheme. For a non-uniform grid such as the one shown in Figure J.1, the forward face concentration can be written using the QUICKEST algorithm as:

$$\left(C_r\right)_f = P_1(x) - \frac{V\Delta t}{2}\left(\frac{dP_1}{dx}\right) - \frac{1}{6}\left[\left(\Delta x_c\right)^2 - \left(V\Delta t\right)^2\right]\left(\frac{d^2P_2}{dx^2}\right) \tag{J.4}$$

where Δx_c is the control-volume length given by ½($\Delta x_{i-1}+\Delta x_i$) and P_1 and P_2 are the first and second order Lagrangian interpolating polynomials written such that:

$$P_1(x) = \frac{x - x_i}{x_{i+1} - x_i}(C_r)_{i+1} + \frac{x_{i+1} - x}{x_{i+1} - x_i}(C_r)_i \tag{J.5}$$

$$\begin{aligned} P_2(x) = {} & \frac{(x - x_i)(x - x_{i-1})}{(x_{i+1} - x_i)(x_{i+1} - x_{i-1})}(C_r)_{i+1} + \frac{(x - x_{i+1})(x - x_{i-1})}{(x_i - x_{i+1})(x_i - x_{i-1})}(C_r)_i \\ & + \frac{(x - x_{i+1})(x - x_i)}{(x_{i-1} - x_{i+1})(x_{i-1} - x_i)}(C_r)_{i-1} \end{aligned} \tag{J.6}$$

where x denotes the position of the forward cell face. The first and the second derivatives of these functions are then evaluated to find the expressions required for the QUICKEST algorithm:

$$\frac{dP_1(x)}{dx} = \frac{1}{x_{i+1} - x_i}(C_r)_{i+1} - \frac{1}{x_{i+1} - x_i}(C_r)_i \tag{J.7}$$

$$\begin{aligned} \frac{d^2P_2(x)}{dx^2} = {} & \frac{2}{(x_{i+1} - x_i)(x_{i+1} - x_{i-1})}(C_r)_{i+1} + \frac{2}{(x_i - x_{i+1})(x_i - x_{i-1})}(C_r)_i \\ & + \frac{2}{(x_{i-1} - x_{i+1})(x_{i-1} - x_i)}(C_r)_{i-1} \end{aligned} \tag{J.8}$$

When substituted back in the interpolation equation, one would obtain the expression for the front cell face concentration value. For the particular case of a uniform grid, the forward cell face concentration value becomes:

$$\begin{aligned} (C_r)_f = {} & \frac{1}{2}\left((C_r)_{i+1} + (C_r)_i\right) - \frac{CN}{2}\left((C_r)_{i+1} - (C_r)_i\right) \\ & - \frac{1}{6}\left[1 - CN^2\right]\left((C_r)_{i+1} - 2(C_r)_i + (C_r)_{i-1}\right) \end{aligned} \tag{J.9}$$

where *CN* is the Courant number given by:

$$CN = \frac{V\Delta t}{\Delta x} \tag{J.10}$$

A similar procedure is implemented for the backward face concentration can be written using the QUICKEST algorithm as:

$$\left(C_r\right)_b = P_1\left(x\right) - \frac{V\Delta t}{2}\left(\frac{dP_1}{dx}\right) - \frac{1}{6}\left[\left(\Delta x_c\right)^2 - \left(V\Delta t\right)^2\right]\left(\frac{d^2P_2}{dx^2}\right) \tag{J.11}$$

where P_1 and P_2 are similar first and second order Lagrangian interpolating polynomials that can be written such that:

$$P_1\left(x\right) = \frac{x - x_{i-1}}{x_i - x_{i-1}}\left(C_r\right)_i + \frac{x_i - x}{x_i - x_{i-1}}\left(C_r\right)_{i-1} \tag{J.12}$$

$$\begin{aligned} P_2\left(x\right) = {} & \frac{\left(x - x_{i-1}\right)\left(x - x_{i-2}\right)}{\left(x_i - x_{i-1}\right)\left(x_i - x_{i-2}\right)}\left(C_r\right)_i + \frac{\left(x - x_i\right)\left(x - x_{i-2}\right)}{\left(x_{i-1} - x_i\right)\left(x_{i-1} - x_{i-2}\right)}\left(C_r\right)_{i-1} \\ & + \frac{\left(x - x_i\right)\left(x - x_{i-1}\right)}{\left(x_{i-2} - x_i\right)\left(x_{i-2} - x_{i-1}\right)}\left(C_r\right)_{i-2} \end{aligned} \tag{J.13}$$

where x now denotes the position of the backward cell face. The first and the second derivatives of these functions are taken to evaluate the expressions required for the QUICKEST algorithm:

$$\frac{dP_1(x)}{dx} = \frac{1}{x_i - x_{i-1}}(C_r)_i - \frac{1}{x_i - x_{i-1}}(C_r)_{i-1} \tag{J.14}$$

$$\frac{d^2P_2(x)}{dx^2} = \frac{2}{(x_i - x_{i-1})(x_i - x_{i-2})}(C_r)_i + \frac{2}{(x_{i-1} - x_i)(x_{i-1} - x_{i-2})}(C_r)_{i-1} + \frac{2}{(x_{i-2} - x_i)(x_{i-2} - x_{i-1})}(C_r)_{i-2} \tag{J.15}$$

When substituted back in the interpolation equation, one would obtain the expression for the back cell face concentration value. Note that for a uniform grid, the backward cell face concentration value becomes:

$$(C_r)_b = \frac{1}{2}\left((C_r)_i + (C_r)_{i-1}\right) - \frac{CN}{2}\left((C_r)_i - (C_r)_{i-1}\right) - \frac{1}{6}\left[1 - CN^2\right]\left((C_r)_i - 2(C_r)_{i-1} + (C_r)_{i-2}\right) \tag{J.16}$$

Hence, for a control-volume *i*, the QUICKEST algorithm uses a total of 4 nodal points to interpolate the forward and backward cell face concentration values giving a third order accurate scheme.

Flux limiting with ULTIMATE method

Although the QUICKEST algorithm introduces significant advances in advection modeling, it still can not fully capture steep gradients. The algorithm creates spurious oscillations in the leading edge of such gradients. These oscillations can be effectively removed by using a flux limiting procedure. Leonard (1991) formulated a universal

limiter to be used in conjunction with the QUICKEST algorithm. The algorithm works as follows:

1. Upstream, central and downstream nodes (i.e., U, C and D) are designated for the node under analysis by using the sign of the flow velocity for each cell face.
2. The variable ADEL is computed for each cell face:

$$ADEL = |DEL| = \left|(C_r)_D^j - (C_r)_U^j\right| \tag{J.17}$$

3. The variable ACURV is computed for each cell face:

$$ACURV = |CURV| = \left|(C_r)_D^j - 2(C_r)_C^j + (C_r)_U^j\right| \tag{J.18}$$

4. If ACURV≥ADEL, there is non-monotonic behavior of concentration and the cell face value is set as:

$$(C_r)_f^j = (C_r)_C^j \tag{J.19}$$

   and proceed to the next cell face.
5. Else, a reference concentration is evaluated for each cell face:

$$(C_r)_{ref} = (C_r)_U^j + \frac{(C_r)_C^j - (C_r)_U^j}{CN} \tag{J.20}$$

6. The cell face concentration is evaluated using standard QUICKEST method.
7. If DEL>0, set:

$$(C_r)_C^j \le (C_r)_f \le \min\left((C_r)_{ref}, (C_r)_D^j\right) \tag{J.21}$$

8. Else, set:

$$\max\left((C_r)_{ref}, (C_r)_D^j\right) \le (C_r)_f \le (C_r)_C^j \tag{J.22}$$

9. Continue to next face and node.

Numerical solution of dispersion, decay and source/sink operators

The dispersion operator does not pose any numerical problems and hence can be accurately discretized by using a central difference scheme as shown in Figure J.1. With non-uniform grid spacing, the dispersion operator is discretized as follows:

$$\frac{\partial}{\partial x}\left(AD_x \frac{\partial C_r}{\partial x}\right) = \frac{1}{\frac{1}{2}(\Delta x_{i-1} + \Delta x_i)}\left[\begin{array}{r}\left(A_f (D_L)_f \frac{(C_r)_{i+1} - (C_r)_i}{\Delta x_i}\right) \\ -\left(A_b (D_L)_b \frac{(C_r)_i - (C_r)_{i-1}}{\Delta x_{i-1}}\right)\end{array}\right] \tag{J.23}$$

When the dispersion, decay and the source/sink operators are discretized at the unknown time level, the final discretized form of the channel transport equation becomes:

$$
\begin{aligned}
&\left(C_r A\right)_i^{j+1} = \left(C_r A\right)_i^{*} \\
&+\frac{\Delta t}{\frac{1}{2}\left(\Delta x_{i-1}+\Delta x_i\right)}\left[\left(A_f^{j+1}\left(D_L\right)_f \frac{\left(C_r\right)_{i+1}^{j+1}-\left(C_r\right)_i^{j+1}}{\Delta x_i}\right)-\left(A_b^{j+1}\left(D_L\right)_b \frac{\left(C_r\right)_i^{j+1}-\left(C_r\right)_{i-1}^{j+1}}{\Delta x_{i-1}}\right)\right] \\
&+\Delta t\left[\begin{array}{l} -k\left(C_r\right)_i^{j+1} A_i^{j+1}+\left(q_{L1}\right)_i^{j+1}\left(C_{L1}^{*}\right)_i^{j+1} \\ \qquad -\left(n_{sed} D_{sed}\right)_i \dfrac{\left(C_g\right)_i^{j+1}-\left(C_r\right)_i^{j+1}}{\Delta z}\left(w_r\right)_i^{j+1}+\left(q_{L2}\right)_i^{j+1}\left(C_{L2}^{*}\right)_i^{j+1} \end{array}\right]
\end{aligned}
\tag{J.24}
$$

Treatment of junctions

Complex channel networks with junctions are not studied extensively within the contaminant transport framework except for the work of Zhang (1998) who has formulated the contaminant transport phenomena in artificial channel networks. In this study, however, the main features of the junction treatment are developed for natural channels in a coupled framework. Since the proposed algorithm in this study solves the transport equation in two separate steps, treatment of junctions must follow the same strategy. Hence, both the explicit advection algorithm and the implicit dispersion/decay/source/sink algorithms must properly treat junctions.

In the advection step, the junction condition must consider the fact that the algorithm is explicit in nature. For explicit treatment of junctions, the method of characteristics is a viable option. In the method of characteristics, the last reach of each

inflowing channel is considered. A forward characteristic is drawn from the unknown concentration value $(C_r)_N^{n+1}$ to the known time line. The concentration value corresponding to the point where the characteristic line cuts the known time line is called the foot of the characteristics and the concentration at this point is essentially the required concentration value. When this is done for all inflowing channels, one would obtain temporary junction concentration values. An advective mass balance is then written using all inflowing channels to compute the concentration value at the most upstream point of the outflowing channel. Then, this concentration is equated to the concentration value at the most downstream points of all inflowing channels satisfying the equality of the concentrations at the junction. In general, a linear interpolation of the two neighboring concentration values at nodes *N-1* and *N* is considered to be sufficiently accurate (Figure J.2). If the position of the foot of the characteristic at the known time line is represented with x_{foot}, then the concentration value at this point is given by:

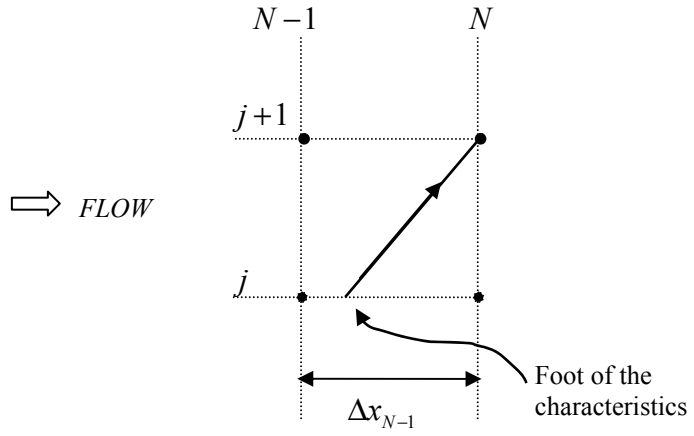

Figure J. 2. Method of characteristics at junctions for advection step

$$x_{foot} = x_N - V\Delta t \tag{J.25}$$

The concentration is then calculated using a linear interpolation function such that:

$$C_{foot}^{j} = \left(C_r\right)_{N-1}^{j} + \frac{x_N - V\Delta t - x_{N-1}}{\Delta x_{N-1}}\left(\left(C_r\right)_{N}^{j} - \left(C_r\right)_{N-1}^{j}\right) \tag{J.26}$$

It is important to note that higher order interpolators could also be used in this operation to increase the accuracy of the solution. However, for practical purposes, a linear interpolator is satisfactory. Finally, the concentration at the unknown time line is equated to the calculated concentration value at the foot of the characteristic such that:

$$\left(C_r\right)_{N}^{j+1} = C_{foot}^{j} \tag{J.27}$$

Once this operation is done for all inflowing channels, one can write an advective mass balance at the junction to find the concentration at the most upstream point of the outflowing channel. For a junction shown in Figure J.3, the junction mass balance is written as:

$$\left(C_r\right)_{1,C3}^{j+1} = \frac{\left(C_r\right)_{N,C1}^{j+1} Q_{N,C1}^{j+1} + \left(C_r\right)_{N,C2}^{j+1} Q_{N,C2}^{j+1}}{Q_{N,C1}^{j+1} + Q_{N,C2}^{j+1}} \tag{J.28}$$

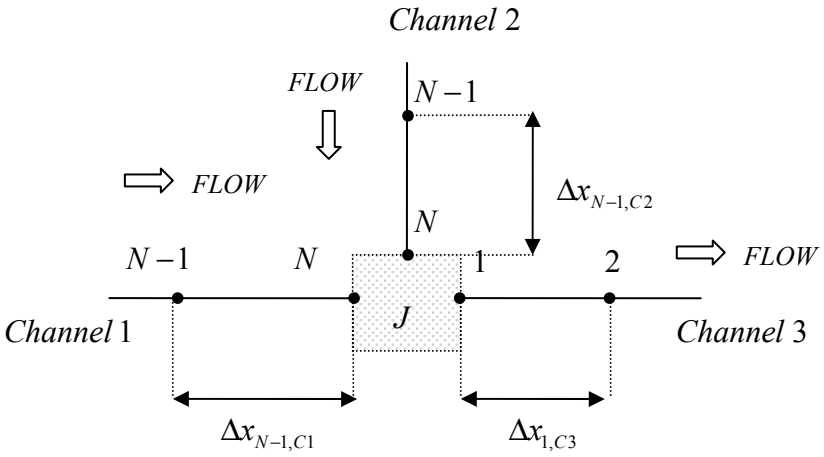

Figure J. 3. Treatment of junctions

where the first subscript represents the channel specific local nodal value and the second subscript stands for the channel this node belongs. Once this concentration is found from the mass balance, it serves as the upstream boundary condition of the outflowing channel. Finally, it is equated to the concentration values at the most downstream nodes of all inflowing channels to provide the downstream boundary value:

$$\begin{aligned} \left(C_r\right)_{N,C1}^{j+1} &= \left(C_r\right)_{1,C3}^{j+1} \\ \left(C_r\right)_{N,C2}^{j+1} &= \left(C_r\right)_{1,C3}^{j+1} \end{aligned} \tag{J.29}$$

The treatment of junctions is slightly different in the dispersion/decay/source/sink operator. Since this operator is implicit in nature, the junction condition must also be treated implicitly. A total mass balance between inflowing channels and the outflowing channel guarantees the satisfaction of mass continuity. A time-weighted mass balance could be written as:

$$\sum_{i=1}^{n}\left[M_{in}^{j+1}\right]_i = M_{out}^{j+1} \tag{J.30}$$

where the total mass flux term for an inflowing or outflowing channel is given as the summation of the dispersive mass flux, decayed mass flux and the mass flux due to source/sink terms:

$$M_{in,out} = AD_L\frac{\partial C_r}{\partial x} - kC_r\forall + q_{L1}C_{L1}^*\frac{\Delta x}{2} - n_{sed}D_{sed}\frac{C_g - C_r}{\Delta z}w_r\frac{\Delta x}{2} + q_{L2}C_{L2}^*\frac{\Delta x}{2} \tag{J.31}$$

After discretizing the mass flux term, one could obtain a junction mass balance for the second step of the advection-dispersion equation solution. As an example, the discretization for the first channel of Figure J.3 is shown below:

$$\begin{aligned} M_{C1} = {} & A_b\left(D_L\right)_b\frac{\left(C_r\right)_{N,C1} - \left(C_r\right)_{N-1,C1}}{\Delta x_{N-1,C1}} - k\left(C_r\right)_{N,C1}A_{N,C1}\frac{\Delta x_{N,C1-1}}{2} + \left(q_{L1}\right)_{N,C1}\left(C_{L1}^*\right)_{N,C1}\frac{\Delta x_{N-1,C1}}{2} \\ & - \left(n_{sed}D_{sed}\right)_i\frac{\left(C_g\right)_{N,C1} - \left(C_r\right)_{N,C1}}{\Delta z}\left(w_r\right)_{N,C1}\frac{\Delta x_{N-1,C1}}{2} + \left(q_{L2}\right)_{N,C1}\left(C_{L2}^*\right)_{N,C1}\frac{\Delta x_{N-1,C1}}{2} \end{aligned} \tag{J.32}$$

This discretization is written for all channels and for both known and unknown time lines and substituted in the above junction mass balance equation. It is then solved for the upstream node of the outflowing channel. Finally, the equality of concentrations at junction nodes is implemented.

APPENDIX K

DERIVATION OF GALERKIN FORM OF GROUNDWATER CONTAMINANT TRANSPORT EQUATION

APPENDIX K

DERIVATION OF GALERKIN FORM OF GROUNDWATER CONTAMINANT TRANSPORT EQUATION

The first step of the derivation of the weak form is to approximate the unknown function over the domain using interpolating functions, $N_j(x,y)$, of the form:

$$C_g(x,y,t) \approx \hat{C}_g(x,y,t) = \sum_{j=1}^{N} \left(\hat{C}_g(t)\right)_j N_j(x,y) \tag{K.1}$$

where $\hat{C}_g(t)$ is the approximate value of the contaminant concentration and N is the total number of nodes in the two-dimensional domain. In essence, the temporal and spatial discretizations are separated from each other in the approximate solution. The nodal values, $(\hat{C}_g(t))_j$, becomes only a function of time and the shape function, $N_j(x,y)$, is now only a function of space. It is also important to note that the shape functions are defined only for its corresponding node. They are zero elsewhere in the domain.

Since the Galerkin method is an approximate technique, the solution given in equation (K.1) does not satisfy the differential equation exactly and a residual occurs. The method states that the weighted average of this residual over the whole domain

becomes zero. If the approximate solution is substituted in the differential equation, one can write the total residual, $\check{R}$, as:

$$\begin{aligned}
&\tilde{R}(x,y,t) = nR_d\left(h_g - z_b\right)\frac{\partial \hat{C}_g}{\partial t} + \left(h_g - z_b\right)q_x\frac{\partial \hat{C}_g}{\partial x} + \left(h_g - z_b\right)q_y\frac{\partial \hat{C}_g}{\partial y} \\
&-\frac{\partial}{\partial x}\left[\left(h_g - z_b\right)nD_{xx}\frac{\partial \hat{C}_g}{\partial x}\right] - \frac{\partial}{\partial x}\left[\left(h_g - z_b\right)nD_{xy}\frac{\partial \hat{C}_g}{\partial y}\right] \\
&-\frac{\partial}{\partial y}\left[\left(h_g - z_b\right)nD_{yx}\frac{\partial \hat{C}_g}{\partial x}\right] - \frac{\partial}{\partial y}\left[\left(h_g - z_b\right)nD_{yy}\frac{\partial \hat{C}_g}{\partial y}\right] \\
&+I\left(C_I^* - \hat{C}_g\right) + \lambda nR_d\left(h_g - z_b\right)\hat{C}_g + K_w n\left(h_g - z_b\right)\hat{C}_g - \hat{C}_g S_y\frac{\partial h_g}{\partial t} \\
&+\sum_{k=1}^{n_w}\left[Q_{w,k}\left(C_{w,k}^* - \hat{C}_g\right)\delta\left(x - x_{w,k}\right)\delta\left(y - y_{w,k}\right)\right] \\
&+\sum_{m=1}^{n_r}\left[\begin{array}{l}\int_0^1\left[q_{L1,m}\left(C_{L1,m}^* - \hat{C}_g\right) - n_{sed,m}D_{sed,m}\dfrac{C_{r,m} - \hat{C}_g}{m_{r,m}}w_{r,m}\right] \\ \sqrt{\left(\dfrac{dg_{x,m}}{du}\right)^2 + \left(\dfrac{dg_{y,m}}{du}\right)^2}\,\delta\left(x - g_{x,m}(u)\right)\delta\left(y - g_{y,m}(u)\right)du\end{array}\right]
\end{aligned} \tag{K.2}$$

The Galerkin finite element method is based on the idea of minimizing this residual over the solution domain by letting the weighed integral residual tend to zero. In this formulation the weighing functions are selected as the interpolating functions used in element level:

$$\iint_\Omega \tilde{R}(x,y,t)\,N_i(x,y)\,d\Omega = 0 \qquad i = 1,2,3,\ldots,N \tag{K.3}$$

For the sake of clarity, the description of the index i running from *1* to N is not repeated in the following equations. When the expression for the residual is substituted in Equation (K.3) and the square root expression is written as the norm of the gradient of parametric vector equation $\mathbf{g} = g_x\mathbf{i} + g_y\mathbf{j}$, the integral simplifies to:

$$\iint_{\Omega}\left\{\begin{array}{l} nR_d\left(h_g - z_b\right)\dfrac{\partial \hat{C}_g}{\partial t} + \left(h_g - z_b\right)q_x\dfrac{\partial \hat{C}_g}{\partial x} + \left(h_g - z_b\right)q_y\dfrac{\partial \hat{C}_g}{\partial y} \\ -\dfrac{\partial}{\partial x}\left[\left(h_g - z_b\right)nD_{xx}\dfrac{\partial \hat{C}_g}{\partial x} + \left(h_g - z_b\right)nD_{xy}\dfrac{\partial \hat{C}_g}{\partial y}\right] \\ -\dfrac{\partial}{\partial y}\left[\left(h_g - z_b\right)nD_{yx}\dfrac{\partial \hat{C}_g}{\partial x} + \left(h_g - z_b\right)nD_{yy}\dfrac{\partial \hat{C}_g}{\partial y}\right] \\ +I\left(C_I^* - \hat{C}_g\right) + \lambda nR_d\left(h_g - z_b\right)\hat{C}_g + K_w n\left(h_g - z_b\right)\hat{C}_g - \hat{C}_g S_y\dfrac{\partial h_g}{\partial t} \\ +\displaystyle\sum_{k=1}^{n_w}\left[Q_{w,k}\left(C_{w,k}^* - \hat{C}_g\right)\delta\left(x - x_{w,k}\right)\delta\left(y - y_{w,k}\right)\right] \\ +\displaystyle\sum_{m=1}^{n_r}\left[\int_0^1\left[q_{L1,m}\left(C_{L1,m}^* - \hat{C}_g\right) - n_{sed,m}D_{sed,m}\dfrac{C_{r,m} - \hat{C}_g}{m_{r,m}}w_{r,m}\right]\right. \\ \qquad\qquad \left.\left|\nabla\mathbf{g}\right|\delta\left(x - g_{x,m}(u)\right)\delta\left(y - g_{y,m}(u)\right)du\right] \end{array}\right\} N_i d\Omega = 0 \tag{K.4}$$

The integration by parts is now applied to the second order derivative terms in the above integral to reduce them to first order and incorporate the natural boundary conditions:

$$\begin{aligned} \iint_{\Omega}\left\{\frac{\partial}{\partial x}\left[\left(h_g - z_b\right)nD_{xx}\frac{\partial \hat{C}_g}{\partial x} + \left(h_g - z_b\right)nD_{xy}\frac{\partial \hat{C}_g}{\partial y}\right]\right\} N_i d\Omega = \\ -\iint_{\Omega}\left[\left(h_g - z_b\right)nD_{xx}\frac{\partial \hat{C}_g}{\partial x} + \left(h_g - z_b\right)nD_{xy}\frac{\partial \hat{C}_g}{\partial y}\right]\frac{\partial N_i}{\partial x}d\Omega \\ +\int_{\Gamma}\left[\left(h_g - z_b\right)nD_{xx}\frac{\partial \hat{C}_g}{\partial x} + \left(h_g - z_b\right)nD_{xy}\frac{\partial \hat{C}_g}{\partial y}\right]N_i n_x d\Gamma \end{aligned} \tag{K.5}$$

$$\iint_{\Omega}\left\{\frac{\partial}{\partial y}\left[\left(h_g-z_b\right)nD_{yx}\frac{\partial \hat{C}_g}{\partial x}+\left(h_g-z_b\right)nD_{yy}\frac{\partial \hat{C}_g}{\partial y}\right]\right\}N_i d\Omega =$$
$$-\iint_{\Omega}\left[\left(h_g-z_b\right)nD_{yx}\frac{\partial \hat{C}_g}{\partial x}+\left(h_g-z_b\right)nD_{yy}\frac{\partial \hat{C}_g}{\partial y}\right]\frac{\partial N_i}{\partial y}d\Omega \qquad \text{(K.6)}$$
$$+\int_{\Gamma}\left[\left(h_g-z_b\right)nD_{yx}\frac{\partial \hat{C}_g}{\partial x}+\left(h_g-z_b\right)nD_{yy}\frac{\partial \hat{C}_g}{\partial y}\right]N_i n_y d\Gamma$$

where n_x and n_y represent the x and y components of unit normal vector. Substituting these expressions and rearranging gives:

$$-\int_{\Gamma}\left\{\begin{array}{l}\left[\left(h_g-z_b\right)nD_{xx}\frac{\partial \hat{C}_g}{\partial x}+\left(h_g-z_b\right)nD_{xy}\frac{\partial \hat{C}_g}{\partial y}\right]N_i n_x+\\ \left[\left(h_g-z_b\right)nD_{yx}\frac{\partial \hat{C}_g}{\partial x}+\left(h_g-z_b\right)nD_{yy}\frac{\partial \hat{C}_g}{\partial y}\right]N_i n_y\end{array}\right\}d\Gamma$$
$$+\iint_{\Omega}\left\{\begin{array}{l}\left[\left(h_g-z_b\right)nD_{xx}\frac{\partial \hat{C}_g}{\partial x}+\left(h_g-z_b\right)nD_{xy}\frac{\partial \hat{C}_g}{\partial y}\right]\frac{\partial N_i}{\partial x}\\ \left[\left(h_g-z_b\right)nD_{yx}\frac{\partial \hat{C}_g}{\partial x}+\left(h_g-z_b\right)nD_{yy}\frac{\partial \hat{C}_g}{\partial y}\right]\frac{\partial N_i}{\partial y}\end{array}\right\}d\Omega$$
$$+\iint_{\Omega}\left\{\begin{array}{l}nR_d\left(h_g-z_b\right)\frac{\partial \hat{C}_g}{\partial t}+\left(h_g-z_b\right)q_x\frac{\partial \hat{C}_g}{\partial x}+\left(h_g-z_b\right)q_y\frac{\partial \hat{C}_g}{\partial y}\\ +I\left(C_I^*-\hat{C}_g\right)+\lambda nR_d\left(h_g-z_b\right)\hat{C}_g+K_w n\left(h_g-z_b\right)\hat{C}_g-\hat{C}_g S_y\frac{\partial h_g}{\partial t}\\ +\sum_{k=1}^{n_w}\left[Q_{w,k}\left(C_{w,k}^*-\hat{C}_g\right)\delta\left(x-x_{w,k}\right)\delta\left(y-y_{w,k}\right)\right]\\ +\sum_{m=1}^{n_r}\left[\int_0^1\left[q_{L1,m}\left(C_{L1,m}^*-\hat{C}_g\right)-n_{sed,m}D_{sed,m}\frac{C_{r,m}-\hat{C}_g}{m_{r,m}}w_{r,m}\right]\right.\\ \left.\left|\nabla\mathbf{g}\right|\delta\left(x-g_{x,m}(u)\right)\delta\left(y-g_{y,m}(u)\right)du\right]\end{array}\right\}N_i d\Omega=0 \qquad \text{(K.7)}$$

In the above form, the boundary integral can be written as a concentration dependent flux boundary condition, Γ_3:

$$\int_{\Gamma}(...)\,N_i d\Gamma = \int_{\Gamma_3}(...)\,N_i d\Gamma_3 \tag{K.8}$$

where it becomes the natural boundary conditions. In addition to the third type boundary, the domain might also have first type boundaries where the known stage is specified. Such boundaries form the essential boundary conditions. At the nodes of essential boundary conditions, the solution is known and the residual vanishes. The integral can be divided into two sections representing influx (source) and outflux (exit) portions such that:

$$\int_{\Gamma_3}(...)\,N_i d\Gamma_3 = \int_{\Gamma_3^{in}}(...)\,N_i d\Gamma_3^{in} + \int_{\Gamma_3^{out}}(...)\,N_i d\Gamma_3^{out} \tag{K.9}$$

Along the influx portion of Γ_3, the variable boundary condition is directly substituted in the corresponding integral to give:

$$\begin{aligned} -\int_{\Gamma_3^{in}} \left\{ \begin{array}{l} \left[\left(h_g - z_b\right) nD_{xx} \dfrac{\partial \hat{C}_g}{\partial x} + \left(h_g - z_b\right) nD_{xy} \dfrac{\partial \hat{C}_g}{\partial y} \right] N_i n_x + \\ \left[\left(h_g - z_b\right) nD_{yx} \dfrac{\partial \hat{C}_g}{\partial x} + \left(h_g - z_b\right) nD_{yy} \dfrac{\partial \hat{C}_g}{\partial y} \right] N_i n_y \end{array} \right\} d\Gamma_3^{in} \\ = \int_{\Gamma_3^{in}} \left[\left(h_g - z_b\right) q_v C_v \right] N_i d\Gamma_3^{in} - \int_{\Gamma_3^{in}} \mathbf{n} \cdot \left[\left(h_g - z_b\right) \mathbf{q} \hat{C}_g \right] N_i d\Gamma_3^{in} \end{aligned} \tag{K.10}$$

For the outflux or exit boundary, the integral is left as it is representing a free exit boundary condition:

$$-\int_{\Gamma_3^{out}} \left\{ \begin{array}{l} \left[\left(h_g - z_b\right) nD_{xx} \dfrac{\partial \hat{C}_g}{\partial x} + \left(h_g - z_b\right) nD_{xy} \dfrac{\partial \hat{C}_g}{\partial y} \right] N_i n_x + \\ \left[\left(h_g - z_b\right) nD_{yx} \dfrac{\partial \hat{C}_g}{\partial x} + \left(h_g - z_b\right) nD_{yy} \dfrac{\partial \hat{C}_g}{\partial y} \right] N_i n_y \end{array} \right\} d\Gamma_3^{out} = -\int_{\Gamma_3^{out}} \mathbf{n} \cdot \left(h_g - z_b\right) n\mathbf{D} \cdot \nabla \hat{C}_g \, N_i d\Gamma_3^{out} \tag{K.11}$$

Therefore, the total boundary integral can be written as:

$$\begin{aligned} &\int_{\Gamma_3^{in}} \left[\left(h_g - z_b\right) q_v C_v \right] N_i d\Gamma_3^{in} - \int_{\Gamma_3^{in}} \mathbf{n} \cdot \left[\left(h_g - z_b\right) \mathbf{q} \hat{C}_g \right] N_i d\Gamma_3^{in} - \int_{\Gamma_3^{out}} \mathbf{n} \cdot \left(h_g - z_b\right) n\mathbf{D} \cdot \nabla \hat{C}_g \, N_i d\Gamma_3^{out} \\ &+ \iint_{\Omega} \left\{ \begin{array}{l} \left[\left(h_g - z_b\right) nD_{xx} \dfrac{\partial \hat{C}_g}{\partial x} + \left(h_g - z_b\right) nD_{xy} \dfrac{\partial \hat{C}_g}{\partial y} \right] \dfrac{\partial N_i}{\partial x} \\ \left[\left(h_g - z_b\right) nD_{yx} \dfrac{\partial \hat{C}_g}{\partial x} + \left(h_g - z_b\right) nD_{yy} \dfrac{\partial \hat{C}_g}{\partial y} \right] \dfrac{\partial N_i}{\partial y} \end{array} \right\} d\Omega \\ &+ \iint_{\Omega} \left\{ \begin{array}{l} nR_d \left(h_g - z_b\right) \dfrac{\partial \hat{C}_g}{\partial t} + \left(h_g - z_b\right) q_x \dfrac{\partial \hat{C}_g}{\partial x} + \left(h_g - z_b\right) q_y \dfrac{\partial \hat{C}_g}{\partial y} \\ + I\left(C_I^* - \hat{C}_g\right) + \lambda nR_d \left(h_g - z_b\right) \hat{C}_g + K_w n \left(h_g - z_b\right) \hat{C}_g - \hat{C}_g S_y \dfrac{\partial h_g}{\partial t} \\ + \sum_{k=1}^{n_w} \left[Q_{w,k} \left(C_{w,k}^* - \hat{C}_g\right) \delta\left(x - x_{w,k}\right) \delta\left(y - y_{w,k}\right) \right] \\ + \sum_{m=1}^{n_r} \left[\int_0^1 \left[q_{L1,m} \left(C_{L1,m}^* - \hat{C}_g\right) - n_{sed,m} D_{sed,m} \dfrac{C_{r,m} - \hat{C}_g}{m_{r,m}} w_{r,m} \right] \right. \\ \left. \qquad \left| \nabla \mathbf{g} \right| \delta\left(x - g_{x,m}(u)\right) \delta\left(y - g_{y,m}(u)\right) du \right] \end{array} \right\} N_i d\Omega = 0 \end{aligned} \tag{K.12}$$

When each term is written explicitly, one would obtain the following:

$$\int_{\Gamma_3^{in}}\left[\left(h_g-z_b\right)q_vC_v\right]N_i d\Gamma_3^{in}-\int_{\Gamma_3^{in}}\mathbf{n}\cdot\left[\left(h_g-z_b\right)\mathbf{q}\hat{C}_g\right]N_i d\Gamma_3^{in}-\int_{\Gamma_3^{out}}\mathbf{n}\cdot\left(h_g-z_b\right)n\mathbf{D}\cdot\nabla\hat{C}_g\,N_i d\Gamma_3^{out}$$
$$+\iint_{\Omega}\left[\left(h_g-z_b\right)nD_{xx}\frac{\partial\hat{C}_g}{\partial x}+\left(h_g-z_b\right)nD_{xy}\frac{\partial\hat{C}_g}{\partial y}\right]\frac{\partial N_i}{\partial x}d\Omega$$
$$+\iint_{\Omega}\left[\left(h_g-z_b\right)nD_{yx}\frac{\partial\hat{C}_g}{\partial x}+\left(h_g-z_b\right)nD_{yy}\frac{\partial\hat{C}_g}{\partial y}\right]\frac{\partial N_i}{\partial y}d\Omega$$
$$+\iint_{\Omega}nR_d\left(h_g-z_b\right)\frac{\partial\hat{C}_g}{\partial t}N_i d\Omega+\iint_{\Omega}\left(h_g-z_b\right)q_x\frac{\partial\hat{C}_g}{\partial x}N_i d\Omega+\iint_{\Omega}\left(h_g-z_b\right)q_y\frac{\partial\hat{C}_g}{\partial y}N_i d\Omega$$
$$+\iint_{\Omega}I\left(C_I^*-\hat{C}_g\right)N_i d\Omega+\iint_{\Omega}\lambda nR_d\left(h_g-z_b\right)\hat{C}_gN_i d\Omega$$
$$+\iint_{\Omega}K_wn\left(h_g-z_b\right)\hat{C}_gN_i d\Omega-\iint_{\Omega}\hat{C}_gS_y\frac{\partial h_g}{\partial t}N_i d\Omega$$
$$+\iint_{\Omega}\sum_{k=1}^{n_w}\left[Q_{w,k}\left(C_{w,k}^*-\hat{C}_g\right)\delta\left(x-x_{w,k}\right)\delta\left(y-y_{w,k}\right)\right]N_i d\Omega$$
$$+\iint_{\Omega}\sum_{m=1}^{n_r}\left[\int_0^1\left[q_{L1,m}\left(C_{L1,m}^*-\hat{C}_g\right)-n_{sed,m}D_{sed,m}\frac{C_{r,m}-\hat{C}_g}{m_{r,m}}w_{r,m}\right]\left|\nabla\mathbf{g}\right|\delta\left(x-g_{x,m}(u)\right)\delta\left(y-g_{y,m}(u)\right)du\right]N_i d\Omega=0 \tag{K.13}$$

Finally, writing the scalar forms of the boundary integrals would yield the weak form of the equation:

$$
\begin{aligned}
&\int_{\Gamma_3^{in}} \left[\left(h_g - z_b\right) q_v C_v \right] N_i d\Gamma_3^{in} - \int_{\Gamma_3^{in}} \left[\left(h_g - z_b\right) \left(q_x n_x + q_y n_y\right) \hat{C}_g \right] N_i d\Gamma_3^{in} \\
&- \int_{\Gamma_3^{out}} \left\{ \begin{array}{l} \left[\left(h_g - z_b\right) nD_{xx} \dfrac{\partial \hat{C}_g}{\partial x} + \left(h_g - z_b\right) nD_{xy} \dfrac{\partial \hat{C}_g}{\partial y} \right] N_i n_x + \\ \left[\left(h_g - z_b\right) nD_{yx} \dfrac{\partial \hat{C}_g}{\partial x} + \left(h_g - z_b\right) nD_{yy} \dfrac{\partial \hat{C}_g}{\partial y} \right] N_i n_y \end{array} \right\} d\Gamma_3^{out} \\
&+ \iint_{\Omega} \left[\left(h_g - z_b\right) nD_{xx} \frac{\partial \hat{C}_g}{\partial x} + \left(h_g - z_b\right) nD_{xy} \frac{\partial \hat{C}_g}{\partial y} \right] \frac{\partial N_i}{\partial x} d\Omega \\
&+ \iint_{\Omega} \left[\left(h_g - z_b\right) nD_{yx} \frac{\partial \hat{C}_g}{\partial x} + \left(h_g - z_b\right) nD_{yy} \frac{\partial \hat{C}_g}{\partial y} \right] \frac{\partial N_i}{\partial y} d\Omega \\
&+ \iint_{\Omega} nR_d \left(h_g - z_b\right) \frac{\partial \hat{C}_g}{\partial t} N_i d\Omega + \iint_{\Omega} \left(h_g - z_b\right) q_x \frac{\partial \hat{C}_g}{\partial x} N_i d\Omega + \iint_{\Omega} \left(h_g - z_b\right) q_y \frac{\partial \hat{C}_g}{\partial y} N_i d\Omega \\
&+ \iint_{\Omega} I \left(C_I^* - \hat{C}_g\right) N_i d\Omega + \iint_{\Omega} \lambda nR_d \left(h_g - z_b\right) \hat{C}_g N_i d\Omega \\
&+ \iint_{\Omega} K_w n \left(h_g - z_b\right) \hat{C}_g N_i d\Omega - \iint_{\Omega} \hat{C}_g S_y \frac{\partial h_g}{\partial t} N_i d\Omega \\
&+ \iint_{\Omega} \sum_{k=1}^{n_w} \left[Q_{w,k} \left(C_{w,k}^* - \hat{C}_g\right) \delta\left(x - x_{w,k}\right) \delta\left(y - y_{w,k}\right) \right] N_i d\Omega \\
&+ \iint_{\Omega} \sum_{m=1}^{n_r} \left[\int_0^1 \left[q_{L1,m} \left(C_{L1,m}^* - \hat{C}_g\right) - n_{sed,m} D_{sed,m} \frac{C_{r,m} - \hat{C}_g}{m_{r,m}} w_{r,m} \right] \right. \\
&\qquad \left. \left|\nabla \mathbf{g}\right| \delta\left(x - g_{x,m}(u)\right) \delta\left(y - g_{y,m}(u)\right) du \right] N_i d\Omega = 0
\end{aligned}
\tag{K.14}
$$

When the approximate solution in (K.1) is substituted in the weak form, one would obtain the following expression:

$$
\begin{aligned}
&\int_{\Gamma_3^{in}}\left[\left(h_g-z_b\right)q_vC_v\right]N_i d\Gamma_3^{in}-\int_{\Gamma_3^{in}}\left[\left(h_g-z_b\right)\left(q_xn_x+q_yn_y\right)\left[\sum_{j=1}^{N}\left(\hat{C}_g\right)_j N_j\right]\right]N_i d\Gamma_3^{in}\\
&-\int_{\Gamma_3^{out}}\left\{\begin{array}{l}\left[\left(h_g-z_b\right)nD_{xx}\dfrac{\partial}{\partial x}\left[\sum_{j=1}^{N}\left(\hat{C}_g\right)_j N_j\right]+\left(h_g-z_b\right)nD_{xy}\dfrac{\partial}{\partial y}\left[\sum_{j=1}^{N}\left(\hat{C}_g\right)_j N_j\right]\right]N_i n_x+\\ \left[\left(h_g-z_b\right)nD_{yx}\dfrac{\partial}{\partial x}\left[\sum_{j=1}^{N}\left(\hat{C}_g\right)_j N_j\right]+\left(h_g-z_b\right)nD_{yy}\dfrac{\partial}{\partial y}\left[\sum_{j=1}^{N}\left(\hat{C}_g\right)_j N_j\right]\right]N_i n_y\end{array}\right\}d\Gamma_3^{out}\\
&+\iint_{\Omega}\left[\left(h_g-z_b\right)nD_{xx}\frac{\partial}{\partial x}\left[\sum_{j=1}^{N}\left(\hat{C}_g\right)_j N_j\right]+\left(h_g-z_b\right)nD_{xy}\frac{\partial}{\partial y}\left[\sum_{j=1}^{N}\left(\hat{C}_g\right)_j N_j\right]\right]\frac{\partial N_i}{\partial x}d\Omega\\
&+\iint_{\Omega}\left[\left(h_g-z_b\right)nD_{yx}\frac{\partial}{\partial x}\left[\sum_{j=1}^{N}\left(\hat{C}_g\right)_j N_j\right]+\left(h_g-z_b\right)nD_{yy}\frac{\partial}{\partial y}\left[\sum_{j=1}^{N}\left(\hat{C}_g\right)_j N_j\right]\right]\frac{\partial N_i}{\partial y}d\Omega\\
&+\iint_{\Omega}nR_d\left(h_g-z_b\right)\frac{\partial}{\partial t}\left[\sum_{j=1}^{N}\left(\hat{C}_g\right)_j N_j\right]N_i d\Omega+\iint_{\Omega}\left(h_g-z_b\right)q_x\frac{\partial}{\partial x}\left[\sum_{j=1}^{N}\left(\hat{C}_g\right)_j N_j\right]N_i d\Omega\\
&+\iint_{\Omega}\left(h_g-z_b\right)q_y\frac{\partial}{\partial y}\left[\sum_{j=1}^{N}\left(\hat{C}_g\right)_j N_j\right]N_i d\Omega+\iint_{\Omega}I\left(C_I^*-\left[\sum_{j=1}^{N}\left(\hat{C}_g\right)_j N_j\right]\right)N_i d\Omega\\
&+\iint_{\Omega}\lambda nR_d\left(h_g-z_b\right)\left[\sum_{j=1}^{N}\left(\hat{C}_g\right)_j N_j\right]N_i d\Omega+\iint_{\Omega}K_w n\left(h_g-z_b\right)\left[\sum_{j=1}^{N}\left(\hat{C}_g\right)_j N_j\right]N_i d\Omega\\
&-\iint_{\Omega}\left[\sum_{j=1}^{N}\left(\hat{C}_g\right)_j N_j\right]S_y\frac{\partial h_g}{\partial t}N_i d\Omega\\
&+\iint_{\Omega}\sum_{k=1}^{n_w}\left[Q_{w,k}\left(C_{w,k}^*-\left[\sum_{j=1}^{N}\left(\hat{C}_g\right)_j N_j\right]\right)\delta\left(x-x_{w,k}\right)\delta\left(y-y_{w,k}\right)\right]N_i d\Omega\\
&+\iint_{\Omega}\sum_{m=1}^{n_r}\left[\int_0^1\left[q_{L1,m}\left(C_{L1,m}^*-\left[\sum_{j=1}^{N}\left(\hat{C}_g\right)_j N_j\right]\right)-n_{sed,m}D_{sed,m}\frac{C_{r,m}-\left[\sum_{j=1}^{N}\left(\hat{C}_g\right)_j N_j\right]}{m_{r,m}}w_{r,m}\right]\right.\\
&\qquad\left.\left|\nabla\mathbf{g}\right|\delta\left(x-g_{x,m}(u)\right)\delta\left(y-g_{y,m}(u)\right)du\right]N_i d\Omega=0
\end{aligned}
$$

(K.15)

Since the nodal values are only a function of time and the shape functions are only a function of spatial coordinates, the above expression can be simplified by taking some of the terms out of the derivatives:

$$
\int_{\Gamma_3^{in}} \left[\left(h_g - z_b \right) q_v C_v \right] N_i d\Gamma_3^{in} - \int_{\Gamma_3^{in}} \left[\left(h_g - z_b \right) \left(q_x n_x + q_y n_y \right) \left[\sum_{j=1}^{N} \left(\hat{C}_g \right)_j N_j \right] \right] N_i d\Gamma_3^{in}
$$

$$
- \int_{\Gamma_3^{out}} \left\{ \begin{array}{l} \left[\left(h_g - z_b \right) n D_{xx} \sum_{j=1}^{N} \left(\hat{C}_g \right)_j \frac{\partial N_j}{\partial x} + \left(h_g - z_b \right) n D_{xy} \sum_{j=1}^{N} \left(\hat{C}_g \right)_j \frac{\partial N_j}{\partial y} \right] N_i n_x + \\ \left[\left(h_g - z_b \right) n D_{yx} \sum_{j=1}^{N} \left(\hat{C}_g \right)_j \frac{\partial N_j}{\partial x} + \left(h_g - z_b \right) n D_{yy} \sum_{j=1}^{N} \left(\hat{C}_g \right)_j \frac{\partial N_j}{\partial y} \right] N_i n_y \end{array} \right\} d\Gamma_3^{out}
$$

$$
+ \iint_{\Omega} \left[\left(h_g - z_b \right) n D_{xx} \sum_{j=1}^{N} \left(\hat{C}_g \right)_j \frac{\partial N_j}{\partial x} + \left(h_g - z_b \right) n D_{xy} \sum_{j=1}^{N} \left(\hat{C}_g \right)_j \frac{\partial N_j}{\partial y} \right] \frac{\partial N_i}{\partial x} d\Omega
$$

$$
+ \iint_{\Omega} \left[\left(h_g - z_b \right) n D_{yx} \sum_{j=1}^{N} \left(\hat{C}_g \right)_j \frac{\partial N_j}{\partial x} + \left(h_g - z_b \right) n D_{yy} \sum_{j=1}^{N} \left(\hat{C}_g \right)_j \frac{\partial N_j}{\partial y} \right] \frac{\partial N_i}{\partial y} d\Omega
$$

$$
+ \iint_{\Omega} n R_d \left(h_g - z_b \right) \sum_{j=1}^{N} N_j \frac{\partial \left(\hat{C}_g \right)_j}{\partial t} N_i d\Omega + \iint_{\Omega} \left(h_g - z_b \right) q_x \sum_{j=1}^{N} \left(\hat{C}_g \right)_j \frac{\partial N_j}{\partial x} N_i d\Omega
$$

$$
+ \iint_{\Omega} \left(h_g - z_b \right) q_y \sum_{j=1}^{N} \left(\hat{C}_g \right)_j \frac{\partial N_j}{\partial y} N_i d\Omega + \iint_{\Omega} I \left(C_I^* - \left[\sum_{j=1}^{N} \left(\hat{C}_g \right)_j N_j \right] \right) N_i d\Omega
$$

$$
+ \iint_{\Omega} \lambda n R_d \left(h_g - z_b \right) \left[\sum_{j=1}^{N} \left(\hat{C}_g \right)_j N_j \right] N_i d\Omega + \iint_{\Omega} K_w n \left(h_g - z_b \right) \left[\sum_{j=1}^{N} \left(\hat{C}_g \right)_j N_j \right] N_i d\Omega
$$

$$
- \iint_{\Omega} \left[\sum_{j=1}^{N} \left(\hat{C}_g \right)_j N_j \right] S_y \frac{\partial h_g}{\partial t} N_i d\Omega
$$

$$
+ \iint_{\Omega} \sum_{k=1}^{n_w} \left[Q_{w,k} \left(C_{w,k}^* - \left[\sum_{j=1}^{N} \left(\hat{C}_g \right)_j N_j \right] \right) \delta \left(x - x_{w,k} \right) \delta \left(y - y_{w,k} \right) \right] N_i d\Omega
$$

$$
+ \iint_{\Omega} \sum_{m=1}^{n_r} \left[\int_0^1 \left[q_{L1,m} \left(C_{L1,m}^* - \left[\sum_{j=1}^{N} \left(\hat{C}_g \right)_j N_j \right] \right) - n_{sed,m} D_{sed,m} \frac{C_{r,m} - \left[\sum_{j=1}^{N} \left(\hat{C}_g \right)_j N_j \right]}{m_{r,m}} w_{r,m} \right] \left| \nabla \mathbf{g} \right| \delta \left(x - g_{x,m}(u) \right) \delta \left(y - g_{y,m}(u) \right) du \right] N_i d\Omega
$$

$$
= 0
$$

(K.16)

Since N_i is defined such that it is non-zero only over elements adjacent to node *i*, the integrations may be performed piecewise over each element and subsequently summed.

$$\sum_{e=1}^{n_e}\left[\int_{\Gamma_3^{in,e}}\left[\left(h_g-z_b\right)q_vC_v\right]N_i d\Gamma_3^{in,e}\right]-\sum_{e=1}^{n_e}\left[\int_{\Gamma_3^{in,e}}\left[\left(h_g-z_b\right)\left(q_xn_x+q_yn_y\right)\sum_{j=1}^{N}\left(\hat{C}_g\right)_j\right]N_jN_i d\Gamma_3^{in,e}\right]$$

$$-\sum_{e=1}^{n_e}\left[\int_{\Gamma_3^{out,e}}\left(h_g-z_b\right)n\begin{Bmatrix}\left[D_{xx}\sum_{j=1}^{N}\left(\hat{C}_g\right)_j\frac{\partial N_j}{\partial x}+D_{xy}\sum_{j=1}^{N}\left(\hat{C}_g\right)_j\frac{\partial N_j}{\partial y}\right]N_in_x+\\ \left[D_{yx}\sum_{j=1}^{N}\left(\hat{C}_g\right)_j\frac{\partial N_j}{\partial x}+D_{yy}\sum_{j=1}^{N}\left(\hat{C}_g\right)_j\frac{\partial N_j}{\partial y}\right]N_in_y\end{Bmatrix}d\Gamma_3^{out,e}\right]$$

$$+\sum_{e=1}^{n_e}\left[\iint_{\Omega^e}\left(h_g-z_b\right)n\left[D_{xx}\sum_{j=1}^{N}\left(\hat{C}_g\right)_j\frac{\partial N_j}{\partial x}\frac{\partial N_i}{\partial x}+D_{xy}\sum_{j=1}^{N}\left(\hat{C}_g\right)_j\frac{\partial N_j}{\partial y}\frac{\partial N_i}{\partial x}\right]d\Omega^e\right]$$

$$+\sum_{e=1}^{n_e}\left[\iint_{\Omega^e}\left(h_g-z_b\right)n\left[D_{yx}\sum_{j=1}^{N}\left(\hat{C}_g\right)_j\frac{\partial N_j}{\partial x}\frac{\partial N_i}{\partial y}+D_{yy}\sum_{j=1}^{N}\left(\hat{C}_g\right)_j\frac{\partial N_j}{\partial y}\frac{\partial N_i}{\partial y}\right]d\Omega^e\right]$$

$$+\sum_{e=1}^{n_e}\left[\iint_{\Omega^e}nR_d\left(h_g-z_b\right)\sum_{j=1}^{N}\frac{\partial\left(\hat{C}_g\right)_j}{\partial t}N_jN_i d\Omega^e\right]$$

$$+\sum_{e=1}^{n_e}\left[\iint_{\Omega^e}\left(h_g-z_b\right)\left[q_x\sum_{j=1}^{N}\left(\hat{C}_g\right)_j\frac{\partial N_j}{\partial x}+q_y\sum_{j=1}^{N}\left(\hat{C}_g\right)_j\frac{\partial N_j}{\partial y}\right]N_i d\Omega^e\right]$$

$$+\sum_{e=1}^{n_e}\left[\iint_{\Omega^e}IC_I^*N_i d\Omega^e\right]-\sum_{e=1}^{n_e}\left[\iint_{\Omega^e}I\sum_{j=1}^{N}\left(\hat{C}_g\right)_jN_jN_i d\Omega^e\right]$$

$$+\sum_{e=1}^{n_e}\left[\iint_{\Omega^e}\lambda nR_d\left(h_g-z_b\right)\sum_{j=1}^{N}\left(\hat{C}_g\right)_jN_jN_i d\Omega^e\right]+\sum_{e=1}^{n_e}\left[\iint_{\Omega^e}K_wn\left(h_g-z_b\right)\sum_{j=1}^{N}\left(\hat{C}_g\right)_jN_jN_i d\Omega^e\right]$$

$$-\sum_{e=1}^{n_e}\left[\iint_{\Omega^e}\sum_{j=1}^{N}\left(\hat{C}_g\right)_jS_y\frac{\partial h_g}{\partial t}N_jN_i d\Omega^e\right]$$

$$+\sum_{e=1}^{n_e}\left[\iint_{\Omega^e}\sum_{k=1}^{n_w}\left[Q_{w,k}\left(C_{w,k}^*-\left[\sum_{j=1}^{N}\left(\hat{C}_g\right)_jN_j\right]\right)\delta\left(x-x_{w,k}\right)\delta\left(y-y_{w,k}\right)\right]N_i d\Omega^e\right]$$

$$+\sum_{e=1}^{n_e}\iint_{\Omega^e}\sum_{m=1}^{n_r}\left[\int_0^1\left[q_{L1,m}\left(C_{L1,m}^*-\left[\sum_{j=1}^{N}\left(\hat{C}_g\right)_jN_j\right]\right)-n_{sed,m}D_{sed,m}\frac{C_{r,m}-\left[\sum_{j=1}^{N}\left(\hat{C}_g\right)_jN_j\right]}{m_{r,m}}w_{r,m}\right]\left|\nabla\mathbf{g}\right|\delta\left(x-g_{x,m}(u)\right)\delta\left(y-g_{y,m}(u)\right)du\right]N_i d\Omega^e$$

$$=0 \qquad \text{(K.17)}$$

The element integrals can be written in matrix form:

$$\mathbf{S^e} \cdot \hat{\mathbf{C}}_\mathbf{g} + \mathbf{M^e} \cdot \frac{d\,\hat{\mathbf{C}}_\mathbf{g}}{dt} = \mathbf{F^e} \tag{K.18}$$

and the element matrices and vectors are defined as follows:

$$\begin{aligned}
\mathbf{S^e} = & -\int_{\Gamma_3^{in,e}} \left[\left(h_g - z_b\right)\left(q_x n_x + q_y n_y\right) \right] N_j N_i d\Gamma_3^{in,e} \\
& - \int_{\Gamma_3^{out,e}} \left(h_g - z_b\right) n \left\{ \left[D_{xx} \frac{\partial N_j}{\partial x} + D_{xy} \frac{\partial N_j}{\partial y} \right] N_i n_x + \left[D_{yx} \frac{\partial N_j}{\partial x} + D_{yy} \frac{\partial N_j}{\partial y} \right] N_i n_y \right\} d\Gamma_3^{out,e} \\
& + \iint_{\Omega^e} \left(h_g - z_b\right) n \left[D_{xx} \frac{\partial N_j}{\partial x}\frac{\partial N_i}{\partial x} + D_{xy} \frac{\partial N_j}{\partial y}\frac{\partial N_i}{\partial x} + D_{yx} \frac{\partial N_j}{\partial x}\frac{\partial N_i}{\partial y} + D_{yy} \frac{\partial N_j}{\partial y}\frac{\partial N_i}{\partial y} \right] d\Omega^e \\
& + \iint_{\Omega^e} \left(h_g - z_b\right) \left[q_x \frac{\partial N_j}{\partial x} + q_y \frac{\partial N_j}{\partial y} \right] N_i d\Omega^e \\
& - \iint_{\Omega^e} I N_j N_i d\Omega^e \\
& + \iint_{\Omega^e} \lambda n R_d \left(h_g - z_b\right) N_j N_i d\Omega^e \\
& + \iint_{\Omega^e} K_w n \left(h_g - z_b\right) N_j N_i d\Omega^e \\
& - \iint_{\Omega^e} S_y \frac{\partial h_g}{\partial t} N_j N_i d\Omega^e \\
& - \iint_{\Omega^e} \sum_{k=1}^{n_w} \left[Q_{w,k} N_j \delta\left(x - x_{w,k}\right) \delta\left(y - y_{w,k}\right) \right] N_i d\Omega^e \\
& + \iint_{\Omega^e} \sum_{m=1}^{n_r} \left[\int_0^1 \left[-q_{L1,m} N_j + n_{sed,m} D_{sed,m} \frac{w_{r,m}}{m_{r,m}} N_j \right] \left|\nabla \mathbf{g}\right| \delta\left(x - g_{x,m}(u)\right) \delta\left(y - g_{y,m}(u)\right) du \right] N_i d\Omega^e
\end{aligned} \tag{K.19}$$

$$\mathbf{M^e} = \iint_{\Omega^e} n R_d \left(h_g - z_b\right) N_j N_i d\Omega^e \tag{K.20}$$

$$
\begin{aligned}
\mathbf{F^e} = & -\int_{\Gamma_3^{in,e}} \left[\left(h_g - z_b \right) q_v C_v \right] N_i d\Gamma_3^{in,e} \\
& - \iint_{\Omega^e} IC_I^* N_i d\Omega^e \\
& - \iint_{\Omega^e} \sum_{k=1}^{n_w} \left[Q_{w,k} C_{w,k}^* \delta\left(x - x_{w,k} \right) \delta\left(y - y_{w,k} \right) \right] N_i d\Omega^e \\
& - \iint_{\Omega^e} \sum_{m=1}^{n_r} \left[\int_0^1 \left[q_{L1,m} C_{L1,m}^* - n_{sed,m} D_{sed,m} \frac{w_{r,m}}{m_{r,m}} C_{r,m} \right] \right. \\
& \qquad \left. \left| \nabla \mathbf{g} \right| \delta\left(x - g_{x,m}(u) \right) \delta\left(y - g_{y,m}(u) \right) du \right] N_i d\Omega^e
\end{aligned}
\tag{K.21}
$$

Finally, the global assembly of these matrices would yield the following matrix equation:

$$
\mathbf{S} \cdot \hat{\mathbf{C}}_\mathbf{g} + \mathbf{M} \cdot \frac{d \hat{\mathbf{C}}_\mathbf{g}}{dt} = \mathbf{F} \tag{K.22}
$$

where **S**, **M** and **F** is generally known as stiffness matrix, mass matrix and load vector, respectively, from the structural mechanics analogy.

APPENDIX L

DERIVATION OF ELEMENT INTEGRAL EQUATIONS FOR GROUNDWATER CONTAMINANT TRANSPORT

APPENDIX L

DERIVATION OF ELEMENT INTEGRAL EQUATIONS FOR GROUNDWATER CONTAMINANT TRANSPORT

The key point in finite element analysis is the derivation of element matrices and vectors that are obtained as a result of element level integrations. These element level matrices and vectors are then later assembled sequentially to obtain their global counterparts. In this study, the element matrices and vectors are [4X4] and {4X1} systems, respectively, since four-nodal linear quadrilateral elements are used to discretize the domain. In what follows first the evaluation of element domain integrals are discussed followed by the discussion of element boundary integrals. Each integral given in equations (K.19), (K.20) and (K.21) are split and written separately with a bullet. They are analyzed such that a procedure for their numerical evaluation is presented.

Derivation of Element Matrices and Vectors within the Domain

For all elements in the domain, a series of integrals presented in (K.19), (K.20) and (K.21) are evaluated to obtain the members of the [4X4] element stiffness and mass

matrices and {4X1} element load vector. Hence, in what follows, each integral is analyzed individually in which subscripts *i* and *j* run from 1 to 4.

- $$\iint_{\Omega^e} \left(h_g - z_b\right) n \left[D_{xx} \frac{\partial N_j}{\partial x} \frac{\partial N_i}{\partial x} + D_{xy} \frac{\partial N_j}{\partial y} \frac{\partial N_i}{\partial x} + D_{yx} \frac{\partial N_j}{\partial x} \frac{\partial N_i}{\partial y} + D_{yy} \frac{\partial N_j}{\partial y} \frac{\partial N_i}{\partial y} \right] d\Omega^e$$

This integral is associated with the dispersive flux term in *x*- and *y*- directions due to the change in contaminant concentration *x*- and *y*- directions as shown in equation (K.19). The basic assumption is that dispersion coefficients, porosity, and aquifer thickness are taken to be constant over an element. Therefore, all of these terms can be taken out of the integral and the integral is separated into its components.

$$\begin{aligned} &\left(h_g - z_b\right) n D_{xx} \iint_{\Omega^e} \frac{\partial N_j}{\partial x} \frac{\partial N_i}{\partial x} d\Omega^e + \left(h_g - z_b\right) n D_{xy} \iint_{\Omega^e} \frac{\partial N_j}{\partial y} \frac{\partial N_i}{\partial x} d\Omega^e \\ &+ \left(h_g - z_b\right) n D_{yx} \iint_{\Omega^e} \frac{\partial N_j}{\partial x} \frac{\partial N_i}{\partial y} d\Omega^e + \left(h_g - z_b\right) n D_{yy} \iint_{\Omega^e} \frac{\partial N_j}{\partial y} \frac{\partial N_i}{\partial y} d\Omega^e \end{aligned} \tag{L.1}$$

Each integral in (L.1) could then be written in local coordinates using the determinant of the Jacobian matrix and the master element concept. At this stage, it is important to transform the partial derivatives with respect to the global coordinates to the partial derivatives with respect to the local coordinates. For example, the derivatives in the first integral could be written as follows as using the chain rule of differentiation and the transformation matrix:

$$\frac{\partial N_i}{\partial x} = \frac{1}{|J|}\left[\left(\sum_{k=1}^{4} y_k \frac{\partial N_k}{\partial \eta}\right)\frac{\partial N_i}{\partial \xi} - \left(\sum_{k=1}^{4} y_k \frac{\partial N_k}{\partial \xi}\right)\frac{\partial N_i}{\partial \eta}\right]$$
$$\frac{\partial N_j}{\partial x} = \frac{1}{|J|}\left[\left(\sum_{k=1}^{4} y_k \frac{\partial N_k}{\partial \eta}\right)\frac{\partial N_j}{\partial \xi} - \left(\sum_{k=1}^{4} y_k \frac{\partial N_k}{\partial \xi}\right)\frac{\partial N_j}{\partial \eta}\right] \quad \text{(L.2)}$$

In these two equations, all the derivatives are simple partials of the shape functions with respect to local coordinates and can be computed easily. Substituting these two derivatives and writing the integral in terms of local coordinates, one would obtain:

$$\iint_{\Omega^e} \frac{\partial N_j}{\partial x}\frac{\partial N_i}{\partial x} d\Omega^e = \int_{-1}^{1}\int_{-1}^{1} \left\{ \begin{array}{l} \frac{1}{|J|}\left[\left(\sum_{k=1}^{4} y_k \frac{\partial N_k}{\partial \eta}\right)\frac{\partial N_i}{\partial \xi} - \left(\sum_{k=1}^{4} y_k \frac{\partial N_k}{\partial \xi}\right)\frac{\partial N_i}{\partial \eta}\right] * \\ \frac{1}{|J|}\left[\left(\sum_{k=1}^{4} y_k \frac{\partial N_k}{\partial \eta}\right)\frac{\partial N_j}{\partial \xi} - \left(\sum_{k=1}^{4} y_k \frac{\partial N_k}{\partial \xi}\right)\frac{\partial N_j}{\partial \eta}\right] \end{array} \right\} |J| d\xi d\eta \quad \text{(L.3)}$$

If the whole expression inside the integral is simplified and written as some function *f*:

$$f(\xi,\eta) = \frac{1}{|J|}\left[\left(\sum_{k=1}^{4} y_k \frac{\partial N_k}{\partial \eta}\right)\frac{\partial N_i}{\partial \xi} - \left(\sum_{k=1}^{4} y_k \frac{\partial N_k}{\partial \xi}\right)\frac{\partial N_i}{\partial \eta}\right] * \left[\left(\sum_{k=1}^{4} y_k \frac{\partial N_k}{\partial \eta}\right)\frac{\partial N_j}{\partial \xi} - \left(\sum_{k=1}^{4} y_k \frac{\partial N_k}{\partial \xi}\right)\frac{\partial N_j}{\partial \eta}\right] \quad \text{(L.4)}$$

the first integral simplifies to:

$$\iint_{\Omega^e} \frac{\partial N_j}{\partial x}\frac{\partial N_i}{\partial x} d\Omega^e = \int_{-1}^{1}\int_{-1}^{1} f(\xi,\eta) d\xi d\eta \quad \text{(L.5)}$$

and evaluated using the Gaussian quadrature:

$$\int_{-1}^{1}\int_{-1}^{1} f(\xi,\eta)d\xi d\eta = \sum_{l=1}^{NSP}\sum_{m=1}^{NSP} w_l w_m f(\xi_m,\eta_l) \tag{L.6}$$

When the above procedure is implemented for all integrals, one could obtain the final form of the dispersion flux integral. The difference between the integrals occurs from the differentiation with respect to x and y coordinates of the shape functions and their corresponding forms in local coordinates. Hence, the function f takes a different form for each of the four integrals such that:

$$f_1(\xi,\eta) = \frac{1}{|J|}\left[\left(\sum_{k=1}^{4} y_k \frac{\partial N_k}{\partial \eta}\right)\frac{\partial N_i}{\partial \xi} - \left(\sum_{k=1}^{4} y_k \frac{\partial N_k}{\partial \xi}\right)\frac{\partial N_i}{\partial \eta}\right] * \left[\left(\sum_{k=1}^{4} y_k \frac{\partial N_k}{\partial \eta}\right)\frac{\partial N_j}{\partial \xi} - \left(\sum_{k=1}^{4} y_k \frac{\partial N_k}{\partial \xi}\right)\frac{\partial N_j}{\partial \eta}\right] \tag{L.7}$$

$$f_2(\xi,\eta) = \frac{1}{|J|}\left[-\left(\sum_{k=1}^{4} x_k \frac{\partial N_k}{\partial \eta}\right)\frac{\partial N_j}{\partial \xi} + \left(\sum_{k=1}^{4} x_k \frac{\partial N_k}{\partial \xi}\right)\frac{\partial N_j}{\partial \eta}\right] * \left[\left(\sum_{k=1}^{4} y_k \frac{\partial N_k}{\partial \eta}\right)\frac{\partial N_i}{\partial \xi} - \left(\sum_{k=1}^{4} y_k \frac{\partial N_k}{\partial \xi}\right)\frac{\partial N_i}{\partial \eta}\right] \tag{L.8}$$

$$f_3(\xi,\eta) = \frac{1}{|J|}\left[\left(\sum_{k=1}^{4} y_k \frac{\partial N_k}{\partial \eta}\right)\frac{\partial N_j}{\partial \xi} - \left(\sum_{k=1}^{4} y_k \frac{\partial N_k}{\partial \xi}\right)\frac{\partial N_j}{\partial \eta}\right] * \left[-\left(\sum_{k=1}^{4} x_k \frac{\partial N_k}{\partial \eta}\right)\frac{\partial N_i}{\partial \xi} + \left(\sum_{k=1}^{4} x_k \frac{\partial N_k}{\partial \xi}\right)\frac{\partial N_i}{\partial \eta}\right] \tag{L.9}$$

$$f_4(\xi,\eta)=\frac{1}{|J|}\left[-\left(\sum_{k=1}^{4}x_k\frac{\partial N_k}{\partial \eta}\right)\frac{\partial N_j}{\partial \xi}+\left(\sum_{k=1}^{4}x_k\frac{\partial N_k}{\partial \xi}\right)\frac{\partial N_j}{\partial \eta}\right]* \left[-\left(\sum_{k=1}^{4}x_k\frac{\partial N_k}{\partial \eta}\right)\frac{\partial N_i}{\partial \xi}+\left(\sum_{k=1}^{4}x_k\frac{\partial N_k}{\partial \xi}\right)\frac{\partial N_i}{\partial \eta}\right] \tag{L.10}$$

where *f1*, *f2*, *f3* and *f4* represent the local functional form of each integrand of the original element integral. Finally, one could obtain the final integral when the corresponding values of the element averaged saturated thickness, porosity and dispersion coefficient are substituted in the original integral giving a final outcome of a [4X4] element matrix.

- $\iint_{\Omega^e} nR_d\left(h_g-z_b\right)N_jN_i d\Omega^e$

This integral is associated with the time rate of change of the contaminant concentration over an element as shown in equation (K.20). The basic assumption is that the retardation coefficient and aquifer porosity are constant over an element. Therefore, all of these terms can be taken out of the integral. Furthermore, the integral is written in local coordinates using the determinant of the Jacobian matrix and the master element concept.

$$\begin{aligned}\iint_{\Omega^e}\left(h_g-z_b\right)nR_dN_jN_i d\Omega^e &= \left(h_g-z_b\right)nR_d\iint_{\Omega^e}N_jN_i d\Omega^e \\ &= \left(h_g-z_b\right)nR_d\int_{-1}^{1}\int_{-1}^{1}N_j(\xi,\eta)N_i(\xi,\eta)|J|\,d\xi d\eta\end{aligned} \tag{L.11}$$

If the integral is evaluated using the Gaussian quadrature, one would obtain:

$$\int_{-1}^{1}\int_{-1}^{1} N_j(\xi,\eta)N_i(\xi,\eta)|J|d\xi d\eta = \sum_{l=1}^{NSP}\sum_{m=1}^{NSP} w_l w_m N_j(\xi_m,\eta_l)N_i(\xi_m,\eta_n)|J(\xi_m,\eta_l)| \quad \text{(L.12)}$$

Finally, the element matrix is written using the above formula and substituting the corresponding values of aquifer thickness, porosity and retardation coefficient. The final outcome of the integral is a [4X4] matrix from each element.

- $\iint_{\Omega^e}(h_g - z_b)\left[q_x\frac{\partial N_j}{\partial x} + q_y\frac{\partial N_j}{\partial y}\right]N_i d\Omega^e$

This integral is associated with the convective flux term in *x*- and *y*- directions as shown in equation (K.19). The basic assumption is that the flux term and the aquifer thickness are taken to be constant values over the element. Therefore, both of these terms can be taken out of the integral and the integral is separated into its components.

$$(h_g - z_b)q_x\iint_{\Omega^e}\frac{\partial N_j}{\partial x}N_i d\Omega^e + (h_g - z_b)q_y\iint_{\Omega^e}\frac{\partial N_j}{\partial y}N_i d\Omega^e \quad \text{(L.13)}$$

Each integral in (L.13) could then be written in local coordinates using the determinant of the Jacobian matrix and the master element concept. At this stage, it is important to transform the partial derivatives with respect to the global coordinates to the partial derivatives with respect to the local coordinates. For example, the derivative in the first

integral could be written as follows as using the chain rule of differentiation and the transformation matrix:

$$\frac{\partial N_j}{\partial x} = \frac{1}{|J|}\left[\left(\sum_{k=1}^{4} y_k \frac{\partial N_k}{\partial \eta}\right)\frac{\partial N_j}{\partial \xi} - \left(\sum_{k=1}^{4} y_k \frac{\partial N_k}{\partial \xi}\right)\frac{\partial N_j}{\partial \eta}\right] \tag{L.14}$$

In this equation, the derivatives are simple partials of the shape functions with respect to local coordinates and can be computed easily. Substituting these derivatives and writing the integral in terms of local coordinates, one would obtain:

$$\iint_{\Omega^e} \frac{\partial N_j}{\partial x} N_i d\Omega^e = \int_{-1}^{1}\int_{-1}^{1} \left\{\frac{1}{|J|}\left[\left(\sum_{k=1}^{4} y_k \frac{\partial N_k}{\partial \eta}\right)\frac{\partial N_j}{\partial \xi} - \left(\sum_{k=1}^{4} y_k \frac{\partial N_k}{\partial \xi}\right)\frac{\partial N_j}{\partial \eta}\right]\right\} N_i |J| d\xi d\eta \tag{L.15}$$

If the whole expression inside the integral is simplified and written as:

$$f(\xi,\eta) = \left[\left(\sum_{k=1}^{4} y_k \frac{\partial N_k}{\partial \eta}\right)\frac{\partial N_j}{\partial \xi} - \left(\sum_{k=1}^{4} y_k \frac{\partial N_k}{\partial \xi}\right)\frac{\partial N_j}{\partial \eta}\right] N_i \tag{L.16}$$

the integral simplifies to:

$$\iint_{\Omega^e} \frac{\partial N_j}{\partial x} N_i d\Omega^e = \int_{-1}^{1}\int_{-1}^{1} f(\xi,\eta) d\xi d\eta \tag{L.17}$$

and evaluated using the Gaussian quadrature:

$$\int_{-1}^{1}\int_{-1}^{1} f(\xi,\eta)d\xi d\eta = \sum_{l=1}^{NSP}\sum_{m=1}^{NSP} w_l w_m f(\xi_m,\eta_l) \qquad \text{(L.18)}$$

When the above procedure is implemented for the other integral, one could obtain the final form of the advective flux integral. The function *f* takes the following form for the second integral:

$$f(\xi,\eta) = \left[-\left(\sum_{k=1}^{4} x_k \frac{\partial N_k}{\partial \eta} \right) \frac{\partial N_j}{\partial \xi} + \left(\sum_{k=1}^{4} x_k \frac{\partial N_k}{\partial \xi} \right) \frac{\partial N_j}{\partial \eta} \right] N_i \qquad \text{(L.19)}$$

Finally, one could obtain the final integral when the corresponding values of that the flux term and the aquifer thickness are substituted in the original integral giving a final outcome of a [4X4] element matrix.

- $\iint_{\Omega^e} I N_j N_i d\Omega^e$

This integral is associated with the mass flux within the infiltrating water as shown in equation (K.19). The basic assumption is that the infiltration rate, *I*, is taken to be constant over the element. Therefore, this term can be taken out of the integral. Furthermore, the integral is written in local coordinates using the determinant of the Jacobian matrix and the master element concept.

$$\iint_{\Omega^e} IN_j N_i d\Omega^e = I\iint_{\Omega^e} N_j N_i d\Omega^e = I\int_{-1}^{1}\int_{-1}^{1} N_j(\xi,\eta)\, N_i(\xi,\eta)\left|J\right| d\xi d\eta \qquad \text{(L.20)}$$

If the integral is evaluated using the Gaussian quadrature, one would obtain:

$$\int_{-1}^{1}\int_{-1}^{1} N_j(\xi,\eta) N_i(\xi,\eta)\left|J\right| d\xi d\eta = \sum_{l=1}^{NSP}\sum_{m=1}^{NSP} w_l w_m N_j(\xi_m,\eta_l) N_i(\xi_m,\eta_n)\left|J(\xi_m,\eta_l)\right| \qquad \text{(L.21)}$$

Finally, the element matrix is written using the above formula and substituting the corresponding infiltration value. The final outcome of the integral is a [4X4] matrix from each element.

- $\iint_{\Omega^e} \lambda n R_d \left(h_g - z_b\right) N_j N_i d\Omega^e$

This integral is associated with the radioactive decay of the contaminant mass as shown in equation (K.19). The basic assumption is that the aquifer thickness, porosity, decay and retardation coefficients are all taken to be constant over the element. Therefore, these terms can be taken out of the integral. Furthermore, the integral is written in local coordinates using the determinant of the Jacobian matrix and the master element concept.

$$\iint_{\Omega^e} \lambda n R_d \left(h_g - z_b\right) N_j N_i d\Omega^e = \lambda n R_d \left(h_g - z_b\right) \iint_{\Omega^e} N_j N_i d\Omega^e$$
$$= \lambda n R_d \left(h_g - z_b\right) \int_{-1}^{1}\int_{-1}^{1} N_j(\xi,\eta) N_i(\xi,\eta) |J| d\xi d\eta \quad \text{(L.22)}$$

If the integral is evaluated using the Gaussian quadrature, one would obtain:

$$\int_{-1}^{1}\int_{-1}^{1} N_j(\xi,\eta) N_i(\xi,\eta) |J| d\xi d\eta = \sum_{l=1}^{NSP}\sum_{m=1}^{NSP} w_l w_m N_j(\xi_m,\eta_l) N_i(\xi_m,\eta_n) |J(\xi_m,\eta_l)| \quad \text{(L.23)}$$

Finally, the element matrix is written using the above formula and substituting the corresponding values of aquifer thickness, porosity, decay and retardation coefficient. The final outcome of the integral is a [4X4] matrix from each element.

- $\iint_{\Omega^e} K_w n \left(h_g - z_b\right) N_j N_i d\Omega^e$

This integral is associated with the biological decay of the contaminant mass as shown in equation (K.19). The basic assumption is that the aquifer thickness, porosity and decay coefficient are all taken to be constant over the element. Therefore, these terms can be taken out of the integral. Furthermore, the integral is written in local coordinates using the determinant of the Jacobian matrix and the master element concept.

$$\iint_{\Omega^e} K_w n\left(h_g - z_b\right) N_j N_i d\Omega^e = K_w n\left(h_g - z_b\right) \iint_{\Omega^e} N_j N_i d\Omega^e$$
$$= K_w n\left(h_g - z_b\right) \int_{-1}^{1}\int_{-1}^{1} N_j(\xi,\eta) N_i(\xi,\eta) |J| d\xi d\eta \quad \text{(L.24)}$$

If the integral is evaluated using the Gaussian quadrature, one would obtain:

$$\int_{-1}^{1}\int_{-1}^{1} N_j(\xi,\eta) N_i(\xi,\eta) |J| d\xi d\eta = \sum_{l=1}^{NSP}\sum_{m=1}^{NSP} w_l w_m N_j(\xi_m,\eta_l) N_i(\xi_m,\eta_n) |J(\xi_m,\eta_l)| \quad \text{(L.25)}$$

Finally, the element matrix is written using the above formula and substituting the corresponding values of aquifer thickness, porosity and decay coefficient. The final outcome of the integral is a [4X4] matrix from each element.

- $\iint_{\Omega^e} S_y \frac{\partial h_g}{\partial t} N_j N_i d\Omega^e$

This integral is associated with the mass stored within the aquifer as shown in equation (K.19). The basic assumption is that the specific yield and the time rate of change of the hydraulic head are taken to be constant over the element. Therefore, these terms can be taken out of the integral. Furthermore, the integral is written in local coordinates using the determinant of the Jacobian matrix and the master element concept.

$$\iint_{\Omega^e} S_y \frac{\partial h_g}{\partial t} N_j N_i d\Omega^e = S_y \frac{\partial h_g}{\partial t} \iint_{\Omega^e} N_j N_i d\Omega^e = S_y \frac{\partial h_g}{\partial t} \int_{-1}^{1}\int_{-1}^{1} N_j(\xi,\eta) N_i(\xi,\eta) |J| d\xi d\eta \quad \text{(L.26)}$$

If the integral is evaluated using the Gaussian quadrature, one would obtain:

$$\int_{-1}^{1}\int_{-1}^{1} N_j(\xi,\eta)N_i(\xi,\eta)|J|d\xi d\eta = \sum_{l=1}^{NSP}\sum_{m=1}^{NSP} w_l w_m N_j(\xi_m,\eta_l)N_i(\xi_m,\eta_n)|J(\xi_m,\eta_l)| \qquad \text{(L.27)}$$

Finally, the element matrix is written using the above formula and substituting the corresponding values for specific yield and time rate of change of hydraulic head. The final outcome of the integral is a [4X4] matrix from each element.

- $\iint_{\Omega^e} IC_I^* N_i d\Omega^e$

This integral is associated with the mass flux within the infiltrating water as shown in equation (K.21). The basic assumption is that the infiltration rate and the contaminant concentration in the infiltrating water are taken to be constant over the element. Therefore, these terms can be taken out of the integral. Furthermore, the integral is written in local coordinates using the determinant of the Jacobian matrix and the master element concept.

$$\iint_{\Omega^e} IC_I^* N_i d\Omega = IC_I^* \iint_{\Omega^e} N_i d\Omega = IC_I^* \int_{-1}^{1}\int_{-1}^{1} N_i(\xi,\eta)|J|d\xi d\eta \qquad \text{(L.28)}$$

If the integral is evaluated using the Gaussian quadrature, one would obtain:

$$\int_{-1}^{1}\int_{-1}^{1} N_i(\xi,\eta)|J|d\xi d\eta = \sum_{l=1}^{NSP}\sum_{m=1}^{NSP} w_l w_m N_i(\xi_m,\eta_l)|J(\xi_m,\eta_l)| \tag{L.29}$$

Finally, the element vector is written using the above formula and substituting the corresponding values of infiltration rate and the contaminant concentration in the infiltrating water. The final outcome of the integral is a {4X1} vector from each element.

- $\iint_{\Omega^e}\sum_{k=1}^{n_w}\left[Q_{w,k}N_j\delta\left(x-x_{w,k}\right)\delta\left(y-y_{w,k}\right)\right]N_i d\Omega^e$

This term represents the contribution of discharge/recharge wells in the domain as shown in equation (K.19). The basic assumption is that well locations coincide with the nodal points. For each well, the corresponding mass flux is included in the stiffness matrix. The domain integral of point source term associated with wells can be simplified using the sifting property of the Dirac-δ function. After implementing the property for each delta function, one would obtain:

$$\begin{aligned}\iint_{\Omega}\sum_{k=1}^{n_w}\left[Q_{w,k}\delta\left(x-x_{w,k}\right)\delta\left(y-y_{w,k}\right)\right]N_i d\Omega \\ = \sum_{k=1}^{n_w} Q_{w,k}\left(x_{w,k},y_{w,k}\right)N_i\left(x_{w,k},y_{w,k}\right)N_j\left(x_{w,k},y_{w,k}\right)\end{aligned} \tag{L.30}$$

At the well point, the basis function evaluates to 1 for that point and 0 for all other points. Therefore, the volumetric flux associated with the well is added to the diagonal element for the particular node:

$$\iint_{\Omega} \sum_{k=1}^{n_w} \left[Q_{w,k} \delta\left(x - x_{w,k}\right) \delta\left(y - y_{w,k}\right) \right] N_i d\Omega = \sum_{k=1}^{n_w} Q_{w,k} \left(x_{w,k}, y_{w,k}\right) \tag{L.31}$$

which is evaluated without any difficulty.

- $\iint_{\Omega^e} \sum_{k=1}^{n_w} \left[Q_{w,k} C^*_{w,k} \delta\left(x - x_{w,k}\right) \delta\left(y - y_{w,k}\right) \right] N_i d\Omega^e$

This term represents the contribution of discharge/recharge wells in the domain as shown in equation (K.21). The basic assumption is that well locations coincide with the nodal points. For each well, the corresponding mass flux is included in the load vector. The domain integral of point source term associated with wells can be simplified using the sifting property of the Dirac-δ function. After implementing the property for each delta function, one would obtain:

$$\begin{aligned} &\iint_{\Omega^e} \sum_{k=1}^{n_w} \left[Q_{w,k} C^*_{w,k} \delta\left(x - x_{w,k}\right) \delta\left(y - y_{w,k}\right) \right] N_i d\Omega^e \\ &\qquad = \sum_{k=1}^{n_w} \left[Q_{w,k} \left(x_{w,k}, y_{w,k}\right) C^*_{w,k} \left(x_{w,k}, y_{w,k}\right) \right] N_i \left(x_{w,k}, y_{w,k}\right) \end{aligned} \tag{L.32}$$

Since the interpolating function takes the value of 1 at the particular node, the expression simplifies to:

$$\iint_{\Omega^e} \sum_{k=1}^{n_w} \left[Q_{w,k} C^*_{w,k} \delta\left(x - x_{w,k}\right) \delta\left(y - y_{w,k}\right) \right] N_i d\Omega^e = \sum_{k=1}^{n_w} Q_{w,k} \left(x_{w,k}, y_{w,k}\right) C^*_{w,k} \left(x_{w,k}, y_{w,k}\right) \quad \text{(L.33)}$$

which is evaluated without any difficulty.

- $$\iint_{\Omega^e} \sum_{m=1}^{n_r} \left[\int_0^1 \left[q_{L1,m} - \frac{n_{sed,m} D_{sed,m} w_{r,m}}{m_{r,m}} \right] N_j N_i \left| \nabla \mathbf{g} \right| \delta\left(x - g_{x,m}(u)\right) \delta\left(y - g_{y,m}(u)\right) du \right] d\Omega^e$$

This integral represents the contribution of flux associated with a line source (i.e, river) as shown in equation (K.19). When linear quadrilateral elements are used to discretize the domain, the sides of the element are straight lines between two nodal points. Therefore, the river (i.e., the line source) becomes a combination of several straight line segments. Each of these segments is defined by the two end points such that the parametric equation of each line segment is written as:

$$\begin{aligned} x &= g_x(u) = x_A + \left(x_B - x_A\right) u \\ y &= g_y(u) = y_A + \left(y_B - y_A\right) u \end{aligned} \quad \text{(L.34)}$$

where points $A(x_A,y_A)$ and $B(x_B,y_B)$ define the global coordinates of the end points of a line segment. For a straight line, the gradient of parametric vector equation **g** is evaluated to be the length of the line segment:

$$|\nabla \mathbf{g}| = \sqrt{\left(\frac{dg_x}{du}\right)^2 + \left(\frac{dg_y}{du}\right)^2} = \sqrt{\left(x_B - x_A\right)^2 + \left(y_B - y_A\right)^2} = L_{AB} \tag{L.35}$$

Furthermore, it is assumed that the lateral flow, porosity, dispersion coefficient, thickness and wetted perimeter at the river/groundwater interface are constant along the element and hence can also be taken out of the integral. It is important to note that if these terms were not constant but were spatially variable such that they would be a function of u, then they could not be taken out of the integral and can only be integrated using numerical integration techniques. After these simplifications, the expression becomes:

$$\iint_{\Omega^e} \sum_{m=1}^{n_r} \left[L_{AB,e,m} \left(q_{L1} - \frac{n_{sed} D_{sed} w_r}{m_r} \right)_{m,e} \int_0^1 N_j N_i \delta\left(x - g_{x,m,e}(u)\right) \delta\left(y - g_{y,m,e}(u)\right) du \right] d\Omega^e \tag{L.36}$$

Since the shape functions are not a function of the parameter u, they can also be taken out of the integral to give:

$$\iint_{\Omega^e} \sum_{m=1}^{n_r} \left[L_{AB,e,m} \left(q_{L1} - \frac{n_{sed} D_{sed} w_r}{m_r} \right)_{m,e} N_j N_i \int_0^1 \delta\left(x - g_{x,m,e}(u)\right) \delta\left(y - g_{y,m,e}(u)\right) du \right] d\Omega^e \tag{L.37}$$

The next step is to perform the integration over the parameter u that can be done using the sifting property of Dirac-δ function. The integral with respect to the parameter u can be performed with either one of the Dirac-δ expressions using the sifting property of the function. After substituting the expressions for g_x and g_y given in equation (L.34), the integral becomes:

$$\int_0^1 \delta\left(x - x_{A,e,m} + \left(x_{A,e,m} - x_{B,e,m}\right)u\right)\delta\left(y - y_{A,e,m} + \left(y_{A,e,m} - y_{B,e,m}\right)u\right)du \qquad \text{(L.38)}$$

If the x-component is selected to perform the integration, the y-component of the Dirac-δ function can be written as some function $h(u)$ such that the integral becomes:

$$\int_0^1 h(u)\,\delta\left(x - x_{A,e,m} + \left(x_{A,e,m} - x_{B,e,m}\right)u\right)du \qquad \text{(L.39)}$$

The expression in the Dirac-δ function can now be rearranged to give:

$$\delta\left(x - x_{A,e,m} + \left(x_{A,e,m} - x_{B,e,m}\right)u\right) = \delta\left(\left(x_{A,e,m} - x_{B,e,m}\right)\left[\frac{x - x_{A,e,m}}{x_{A,e,m} - x_{B,e,m}} + u\right]\right) \qquad \text{(L.40)}$$

Since the term ($x_{A,e,m}$-$x_{B,e,m}$) is a constant, it can be written as:

$$\delta\left(x - x_{A,e,m} + \left(x_{A,e,m} - x_{B,e,m}\right)u\right) = \frac{1}{\left|x_{A,e,m} - x_{B,e,m}\right|}\delta\left(\left[\frac{x - x_{A,e,m}}{x_{A,e,m} - x_{B,e,m}} + u\right]\right) \qquad \text{(L.41)}$$

Rewriting the Dirac-δ function gives:

$$\delta\left(x-x_{A,e,m}+\left(x_{A,e,m}-x_{B,e,m}\right)u\right)=\frac{1}{\left|x_{A,e,m}-x_{B,e,m}\right|}\delta\left(u-\frac{x-x_{A,e,m}}{x_{B,e,m}-x_{A,e,m}}\right) \tag{L.42}$$

Since the derivative of the Dirac-δ function is the Heaviside step function by using the sifting property (Harris and Stocker, 1998), the integration over *u* yields:

$$\begin{aligned}\int_0^1 h(u)\frac{1}{\left|x_{A,e,m}-x_{B,e,m}\right|}\delta\left(u-\frac{x-x_{A,e,m}}{x_{B,e,m}-x_{A,e,m}}\right)du \\ =\frac{1}{\left|x_{A,e,m}-x_{B,e,m}\right|}h\left(\frac{x-x_{A,e,m}}{x_{B,e,m}-x_{A,e,m}}\right)H\left(u-\frac{x-x_{A,e,m}}{x_{B,e,m}-x_{A,e,m}}\right)\Bigg|_{u=0}^{u=1}\end{aligned} \tag{L.43}$$

where *H* is the Heaviside step function. Evaluating this function at two points gives:

$$H\left(u-\frac{x-x_{A,e,m}}{x_{B,e,m}-x_{A,e,m}}\right)\Bigg|_{t=0}^{t=1}=H\left(\frac{x_{B,e,m}-x}{x_{B,e,m}-x_{A,e,m}}\right)-H\left(\frac{x-x_{A,e,m}}{x_{B,e,m}-x_{A,e,m}}\right) \tag{L.44}$$

Along the line where $x_{A,e,m}\leq x\leq x_{B,e,m}$, the Heaviside function expression above is calculated to be 1, and 0 elsewhere. After evaluating the function *h(u)* and substituting, the integral with respect to parameter *u* yields:

$$\int_0^1 \delta\left(x - x_{A,e,m} + \left(x_{A,e,m} - x_{B,e,m}\right)u\right)\delta\left(y - y_{A,e,m} + \left(y_{A,e,m} - y_{B,e,m}\right)u\right)du$$
$$= \frac{1}{\left|x_{A,e,m} - x_{B,e,m}\right|}\delta\left(y - y_{A,e,m} + \left(y_{A,e,m} - y_{B,e,m}\right)\left(\frac{x - x_{A,e,m}}{x_{B,e,m} - x_{A,e,m}}\right)\right) \quad \text{(L.45)}$$

This term can now be substituted back in the general line source term to give:

$$\iint_{\Omega^e}\sum_{m=1}^{n_r}\left[L_{AB,e,m}\left(q_{L1} - \frac{n_{sed}D_{sed}w_r}{m_r}\right)_{m,e} N_j N_i \frac{1}{\left|x_{A,e,m} - x_{B,e,m}\right|} \delta\left(y - y_{A,e,m} + \left(y_{A,e,m} - y_{B,e,m}\right)\left(\frac{x - x_{A,e,m}}{x_{B,e,m} - x_{A,e,m}}\right)\right)\right]d\Omega^e \quad \text{(L.46)}$$

Taking the constant terms out of the domain integral and rearranging gives:

$$\frac{L_{AB,e,m}}{\left|x_{A,e,m} - x_{B,e,m}\right|}\iint_{\Omega^e}\left[\left(q_{L1} - \frac{n_{sed}D_{sed}w_r}{m_r}\right)_{m,e} N_j N_i \delta\left(y - y_{A,e,m} + \left(y_{A,e,m} - y_{B,e,m}\right)\left(\frac{x - x_{A,e,m}}{x_{B,e,m} - x_{A,e,m}}\right)\right)\right]d\Omega^e \quad \text{(L.47)}$$

Focusing on the domain integral, the expression in front of the Dirac-δ function is treated as a function and the element integral can be evaluated using the sifting property and the Heaviside function:

$$\iint_{\Omega^e}\left(q_{L1}-\frac{n_{sed}D_{sed}w_r}{m_r}\right)_{m,e}N_jN_i\delta\left(y-y_{A,e,m}+\left(y_{A,e,m}-y_{B,e,m}\right)\left(\frac{x-x_{A,e,m}}{x_{B,e,m}-x_{A,e,m}}\right)\right)d\Omega^e=$$

$$\int_{x^e}\left[\begin{array}{c}\left(q_{L1}-\frac{n_{sed}D_{sed}w_r}{m_r}\right)_{m,e}\left(x,y_{A,e,m}+\left(y_{B,e,m}-y_{A,e,m}\right)\left(\frac{x-x_{A,e,m}}{x_{B,e,m}-x_{A,e,m}}\right)\right)\\ N_j\left(x,y_{A,e,m}+\left(y_{B,e,m}-y_{A,e,m}\right)\left(\frac{x-x_{A,e,m}}{x_{B,e,m}-x_{A,e,m}}\right)\right)\\ N_i\left(x,y_{A,e,m}+\left(y_{B,e,m}-y_{A,e,m}\right)\left(\frac{x-x_{A,e,m}}{x_{B,e,m}-x_{A,e,m}}\right)\right)\end{array}\right]dx^e \quad \text{(L.48)}$$

where the parenthesis after the terms (q_{L1} - $n_{sed}D_{sed}w_r/m_r$), N_j and N_i show at which (x,y) position they are evaluated. In this equation, all terms are reduced to a single variable (i.e., x) that is valid along the line segment. Therefore, the integral with respect to x will be performed between the two end points of the line segment. If one assumes that the (q_{L1} - $n_{sed}D_{sed}w_r/m_r$) term is constant along the line segment and the functional parenthesis is dropped out for N_j and N_i for simplicity, one would obtain the following:

$$\left(q_{L1}-\frac{n_{sed}D_{sed}w_r}{m_r}\right)_{m,e}\int_{x_{A,e,m}}^{x_{B,e,m}}N_jN_idx^e \quad \text{(L.49)}$$

It is important to note that the shape functions are evaluated along the line segment. The integration of the shape functions along the line can be done using global coordinates or local coordinates. The result is a [2X2] matrix. Below, a sample integration using global coordinates is shown for the (1,1) position such that:

$$\int_{x_{A,e,m}}^{x_{B,e,m}} N_j N_i dx^e = \int_{x_{A,e,m}}^{x_{B,e,m}} \left(\frac{x - x_{A,e,m}}{x_{B,e,m} - x_{A,e,m}} \right) \left(\frac{x - x_{A,e,m}}{x_{B,e,m} - x_{A,e,m}} \right) dx^e = \frac{1}{3} \left(x_{B,e,m} - x_{A,e,m} \right) \quad \text{(L.50)}$$

The other positions follow the same idea. When the result of the integration is substituted in the original term and necessary simplifications are made, one would obtain:

$$\left(q_{L1} - \frac{n_{sed} D_{sed} w_r}{m_r} \right)_{m,e} \frac{L_{AB,e,m}}{3} \quad \text{(L.51)}$$

The coefficient of the length of the line changes for other positions such that it is 1/3 for positions i = j and 1/6 for i ≠ j.

- $$\iint_{\Omega^e} \sum_{m=1}^{n_r} \left[\int_0^1 \left[q_{L1,m} C^*_{L1,m} - n_{sed,m} D_{sed,m} \frac{w_{r,m}}{m_{r,m}} C_{r,m} \right] |\nabla \mathbf{g}| \, \delta\left(x - g_{x,m}(u) \right) \delta\left(y - g_{y,m}(u) \right) du \right] N_i d\Omega^e$$

This integral represents the contribution of mass flux associated with a line source (i.e, river) as shown in equation (K.21). Following the steps shown in the above integral, the problem reduces to the evaluation of the following integral:

$$\int_{x^e} N_i dx^e = \int_{x_{A,e,m}}^{x_{B,e,m}} N_i dx^e \quad \text{(L.52)}$$

The integration of the shape functions along the line can be done using global coordinates or local coordinates. The result is now a {2X1} vector. Below, the integration is shown for the (1,1) position such that:

$$\int_{x_{A,e,m}}^{x_{B,e,m}} N_i dx^e = \int_{x_{A,e,m}}^{x_{B,e,m}} \left(\frac{x - x_{A,e,m}}{x_{B,e,m} - x_{A,e,m}} \right) dx^e = \frac{1}{2}\left(x_{B,e,m} - x_{A,e,m}\right) \tag{L.53}$$

When the result of the integration is substituted in the original term, one would obtain:

$$\left[q_{L1,m} C^*_{L1,m} - n_{sed,m} D_{sed,m} \frac{\left(w_r\right)_m}{\left(m_r\right)_m} C_{r,m} \right]_{e,m} \frac{L_{AB,e,m}}{2} \tag{L.54}$$

The result is the same for the other position (2,1).

Derivation of Boundary Element Matrices and Vectors

Elements involving a boundary where a natural boundary condition is specified require the computation of boundary integrals. In these integrals, the integration is performed over the global boundary coordinate $d\Gamma^e$ along the boundary of the element. To simplify the integration process, the integrands must be written on the master element using the local coordinate system and must also be specified for a particular side of the element, which in turn requires that the shape functions are expressed for the particular boundary side of the element. As seen in Figure E.1, the boundary of the element can be any side of the quadrilateral depending on its position in the analysis domain. In order to

write the shape functions along each side, appropriate values of ξ and η are substituted for the general shape function formulae.

The global boundary coordinate Γ is mapped to a local boundary coordinate a ($-1 \le a \le 1$) for each side as shown in Figure E.1. The local coordinates holds the values ξ = a, η = -1 for side 1, ξ = 1, η = a for side 2, ξ = -a, η = 1 for side 3 and ξ = -1, η = -a for side 4. Using these values, one would obtain the following four shape functions for each side of the element:

$$\begin{aligned} SIDE \quad 1: \quad & \left[\frac{1-a}{2}, \frac{1+a}{2}, 0, 0\right] \\ SIDE \quad 2: \quad & \left[0, \frac{1-a}{2}, \frac{1+a}{2}, 0\right] \\ SIDE \quad 3: \quad & \left[0, 0, \frac{1-a}{2}, \frac{1+a}{2}\right] \\ SIDE \quad 4: \quad & \left[\frac{1+a}{2}, 0, 0, \frac{1-a}{2}\right] \end{aligned} \tag{L.55}$$

If the values of -1 and +1 are substituted for a in the above formulae, one would indeed obtain the fact that shape functions are equal to 1 at the node it is written for and 0 at all other nodes of the element. The integral over the element in global coordinates must also be transformed to an integral over the master element in local coordinates. This transformation introduces the determinant of the Jacobian between global boundary and local boundary coordinates.

$$\int_{\Gamma^e} f(B) d\Gamma^e = \int_{-1}^{1} f(a) |J_a| da \tag{L.56}$$

where J_a is the Jacobian of the boundary and the incremental boundary coordinate in global coordinate system, *dB*, can be written as follows according to the Figure E.2:

$$d\Gamma = \sqrt{(dx)^2 + (dy)^2} \tag{L.57}$$

Dividing both sides of this relationship with differential length, *da*, would give the following relationship between the global and local boundary coordinate:

$$\frac{d\Gamma}{da} = \sqrt{\left(\frac{dx}{da}\right)^2 + \left(\frac{dy}{da}\right)^2} \qquad \Rightarrow \qquad d\Gamma = J_a da \tag{L.58}$$

Therefore, the Jacobian of the boundary is written as:

$$J_a = \sqrt{\left(\frac{dx}{da}\right)^2 + \left(\frac{dy}{da}\right)^2} \tag{L.59}$$

where *da* will always take the value of 2 since it is the length of any side on the master element. Before we proceed with evaluating the boundary integrals, one must write the global derivatives of the shape functions in local boundary coordinate. In order to implement this transformation from global to local coordinate, derivatives of these shape functions with respect to local coordinates are evaluated using the chain rule of differentiation:

$$\frac{\partial N_i}{\partial x} = \frac{\partial N_i}{\partial a}\frac{\partial a}{\partial x}$$
$$\frac{\partial N_i}{\partial y} = \frac{\partial N_i}{\partial a}\frac{\partial a}{\partial y} \tag{L.60}$$

which can be represented in matrix form as:

$$\begin{bmatrix} \frac{\partial N_i}{\partial x} \\ \frac{\partial N_i}{\partial y} \end{bmatrix} = \frac{\partial N_i}{\partial a}\begin{bmatrix} \frac{\partial a}{\partial x} \\ \frac{\partial a}{\partial y} \end{bmatrix} \tag{L.61}$$

The derivatives of the shape functions with respect to local coordinates can easily be computed as follows:

$$\frac{\partial N_1}{\partial a} = -\frac{1}{2} \qquad \frac{\partial N_2}{\partial a} = +\frac{1}{2} \tag{L.62}$$

Moreover, one can simplify the transformation between global and local coordinates as:

$$x = x(a) = \sum_{i=1}^{2} x_i N_i(a)$$
$$y = y(a) = \sum_{i=1}^{2} y_i N_i(a) \tag{L.63}$$

When these expressions are written and simplified for *a*, one can obtain the derivatives with respect to *x* and *y* as:

$$\begin{bmatrix} \dfrac{\partial a}{\partial x} \\ \dfrac{\partial a}{\partial y} \end{bmatrix} = \begin{bmatrix} \dfrac{2}{x_2 - x_1} \\ \dfrac{2}{y_2 - y_1} \end{bmatrix} \tag{L.64}$$

It is now possible to complete the transformation of the shape function derivatives by using this matrix and the derivatives of the shape functions with respect to local coordinates. Using these fundamental concepts, the boundary integrals can be evaluated as follows:

- $\int\limits_{\Gamma_3^{in,e}} \left[\left(h_g - z_b \right) \left(q_x n_x + q_y n_y \right) \right] N_j N_i d\Gamma_3^{in,e}$

This integral represents the contribution of influx Cauchy boundary condition as shown in equation (K.19). The basic assumption is that aquifer thickness and Darcy velocity are constant over the boundary side of the element. Therefore, these terms can be taken out of the integral.

$$\int\limits_{\Gamma_3^{in,e}} \left[\left(h_g - z_b \right) \left(q_x n_x + q_y n_y \right) \right] N_j N_i d\Gamma_3^{in,e} = \left[\left(h_g - z_b \right) \left(q_x n_x + q_y n_y \right) \right] \int\limits_{\Gamma_3^{in,e}} N_j N_i d\Gamma_3^{in,e} \tag{L.65}$$

Furthermore, the integral is written in local coordinates using the determinant of the Jacobian matrix and the master element concept. At this stage, it is important to transform the shape functions with respect to the global coordinates to the shape function with respect to the local coordinates.

$$\int_{\Gamma_3^{in,e}} N_j N_i d\Gamma_3^{in,e} = \int_{-1}^{1} N_j N_i \left|J_a\right| da \tag{L.66}$$

and can further be simplified since the Jacobian is simply one half the length of the boundary side.

$$\int_{\Gamma_3^{in,e}} N_j N_i d\Gamma_3^{in,e} = \frac{L_e}{2} \int_{-1}^{1} N_j N_i da \tag{L.67}$$

It is important to note that this integral is simple and does not need numerical integration. It can be integrated exactly using the non-zero shape functions to obtain 2/6 for i = j and 1/6 for i ≠ j, regardless of the side and the associated nodes of the element. Therefore, the final outcome of this boundary integral is a [2X2] vector from each boundary element.

- $\int_{\Gamma_3^{in,e}} \left[\left(h_g - z_b\right) q_v C_v\right] N_i d\Gamma_3^{in,e}$

This integral represents the contribution of influx Cauchy boundary condition as shown in equation (K.21). The basic assumption is that the aquifer thickness, volumetric

inflow rate and contaminant concentration in the inflow are constant over the boundary of the element. Therefore, they can be taken out of the integral to yield:

$$\int_{\Gamma_3^{in,e}} \left[\left(h_g - z_b \right) q_v C_v \right] N_i d\Gamma_3^{in,e} = \left(h_g - z_b \right) q_v C_v \int_{\Gamma_3^{in,e}} N_i d\Gamma_3^{in,e} \tag{L.68}$$

Furthermore, the integral is written in local coordinates using the determinant of the Jacobian matrix and the master element concept. At this stage, it is important to transform the shape functions with respect to the global coordinates to the shape function with respect to the local coordinates.

$$\int_{\Gamma_3^{in,e}} N_i d\Gamma_3^{in,e} = \int_{-1}^{1} N_i \left| J_a \right| da \tag{L.69}$$

and can further be simplified since the Jacobian is simply one half the length of the boundary side.

$$\int_{\Gamma_3^{in,e}} N_i d\Gamma_3^{in,e} = \frac{L_e}{2} \int_{-1}^{1} N_i da \tag{L.70}$$

As before, this integral is simple and does not need numerical integration. It can be integrated exactly to obtain 1 regardless of the side and the associated nodes of the element. Therefore, the final outcome of this boundary integral is a {2X1} vector from each boundary element.

- $$\int_{\Gamma_3^{out,e}} \left(h_g - z_b\right) n \left\{ \left[D_{xx} \frac{\partial N_j}{\partial x} + D_{xy} \frac{\partial N_j}{\partial y} \right] N_i n_x + \left[D_{yx} \frac{\partial N_j}{\partial x} + D_{yy} \frac{\partial N_j}{\partial y} \right] N_i n_y \right\} d\Gamma_3^{out,e}$$

This integral represents the contribution of outflux Cauchy boundary condition as shown in equation (K.19). The basic assumption is that the aquifer thickness, porosity and dispersion coefficients are constant over the boundary of the element. Therefore, they can be taken out of the integral to yield:

$$\begin{aligned} &\left(h_g - z_b\right) n D_{xx} n_x \int_{\Gamma_3^{out,e}} \frac{\partial N_j}{\partial x} N_i d\Gamma_3^{out,e} + \left(h_g - z_b\right) n D_{xy} n_x \int_{\Gamma_3^{out,e}} \frac{\partial N_j}{\partial y} N_i d\Gamma_3^{out,e} \\ &+ \left(h_g - z_b\right) n D_{yx} n_y \int_{\Gamma_3^{out,e}} \frac{\partial N_j}{\partial x} N_i d\Gamma_3^{out,e} + \left(h_g - z_b\right) n D_{yy} n_y \int_{\Gamma_3^{out,e}} \frac{\partial N_j}{\partial y} N_i d\Gamma_3^{out,e} \end{aligned} \tag{L.71}$$

Furthermore, the integral is written in local coordinates using the determinant of the Jacobian matrix and the master element concept. At this stage, it is important to transform the partial derivatives with respect to the global coordinates to the partial derivatives with respect to the local coordinates. Using the chain rule of differentiation and the transformation matrix, the partial derivative of the shape functions is written as:

$$\begin{aligned} \frac{\partial N_j}{\partial x} &= \frac{\partial N_j}{\partial a} \frac{\partial a}{\partial x} \\ \frac{\partial N_j}{\partial y} &= \frac{\partial N_j}{\partial a} \frac{\partial a}{\partial y} \end{aligned} \tag{L.72}$$

In this equation, the derivatives are simple partials of the shape functions with respect to local coordinates as shown above. Substituting this expression and writing the first integral in terms of local coordinates, one would obtain:

$$\int_{\Gamma_3^{out,e}} \frac{\partial N_j}{\partial x} N_i d\Gamma_3^{out,e} = \int_{-1}^{1} \frac{\partial N_j}{\partial a} \frac{\partial a}{\partial x} N_i |J| da \tag{L.73}$$

If the whole expression inside the integral is simplified and written as:

$$f(a) = \frac{\partial N_j}{\partial a} \frac{\partial a}{\partial x} N_i |J| \tag{L.74}$$

the integral simplifies to:

$$\int_{\Gamma_3^{out,e}} \frac{\partial N_j}{\partial x} N_i d\Gamma_3^{out,e} = \int_{-1}^{1} f(a)\, da \tag{L.75}$$

and evaluated using the Gaussian quadrature:

$$\int_{-1}^{1} f(a) da = \sum_{m=1}^{NSP} w_m f(a) \tag{L.76}$$

When the above procedure is implemented for other integrals, one could obtain the final form of the outflux Cauchy boundary condition integral. The only difference between the

integrals occurs from the differentiation with respect to x and y coordinates of the shape functions and their corresponding forms in local coordinates. Hence, the function f takes one of the following two forms for integrals with shape function derivatives with respect to x- and y- directions such that:

$$f_1(a) = \frac{\partial N_j}{\partial a}\frac{\partial a}{\partial x} N_i |J| \tag{L.77}$$

$$f_2(a) = \frac{\partial N_j}{\partial a}\frac{\partial a}{\partial y} N_i |J| \tag{L.78}$$

Finally, the element matrix is written using the above formulae and substituting the saturated aquifer thickness, porosity and dispersion coefficients. The final outcome of the integral is a [2X2] element matrix.

REFERENCES

Abbott, M.B., Bathurst, J.C., Cunge, J.A., O'Connel, P.E. and Rasmussen, J. (1986a). "An introduction to the European Hydrological System – Systeme Hydrologique Europeen, "SHE", 1:History and philosophy of a physically-based, distributed modeling system." *Journal of Hydrology*, Vol. 87, pp. 45-59.

Abbott, M.B., Bathurst, J.C., Cunge, J.A., O'Connel, P.E. and Rasmussen, J. (1986b). "An introduction to the European Hydrological System – Systeme Hydrologique Europeen, "SHE", 2:Structure of a physically-based, distributed modeling system." *Journal of Hydrology*, Vol. 87, pp. 61-77.

Abbott, M.B. and Refsgaard, J.C. (1996). *Distributed Hydrological Modelling*. Kluwer Academic Publishers,321p.

Adam, Y. (1977). "Highly accurate compact implicit methods and boundary conditions." *Journal of Computational Physics*, Vol. 24, pp. 10-22.

Akan, A.O. (1987). "Pollutant washoff by overland flow." *Journal of Environmental Engineering,* Vol. 113, No. 4, pp. 811-823.

Akan, A.O. and Yen, B.C. (1981a). "Mathematical model of shallow water flow over porous media." *Journal of the Hydraulics Division, ASCE*, Vol. 107, No. HY4, pp. 479-494.

Akan, A.O. and Yen. B.C. (1981b). "Diffusion-wave flood routing in channel networks." *Journal of the Hydraulics Division, ASCE*, Vol. 107, No. HY 6, pp. 719-732.

Akanbi, A. A. and Katopodes, N. D. (1988). "Model for flood propagation on initially dry land." *Journal of Hydraulic Engineering,* Vol.114, No.7, pp. 689-706.

Amein, M. (1966). "Stream flow Routing on Computer by Characteristics." *Water Resources Research*, Vol. 2, No. 1, pp. 123-130.

Amein, M. and Chu, H.L. (1975). "Implicit Numerical Modeling of Unsteady Flows." *Journal of Hydraulics Division, ASCE*, Vol. 101, No. HY 6, pp. 93-108.

Amein, M. and Fang, C. S. (1970). "Implicit flood routing in natural channels." *Journal of the Hydraulics Division, ASCE*, Vol. 96, No. HY 12, pp. 2481-2500.

Aral, M.M. (1990). *Groundwater modeling in multilayer aquifers: Unsteady flow.* Lewis Publishers, Inc. 143p.

Aral, M.M., Mayer, P.G. and Maslia, M.L. (1980). *Mathematical modeling of aquatic dispersion of effluents.* Final Project Report No: E-20-604, School of Civil Engineering, Georgia Institute of Technology, Atlanta, Georgia, 87p.

Aral, M.M. and Gunduz, O. (2003). "Scale effects in large scale watershed modeling." In *Advances in Hydrology - Proceedings of the International Conference on Water and Environment: WE-2003*, edited by V.P. Singh and R.N. Yadava, Allied Publishers Pvt. Limited, pp. 37-51.

Baltzer, R.A. and Lai, C. (1968). "Computer simulation of unsteady flows in waterways." *Journal of Hydraulics Division, ASCE*, Vol. 94, No. HY 4, pp. 1083-1117.

Barry, D.A., Parlange, J.Y., Sander, G.C. and Sivaplan, M. (1993). "A class of exact solutions for Richards' equation." *Journal of Hydrology,* Vol. 142, pp. 29-46.

Basco, D.R. (1984). *An implicit, wiggle free and accurate upstream finite difference algorithm for the one dimensional transport-diffusion equation*. US Army Corps of Engineers, Environmental Impact Research Program*,* Miscalleneous Paper EL-84-4, 49p.

Bear, J. (1972). *Dynamics of Fluids in Porous Media*. Elsevier, Inc., New York, 764p.

Bear, J. (1979). *Hydraulics of Groundwater*. McGraw Hill, Inc., New York, 569p.

Bear, J. and Verrujit, A. (1987). *Modeling Groundwater Flow and Pollution.* D. Reidel Publishing Company, Dordrecht, Holland, 414p.

Bedford, K.W., Sykes, R.M. and Libicki, C. (1983). "Dynamic advective water quality model for rivers." *Journal of Environmental Engineering*, Vol. 109, No. 3, pp. 535-554.

Bencala, K.E. (1983). "Simulation of solute transport in a mountain pool-and-riffle stream with a kinetic mass transfer model for sorption." *Water Resources Research*, Vol. 19, No. 3, pp. 732-738.

Bencala, K.E. and Walters, R.A. (1983). "Simulation of solute transport in a mountain pool-riffle stream: a transient storage model." *Water Resources Research*, Vol. 19, No. 3, pp. 718-724.

Bentley, L.R. and Pinder, G.F. (1992). "Eulerian-Lagrangian solution of the vertically averaged groundwater transport equation." *Water Resources Research*, Vol. 28, No. 11, pp. 3011-3020.

Beven, K., Calver A. and Morris, E.M. (1987). "The Institute of Hydrology distributed model." *Institute of Hydrology Report:98,* Wallingford, U.K.

Binning, P. and Celia, M.A. (1995). "A finite volume Eulerian-Lagrangian localized adjoint method for solution of the contaminant transport equations in two dimensional multiphase flow systems." *Water Resources Research*, Vol. 32, No. 1, pp. 103-114.

Blandford, G.E. and Ormsbee, L.E. (1993). "A diffusion wave finite element model for channel networks." *Journal of Hydrology*, Vol.142, pp. 99-120.

Bradford, S.F. and Katopodes, N.D. (1998). "Non-hydrostatic model for surface irrigation." *Journal of Irrigation and Drainage Engineering*, Vol. 124, No. 4, pp. 200-212.

Bradford, S.F. and Sanders, B.F. (2002). "Finite-volume model for shallow-water flooding of arbitrary topography.", *Journal of Hydraulic Engineering*, Vol.128, No.3, pp. 289-298.

Brooks, R.H. and Corey, A.T. (1964). "Hydraulic properties of porous media." *Hydrology PaperNo:3*, Civil Engineering Department, Colorado State University, Fort Collins, CO.

Brunner, G.W. (2002). *HEC-RAS: River analysis system User's Manual.* U.S. Army Corps of Engineers Hydrologic Engineering Center, CPD-68, 420p.

Caldwell, M.M., Matson, P.A., Wessman, C. and Gamon, J.. (1993). "Prospects for scaling." In *Scaling Physiological Processes: Leaf to Globe*, edited by J.R. Ehleringer and C.B. Field, pp. 223-230.

Campbell, G.S. (1974). "A simple method for determining unsaturated conductivity from moisture retention data." *Soil Science*, Vol.117, pp. 311-314.

Carsel, R. F. and Parrish, R. S., (1988). "Developing joint probability distributions of soil water retention characteristics." *Water Resources Research*, Vol. 24, No. 5, pp. 755-769.

Celia, M.A., Bouloutas, E.T. & Zarba, R.L. (1990). "A general mass-conservative numerical solution for the unsaturated flow equation." *Water Resources Research*, Vol. 26, No. 7, pp. 1483-1496.

Chang, T.J., Hsu, M.H., Teng, W.H. and Huang, C.J. (2000). "A GIS-assisted distributed watershed model for simulating flooding and inundation." *Journal of the American Water Resources Association*, Vol. 36, No. 5, pp. 975-988.

Chapra, S.C. and Canale, R.P. (2002). *Numerical Methods for Engineers*, McGraw Hill, New York, NY, 926p.

Chaundhry, Y. M. and Contractor, D. N. (1973). "Application of implicit method to surges in channels." *Water Resources Research*, Vol. 9, No. 6, pp. 1605-1612.

Chen, Y. and Falconer, R.A. (1992). "Advection-diffusion modeling using the modified QUICK scheme." *International Journal for Numerical Methods in Fluids*, Vol. 15, pp. 1171-1196.

Chen, Y. and Falconer, R.A. (1994). "Modified forms of the third-order convection, second-order diffusion scheme for the advection-diffusion equation." *Advances in Water Resources*, Vol. 17, pp. 147-170.

Chen, J.M., Tan, Y.C. and Chen, C.H. (2003). "Analytical solutions of one-dimensional infiltration before and after poinding." *Hydrological Processes*, Vol. 17, pp. 815-822.

Choi, G.W. and Molinas, A. (1993). "Simultaneous solution algorithm for channel network modeling." *Water Resources Research*, Vol. 29, No. 2, pp. 321-328.

Chow, V.T. (1959). *Open Channel Hydraulics.* McGraw Hill Inc, 680p.

Chow, V.T., Ben-Zvi, A. (1973). "Hydrodynamic Modeling of Two-Dimensional Watershed Flow." *Journal of the Hydraulics Division, ASCE*, Vol.99, No. HY11, pp. 2023-2040.

Chu, P.C. and Fan, C. (1998). "A three-point combined compact difference scheme." *Journal of Computational Physics*, Vol. 140, pp. 370-399.

Chu, P.C. and Fan, C. (1999). "A three-point sixth order non-uniform combined compact difference scheme." *Journal of Computational Physics*, Vol. 148, pp. 663-674.

Clapp, R.B. and Hornberger, G.M. (1978). "Empirical equations for some hydraulic properties." *Water Resources Research*, Vol. 14, No. 4, pp. 601-604.

Cooley, R.L. and Moin, S.A. (1976). "Finite element solution of Sanint-Venant equations." *Journal of the Hydraulics Division, ASCE*, Vol.102, No. HY6, pp. 759-775.

Corwin, D.L. and Waggoner, B.L. (1990). *TETRANS: Solute transport modeling software user's guide (IBM- Compatible Version 1.5).* U.S. Salinity Laboratory, Agricultural Research Service, U.S. Department of Agriculture, Riverside, California, 120p.

DeLong, L.L. (1986). "Extension of the Unsteady One-Dimensional Open-Channel Flow Equations for Flow Simulation in Meandering Channels with Flood Plains." *Selected Papers in Hydrological Science,* U.S. Geological Survey Water Supply Paper 2220, pp. 101-105.

DeLong, L.L. (1989). "Mass Conservation: 1-D Open Channel Flow Equations." *Journal of Hydraulic Engineering, ASCE*, Vol. 115, pp. 263-269.

Deng, Z.Q., Singh, V.P. and Bengtsson, L. (2001). "Longitudinal dispersion coefficient in straight rivers." *Journal of Hydraulic Engineering,* Vol. 127, No. 11, pp. 919-927.

Di Giammarco, P., Giardino, P.T., Rametta, F. and Todini, E. (1994). "Integrated catchment modeling and meso-scale hydrology." In *Advances in Distributed Hydrology*, edited by R. Rosso, A. Peano, I. Becchi and G.A. Bemporad, Water Resources, Highland Ranch, Colorado, pp. 247-292.

Di Giammarco, P., Todini, E. & Lamberti, P. (1996). "A conservative finite elements approach to overland flow: the control volume finite element formulation." *Journal of Hydrology*, Vol. 175, pp. 267-291.

Dingman, S. L. (1994). *Physical Hydrology*. Prentice Hall, Inc., 575 p.

Donigian, A.S., Bicknell, B.R. and Imhoff, J.C. (1995). "Hydrological Simulation Program-Fortran." In *Computer Models of Watershed Hydrology*, edited by V.P. Singh, pp.395-442.

Dronkers, J.J. (1964). *Tidal Computations in Rivers and Coastal Waters.* North-Holland Publishing Company, Amsterdam, 518p.

Dutta, D., Herath, S. and Musiake, K. (2000). "Flood inundation simulation in a river basin using a physically-based distributed hydrologic model." *Hydrological Processes*, Vol.14, No.3, pp. 497-519.

Elder, J.W. (1959). "The dispersion of a marked fluid in turbulent shear flow." *Journal of Fluid Mechanics*, Vol. 5, No. 4, pp. 544-560.

El-Hames, A.S. and Richards, K.S. (1998). "An integrated, physically-based model for arid region flash flood prediction capable of simulating dynamic transmission loss." *Hydrological Processes*, Vol. 12, No. 8, pp. 1219-1232.

Engman, E. T. (1986). "Roughness Coefficients for Routing Surface Runoff." *Journal of Irrigation and Drainage Engineering*, Vol.112, No.1, pp. 39-53.

Esteves, M., Faucher, X., Galle, S. and Vauclin, M. (2000). "Overland flow and infiltration modeling for small plots during unsteady rain: Numerical results versus observed values." *Journal of Hydrology*, Vol. 228, pp. 265-282.

Ewen, J. Parkin, G and O'Connell, P.E. (2000). "SHETRAN: distributed river basin flow and transport modeling system." *Journal of Hydrologic Engineering,* Vol. 5, No. 3, pp. 250-258.

Falconer, R.A. and Liu, S. (1988). "Modeling solute transport using QUICK scheme." *Journal of Environmental Engineering*, Vol. 114, No. 1, pp. 3-20.

Faust, C.R., Sims, P.N., Spalding, C.P., Andersen, P.F. and Stephenson, D.E. (1990). *FTWORK: A three dimensional groundwater flow and solute transport code*. WRSC-RP-89-1085, Westinghouse Savannah River Company, Aiken, SC.

Feddes, R.A., Kabat, P., Van Bakel, P.J.T., Bronswijk J.J.B. and Halbertsma, J. (1988). "Modeling soil water dynamics in the unsaturated zone – State of the art." *Journal of Hydrology*, Vol. 100, pp. 69-111.

Feng, K. and Molz, F. J. (1997). "A 2-D, diffusion-based, wetland flow model." *Journal of Hydrology*, Vol.196, pp. 230-250

Fiedler, F.R. and Ramirez, J.A. (2000). "A numerical method for simulating discontinuous shallow flow over an infiltrating surface." *International Journal for Numerical Methods in Fluids,* Vol. 32, pp. 219-240.

Fischer, H.B. (1966). *Longitudinal dispersion in laboratory and natural streams.* Report No. KH-R-12, Keck Laboratory of Hydraulics and Water Resources, California Institute of Technology, Pasadena, California.

Fischer, H.B. (1968). "Dispersion predictions in natural streams." *Journal of the Sanitary Engineering Division, ASCE*, Vol. 94, No. SA5, pp. 927-943.

Fischer, H.B. (1975). "Discussion of 'Simple method for predicting dispersion in streams', by R.S. McQuivey and T.N. Keefer." *Journal of the Environmental Engineering Division, ASCE*, Vol. 101, No. EE3, pp. 453-455.

Fischer, H.B., List, E.J.., Koh, R.C.Y., Imberger, J. and Brooks, N.H. (1979). *Mixing in Inland and Coastal Waters.* Academic Press, NewYork, NY, 302p.

Fread, D. L. (1974). *Numerical properties of implicit four point finite difference equations of unsteady flow.* NOAA Technical Memo NWS HYDRO-18, U.S. Department of Commerce, National Weather Service, Silver Spring, Maryland.

Fread, D.L. (1976). "Flood Routing in Meandering Rivers with Flood Plains." *RIVERS '76: Symposium on Inland Waterways for Navigation, Flood Control and Water Diversions, August 10-12, 1976.* Colorado State University, Fort Collins, CO, Vol.1, pp.16-35.

Fread, D. L. (1985). "Chapter 14: Channel Routing." *Hydrological Forecasting,* edited by M. G. Anderson and T. P. Burt, John Wiley and Sons Ltd, pp. 437-503.

Fread, D.L. (1993). "Flow Routing." *Handbook of Hydrology*, edited by D.R. Maidment, McGraw-Hill, Inc. pp. 10.1-10.36.

Freeze, R.A. (1972a). "Role of subsurface flow in generating surface runoff: 1. Base flow contributions to channel flow." *Water Resources Research*, Vol. 8, No. 3, pp. 609-623.

Freeze, R.A. (1972b). "Role of subsurface flow in generating surface runoff: 2. Upstream source areas." *Water Resources Research*, Vol. 8, No. 5, pp. 1272-1283.

Frind, E.O. and Verge, M.J. (1978). "Three dimensional modeling of groundwater flow systems." *Water Resources Research*, Vol. 14, No. 5, pp. 844-856.

Gandolfi, C. and Savi, F. (2000). "A mathematical model for the coupled simulation of surface runoff and infiltration." *Journal of Agricultural Engineering Research*, Vol.75, pp. 49-55.

Garcia-Navarro, P, Playan, E. And Zapata, N. (2000). "Solute transport modeling in overland flow applied to fertigation." *Journal of Irrigation and Drainage Engineering*, Vol. 126, No. 1, pp. 33-40.

Geisdal, T. and Teigland, R. (1998). "Accuracy and stability of semi-implicit finite difference advection schemes." *Communications in Numerical Methods in Engineering*, Vol. 14, pp. 647-655.

Glass, J. and Rodi, W. (1982). "A higher order numerical scheme for scalar transport." *Computer Methods in Applied Mechanics and Engineering*, Vol. 31, pp. 337-358.

Gottardi, G. and Venutelli, M. (1993a). "RICHARDS: Computer model for the numerical simulation of one-dimensional infiltration into unsaturated soil." *Computers and Geosciences*, Vol. 19, No. 9, pp. 1239-1266.

Gottardi, G. and Venutelli, M. (1993b). "A control volume finite element model for two dimensional overland flow." *Advances in Water Resources,* Vol.16, pp. 277-284.

Gottardi, G. and Venutelli, M. (1997). "LANDFLOW: Computer program for the numerical simulation of two-dimensional overland flow." *Computers and Geosciences,* Vol.23, No. 1, pp. 77-89.

Govindaraju, R.S. and Kavvas, M.L. (1991). "Dynamics of moving boundary overland flows over infiltrating surfaces at hillslopes." *Water Resources Research*, Vol. 27, No. 8, pp. 1885-1898.

Grayson, R.B., Moore, I.D. and McHahon, T.A. (1992). "Physically-based hydrological modeling 1: A terrain-based model for investigative purposes." *Water Resources Research*, Vol. 28, No. 10. pp. 2639-2658.

Gunduz, O. and Aral, M.M. (2003a). *A simultaneous solution approach for coupled surface and subsurface flow modeling.* Report no: MESL-02-03, Multimedia Environmental Simulations Laboratory Report, School of Civil and Environmental Engineering, Georgia Institute of Technology, Atlanta, Georgia, 98p.

Gunduz, O. and Aral, M.M. (2003b). "Simultaneous solution of coupled surface water/groundwater flow systems." In *River Basin Management II,* edited by C.A. Brebbia, pp. 25-33.

Gunduz, O. and Aral, M.M. (2003c). "An integrated model of surface and subsurface flows." In *Water Resources Management II*, edited by C.A. Brebbia, pp. 367-376.

Gunduz, O. and Aral, M.M. (2004a). "A Dirac-delta function notation for source/sink terms in groundwater flow." *Journal of Hydrologic Engineering* (submitted).

Gunduz, O. and Aral, M.M. (2004b). "River networks and groundwater flow: A simultaneous solution of a coupled system." *Journal of Hydrology* (submitted).

Green, W.H. and Ampt, G.A. (1911). "Studies on soil physics: 1. Flow of air and water through soils." *Journal of Agricultural Science*, Vol. 4, pp. 1-24.

Harris, J.W. and Stocker H., 1998. *Handbook of Mathematics and Computational Science*. Springer-Verlag, Inc., New York, 1028p.

Havno, K., Madsen, M.N. and Dorge, J. (1995). "MIKE 11 – A generalized river modeling package." In *Computer Models of Watershed Hydrology*, edited by V.P. Singh, pp.733-782.

Heatwole, C.D., Shanholtz, V.O. and Ross, B.B. (1982). "Finite element model to describe overland flow on an infiltrating watershed." *Transactions of the ASAE,* Vol. 25. pp. 630-637.

Hills, R.G., Porro, I., Hudson, D.B. and Wierenga, P.J. (1989). "Modeling one-dimensional infiltration into very dry soils 1. Model development and evaluation." *Water Resources Research*, Vol. 25, No. 6, pp. 1259-1269.

Hirsch, R.S. (1975). "Higher order accurate difference solutions of fluid mechanics problems by a compact differencing technique." *Journal of Computational Physics*, Vol. 19, pp. 90-109.

Hogarth, W.L. and Parlange, J.Y. (2000). "Application and improvement if a recent approximate analytical solution of Richards' equation." *Water Resources Research*, Vol. 36, No. 7, pp. 1965-1968.

Holly, F.M.Jr. and Preissmann, A. (1977). "Accurate calculation of transport in two-dimensions." *Journal of Hydraulics Division ASCE*, Vol. 103, No. HY11, pp. 1259-1277.

Hong, L.D., Akiyama J. and Ura, M. (1994). "Efficient mass-conservative numerical solution for the two-dimensional unsaturated flow equation." *Journal of Hydroscience and Hydraulic Engineering*, Vol. 11, No. 2, pp. 1-18.

Hong, S. and Mostaghimi, S. (1997). "Comparison of 1-D and 2-D modeling of overland runoff and sediment transport." *Journal of the Americal Water Resources Association,* Vol. 33, No. 5, pp. 1103-1116.

Horton, R.E., 1933. "The role of infiltration in the hydrologic cycle." *Transactions of the American Geophysical Union*, Vol. 14, pp. 446-460.

Hromadka II, T. V. and Lai, C. (1985). "Solving the two dimensional diffusion flow model." *Proceedings of the Speciality Conference* Sponsored by ASCE, Lake Buena Vista, FL. pp.555-562.

Hromadka II, T. V. and Yen, C. C. (1986). "A Diffusion Hydrodynamic model (DHM)." *Advances in Water Resources*, Vol.9, No.9, pp.118-170.

Huang, K., Mohanty B.P. and van Genuchten, M.Th. (1996). "A new convergence criterion for the modified Picard iteration method to solve the variably saturated flow equation." *Journal of Hydrology*, Vol. 260, pp. 69-91.

Huyakorn, P.S., Mercer, J.W. and Ward, D.S. (1985). "Finite element matrix and mass balance computational schemes for transport in variably saturated porous media." *Water Resources Research*, Vol. 21, No. 3, pp. 346-358.

Huyakorn, P.S., Jones, B.G. and Andersen, P.F. (1986). "Finite element algorithms for simulating three dimensional groundwater flow and solute transport in multilayer systems." *Water Resources Research*, Vol. 22, No. 3. pp. 361-374.

Islam, M.R. and Chaudhry, M.H. (1997). "Numerical solution of transport equation for applications in environmental hydraulics and hydrology". *Journal of Hydrology*, Vol. 191, pp. 106-121.

Iwasa, Y. and Aya, S. (1991). "Predicting longitudinal dispersion coefficient in open channel flows." *Proceedings of the International Symposium on Environmental Hydrology*, *HongKong*, pp. 505-510.

Izzard, C.F. (1946). "Hydraulics of runoff from developed surfaces." *Highway Research Board, Proceedings of the 26th Annual Meeting*, pp. 129-150.

James, W.P. and Kim, K.W. (1990). "A distributed dynamic watershed model." *Water Resources Bulletin*, Vol. 26, No. 4, pp. 587-596.

Jaque, D.T. and Ball, J.E. (1994). "Numerical simulation of advective-diffusive mass transport." *Journal of Hydroscience and Hydraulic Engineering*, Vol. 11, No. 2, pp. 49-56.

Jarvis, P.G. (1995). "Scaling processes and problems." *Plant, Cell, and Environment*, Vol. 18, pp. 1079-1089.

Jha, R., Herath, S. and Musiake, K. (2000). "River network solution for a distributed hydrological model and applications." *Hydrological Processes*, Vol. 14, pp. 575-592.

Jobson, H.E. (1987). "Lagrangian model of nitrogen kinetics in the Chattahoochee River." *Journal of Environmental Engineering*, Vol. 113, No. 2, pp. 223-242.

Judah, O.M., Shanholtz, V.O. and Contractor, D.N. (1975). "Finite element simulation of flood hydrographs." *Transactions of the ASAE,* Vol. 18, No. 3, pp. 518-522.

Julien, P.Y., Saghafian B. and Ogden, F.L. (1995). "Raster-based hydrological modeling of spatially-varied surface runoff." *Water Resources Bulletin*, Vol. 31, No. 3, pp. 523-536.

Kashefipour, S.M. and Falconer, R.A. (2002). "Longitudinal dispersion coefficients in natural channels." *Water Research*, Vol. 36, pp. 1596-1608.

Katopodes, N. and Strelkoff, T. (1979). "Two-dimensional shallow water wave models." *Journal of Engineering Mechanics ASCE,* Vol. 105, No. EM2, pp. 317-334.

Kawahara, M. and Yokoyama, T. (1980). "Finite element method for direct runoff flow." *Journal of the Hydraulics Division, ASCE*, Vol.106, No. HY4, pp. 519-534.

Komatsu, T., Holly, F.M.Jr., Nakashiki, N. and Ohgushi, K. (1985). "Numerical calculation of pollutant transport in one and two dimensions." *Journal of Hydroscience and Hydraulic Engineering*, Vol. 3, No. 2, pp. 15-30.

Koussis, A.D. and Rodriguez-Mirasol, J. (1998). "Hydraulic estimation of dispersion coefficient for streams." *Journal of Hydraulic Engineering,* Vol. 124, No. 3, pp. 317-320.

LaBolle, E.M., Fogg, G.E. and Tompson, A.F.B. (1996). "Random walk simulation of transport in heterogeneous porous media: Local mass conservation problem and implementation methods." *Water Resources Research*, Vol. 32, No. 3, pp. 583-593.

Lal, A.M.W. (1998). "Weighted implicit finite-volume model for overland flow." *Journal of Hydraulic Engineering,* Vol.124, No.9, pp. 941-950.

Leonard, B.P. (1979). "A stable and accurate convective modeling procedure based on quadratic upstream interpolation." *Computer Methods in Applied Mechanics and Engineering*, Vol. 19, pp. 59-98.

Leonard, B.P. (1991). "The ULTIMATE conservative difference scheme applied to unsteady one-dimensional advection." *Computer Methods in Applied Mechanics and Engineering*, Vol. 88, pp. 17-74.

Leonard, B.P. and Noye, B.J. (1989). "Second and third order two-level implicit FDM's for unsteady one-dimensional convection-diffusion." *Computational Techniques and Applications CTAC-89*, edited by W.L. Hogart and B.J. Noye, pp. 311-317.

Liggett, J.A. and Woolhiser, D.A. (1967). "Difference Solutions of Shallow Water Equation." *Journal of Engineering Mechanics Division, ASCE.* Vol. 95 No. EM-2, pp. 39-71.

Lin, Y. and Medina Jr., M.A. (2003). "Incorporating transient storage in conjunctive stream-aquifer modeling." *Advances in Water Resources,* Vol. 26, No. 9, pp. 1001-1019.

Liu, H. (1977). "Predicting dispersion coefficient of streams." *Journal of the Environmental Engineering Division, ASCE*, Vol. 103, No. EE1, pp. 59-69.

Magazine, M.K., Pathak, S.K. and Pande, P.K. (1988). "Effect of bed and side roughness on dispersion in open channels." *Journal of Hydraulic Engineering,* Vol. 114, No. 7, pp. 766-782.

Manson, J.R. and Wallis, S.G. (1995). "An accurate numerical algorithm for advective transport". *Communications in Numerical Methods in Engineering*, Vol. 11. pp. 1039-1045.

Manson, J.R. and Wallis, S.G. (2000). "A conservative, semi-Lagrangian fate and transport model for fluvial systems – 1. Theoretical development." *Water Research*, Vol. 34, No. 15, pp. 3769-3777.

Manson, J.R., Wallis, S.G. and Hope, D. (2001). "A conservative semi-Lagrangian transport model for rivers with transient storage zones." *Water Resources Research*, Vol. 37, No. 12, pp. 3321-3329.

Marceau, D. (1999) "The scale issue in social and natural sciences." *Canadian Journal of Remote Sensing*, Vol. 25, No. 4, pp. 347-356.

Marcus, K.B. and Julien, P.Y. (1990). "Two dimensional modeling of overland flow." *Hydraulics/Hydrology of Arid Lands*, Proceedings of the International Symposium, Hydraulics Division of ASCE and Irrigation and Drainage Division of ASCE, 07/30-08/02 1990, San Diego, CA. pp. 256-261.

Marinelli, F. and Durnford, D.S. (1998). "Semi-analytical solution to Richards' equation for layered porous media." *Journal of Irrigation and Drainage Engineering, ASCE*, Vol. 124, No. 6, pp. 290-299.

Marino, M.A. (1967). "Hele-Shaw model study of the growth and decay of groundwater ridges." *Journal of Geophysical Research*, Vol. 72, No. 4, pp. 1195-1205.

Marino, M.A. and Luthin, J.N. (1982). *Seepage and Groundwater*. Developments in Water Science 13, Elsevier Scientific Publishing Company, 489p.

McBride, G.B. and Rutherford, J.C. (1984). "Accurate modeling of river pollutant transport." *Journal of Environmental Engineering*, Vol. 110, No. 4, pp. 808-827.

McDonald, M.G. and Harbaugh, A.W. (1988). "A modular three-dimensional finite difference groundwater flow model." *U.S. Geological Survey Techniques of Water Resources Investigations,* Book 6, Chapter A1, 586p.

McQuivey, R.S. and Keefer, T.N. (1974). "Simple method for predicting dispersion in streams." *Journal of the Environmental Engineering Division, ASCE*, Vol. 100, No. EE4, pp. 997-1011.

Miller, C.T., Williams, G.A., Kelley, C.T. & Tocci, M.D. (1998). "Robust solution of Richards' equation for non-uniform porous media." *Water Resources Research*, Vol. 34, No. 10, pp. 2599-2610.

Milly, P.C.D. (1985). "A mass-conservative procedure for time-stepping in models of unsaturated flow." *Advances in Water Resources*, Vol. 8, No. 3, pp. 32-36.

Moore, I.D. and Foster, G.R. (1990). "Chapter 7: Hydraulics of Overland Flow." In *Process Studies in Hill Slope Hydrology,* edited by M.G. Anderson and T.P. Burt, John Wiley ans Sons Ltd., pp. 215-254.

Morita, M. and Yen, B.C. (2002). "Modeling of conjunctive two-dimensional surface-three dimensional subsurface flows." *Journal of Hydraulic Engineering*, ASCE, Vol. 128, No. 2, pp. 184-200.

Motha, J. A. and Wigham, J. M. (1995). "Modeling overland flow with seepage." *Journal of Hydrology*, Vol.169, pp. 265-280.

Mualem, Y. (1976). "A new model for predicting the hydraulic conductivity of unsaturated porous media." *Water Resources Research*, Vol. 12, No. 3, pp. 513-522.

Narasimhan, T.N. and Witherspoon, P.A. (1977). "Numerical model for saturated-unsaturated flow in deformable porous media: 1. Theory." *Water Resources Research*, Vol. 13, No. 3, pp. 657-664.

Narasimhan, T.N., Witherspoon, P.A. and Edwards A.L. (1978). "Numerical model for saturated-unsaturated flow in deformable porous media: 2. The algorithm", *Water Resources Research*, Vol.14, No.2, pp. 255-261.

Neuman, S.P., 1973. "Saturated-unsaturated seepage by finite elements", *Journal of Hydraulics Division ASCE,* Vol. 99, No. HY12, pp. 2233-2250.

Neuman, S.P. (1984). "Adaptive Eulerian-Lagrangian finite element method for advection-dispersion." *International Journal for Numerical Methods in Engineering*, Vol. 20, pp. 321-337.

Noye, B.J. (1990). "A new third-order finite difference method for transient one-dimensional advection-diffusion." *Communications in Applied Numerical Methods*, Vol. 6, pp. 279-288.

Ogata, A. and Banks, R.B. (1961). "A solution of the differential equation of longitudinal dispersion in porous media." *Professional Paper No. 411-A*, U.S. Geological Survey, Washington, D.C.

Oliveira, A. and Baptista, A.M. (1995). "A comparison of integration and interpolation Eulerian-Lagrangian methods." *International Journal for Numerical Methods in Fluids*, Vol. 21, pp. 183-204.

Pan, L. and Wierenga, P.J. (1995). "A transformed pressure head-based approach to solve Richards' equation for variably saturated soils." *Water Resources Research*, Vol. 31, No. 4, pp. 925-931.

Pan, L., Warrick, A.W. and Wierenga, P.J. (1996). "Finite element methods for modeling water flow in variably saturated porous media: Numerical oscillation and mass-distributed schemes." *Water Resources Research*, Vol. 32, No. 6, pp. 1883-1889.

Pan, L. and Wierenga, P.J. (1997). "Improving numerical modeling of two dimensional water flow in variably saturated, heterogeneous porous media." *Soil Science Society of America Journal*, Vol. 61, No. 2, pp. 335-346.

Paniconi, C., Aldama A.A. and Wood, E.F. (1991). "Numerical evaluation of iterative and non-iterative methods for the solution of the nonlinear Richards' equation." *Water Resources Research*, Vol. 27, No. 6, pp. 1147-1163.

Philip, J.R. (1957). "The theory of infiltration: 1. The infiltration equation and its solution." *Soil Science*, Vol. 83, No. 5, pp. 345-357.

Philip, J.R. (1969). "Theory of infiltration." *Advances in Hydroscience,* Vol. 5, pp. 215-296.

Pinder, G.F. and Sauer, S.P. (1971). "Numerical simulation of flood wave modification due to bank storage effects." *Water Resources Research*, Vol. 7, No. 1, pp. 63-70.

Playan, E., Walker, W.R. and Merkey, G.P. (1994). "Two-dimensional simulation of basin irrigation, 1: Theory." *Journal of Irrigation and Drainage Engineering*, Vol. 120, No. 5, pp. 837-856.

Preissmann, A. (1961). "Propagation of translatory waves in channels and rivers." *Proceedings of the First Congress of French Association for Computation*, Grenoble, France, pp. 433-442.

Radwan, S.F. (1999). "On the fourth order accurate compact ADI scheme for solving the unsteady non-linear coupled Burger's equation." *Journal of Nonlinear Mathematical Physics*, Vol. 6. No.1, pp. 13-34.

Rathfelder, K. and Abriola, L. M. (1994). "Mass-conservative numerical solutions of the head-based Richards' equation." *Water Resources Research*, Vol. 30, No. 9, pp. 2579-2586.

Ravi, V. and Johnson, J.A. (1993). *VLEACH: A One-Dimensional Finite Difference Vadose Zone Leaching Model.* U.S. Environmental Protection Agency Robert S. Kerr Environmental Research Laboratory, Center for Subsurface Modeling Support, Ada, Oklahoma, 65p.

Refsgaard, J.C. and Storm, B. (1995). "MIKE SHE." In *Computer Models of Watershed Hydrology*, edited by V.P. Singh, pp.809-846.

Ristenpart, E. and Wittenberg, D. (1991). "Hydrodynamic water quality simulation – an approximative solution." *Water Science and Technology*, Vol. 24, No. 6, pp. 157-163.

Romano, N., Brunone B. and Santini, A. (1998). "Numerical analysis of one-dimensional unsaturated flow in layered soils." *Advances in Water Resources*, Vol. 21, pp. 315-324.

Ross, B.B., Contractor, D.N. and Shanholtz, V.O. (1977). "Finite element simulation of overland flow and channel flow." *Transactions of the ASAE,* Vol. 20, No. 4, pp. 705-712.

Ross, B.B., Contractor, D.N. and Shanholtz, V.O. (1979). "A finite element model of overland flow and channel flow for assessing the hydrological impact of land use change." *Journal of Hydrology*, Vol. 41, pp. 11-30.

Runkel, R.L. and Chapra, S.C. (1993). "An efficient numerical solution of the transient storage equations for solute transport in small streams." *Water Resources Research*, Vol. 29, No. 1, pp. 211-215.

Runkel, R.L. (1998). *One-dimensional transport with inflow and storage (OTIS): a solute transport model for streams and rivers*. U.S. Geological Survey Water Resources Investigations Report, No. 98-4018, 73p.

Sander, G.C., Parlange, J.Y., Kuhnel, V., Hogarth, W.L., Lockington, D. and O'Kane, J.P.J. (1988). "Exact nonlinear solution for constant flux infiltration." *Journal of Hydrology*, Vol. 97, pp. 341-346.

Seo, I.W. and Cheong, T.S. (1998). "Predicting longitudinal dispersion coefficient in natural streams." *Journal of Hydraulic Engineering,* Vol. 124, No. 1, pp. 25-32.

Shakill, B.S. and Johnson, L.E. (2000). "F2D: A kinematic distributed watershed rainfall-runoff model." *NOAA Technical Memorandum OAR FSL-24,* Forecast Systems Laboratory, Boulder, CO, 28p.

Simunek, J., Sejna, M. and van Genuchten, M. Th. (1998). *The HYDRUS 1-D Software Package for Simulating the One-Dimensional Movement of Water, Heat and Multiple Solutes in Variably-Saturated Media*. U.S. Salinity Laboratory, Agricultural Research Service, U.S. Department of Agriculture, Riverside, California, 165p.

Singh, V.P. (1995). "Watershed Modeling." In *Computer Models of Watershed Hydrology*, edited by V.P. Singh, pp. 1-22.

Singh, V.P. and Bhallamudi, S.M. (1998). "Conjunctive surface-subsurface modeling of overland flow." *Advances in Water Resources*, Vol. 21, pp. 567-579.

Smith, R.E. and Woolhiser, D.A. (1971). "Overland flow on an infiltrating surface." *Water Resources Research*, Vol. 7, No. 4, pp. 899-913.

Spotz, W.F. and Carey, G.F. (2001). "Extension of high-order compact schemes to time dependent problems." *Numerical Methods in Partial Differential Equations*, Vol. 17, pp. 657-672.

Srivastava, R. and Yeh, T.C.J. (1991). "Analytical solutions for one-dimensional, transient, intilration toward the water table in homogeneous and layered soils." *Water Resources Research*, Vol. 27, No. 5, pp. 753-762.

Stamou, A. I. (1991). "Numerical modeling of water quality in rivers using the QUICK scheme." *Advances in Water Resources Technology*, edited by G. Tsakiris, pp. 397-405.

Stamou, A. I. (1992). "Improving the numerical modeling of river water quality by using higher order difference schemes." *Water Research*, Vol. 26, No. 12, pp. 1563-1570.

STATSGO (1998). State soil geographic (STATSGO) database of Georgia. Georgia GIS Data Clearinghouse: http://gis1.state.ga.us

Stephenson, D. and Meadows, M.E. (1986). *Kinematic Hydrology and Modeling*. Developments in Water Science, Vol.26. 250p.

Still, D.A. and Shih, S.F. (1985). "Using Landsat data to classify land use for assessing the basinwide runoff index." *Water Resources Bulletin*, Vol. 21, No. 6, pp. 931-940.

Stoker, J.J. (1953). "Numerical solution of flood prediction and river regulation problems: Derivation of basic theory and formulation of numerical methods of attack." Report No. IMM-NYU-200, New York University, Institute of Mathematical Science, New York.

Streeter, V. L. and Wylie, E. B. (1967). *Hydraulic Transients.* McGraw Hill Book Co., pp. 239-259.

Strelkoff, T. (1969). "One dimensional equations of open channel flow." *Journal of Hydraulics Division, ASCE*, Vol. 95, No. HY 3, pp. 861-876.

Strelkoff, T. (1970). "Numerical Solution of Saint-Venant Equations." *Journal of Hydraulics Division, ASCE*, Vol. 96, No. HY 1, pp. 223-252.

Sturm, T. W. (2001). *Open Channel Hydraulics*. McGraw Hill Inc., 493p.

Szymkiewicz, R. (1991). "Finite element method for the solution of the Saint Venant equations in an open channel network." *Journal of Hydrology*, Vol. 122, pp. 275-287.

Tayfur, G., Kavvas M.L., Govindaraju, R.S. and Storm, D.E. (1993). "Applicability of St. Venant equations for two-dimensional overland flows over rough infiltrating surfaces." *Journal of Hydraulic Engineering, ASCE*, Vol. 119, No. 1, pp. 51-63.

Taylor, G.I. (1954). "Dispersion of matter in turbulent flow through a pipe." *Proceedings of the Royal Society, London, U.K. Series – A*, Vol. 223, pp. 446-468.

Tocci, M.D., Kelley C.T. and Miller, C.T. (1997). "Accurate and economical solution of the pressure-head form of Richards' equation by the method of lines." *Advances in Water Resources*, Vol. 20, No. 1, pp. 1-14.

Tompson, A.F.B. and Gelhar, L.W. (1990). "Numerical simulation of solute transport in three dimensional randomly heterogeneous media." *Water Resources Research*, Vol. 26, No. 10, pp. 2541-2562.

Tracy, F.T. (1995). "1-D, 2-D and 3-D analytical solutions of unsaturated flow in groundwater." *Journal of Hydrology*, Vol. 170, pp. 199-214.

Tucci, C.E.M. and Chen, Y.H. (1981). "Unsteady water quality model for river network." *Journal of the Water Resources Planning and Management Division ASCE*, Vol. 107, No. WR2, pp. 477-493.

Valenzuela, C. and Aral, M.M. (2004). "Application of HSPF to the Lower Altamaha River Basin." Report no: MESL-02-04, Multimedia Environmental Simulations Laboratory Report, School of Civil and Environmental Engineering, Georgia Institute of Technology, Atlanta, Georgia (in preparation).

Van Dam, J.C. and Feddes, R.A. (2000). "Numerical simulation of infiltration, evaporation and shallow groundwater levels with the Richards' equation." *Journal of Hydrology*, Vol. 233, pp. 72-85.

Van Genuchten, M. Th. (1980). "A closed-form equation for predicting the hydraulic conductivity of unsaturated soils." *Soil Science Society of America Journal*, Vol. 44, pp. 892-898.

Van Genuchten, M.Th. (1982). "A comparison of numerical solutions of the one-dimensional unsaturated-saturated flow and mass transport equations." *Advances in Water Resources*, Vol. 5, No. 3, pp. 47-55.

Van Genuchten, M.Th. and Alves, W.J. (1982). *Analytical solutions of the one-dimensional convective-dispersive solute transport equation*. U.S. Department of Agriculture, Technical Bulletin No. 1661, 151p.

Vanderkwaak, J.E. and Loague, K. (2001). "Hydrologic-response simulations for the R-5 catchment with a comprehensive physics-based model." *Water Resources Research*, Vol. 37, No. 4, pp. 999-1013.

Voss, C.I. (1984). *SUTRA: A finite element simulation model for saturated-unsaturated, fluid density dependent groundwater flow with energy transport or chemical reactive single species solute transport.* US Geological Survey, Water Resources Investigations Report 84-4369.

Wallach, R. and Shabtai, R. (1992). "Surface runoff contamination by soil chemicals: simulations for equilibrium and first-order kinetics." *Water Resources Research*, Vol. 28, No. 1, pp. 167-173.

Wallach, R., Grigorin G. and Rivlin, J. (1997). "The errors in surface runoff prediction by neglecting the relationship between infiltration rate and overland flow depth." *Journal of Hydrology*, Vol. 200, pp. 243-259.

Wallach, R., Grigorin, G. and Rivlin, J. (2001). "A comprehensive mathematical model for transport of soil-dissolved chemicals by overland flow." *Journal of Hydrology*, Vol.247, pp. 85-99.

Wang, H. Q. and Lacroix, M. (1997). "Optimal weighing in the finite difference solution of the convection-dispersion equation." *Journal of Hydrology*, Vol. 200, pp. 228-242.

Warrick, A.W. (1975). "Analytical solutions to the one-dimensional linearized moisture flow equation for arbitrary input." *Soil Science*, Vol 120, No. 2, pp. 79-84.

Warrick, A.W., Lomen, D.O. and Islas, A. (1990). "An analytical solution to Richards' equation for a draining soil profile." *Water Resources Research*, Vol. 26, No. 2, pp. 253-258.

Warrick, A.W., Islas, A. and Lomen, D.O. (1991). "An analytical solution to Richards' equation for time-varying infiltration." *Water Resources Research*, Vol. 27, No. 5, pp. 253-258.

Weiyan, T. (1992). *Shallow Water Hydrodynamics*. Elsevier Science Publishers, Amsterdam, 434p.

Williams, G.A. and Miller, C.T. (1999). "An evaluation of temporally adaptive transformation approaches for solving Richards' equation." *Advances in Water Resources*, Vol. 22, No. 8, pp. 831-840.

Williams, G.A., Miller C.T. and Kelley, C.T. (2000). "Transformation approaches for simulating flow in variably saturated porous media." *Water Resources Research*, Vol. 36, No. 4, pp. 923-934.

Wylie, E.B. (1970). "Unsteady Free Surface Flow Computation." *Journal of Hydraulics Division, ASCE*, Vol. 96, No. HY 11, pp. 2241-2251.

Yan, M. and Kahawita, R. (2000). "Modeling the fate of pollutant in overland flow." *Water Research*, Vol. 34, No. 13, pp. 3335-3344.

Yeh, G.T. (1999). *Computational Subsurface Hydrology: Fluid Flows*. Kluwer Academic Publishers, Norvell, Massachusetts, 277p.

Yeh, G.T., Cheng, H.P., Cheng, J.R., Lin, H.C. and Martin, W.D. (1998). *A numerical model simulating water flow and contaminant and sediment transport in watershed systems of 1-D stream-river network, 2-D overland regime and 3-D subsurface media (WASH123D: Version 1.0*). Technical Report CHL-98-19. Waterway Experiment Station, U. S. Army Corps of Engineering, Vicksburg, MS.

Yeh, T.C., Srivastava, R., Guzman, A. and Harter, T. (1993). "A numerical model for water flow and chemical transport in variably saturated porous media." *Groundwater*, Vol. 31, No. 4, pp. 634-644.

Yu, T.S. and Li, C.W. (1994). "Efficient higher order backward characteristics schemes for transient advection." *International Journal for Numerical Methods in Fluids*, Vol. 19, pp. 997-1021.

Zhang, Y. (1998). *Numerical modeling of shock wave propagation and contaminant fate and transport in open channel networks*. Ph.D. Dissertation, Georgia Institute of Technology, Atlanta, GA, USA. 332p.

Zhang, R., Huang, K. and van Genuchten, M.T. (1993). "An efficient Eulerian-Lagrangian method for solving solute transport problems in steady and transient flow fields." *Water Resources Research*, Vol. 29, No. 12, pp. 4131-4138.

Zhang, X. and Ewen, J. (2000). "Efficient method for simulating gravity-dominated water flow in unsaturated soils." *Water Resources Research*, Vol. 36, No. 9, pp. 2777-2780.

Zhang, X., Bengough, A.G., Crawford J. W. and Young, I. M. (2002). "Efficient methods for solving water flow in variably saturated soils under prescribed flux infiltration." *Journal of Hydrology*, Vol. 260, pp. 75-87.

Zhang, W. and Cundy, T.W. (1989). "Modeling of two-dimensional overland flow." *Water Resources Research*, Vol. 25, No. 9, pp. 2019-2035.

Zhao, D.H., Shen, H.W., Tabios, G.Q., Lai, J.S. and Tan, W.Y. (1994). "Finite volume two dimensional unsteady flow model for river basins." *Journal of Hydraulic Engineering, ASCE*, Vol. 120, No. 7, pp. 863-883.

Zienkiewicz, O.C. and Taylor, R.L. (1989). *The Finite Element Method: Volume 1 Basic Formulation and Linear Problems*. McGraw-Hill Book Company, 648p.

VITA

The author was born on November 15, 1972 in Ankara, Turkey. He received his Bachelor of Science degree in Environmental Engineering from the Department of Environmental Engineering of Middle East Technical University in Ankara, Turkey in June 1994. After his graduation, he became a graduate research and teaching assistant in the same program and continued his studies towards his master's degree. He received his Master of Science degree in Environmental Engineering from the same department in June 1997, for which, he received the "Best Thesis Award - 1997". He later joined Prof. Dr. Mustafa N. Parlar Research and Education Foundation of Middle East Technical University and worked as a project coordinator for one year. He was later awarded a Doctoral scholarship by the Turkish Council of Higher Education. Mr. Gunduz started his Ph.D. education in the School of Civil and Environmental Engineering of Georgia Institute of Technology in September 1998. He received his Master of Science in Civil Engineering degree from the same school in December 2000. His research interests include hydrologic and hydraulic modeling of watershed processes, numerical modeling and GIS applications of surface and subsurface flow systems.